

Uniwersytet im. Adama Mickiewicza w Poznaniu

Wydział Chemii

## **ROZPRAWA DOKTORSKA**

**mgr Natalia Berdzik**

**Nowe pochodne graminy – synteza, analiza spektroskopowa  
oraz ocena aktywności biologicznej**

**New gramine derivatives - synthesis, spectroscopic analysis and  
biological activity**

W formie spójnego tematycznie cyklu artykułów opublikowanych  
w czasopismach naukowych

Promotor: prof. UAM dr hab. Beata Jasiewicz

Poznań 2024



*Składam serdeczne podziękowania  
Prof. UAM dr hab. Beacie Jasiewicz  
za poświęcony czas oraz pomoc  
w opracowaniu niniejszej pracy*

*Chciałabym podziękować również  
Prof. UAM dr hab. Tomaszowi Pospiesznemu,  
dr Hannie Koenig, dr Arlecie Sierakowskiej  
za cenne wskazówki, sugestie i uwagi  
oraz prof. UAM dr hab. Lucynie Mrówczyńskiej  
za pomoc w realizacji badań biologicznych*

*Dziękuję Mildzie i Kamilowi  
za współpracę i przyjazną atmosferę.*

*Pragnę serdecznie podziękować  
mojemu Wojtkowi, rodzinie i przyjaciołom  
za ogromne wsparcie, motywację i zrozumienie.*



# Spis treści

Życiorys naukowy.....	1
Lista publikacji.....	2
Wstęp i cel pracy.....	4
<b>Część literaturowa</b> .....	<b>6</b>
1. Charakterystyka i reaktywność indolu.....	7
2. Naturalne pochodne indolu .....	13
2.1. Związki indolu pochodzenia zwierzęcego .....	14
2.2. Związki indolu pochodzenia roślinnego .....	15
3. Syntetyczne pochodne indolu o znaczeniu farmakologicznym.....	19
3.1. Pochodne indolu o właściwościach przeciwzapalnych.....	19
3.2. Pochodne indolu o właściwościach antynowotworowych.....	21
3.3. Tryptany - analogi indolu stosowane w leczeniu migreny.....	22
3.4. Pochodne indolu o znaczeniu przeciwdrobnoustrojowym.....	24
3.5. Przeciwwirusowe pochodne indolu .....	26
3.6. Pochodne indolu o właściwościach antyoksydacyjnych.....	27
3.7. Mechanizmy działania antyoksydantów na przykładzie indolo-3-karbinolu .....	31
4. Gramina jako związek wyjściowy w syntezie nowych pochodnych indolu .....	34
4.1. Reaktywność cząsteczki graminy .....	34
4.2. Pochodne graminy o znaczeniu biologicznym.....	37
<b>Wyniki badań</b> .....	<b>39</b>
1. Pochodne pierwszej grupy .....	40
2. Pochodne drugiej grupy .....	53
3. Pochodne trzeciej grupy.....	58
Podsumowanie .....	62
Spis rysunków.....	65
Schematy przeprowadzonych syntez .....	68

Literatura.....	71
Streszczenie rozprawy doktorskiej .....	90
Publikacje wchodzące w skład rozprawy doktorskiej i materiały uzupełniające .....	92

## **Życiorys naukowy**

Urodziłam się 13 maja 1996 roku w Szczecinie. W 2015 roku ukończyłam Liceum Ogólnokształcące im. Noblistów Polskich w Pyrzycach.

W październiku 2015 roku rozpoczęłam studia na Wydziale Chemii im. Adama Mickiewicza w Poznaniu wybierając, jako specjalność, chemię biologiczną. Pracę licencjacką realizowałam w zakładzie Chemii Związków Heterocyklicznych. Tematem moich badań była synteza nowych pochodnych nikotyny. W roku 2018, w ramach pracy magisterskiej rozpoczęłam badania nad syntezą nowych pochodnych graminy o potencjalnej aktywności antyoksydacyjnej, które wykonywałam w Zakładzie Produktów Bioaktywnych. Zarówno pracę licencjacką jak i magisterską przygotowywałam pod opieką Pani Prof. UAM dr hab. Beaty Jasiewicz. Zainteresowanie tematyką alkaloidów indolowych kontynuowałam na studiach w Szkole Doktorskiej Nauk Ścisłych, które rozpoczęłam w październiku 2020 roku.

W czasie mojej nauki w Szkole Doktorskiej prowadziłam również badania hemokompatybilności i aktywności antyoksydacyjnej otrzymanych przeze mnie związków. Wspomniane prace wykonywałam w Zakładzie Biologii Komórki na Wydziale Biologii UAM przy wsparciu Pani Prof. UAM dr hab. Lucyny Mrówczyńskiej.

Wyniki swoich badań przedstawiłam na kilku konferencjach krajowych w postaci posterów oraz komunikatów ustnych. Jestem współautorką czterech publikacji w czasopismach z listy filadelfijskiej oraz siedmiu rozdziałów w monografiach.

## Lista publikacji

### Publikacje wchodzące w skład rozprawy doktorskiej

- P1.** Kozanecka-Okupnik, W., Sierakowska, A., **Berdzik, N.**, Kowalczyk, I., Mrówczyńska, L., Jasiewicz, B. New triazole-bearing gramine derivatives – synthesis, structural analysis and protective effect against oxidative haemolysis. *Natural Product Research*, **2022**, 36(13), 3413–3419. <https://doi.org/10.1080/14786419.2020.1864364>
- P2.** **Berdzik, N.**, Jasiewicz, B., Ostrowski, K., Sierakowska, A., Szlaużys, M., Nowak, D., Mrówczyńska, L. Novel gramine-based bioconjugates obtained by click chemistry as cytoprotective compounds and potent antibacterial and antifungal agents. *Natural Product Research*, **2023**, 1–7. <https://doi.org/10.1080/14786419.2023.2261139>
- P3.** **Berdzik, N.**, Koenig, H., Mrówczyńska, L., Nowak, D., Jasiewicz, B., Pospieszny, T. Synthesis and Hemolytic Activity of Bile Acid-Indole Bioconjugates Linked by Triazole. *Journal of Organic Chemistry*, **2023**, 88(24), 16719–16734 <https://doi.org/10.1021/acs.joc.3c00815>
- P4.** Babijczuk, K., **Berdzik, N.**, Nowak, D., Warżajtis, B., Rychlewska, U., Starzyk, J., Mrówczyńska, L., Jasiewicz, B. Novel C3-Methylene-Bridged Indole Derivatives with and without Substituents at N1: The Influence of Substituents on Their Hemolytic, Cytoprotective, and Antimicrobial Activity. *International Journal of Molecular Sciences*, **2024**, 25(10), 5364, <https://doi.org/10.3390/ijms25105364>

### Rozdziały w monografiach

- 1.** **Berdzik, N.**, Sierakowska, A., Kozanecka-Okupnik, W., Jasiewicz, B., Mrówczyńska, L. Biological activity of new indole derivatives, *The Book of Articles*. National Scientific Conference “e-Factory of Science” V edition, **2021**, 6-16,
- 2.** **Berdzik, N.**, Sierakowska, A., Jasiewicz, B. Synteza i analiza spektroskopowa nowych pochodnych indolu. *Nauka i przemysł-metody spektroskopowe w praktyce, nowe wyzwania i możliwości*. Hubicki Zbigniew (red.), **2021**, vol. 1, Lublin, Uniwersytet Marii Curie-Skłodowskiej w Lublinie, s.114-117, ISBN 9788322795040
- 3.** Sierakowska, A., **Berdzik, N.**, Jasiewicz, B. Synteza i analiza spektroskopowa nowych pochodnych kofeiny. *Nauka i przemysł-metody spektroskopowe w praktyce, nowe wyzwania i możliwości*. Hubicki Zbigniew (red.), **2021**, vol. 1, Lublin, Uniwersytet Marii Curie-Skłodowskiej w Lublinie, s.109-113, ISBN 9788322795040



4. **Berdzik, N.**, Sierakowska, A., Ostrowski, K., Jasiewicz, B. Synthesis of new indole dimers with triazole ring, The Book of Articles. National Scientific Conference "Knowledge – Key to Success" VI edition, **2022**, 5-13, ISBN: 978-83-963887-0-4
5. Ostrowski, K., Sierakowska, A., **Berdzik, N.**, Jasiewicz, B. Click chemistry as a tool for the synthesis of new caffeine derivatives, The Book of Articles. National Scientific Conference "Knowledge – Key to Success" VI edition, **2022**, 46-52, ISBN: 978-83-963887-0-4
6. Szlauzys, M., **Berdzik, N.**, Ostrowski, K., Jasiewicz, B. Synthesis of new indole-uracil bioconjugates with potent biological activity, The Book of Articles. National Scientific Conference "e-Factory of Science" IX edition, **2023**, 87-94, ISBN: 978-83-967915-2-8
7. **Berdzik, N.**, Jasiewicz, B., Starzyk, J. Synteza, analiza spektroskopowa oraz wstępna ocena aktywności biologicznej nowych estrów indolowych. Na pograniczu chemii, biologii i fizyki – rozwój nauk. Tom 5/Szłyk Edward (red.), **2023**, Wydawnictwo Naukowe Uniwersytetu Mikołaja Kopernika, 9-18, ISBN 9788323152590

#### Udział w konferencjach naukowych

1. **Berdzik, N.**, Sierakowska, A., Kozanecka-Okupnik, W., Jasiewicz, B., Mrówczyńska, L. Aktywność biologiczna nowych pochodnych indolu, e-Factory of Science, 10.04.2021, on-line
2. **Berdzik, N.**, Sierakowska, A., Jasiewicz, B. Synteza i analiza nowych pochodnych indolu, Nauka i przemysł - metody spektroskopowe w praktyce, nowe wyzwania i możliwości, 29.06.2021, on-line
3. Kurek, J. Sierakowska, A., **Berdzik, N.**, Jasiewicz, B. Związki naturalne w ochronie upraw, II EU Green Week, 1.06.2021, on-line
4. **Berdzik, N.**, Sierakowska, A., Ostrowski, K., Jasiewicz, B. Synthesis of new indole dimers with triazole ring, National Scientific Conference "Knowledge – Key to Success" VI edition, 22.01.2022, on-line
5. **Berdzik, N.**, Jasiewicz, B., Koenig, H., Pospieszny, T. Synteza nowych pochodnych zawierających układ indolowy, triazolowy oraz steroidowy. IV Ogólnopolskie Sympozjum Chemii Bioorganicznej, Organicznej i Biomateriałów, 3.12.2022, Poznań
6. **Berdzik, N.**, Jasiewicz, B., Starzyk, J. Synteza, analiza spektroskopowa oraz wstępna ocena aktywności biologicznej nowych estrów indolowych. XVI Kopernikańskie Seminarium Doktoranckie, 29-30.06.2023, Toruń

## - Wstęp i cel pracy –

Badania dotyczące zjawiska braku równowagi między stężeniem wolnych rodników, a skutecznością mechanizmów antyoksydacyjnych organizmu, nazywanego stresem oksydacyjnym, dowodzą, że ma on udział w patofizjologii wielu poważnych chorób, w tym nowotworów, czy chorób neurodegeneracyjnych, takich jak choroby Alzheimera i Parkinsona. Współczesna medycyna nadal zmaga się ze znalezieniem skutecznych leków, które byłyby efektywne w zwalczaniu tych chorób. Dlatego niezmiernie ważnym zagadnieniem jest projektowanie nowych związków o potencjalnej aktywności antyoksydacyjnej. W poszukiwaniu nowych związków aktywnych biologicznie szczególną uwagę zwraca się na związki naturalne, izolowane z roślin, które stanowią punkt wyjścia do modyfikacji chemicznych. Jednym z nich jest alkaloid indolowy, gramina. Zarówno graminę, jak i jej pochodne cechuje wysoka bioaktywność. Poprzez zastosowanie odpowiednich modyfikacji cząsteczki graminy i łączenie jej z innymi biologicznie aktywnymi molekułami możliwe jest zwiększanie potencjału terapeutycznego i obszarów zastosowania otrzymanych pochodnych. To zainspirowało mnie do podjęcia badań w tym obszarze.

**Za cel swojej pracy doktorskiej wybrałam syntezę nowych pochodnych graminy o potencjalnym działaniu antyoksydacyjnym. Praca obejmuje syntezę trzech grup związków (pochodnych indolu), ich charakterystykę spektroskopową, badania *in silico* oraz badania aktywności antyoksydacyjnej *in vitro*.**

Pierwszą grupę stanowią związki **indolowo-triazolowe zawierające linkery alifatyczne o różnej długości łańcucha węglowego**. Do tej grupy wchodzi również **pochodne zawierające dodatkowo ugrupowanie fenyłowe z podstawnikami azydometylenowymi lub pierścieniami ftalimidowymi**. Zbadałam cytotoksyczność tych pochodnych wobec erytrocytów ludzkich oraz **aktywność protekcyjną** wobec indukowanej przez AAPH hemolizie czerwonych krwinek.

Według danych literaturowych kwasy żółciowe powodują rozpad czerwonych krwinek i uwolnienie hemoglobiny do osocza krwi (hemoliza). Badania prowadzone w ubiegłych latach w naszej grupie badawczej, wykazały, że znacznie niższą aktywność hemolityczną wykazują sole pochodnych kwasów żółciowych i graminy. Aby przekonać się czy i w jakim stopniu obecność **ugrupowania triazolowego wpłynie na aktywność**

**hemolityczną koniugatów indolu i kwasów żółciowych otrzymałam serię biokonjugatów acetylowych i formylowych pochodnych kwasów żółciowych i indolu połączonych ugrupowaniem triazolowym.**

Najbardziej preferowaną drogą modyfikacji układu indolowego jest podstawienie pierścienia pirolowego w pozycji C3. Literatura obfituje w przykłady podstawionych w pozycji C3 indoli o różnorodnych właściwościach biologicznych. Kolejnym sposobem modyfikacji pierścienia indolu, może być substytucja zachodząca na heterocyklicznym atomie azotu – w pozycji N1. Opisanych w literaturze *N*-podstawionych pochodnych indolu jest jednak znacznie mniej. Dlatego też trzecią grupę pochodnych, wchodzących w skład mojej pracy doktorskiej, stanowią ***N*-podstawione estrowe pochodne 3-etoksymetyloindolu**, związku który wykazał obiecującą aktywność cytoprotekcyjną przed hemolizą wywołaną stresem oksydacyjnym. Ważnym aspektem było **określenie wpływu modyfikacji pozycji N1 na aktywność antyoksydacyjną otrzymanych pochodnych.**

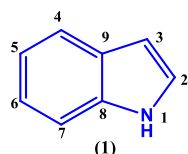
Swoje badania postanowiłam poszerzyć o analizę **aktywności przeciwbakteryjnej i przeciwgrzybiczej** niektórych, nowo otrzymanych pochodnych wobec wybranych gatunków grzybów i bakterii oraz w badaniach *in silico* definiując powinowactwo pochodnych indolu do miejsc aktywnych określonych domen białkowych **wykorzystując dokowanie molekularne.**

Wszystkie wyniki zawarte w tej pracy zostały opublikowane w czasopismach naukowych o zasięgu międzynarodowym.

**- CZEŚĆ LITERATUROWA -**

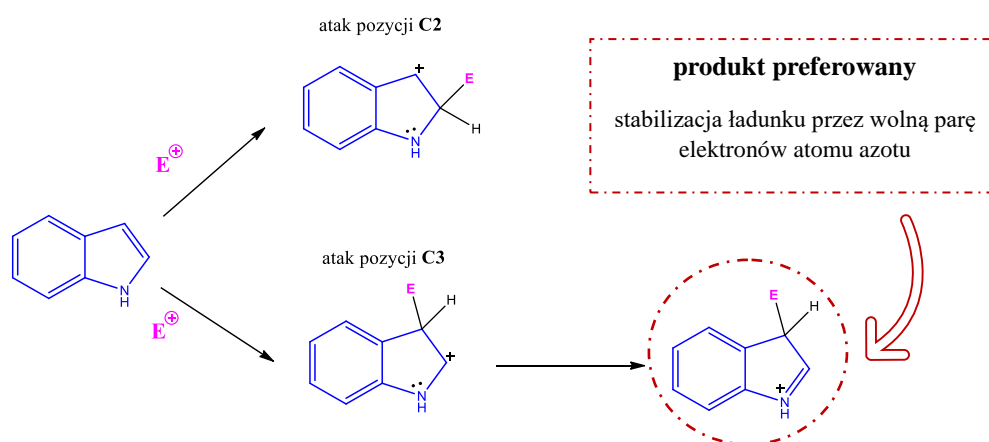
## 1. Charakterystyka i reaktywność indolu

Indol (2,3-benzopirrol) (Rys. 1) jest słabo zasadowym związkiem aromatycznym składającym się z dwóch skondensowanych pierścieni: pięciocząłowego pierścienia pirolowego i sześciocząłowego pierścienia benzenowego [1].



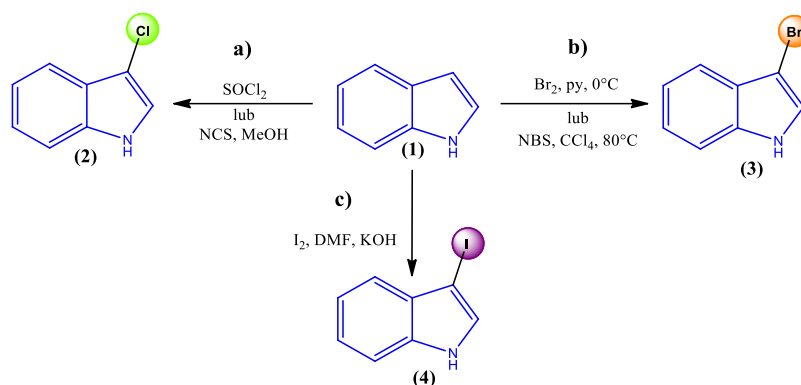
Rysunek 1. Struktura cząsteczki indolu

Posiada nadmiar zdelokalizowanych elektronów  $\pi$ , co czyni jego cząsteczkę wysoce reaktywną w stosunku do klasycznych reakcji substytucji elektrofilowej, takich jak protonowanie, halogenowanie, alkilowanie i acylowanie. Pozycja C3 pierścienia pirolowego jest najbardziej reaktywnym miejscem niepodstawionego układu indolu ze względu na większą stabilność termodynamiczną związku pośredniego utworzonego przez protonowanie (Rys. 2) [1-7].



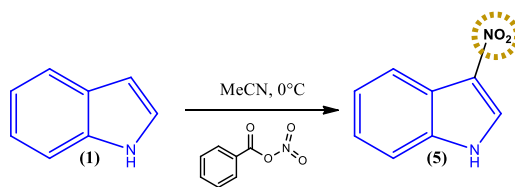
Rysunek 2. Reakcje substytucji elektrofilowej zachodzącej w pozycjach C2 i C3 pierścienia indolu

Na rysunku 3 przedstawiłam schematy reakcji: a) chlorowania; b) bromowania; c) jodowania indolu. Powstałe 3-halogenoindole są jednak bardzo niestabilne, szczególnie w środowisku kwasowym [1,2,8-10].



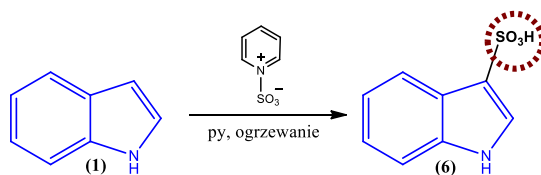
Rysunek 3. Schemat reakcji halogenowania indolu

Nitrowanie indolu przy użyciu klasycznej mieszaniny nitrującej (mieszanina stężonych  $\text{HNO}_3$  i  $\text{H}_2\text{SO}_4$ ) prowadzi do otrzymania trudnych w obróbce produktów, prawdopodobnie z powodu polimeryzacji indolu katalizowanej kwasem. 3-Nitroindol (5) można otrzymać w łagodniejszych warunkach, stosując azotan benzoilu (Rys. 4) [1,8,9,11].



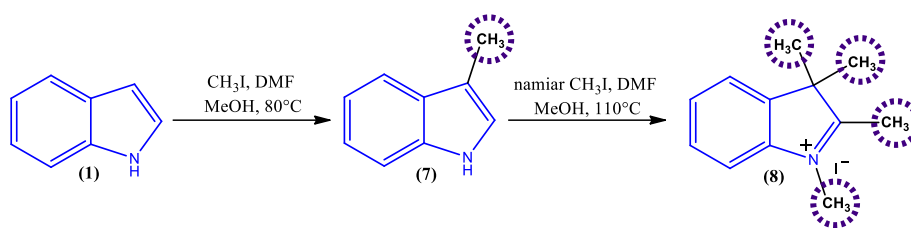
Rysunek 4. Schemat reakcji nitrowania indolu

Ogrzewanie indolu i kompleksu pirydyna – tlenek siarki (VI) w pirydynie prowadzi do sulfonowania indolu w pozycji C3 i utworzenia kwasu indolo-3-sulfonowego (6) (Rys. 5) [1,8,9,12].



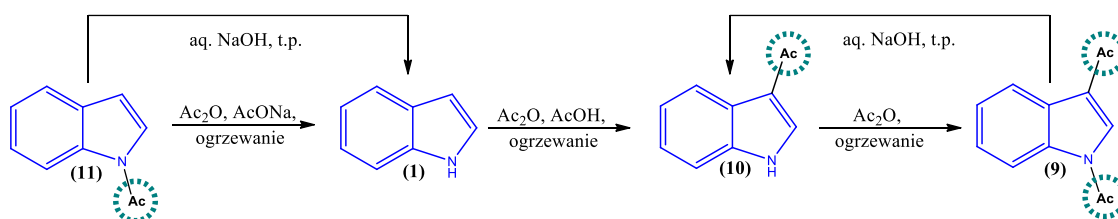
Rysunek 5. Schemat reakcji sulfonowania indolu

Indol nie reaguje z halogenkami alkilu w temperaturze pokojowej. Reakcja indolu z jodometanem w dimetyloformamidzie zachodzi dopiero w temperaturze około  $80^\circ\text{C}$  i skutkuje utworzeniem 3-metyloindolu (skatolu). W miarę wzrostu temperatury, zachodzi dalsze metylowanie do powstania jodku 1,2,3,3-tetrametylo-3*H*-indolu (Rys. 6) [2,8,9].



Rysunek 6. Schemata reakcji metylowania indolu

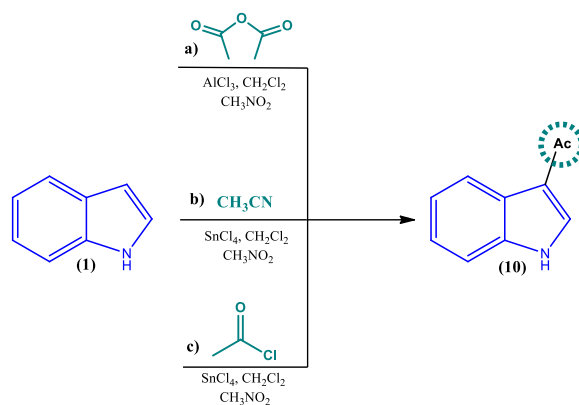
Indol w reakcji z bezwodnikiem octowym w kwasie octowym, w temperaturze powyżej  $140^\circ\text{C}$ , tworzy głównie 1,3-diacetyloindol (9) oraz, w mniejszych ilościach, 3- i *N*-acetyloindol (10 i 11). Z kolei acetylowanie indolu w obecności octanu sodu prowadzi wyłącznie do otrzymania *N*-acetyloindolu (11). 3-Acetyloindol (10) można otrzymać poprzez hydrolizę 1,3-diacetyloindolu (9) w warunkach zasadowych (Rys. 7) [1,2,8,9].



Rysunek 7. Schemat reakcji acetylowania indolu

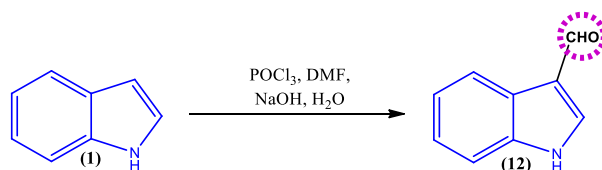
Powyżej opisane reakcje acetylowania indolu w bezwodniku octowym mogą skutkować niską wydajnością reakcji ze względu na konkurencyjne tworzenie się produktów *N*-, 3- lub 1,3-dipodstawionych oraz występowanie innych reakcji ubocznych, często obserwowanych w środowisku kwasowym, takich jak samopolimeryzacja indolu.

3-Acetyloindol (10) można otrzymać także w warunkach Friedla-Craftsa wykorzystując bezwodniki (Rys. 8a), nityle (Rys. 8b) lub chlorki kwasowe (Rys. 8c) w obecności kwasów Lewisa. Reakcje te prowadzą do regioselektywnego otrzymania 3-acetyloindolu z zachowaniem wysokich wydajności reakcji [10,13].



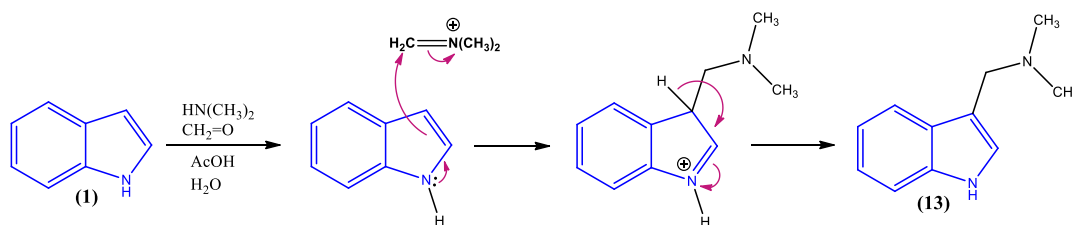
Rysunek 8. Acetylowanie indolu w warunkach Friedla-Craftsa

Reakcja Vilsmeiera-Haacka jest bardzo efektywną metodą formylowania bogatych w elektrony związków aromatycznych. Indolo-3-aldehyd (12) można otrzymać przez bezpośrednie formylowanie indolu dimetyloformamidem, stosując trichlorek fosforu jako katalizator (Rys. 9) [1,2,8,9,14].



Rysunek 9. Schemat reakcji formylowania indolu metodą Vilsmeiera-Haacka

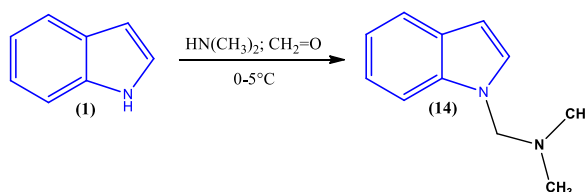
Jedną z głównych metod wprowadzania grupy dimetyloaminometylowej do aktywowanych układów aromatycznych poprzez reakcję z aminą i formaldehydem jest aminometylacja Mannicha. Indol w warunkach reakcji Mannicha, katalizowanej kwasem octowym (lub  $\text{ZnCl}_2$ ), prowadzi do utworzenia graminy (13) – ważnego alkaloidu indolowego (Rys. 10) [1,2,8,9,14].



Rysunek 10. Mechanizm katalizowanej kwasem octowym reakcji Mannicha prowadzącej do utworzenia graminy

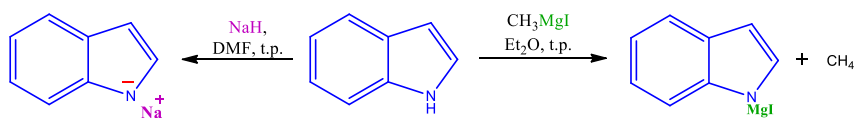


W przypadku cząsteczki indolu, warunki reakcji Mannicha mają istotny wpływ na jej kierunek. Przy wykorzystaniu metody aminometylacji Mannicha możliwe jest także uzyskanie *N*-dimetyloaminometyloindolu (14) poprzez obniżenie temperatury reakcji do 0-5°C (Rys. 11) [14].



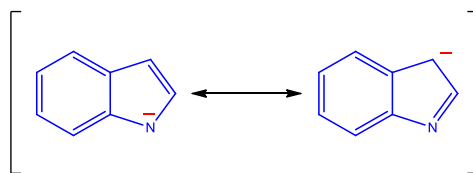
Rysunek 11. Schemat reakcji Mannicha zachodzącej w obniżonej temperaturze

Grupa aminowa pierścienia heterocyklicznego jest słabym nukleofilem, dlatego podstawienie pozycji N1 jest możliwe tylko wtedy, gdy kwaśny proton grupy -NH zostanie usunięty w celu wytworzenia silnie naładowanego nukleofila. Atom wodoru związany z heterocyklicznym atomem azotu indolu jest znacznie bardziej kwaśny ( $pK_a=16,2$ ) niż w innych aromatycznych aminach ( $pK_a$  aniliny wynosi 30,7). Pod wpływem bardzo mocnych zasad (wodorek sodu, *n*-butylolit lub alkiłowy odczynnik Grignarda) *N*-niepodstawiony indol przekształca się w odpowiedni anion indolilowy (Rys. 12) [2,8,9].



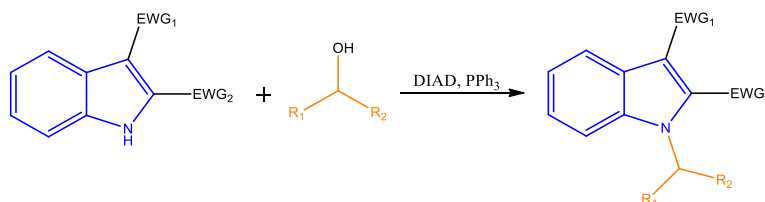
Rysunek 12. Reakcja indolu z mocnymi zasadami

Anion indolilowy ma dwie główne struktury mezomeryczne (Rys. 13), w których ładunek ujemny znajduje się głównie na atomie azotu i atomie węgla C3. Z tego względu anion indolilowy zachowuje się jak ambidentny nukleofil: w zależności od warunków reakcji podstawienie może zachodzić w pozycjach C3 lub w N1.



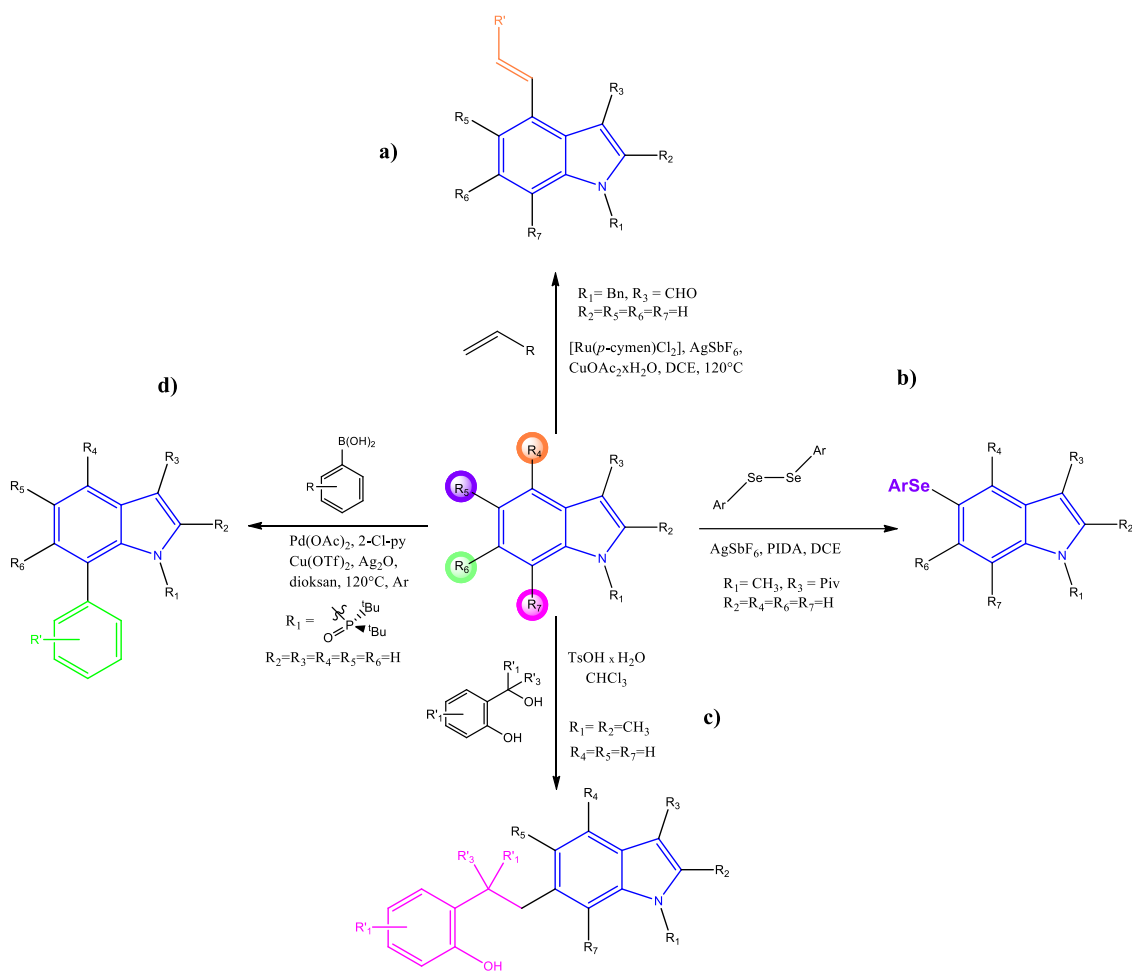
Rysunek 13. Struktury mezomeryczne anionu indolilowego

Reakcja Mitsunobu jest jedną z metod *N*-alkilowania pochodnych indolu przy użyciu alkoholi, tryfenylofosfiny (PPh<sub>3</sub>) oraz azodikarboksylanu diizopropylu (DIAD). Jednakże, aby zwiększyć kwasowość atomu wodoru grupy -NH indolu, wymagane jest podstawienie pozycji C2 lub C3 pierścienia indolowego podstawnikami wyciągającymi elektrony (EWG) (Rys. 14) [15].



Rysunek 14. Schemat alkilowania indolu w pozycji N1 przy użyciu reakcji Mitsunobu

W porównaniu do pierścienia pirolowego, dostęp do mniej aktywowanego pierścienia benzenowego pozostaje dużym wyzwaniem. Opracowano jednak kilka metod na wprowadzanie podstawników w pozycje C4-C7 układu indolowego. Reakcja *N*-benzylindolu, podstawionego w pozycji C3 grupą formylową, z odpowiednimi akrylanami, przy zastosowaniu katalizatorów rutenowych i srebrnych, prowadzi do selektywnego otrzymania C4-podstawionych indoli (Rys. 15a) [16]. Regioselektywne selenowanie w pozycji C5 jest natomiast możliwe poprzez zastosowanie AgSbF<sub>6</sub> i (diacetoksy)jodobenzenu (PIDA) jako katalizatora (Rys. 15b) [17]. Z kolei 2,3-dimetyloindol, w katalizowanej kwasem *p*-toluenosulfonowym (TsOH), reakcji z alkoholami *o*-hydroksybenzylowymi tworzy pochodne podstawione w pozycji C6 (Rys. 15c) [18]. Podstawienie atomu azotu pierścienia pirolowego indolu grupami takimi jak grupa silylowa i piwalowa (Piv), okazało się mieć wpływ kierunkowy na regioselektywność reakcji borowania, olefinowania i amidowania w pozycji C7. Arylowanie atomu węgla C7 z wysoką regioselektywnością następuje w wyniku reakcji *N*-podstawionego indolu z kwasami fenyloboronowymi (Rys. 15d) [9,19,20].



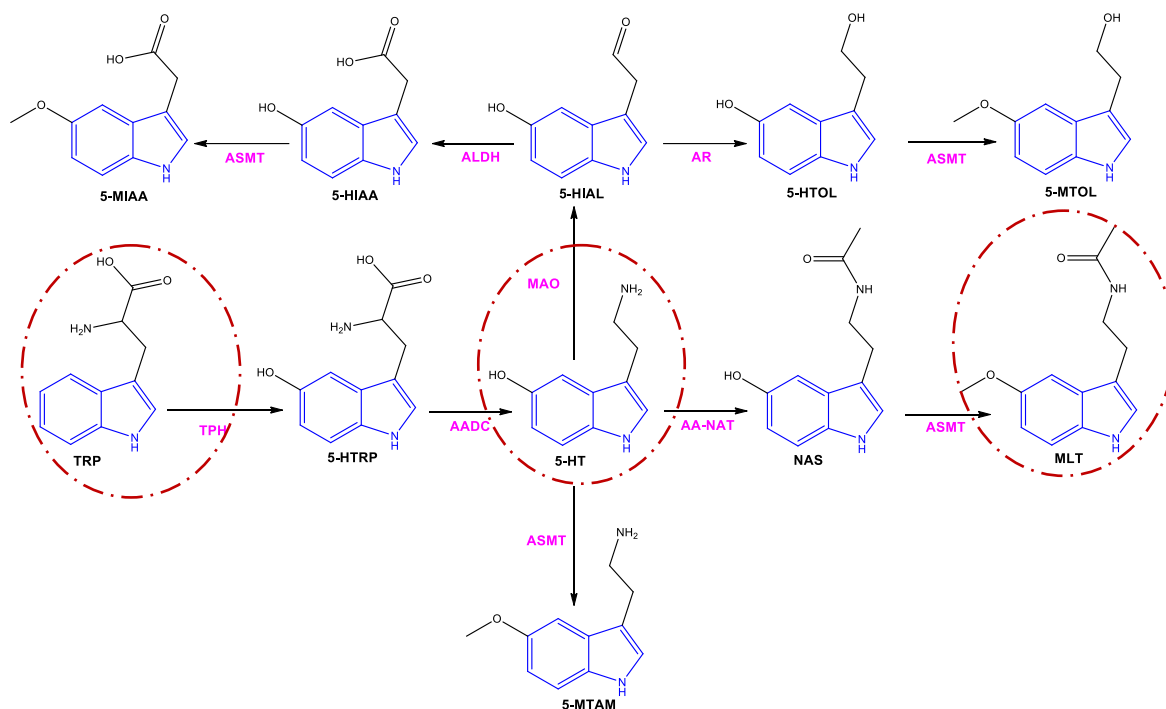
Rysunek 15. Reaktywność pierścienia benzenowego indolu

## 2. Naturalne pochodne indolu

Skondensowany układ pierścieni indolu zawarty jest zarówno w związkach pochodzenia zwierzęcego, jak i roślinnego. Indol jest budulcem niezwykle zróżnicowanego szeregu biologicznie istotnych związków naturalnych poczynając od prostych pochodnych takich jak serotonina, po złożone cząsteczki alkaloidów, które znalazły zastosowanie kliniczne, takich jak przeciwnowotworowa winblastyna, czy przeciwnadciśnieniowa rezerpina [21-23].

## 2.1. Związki indolu pochodzenia zwierzęcego

Prekursorem pochodnych indolu występujących w tkankach zwierzęcych jest tryptofan (TRP) [24,25]. Indoloaminy będące produktami metabolizmu tryptofanu (Rys. 16) wydzielane są głównie przez szyszynkę.



Rysunek 16. Schemat metabolizmu tryptofanu

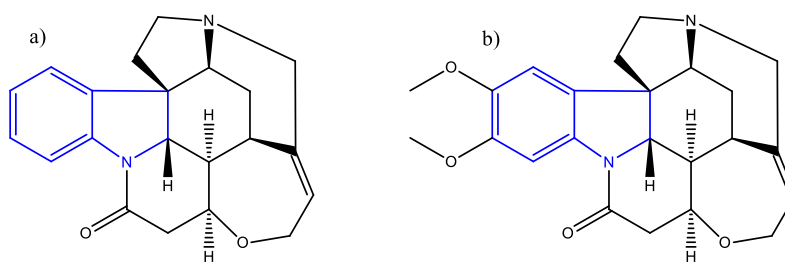
Tryptofan jest hydroksylowany przez hydroksylazę tryptofanu (TRH) do 5-hydroksytryptofanu (5-HTRP), który za pomocą dekarboksylazy aminokwasów aromatycznych (AADC) jest dekarboksylowany do serotoniny (5-hydroksytryptaminy, 5-HT) [25-29]. Serotonina jest kluczowym neuroprzekaźnikiem w ośrodkowym układzie nerwowym (OUN). Odgrywa istotną rolę w funkcjach mózgu, takich jak regulacja nastroju, snu i apetytu. Serotonina jest także składnikiem różnych leków psychoaktywnych wykazujących działanie przeciwdepresyjne, przeciwpsychotyczne, przeciwłkowe, empatogenne lub psychodeliczne, w zależności od specyficznych interakcji z układem serotoninowym, a także innymi neuromodulatorami, takimi jak noradrenalina, dopamina i oksytocyna [27-29]. 5-HT stanowi punkt wyjścia dla kilku szlaków metabolicznych w metabolizmie tryptofanu, najlepiej zbadana jest jednak jej przemiana w melatoninę (MLT), która obejmuje dwa etapy. W pierwszym etapie 5-hydroksytryptamina, za pomocą *N*-acetylotransferazy aryloalkiloaminowej (AA-NAT), jest acetylowana do *N*-acetyloserotoniny (NAS). Drugi etap obejmuje metylację NAS przez *O*-metylotransferazę

*N*-acetyloserotoniny (ASMT) do metaltioniny (MLT). Serotonina może być także bezpośrednio metylowana przez ASMT do 5-metoksytryptaminy (5-MTAM). Oksydacyjna deaminacja serotoniny za pomocą monoaminoosydazy (MAO) prowadzi do utworzenia aldehydu 5-hydroksyindolooctowego (5-HIAL). Aldehyd ten jest utleniany przez dehydrogenazę aldehydową (ALDH) do kwasu 5-hydroksyindolooctowego (5-HIAA), który jest metylowany przez ASMT i tworzy kwas 5-metoksyindolooctowy (5-MIAA). Natomiast redukcja 5-HIAL przez reduktazę aldozową (AR) prowadzi do powstania 5-hydroksytryptofolu (5-HTOL), który pod wpływem ASMT przekształcany jest w 5-metoksytryptofol (5-MTOL) [25-29].

## **2.2. Związki indolu pochodzenia roślinnego**

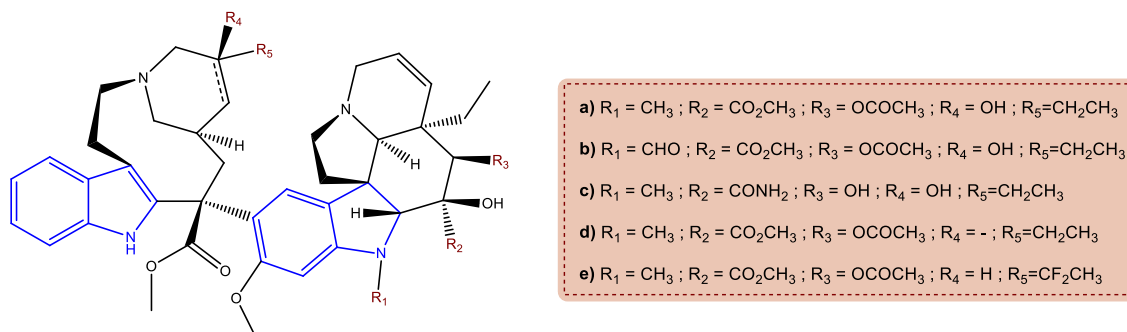
Największą grupę związków indolu pochodzenia roślinnego stanowią alkaloidy indolowe. Alkaloidami nazywamy związki głównie pochodzenia roślinnego o charakterze zasadowym, zawierające co najmniej jeden, przeważnie heterocykliczny atom azotu. Znaczną grupę tych związków stanowią alkaloidy indolowe, które charakteryzują się różnorodną bioaktywnością [30].

Strychnina (Rys. 17a) i brucyna (Rys. 17b) to alkaloidy obecne w nasionach kulczyby wroniego oka (*Strychnos nux vomica L.*) - drzewa rosnącego w Chinach i krajach Azji Południowej. Cząsteczki tych związków zawierają w swojej strukturze ugrupowanie indolowe i są silnymi toksynami. Strychnina wykazuje znacznie silniejsze działanie neurotoksyczne od brucyny. Wynika to z silnie antagonistycznego działania wobec receptorów glicyny, blokowania aktywności różnych typów mięśni oraz neuronalnych nikotynowych receptorów acetylocholin. Dawka śmiertelna strychniny wynosi od 50 do 100 mg, a najczęstszą przyczyną śmierci jest niewydolność oddechowa. Ze względu na swoją toksyczność strychnina stosowana jest głównie jako trucizna, np. w środkach gryzoniobójczych. Wykazano również farmakologiczne działanie strychniny i brucyny w zakresie przeciwnowotworowym, przeciwbólowym i przeciwzapalnym, przy czym brucyna charakteryzuje się niższą toksycznością i większą wartością terapeutyczną [31-35].



Rysunek 17. Struktura cząsteczek strychniny i brucyny

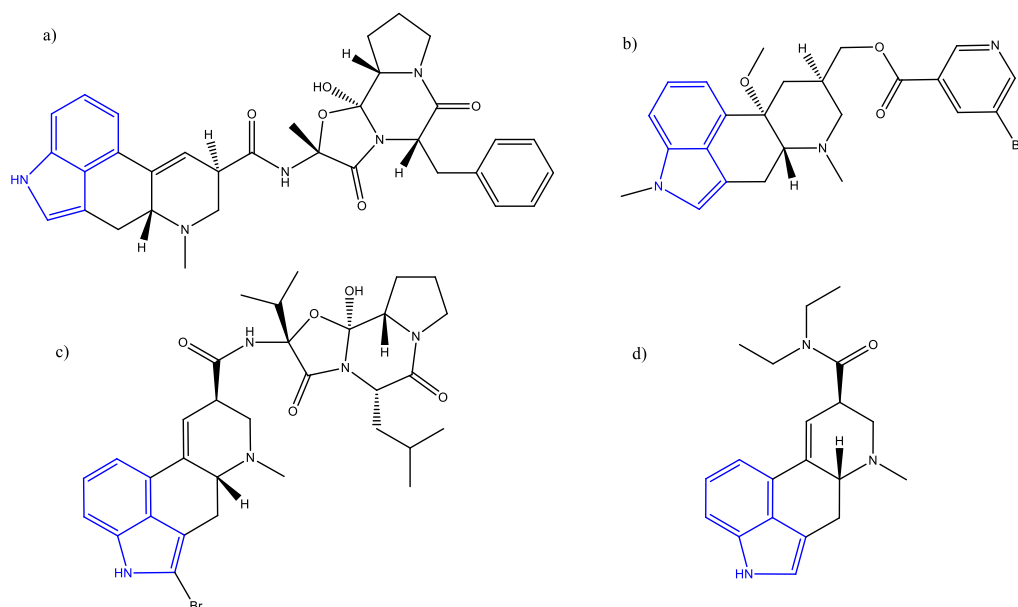
Alkaloidy Vinca (alkaloidy barwinka różyczkowego) to grupa związków chemicznych zawierających układ pierścieni indolu, pozyskiwana z barwinka różyczkowego (*Vinca Rosea* znany również jako *Catharanthus Roseus*). Alkaloidy Vinca znalazły zastosowanie w leczeniu cukrzycy oraz wysokiego ciśnienia krwi, jednak szczególną rolę odgrywają w terapiach przeciwnowotworowych. Obecnie w zastosowaniu klinicznym znajduje się pięć alkaloidów bawrinka: naturalnie występujące winblastyna (Rys. 18a) i winkrystyna (Rys. 18b) oraz półsyntetyczne pochodne windezyny (Rys. 18c) – stosowane klinicznie tylko w kilku krajach – winorelbina (Rys. 18d) oraz winflunina (Rys. 18e), zatwierdzona przez Europejską Agencję Leków (EMA) w 2012 r. w leczeniu przerzutowego i zaawansowanego raka nabłonka dróg moczowych [22,36-38].



Rysunek 18. Struktury cząsteczek alkaloidów Vinca będących w zastosowaniu klinicznym

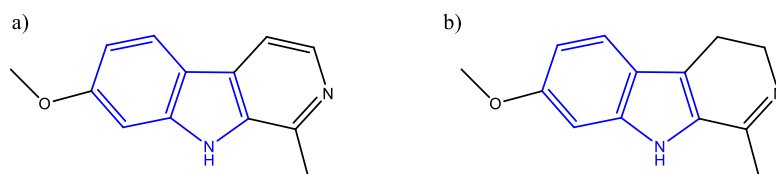
Alkaloidy sporyszu są kolejną grupą związków zaliczaną do alkaloidów indolowych. Są to mykotoksyny wytwarzane przez przetrwalniki buławinka czerwonego (*Claviceps purpurea*) – grzyba wywołującego choroby zbóż i traw, toksycznego także dla ludzi i zwierząt. Przewlekłe zatrucie sporyszem (ergotyzm) było powszechne w Europie w średniowieczu w wyniku spożycia chleba wyprodukowanego ze skażonego żyta. Z upływem lat zaczęto wykorzystywać alkaloidy sporyszu w celach medycznych, głównie w leczeniu chorób ośrodkowego układu nerwowego. Ergotaminę (Rys. 19a) stosuje się

w leczeniu ostrych napadów migreny. Bromokryptyna (Rys. 19b), syntetyczna pochodna  $\alpha$ -ergokryptyny stosowana jest w leczeniu choroby Parkinsona i hiperprolaktynemii. Nicergolina (Rys. 19c) jest pochodną kwasu D-lizerginowego, którą wykorzystuje się w leczeniu demencji i chorób naczyniowych, takich jak zakrzepica mózgu [39-42]. Dietyloamid kwasu lizergowego (LSD) (Rys. 19d) znany jest ze swojej silnej aktywności psychodelicznej. Z względu na właściwości psychoaktywne LSD pojawiło się duże zainteresowanie jego potencjalnym zastosowaniem jako środka terapeutycznego w psychiatrii. LSD stosowano w leczeniu lęków, depresji, chorób psychosomatycznych i uzależnień. Większość badań nie została przeprowadzona według współczesnych standardów, a w 1967 roku LSD został zakazany, co spowodowało zaprzestanie terapii z jego wykorzystaniem. Ponowne zainteresowanie badaniami nad LSD i jego potencjałem terapeutycznym w psychiatrii zajęło kilka dziesięcioleci [42,43].



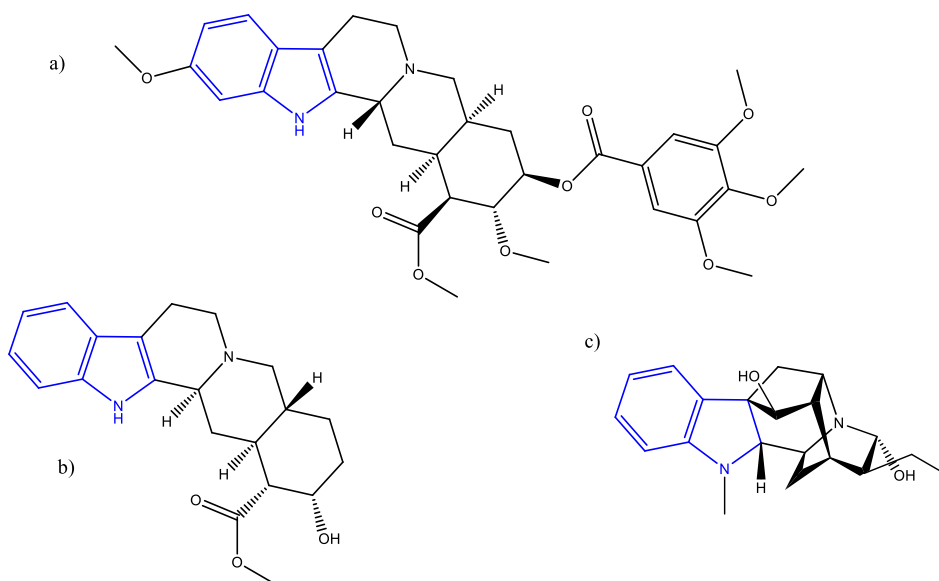
Rysunek 19. Struktury cząsteczek wybranych alkaloidów sporyszu

Harmina i harmalina (Rys. 20) występują w roślinach rodzaju *Peganum* i znane są głównie z działania psychoaktywnego. Są także składnikami Ayahuaski, halucynogennego napoju spożywanego podczas rytuałów przez plemiona amazońskie. Poza działaniem psychotropowym, alkaloidy te wykazały również potencjał przeciwnowotworowy, przeciwzapalny, neuroprotektynny i przeciwcukrzycowy [44-47].



Rysunek 20. Struktury cząsteczek: a) harminy i b) harmaliny

Rezerpina, johimbina i ajmalina (Rys. 21) to alkaloidy indolowe wyizolowane z korzeni rauwolfii zmijowej (*Rauwolfia serpentina*). Rezerpina od wielu lat stosowana jest w leczeniu wysokiego ciśnienia krwi, jednak wraz z wprowadzeniem nowych leków przeciwnadciśnieniowych wykorzystanie rezerpiny w farmakoterapii drastycznie spadło. Johimbina wykorzystywana jest jako stosunkowo bezpieczny środek terapeutyczny przy trudnościach seksualnych, natomiast ajmalina wykazuje silne działanie antyarytmiczne i obniżające ciśnienie krwi [23,48,49].



Rysunek 21. Struktury cząsteczek: a) rezerpiny; b) johimbiny; c) ajmaliny

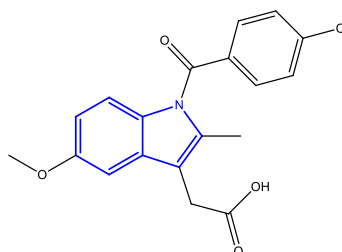


### 3. Syntetyczne pochodne indolu o znaczeniu farmakologicznym

W ostatnich latach indol stał się powszechnie stosowanym szkieletem molekularnym umożliwiającym rozwój i projektowanie nowych leków, w szczególności środków przeciwzapalnych, antynowotworowych, przeciwdrobnoustrojowych, przeciwwirusowych oraz stosowanych w leczeniu migreny i mdłości [50].

#### 3.1. Pochodne indolu o właściwościach przeciwzapalnych

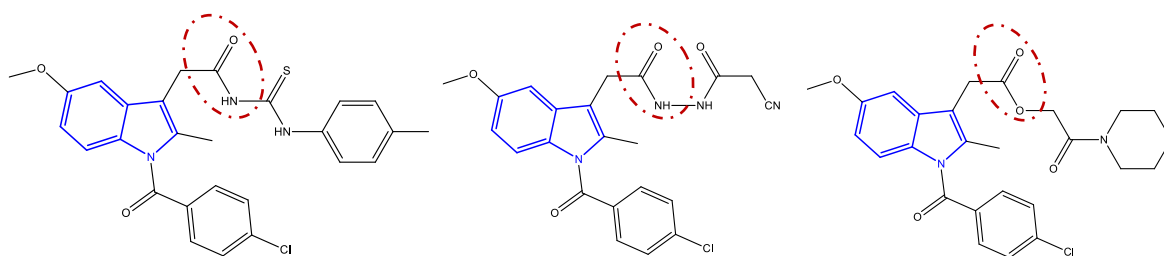
Jednym z najbardziej znanych, komercyjnie dostępnych, związków indolu jest Indometacyna (Rys. 22) – pochodna kwasu octowego, zaliczana do grupy Niesteroidowych Leków Przeciwzapalnych (*ang. NSAIDs, Non-steroidal anti-inflammatory drugs*). Indometacyna, obok aspiryny, była jednym ze związków zastosowanych przez Johna Vane'a w 1971 r. do odkrycia istotnej aktywności niesteroidowych leków przeciwzapalnych (NLPZ) jako inhibitora prostaglandyn, co później doprowadziło do zdobycia przez niego, oraz Bergströma i Samuelssona, Nagrody Nobla w dziedzinie Fizjologii lub Medycyny w 1982 r [51].



Rysunek 22. Wzór strukturalny Indometacyny (kwasu 2-(1-(4-chlorobenzoilo)-5-metoksy-2-metylo-1H-indol-3-ilo)octowego).

Indometacyna działa jak większość innych NLPZ. Aktywność indometacyny polega na hamowaniu syntezy prostaglandyn. Prostaglandyny, wytwarzane głównie przez enzymy cyklooksygenazy (COX), są krytycznymi mediatorami stanu zapalnego, gorączki i bólu. Utrzymują także czynność nerek, błonę śluzową przewodu pokarmowego i aktywność płytek krwi. Inhibicja enzymów COX przez NLPZ może wyjaśniać niektóre działania niepożądane tych leków. COX-1 bierze udział w wytwarzaniu tromboksanu A<sub>2</sub> (krytycznego mediatora agregacji płytek krwi), zatem hamowanie tego enzymu jest prawdopodobnie odpowiedzialne za przeciwpłytkowe działanie NLPZ. COX-1 jest odpowiedzialny również za utrzymanie błony śluzowej przewodu pokarmowego, podczas gdy poziom COX-2 ulega zwiększeniu

w tkankach objętych stanem zapalnym i wytwarza prostaglandyny odpowiedzialne za stan zapalny, gorączkę i ból. W rezultacie NLPZ selektywne wobec COX-2 mogą powodować mniej skutków ubocznych związanych z przewodem pokarmowym. Indometacyna działa nieselektywnie, wobec obu izoform cyklooksygenazy prowadząc do poważnych powikłań, takich jak wrzody żołądka i toksyczność nerkowa [51-54]. Nieselektywne hamowanie obu enzymów COX przypisuje się działaniu ugrupowania COOH, dlatego naukowcy skupiają się na odpowiednich modyfikacjach cząsteczki indometacyny, które mają zwiększyć selektywność wobec izoformy COX-2 [55,56]. W literaturze znane są pochodne estrowe i amidowe indometacyny (Rys. 23), które wykazały skuteczne działanie przeciwzapalne, a przy tym także wysoką selektywność wobec COX-2 [55-58].

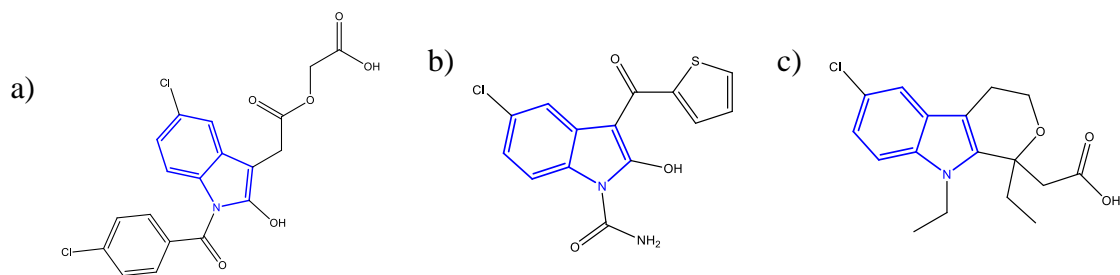


Rysunek 23. Pochodne indometacyny o właściwościach przeciwzapalnych selektywne wobec COX-2 [6, 8]

Acemetacyna (Rys. 24a) może stanowić użyteczną alternatywę dla konwencjonalnych NLPZ w leczeniu stanów zapalnych i bólu. Jest to pochodna estru karboksymetylowego indometacyny i wykazuje umiarkowaną selektywność wobec COX-1. Acemetacyna jest często określana jako prolek indometacyny, ponieważ w obecności leukocytów lub tkanki błony śluzowej żołądka zostaje przekształcona w indometacynę. Prawdopodobnie dlatego powoduje mniejsze uszkodzenie żołądka niż indometacyna [50,59].

Tenidap (Rys. 24b) (opracowany przez firmę Pfizer), inhibitor COX/5-LOX, jest potencjalnym lekiem przeciwzapalnym, modulującym cytokiny o działaniu przeciwreumatoidalnym. Został on jednak odrzucony przez Agencję Żywności i Leków w 1996r. ze względu na doniesienia o toksyczności dla wątroby i nerek [50,60].

Etodolak (Rys. 24c) jest to niesteroidowy lek przeciwzapalny działający jako selektywny inhibitor COX-2. Powoduje zmniejszenie poziomu prostaglandyn w organizmie przy lepszej tolerancji ze strony przewodu pokarmowego. Środek ten ma zastosowanie w leczeniu choroby zwyrodnieniowej stawów i reumatoidalnego zapalenia stawów [50,61,62].



Rysunek 24. Wzory strukturalne: a) Acemetacyn, b) Tenidapu, c) Etodolaku.

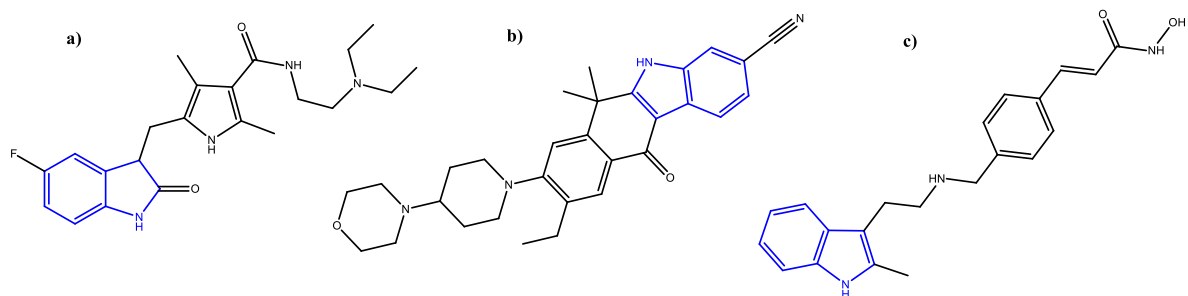
### 3.2. Pochodne indolu o właściwościach antynowotworowych

Rak jest globalnym problemem zdrowia publicznego, odpowiedzialnym za jedną szóstą zgonów wśród całej ludzkiej populacji. Ukierunkowanie leków, szczególnie na określone geny i białka zaangażowane we wzrost i przeżycie komórek nowotworowych, jest jednym z głównych celów badań na całym świecie [63-65]. Wiele leków stosowanych w terapiach przeciwnowotworowych opartych jest na strukturze indolu.

Sunitynib (Rys. 25a) to wielokierunkowy inhibitor kinazy tyrozynowej, który ma silne działanie antyangiogenne i przeciwnowotworowe. Sunitynib jest standardowym terapeutycznym w leczeniu pierwszego rzutu w przypadku przerzutowego raka nerkowokomórkowego (mRCC) [50,66-68].

Alectinib (Rys. 25b) jest wysoce selektywnym inhibitorem kinazy chłoniaka anaplastycznego drugiej generacji (ALK). Ta pochodna indolowa stosowana jest w leczeniu niedrobnokomórkowego rak płuca (NSCLC) [50,65,68].

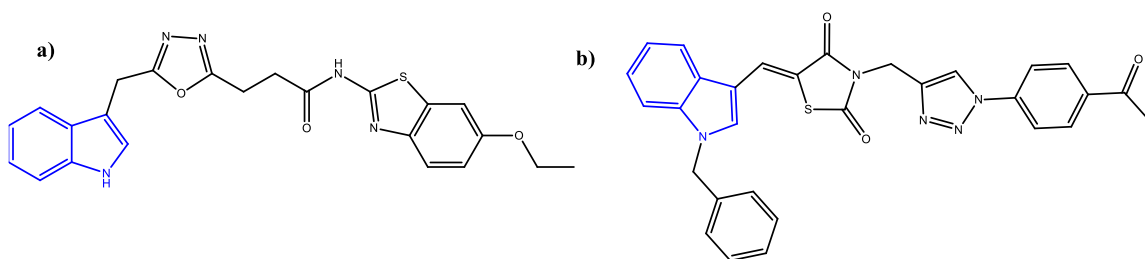
Panobinostat (Rys. 25c) jest pochodną indolowego kwasu hydroksamowego. Wykazuje nieselektywną inhibicję wobec deacetylazy histonowej (HDAC) oraz zdolność do uwrażliwiania opornych na leczenie komórek szpiczaka mnogiego w badaniach przedklinicznych, a także u pacjentów z RRMM (*ang. Relapsed/refractory multiple myeloma* - nawracający/oporny na leczenie szpiczak mnogi) w badaniach klinicznych [50,65,68]. Panobinostat w 2022 roku został uznany przez Europejską Agencję Leków (EMA) za lek sierocy (niemający innych odpowiedników, *ang. „orphan drug”*) do leczenia nowotworów glejowych [69].



Rysunek 25. Struktury leków stosowanych w terapiach przeciwnowotworowych: a) Sunitynib, b) Alectinib, c) Panobinostat

Ze względu na wielopostaciowy charakter chorób nowotworowych nieustannie trwają badania nad projektowaniem nowych terapeutyków. Modyfikacje cząsteczki indolu od wielu lat przyczyniają się do otrzymywania potencjalnych środków przeciwnowotworowych.

Badania z 2020 opisują otrzymanie pochodnej indolu z podstawnikiem 6-etoksybenzotiazolowym (Rys. 26a), która w badaniach *in vitro* wykazała cytotoksyczność wobec linii komórkowych ludzkiego raka jelita grubego (HCT116), gruczolakoraka płuc (A549) oraz czerniaka (A375) [70]. Z kolei, w 2022 roku opisano aktywność przeciwnowotworową pochodnej indolu zawierającej ugrupowania tiazolidynedionowe oraz triazolowe z podstawnikiem acetylofenylowym (Rys. 26b) przeciwko ludzkim liniom komórek nowotworowych HCT116 (rak jelita grubego), PC3 (rak prostaty), HePG2 (rak wątrobowokomórkowy) i MCF7 (rak sutka) [71].



Rysunek 26. Pochodne indolowe o właściwościach przeciwnowotworowych

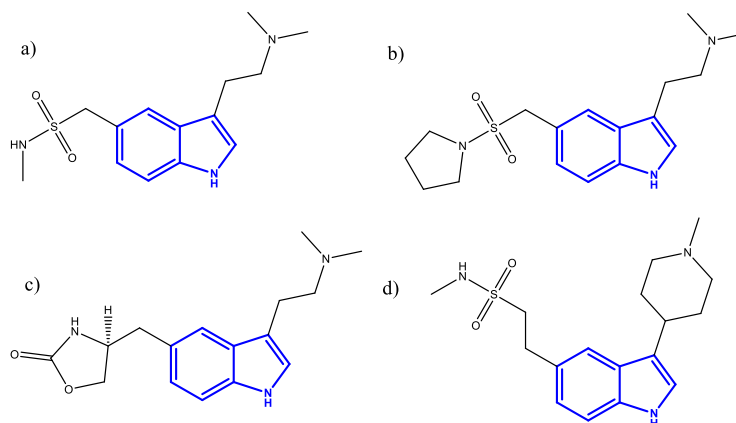
### 3.3. Tryptany - analogi indolu stosowane w leczeniu migreny

Migrena to złożone zaburzenie mózgu, które można wytłumaczyć interakcją czynników genetycznych i środowiskowych. Charakteryzuje się silnym bólem głowy związanym z nudnościami, światłowstrętem i/lub fonofobią [72-74]. Patofizjologiczne mechanizmy

migreny nie są w pełni poznane, ale ogólnie przyjmuje się, że zaburzenie to dotyczy zarówno obwodowego, jak i ośrodkowego układu nerwowego, a także mechanizmów naczyniowych i zapalnych [72,75]. Leki, które można zastosować w leczeniu ataku migreny, obejmują niesteroidowe leki przeciwzapalne (NLPZ) i inne leki przeciwbólowe, aczkolwiek nie są to leki dedykowane do leczenia jedynie migreny i często bywają nieskuteczne. Pierwszym lekiem opracowanym ściśle w kierunku leczenia migreny był alkaloid indolowy, Ergotamina, która może wywoływać zwężenie naczyń krwionośnych i działa jako agonista wielu receptorów, w tym serotoniny, dopaminy i (nor)adrenaliny [72, 76]. Kluczową rolę we współczesnych terapiach przeciwmigrenowych odgrywają receptory serotoninowe (5-hydroksytryptaminy, 5-HT). Serotonina została zidentyfikowana jako substancja zwężająca naczynia krwionośne i sugeruje się, że jej niski poziom w osoczu krwi odgrywa rolę w patofizjologii migreny. [72,75,77].

Selektywnymi agonistami receptorów serotoninowych 5-HT<sub>1B</sub> i 5-HT<sub>1D</sub> są pochodne indolowe z grupy tryptanów [72,75]. Prawie wszystkie tryptany zawierają w łańcuchu bocznym przyłączonym w pozycji C3 ugrupowania indolowego grupę aminową (tak jak w przypadku cząsteczki serotoniny). Główną różnicą strukturalną wśród tej grupy leków jest budowa łańcucha bocznego zlokalizowanego w pozycji C5 układu indolowego. Najczęściej obecne postawniki to sulfonamidy i sulfony, heterocykle, takie jak triazol, 2-oksazolidon, oraz karboksyamidy [78,79].

Pierwszym lekiem selektywnie ukierunkowanym na receptory 5-HT<sub>1</sub> był sumatryptan (Rys. 27a). Lek ten ma trzy przypuszczalne mechanizmy działania terapeutycznego: zwęża rozszerzone naczynia krwionośne opon mózgowo-rdzeniowych, hamuje uwalnianie neuropeptydów wazoaktywnych oraz zmniejsza transmisję sygnału bólowego [72,80]. Sumatryptan nie przenika przez barierę krew-mózg ze względu na jego niską lipofilowość, co spowodowało wzbogacenie tej grupy leków o nowe substancje, takie jak, almotryptan, zolmitryptan, czy naratryptan (Rys.27b-d), wykazujące większą biodostępność od sumatryptanu [78-81].

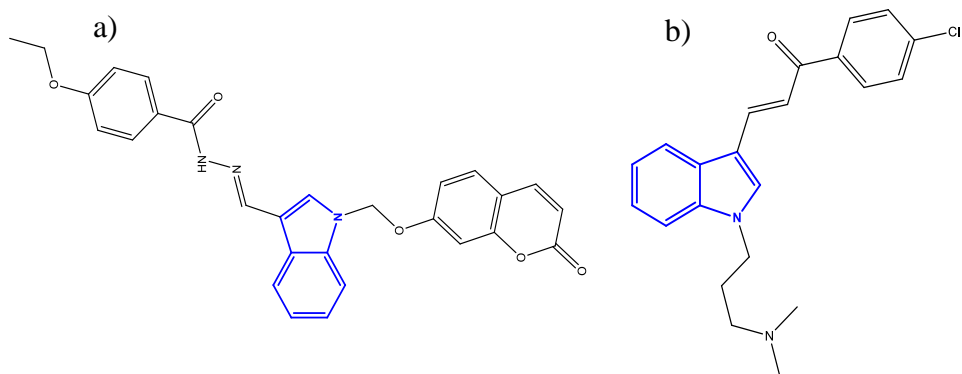


Rysunek 27. Struktury cząsteczek leków przeciwmigrenowych: a) sumatriptan; b) almotriptan; c) zolmitriptan; d) naratriptan

### 3.4. Pochodne indolu o znaczeniu przeciwdrobnoustrojowym

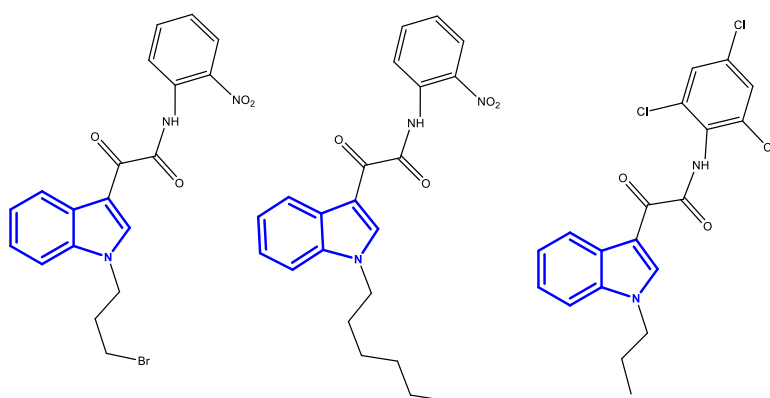
Infekcje bakteryjne są główną przyczyną niektórych chorób charakteryzujących się wysoką śmiertelnością, takich jak tyfus, gruźlica, dżuma, błonica, cholera, czerwonka i zapalenie płuc. Natomiast grzyby chorobotwórcze mogą wydzielać toksyny i metabolity szkodliwe dla ludzi, zwierząt i roślin [82,83].

Chociaż istnieje wiele środków przeciwdrobnoustrojowych dostępnych na rynku, zdolność mikroorganizmów do tworzenia zmutowanych szczepów, czy wytworzenie przez nie lekooporności generuje potrzebę projektowania nowych substancji o potencjalnej aktywności przeciwbakteryjnej i przeciwgrzybiczej. Niektóre analogi indolu opisane w literaturze wykazały efekt przeciwdrobnoustrojowy. Tiwari, Kirar, Banerjee i inni zsyntezowali serię *N*-podstawionych pochodnych indolu, które wykazały aktywność wobec bakterii Gram dodatnich *Bacillus subtilis* (Rys. 28a) oraz grzybów z gatunku *Candida viswanathii* (Rys 28b) [83].



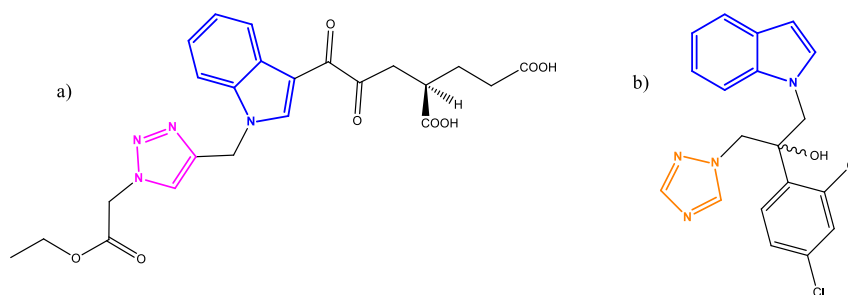
Rysunek 28. Pochodne indolu o właściwościach przeciwbakteryjnych i przeciwgrzybiczych

Jain, Utreja, Sharma wykazali, że pochodne z podstawnikami alkilowymi lub bromoalkilowymi w pozycji N1 efektywnie hamują wzrost populacji bakterii szczepów *Pseudomonas oryzaehabitans* i *Pseudomonas aeruginosa* [84]. Struktury najbardziej aktywnych pochodnych przedstawiłam na rysunku poniżej (Rys. 29).



Rysunek 29. N-podstawione pochodne indolu o właściwościach przeciwbakteryjnych

Znane są również hybrydy triazolowo-indolowe (Rys. 30) o działaniu przeciwgrzybiczym wobec niektórych gatunków grzybów z rodzaju *Candida*. Pochodna indolu z pierścieniem 1,2,3-triazolowym (Rys. 30a) wykazała aktywność przeciw *Candida albicans* [85], natomiast związek z ugrupowaniem indolowym oraz 1,2,4-triazolowym (Rys. 30b) efektywnie hamował rozwój gatunków *Candida glabrata* oraz *Candida krusei* [86].



Rysunek 30. Pochodne indolowo-triazolowe o działaniu przeciwwirusowymprzeciwwirusowym

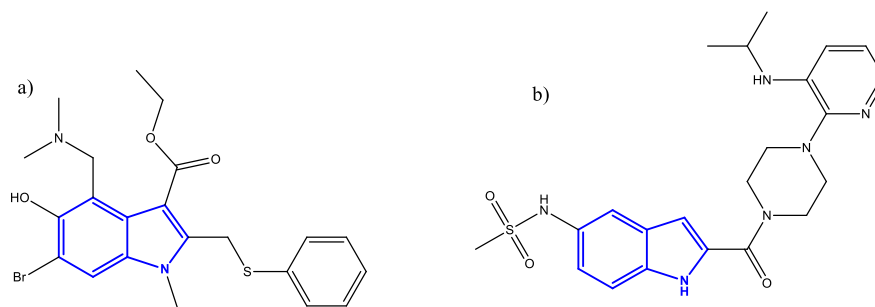
### 3.5. Przeciwwirusowe pochodne indolu

Choroby wirusowe są infekcjami niezwykle powszechnymi. Do najbardziej znanych chorób wirusowych zaliczamy: przeziębienie, grypę, ospę wietrzną, opryszczkę, zapalenie żołądka i jelit (grypa żołądkowa), AIDS wywołane ludzkim wirusem niedoboru odporności HIV, zapalenie wątroby (WZW), Choroba Heinego-Medina wywoływana przez wirusa Polio, choroby wirusowe wywołane wirusami Ebola, HPV, a także ciężki ostry zespół oddechowy wywołany wirusem SARS-CoV-1, który jeszcze bardziej uwypuklił deficyt związków przeciwwirusowych, odpowiednich do bezzwłocznego zastosowania w leczeniu nawracających lub pojawiających się chorób wirusowych [87-89].

Jednym z aktywnych biologicznie związków indolu jest Umifenovir (Rys. 31a) (sprzedawany pod marką Arbidol) jest lekiem przeciwwirusowym licencjonowanym w Rosji i Chinach do stosowania zapobiegawczego i leczenia zakażeń ludzką grypą typu A i B, a także powikłań pogrypowych. Umifenovir cechuje się szerokim spektrum działania, jest aktywny również przeciwko wirusom powodującym wirusowe zapalenie wątroby typu B i C; wirusowi Ebola i opryszczki; SARS oraz niektórym flawiwirusom, w tym wirusowi Zika, Zachodniego Nilu i kleszczowego zapalenia mózgu [89-92].

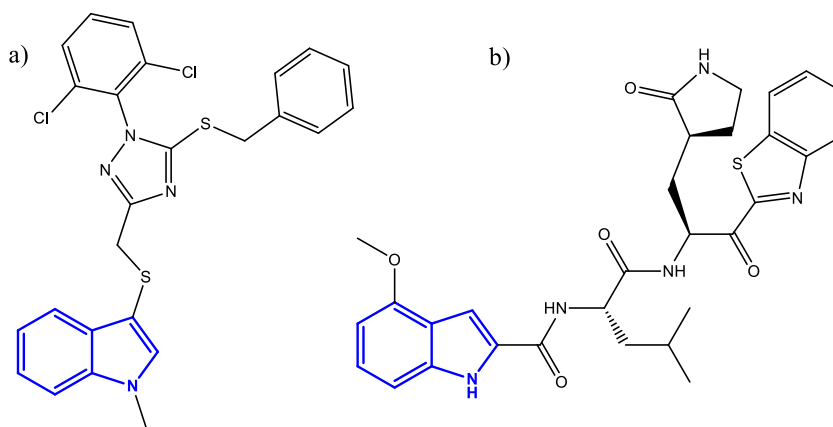
Delawirdyna (Rys. 31b) jest nienukleozydowym inhibitorem odwrotnej transkryptazy (NNRTI) pierwszej generacji. Została zatwierdzona przez FDA w 1997 r. do leczenia ludzkiego wirusa niedoboru odporności typu 1 (HIV-1). Stosowana była w ramach wysoce aktywnej terapii przeciwretrowirusowej (HAART - *ang. highly active antiretroviral therapy*). Obecnie wycofana z użycia ze względu na pojawianie się licznych działań niepożądanych, niewygodne dawkowanie (trzy razy dziennie) oraz pojawienie się skuteczniejszych preparatów drugiej generacji [89,93,94].





Rysunek 31. Leki zawierające cząsteczkę indolu o aktywności przeciwwirusowej: a) Umifenovir; b) Delawirdyna

Aktywność przeciwwirusowa pochodnych indolu nadal jest przedmiotem badań wielu naukowców na całym świecie. Przedstawiona na poniższym rysunku (Rys. 32a) hybryda triazolowo-indolowa wykazała obiecującą aktywność wobec wirusa grypy typu A [95], natomiast związek zawierający ugrupowanie indolowe (Rys. 32b) i benzotiazolowe całkowicie blokuje infekcję SARS CoV-2 *in vitro* bez wykrywalnej cytotoksyczności [96].



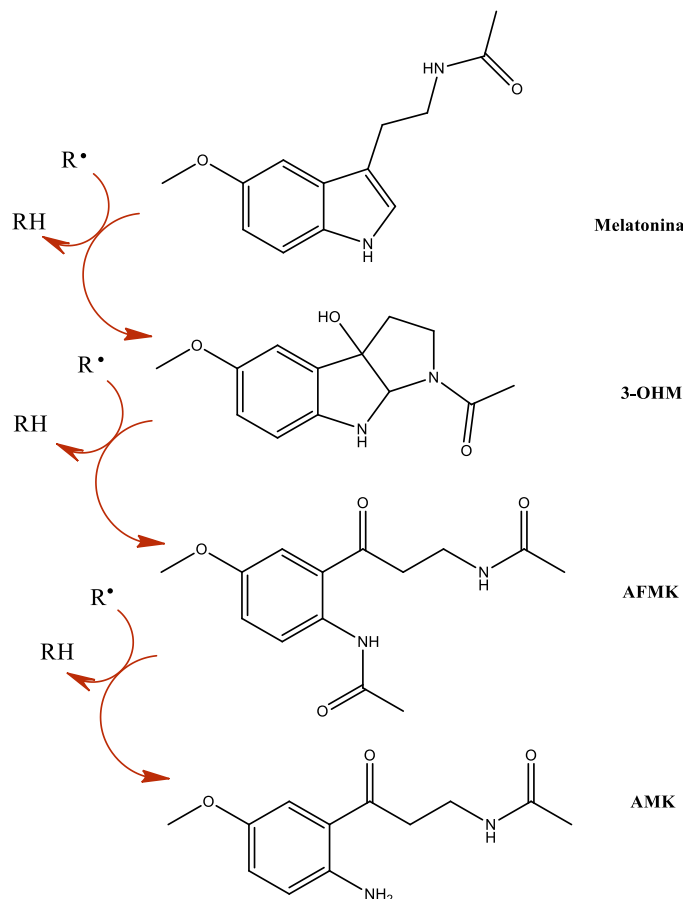
Rysunek 32. Pochodne indolu o aktywności przeciwwirusowej

### 3.6. Pochodne indolu o właściwościach antyoksydacyjnych

Związki indolowe są bardzo skutecznymi przeciwutleniaczami, chroniącymi zarówno lipidy, jak i białka przed peroksydacją. Bogata w elektrony struktura indolu determinuje aktywność antyoksydacyjną jego pochodnych w układach biologicznych [97,98].

Jednym z najobszerniej opisanych analogów indolu wykazującym właściwości antyoksydacyjne jest melatonina. Jest to neurohormon wytwarzany i uwalniany głównie przez szyszynkę, ale także przez układ trawienny, komórki krwi, soczewkę i siatkówkę oka, nerki, tarczycę, jajniki, mózdzek, żółć, szpik kostny i płyn mózgowo-rdzeniowy [99-101]. Melatonina odpowiedzialna jest głównie za regulowanie dobowego rytmu funkcji

fizjologicznych u ssaków. Hormon ten jest także niezwykle skuteczny w redukowaniu stresu oksydacyjnego [97,99]. Jego działanie polega na bezpośredniej neutralizacji reaktywnych form tlenu (RFT) i reaktywnych form azotu (RFA) oraz pośredniej stymulacji enzymów antyoksydacyjnych przy jednoczesnym tłumieniu aktywności enzymów prooksydacyjnych. Aromatyczny pierścień indolowy melatoniny wychwytuje RFT i RFA, a efekt ten jest potęgowany przez dalszą aktywność przeciwutleniającą produktów reakcji i metabolitów melatoniny w sposób kaskadowy (Rys. 33).

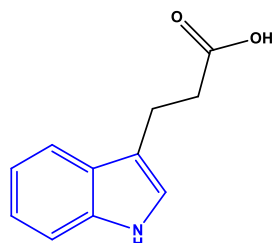


Rysunek 33. Kaskadowa reakcja melatoniny i jej metabolitów z wolnymi rodnikami

W reakcji z rodnikiem hydroksylowym  $HO^\bullet$  melatonina ulega przemianom w metabolit przejściowy - cykliczną 3-hydroksymelatoninę (3-OHM), która również jest silnym zmiataczem wolnych rodników. Następnie, w wyniku utleniania, powstaje *N1*-acetylo-*N1*-formylo-5-metoksykynuramina (AFMK). Deformylacja AFMK prowadzi do wytworzenia *N2*-acetylo-5-metoksykinuraminy (AMK) [99,101,102].

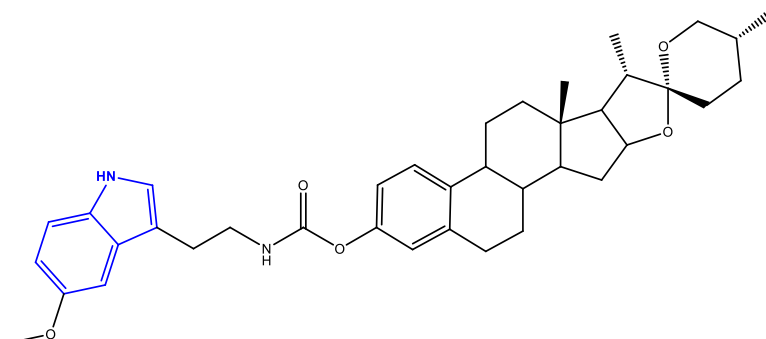
Kwas indolo-3-propionowy (IPA) (Rys. 34) jest produktem deaminacji tryptofanu, wytwarzanym przez bakterie *Clostridium sporogenes* i *Peptostreptococcus anaerobius*

w jelitach i, podobnie jak melatonina, skutecznie neutralizuje rodniki HO<sup>•</sup> [103-106]. IPA pełni rolę ochronną na poziomie komórkowym i tkankowym, ograniczając stany zapalne, peroksydację lipidów i powstawanie wolnych rodników. Kwas indolo-3-propionowy uznaje się za kluczowy związek w opracowaniu strategii terapeutycznej w leczeniu choroby Alzheimera i innych chorób neurodegeneracyjnych [106,107].



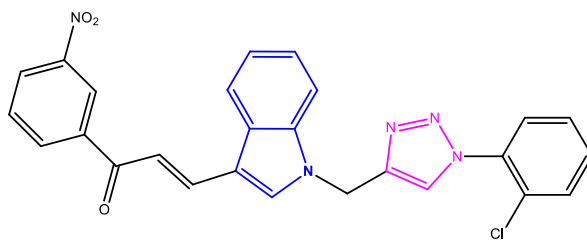
Rysunek 34. Kwas indolilo-3-propionowy (IPA)

W literaturze opisane są także syntetyczne pochodne indolu o potencjalnej aktywności antyoksydacyjnej. Hybryda steroidowo-indolowa przedstawiona na rysunku 35 wykazała skuteczne działanie farmakologiczne przeciwko uszkodzeniom komórkowym wywołanym przez H<sub>2</sub>O<sub>2</sub>, 6-OHDA (6-hydroksydopaminę) i beta amyloid [108].



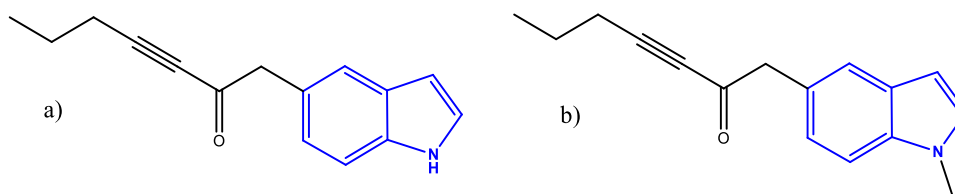
Rysunek 35. Hybryda steroidowo-indolowa o właściwościach przeciwutleniających

Dipodstawiona pochodna indolu zawierająca pierścień 1,2,3-triazolowy (Rys. 36) zmiatała wolne rodniki DPPH (2,2-difenylo-1-pikrylohydrazyl) w stopniu zbliżonym (68%) do kwasu askorbinowego (78%) [109].



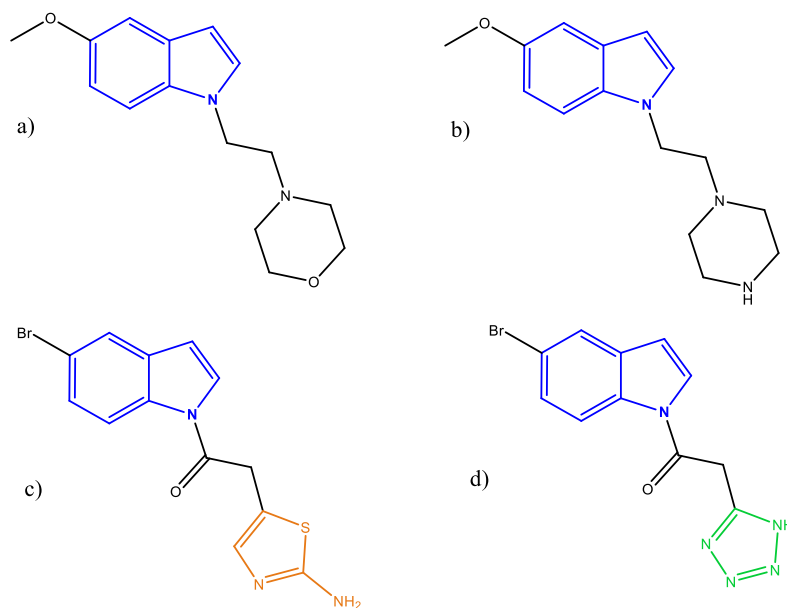
Rysunek 36. Pochodna triazolowo-indolowa

Związki z nienasyconym łańcuchem bocznym w pozycji C5 pierścienia indolowego okazały się neutralizować wolne rodniki porównywalnie do pochodnej witaminy E - Troloxu (substancji używanej jako wzorzec w badaniach właściwości antyoksydacyjnych) (99%). Pochodna przedstawiona na rysunku 37a wykazała 90%-skuteczność, natomiast podstawienie w pozycji N1 (Rys. 37b) nieznacznie obniżyło potencjał antyoksydacyjny cząsteczki (79%) [110].



Rysunek 37. Pochodne indolu z nienasyconym łańcuchem bocznym w pozycji C5

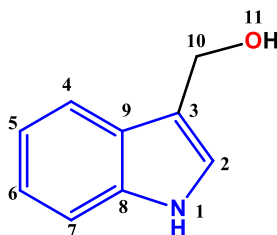
Wysoki potencjał antyoksydacyjny w testach z DPPH wykazały także *N*-podstawione analogi melatoniny (Rys. 38a i 38b) [111] oraz *N*-acylowe bromopochodne indolu z ugrupowaniem tiazolowym lub tetrazolowym (Rys. 49c i 49d) [112].



Rysunek 38. N-podstawione pochodne indolu o właściwościach antyoksydacyjnych

### 3.7. Mechanizmy działania antyoksydantów na przykładzie indolo-3-karbinolu

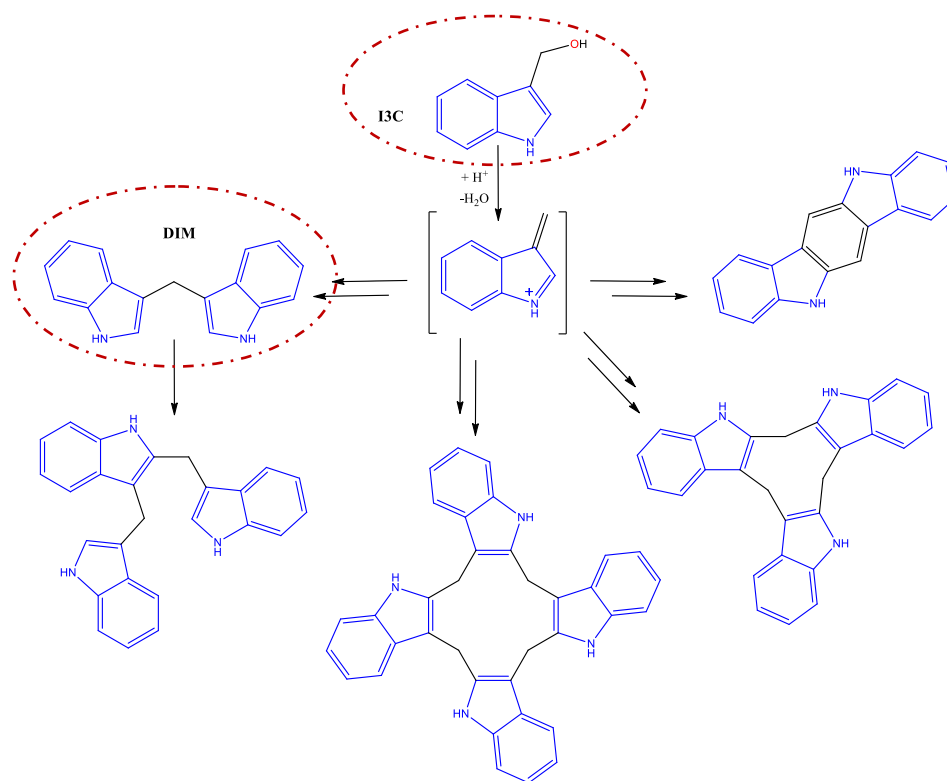
Indolo-3-karbinol (I3C) (Rys. 39) jest substancją fitochemiczną wytwarzaną przez rozkład glukobrassicyny, glukozynolanu występującego w warzywach z rodziny *Brassicaceae*, znanych jako warzywa kapustne [113]. I3C znany jest z efektywnego działania chemoprewencyjnego. Wykazuje aktywność wobec kilku typów nowotworów u ludzi tj. czerniaka, nowotworu piersi, prostaty, płuc, jelita grubego, białaczki i raka szyjki macicy. Opisano również jego działanie przeciwzapalne [114,115].



Rysunek 39. Struktura cząsteczki indolo-3-karbinolu

W warunkach kwasowych *in vivo*, ze względu na wysoką niestabilność, I3C jest zwykle przekształcany w ponad 15 oligomerycznych i dimerycznych związków bioaktywnych (Rys. 40). Metabolitem odgrywającym szczególną rolę w działaniu prozdrowotnym I3C jest jego dimer - 3'3-diindolilometan (DIM). DIM jest potencjalnym środkiem mogącym znaleźć

zastosowanie w profilaktyce stanów zapalnych, otyłości, cukrzycy, chorób układu krążenia, nowotworów, nadciśnienia, chorób neurodegeneracyjnych, a także osteoporozy [115-117].



Rysunek 40. Dimeryczne, trimeryczne i tetrameryczne metabolity I3C

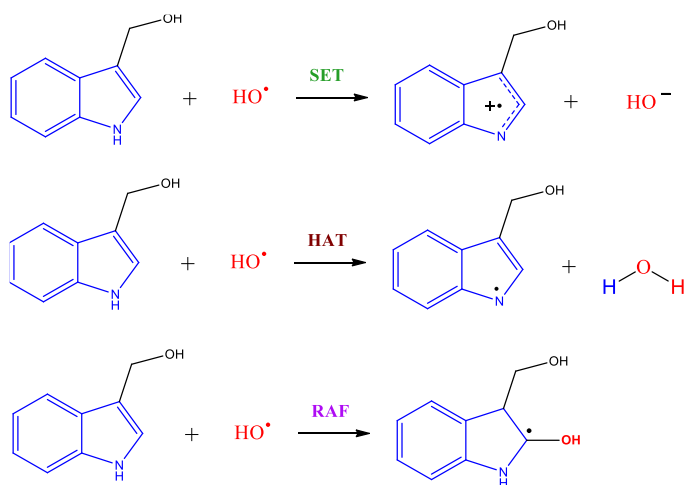
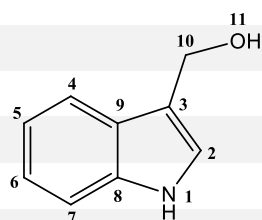
Badania eksperymentalne dowodzą, że I3C i jego pochodne są potencjalnymi zmiataczami wolnych rodników, przy czym niektóre pochodne wykazały wyższą aktywność przeciwutleniającą (wyrażoną wartościami  $IC_{50}$ ) niż witamina E ( $\alpha$ -tokoferol) w badaniach z DPPH [118,119].

Quan V. Vo wraz z zespołem zbadali aktywność przeciwutleniającą *in silico* indolo-3-karbinolu i jego pochodnych w stosunku do rodnika hydroksylowego w środowisku wodnym i lipidowym za pomocą obliczeń termodynamicznych i kinetycznych [118,119]. Działanie antyoksydacyjne I3C wobec rodnika hydroksylowego oparte jest głównie na mechanizmie RAF (*radical adduct formation*), szczególnie dominuje ono w środowisku lipidowym. Mechanizm SET (*single electron transfer*) może zachodzić jedynie w rozpuszczalniku polarnym. Najbardziej reaktywne pozycje cząsteczki I3C określono za pomocą obliczeń energii swobodnej Gibbsa (Tab. 1). Wykazano, że dla mechanizmu RAF jest to pozycja C2 (zarówno w środowisku wodnym jak i lipidowym), natomiast dla mechanizmu HAT

(hydrogen atom transfer) najbardziej korzystne będą pozycje N1 oraz C10. Równania potencjalnie zachodzących reakcji pomiędzy I3C a rodnikiem hydroksylowym przedstawiłam na rysunku 41 [118,119].

Tabela 1. Energia swobodna Gibbsa ( $\Delta G^\circ$ ) reakcji pomiędzy I3C i rodnikiem  $\text{HO}^\bullet$  w badanych rozpuszczalnikach (kcal/mol)

Mechanizm	Pozycja	Rozpuszczalnik		
		Woda	Etanian pentylu	
<b>SET</b>	-	-0,5	46,5	
<b>HAT</b>	N1	-28,5	-24,5	
	O11	-13,6	-13,5	
	C2	1,3	1,9	
	C4	-7,9	-4,9	
	C5	-7,4	-5,3	
	C6	-7,4	-5,3	
	C7	-6,9	-4,7	
	C10	-35,1	-31,2	
	<b>RAF</b>	C2	-19,6	-19,5
		C3	-12,4	-11,7
C4		-12,2	-12,4	
C5		-6,0	-5,1	
C6		-8,5	-7,9	
C7		-11,6	-11,7	
C8		1,2	1,1	
C9		7,9	6,4	

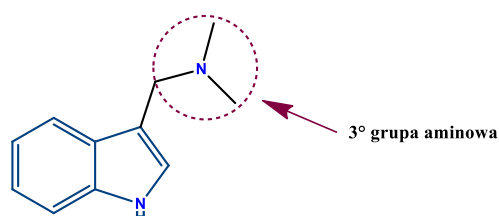


Rysunek 41. Proponowane mechanizmy antyoksydacyjne I3C

## 4. Gramina jako związek wyjściowy w syntezie nowych pochodnych indolu

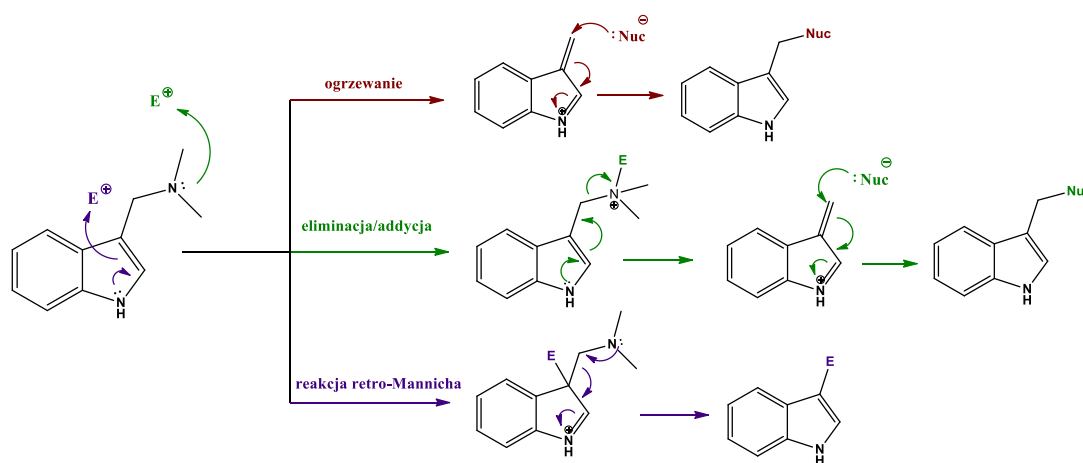
### 4.1. Reaktywność cząsteczki graminy

Gramina (Rys. 42) [3-(dimetyloaminometylo)indol] jest alkaloidem indolowym izolowanym z roślin należących do rodziny wiechlinowatych (*Poaceae*), takich jak lasecznica trzcinowata (*Arundo donax L.*), owies zwyczajny (*Avena sativa L.*), jęczmień zwyczajny (*Hordeum vulgare L.*) oraz pszenica zwyczajna (*Triticum aestivum L.*). Gramina jest zasadą Mannicha, zbudowaną z ugrupowania indolowego, które w pozycji C3 zawiera podstawnik dimetyloaminometylowy [120,121].



Rysunek 42. Budowa cząsteczki graminy

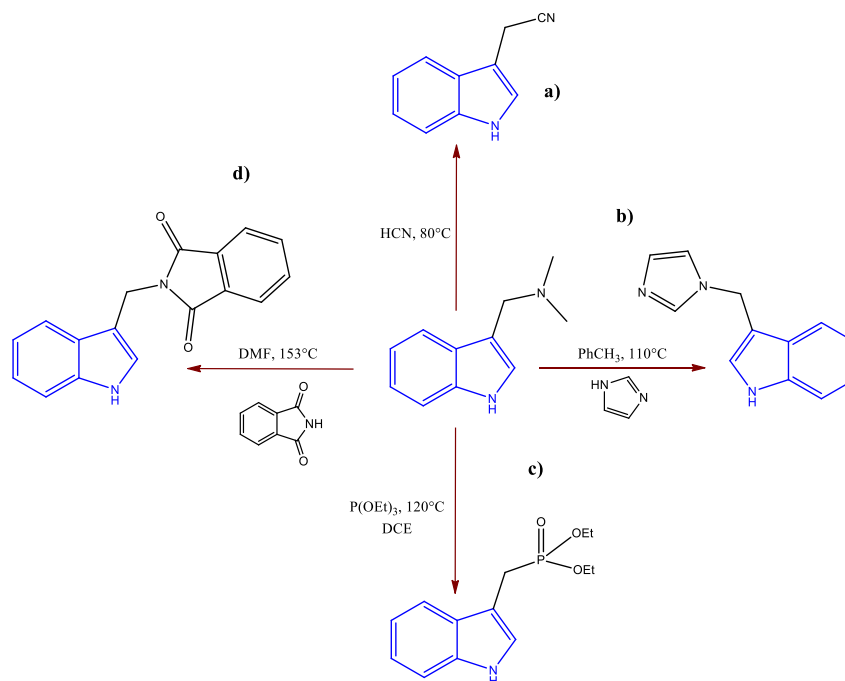
Trzeciorzędowa grupa aminowa obecna w łańcuchu bocznym indolu może być łatwo przekształcona w czwartorzędową sól amoniową, będącą doskonałą grupą odchodzącą, lub usunięta pod wpływem wysokiej temperatury ( $>80^{\circ}\text{C}$ ), czy na drodze reakcji retro-Mannicha (Rys. 43). Z tego względu gramina jest doskonałym związkiem wyjściowym do otrzymania szeregu nowych związków indolu podstawionych w pozycji C3 [121-126].



Rysunek 43. Przykładowe mechanizmy reakcji, jakim ulega gramina

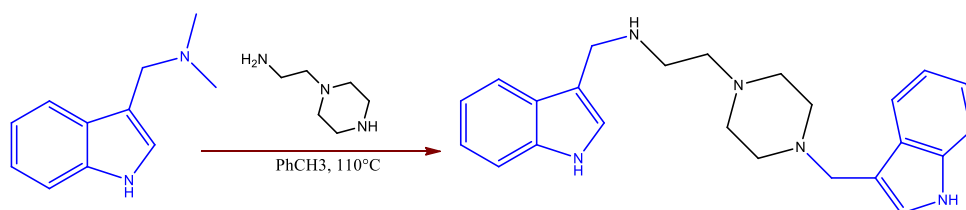


Ogrzewanie graminy w wysokiej temperaturze z cząsteczkami o charakterze nukleofilowym skutkuje substytucją indolu w pozycji C3. Na rysunku 44 przedstawiłam schematy reakcji graminy z cyjanowodorem (a), imidazolem w toluenie (b), fosforanem trietylu w dichloroetanie (c) oraz ftalimidem w dimetyloformamidzie (d) [122,127,128].



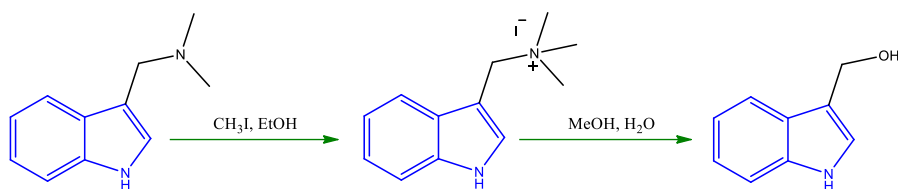
Rysunek 44. Schematy reakcji graminy z nukleofilami

Ogrzewanie graminy w toluenie z 2-piperazynietyloaminą prowadzi do powstania pochodnej bisindolowej (Rys. 45) [122].



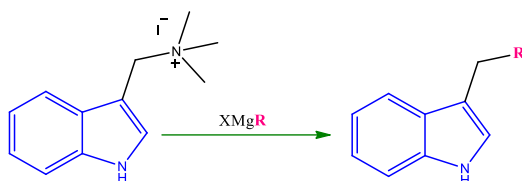
Rysunek 45. Schemat reakcji otrzymywani bisindolowej pochodnej graminy

Reakcja graminy i jodku metylu prowadzi do otrzymania czwartorzędowej soli amoniowej, metylojodku graminy, który w reakcji z alkoholem metylowym tworzy 3-hydroksymetyloindol, zwany potocznie indolo-3-karbinolem (I3C) (Rys. 46) [122,129].



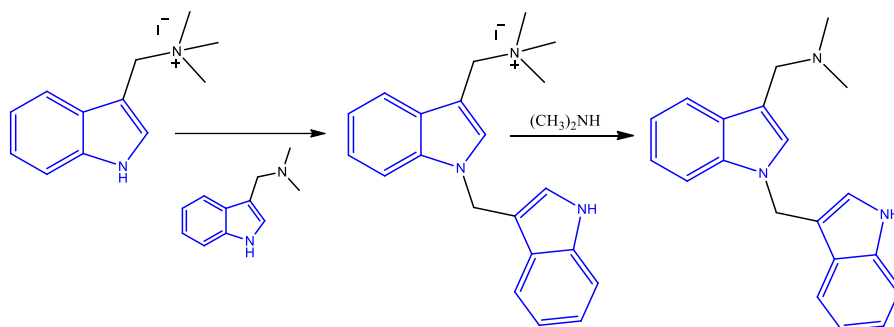
Rysunek 46. Schemat syntezy indolo-3-karbinolu

Poddawanie metylojodku graminy reakcjom z odczynnikami Grignarda jest znakomitym narzędziem do wydłużania łańcucha bocznego indolu (Rys. 47) [122,130] .



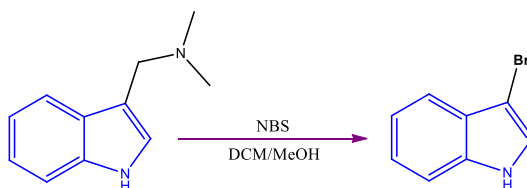
Rysunek 47. Schemat reakcji metylojodku graminy z odczynnikami Grignarda

Reakcja graminy z jej czwartorzędową solą może prowadzić do dimeryzacji alkaloidu, nawet w temperaturze pokojowej (Rys. 48) [122].



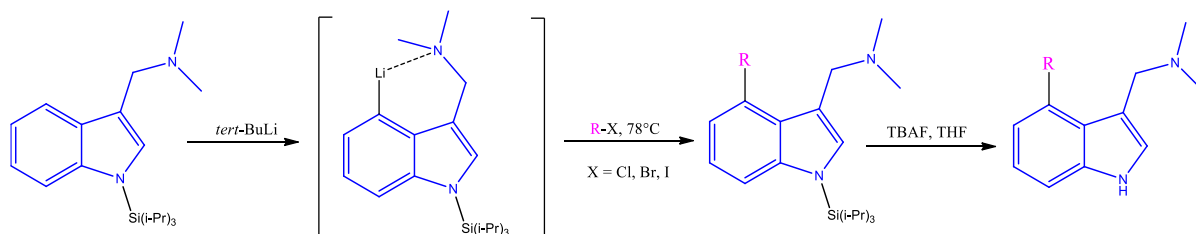
Rysunek 48. Dimeryzacja graminy

Gramina w reakcji z *N*-bromosukcynoimidem (NBS) tworzy 3-bromoindol. Reakcja obejmuje bromowanie indolu w pozycji C3, a następnie odejście grupy dimetyloaminowej (reakcja retro-Mannicha) (Rys. 49) [122,124,128].



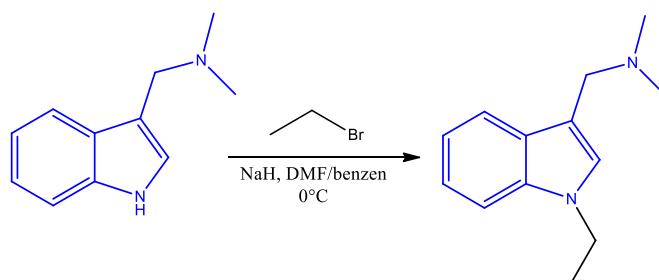
Rysunek 49. Schemat reakcji otrzymywania 3-bromoindolu

Litowanie *N*-podstawionej triizopropylsililem ( $\text{Si}(i\text{-Pr})_3$ ) graminy prowadzi do powstania metaloorganicznego produktu pośredniego, który w reakcji z odpowiednim halogenkiem alkilu tworzy pochodną graminy alkilowaną w pozycji C4 indolu. Pozycję N1 można odblokować stosując fluorek tetra-*n*-butyloamonu (TBAF) (Rys. 50) [131].



Rysunek 50. Synteza 4-alkilograminy

Alkilowanie graminy bromkiem etylu w temperaturze  $0^\circ\text{C}$  w mieszaninie DMF/benzen w obecności wodoru sodu pozwoliło otrzymać *N*-etylograminę z wydajnością 40% (Rys. 51) [122].

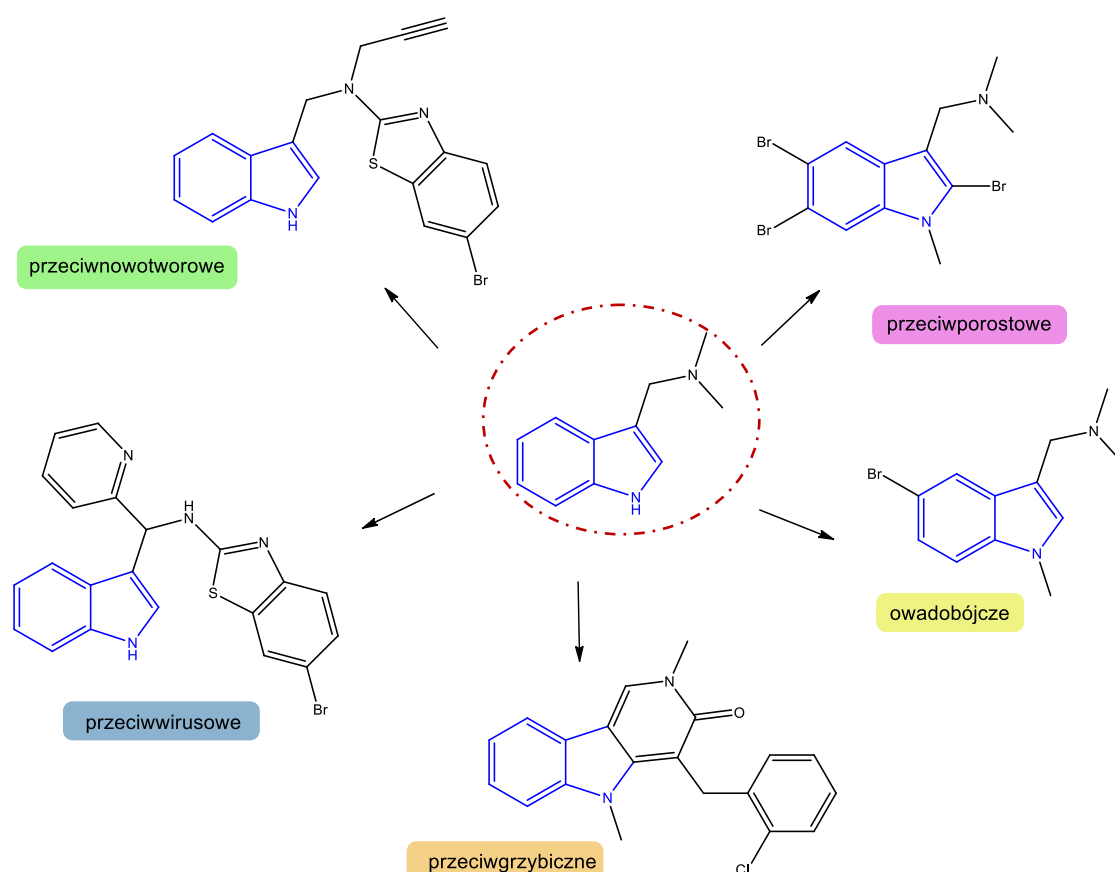


Rysunek 51. *N*-alkilowanie graminy bromkiem etylu

#### 4.2. Pochodne graminy o znaczeniu biologicznym

Zarówno gramina, jak i jej pochodne wykazują szeroką gamę aktywności biologicznej (Rys. 52). 3-(Dimetyloaminometylo)indol rozluźnia mięśnie gładkie oskrzeli oraz naczynia krwionośne, łagodzi zapalenie oskrzeli, nerek i objawy astmy oskrzelowej [122]. Badania na bezkręgowcach wykazały, że gramina jest antagonistą 5-HT w synapsach neuronalnych, ze względu na podobieństwa strukturalne do serotoniny [131-133]. Opisano również potencjalne działanie graminy w leczeniu patologicznego przerostu mięśnia sercowego [134]. Pochodne tego alkaloidu hamowały także namnażanie się komórek raka żołądka, jamy ustnej, płuc, okrężnicy oraz wątroby [131,135,136]. Ponadto pochodne graminy działają przeciw Enterowirusowi 71 wywołującemu choroby i chorób rąk, stóp i jamy ustnej u ludzi, a także wirusa mozaiki tytoniu (TMV) [131,137,138]. Badania aktywności przeciwbakteryjnej

graminy i jej analogów udowodniły ich potencjalne działanie hamujące strefy wzrostu bakterii rodzaju *Novosphingobium* i *Massilia* oraz szczepów *Escherichia coli*, *Staphylococcus aureus* i *Klebsiella pneumoniae* [131,139-143]. Pochodne graminy wykazały aktywność przeciwgrzybiczą wobec gatunków *Blumeria graminis*, *Fusarium graminearum*, *Candida glabrata*, *Aspergillus Niger* oraz *Phytophthora piricola* [131,138,144,145]. Obecność opisywanego alkaloidu indolowego w tkankach roślinnych pełni między innymi rolę obronną, dlatego jest on znany ze swojego działania owadobójczego, głównie w stosunku do mszyc, słonecznicy orzechówki, skoczków brunatnych i chrząszczy [132,146-148]. Bromopochodna graminy (2,5,6-tribromo-1-metylogramina) pełni istotną funkcję w ochronie przeciwporostowej [149,150].



Rysunek 52. Przykładowe bioaktywne pochodne graminy o właściwościach przeciwnowotworowych, przeciwwirusowych, przeciwgrzybiczych, owadobójczych i przeciwporostowych.

**- WYNIKI BADAŃ -**

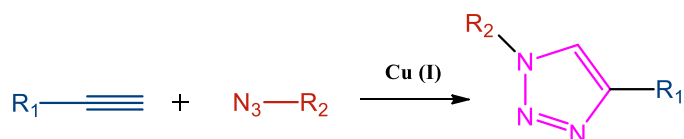
Indol od wielu lat stanowi modelowy związek do projektowania nowych środków o potencjalnym zastosowaniu terapeutycznym. Jego cząsteczka występuje w szeregu różnych substancji pochodzenia naturalnego, jak i związkach syntetycznych stosowanych w farmakologii i przemyśle. Pomimo występowania licznych analogów indolu o znaczeniu farmakologicznym, istnieje ciągle zapotrzebowanie na syntezę nowych pochodnych wykazujących lepsze, bardziej wszechstronne zastosowanie, a także mniejszą toksyczność.

W części literaturowej (str. 34-37) opisałam szeroki zakres możliwości modyfikacji cząsteczki alkaloidu indolowego, graminy. Ze względu na tę reaktywność, to właśnie **graminę wykorzystałam jako związek wyjściowy do syntezy wszystkich nowych pochodnych indolu będących przedmiotem tej pracy.**

## 1. Pochodne pierwszej grupy

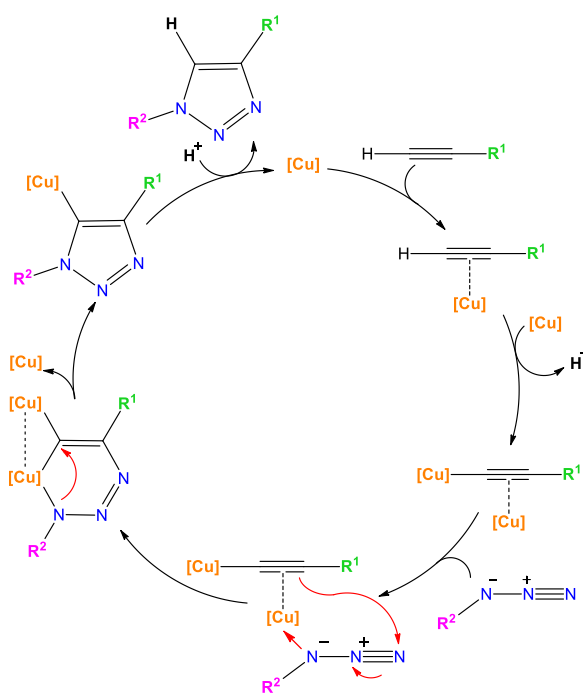
Łączenie ze sobą różnych cząsteczek bioaktywnych pozwala na otrzymywanie nowych związków chemicznych wykazujących bardziej zróżnicowane spektrum aktywności biologicznej. Niezwykle użyteczną metodą tworzenia biokonjugatów są reakcje chemii click. Reakcje te cechuje wysoka selektywność i wydajność, odporność na warunki wodne i tlenowe, stosowanie nietoksycznych rozpuszczalników oraz niewielka ilość produktów ubocznych, które można łatwo usunąć. W wyniku tych reakcji dochodzi nie tylko do związania ze sobą dwóch fragmentów molekularnych, ale także do utworzenia pierścienia 1,2,3-triazolowego, który również jest cząsteczką biologicznie atrakcyjną.

Najczęściej stosowaną reakcją „chemii click”, jest katalizowana jonami miedzi (I) cykloaddycja azydkowo-alkinowa (CuAAC – ang.: copper(I) catalyzed azide-alkyne cycloaddition), opisana w 2001 r. przez Sharplessa i Meldala, którzy za swoje badania dwadzieścia jeden lat później otrzymali nagrodę Nobla w dziedzinie chemii [151-153]. CuAAC jest rodzajem 1,3-dipolarnej cykloaddycji Huisgena polegającej na tworzeniu 1,4-dipodstawionych 1,2,3-triazoli pomiędzy organicznym azydkiem i terminalnym alkinem (Rys. 53).



Rysunek 53. Schemat reakcji CuAAC

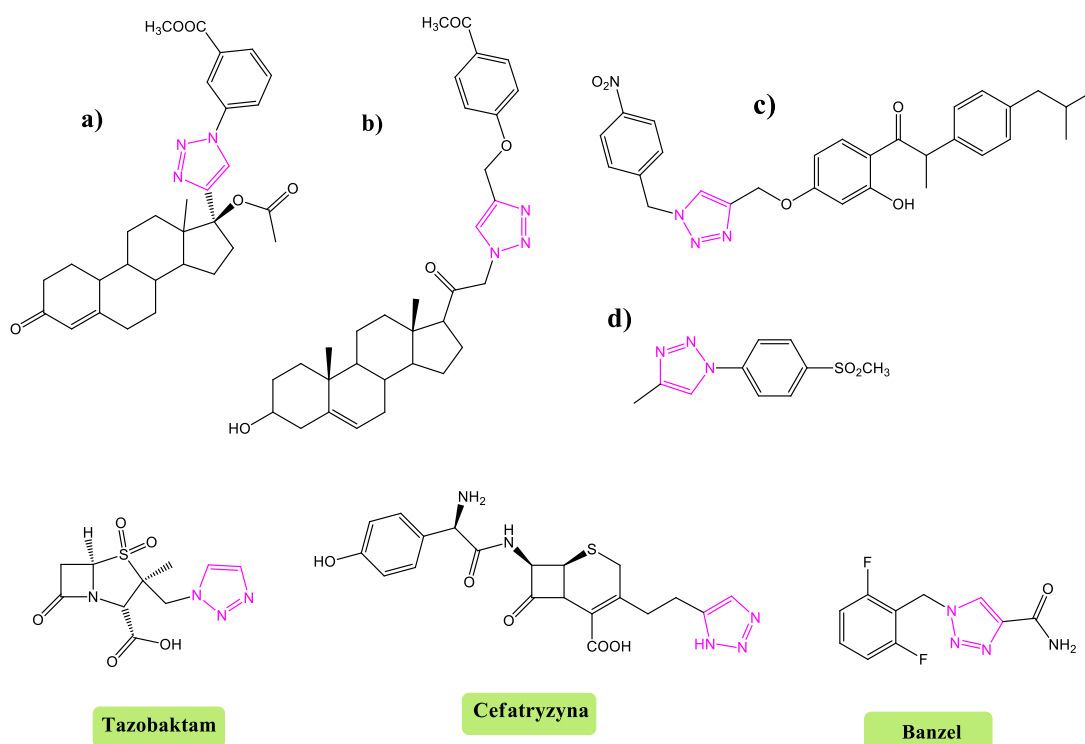
Niekatalizowana reakcja 1,3-dipolarnej cykloaddycji Huisgena pomiędzy azydkami organicznymi i alkinami jest mało efektywna ze względu na wymagania dotyczące wysokiej temperatury, powolną kinetykę reakcji i tworzenie izomerów strukturalnych (1,4- i 1,5 - dipodstawionych triazoli) oraz ze względu na brak selektywności. Wprowadzenie katalizatora miedziowego umożliwiło przebieg cykloaddycji w krótkim czasie, przy zastosowaniu łagodnych warunków reakcji oraz z regioselektywnością dla 1,4-dipodstawionego adduktu. Mechanizm reakcji click przedstawiłam na rysunku 54.



Rysunek 54. Mechanizm reakcji CuAAC

Pierścień 1,2,3-triazolowy występujący w cząsteczkach produktów reakcji click nie jest jedynie pasywnym łącznikiem, wykazuje on kilka korzystnych właściwości fizykochemicznych, takich jak duży moment dipolowy, oddziaływanie  $\pi$ - $\pi$  z pierścieniami aromatycznymi (np. fenyłowymi), tworzenie wiązań wodorowych czy koordynacja z jonami metali, a także dobrą rozpuszczalność w wodzie i wysoką stabilność w warunkach fizjologicznych. Choć ugrupowanie triazolowe nie występuje w naturze, jego właściwości umożliwiają mu swobodne wiązanie się z różnymi receptorami w układach biologicznych. Chemia click ułatwia łączenie ze sobą różnych fragmentów molekularnych, jednocześnie wzbogacając powstały koniugat o atrakcyjny biologicznie układ triazolowy. Reakcja CuAAC

jest niezwykle wydajnym narzędziem syntetycznym stosowanym przy projektowaniu bibliotek związków aktywnych biologicznie. Pochodne triazolowe znalazły zastosowanie jako środki przeciwnowotworowe, przeciwbakteryjne, przeciwwirusowe, antyoksydacyjne, przeciwpadaczkowe, przeciwzapalne oraz przeciwgrzybicze [85,153-160]. Niektóre pochodne 1,2,3-triazolowe stosowane są już w terapiach klinicznych. Do takich leków należą między innymi przeciwbakteryjne tazobaktam i cefatryzyna, oraz Banzel<sup>®</sup> stosowany w leczeniu padaczki (Rys. 55) [161,162].



Rysunek 55. Wybrane pochodne triazolowe o właściwościach przeciwnowotworowych (a i b); przeciwbakteryjnych (c); przeciwzapalnych (d) oraz struktury leków zawierających pierścień 1,2,3-triazolowy

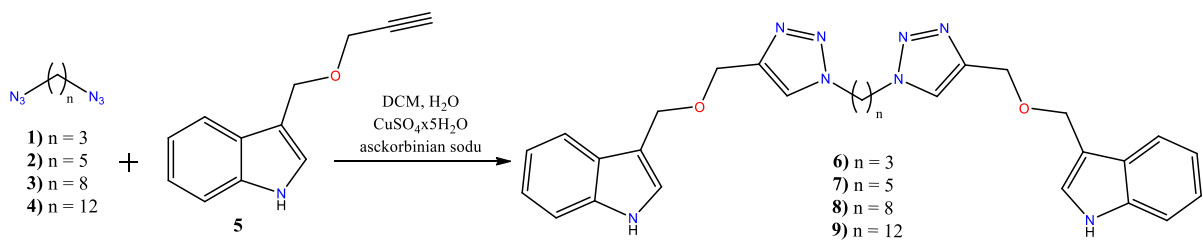
Przeciwutleniacze odgrywają znaczącą rolę w ochronie organizmu przed stanami patologicznymi wywołanymi reaktywnymi formami tlenu (RFT) i azotu (RFA) powstającymi w wielu procesach egzogennych i endogennych [163,164]. Wyróżniamy dwa typy RFT i RFA: rodniki obejmujące anionorodniki ponadtlenkowe ( $O_2^{\cdot-}$ ), rodniki tlenowe ( $O_2^{\cdot}$ ), hydroksylowe ( $OH^{\cdot}$ ), rodniki alkoksyłowe ( $RO^{\cdot}$ ), rodniki nadtlenkowe ( $ROO^{\cdot}$ ), rodniki tlenku azotu ( $NO^{\cdot}$ ) i dwutlenku azotu ( $NO_2^{\cdot}$ ) oraz nierodniki takie jak: nadtlenek wodoru ( $H_2O_2$ ), tlen singletowy ( $^1O_2$ ), ozon ( $O_3$ ), kwas azotowy (III) ( $HNO_2$ ), kation nitrozyłowy



(NO<sup>+</sup>), kation nitronowy (NO<sub>2</sub><sup>+</sup>), anion nitroksylowy (NO<sup>-</sup>), trójtlenek diazotu (N<sub>2</sub>O<sub>3</sub>), tetratlenek diazotu (N<sub>2</sub>O<sub>4</sub>), nadtlenki organiczne (ROOH), nadtlenoazotyn (ONOOH) i aldehydy (HCOR) [165]. Wolne rodniki są indywiduami niezwykle reaktywnymi ze względu na obecność niesparowanego elektronu. Niski poziom wolnych rodników, wytwarzanych w naturalnym metabolizmie komórkowym, nie jest szkodliwy dla naszego organizmu. Wolne rodniki uczestniczą w procesach biochemicznych, a ich nadmiar jest kontrolowany przez przeciwutleniacze. Jednakże brak równowagi pomiędzy stężeniem RFT i przeciwutleniaczy może być przyczyną wielu poważnych zaburzeń. Ten brak równowagi, związany ze wzrostem reaktywnych form tlenu, nazywany jest stresem oksydacyjnym. Niekontrolowana produkcja RFT, związana ze słabym mechanizmem ochronnym, prowadzi do peroksydacji lipidów, karbonylacji białek, tworzenia adduktów karbonylowych (aldehyd/keton), nitrowania, sulfoksydacji, uszkodzeń DNA, takich jak pęknięcia nici, usunięcie nukleotydów, modyfikacja zasad i krzyżowanie połączeń białko-DNA [166-168]. Stres oksydacyjny jest powiązany z wieloma chorobami, takimi jak nowotwory, cukrzyca, otyłość, przerost serca, choroby Alzheimera i Parkinsona, miażdżyca i malaria [164,167,168].

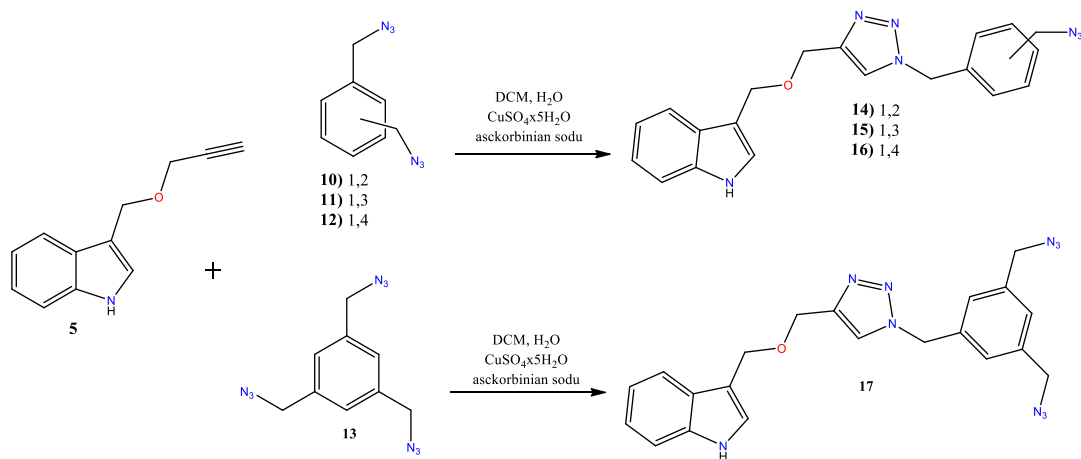
Istnieje szeroka gama naturalnych i endogennych przeciwutleniaczy. Peroksydaza glutationowa (GSH-Px), dysmutaza ponadtlenkowa (SOD) i katalaza (CAT) to enzymy zaangażowane w mechanizm antyoksydacyjny organizmu [97,98,165-170]. Naturalne, egzogenne przeciwutleniacze, takie jak witamina C lub E, karotenoidy i flawonoidy, mogą być dostarczane z pożywienia lub wraz z suplementami diety [170]. Ze względu na wpływ stresu oksydacyjnego na patofizjologię różnych chorób, rośnie również zainteresowanie syntezą związków o właściwościach przeciwutleniających [163,170].

Dimeryczne pochodne indolu, takie jak opisany w części literaturowej (str. 31-33) suplement diety, 3,3'-diindolilometan (DIM), wykazują szerokie spektrum aktywności biologicznej, w tym działanie przeciwutleniające [171-173]. Aktywność antyoksydacyjną wykazał także inny bis-indolowy związek pochodzenia naturalnego – indygo, a także syntetyczne bis-indolowe zasady Schiffa oraz pochodne  $\beta$ -laktamowe [174-176]. Zainspirowana tymi faktami swoje badania rozpoczęłam od **syntezy dimerów indolu zawierających dodatkowo ugrupowanie triazolowe (Schemat 1). Stosując metodę CuAAC uzyskałam cztery nowe, symetryczne dimery indolu i triazolu z łącznikami alifatycznymi (6-9).**



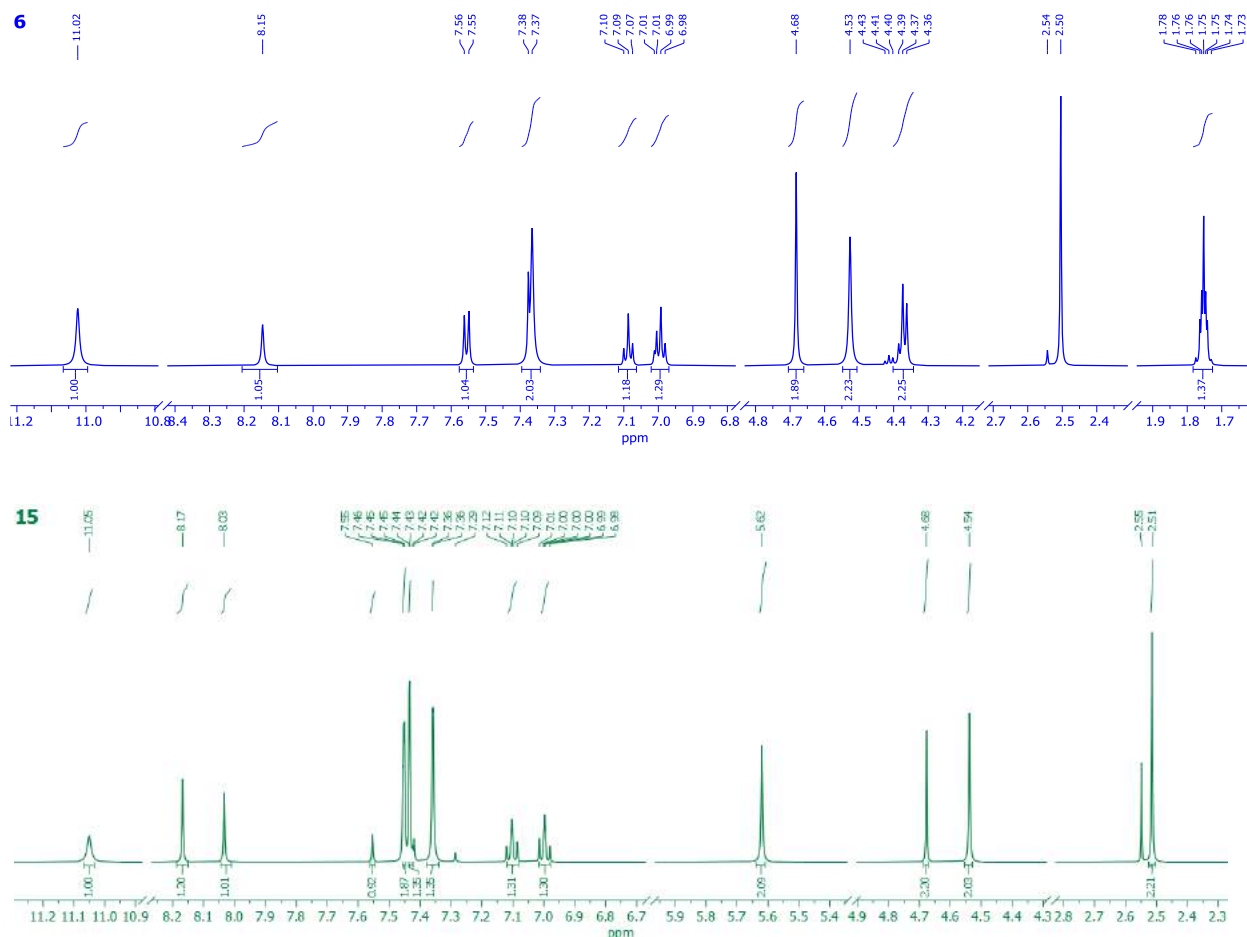
Schemat 1. Synteza dimerów triazolowo-indolowych

Interesującym zagadnieniem wydało mi się porównanie aktywności biologicznej otrzymanych dimerów zawierających linkery alifatyczne (6-9) z aktywnością analogicznych dimerów i trimeru z łącznikiem arylowym. **Z tego względu kolejnym etapem mojej pracy było przeprowadzenie serii reakcji chemii click 3-propargiloksymetyloindolu (5) z azydkami 1,2-, 1,3- i 1,4-dimetylobenzenu oraz 1,3,5-trimetylobenzenu (10-13, Schemat 2).** Efektem przeprowadzonych syntez było jednak **otrzymanie monomerycznych pochodnych indolu zawierających ugrupowanie triazolowe oraz azydo- lub diazydometylobenzenowe (14-17).** Pomimo użycia dwukrotnego nadmiaru pochodnej propargilowej 5, cykloaddycji uległa tylko jedna grupa azydkowa przyłączona do pierścienia benzeny, co potwierdziłam poprzez analizę widm <sup>1</sup>H i <sup>13</sup>C NMR otrzymanych produktów [P2]. Powstanie wyłącznie monomerów uwarunkowane było prawdopodobnie zbyt wysoką gęstością elektronową wynikającą z małej odległości pomiędzy pierścieniem triazolowym a pierścieniem benzenowym.



Schemat 2. Synteza triazolowych pochodnych indolu z pierścieniem benzenowym

Na rysunku 56 przedstawiłam widma przykładowych związków dla serii dimerów (związek **6** z łącznikiem propylowym) oraz pochodnych monomerycznych z ugrupowaniem azydkowym (związek **15** podstawiony w pozycjach 1,3).

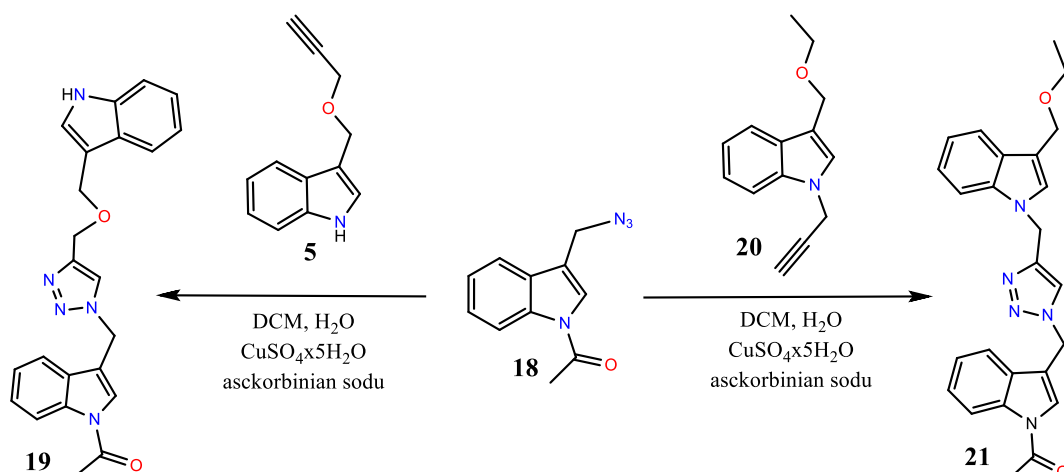


Rysunek 56. Widma  $^1\text{H}$  NMR pochodnych **6** i **15**

Jak widać na rysunku 56 liczba i integracja sygnałów na widmie  $^1\text{H}$  NMR pochodnej **6** wyraźnie świadczy o otrzymaniu pochodnej dimerycznej. Singlet występujący przy wartości 11,02 ppm odpowiada dwóm protonom grup aminowych pierścieni indolu. Sygnały w zakresie 8,03–6,98 ppm pochodzą od protonów pierścieni aromatycznych. Proton pierścienia triazolowego występuje jako singlet przy 8,17 ppm. Przy wartościach 4,68 i 4,53 ppm pojawia się osiem protonów czterech grup  $-\text{CH}_2$  należących do grup eterowych znajdujących się w łańcuchach bocznych pierścieni indolu. Multiplet w zakresie 4,43–4,36 ppm odpowiada czterem protonom dwóch grup  $\text{CH}_2$  łańcucha propylowego, pozostałe dwa protony łańcucha węglowego dają kwintet w zakresie 1,78–1,73 ppm.

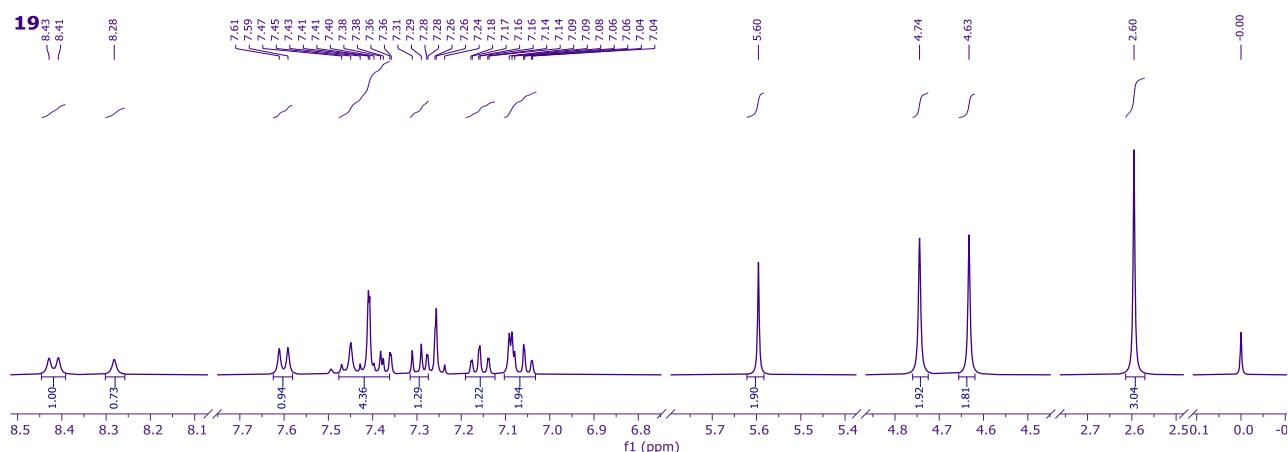
Analiza widma  $^1\text{H}$  NMR pochodnej **15** potwierdza obecność protonu grupy -NH (11,05 ppm) oraz pozostałych protonów pierścienia indolu (8,03–6,98 ppm). Proton pierścienia triazolowego występuje przy 8,17 ppm. W zakresie 7,55–7,29 ppm, obok sygnałów pochodzących od pierścienia indolu, pojawiają się również sygnały pierścienia benzenowego. Przy niższych wartościach przesunięcia chemicznego obserwujemy dwa singlety, przy 5,62 oraz 4,68 ppm, należące do dwóch grup -CH<sub>2</sub> grupy eterowej, natomiast singlety przy 4,54 oraz 2,51 ppm odpowiadają dwóm grupom metylenowym przyłączonym do pierścienia benzenowego. Nie są one równo cenne, co wyklucza powstanie pochodnej dimerycznej. Sygnał przy 4,54 ppm odpowiada protonom grupy metylenowej znajdującej się pomiędzy pierścieniem triazolowym a pierścieniem benzenowym, natomiast protony przyłączone do grupy -N<sub>3</sub> pojawiają się przy wartości 2,51 ppm.

Dodatkowo otrzymałam nowe dipodstawione pochodne indolu (**18** i **20**), które stanowiły substraty do syntezy konjugatów zawierających dwa ugrupowania indolowe różnie podstawione połączone pierścieniem triazolowym (**19** i **21**, Schemat 3).



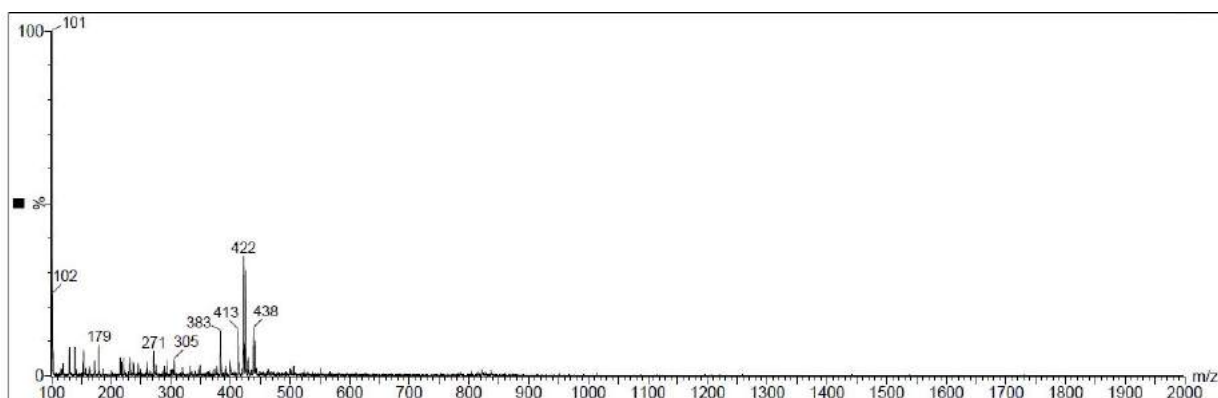
Schemat 3. Synteza pochodnych **19** i **21**

Na podstawie przedstawionego na rysunku 57 widma  $^1\text{H}$  NMR pochodnej **19** można potwierdzić otrzymanie związku o strukturze przedstawionej na Schemacie 4. Jak możemy zaobserwować, w zakresie 8,43–7,04 ppm widnieją sygnały odpowiadające protonom pierścieni indolu. Ze względu na różne otoczenie elektronowe obydwu pochodnych indolu tworzących związek **19**, sygnały te są przesunięte względem siebie. Pochodna **19** jest niesymetryczna. Podobną zależność obserwujemy w przypadku pochodnej **21**.



Rysunek 57. Widmo  $^1\text{H}$  NMR pochodnej **19**

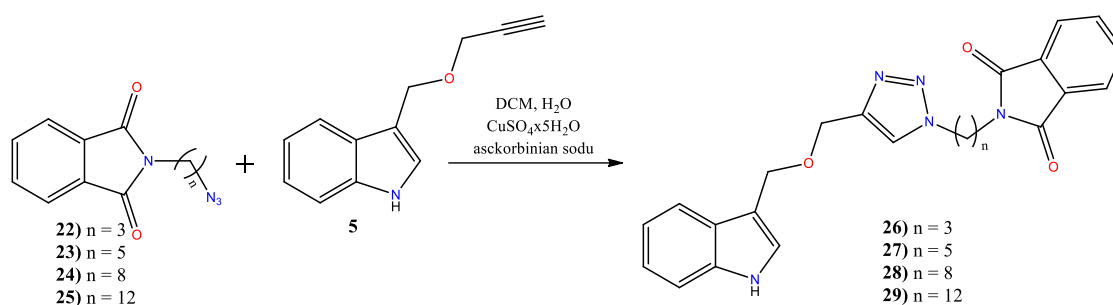
Analiza widm masowych ESI-MS pochodnych **19** i **21** wskazuje na otrzymanie cząsteczek o masach 399 oraz 427 u, co odpowiada masom molowym cząsteczek **19** i **21**. Jako przykład na rysunku 58 przedstawiłam widmo masowe pochodnej **19**, gdzie obserwujemy jony pseudomolekularne powstałe poprzez przyłączenie do cząsteczki związku **19** kationów metali takich jak sód ( $422 [\text{M}+\text{Na}]^+$ ), czy potas ( $438 [\text{M}+\text{K}]^+$ ).



Rysunek 58. Widmo ESI-MS pochodnej **19**

Jednym z kluczowych substratów do syntezy różnych związków biologicznie aktywnych jest ftalimid. W literaturze możemy znaleźć przykłady pochodnych ftalimidu wykazujących działanie przeciwzapalne, przeciwbólowe, przeciwnowotworowe, przeciwdrobnoustrojowe i przeciwdrgawkowe [177,178]. Znane są także pochodne ftalimidu o właściwościach antyoksydacyjnych [179-181]

Zważając na aktywność przeciwutleniającą zarówno pochodnych indolu jak i ftalimidu uznałam, że połączenie tych dwóch ugrupowań może spowodować efekt synergiczny i uzyskam związki o jeszcze lepszych właściwościach antyoksydacyjnych. W związku z powyższym otrzymałam serię **pochodnych indolowo-ftalimidowych połączonych łańcuchami alifatycznymi i pierścieniem triazolowym (26-29, Schemat 4)**. Substratami do przeprowadzonej reakcji CuAAC były *N*-azydoalkiloftalimidy o różnej długości łańcucha alifatycznego (22-25) oraz, zawierający terminalne wiązanie potrójne, 3-propargiloksymetyloindol (5) [P1].

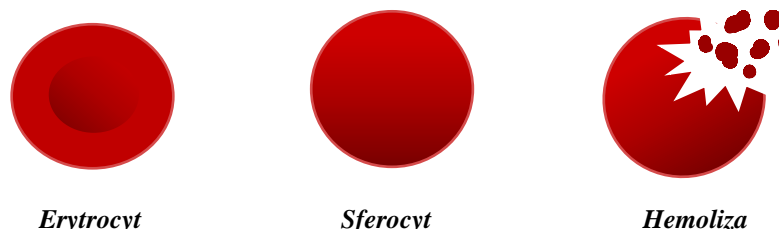


Schemat 4. Synteza triazolowych pochodnych indolu i ftalimidu

Strukturę związków 26-29 potwierdziłam za pomocą metod spektroskopowych. Na widmach  $^1\text{H}$  NMR wszystkich nowych triazolowych pochodnych indolu i ftalimidu charakterystyczny singlet atomu wodoru pierścienia triazolowego obserwujemy w zakresie 8,05–8,00 ppm. Sygnały pochodzące od protonów pierścieni aromatycznych indolu i ftalimidu występują w zakresie 7,86-7,50 ppm. Protony grup metylenowych grupy eterowej możemy zaobserwować w przedziale 5,30-4,52 ppm, natomiast przy niższych wartościach przesunięcia chemicznego pojawiają się sygnały protonów wchodzących w skład łańcucha alifatycznego. Na widmach FT-IR występują charakterystyczne pasma absorpcji z maksimum przy ok.  $3400\text{ cm}^{-1}$  charakterystyczne dla drgań rozciągających wiązania N-H grupy aminowej ugrupowania indolu oraz pasma absorpcji, przy wartościach ok.  $1700\text{ cm}^{-1}$ , wskazujące na obecność wiązań C=O grup karbonylowych cząsteczki ftalimidu.

Erytrocyty są modelami komórkowymi wykorzystywanymi w badaniach aktywności biologicznej związków *in vitro*. Obecna w erytrocytach hemoglobina transportuje tlen dlatego jest ona szczególnie narażona na działanie RFT. Ekspozycja erytrocytów na stres oksydacyjny może w konsekwencji skutkować przerwaniem błony komórkowej czerwonych krwinek prowadzącym do hemolizy (Rys. 59), czyli uwolnienia hemoglobiny z erytrocytów

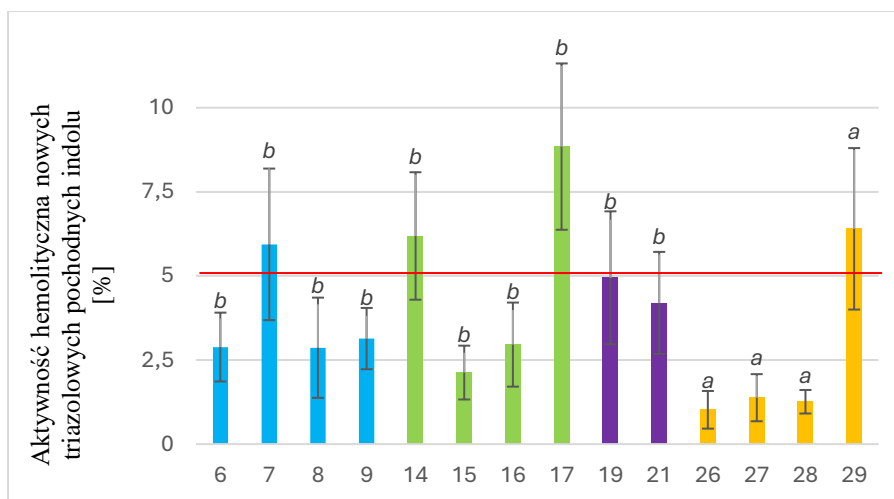
do osocza krwi. Dlatego jednym z głównych kryteriów ograniczających zastosowanie nowych związków bioaktywnych mających kontakt z krwią jest ocena ich hemokompatybilności [182-184].



Rysunek 59. Proces hemolizy

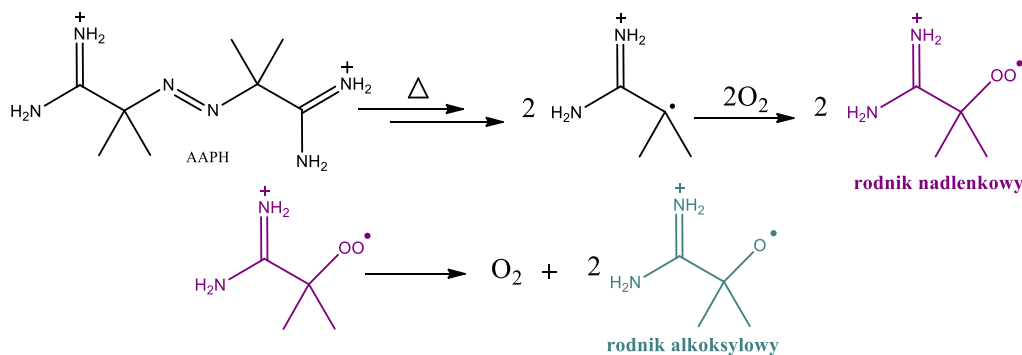
Wszystkie związki wchodzące w skład pierwszej grupy otrzymanych przeze mnie pochodnych zbadalam, we współpracy z Zakładem Biologii Komórki Wydziału Biologii UAM, pod kątem **aktywności cytotoksycznej względem erytrocytów ludzkich oraz aktywności protekcyjnej wobec indukowanej przez AAPH hemolizie czerwonych krwinek [P1,P2].**

Większość otrzymanych przeze mnie triazolowych pochodnych indolu, z wyjątkiem pochodnych **7, 14, 17 i 29** wykazała aktywność hemolityczną wobec erytrocytów ludzkich na poziomie mniejszym niż 5%, co wskazuje na ich hemokompatybilność (Rys. 60). Wśród pochodnych dimerycznych **6-9** nie zauważyłam związku między budową strukturalną związków a ich cytotoksycznością, hemolityczna jest tylko pochodna z łańcuchem pentylowym (**7**). Brak hemokompatybilności u pochodnych z ugrupowaniem azydometylobenzenowym może być związana z położeniem podstawnika azydometyloвого względem pierścienia triazolowego – zarówno pochodna **14** jak i **17** zawierają pierścień benzenowy podstawiony w pozycji 1,2, która znajduje się najbliżej pierścienia triazolowego. Pochodna **17** zawiera dwa podstawniki z grupą azydkową, co również może wpływać na jej hemolityczność. Natomiast spośród pochodnych indolowo-ftalimidowych **26-29**, cytotoksyczna okazała się pochodna z najdłuższym, dodecyłowym, łańcuchem węglowym (**29**) [P1,P2].



Rysunek 60. Aktywność hemolityczna nowych triazolowych pochodnych indolu [%]. Kolorem niebieskim zaznaczyłam dimeryczne pochodne indolu z linkerami alifatycznymi, kolorem zielonym – pochodne z dodatkowym pierścieniem benzenowym, kolorem fioletowym pochodne diindolowe, natomiast kolorem żółtym związki indolowo-ftalimidowe; Dane zawarte: <sup>a</sup>[P1], <sup>b</sup>[P2]

AAPH (2,2'-chlorowodorku-azobis(2-amidynopropanu) to związek, który pod wpływem temperatury rozkłada się z wytworzeniem rodników nadtlenkowych i alkoksylowych (Rys. 61).

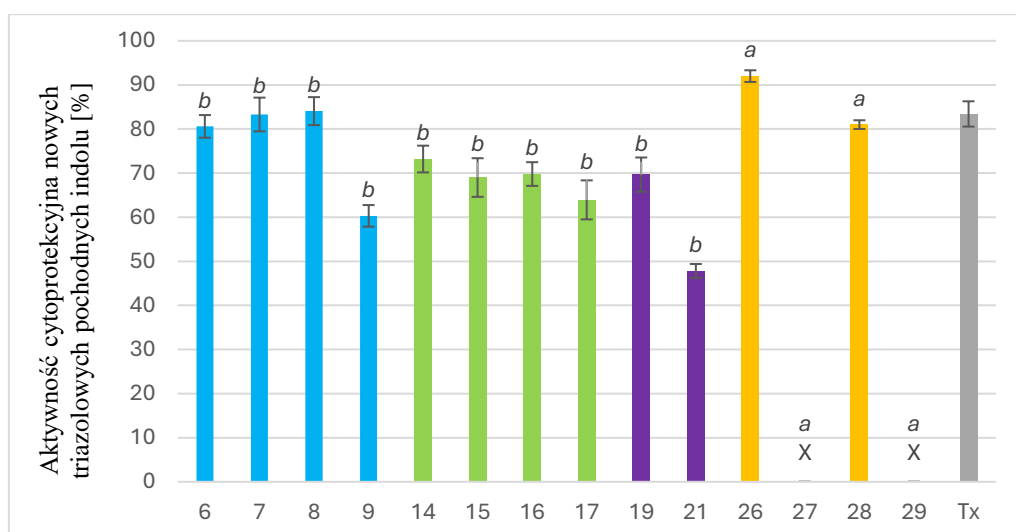


Rysunek 61. Mechanizm termicznego rozkładu AAPH

Znaczna część pochodnych pierwszej grupy skutecznie chroniła czerwone krwinki przed hemolizą indukowaną przez rodniki powstające w wyniku rozpadu AAPH (Rys. 62) [185]. Co ciekawe, pochodne indolowo-ftalimidowe z łańcuchem pentyłowym i dodecyłowym (**27** i **29**), nie wykazały żadnej aktywności protekcyjnej, natomiast dimery indolowe zawierające linkery alifatyczne o tej samej liczbie atomów węgla (**7** i **9**) efektywnie zmiatały wolne rodniki. Interesująca jest także niska aktywność cytoprotekcyjna pochodnej zawierającej dwa dipodstawione ugrupowania indolowe (**21**). W porównaniu do pozostałych



analogów diindolowych działanie protekcyjne pochodnej **21**, zawierającej dwa dipodstawione (w pozycjach C3 i N1) ugrupowania indolowe, jest najslabsza [**P1**,**P2**]. Może to wynikać z podstawienia atomu azotu obu ugrupowań indolowych wchodzących w skład tej cząsteczki. Aktywność przeciwnadciwnikowa pochodnych indolu związana jest z aromatycznym charakterem ugrupowania indolowego zawierającego grupę NH. Wolne rodniki są neutralizowane poprzez przeniesienie atomu wodoru lub elektronów z układu indolu (odpowiednio mechanizmy HAT i SET), na skutek utworzenia stabilizowanego rezonansem rodnika indolilowego [186,187,**P2**].



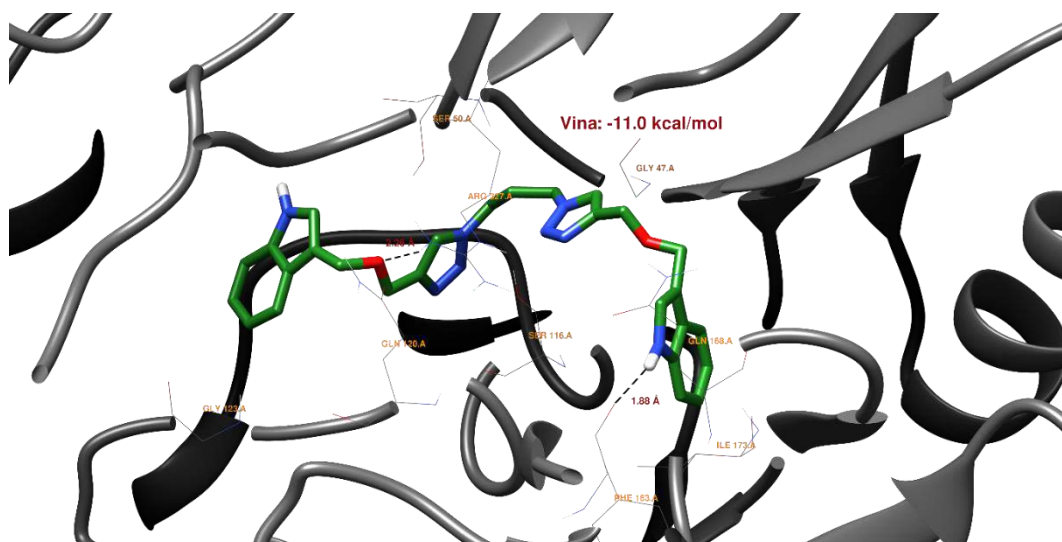
Rysunek 62. Aktywność cytoprotekcyjna nowych triazolowych pochodnych indolu [%]. Badanie wykonane dla stężenia 0,1 mg/mL w porównaniu do Troloxu (Tx) jako odniesienia. Kolorem niebieskim zaznaczyłam dimeryczne pochodne indolu z linkerami alifatycznymi, kolorem zielonym – pochodne z dodatkowym pierścieniem benzenowym, kolorem żółtym związki indolowo-ftalimidowe, natomiast kolorem fioletowym pochodne diindolowe; Dane zawarte: <sup>a</sup>[**P1**], <sup>b</sup>[**P2**]

Dla wszystkich pochodnych pierwszej grupy przeprowadziłam także badania *in silico* parametrów ADME (ang.: *absorption, distribution, metabolism, excretion* – wchłanianie, dystrybucja, metabolizm, wydalanie) określające profil farmakokinetyczny potencjalnego kandydata na lek. Większość związków spełnia regułę Lipińskiego: masa cząsteczkowa  $\leq 500$ , liczba donorów wiązań wodorowych  $\leq 5$ , liczba akceptorów wiązań wodorowych  $\leq 10$  i wartości współczynnika podziału oktanol-woda ( $\log P$ )  $\leq 5$ . Wyjątek stanowią pochodne **7-9** oraz **29**, których masa cząsteczkowa przekracza wartość 500 g/mol. Wartości parametrów ADME analizowanych związków zestawiałam w Tabeli 2.

Tabela 2. Właściwości fizykochemiczne związków należących do pierwszej grupy pochodnych indolowych

Związek	HBA	HBD	log $P_{o/w}$	M [g/mol]
6	6	2	2,87	496,56
7	6	2	3,56	524,62
8	6	2	4,57	566,70
9	6	2	5,96	622,80
14	6	1	2,95	373,41
15	6	1	2,91	373,41
16	6	1	2,91	373,41
17	9	1	2,99	428,45
19	4	0	3,37	427,50
21	4	1	3,03	399,45
26	5	1	2,63	415,44
27	5	1	3,24	443,50
28	5	1	4,16	485,58
29	5	1	5,65	541,68

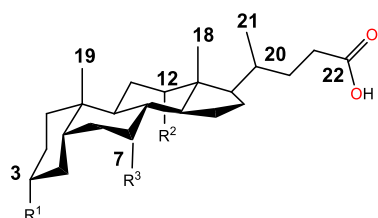
Spośród pochodnych pierwszej grupy do predykcji aktywności przeciwdrobnoustrojowej wybrałam związki **6**, **8**, **15** oraz **19**, ze względu na ich niską cytotoksyczność i równocześnie wysoką aktywność cytoprotekcyjną. Związki te wykazały potencjalną aktywność przeciwbakteryjną oraz przeciwgrzybiczną określoną na podstawie powinowactwa do receptorów białkowych bakterii *Escherichia Coli* (2Q85) oraz grzybów z gatunku *Candida Albicans* (5V5Z) zdefiniowanych na podstawie metody **dokowania molekularnego**. Prawdopodobne oddziaływania jakie mogą wystąpić pomiędzy badanymi ligandami a receptorem bakterii *E. Coli* przedstawiłam na przykładzie związku **6** na rysunku poniżej (Rys. 63).



Rysunek 63. Struktura pochodnej 6 w miejscu aktywnym domeny białka 2Q85 z możliwymi wiązaniemii wodorowymi zaznaczonymi jako czarne linie przerywane.

## 2. Pochodne drugiej grupy

Kwasy żółciowe (np. litocholowy, deoksycholowy i cholowy; Rys. 64), syntetyzowane w organizmie wszystkich kręgowców, stanowią główne produkty metabolizmu cholesterolu.



**Kwas litocholowy**  $R^1 = \text{OH}, R^2 = R^3 = \text{H}$

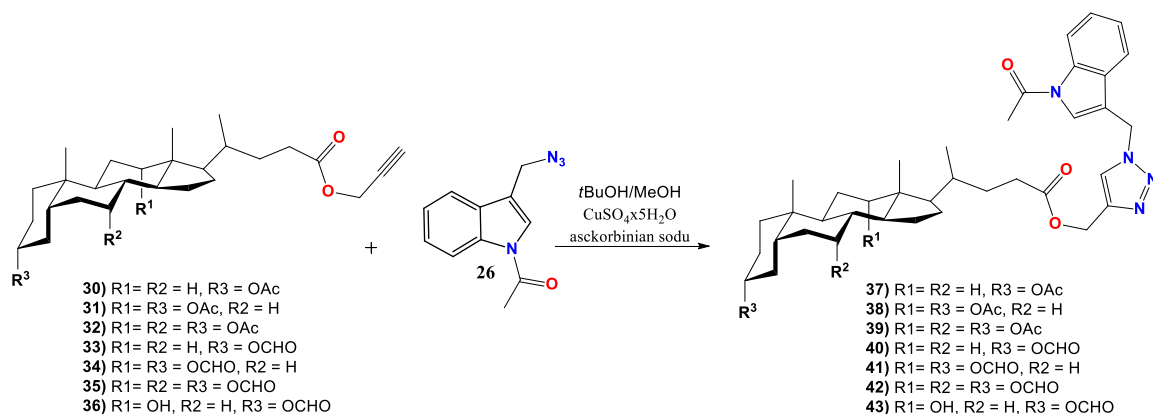
**Kwas deoksycholowy**  $R^1 = \text{OH}; R^2 = \text{OH}, R^3 = \text{H}$

**Kwas cholowy**  $R^1 = R^2 = R^3 = \text{OH}$

Rysunek 64. Struktura kwasów litocholowego, deoksycholowego oraz cholowego

Ich właściwości fizyko-chemiczne, takie jak, wysoka stabilność, biokompatybilność i amfifilowość sprawiają, że kwasy żółciowe i ich pochodne pełnią ważne funkcje w układach biologicznych, w tym regulację metaboliczną, ochronę przeciwdrobnoustrojową i solubilizację lipidów podczas trawienia. Kwasy żółciowe wykazują wysoką zdolność do penetracji i rozbijania membran biologicznych. Udowodniono, że mogą one uszkadzać błony erytrocytów, a także indukować kurczenie się komórek, co prowadzi do uwalniania przez nie materiałów wewnątrzkomórkowych [188-190]. Badania przeprowadzone wcześniej w naszej grupie badawczej wykazały, że połączenie cząsteczki gramininy z pochodnymi kwasów

żółciowych wpływa na obniżenie ich aktywności hemolitycznej [191,192]. Wpływ cząsteczki graminy na cytotoksyczność kwasów żółciowych wzbudził moje zainteresowanie, dlatego postanowiłam przeprowadzić kolejne modyfikacje i otrzymać, metodą chemii click, pochodne indolu i kwasów żółciowych wzbogacone dodatkowo ugrupowaniem triazolowym (37-43, Schemat 5) [P3].

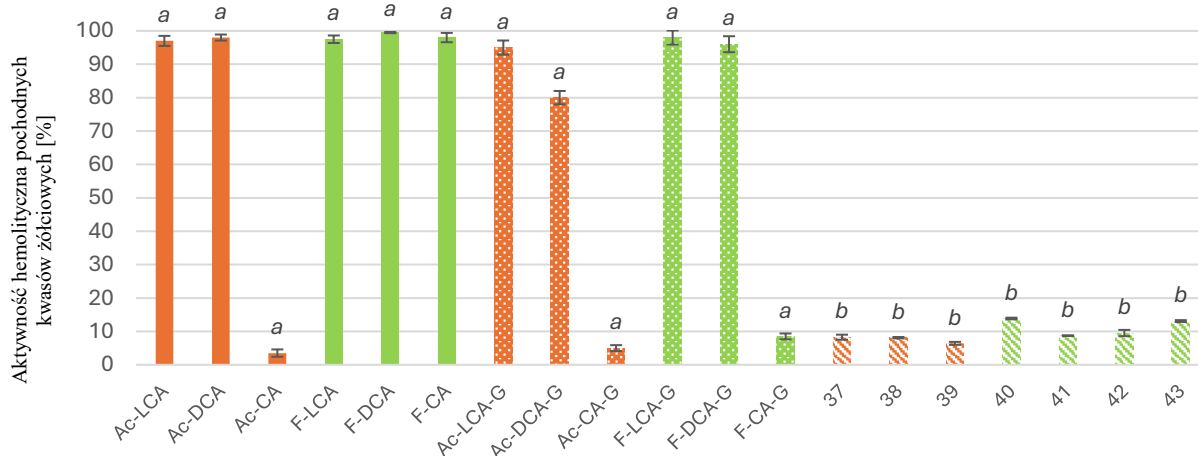


Schemat 5. Synteza triazolowych pochodnych indolu i kwasów żółciowych

Struktury otrzymanych produktów potwierdziłam za pomocą metod spektroskopowych. Na widmach  $^1\text{H}$  NMR wszystkich nowych triazolowych konjugatów indolowo-steroidowych, w zakresie 7,58–7,57 ppm, widoczny jest sygnał diagnostyczny dla protonu pierścienia triazolowego. Dla pochodnych formylowych 40-43 obserwujemy dodatkowy sygnał w zakresie 8,11–8,02 ppm charakterystyczny dla grupy -OCHO. Sygnały odpowiadające protonom pierścienia aromatycznego ugrupowania indolowego pojawiają się w zakresie 8,43–7,28 ppm u wszystkich nowych biokonjugatów. Bardzo charakterystyczne sygnały w zakresie 0,69–0,59, 0,94–0,90 oraz 0,90–0,74 ppm dają także trzy grupy metylowe układu steroidowego. Na widmach  $^{13}\text{C}$  NMR pochodnych 37-43 widoczne są charakterystyczne sygnały dla atomów węgla grup karbonylowych (grup acetylowych, formylowych i grupy estrowej) znajdujące się w regionie ok. 170 ppm. Sygnały diagnostyczne dla atomów węgla pierścienia 1,2,3-triazolowego obserwuje się w zakresie 143,4-143,3 i 123,6–123,5 ppm. Atomy węgla pierścieni indolu występują w zakresie 136,0-115,6 ppm. Na widmach FT-IR pochodnych 37-43 możemy zaobserwować pasma drgań charakterystyczne dla wiązań =C-H (ok. 3100  $\text{cm}^{-1}$ ), -C-H (ok. 2900-2800  $\text{cm}^{-1}$ ), C=O (1700  $\text{cm}^{-1}$ ). Dla pochodnej 43 możemy zaobserwować dodatkowo szerokie pasmo absorpcji z maximum przy 3435  $\text{cm}^{-1}$  pochodzące od drgań rozciągających wiązań grupy hydroksylowej.

Sprawdziłam również, jaki wpływ miały zastosowane przeze mnie modyfikacje na cytotoksyczność otrzymanych związków.

Jak widać na poniższym wykresie (Rys. 65) acetylowe pochodne kwasów lithocholowego i deoksycholowego, a także formylowe pochodne wszystkich przebadanych kwasów żółciowych (lithocholowego, deoksycholowego i cholowego) wykazały bardzo wysoką aktywność cytotoksyczną. Połączenie tych pochodnych z cząsteczką graminy nie wpłynęło znacząco na obniżenie aktywności hemolitycznej otrzymanych związków. Otrzymane przeze mnie konjugaty indolu i pochodnych kwasów żółciowych z pierścieniem triazolowym, jako elementem łączącym (**37-43**), cechuje znacznie niższa cytotoksyczność w porównaniu z ich analogami bez ugrupowania triazolowego [192, **P3**].



Rysunek 65. Aktywność hemolityczna acetylowych (kolor pomarańczowy) oraz formylowych (kolor zielony) pochodnych kwasów żółciowych (Ac/F-LCA, Ac/F-DCA, Ac/F-CA), ich soli z gramina (Ac/F-LCA-G, Ac/F-DCA-G, Ac/F-CA-G) oraz związków 37-40 [%]. Badanie wykonane dla stężenia 0,1 mg/mL.  
Dane zawarte: <sup>a</sup> [11], <sup>b</sup> [P3]

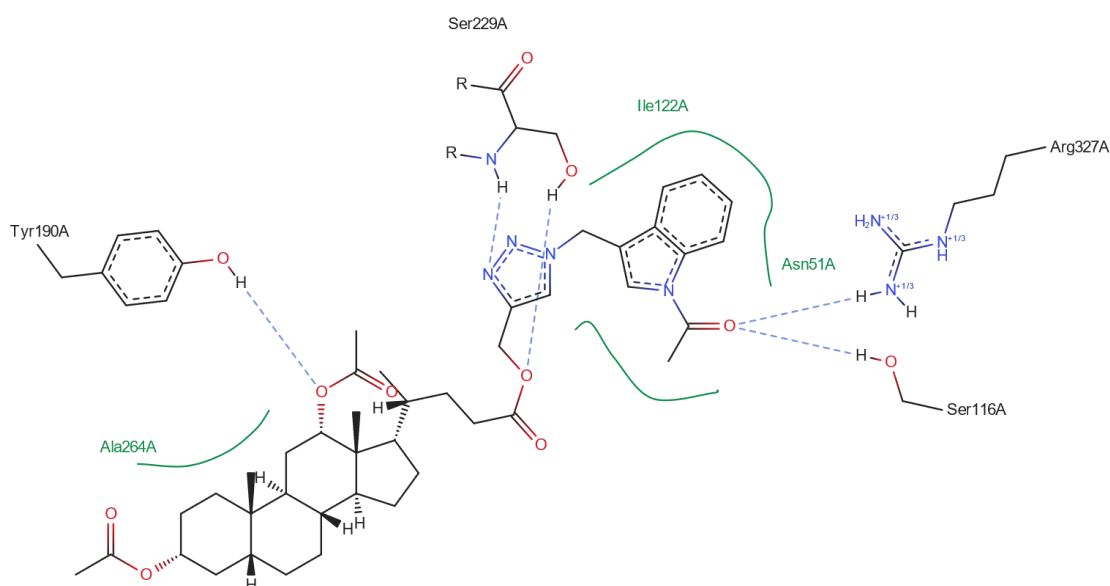
Metody modelowania molekularnego pozwoliły na predykcję potencjalnej aktywności przeciwdrobnoustrojowej pochodnej diacetylowej (**38**) i diformylowej (**41**) kwasu deoksycholowego, oraz jej monopodstawionego analogu, zawierającego jedną niepodstawioną grupę hydroksylową (**43**), a także porównanie wpływu konkretnych grup (acetylowa, formylowa, hydroksylowa) na ich interakcje z określonymi domenami białkowymi bakterii szczepu *Escherichia Coli* (2Q85) oraz grzybów gatunku *Candida Albicans* (5V5Z). Wszystkie przebadane pochodne (**38**, **41**, **43**) wykazały potencjalną aktywność przeciwbakteryjną i przeciwgrzybiczną [P3]. Na poniższych rysunkach przedstawiono sposób, w jaki ligandy **38**, **41** oraz **43** oddziałują z domeną białka 2Q85.

W przypadku diacetylowej pochodnej **38** pomiędzy domeną liganda i białka może powstać wiązanie wodorowe pomiędzy tlenem jednej z grup acetylowych układu

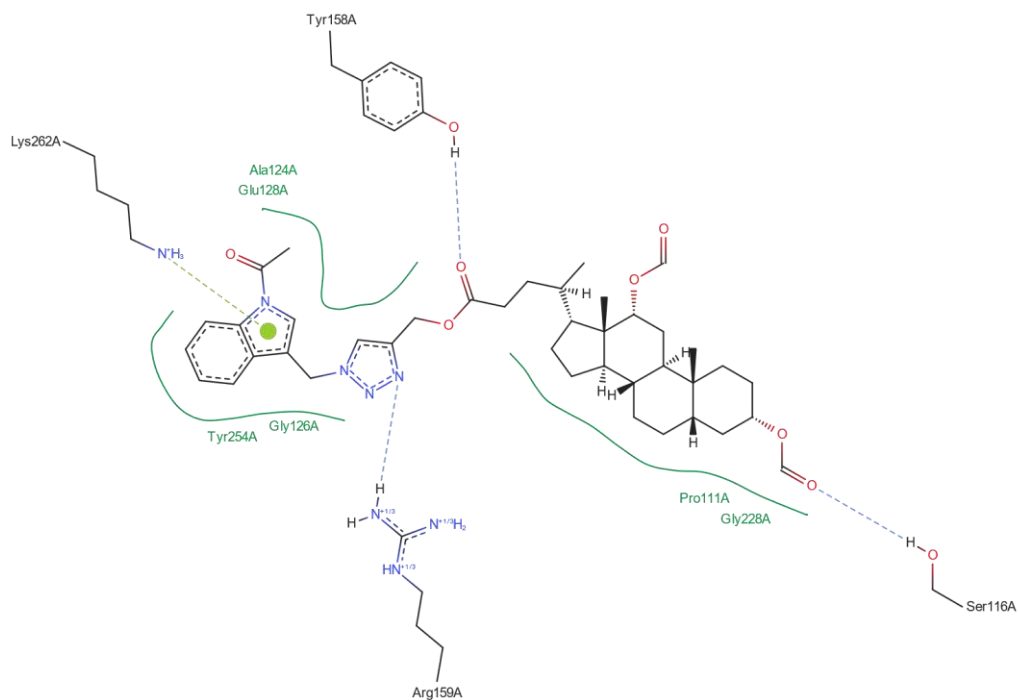
steroidowego, a resztą aminokwasu TYR-190. Na rysunku 66 możemy zauważyć, że pomiędzy tlenem grupy estrowej łączącej układ steroidowy z pierścieniem triazolowym oraz atomem azotu tego pierścienia a resztą seryny (SER-229) mogą powstać dwa dodatkowe wiązania wodorowe. W tworzeniu wiązań wodorowych z resztą aminokwasów ARG-327 oraz SER-116 bierze udział atom tlenu grupy acetylowej przyłączonej do pierścienia indolowego.

Interakcje diformylowej pochodnej **41** z domeną białka 2Q85 (Rys. 67) polegają na prawdopodobnym tworzeniu wiązań wodorowych pomiędzy karbonyłowymi atomami tlenu grupy estrowej i formylowej liganda a resztą aminokwasów TYR-158 oraz SER-116. Atom azotu pierścienia triazolowego oddziałuje natomiast z resztą ARG-159. Dodatkowo pierścień pirolowy układu indolowego może uczestniczyć w oddziaływaniach kation-pi z resztą LYS-262.

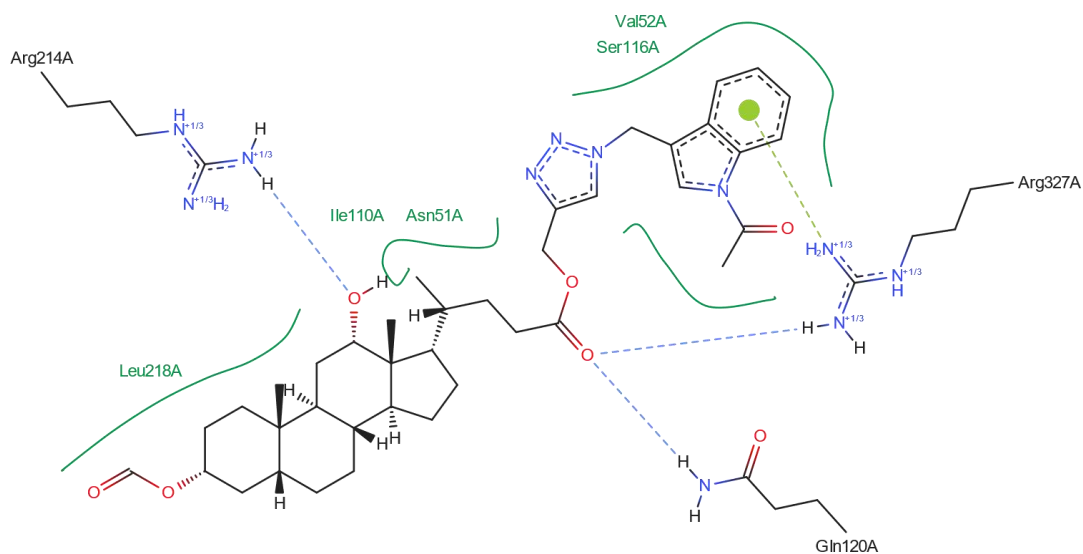
Atom tlenu niepodstawionej grupy hydroksylowej pochodnej formylowej **43** (Rys. 68) może wiązać się poprzez wiązanie wodorowe z resztą argininy ARG-214. Karbonylowy atom tlenu grupy estrowej może oddziaływać za pomocą wiązań wodorowych z resztami glutaminy GLN-120 oraz argininy ARG-327. Rysunek 57 wskazuje także na oddziaływane kation-pi pierścienia indolowego i ARG-327 [P3].



Rysunek 66. Struktura pochodnej **38** wewnątrz miejsca aktywnego domeny białka 2Q85 z zaznaczonymi interakcjami: zielone linie ciągłe – oddziaływanie hydrofobowe i niebieskie linie przerywane – wiązanie wodorowe.



Rysunek 67. Struktura pochodnej **41** wewnątrz miejsca aktywnego domeny białka 2Q85 z zaznaczonymi interakcjami: zielone linie ciągłe – oddziaływanie hydrofobowe, niebieskie linie przerywane – wiązanie wodorowe, zielone linie przerywane – oddziaływania kation-pi.

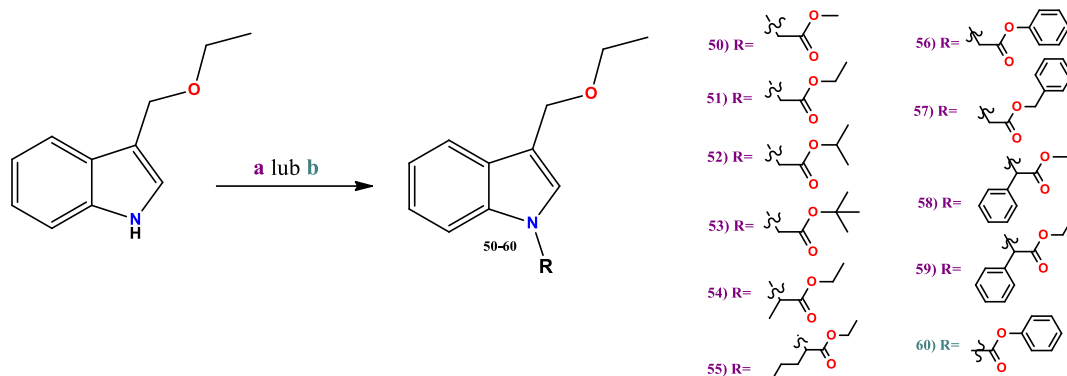


Rysunek 68. Struktura pochodnej **43** wewnątrz miejsca aktywnego domeny białka 2Q85 z zaznaczonymi interakcjami: zielone linie ciągłe – oddziaływanie hydrofobowe, niebieskie linie przerywane – wiązanie wodorowe, zielone linie przerywane – oddziaływania kation-pi.

Oddziaływania ligandów **38**, **41** i **43** z domeną białkową *Candida Albicans* (5V5Z) opisane zostały w publikacji **P3**.

### 3. Pochodne trzeciej grupy

Ze względu na predyspozycje układu indolowego do ulegania reakcjom substytucji elektrofilowej w pozycji C3, to właśnie ten sposób modyfikacji jest najczęściej stosowany przy syntezie nowych pochodnych indolu. W naszej grupie badawczej otrzymano szereg związków indolu podstawionych w pozycji C3 wykazujących wysoki potencjał antyoksydacyjny. Jednym z takich związków jest 3-etoksymetyloindol, który w testach z AAPH wykazał aktywność cytoprotekcyjną (79%) zbliżoną do aktywności wzorca – Troloxu (86%) [127]. Przeprowadzono także badania które wykazały, że podstawienie atomu azotu indolo-3-karbinolu grupą acetylową znacznie obniża aktywność cytoprotekcyjną jego prekursora. Z kolei *N*-acetylowa pochodna indolu podstawiona w pozycji C3 ugrupowaniem piperidynotiokarbaminianowym wykazuje wysoką aktywność przeciwutleniającą [P4]. Z danych literaturowych wynika, że znane są pochodne indolu podstawione w pozycji N1 o właściwościach antyoksydacyjnych [193-195]. Mając na uwadze powyższe fakty, postanowiłam zbadać, jaki wpływ będzie miało podstawienie pozycji N1 analogów indolu na ich aktywność przeciwutleniającą. W konsekwencji tego, trzecią grupę zsyntezowanych przeze mnie pochodnych stanowią ***N*-podstawione estrowe pochodne indolu zawierające w pozycji C3 grupę etoksymetylową (51-60, Schemat 6) [P4].**



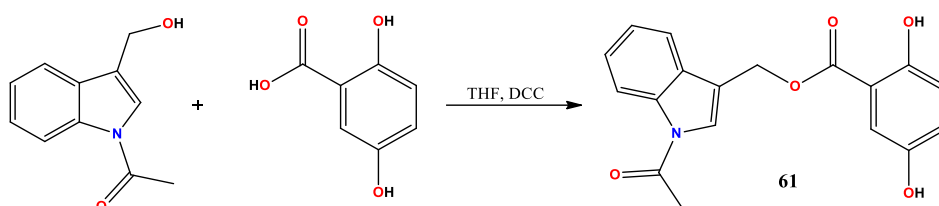
Schemat 6. Synteza *N*-podstawionych pochodnych indolu (**a**: BrR, NaH, DMF; **b**: kwas benzoesowy, PPh<sub>3</sub>, NBS, CH<sub>2</sub>Cl<sub>2</sub>, Et<sub>3</sub>N)

Kwas salicylowy (kwas 2-hydroksybenzoesowy) jest jednym z najszerzej opisanych związków o właściwościach przeciwgorączkowych, przeciwreumatycznych i przeciwbólowych. Wykazuje także działanie antyoksydacyjne dzięki obecności m.in. grupy



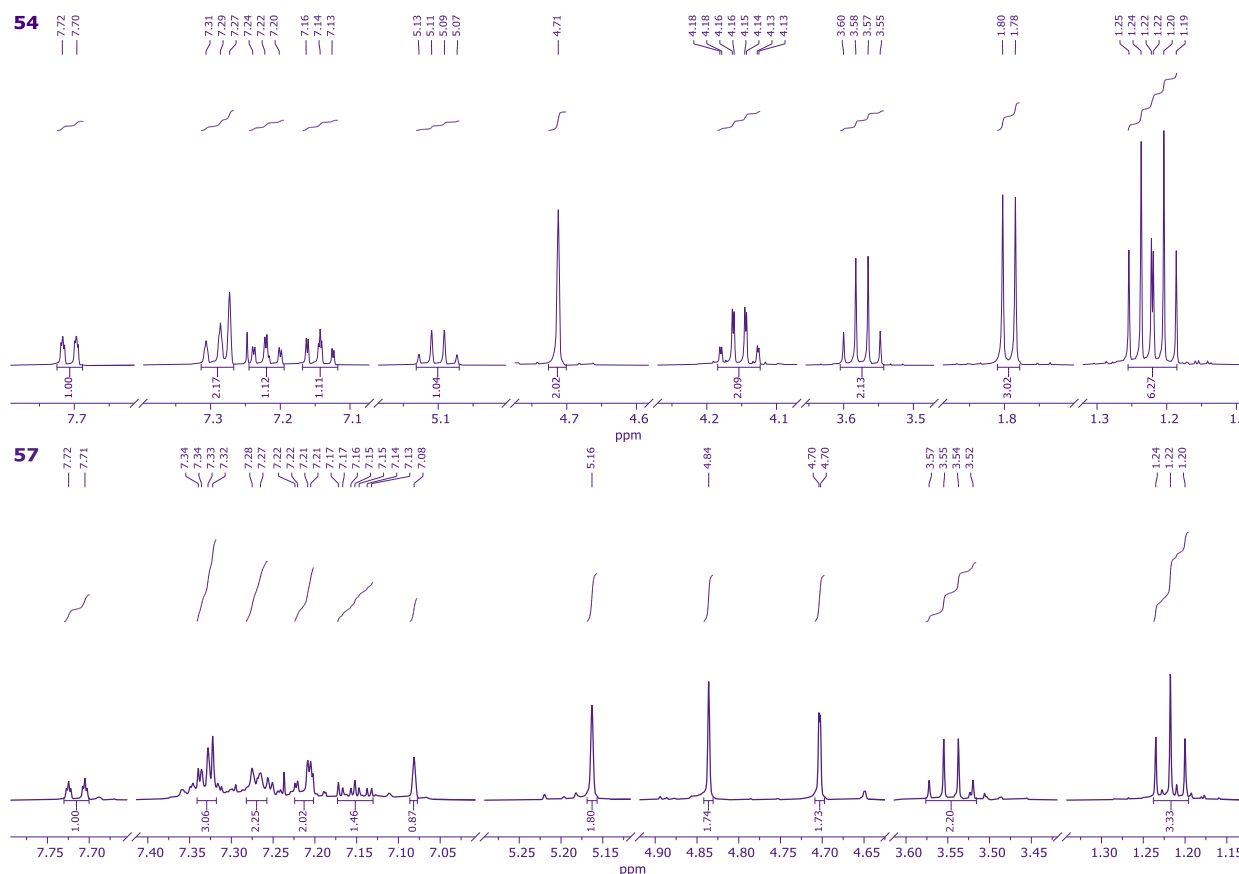
fenolowej. Według Velika B. & Kron I. oraz Foki M. C. fenole redukują poziom utleniania związków organicznych poprzez przeniesienie atomu wodoru z grupy OH na rodniki ponadtlenkowe [196,197].

Ze względu na opisane powyżej właściwości pochodnych fenolowych, uznałam, iż ciekawym aspektem mojej pracy będzie zbadanie aktywności antyoksydacyjnej pochodnej indolowej zawierającej dodatkowo ugrupowanie fenolowe. W związku z tym grupę pochodnych estrowych poszerzyłam o ester *N*-acetylo-3-metyloindolu i kwasu 2,5-dihydroksybenzoesowego (**61**, Schemat 7).



Schemat 7. Synteza pochodnej 61

Metody spektroskopowe pozwoliły na określenie struktur otrzymanych pochodnych. Na widmach  $^1\text{H}$  NMR związków **50-61**, w zakresie 8,41-6,19 ppm, obecne są sygnały charakterystyczne dla protonów pierścieni aromatycznych układu indolu oraz pierścieni benzenowych podstawników. Protony grup metylenowych należących do grupy eterowej występują jako dublety lub singlety przy wartościach około 5,50-4,15 ppm. Charakterystycznym sygnałem widocznym na widmach  $^{13}\text{C}$  NMR jest sygnał należący do karbonylowego atomu węgla obecny przy około 170 ppm. Atomy węgla pierścieni indolu oraz pierścienia benzenowego obecne są natomiast w zakresie 158-109 ppm. Na poniższym rysunku (Rys. 69) przedstawiłam przykładowe widma protonowe pochodnych z podstawnikami propanianoetylowym (**54**) oraz octanobenzylowym (**57**).



Rysunek 69. Widma  $^1\text{H}$  NMR pochodnych **54** i **57**

Widmo FT-IR estru pochodnej indolu z kwasem 2,5-dihydroksybenzoesowym **61** zawiera bardzo charakterystyczne szerokie pasmo absorpcji, z maximum przy  $3215\text{ cm}^{-1}$ , diagnostyczne dla drgań wiązań grup hydroksylowych. Pasma absorpcji w zakresie  $3050\text{-}2800\text{ cm}^{-1}$  odpowiadają drganiom wiązania C-H pierścieni aromatycznych i łańcuchów alifatycznych. Intensywne pasmo odpowiadające drganiom rozciągającym grupy karbonylowej zlokalizowane jest przy około  $1700\text{ cm}^{-1}$  (**16**, **18**, **20-30**).

Badania cytotoksyczności wykazały, że większość otrzymanych przeze mnie *N*-podstawionych pochodnych indolu działa hemolitycznie wobec erytrocytów ludzkich (**51**, **53**, **55-57**, **59-61**) w stężeniu  $0,1\text{ mg/mL}$ . Spośród związków zawierających podstawnik fenylowy, tylko pochodna **58** nie powodowała hemolizy krwinek czerwonych. Do związków hemokompatybilnych zaliczają się także trzy pochodne z podstawnikiem alifatycznym (**50**, **52**, **54**) Aktywność cytotoksyczna otrzymanych przeze mnie *N*-podstawionych pochodnych indolu może być determinowana obecnością hydrofobowych podstawników estrowych w pozycji N1, które umożliwiają penetrację dwuwarstwy fosfolipidowej

erytrocytów. Obniżenie stężenia badanych związków **50-61** do 0,01 mg/mL zredukowało ich aktywność hemolityczną, co pozwoliło na analizę ich właściwości cytoprotekcyjnych [P4].

Z przeprowadzonych badań wynika, że podstawienie heterocyklicznego atomu azotu indolu wpłynęło niekorzystnie na aktywność cytoprotekcyjną jego pochodnych. Spośród związków **50-61**, najwyższą aktywność przeciwutleniającą wobec indukowanej przez AAPH hemolizie krwinek czerwonych wykazały związki z podstawnikami fenylooctanoetylowym (**59**) (31%), pentanianometylowym (**55**) (20%) i benzoesowym **60** (19%) w porównaniu do Troloxu (52%). Pozostałe *N*-podstawione pochodne indolu wykazały bardzo niską aktywność antyoksydacyjną [P4].

Ze względu na wysoką aktywność przeciwutleniającą pochodnych fenolu spodziewałam się, iż połączenie równie aktywnej biologicznie cząsteczki, jaką jest indol, z kwasem 2,5-dihydroksybenzoesowym będzie prowadzić do otrzymania nowego związku o analogicznych lub lepszych właściwościach antyoksydacyjnych. Wbrew moim oczekiwaniom pochodna **61** nie wykazała znaczącej aktywności przeciwutleniającej. Dane literaturowe wskazują, że niektóre *N*-podstawione pochodne indolu wykazują aktywność przeciwdrobnoustrojową [198-200]. Dlatego postanowiłam określić aktywność przeciwbakteryjną i przeciwgrzybiczną pochodnych **50-61** w badaniach prowadzonych we współpracy z Katedrą Gleboznawstwa i Mikrobiologii, Wydziału Rolnictwa, Ogrodnictwa i Bioinżynierii, Uniwersytetu Przyrodniczego w Poznaniu, wobec wybranych gatunków bakterii i grzybów [P4].

Aktywność przeciwbakteryjną związków **50-61** określono wobec szczepów bakterii *Micrococcus luteus*, *Bacillus subtilis*, *Escherichia coli* oraz *Pseudomonas fluorescens*, jako zdolność do hamowania ich wzrostu. Najlepszym inhibitorem okazał się związek **53** (z podstawnikiem octano-*tert*-butylowym), który hamował wzrost bakterii gatunku *Bacillus subtilis*. U pozostałych pochodnych nie zaobserwowano istotnej aktywności przeciwbakteryjnej [P4].

Do zbadania aktywności przeciwgrzybiczej związków **50-61** wykorzystano grzyby gatunków *Alternaria alternata*, *Fusarium culmorum*, *Trichoderma harzianum*, *Trichoderma atroviride* oraz *Botrytis cinerea*. Pochodne z podstawnikami octanometylowym (**50**), propanianoetylowym (**54**), fenylooctanometylowym (**58**) i fenylooctanoetylowym (**59**) wykazały najwyższą aktywność przeciwgrzybiczną. Otrzymane przeze mnie *N*-podstawione pochodne indolu okazały się najefektywniej hamować rozwój grzybów gatunku *Trichoderma atroviride*. Większość związków należących do trzeciej grupy opisywanych pochodnych może być rozważana jako potencjalne substancje o działaniu przeciwgrzybiczym [P4].

## Podsumowanie

Celem naukowym niniejszej rozprawy doktorskiej było otrzymanie nowych pochodnych indolu o potencjalnej aktywności antyoksydacyjnej, które w przyszłości mogłyby znaleźć zastosowanie w farmakologii. Dodatkowym aspektem mojej pracy było określenie aktywności przeciwbakteryjnej i przeciwgrzybiczej, wybranych nowo otrzymanych pochodnych i tym samym poszerzenia obszaru ich potencjalnego zastosowania.

Wszystkie nowo otrzymane związki scharakteryzowałam poprzez analizę widm NMR i FT-IR oraz (dla większości pochodnych) za pomocą spektrometrii mas EI-MS lub ESI-MS.

Wszystkie badania aktywności hemolitycznej i cytoprotekcyjnej przeprowadzono we współpracy z Zakładem Biologii Komórki Wydziału Biologii UAM. Część tych badań wykonałam samodzielnie.

Badania aktywności przeciwbakteryjnej i przeciwgrzybiczej zostały zrealizowane we współpracy z Katedrą Gleboznawstwa i Mikrobiologii, Wydziału Rolnictwa, Ogrodnictwa i Bioinżynierii, Uniwersytetu Przyrodniczego w Poznaniu.

Badania dokowania molekularnego przeprowadzono w Zakładzie Chemii Kwantowej Wydziału Chemii UAM.

Procedury syntezy nowych pochodnych, ich charakterystyka spektroskopowa oraz pozostałe wyniki badań zostały przedstawione w czterech publikacjach naukowych [P1-P4].

### W wyniku przeprowadzonych badań:

- Łącznie zsyntezowałam trzydzieści pięć nowych pochodnych indolu;
- Nowa pochodna indolu zawierająca łańcuch *n*-propargilowy przyłączony do heterocyklicznego atomu azotu pierścienia indolowego oraz nowa pochodna zawierająca ugrupowanie azydkowe w łańcuchu bocznym pozycji C3 posłużyły mi jako substraty do syntezy pochodnych diindolowych;
- Przy zastosowaniu metody chemii click, otrzymałam czternaście nowych triazolowych pochodnych indolu w tym: cztery pochodne zawierające dodatkowo ugrupowanie ftalimidowe, cztery pochodne dimeryczne z linkerami alifatycznymi, trzy izomery pochodnych z dodatkowym dipodstawionym pierścieniem benzenowym oraz jeden analog tripodstawiony oraz dwie pochodne diindolowe;

- Metodą chemii click, uzyskałam siedem nowych pochodnych indolowo-steroidowych zawierających także pierścień 1,2,3-triazolowy;
- Przeprowadziłam reakcje 3-etoksymetyloindolu z serią bromoestrów, w skutek czego otrzymałam 10 nowych *N*-podstawionych estrowych pochodnych indolu;
- Dodatkowo, w reakcjach z pochodnymi kwasów benzoesowych, uzyskałam dwie estrowe pochodne indolu
- Otrzymane związki scharakteryzowałam spektroskopowo ( $^1\text{H}$  NMR,  $^{13}\text{C}$  NMR, FT-IR, MS)
- Znaczna część otrzymanych przeze mnie pochodnych okazała się być biokompatybilna wobec erytrocytów ludzkich;
- Znaczna część związków wykazała aktywność protekcyjną wobec wywołanej przez AAPH hemolizie krwinek czerwonych; część badań biologicznych przeprowadziłam samodzielnie;
- Badania przeprowadzone z użyciem metod *in silico*, a także metod eksperymentalnych, wykazały potencjalną aktywność przeciwgrzybiczną niektórych nowo otrzymanych związków;
- Za pomocą metod teoretycznych oceniłam właściwości fizykochemiczne wybranych związków w oparciu o reguły Lipińskiego i Vebera, większość badanych związków spełnia kryteria tych reguł.

Tabela 3. Porównanie numeracji związków zawartej w niniejszej pracy do numeracji obowiązującej w poszczególnych publikacjach **P1-P4**.

Rozprawa doktorska	Publikacja	Rozprawa doktorska	Publikacja
Publikacja 1 [P1]		Publikacja 3 [P2]	
26	24	37	19
27	25	38	20
28	26	39	21
29	26	40	15
Publikacja 2 [P2]		41	16
6	5	42	17
7	6	43	18
8	7	18	4
8	8	Publikacja 4 [P4]	
14	9	50	18
15	10	51	19
16	11	52	20
17	12	53	21
18	3	54	22
19	13	55	23
20	4	56	24
21	14	57	25
		58	26
		59	27
		60	17
		61	29

## Spis rysunków

Rysunek 1. Struktura cząsteczki indolu

Rysunek 2. Reakcje substytucji elektrofilowej zachodzącej w pozycjach C2 i C3 pierścienia indolu

Rysunek 3. Schemat reakcji halogenowania indolu

Rysunek 4. Schemat reakcji nitrowania indolu

Rysunek 5. Schemat reakcji sulfonowania indolu

Rysunek 6. Schemat reakcji metylowania indolu

Rysunek 7. Schemat reakcji acetylowania indolu

Rysunek 8. Acetylowanie indolu w warunkach Friedla-Craftsa

Rysunek 9. Schemat reakcji formylowania indolu metodą Vilsmeiera-Haacka

Rysunek 10. Mechanizm katalizowanej kwasem octowym reakcji Mannicha prowadzącej do utworzenia graminy

Rysunek 11. Schemat reakcji Mannicha zachodzącej w obniżonej temperaturze

Rysunek 12. Struktury mezomeryczne anionu indolilowego

Rysunek 13. Schemat alkilowania indolu w pozycji N1 przy użyciu reakcji Mitsunobu

Rysunek 14. Reaktywność pierścienia benzenowego indolu

Rysunek 15. Schemat metabolizmu tryptofanu

Rysunek 16. Struktura cząsteczek strychniny i brucyny

Rysunek 17. Struktury cząsteczek alkaloidów Vinca będących w zastosowaniu klinicznym

Rysunek 18. Struktury cząsteczek wybranych alkaloidów sporyszu

Rysunek 19. Struktury cząsteczek: a) harminy i b) harmaliny

Rysunek 20. Struktury cząsteczek: a) harminy i b) harmaliny

Rysunek 21. Struktury cząsteczek: a) rezerpiny; b) johimbiny; c) ajmaliny

Rysunek 22. Wzór strukturalny Indometacyny (kwasu 2-(1-(4-chlorobenzoylo)-5-metoksy-2-metylo-1H-indol-3-ilo)octowego)

Rysunek 23. Pochodne indometacyny o właściwościach przeciwzapalnych selektywne wobec COX-2

Rysunek 24. Wzory strukturalne: a) Acemetacyny, b) Tenidapu, c) Etodolaku

Rysunek 25. Struktury leków stosowanych w terapiach przeciwnowotworowych: a) Sunitynib, b) Alectinib, c) Panobinostat

Rysunek 26. Pochodne indolowe o właściwościach przeciwnowotworowych

Rysunek 27. Struktury cząsteczek leków przeciwmigrenowych: a) sumatryptan; b) almotryptan; c) zolmitryptan; d) naratryptan

*Rysunek 28.* Pochodne indolu o właściwościach przeciwbakteryjnych i przeciwgrzybiczych

*Rysunek 29.* N-podstawione pochodne indolu o właściwościach przeciwbakteryjnych

*Rysunek 30.* Pochodne indolowo-triazolowe o działaniu przeciwgrzybiczymprzeciwgrzybicznym

*Rysunek 31.* Leki zawierające cząsteczkę indolu o aktywności przeciwwirusowej:  
a) Umifenovir; b) Delawirdyna

*Rysunek 32.* Pochodne indolu o aktywności przeciwwirusowej

*Rysunek 33.* Kaskadowa reakcja melatoniny i jej metabolitów z wolnymi rodnikami

*Rysunek 34.* Kwas indolilo-3-propionowy (IPA)

*Rysunek 35.* Hybryda steroidowo-indolowa o właściwościach przeciwutleniających

*Rysunek 36.* Pochodna triazolowo-indolowa

*Rysunek 37.* Pochodne indolu z nienasyconym łańcuchem bocznym w pozycji C5

*Rysunek 38.* N-podstawione pochodne indolu o właściwościach antyoksydacyjnych

*Rysunek 39.* Struktura cząsteczki indolo-3-karbinolu

*Rysunek 40.* Dimeryczne, trimeryczne i tetrameryczne metabolity I3C

*Rysunek 41.* Proponowane mechanizmy antyoksydacyjne I3C

*Rysunek 42.* Budowa cząsteczki graminy

*Rysunek 43.* Przykładowe mechanizmy reakcji, jakim ulega gramina

*Rysunek 44.* Schematy reakcji graminy z nukleofilami

*Rysunek 45.* Schemat reakcji otrzymywani bisindolowej pochodnej graminy

*Rysunek 46.* Schemat syntezy indolo-3-karbinolu

*Rysunek 47.* Schemat reakcji metylojodku graminy z odczynnikami Grignarda

*Rysunek 48.* Dimeryzacja graminy

*Rysunek 49.* Schemat reakcji otrzymywania 3-bromoindolu

*Rysunek 50.* Synteza 4-alkilograminy

*Rysunek 51.* N-alkilowanie graminy bromkiem etylu

*Rysunek 52.* Przykładowe bioaktywne pochodne graminy o właściwościach przeciwnowotworowych, przeciwwirusowych, przeciwgrzybiczych, owadobójczych i przeciwporostowych

*Rysunek 53.* Schemat reakcji CuAAC

*Rysunek 54.* Mechanizm reakcji CuAAC

*Rysunek 55.* Wybrane pochodne triazolowe o właściwościach przeciwnowotworowych (a i b); przeciwbakteryjnych (c); przeciwzapalnych (d) oraz struktury leków zawierających pierścień 1,2,3-triazolowy



*Rysunek 56.* Widma  $^1\text{H}$  NMR pochodnych 6 i 15

*Rysunek 57.* Widmo  $^1\text{H}$  NMR pochodnej 19

*Rysunek 58.* Widmo ESI-MS pochodnej 19

*Rysunek 59.* Proces hemolizy

*Rysunek 60.* Aktywność hemolityczna nowych triazolowych pochodnych indolu [%]

*Rysunek 61.* Mechanizm termicznego rozkładu AAPH

*Rysunek 62.* Aktywność cytoprotekcyjna nowych triazolowych pochodnych indolu [%]

*Rysunek 63.* Struktura pochodnej 6 w miejscu aktywnym domeny białka 2Q85 z możliwymi wiązaniami wodorowymi zaznaczonymi jako czarne linie przerywane

*Rysunek 64.* Struktura kwasów litcholowego, deoksycholowego oraz cholowego

*Rysunek 65.* Aktywność hemolityczna acetylowych oraz formylowych pochodnych kwasów żółciowych, ich soli z graminą oraz związków 37-40 [%]

*Rysunek 66.* Struktura pochodnej 38 wewnątrz miejsca aktywnego domeny białka 2Q85 z zaznaczonymi interakcjami

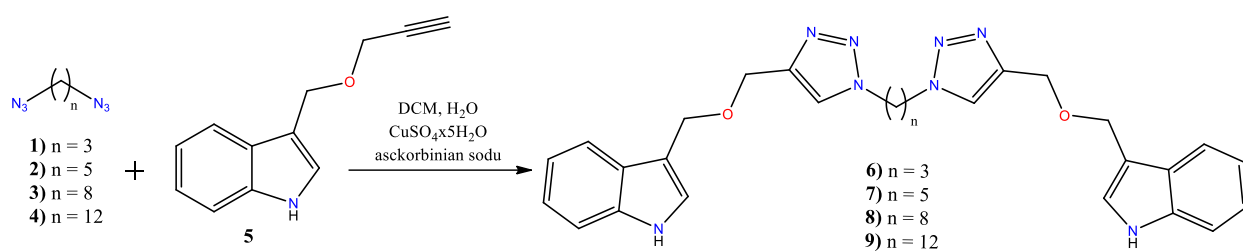
*Rysunek 67.* Struktura pochodnej 41 wewnątrz miejsca aktywnego domeny białka 2Q85 z zaznaczonymi interakcjami

*Rysunek 68.* Struktura pochodnej 43 wewnątrz miejsca aktywnego domeny białka 2Q85 z zaznaczonymi interakcjami

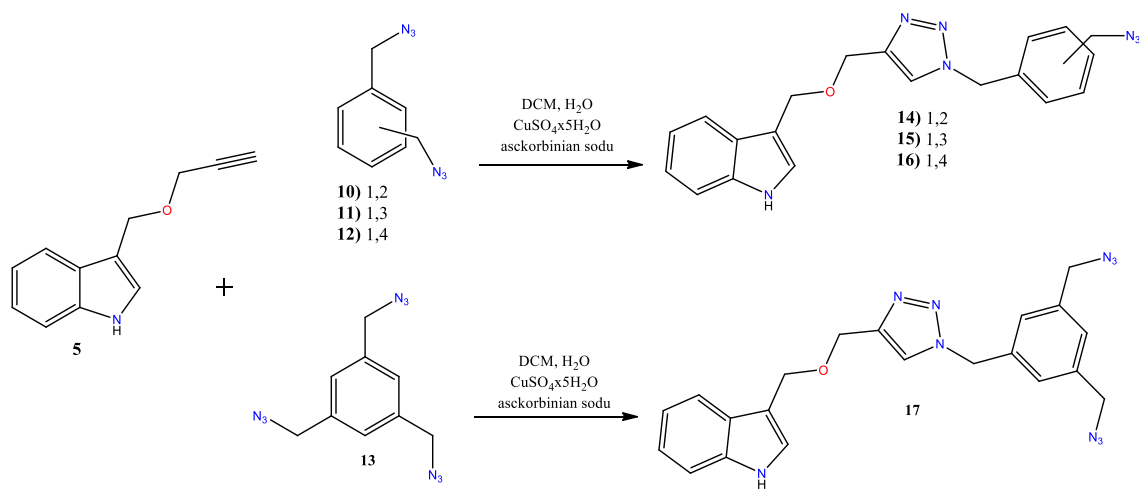
*Rysunek 69.* Widma  $^1\text{H}$  NMR pochodnych 54 i 57

# Schematy przeprowadzonych syntez

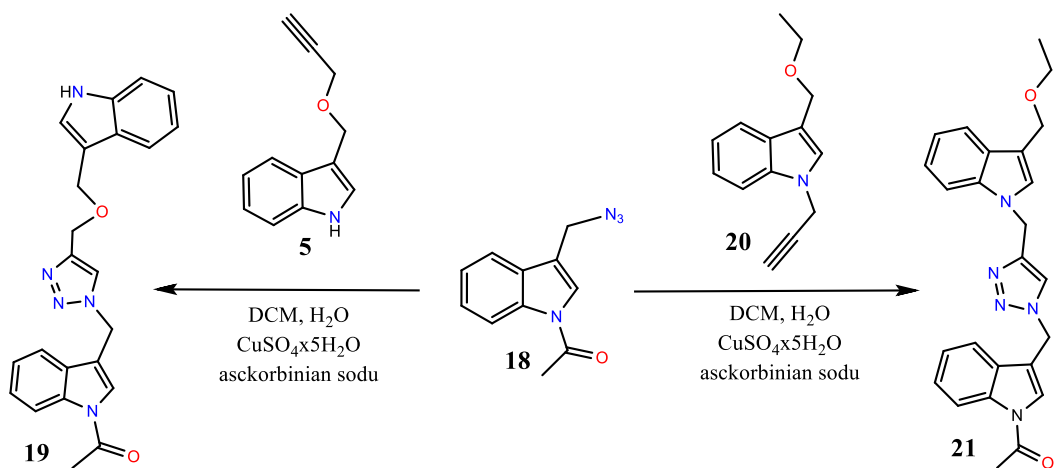
## I. Pierwsza grupa pochodnych



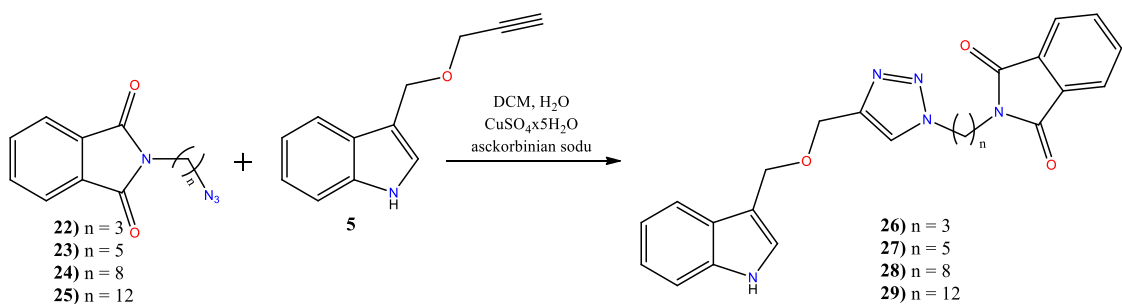
Schemat 1. Synteza dimerów triazolowo-indolowych



Schemat 2. Synteza triazolowych pochodnych indolu z pierścieniem benzenowym

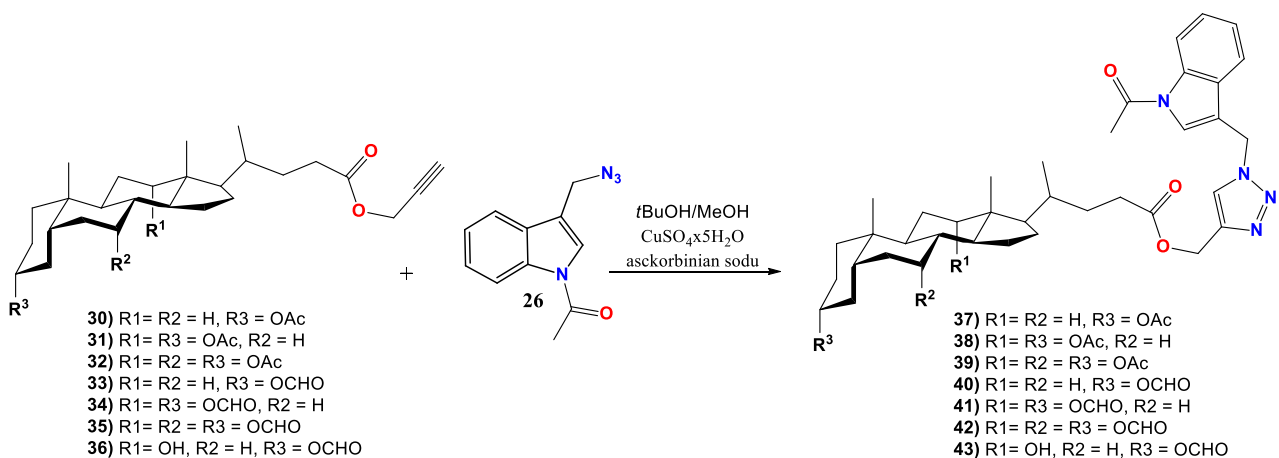


*Schemat 3. Synteza pochodnych 19 i 21*



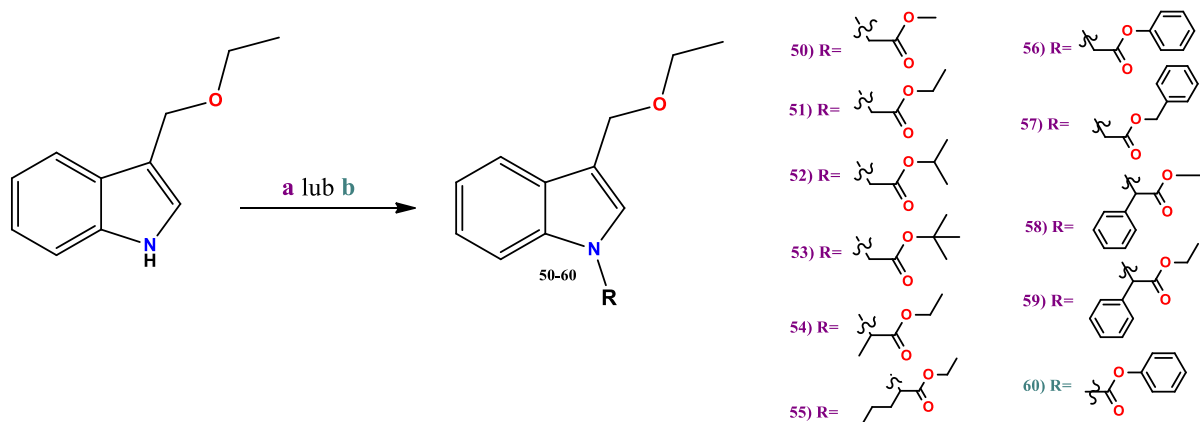
*Schemat 4. Synteza triazolowych pochodnych indolu i ftalimidu*

## II. Druga grupa pochodnych

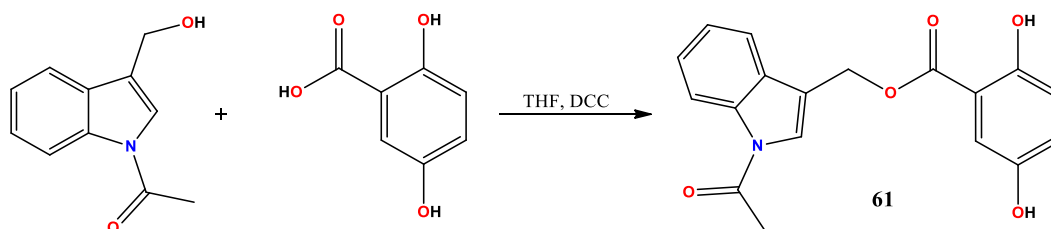


*Schemat 5. Synteza triazolowych pochodnych indolu i kwasów żółciowych*

### III. Trzecia grupa pochodnych



**Schemat 6. Synteza N-podstawionych pochodnych indolu (a: BrR, NaH, DMF; b: kwas benzoesowy, PPh<sub>3</sub>, NBS, CH<sub>2</sub>Cl<sub>2</sub>, Et<sub>3</sub>N)**



**Schemat 7. Synteza pochodnej 61**

## Literatura

- [1] Omar, F., Tareq, A. M., Alqahtani, A. M., Dhama, K., Sayeed, M. A., Emran, T. Bin, & Simal-gandara, J. (2021). Plant-Based Indole Alkaloids: A Comprehensive Overview from a Pharmacological Perspective. *Molecules*, 15;26(8):2297. <https://doi.org/10.3390/molecules26082297>
- [2] Sundberg, R. J. (2010). Electrophilic substitution reactions of indoles. *Heterocyclic Scaffolds II: Reactions and Applications of Indoles*, 47-115.
- [3] Bartoli, G., Bencivenni, G., & Dalpozzo, R. (2010). Organocatalytic strategies for the asymmetric functionalization of indoles. *Chemical Society Reviews*, 39(11), 4449–4465. <https://doi.org/10.1039/b923063g>
- [4] Trubitsõn, D., & Kanger, T. (2020). Enantioselective catalytic synthesis of N-alkylated indoles. *Symmetry*, 12(7). <https://doi.org/10.3390/sym12071184>
- [5] Gribble, G. W. (2003). Novel chemistry of indole in the synthesis of heterocycles. *Pure and Applied Chemistry*, 75(10), 1417–1432. <https://doi.org/10.1351/pac200375101417>
- [6] Ibrahim, M. A. (2010). Synthesis and chemistry of 4-amino-1,2,4-triazin-5-ones. *Heterocycles*, 81(6), 1393–1418. <https://doi.org/10.3987/REV-10-668>
- [7] Bandini, M. (2013). Electrophilicity: The “dark-side” of indole chemistry. *Organic and Biomolecular Chemistry*, 11(32), 5206–5212. <https://doi.org/10.1039/c3ob40735g>
- [8] Sundberg, R. (2012). The Chemistry of Indoles. *Organic Chemistry; A Series of Monographs*. Tom 18; Elsevier
- [9] Stockman, R. A. (2007). Heterocyclic chemistry. *Annual Reports on the Progress of Chemistry - Section B*, 103, 107–124. <https://doi.org/10.1039/b614418g>
- [10] Ahmad, T., Khan, S., & Ullah, N. (2022). Recent Advances in the Catalytic Asymmetric Friedel – Crafts Reactions of Indoles. *ACS Omega*, 7(40), 35446–35485. <https://doi.org/10.1021/acsomega.2c05022>
- [11] Berti, G. Da Settimo, A. Nannipieri, E. (1968). The reactions of some indole derivatives with benzoyl nitrate. Novel oxidative coupling reactions of 2-methylindoles. *Journal of the Chemical Society C: Organic*, 2145-215. <https://doi.org/10.1039/J396800021451>
- [12] Smith, G. F., & Taylor, D. A. (1973). The sulphonation of indole and some of its simple alkyl derivatives. *Tetrahedron*, 29(4), 669–672. [https://doi.org/10.1016/0040-4020\(73\)85012-4](https://doi.org/10.1016/0040-4020(73)85012-4)
- [13] Ottoni, O., De Neder, A. V. F., Dias, A. K. B., Cruz, R. P. A., & Aquino, L. B. (2001). Acylation of indole under friedel - Crafts conditions - An improved method to obtain 3-acylindoles regioselectively. *Organic Letters*, 3(7), 1005–1007. <https://doi.org/10.5555/ol007056i>

- [14] Semenov, B. B., & Yurovskaya, M. A. (2005). Methods for the synthesis of isogramines and their chemical properties. (Review). *Chemistry of Heterocyclic Compounds*, 41(4), 407–425. <https://doi.org/10.1007/s10593-005-0164-x>
- [15] Ling, L., Cao, J., Hu, J., & Zhang, H. (2017). Copper-catalyzed: N-alkylation of indoles by N-tosylhydrazones. *RSC Advances*, 7(45), 27974–27980. <https://doi.org/10.1039/c7ra03765a>
- [16] Lanke, V., & Ramaiah Prabhu, K. (2013). Regioselective synthesis of 4-substituted indoles via C-H activation: A ruthenium catalyzed novel directing group strategy. *Organic Letters*, 15(24), 6262–6265. <https://doi.org/10.1021/ol4031149>
- [17] Song, W. H., Shi, J., Chen, X., & Song, G. (2020). Silver-Catalyzed Remote C5-H Selenylation of Indoles. *Journal of Organic Chemistry*, 85(17), 11104–11115. <https://doi.org/10.1021/acs.joc.0c00921>
- [18] Wu, Q., Li, G. L., Yang, S., Shi, X. Q., Huang, T. Z., Du, X. H., & Chen, Y. (2019). A chemo- and regioselective C6-functionalization of 2,3-disubstituted indoles: Highly efficient synthesis of diarylindol-6-ylmethanes. *Organic and Biomolecular Chemistry*, 17(13), 3462–3470. <https://doi.org/10.1039/c9ob00283a>
- [19] Yang, Y., & Shi, Z. (2018). Regioselective direct arylation of indoles on the benzenoid moiety. *Chemical Communications*, 54(14), 1676–1685. <https://doi.org/10.1039/c7cc08752g>
- [20] Wen, J., & Shi, Z. (2021). From C4 to C7: Innovative Strategies for Site-Selective Functionalization of Indole C-H Bonds. *Accounts of Chemical Research*, 54(7), 1723–1736. <https://doi.org/10.1021/acs.accounts.0c00888>
- [21] Inman, M., & Moody, C. J. (2013). Indole synthesis-something old, something new. *Chemical Science*, 4(1), 29–41. <https://doi.org/10.1039/c2sc21185h>
- [22] Moudi M, Go R, Yien CYS, Nazre M. (2013). Vinca alkaloids. *International Journal of Preventive Medicine*, 4, 1231–1235.
- [23] Verma, K., Paliwal, S., Swapnil S. (2022). Therapeutic potential of reserpine in metabolic syndrome: An evidence based study. *Pharmacological Research*, 186, 106531. <https://doi.org/10.1016/j.phrs.2022.106531>.
- [24] Kerzarea, D. R., & Khedekar, P. B. (2016). Indole Derivatives acting on Central Nervous System – Review. *Journal of Pharmaceutical Science and Bioscientific Research*, 6(2271), 144–156.
- [25] Ziółkowska, N., Lewczuk, B., & Prusik, M. (2018). Diurnal and circadian variations in indole contents in the goose pineal gland. *Chronobiology International*, 35(11), 1560–1575. <https://doi.org/10.1080/07420528.2018.1496926>
- [26] Ligneul, Romain et al. (2023) Serotonin, *Current Biology*, 33(23), 1216–1221, <https://doi.org/10.1016/j.cub.2023.09.068>

- [27] Gonçalves, A. C., Nunes, A. R., Alves, G., & Silva, L. R. (2021). Serotonin and Melatonin: Plant Sources, Analytical Methods, and Human Health Benefits. *Revista Brasileira de Farmacognosia*, 31(2), 162–175. <https://doi.org/10.1007/s43450-021-00141-w>
- [28] Lewczuk, B., Ziółkowska, N., Prusik, M., & Przybylska-Gornowicz, B. (2014). Diurnal profiles of melatonin synthesis-related indoles, catecholamines and their metabolites in the duck pineal organ. *International Journal of Molecular Sciences*, 15(7), 12604–12630. <https://doi.org/10.3390/ijms150712604>
- [29] Sánchez, S., Sánchez, C. L., Paredes, S. D., Rodriguez, A. B., & Barriga, C. (2008). The effect of tryptophan administration on the circadian rhythms of melatonin in plasma and the pineal gland of rats. *Journal of Applied Biomedicine*, 6(4), 177–186. <https://doi.org/10.32725/jab.2008.021>
- [30] Fagundes, P., Sandri, G., Escalona, A., & Moura, S. (2020). Indole alkaloids: 2012 until now, highlighting the new chemical structures and biological activities. *Fitoterapia*, 143 104558. <https://doi.org/10.1016/j.fitote.2020.104558>
- [31] Saito, Y., Kotono, Y., Yasutomo, S., Kenichiro, I. (2020). Selective Transformation of Strychnine and 1,2-Disubstituted Benzenes by C–H Borylation. *Chem*, 6(4), 985 – 993. <https://doi.org/10.1016/j.chempr.2020.02.004>
- [32] Liu, F., Wang, X., Han, X., Tan, X., & Kang, W. (2015). Cytotoxicity and DNA interaction of brucine and strychnine-two alkaloids of semen strychni. *International Journal of Biological Macromolecules*, 77, 92–98. <https://doi.org/10.1016/j.ijbiomac.2015.03.017>
- [33] Chen, J., Qu, Y., Wang, D., Peng, P., Cai, H., Gao, Y., Chen, Z., & Cai, B. (2014). Pharmacological evaluation of total alkaloids from nux vomica: Effect of reducing strychnine contents. *Molecules*, 19(4), 4395–4408. <https://doi.org/10.3390/molecules19044395>
- [34] Hong, B., Grzech, D., Caputi, L. et al. (2022). Biosynthesis of strychnine. *Nature*, 607, 617–622. <https://doi.org/10.1038/s41586-022-04950-4>
- [35] Lu L, Huang R, Wu Y, Jin J-M, Chen H-Z, Zhang L-J and Luan X (2020) Brucine: A Review of Phytochemistry, Pharmacology, and Toxicology. *Frontiers in Pharmacology*, 11, 377. <https://doi.org/10.3389/fphar.2020.00377>
- [36] Leas, D., Schultz, D. C., & Huigens, R. (2023). Chemical Reactions of Indole Alkaloids That Enable Rapid Access to New Scaffolds for Discovery. *SynOpen*, 165–185. <https://doi.org/10.1055/a-2048-8412>
- [37] Zhang, Y., Yang, S. H., & Guo, X. L. (2017). New insights into Vinca alkaloids resistance mechanism and circumvention in lung cancer. *Biomedicine and Pharmacotherapy*, 96, 659–666. <https://doi.org/10.1016/j.biopha.2017.10.041>
- [38] Martino, E., Casamassima, G., Castiglione, S., Cellupica, E., Pantalone, S., Papagni, F., Rui, M., Siciliano, A. M., & Collina, S. (2018). Vinca alkaloids and analogues as

- anti-cancer agents: Looking back, peering ahead. *Bioorganic and Medicinal Chemistry Letters*, 28(17), 2816–2826. <https://doi.org/10.1016/j.bmcl.2018.06.044>
- [39] Jastrzębski, M. K., Kaczor, A. A., & Wróbel, T. M. (2022). Methods of Lysergic Acid Synthesis—The Key Ergot Alkaloid. *Molecules*, 27(21). <https://doi.org/10.3390/molecules27217322>
- [40] Sharma, N., Sharma, V., Manikyam, H., & Krishna, A. (2016). Ergot Alkaloids: A Review on Therapeutic Applications. *European Journal of Medicinal Plants*, 14(3), 1–17. <https://doi.org/10.9734/ejmp/2016/25975>
- [41] Chen, J. J., Han, M. Y., Gong, T., Yang, J. L., & Zhu, P. (2017). Recent progress in ergot alkaloid research. *RSC Advances*, 7(44), 27384–27396. <https://doi.org/10.1039/c7ra03152a>
- [42] Young, C. A., Schardl, C. L., Panaccione, D. G., Florea, S., Takach, J. E., Charlton, N. D., Moore, N., Webb, J. S., & Jaromczyk, J. (2015). Genetics, genomics and evolution of ergot alkaloid diversity. *Toxins*, 7(4), 1273–1302. <https://doi.org/10.3390/toxins7041273>
- [43] Fuentes, J. J., Fonseca, F., Elices, M., Farré, M., & Torrens, M. (2020). Therapeutic Use of LSD in Psychiatry: A Systematic Review of Randomized-Controlled Clinical Trials. *Frontiers in Psychiatry*, 10, 1–14. <https://doi.org/10.3389/fpsy.2019.00943>
- [44] Moloudizargari, M., Mikaili, P., Aghajanshakeri, S., Asghari, M., & Shayegh, J. (2013). Pharmacological and Therapeutic effects of Peganum harmala and its main alkaloids. *Pharmacognosy Reviews*, 7(14), 199–212. <https://doi.org/10.4103/0973-7847.120524>
- [45] Brito-da-costa, A. M., Dias-da-silva, D., Gomes, N. G. M., Dinis-oliveira, R. J., & Madureira-carvalho, Á. (2020). Toxicokinetics and toxicodynamics of ayahuasca alkaloids N,N-dimethyltryptamine (DMT), harmine, harmaline and tetrahydroharmine: Clinical and forensic impact. *Pharmaceuticals*, 13(11), 1–39. <https://doi.org/10.3390/ph13110334>
- [46] Zhang, L., Li, D. & Yu, S. (2020). Pharmacological effects of harmine and its derivatives: a review. *Archives of Pharmacol Research*. 43, 1259–1275. <https://doi.org/10.1007/s12272-020-01283-6>
- [47] Khan, F. A., Maalik, A., Iqbal, Z., & Malik, I. (2013). Recent pharmacological developments in  $\beta$ -carboline alkaloid “harmaline.” *European Journal of Pharmacology*, 721(1–3), 391–394. <https://doi.org/10.1016/j.ejphar.2013.05.003>
- [48] Singh, M., Kaur, R., Rajput, R., & Mathur, G. (2017). Evaluating the therapeutic efficiency and drug targeting ability of alkaloids present in Rauwolfia serpentina. *International Journal of Green Pharmacy*, 11(3), 132–142.



- [49] Jabir, N. R., Firoz, C. K., Zughaibi, T. A., Alsaadi, M. A., Abuzenadah, A. M., Al-Asmari, A. I., Alsaieedi, A., Ahmed, B. A., Ramu, A. K., & Tabrez, S. (2022). A literature perspective on the pharmacological applications of yohimbine. *Annals of Medicine*, 54(1), 2861–2875. <https://doi.org/10.1080/07853890.2022.2131330>
- [50] Chadha, N., & Silakari, O. (2017). Indoles as therapeutics of interest in medicinal chemistry: Bird's eye view. *European Journal of Medicinal Chemistry*, 134, 159–184. <https://doi.org/10.1016/j.ejmech.2017.04.003>
- [51] Villar-Martínez, M. D., Moreno-Ajona, D., Chan, C., & Goadsby, P. J. (2021). Indomethacin-responsive headaches—A narrative review. *Headache*, 61(5), 700–714. <https://doi.org/10.1111/head.14111>
- [52] Bhat, M. A., Mohamed, A. A. O., Mohammad, R., Ansari, M. A., Abuelizz, H. A., Bakheit, A. H., & Naglah, A. M. (2018). Indole derivatives as cyclooxygenase inhibitors: Synthesis, biological evaluation and docking studies. *Molecules*, 23(6). <https://doi.org/10.3390/molecules23061250>
- [53] Lucas, S. (2016). The Pharmacology of Indomethacin. *Headache*, 56(2), 436–446. <https://doi.org/10.1111/head.12769>
- [54] Kassab, S. E., Khedr, M. A., Ali, H. I., & Abdalla, M. M. (2017). Discovery of new indomethacin-based analogs with potentially selective cyclooxygenase-2 inhibition and observed diminishing to PGE2 activities. *European Journal of Medicinal Chemistry*, 141, 306–321. <https://doi.org/10.1016/j.ejmech.2017.09.056>
- [55] Xu, S., Jashim Uddin, M., Banerjee, S., Duggan, K., Musee, J., Kiefer, J. R., Ghebreselasie, K., Rouzer, C. A., & Marnett, L. J. (2019). Fluorescent indomethacin-dansyl conjugates utilize the membrane-binding domain of cyclooxygenase-2 to block the opening to the active site. *Journal of Biological Chemistry*, 294(22), 8690–8698. <https://doi.org/10.1074/jbc.RA119.007405>
- [56] Abdellatif, K. R. A., Abdelall, E. K. A., Elshemy, H. A. H., El-Nahass, E. S., Abdel-Fattah, M. M., & Abdelgawad, Y. Y. M. (2021). New indomethacin analogs as selective COX-2 inhibitors: Synthesis, COX-1/2 inhibitory activity, anti-inflammatory, ulcerogenicity, histopathological, and docking studies. *Archiv Der Pharmazie*, 354(4), 1–13. <https://doi.org/10.1002/ardp.202000328>
- [57] Kalgutkar, A. S., Crews, B. C., Saleh, S., Prudhomme, D., & Marnett, L. J. (2005). Indolyl esters and amides related to indomethacin are selective COX-2 inhibitors. *Bioorganic and Medicinal Chemistry*, 13(24), 6810–6822. <https://doi.org/10.1016/j.bmc.2005.07.073>
- [58] Khanna, S., Madan, M., Vangoori, A., Banerjee, R., Thaimattam, R., Jafar Sadik Basha, S. K., Ramesh, M., Casturi, S. R., & Pal, M. (2006). Evaluation of glycolamide esters of indomethacin as potential cyclooxygenase-2 (COX-2) inhibitors. *Bioorganic and Medicinal Chemistry*, 14(14), 4820–4833. <https://doi.org/10.1016/j.bmc.2006.03.023>

- [59] Simon, L.S. (1996). Actions and toxicity of nonsteroidal anti-inflammatory drugs. *Current Opinion in Rheumatology*, 8, 169-175.
- [60] Chávez-Piña, A. E., McKnight, W., Dickey, M., Castañeda-Hernández, G., & Wallace, J. L. (2007). Mechanisms underlying the anti-inflammatory activity and gastric safety of acemetacin. *British Journal of Pharmacology*, 152(6), 930–938. <https://doi.org/10.1038/sj.bjp.0707451>
- [61] Abdulhamza, H. M., & Farhan, M. S. (2021). Synthesis, characterization and preliminary anti-inflammatory evaluation of new fenoprofen hydrazone derivatives. *Iraqi Journal of Pharmaceutical Sciences*, 29(2), 239–244. <https://doi.org/10.31351/vol29iss2pp239-244>
- [62] Shirinzadeh, H., Neuhaus, E., Ince Erguc, E., Tascioglu Aliyev, A., Gurer-Orhan, H., & Suzen, S. (2020). New indole-7-aldehyde derivatives as melatonin analogues; synthesis and screening their antioxidant and anticancer potential. *Bioorganic Chemistry*, 104, 104219. <https://doi.org/10.1016/j.bioorg.2020.104219>
- [63] Debela, D. T., Muzazu, S. G. Y., Heraro, K. D., Ndalama, M. T., Mesele, B. W., Haile, D. C., Kitui, S. K., & Manyazewal, T. (2021). New approaches and procedures for cancer treatment: Current perspectives. *SAGE Open Medicine*, 9. <https://doi.org/10.1177/20503121211034366>
- [64] Siegel, R. L., Miller, K. D., Wagle, N. S., & Jemal, A. (2023). Cancer statistics, 2023. *CA: A Cancer Journal for Clinicians*, 73(1), 17–48. <https://doi.org/10.3322/caac.21763>
- [65] Dhiman, A., Sharma, R., & Singh, R. K. (2022). Target-based anticancer indole derivatives and insight into structure–activity relationship: A mechanistic review update (2018–2021). *Acta Pharmaceutica Sinica B*, 12(7), 3006–3027. <https://doi.org/10.1016/j.apsb.2022.03.021>
- [66] Faivre, S., Demetri, G., Sargent, W., & Raymond, E. (2007). Molecular basis for sunitinib efficacy and future clinical development. *Nature Reviews Drug Discovery*, 6(9), 734–745. <https://doi.org/10.1038/nrd2380>
- [67] Moran, M., Nickens, D., Adcock, K., Bennetts, M., Desscan, A., Charnley, N., & Fife, K. (2019). Sunitinib for Metastatic Renal Cell Carcinoma: A Systematic Review and Meta-Analysis of Real-World and Clinical Trials Data. *Targeted Oncology*, 14(4), 405–416. <https://doi.org/10.1007/s11523-019-00653-5>
- [68] Berdeja, J. G., Laubach, J. P., Richter, J., Stricker, S., Spencer, A., Richardson, P. G., & Chari, A. (2021). Panobinostat From Bench to Bedside: Rethinking the Treatment Paradigm for Multiple Myeloma. *Clinical Lymphoma, Myeloma and Leukemia*, 21(11), 752–765. <https://doi.org/10.1016/j.clml.2021.06.020>
- [69] Russo, E., Grondona, C., Brullo, C., Spallarossa, A., Villa, C., & Tasso, B. (2023). Indole Antitumor Agents in Nanotechnology Formulations: An Overview. *Pharmaceutics*, 15(7). <https://doi.org/10.3390/pharmaceutics15071815>

- [70] Sever, B., Altıntop, M. D., Özdemir, A., Çiftçi, G. A., Ellakwa, D. E., Tateishi, H., Radwan, M. O., Ibrahim, M. A. A., Otsuka, M., Fujita, M., Ciftci, H. I., & Ali, T. F. S. (2020). In Vitro and In Silico Evaluation of Anticancer Activity of New Indole-Based 1,3,4-Oxadiazoles as EGFR and COX-2 Inhibitors. *Molecules*, 25(21). <https://doi.org/10.3390/molecules25215190>
- [71] Perike, N., Edigi, P. K., Nirmala, G., Thumma, V., Bujji, S., & Naikal, P. S. (2022). Synthesis, Anticancer Activity and Molecular Docking Studies of Hybrid Molecules Containing Indole-Thiazolidinedione-Triazole Moieties. *ChemistrySelect*, 7(47). <https://doi.org/10.1002/slct.202203778>
- [72] de Vries, T., Villalón, C. M., & MaassenVanDenBrink, A. (2020). Pharmacological treatment of migraine: CGRP and 5-HT beyond the triptans. *Pharmacology and Therapeutics*, 211, 107528. <https://doi.org/10.1016/j.pharmthera.2020.107528>
- [73] Steiner, T.J., Stovner, L.J. (2023). Global epidemiology of migraine and its implications for public health and health policy. *Nature Reviews Neurology*, 19, 109–117. <https://doi.org/10.1038/s41582-022-00763-1>
- [74] Grangeon, L., Lange, K. S., Waliszewska-Prosół, M., Onan, D., Marschollek, K., Wiels, W., Mikulenska, P., Farham, F., Gollion, C., & Ducros, A. (2023). Genetics of migraine: where are we now? *Journal of Headache and Pain*, 24(1), 1–23. <https://doi.org/10.1186/s10194-023-01547-8>
- [75] Giniatullin, R. (2022). 5-hydroxytryptamine in migraine: The puzzling role of ionotropic 5-HT<sub>3</sub> receptor in the context of established therapeutic effect of metabotropic 5-HT<sub>1</sub> subtypes. *British Journal of Pharmacology*, 179(3), 400–415. <https://doi.org/10.1111/bph.15710>
- [76] González-Hernández, A., Marichal-Cancino, B. A., Lozano-Cuenca, J., Maassen Van Den Brink A., Villalón, C.M. (2019) Functional Characterization of the Prejunctional Receptors Mediating the Inhibition by Ergotamine of the Rat Perivascular Sensory Peptidergic Drive. *ACS Chemical Neuroscience*, 10(7), 3173-3182. <https://doi.org/10.1021/acscemneuro.8b00611>.
- [77] Villalón, C.M., Van Den Brink, A. M. (2017). The Role of 5-Hydroxytryptamine in the Pathophysiology of Migraine and its Relevance to the Design of Novel Treatments. *Mini-Reviews in Medicinal Chemistry*, 17(11), 928-938. <https://doi.org/10.2174/1389557516666160728121050>.
- [78] Ramachandran, R., Schramm, S., & Schaefer, B. (2023). Migraine drugs. *ChemTexts* 9(2). <https://doi.org/10.1007/s40828-023-00178-5>
- [79] Cameron, C., Kelly, S., Hsieh, S. C., Murphy, M., Chen, L., Kotb, A., Peterson, J., Coyle, D., Skidmore, B., Gomes, T., Clifford, T., & Wells, G. (2015). Triptans in the Acute Treatment of Migraine: A Systematic Review and Network Meta-Analysis. *Headache*, 55(S4), 221–235. <https://doi.org/10.1111/head.12601>

- [80] Derry, C. J., Derry, S., & Moore, R. A. (2012). Sumatriptan (oral route of administration) for acute migraine attacks in adults. *Cochrane Database of Systematic Reviews*, 2, 1465-1858. <https://doi.org/10.1002/14651858.CD008615.pub2>
- [81] Tepper, S. J., & Rapoport, A. M. (1999). The triptans: A summary. *CNS Drugs*, 12(5), 403–417. <https://doi.org/10.2165/00023210-199912050-00007>
- [82] Al-Wabli, R. I., Alsulami, M. A., Bukhari, S. I., Moubayed, N. M. S., Al-Mutairi, M. S., & Attia, M. I. (2021). Design, synthesis, and antimicrobial activity of certain new indole-1,2,4 triazole conjugates. *Molecules*, 26(8), 1–13. <https://doi.org/10.3390/molecules26082292>
- [83] Tiwari, S., Kirar, S., Banerjee, U. C., Neerupudi, K. B., Singh, S., Wani, A. A., Bharatam, P. V., & Singh, I. P. (2020). Synthesis of N-substituted indole derivatives as potential antimicrobial and antileishmanial agents. *Bioorganic Chemistry*, 99, 103787. <https://doi.org/10.1016/j.bioorg.2020.103787>
- [84] Jain, P., Utreja, D., & Sharma, P. (2020). An efficacious synthesis of N-1-, C-3-substituted indole derivatives and their antimicrobial studies. *Journal of Heterocyclic Chemistry*, 57(1), 428–435. <https://doi.org/10.1002/jhet.3799>
- [85] Pawar, K., Yadav, A., Prasher, P., Mishra, S., Singh, B., Singh, P., & Komath, S. S. (2015). Identification of an indole-triazole-amino acid conjugate as a highly effective antifungal agent. *MedChemComm*, 6(7), 1352–1359. <https://doi.org/10.1039/c5md00156k>
- [86] Pagniez, F., Lebouvier, N., Na, Y. M., Ourliac-Garnier, I., Picot, C., Le Borgne, M., & Le Pape, P. (2020). Biological exploration of a novel 1,2,4-triazole-indole hybrid molecule as antifungal agent. *Journal of Enzyme Inhibition and Medicinal Chemistry*, 35(1), 398–403. <https://doi.org/10.1080/14756366.2019.1705292>
- [87] Adamson, C. S., Chibale, K., Goss, R. J. M., Jaspars, M., Newman, D. J., & Dorrington, R. A. (2021). Antiviral drug discovery: Preparing for the next pandemic. *Chemical Society Reviews*, 50(6), 3647–3655. <https://doi.org/10.1039/d0cs01118e>
- [88] Waheed, Y., Sah, R., & Muhammad, K. (2023). Recent Developments in Vaccines for Viral Diseases. *Vaccines*, 11(2), 18–21. <https://doi.org/10.3390/vaccines11020198>
- [89] Zhang, M. Z., Chen, Q., & Yang, G. F. (2015). A review on recent developments of indole-containing antiviral agents. *European Journal of Medicinal Chemistry*, 89, 421–441. <https://doi.org/10.1016/j.ejmech.2014.10.065>
- [90] Leneva, I., Kartashova, N., Poromov, A., Gracheva, A., Korchevaya, E., Glubokova, E., Borisova, O., Shtro, A., Loginova, S., Shchukina, V., Khamitov, R., & Faizuloev, E. (2021). Antiviral activity of umifenovir in vitro against a broad spectrum of coronaviruses, including the novel sars-cov-2 virus. *Viruses*, 13(8). <https://doi.org/10.3390/v13081665>

- [91] Shumyantseva, V. V., Bulko, T. V., Agafonova, L. E., Pronina, V. V., & Kostryukova, L. V. (2023). Comparative Analysis of the Interaction between the Antiviral Drug Umifenovir and Umifenovir Encapsulated in Phospholipids Micelles (Nanosome/Umifenovir) with dsDNA as a Model for Pharmacogenomic Analysis by Electrochemical Methods. *Processes*, 11(3). <https://doi.org/10.3390/pr11030922>
- [92] Yi, W., Jia, C., Yang, Z., Fan, H., Li, M., & Lv, Z. (2023). Effect of umifenovir (arbidol) versus standard care on clinical outcome in patients with COVID-19: a retrospective cohort study. *Therapeutic Advances in Respiratory Disease*, 17, 1–8. <https://doi.org/10.1177/17534666231183811>
- [93] Li, G., Wang, Y., & De Clercq, E. (2022). Approved HIV reverse transcriptase inhibitors in the past decade. *Acta Pharmaceutica Sinica B*, 12(4), 1567–1590. <https://doi.org/10.1016/j.apsb.2021.11.009>
- [94] Szulta, S., Balewski, Ł., Literska, L., & Kornicka, A. (2021). Indole derivatives with therapeutic properties. *Farmacja Polska*, 77(6), 382–394. <https://doi.org/10.32383/farmpol/141381>
- [95] Ji, K.; Zhang, G.N.; Zhao, J.Y.; Zhu, M.; Wang, M.H.; Wang, J.X.; Cen, S.; Wang, Y.C.; Li, W.Y. (2022). Design, synthesis, and anti-influenza A virus activity evaluation of novel indole containing derivatives of triazole. *Bioorganic & Medicinal Chemistry Letters*, 64, 128681. <https://doi.org/10.1016/j.bmcl.2022.128681>.
- [96] Hattori, S., Higashi-Kuwata, N., Hayashi, H., Allu, S. R., Raghavaiah, J., Bulut, H., Das, D., Anson, B. J., Lendy, E. K., Takamatsu, Y., Takamune, N., Kishimoto, N., Murayama, K., Hasegawa, K., Li, M., Davis, D. A., Kodama, E. N., Yarchoan, R., Wlodawer, A., Mitsuya, H. (2021). A small molecule compound with an indole moiety inhibits the main protease of SARS-CoV-2 and blocks virus replication. *Nature Communications*, 12(1), 1–12. <https://doi.org/10.1038/s41467-021-20900-6>
- [97] Süzen, S. (2007). Antioxidant Activities of Synthetic Indole Derivatives and Possible Activity Mechanisms. *Bioactive Heterocycles*, 5, 145–178. [https://doi.org/10.1007/7081\\_2007\\_074](https://doi.org/10.1007/7081_2007_074)
- [98] Azouzi, S., Santuz, H., Morandat, S., Pereira, C., Côté, F., Hermine, O., El Kirat, K., Colin, Y., Le Van Kim, C., Etchebest, C., & Amireault, P. (2017). Antioxidant and Membrane Binding Properties of Serotonin Protect Lipids from Oxidation. *Biophysical Journal*, 112(9), 1863–1873. <https://doi.org/10.1016/j.bpj.2017.03.037>
- [99] Zhang, H. M., Zhang, Y. (2014) Melatonin: a well-documented antioxidant with conditional pro-oxidant actions. *Journal of Pineal Research*, 57(2), 131–46. <https://doi.org/10.1111/jpi.12162>.
- [100] Chrustek, A., & Olszewska-Słonina, D. (2021). Melatonin as a powerful antioxidant. *Acta Pharmaceutica*, 71(3), 335–354. <https://doi.org/10.2478/acph-2021-0027>
- [101] Bantounou, M., Plascevic, J., & Galley, H. F. (2022). Melatonin and Related Compounds: Antioxidant and Inflammatory Actions. *Antioxidants*, 11(3). <https://doi.org/10.3390/antiox11030532>

- [102] Tan, D. X., Manchester, L. C., Esteban-Zubero, E., Zhou, Z., & Reiter, R. J. (2015). Melatonin as a potent and inducible endogenous antioxidant: Synthesis and metabolism. *Molecules*, 20(10), 18886–18906. <https://doi.org/10.3390/molecules201018886>
- [103] Kim, C. S., Jung, S., Hwang, G. S., & Shin, D. M. (2023). Gut microbiota indole-3-propionic acid mediates neuroprotective effect of probiotic consumption in healthy elderly: A randomized, double-blind, placebo-controlled, multicenter trial and in vitro study. *Clinical Nutrition*, 42(6), 1025–1033. <https://doi.org/10.1016/j.clnu.2023.04.001>
- [104] Rynkowska, A., Stepniak, J., & Karbownik-Lewińska, M. (2021). Melatonin and indole-3-propionic acid reduce oxidative damage to membrane lipids induced by high iron concentrations in porcine skin. *Membranes*, 11(8), 3–10. <https://doi.org/10.3390/membranes11080571>
- [105] Konopelski, P., & Mogilnicka, I. (2022). Biological Effects of Indole-3-Propionic Acid, a Gut Microbiota-Derived Metabolite, and Its Precursor Tryptophan in Mammals' Health and Disease. *International Journal of Molecular Sciences*, 23(3). <https://doi.org/10.3390/ijms23031222>
- [106] Iwan, P.; Stepniak, J.; Karbownik-Lewinska, M. (2021). Cumulative Protective Effect of Melatonin and Indole-3-Propionic Acid against KIO<sub>3</sub>—Induced Lipid Peroxidation in Porcine Thyroid. *Toxics*, 9, 89. <https://doi.org/10.3390/toxics9050089>
- [107] Anastassova, N., Stefanova, D., Hristova-Avakumova, N., Georgieva, I., Kondeva-Burdina, M., Rangelov, M., Todorova, N., Tzoneva, R., & Yancheva, D. (2023). New Indole-3-Propionic Acid and 5-Methoxy-Indole Carboxylic Acid Derived Hydrazone Hybrids as Multifunctional Neuroprotectors. *Antioxidants*, 12(4), 977. <https://doi.org/10.3390/antiox12040977>
- [108] Zhou, L. C., Liang, Y. F., Huang, Y., Yang, G. X., Zheng, L. L., Sun, J. M., Li, Y., Zhu, F. L., Qian, H. W., Wang, R., & Ma, L. (2021). Design, synthesis, and biological evaluation of diosgenin-indole derivatives as dual-functional agents for the treatment of Alzheimer's disease. *European Journal of Medicinal Chemistry*, 219, 113426. <https://doi.org/10.1016/j.ejmech.2021.113426>
- [109] Aneja, B., Arif, R., Perwez, A., Napoleon, J. V., Hasan, P., Rizvi, M. M. A., Azam, A., Rahisuddin, & Abid, M. (2018). N-Substituted 1,2,3-Triazolyl-Appended Indole-Chalcone Hybrids as Potential DNA Intercalators Endowed with Antioxidant and Anticancer Properties. *ChemistrySelect*, 3(9), 2638–2645. <https://doi.org/10.1002/slct.201702913>
- [110] Iacopetta, D., Catalano, A., Ceramella, J., Barbarossa, A., Carocci, A., Fazio, A., La Torre, C., Caruso, A., Ponassi, M., Rosano, C., Franchini, C., & Sinicropi, M. S. (2020). Synthesis, anticancer and antioxidant properties of new indole and pyranoindole derivatives. *Bioorganic Chemistry*, 10, 104440. <https://doi.org/10.1016/j.bioorg.2020.104440>

- [111] Kumari, A., Singh, R. K. (2022). Synthesis, Molecular Docking and Biological Evaluation of N-Substituted Indole Derivatives as Potential Anti-Inflammatory and Antioxidant Agents. *Chemistry & Biodiversity*, 19(9), e202200290. <https://doi.org/10.1002/cbdv.202200290>
- [112] Jagadeesan, S., & Karpagam, S. (2023). Novel series of N-acyl substituted indole based piperazine, thiazole and tetrazoles as potential antibacterial, antifungal, antioxidant and cytotoxic agents, and their docking investigation as potential Mcl-1 inhibitors. *Journal of Molecular Structure*, 1271, 134013. <https://doi.org/10.1016/j.molstruc.2022.134013>
- [113] Singh, A. A., Patil, M. P., Kang, M. J., Niyonizigiye, I., & Kim, G. Do. (2021). Biomedical application of Indole-3-carbinol: A mini-review. *Phytochemistry Letters*, 41, 49–54. <https://doi.org/10.1016/j.phytol.2020.09.024>
- [114] Centofanti, F., Alonzi, T., Latini, A., Spitalieri, P., Murdocca, M., Chen, X., Cui, W., Shang, Q., Goletti, D., Shi, Y., Duranti, A., Tomino, C., Biancolella, M., Sangiuolo, F., Capobianchi, M. R., Jain, S., Novelli, G., & Pandolfi, P. P. (2022). Indole-3-carbinol in vitro antiviral activity against SARS-Cov-2 virus and in vivo toxicity. *Cell Death Discovery*, 8(1). <https://doi.org/10.1038/s41420-022-01280-2>
- [115] Amarakoon, D., Lee, W., Tamia, G., & Lee, S. (2023). Indole-3-Carbinol: Occurrence, Health-Beneficial Properties, and Cellular / Molecular Mechanisms. *Annual Review of Food Science and Technology*, 14, 347–366. <https://doi.org/10.1146/annurev-food-060721-025531>
- [116] Du, H., Zhang, X., Zeng, Y., Huang, X., Chen, H., Wang, S., Wu, J., Li, Q., Zhu, W., Li, H., Liu, T., Yu, Q., Wu, Y., & Jie, L. (2019). A Novel Phytochemical, DIM, Inhibits Proliferation, Migration, Invasion and TNF- $\alpha$  Induced Inflammatory Cytokine Production of Synovial Fibroblasts From Rheumatoid Arthritis Patients by Targeting MAPK and AKT/mTOR Signal Pathway. *Frontiers in Immunology*, 10, 1–13. <https://doi.org/10.3389/fimmu.2019.01620>
- [117] Weng, J. R., Tsai, C. H., Kulp, S. K., Chen, C. S. (2008). Indole-3-carbinol as a chemopreventive and anti-cancer agent. *Cancer Letters*, 18, 262(2), 153-163. <https://doi.org/10.1016/j.canlet.2008.01.033>. Epub 2008 Mar 7.
- [118] Vo, Q. V., & Mechler, A. (2020). In Silico Study of the Radical Scavenging Activities of Natural Indole-3-Carbinols. *Journal of Chemical Information and Modeling*, 60(1), 316–321. <https://doi.org/10.1021/acs.jcim.9b00917>
- [119] Vo, Q. V., Van Bay, M., Nam, P. C., & Mechler, A. (2019). Hydroxyl Radical Scavenging of Indole-3-Carbinol: A Mechanistic and Kinetic Study. *ACS Omega*, 4(21), 19375–19381. <https://doi.org/10.1021/acsomega.9b02782>
- [120] Frolidi, G., Silvestrin, B., Dorigo, P., & Caparrotta, L. (2004). Gramine: A vasorelaxing alkaloid acting on 5-HT<sub>2A</sub> receptors. *Planta Medica*, 70(4), 373–375. <https://doi.org/10.1055/s-2004-818953>

- [121] Pathak, M. P., Policegoudra, R. S., Goyary, D., Das, A., Mandal, S., Chakraborti, S., Bora, N. S., Islam, J., Patowary, P., Raju, P. S., & Chattopadhyay, P. (2018). Safety evaluation of an oat grain alkaloid gramine by genotoxicity assays. *Drug and Chemical Toxicology*, 41(2), 147–154. <https://doi.org/10.1080/01480545.2017.1322605>
- [122] Semenov, B. B., & Granik, V. G. (2004). Chemistry of N-(1H-indol-3-ylmethyl)-N,N-dimethylamine (gramine): A review. *Pharmaceutical Chemistry Journal*, 38(6), 287–310. <https://doi.org/10.1023/B:PHAC.0000048140.06266.63>
- [123] Jones, D. T., Artman, G. D., & Williams, R. M. (2007). Coupling of activated esters to gramines in the presence of ethyl propiolate under mild conditions. *Tetrahedron Letters*, 48(7), 1291–1294. <https://doi.org/10.1016/j.tetlet.2006.12.016>
- [124] Kalepu, J., Gandeepan, P., Ackermann, L., & Pilarski, L. T. (2018). C4-H indole functionalisation: Precedent and prospects. *Chemical Science*, 9(18), 4203–4216. <https://doi.org/10.1039/c7sc05336c>
- [125] Chauder, B., Larkin, A., & Snieckus, V. (2002). Rapid route to 3,4-substituted indoles via a directed ortho metalation-retro-Mannich sequence. *Organic Letters*, 4(5), 815–817. <https://doi.org/10.1021/ol017310m>
- [126] Masui, H., Kanda, S., & Fuse, S. (2023). Verification of preparations of (1H-indol-3-yl) methyl electrophiles and development of their microflow rapid generation and substitution. *Communications Chemistry*, 6(1), 1–10. <https://doi.org/10.1038/s42004-023-00837-1>
- [127] Jasiewicz, B., Kozanecka-Okupnik, W., Przygodzki, M., Warzajtis, B., Rychlewska, U., Pospieszny, T., & Mrówczyńska, L. (2021). Synthesis, antioxidant and cytoprotective activity evaluation of C-3 substituted indole derivatives. *Scientific Reports*, 11(1), 1–14. <https://doi.org/10.1038/s41598-021-94904-z>
- [128] Shengmei Guo, Zhebin Zhang, Jianxin Xu, Sen Li, Prof. Zhengjiang Fu, Prof. Hu Cai. (2019). Acid and 1, 2-Dichloroethane Co-Promoted Substitution of the Amino Groups in Gramine and its Analogues with Trialkyl Phosphites. *Chemistry Select*, 4(48), 14111–14113
- [129] Schramm, Charles H. (1951). Gramine Methiodide. *Journal of the American Chemical Society*, 73(6), 2961–2962
- [130] Snyder, H. R.; Eliel, E. L.; Charnahan, R. E. (1951). Alkylation of Grignard Reagents by Quaternary Ammonium Salts. A Novel Synthesis of 1,3-Dialkylindoles. *Journal of the American Chemical Society*, 73(3), 970–973. <https://doi.org/10.1021/ja01147a024>
- [131] Zhang, J., Jia, Q., Li, N., Gu, L., Dan, W., & Dai, J. (2023). Recent Developments of Gramine: Chemistry and Biological Activity. *Molecules*, 28(15). <https://doi.org/10.3390/molecules28155695>
- [132] Parcheta, M., Świsłocka, R., Orzechowska, S., Akimowicz, M., Choińska, R., & Lewandowski, W. (2021). Recent developments in effective antioxidants: The



- structure and antioxidant properties. *Materials*, 14(8), 1–24. <https://doi.org/10.3390/ma14081984>
- [133] Yin, X. J., Huang, X. Y., Ma, Y. B., Geng, C. A., Li, T. Z., Chen, X. L., Yang, T. H., Zhou, J., Zhang, X. M., & Chen, J. J. (2017). Bioactivity-guided synthesis of gramine derivatives as new MT1 and 5-HT1A receptors agonists. *Journal of Asian Natural Products Research*, 19(6), 610–622. <https://doi.org/10.1080/10286020.2017.1323885>
- [134] Xu, L., Su, Y., Yang, X., Bai, X., Wang, Y., Zhuo, C., & Meng, Z. (2023). Phytomedicine Gramine protects against pressure overload-induced pathological cardiac hypertrophy through Runx1-TGFBR1 signaling. *Phytomedicine*, 114, 154779. <https://doi.org/10.1016/j.phymed.2023.154779>
- [135] Zhang, X. H., Guo, Q., Wang, H. Y., Li, Y. H., Khamis, M. Y., Ma, L. Y., Wang, B., & Liu, H. M. (2021). Gramine-based structure optimization to enhance anti-gastric cancer activity. *Bioorganic Chemistry*, 107, 104549. <https://doi.org/10.1016/j.bioorg.2020.104549>
- [136] Ramu, A., Kathiresan, S., Ramadoss, H., Nallu, A., Kaliyan, R., & Azamuthu, T. (2018). Gramine attenuates EGFR-mediated inflammation and cell proliferation in oral carcinogenesis via regulation of NF-κB and STAT3 signaling. *Biomedicine and Pharmacotherapy*, 98, 523–530. <https://doi.org/10.1016/j.biopha.2017.12.049>
- [137] Wei, Y., Shi, L., Wang, K., Liu, M., Yang, Q., Yang, Z., & Ke, S. (2014). Discovery of gramine derivatives that inhibit the early stage of EV71 replication in vitro. *Molecules*, 19(7), 8949–8964. <https://doi.org/10.3390/molecules19078949>
- [138] Lu A, Wang T, Hui H, Wei X, Cui W, Zhou C, Li H, Wang Z, Guo J, Ma D, Wang Q. (2019). Natural Products for Drug Discovery: Discovery of Gramines as Novel Agents against a Plant Virus. *Journal of Agricultural and Food Chemistry*, 67(8) 2148–2156 <https://doi.org/10.1021/acs.jafc.8b06859>
- [139] Yang, C.; Yu, Y.; Sun, W.; Xia, C. (2014) Indole derivatives inhibited the formation of bacterial biofilm and modulated Ca<sup>2+</sup> efflux in diatom. *Marine Pollution Bulletin*, 88, 62–69. <https://doi.org/10.1016/j.marpolbul.2014.09.027>
- [140] Fu, R.; Lu, L.; Li, Z.; Yu, Q.; Zhang, X. (2014). Antibacterial effects of 31 kinds of traditional chinese medicine monomers on MRSA in vitro. *Chinese Pharmaceutical Journal*, 23, 20–21. <https://doi.org/10.3389%2Ffmicb.2015.00479>
- [141] Maver, M.; Escudero-Martinez, C.; Abbott, J.; Morris, J.; Hedley, P.E.; Mimmo, T.; Bulgarelli, D. (2021). Applications of the indole-alkaloid gramine modulate the assembly of individual members of the barley rhizosphere microbiota. *PeerJ*, 9, e12498. <https://doi.org/10.7717/peerj.12498>
- [142] Schütz, V.; Frindte, K.; Cui, J.; Zhang, P.; Hacquard, S.; Schulze-Lefert, P.; Knief, C.; Schulz, M.; Dörmann, P. (2021). Differential impact of plant secondary metabolites on the soil microbiota. *Frontiers in Microbiology*, 12, 666010. <https://doi.org/10.3389/fmicb.2021.666010>

- [143] Xia, X., Huan, Q., Huang, Y., Liu, Z., Liu, Y., Li, R., Wang, M., Wang, Z. (2024). Gramine sensitizes *Klebsiella pneumoniae* to tigecycline killing, *Phytomedicine*, 126, 155421, <https://doi.org/10.1016/j.phymed.2024.155421>.
- [144] Matsuo, H.; Taniguchi, K.; Hiramoto, T.; Yamada, T.; Ichinose, Y.; Toyoda, K.; Takeda, K.; Shiraishi, T. (2001). Gramine increase associated with rapid and transient systemic resistance in barley seedlings induced by mechanical and biological stresses. *Plant and Cell Physiology*, 42, 1103–1111. <https://doi.org/10.1093/pcp/pce139>
- [145] Schreiber, K.J.; Nasmith, C.G.; Allard, G.; Singh, J.; Subramaniam, R.; Desveaux, D. (2011). Found in translation: High-throughput chemical screening in *Arabidopsis thaliana* identifies small molecules that reduce fusarium head blight disease in wheat. *Molecular Plant-Microbe Interactions*, 24, 640–648. <https://doi.org/10.1094/mpmi-09-10-0210>
- [146] Wollein, U.; Bracher, F. (2011). The gramine route to pyrido[4,3-b]indol-3-ones-identification of a new cytotoxic lead. *Scientia Pharmaceutica*, 79, 59–68. <https://doi.org/10.3797/scipharm.1011-11>
- [147] Yang, J.; Kong, X.-D.; Zhu-Salzman, K.; Qin, Q.-M.; Cai, Q.N. (2021). The key glutathione S-transferase family genes involved in the detoxification of rice gramine in brown planthopper *Nilaparvata lugens*. *Insects*, 12, 1055. <https://doi.org/10.3390/insects12121055>
- [148] Cai, Q. N., Han, Y., Cao, Y. Z., Hu, Y., Zhao, X., & Bi, J. L. (2009). Detoxification of gramine by the cereal aphid sitobion avenae. *Journal of Chemical Ecology*, 35(3), 320–325. <https://doi.org/10.1007/s10886-009-9603-y>
- [149] Iwata, S., Saito, S. Y., Kon-ya, K., Shizuri, Y., & Ohizumi, Y. (2001). Novel marine-derived halogen-containing gramine analogues induce vasorelaxation in isolated rat aorta. *European Journal of Pharmacology*, 432(1), 63–70. [https://doi.org/10.1016/S0014-2999\(01\)01476-5](https://doi.org/10.1016/S0014-2999(01)01476-5)
- [150] Feng, K., Li, X., & Yu, L. (2018). Synthesis, antibacterial activity, and application in the antifouling marine coatings of novel acylamino compounds containing gramine groups. *Progress in Organic Coatings*, 118, 141–147. <https://doi.org/10.1016/j.porgcoat.2017.10.027>
- [151] Kolb, H. C., Finn, M. G., & Sharpless, K. B. (2001). Click Chemistry: Diverse Chemical Function from a Few Good Reactions. *Angewandte Chemie - International Edition*, 40(11), 2004–2021. [https://doi.org/10.1002/1521-3773\(20010601\)40:11<2004::AID-ANIE2004>3.0.CO;2-5](https://doi.org/10.1002/1521-3773(20010601)40:11<2004::AID-ANIE2004>3.0.CO;2-5)
- [152] Zaia, J. (2023). The 2022 Nobel Prize in Chemistry for the development of click chemistry and bioorthogonal chemistry. *Analytical and Bioanalytical Chemistry*, 415(4), 527–532. <https://doi.org/10.1007/s00216-022-04483-9>
- [153] Geng, Z., Shin, J. J., Xi, Y., & Hawker, C. J. (2021). Click chemistry strategies for the accelerated synthesis of functional macromolecules. *Journal of Polymer Science*, 59(11), 963–1042. <https://doi.org/10.1002/pol.20210126>

- [154] Singh, M. S., Chowdhury, S., & Koley, S. (2016). Advances of azide-alkyne cycloaddition-click chemistry over the recent decade. *Tetrahedron*, 72(35), 5257–5283. <https://doi.org/10.1016/j.tet.2016.07.044>
- [155] H. Zhou, C., & Wang, Y. (2012). Recent Researches in Triazole Compounds as Medicinal Drugs. *Current Medicinal Chemistry*, 19(2), 239–280. <https://doi.org/10.2174/092986712803414213>
- [156] Aufort, M., Herscovici, J., Bouhours, P., Moreau, N., & Girard, C. (2008). Synthesis and antibiotic activity of a small molecules library of 1,2,3-triazole derivatives. *Bioorganic and Medicinal Chemistry Letters*, 18(3), 1195–1198. <https://doi.org/10.1016/j.bmcl.2007.11.111>
- [157] Meldal, M., & Diness, F. (2020). Recent Fascinating Aspects of the CuAAC Click Reaction. *Trends in Chemistry*, 2(6), 569–584. <https://doi.org/10.1016/j.trechm.2020.03.007>
- [158] Ajmal, M., Mahato, A.K., Khan, M., Rawat, S., Husain, A., Almalki, E.B., Alzahrani, M.A., Haque, A., Hakme, M.J., Albalawi, A.S., Rashid, M. (2024). Significance of Triazole in Medicinal Chemistry: Advancement in Drug Design, Reward and Biological Activity. *Chemistry & Biodiversity*, e202400637. <https://doi.org/10.1002/cbdv.202400637>
- [159] Xu, G., Zhao, J., Jiang, Y., Zhang, P., & Li, W. (2016). Design, synthesis and antifungal activity of novel indole derivatives linked with the 1,2,3-triazole moiety via the CuAAC click reaction. *Journal of Chemical Research*, 40(5), 269–272. <https://doi.org/10.3184/174751916X14597828245275>
- [160] Kharb, R., Sharma, P. C., & Yar, M. S. (2011). Pharmacological significance of triazole scaffold. *Journal of Enzyme Inhibition and Medicinal Chemistry*, 26(1), 1–21. <https://doi.org/10.3109/14756360903524304>
- [161] Alam, M. M. (2022). 1,2,3-Triazole hybrids as anticancer agents: A review. *Archiv Der Pharmazie*, 355(1). <https://doi.org/10.1002/ardp.202100158>
- [162] Kharb, R., Sharma, P. C., & Yar, M. S. (2011). Pharmacological significance of triazole scaffold. *Journal of Enzyme Inhibition and Medicinal Chemistry*, 26(1), 1–21. <https://doi.org/10.3109/14756360903524304>
- [163] Gulcin, İ. (2020). Antioxidants and antioxidant methods: an updated overview. *Archives of Toxicology*, 94(3), 651–715. <https://doi.org/10.1007/s00204-020-02689-3>
- [164] Hajam, Y. A., Rani, R., Ganie, S. Y., Sheikh, T. A., Javaid, D., Qadri, S. S., Pramodh, S., Alsulimani, A., Alkhanani, M. F., Harakeh, S., Hussain, A., Haque, S., & Reshi, M. S. (2022). Oxidative Stress in Human Pathology and Aging: Molecular Mechanisms and Perspectives. *Cells*, 11(3), 552. <https://doi.org/10.3390/cells11030552>
- [165] Santo, A., Zhu, H., & Li, Y. R. (2016). Free Radicals: From Health to Disease. *Reactive Oxygen Species*, October. <https://doi.org/10.20455/ros.2016.847>

- [166] García-Caparrós, P., De Filippis, L., Gul, A., Hasanuzzaman, M., Ozturk, M., Altay, V., & Lao, M. T. (2021). Oxidative Stress and Antioxidant Metabolism under Adverse Environmental Conditions: a Review. *Botanical Review*, 87(4), 421–466. <https://doi.org/10.1007/s12229-020-09231-1>
- [167] Neha, K., Haider, M. R., Pathak, A., & Yar, M. S. (2019). Medicinal prospects of antioxidants: A review. *European Journal of Medicinal Chemistry*, 178, 687–704. <https://doi.org/10.1016/j.ejmech.2019.06.010>
- [168] Pisoschi, A. M., Pop, A., Iordache, F., Stanca, L., Predoi, G., & Serban, A. I. (2021). Oxidative stress mitigation by antioxidants - An overview on their chemistry and influences on health status. *European Journal of Medicinal Chemistry*, 209, 112891. <https://doi.org/10.1016/j.ejmech.2020.112891>
- [169] Parcheta, M., Świsłocka, R., Orzechowska, S., Akimowicz, M., Choińska, R., & Lewandowski, W. (2021). Recent developments in effective antioxidants: The structure and antioxidant properties. *Materials*, 14(8), 1–24. <https://doi.org/10.3390/ma14081984>
- [170] Munteanu, I. G., & Apetrei, C. (2021). Analytical methods used in determining antioxidant activity: A review. *International Journal of Molecular Sciences*, 22(7). <https://doi.org/10.3390/ijms22073380>
- [171] Jayakumar, P., Pugalendi, K.V. & Sankaran, M. (2014). Attenuation of hyperglycemia-mediated oxidative stress by indole-3-carbinol and its metabolite 3, 3'-diindolylmethane in C57BL/6J mice. *Journal of Physiology and Biochemistry*, 70, 525–534. <https://doi.org/10.1007/s13105-014-0332-5>
- [172] Fan S, Meng Q, Saha T, Sarkar FH, Rosen EM. (2009). Low concentrations of diindolylmethane, a metabolite of indole-3-carbinol, protect against oxidative stress in a BRCA1-dependent manner. *Cancer Research*, 1; 69(15), 6083-6091. <https://doi.org/10.1158/0008-5472.CAN-08-3309>.
- [173] Li Y, Kong D, Ahmad A, Bao B, Sarkar FH. (2013). Antioxidant function of isoflavone and 3,3'-diindolylmethane: are they important for cancer prevention and therapy? *Antioxidants & Redox Signaling*. 10; 19(2), 139-150. <https://doi.org/10.1089/ars.2013.5233>. Epub 2013 Mar 14. PMID: 23391445; PMCID: PMC3689155.
- [174] Mizobuti, D. S., da Rocha, G. L., da Silva, H. N. M., Covatti, C., de Lourenço, C. C., Pereira, E. C. L., Salvador, M. J., & Minatel, E. (2022). Antioxidant effects of bis-indole alkaloid indigo and related signaling pathways in the experimental model of Duchenne muscular dystrophy. *Cell Stress and Chaperones*, 27(4), 417–429. <https://doi.org/10.1007/s12192-022-01282-0>
- [175] Singhal, S., Khanna, P., Khanna, L. (2021). Synthesis, comparative in vitro antibacterial, antioxidant and UV fluorescence studies of bis indole Schiff bases and molecular docking with ct-DNA and SARS-CoV-2 Mpro. *Luminescence*, 36(6), 1531. <https://doi.org/10.1002/bio.4098>

- [176] Ranjbari, S., Jarrahpour, A., Kianpour, S., Sepehri, S., Heiran, R., Ghasemi, Y., Turos, E. (2023). Molecular docking, synthesis and evaluation of the antimicrobial, antiproliferative, and antioxidant properties of  $\beta$ -lactam bisindoles, *Journal of Molecular Structure*, 1294(2), 136298, <https://doi.org/10.1016/j.molstruc.2023.136298>
- [177] Almeida L.M., Oliveira M., Ivan P.R., Marina, P. (2020). Advances in Synthesis and Medicinal Applications of Compounds Derived from Phthalimide, *Current Organic Synthesis*, 17 (4), 252-270. <https://dx.doi.org/10.2174/1570179417666200325124712>
- [178] Khatab, H.A., Hammad, S.F., El-Fakharany, E.M., Hashem, A.I., & Eman A. E. El-Helw, E.A.E. (2023). Synthesis and cytotoxicity evaluation of novel 1,8-acridinedione derivatives bearing phthalimide moiety as potential antitumor agents. *Scientific Reports*, 13, 15093. <https://doi.org/10.1038/s41598-023-41970-0>
- [179] Karthik, C.S., Mallesha, L., Mallu, P. (2015). Investigation of Antioxidant Properties of Phthalimide Derivatives. *Canadian Chemical Transactions*, 3, 199-206. <https://doi.org/10.13179/canchemtrans.2015.03.02.0194>.
- [180] Bisht, A.S., Bisht, R. (2021). Microwave assisted synthesis of phthalimide amino derivatives with their antioxidant potential. *Current Trends in Pharmacy and Pharmaceutical Chemistry*, 3(3), 23-27. <http://dx.doi.org/10.18231/j.ctppc.2021.007>
- [181] Kumar, C. S. C., Loh, W. S., Chandraju, S., Win, Y. F., Tan, W. K., Quah, C. K., Fun, H. K. (2015). Synthesis, structural and antioxidant studies of some novel N-ethyl phthalimide esters. *PLoS ONE*, 10(3), 1–23. <https://doi.org/10.1371/journal.pone.0119440>
- [182] Podsiedlik, M., Markowicz-Piasecka, M., Sikora, J. (2020). Erythrocytes as model cells for biocompatibility assessment, cytotoxicity screening of xenobiotics and drug delivery, *Chemico-Biological Interactions*, 332, 109305. <https://doi.org/10.1016/j.cbi.2020.109305>.
- [183] Lippi, G., Blanckaert, N., Bonini, P., Green, S., Kitchen, S., Palicka, V., Vassault, A. J., & Plebani, M. (2008). Haemolysis: An overview of the leading cause of unsuitable specimens in clinical laboratories. *Clinical Chemistry and Laboratory Medicine*, 46(6), 764–772. <https://doi.org/10.1515/CCLM.2008.170>
- [184] Weber, M., Steinle, H., Golombek, S., Hann, L., Schlensak, C., Wendel, H. P., & Avci-Adali, M. (2018). Blood-Contacting Biomaterials: In Vitro Evaluation of the Hemocompatibility. *Frontiers in Bioengineering and Biotechnology*, 6. <https://doi.org/10.3389/fbioe.2018.00099>
- [185] Zhang, L., Yadav, S., John Wang, Y., Mozziconacci, O., & Schöneich, C. (2018). Dual Effect of Histidine on Polysorbate 20 Stability: Mechanistic Studies. *Pharmaceutical Research*, 35(2). <https://doi.org/10.1007/s11095-017-2321-1>
- [186] Süzen, S. (2007). Antioxidant Activities of Synthetic Indole Derivatives and Possible Activity Mechanisms. In: Khan, M.T.H. (eds) Bioactive Heterocycles V. *Topics in*

*Heterocyclic Chemistry*, vol 11. Springer, Berlin, Heidelberg.  
[https://doi.org/10.1007/7081\\_2007\\_074](https://doi.org/10.1007/7081_2007_074)

- [187] Silveira, C.C., Mendes, S.R., Soares, J.R., Victoria, F.N., Martinez, D.M., Savegnago, L. (2013). Synthesis and antioxidant activity of new C-3 sulfenyl indoles. *Tetrahedron Letters*. 54(36), 4926–4929. <https://doi.org/10.1016/j.tetlet.2013.07.004>.
- [188] Di Gregorio, M.C., Cautela, J., & Galantini, L. (2021). Physiology and physical chemistry of bile acids. *International Journal of Molecular Sciences*, 22(4), 1–23. <https://doi.org/10.3390/ijms22041780>
- [189] Gvoic, M., Vukmirovic, S., Al-Salami, H., Mooranian, A., Mikov, M., & Stankov, K. (2021). Bile acids as novel enhancers of CNS targeting antitumor drugs: a comprehensive review. *Pharmaceutical Development and Technology*, 26(6), 617–633. <https://doi.org/10.1080/10837450.2021.1916032>
- [190] Lang, E., Pozdeev, V. I., Gatidis, S., Qadri, S. M., Häussinger, D., Kubitz, R., Herebian, D., Mayatepek, E., Lang, F., Lang, K. S., & Lang, P. A. (2016). Bile acid-induced suicidal erythrocyte death. *Cellular Physiology and Biochemistry*, 38(4), 1500–1509. <https://doi.org/10.1159/000443091>
- [191] Kozanecka, W., Mrówczyńska, L., Pospieszny, T., Jasiewicz, B., & Gierszewski, M. (2015). Synthesis, spectroscopy, theoretical and biological studies of new gramine-steroids salts and conjugates. *Steroids*, 98, 92–99. <https://doi.org/10.1016/j.steroids.2015.03.003>
- [192] Kozanecka-Okupnik, W., Jasiewicz, B., Pospieszny, T., Matuszak, M., & Mrówczyńska, L. (2017). Haemolytic activity of formyl- and acetyl-derivatives of bile acids and their gramine salts. *Steroids*, 126, 50–56. <https://doi.org/10.1016/j.steroids.2017.07.003>
- [193] Aboul-Enein, H. Y., Kruk, I., Lichszteld, K., Michalska, T., Kladna, A., Marczyński, S., & Ölgen, S. (2004). Scavenging of reactive oxygen species by N-substituted indole-2 and 3-carboxamides. *Luminescence*, 19(1), 1–7. <https://doi.org/10.1002/bio.748>
- [194] Bozkaya, P., Ölgen, S., Çoban, T., & Nebİoglu, D. (2007). Synthesis of N-substituted indole-2-carboxamides and investigation of their biochemical responses against free radicals. *Journal of Enzyme Inhibition and Medicinal Chemistry*, 22(3), 319–325. <https://doi.org/10.1080/14756360601114742>
- [195] Ölgen, S., Kiliç, Z., Ada, A. O., & Çoban, T. (2007). Synthesis and evaluation of novel N - H and N-substituted indole-2- and 3-carboxamide derivatives as antioxidants agents. *Journal of Enzyme Inhibition and Medicinal Chemistry*, 22(4), 457–462. <https://doi.org/10.1080/14756360701228491>
- [196] Velika, B., & Kron, I. (2012). Antioxidant properties of benzoic acid derivatives against Superoxide radical. *Free Radicals and Antioxidants*, 2(4), 62–67. <https://doi.org/10.5530/ax.2012.4.11>

- [197] Foti, M.C. (2007). Antioxidant properties of phenols. *The Journal of Pharmacy and Pharmacology*, 59(12), 1673-85. <https://doi.org/10.1211/jpp.59.12.0010>.
- [198] Chen, Y., Li, H., Liu, J., Zhong, R., Li, H., Fang, S., Liu, S., Lin, S. (2021). Synthesis and biological evaluation of indole-based peptidomimetics as antibacterial agents against Gram-positive bacteria, *European Journal of Medicinal Chemistry*, 226, 113813. <https://doi.org/10.1016/j.ejmech.2021.113813>.
- [199] Li, H., Wu, S., Yang, X., He, H., Wu, Z., Song, B., Song, R. (2022). Synthesis, Antibacterial Activity, and Mechanisms of Novel Indole Derivatives Containing Pyridinium Moieties. *Journal of Agricultural and Food Chemistry*, 70(39), 12341-<https://doi.org/10.1021/acs.jafc.2c04213>
- [200] Jagadeesan, S., Karpagam, S. (2023). Novel series of *N*-acyl substituted indole based piperazine, thiazole and tetrazoles as potential antibacterial, antifungal, antioxidant and cytotoxic agents, and their docking investigation as potential Mcl-1 inhibitors, *Journal of Molecular Structure*, 1271, 134013, <https://doi.org/10.1016/j.molstruc.2022.134013>.

Streszczenie rozprawy doktorskiej

**„Nowe pochodne graminy – synteza, analiza spektroskopowa  
oraz ocena aktywności biologicznej”**

mgr Natalia Berdzik

promotor: prof. UAM dr hab. Beata Jasiewicz

Celem mojej pracy doktorskiej było otrzymanie nowych pochodnych indolowych o potencjalnych właściwościach antyoksydacyjnych. Poprzez zastosowanie odpowiednich modyfikacji cząsteczki graminy otrzymałam trzy grupy nieznanych dotąd związków.

Stosując metodę chemii klik otrzymałam dimery indolowo-triazolowe zawierające łączniki alifatyczne o różnej długości łańcucha węglowego oraz pochodne z dodatkowym ugrupowaniem fenylowym lub pierścieniem ftalimidowym. Przy wykorzystaniu warunków reakcji chemii klik otrzymałam również związki zawierające ugrupowania indolowe, triazolowe oraz steroidowe. W ostatnim etapie pracy przeprowadziłam reakcje prowadzące do otrzymania serii *N*-podstawionych estrów indolu.

Otrzymane pochodne scharakteryzowałam za pomocą metod spektroskopowych  $^1\text{H}$  NMR,  $^{13}\text{C}$  NMR, FT-IR oraz MS. Za pomocą metod *in silico* oceniłam również właściwości fizykochemiczne wybranych związków.

Przy współpracy z Wydziałem Biologii UAM określiłam hemokompatybilność wszystkich nowo otrzymanych pochodnych. Większość z tych związków przebadalam również pod kątem ich aktywności cytoprotekcyjnej. Dodatkowym aspektem mojej pracy była wstępna ocena właściwości przeciwbakteryjnych i przeciwgrzybiczych wybranych związków, określonych na podstawie badań eksperymentalnych, przeprowadzonych we współpracy z Uniwersytetem Przyrodniczym w Poznaniu, oraz z wykorzystaniem metod dokowania molekularnego.



Summary of doctoral dissertation

**"New gramine derivatives - synthesis, spectroscopic analysis  
and biological activity"**

mgr Natalia Berdzik

supervisor: prof. UAM, dr hab. Beata Jasiewicz

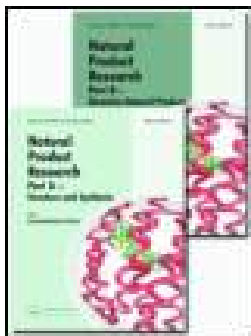
The aim of my Ph.D. thesis was to obtain new indole derivatives with potential antioxidant properties. By appropriate modifications of the gramine molecule, three groups of previously unknown compounds were obtained.

Using click chemistry, indole-triazole dimers with aliphatic linkers of different carbon chain lengths and derivatives with an additional phenyl moiety or phthalimide ring were obtained. Compounds containing indole, triazole and steroid groups were also obtained using click chemistry reaction conditions. In the last stage of my work, reactions leading to the preparation of a series of *N*-substituted indole esters were carried out.

The obtained derivatives were characterized by spectroscopic methods  $^1\text{H}$  NMR,  $^{13}\text{C}$  NMR, FT-IR and MS. The physicochemical properties of selected compounds were determined by theoretical methods.

In cooperation with the Faculty of Biology of Adam Mickiewicz University, the hemocompatibility of all newly obtained derivatives was determined. Most of these compounds were tested for their cytoprotective activity. Another aspect was the preliminary study of antibacterial and antifungal properties of selected compounds based on experimental research carried out in cooperation with the University of Life Sciences in Poznań and by molecular docking methods.

**PUBLIKACJE WCHODZĄCE W SKŁAD  
ROZPRAWY DOKTORSKIEJ  
I MATERIAŁY UZUPEŁNIAJĄCE**



# Natural Product Research

Formerly Natural Product Letters

ISSN: (Print) (Online) Journal homepage: <https://www.tandfonline.com/loi/gnpl20>

## New triazole-bearing gramine derivatives – synthesis, structural analysis and protective effect against oxidative haemolysis

W. Kozanecka-Okupnik , A. Sierakowska , N. Berdzik , I. Kowalczyk , L. Mrówczyńska & B. Jasiewicz

To cite this article: W. Kozanecka-Okupnik , A. Sierakowska , N. Berdzik , I. Kowalczyk , L. Mrówczyńska & B. Jasiewicz (2020): New triazole-bearing gramine derivatives – synthesis, structural analysis and protective effect against oxidative haemolysis, Natural Product Research, DOI: [10.1080/14786419.2020.1864364](https://doi.org/10.1080/14786419.2020.1864364)

To link to this article: <https://doi.org/10.1080/14786419.2020.1864364>



Published online: 24 Dec 2020.



Submit your article to this journal [↗](#)



View related articles [↗](#)



View Crossmark data [↗](#)



## New triazole-bearing gramine derivatives – synthesis, structural analysis and protective effect against oxidative haemolysis

W. Kozanecka-Okupnik<sup>a</sup>, A. Sierakowska<sup>a</sup>, N. Berdzik<sup>a</sup>, I. Kowalczyk<sup>a</sup>, L. Mrówczyńska<sup>b</sup> and B. Jasiewicz<sup>a</sup>

<sup>a</sup>Faculty of Chemistry, Adam Mickiewicz University, Poznań, Poland; <sup>b</sup>Faculty of Biology, Adam Mickiewicz University, Poznań, Poland

### ABSTRACT

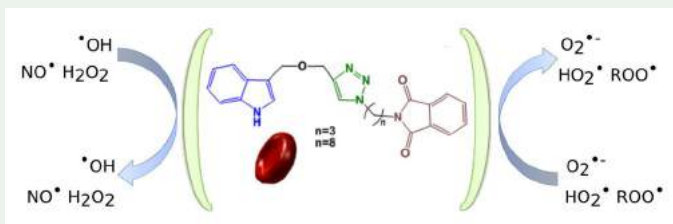
The new series of triazole-bearing gramine derivatives were synthesized through a CuAAC procedure. The structures of all newly obtained compounds were confirmed by spectroscopic analysis and DFT methods. The obtained derivatives were screened for their protective potency against oxidative haemolysis induced by free radicals generated from 2,2'-azobis(2-methylpropionamide) dihydrochloride (AAPH). Our work demonstrates that derivatives with propyl or octyl linker and phthalimide group associated with indole-triazole moiety, which have a folded structure, effectively protect human erythrocytes against oxidative stress-induced haemolysis.

### ARTICLE HISTORY

Received 29 July 2020  
Accepted 10 December 2020

### KEYWORDS


Gramine; indol; click reaction; haemolysis; human erythrocytes; oxidative stress



## 1. Introduction

Indole derivatives, present in natural compounds such as L-tryptophan, serotonin and melatonin, are of particular importance due to their biological properties (Chiou et al. 2010; Lee et al. 2010; Rao et al. 2011; Pawar et al. 2015; Garg et al. 2019). Many indole compounds show antioxidant properties manifested by their ability to scavenge reactive oxygen species (ROS) (Herraiz and Galisteo 2004; Survase et al. 2019). Gramine, a natural indole alkaloid, has been widely used as a pharmaceutical lead scaffold for constructing various biologically active indole-containing compounds (Hong et al.

CONTACT B. Jasiewicz  [beatakoz@amu.edu.pl](mailto:beatakoz@amu.edu.pl)

 Supplemental data for this article can be accessed at <https://doi.org/10.1080/14786419.2020.1864364>.

© 2020 Informa UK Limited, trading as Taylor & Francis Group

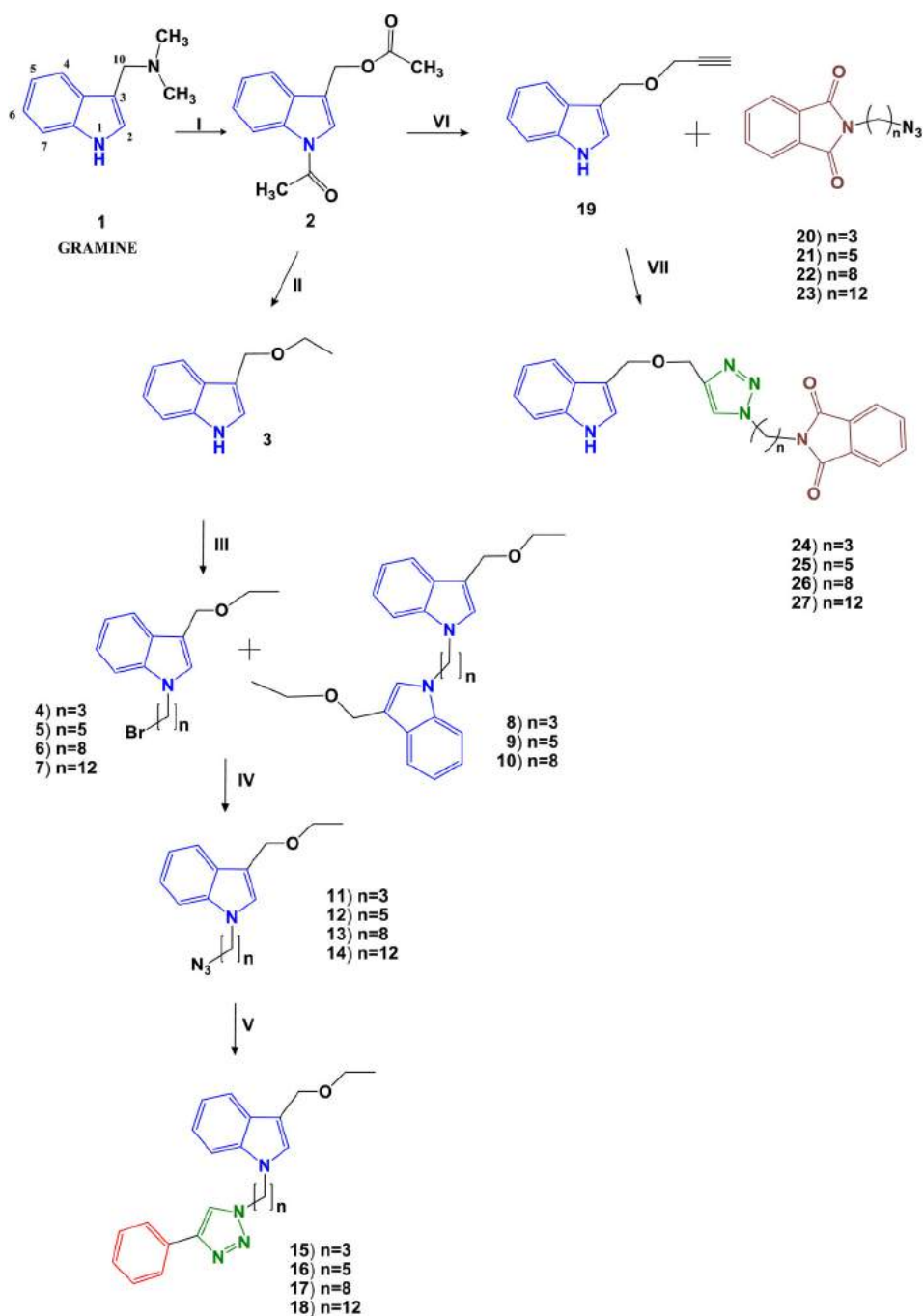
2009; Li et al. 2009; Suzen et al. 2012). Some of the gramine-uracil conjugates protect the human erythrocytes (RBC) against the oxidative stress-induced haemolysis (Kozanecka-Okupnik et al. 2018). Gramine can also modify the membrane-perturbing activity of select steroids and protect against RBC membrane disturbances (Kozanecka-Okupnik et al. 2017). Encouraged with the above findings and in continuation of our work on the synthesis of biologically active alkaloids derivatives, herein, we report the synthesis and structural analysis, as well as the cytoprotective properties of several novel triazole-bearing indoles. Introduction of a 1,2,3-triazole ring to the parent molecule often lead to new, potentially biologically active compounds. For example, indole–triazole conjugates are selective inhibitors and inducers of bacterial biofilms (Minvielle et al. 2013), indole–triazole–amino acid conjugates are a highly effective antifungal agents (Rao et al. 2011). Therefore, a combination of triazole pharmacophore with an alkaloid molecule should allow the promise of new drugs. RBCs are the main cellular components of human blood; therefore, the haemocompatibility of potential blood-contacting compounds is evaluated using RBC (Kozanecka-Okupnik et al. 2017, 2018). *In vitro* haemocompatibility assays, including haemolysis and RBC shape-transformation tests, are used to assess the membrane-partitioning potential of compounds (Malczewska-Jaskóła et al. 2016; de la Harpe et al. 2019). Any harmful effects of the compound tested on the RBC membrane molecular structure do not allow its use for *in vivo* biomedical studies (Farag and Alagawany 2018).

## 2. Results and discussion

### 2.1. Chemistry

The synthesis of new compounds is illustrated in Scheme 1. Compound **2** was prepared *via* the reaction of gramine (**1**) with acetic anhydride. The reaction of compound **2** with ethyl or propargyl alcohol gives the indole analogues **3** and **19**, respectively. The  $^1\text{H}$  NMR spectrum of **3** shows signals near 3.58 ppm and at 1.24 ppm characteristic of the ethoxy group. In contrast, signals from the methylene group and hydrogen atom from the alkyne group (compound **19**) are present at 4.16 and 2.47 ppm, respectively. The absorption bands at  $1079\text{ cm}^{-1}$  (**3**) and  $2095$  (**19**) in the FT-IR spectra confirmed the presence of C-O-C and  $-\text{C}\equiv\text{CH}$  groups in the structure. In the EI-MS spectra of **3** and **19**, the molecular ions are observed at  $m/z=175$  and  $m/z=185$ , respectively. Lower than expected yields for the alkylation step led to identification of compounds **8–10** linked by an alkyl linker (Scheme 1), in addition to the desired products **4–7**. The lowest yield (20%) was noted for the reaction of compound **3** with 1,12-dibromoundecane. In the case of this reaction, no dimer was obtained.

In the  $^1\text{H}$  NMR spectrum of compound **4**, in addition to signals from the 3-ethoxy-indole-3-carbinol molecule (except for the signal from the *N1* hydrogen atom), there are signals from methylene groups of the alkyl chain. The triplets at 4.27 ppm and 3.29 ppm correspond to the hydrogen atoms of the methylene group at the indole ring and to the hydrogen atoms of the methylene group adjacent to the bromine atom, respectively whereas hydrogen atoms from the third methylene group of the propyl chain are present in the range of 2.34–2.28 ppm (Figure S1, supplementary materials). The signal from the hydrogen atoms of the methylene group at the indole



**Scheme 1.** Synthesis of gramine derivatives 2–19: (I) acetic anhydride, temp. 5 h; (II) ethanol, 10% NaOH; (III) 50% NaOH, PhCH<sub>3</sub>, TBAB, Br(CH<sub>2</sub>)<sub>n</sub> Br; (IV) NaN<sub>3</sub>, acetone/water; (V) phenylacetylene, sodium ascorbate, CuSO<sub>4</sub>·5H<sub>2</sub>O, CH<sub>2</sub>Cl<sub>2</sub>/H<sub>2</sub>O (1:1); (VI) propargyl alcohol, 10% NaOH; (VII) sodium ascorbate, CuSO<sub>4</sub>·5H<sub>2</sub>O, CH<sub>2</sub>Cl<sub>2</sub>/H<sub>2</sub>O (1:1).

ring for dimer **8** is present at 4.06 ppm in the form of a triplet and corresponds to four hydrogen atoms whereas hydrogen atoms from the central methylene group are present in the range of 2.43–2.34 ppm (Figure S2, [supplementary materials](#)). MS spectra of all bromide compounds (**4–7**) show signals characteristic to the presence of 1:1 M + 2 isotope of bromine atoms. For example, in the EI-MS spectrum of compound **4** (Fig. S3a) we can observe two peaks of 100% intensity in the molecular ion region, depending on which bromine isotope (79 or 81) ion contains, at  $m/z = 295$  and  $m/z = 297$ , respectively. In the EI-MS spectrum of compound **8**, a signal from a molecular ion is observed at  $m/z = 390$  (50% intensity) (Figure S3b, [supplementary materials](#)). The lack of the signals from the bromine atom additionally confirms the proposed structure of the compound. The detailed analysis of  $^1\text{H}$  NMR, EI-MS and FT-IR spectra of the remaining bromides **5–7** and dimers **9, 10** are presented in Experimental part. 3-Ethoxy-indole-3-carbinol *N*-alkyl bromides **4–7** were converted into respective 3-ethoxy-indole-3-carbinol *N*-alkyl azides **11–14**, which together with phthalimide *N*-alkyl azides **20–23** were further modified into new triazole products **15–18** and **24–27** (Scheme 1). In the  $^1\text{H}$  NMR spectra of all new triazole derivatives **15–18** and **24–27**, the characteristic singlet of hydrogen atom of triazole ring is observed in the range of 8.05–7.58 ppm. Signals near 4.70 ppm (compounds **15–18**) correspond to hydrogen atoms of methylene groups ( $-\text{CH}_2\text{-O}-$ ); signals from the hydrogen atoms of the ethoxy group are in the range of 3.64–3.49 ppm ( $-\text{O-CH}_2-$ ) and at 1.19–1.29 ppm  $-\text{CH}_3$  while the signals of the hydrogen atoms of the phenyl ring are observed in the range of 7–8 ppm. Moreover, in all this spectra we can see signals from hydrogen atoms of the indole ring in the range of 7.82–6.95 ppm. In  $^1\text{H}$  NMR spectra of **24–27**, in addition to the signals of the indole moiety and the triazole ring, signals from the phthalimide ring in the range of 7.70–7.90 ppm are also present. The representative  $^1\text{H}$  NMR spectrum of compound **15** is shown in Fig. S4, [supplementary materials](#). Detailed spectroscopic analysis of compounds **15–18** and **24–27** are presented in Experimental part.

## 2.2. Biological activity

The haemolytic activity of the derivatives and their effect on RBC shape were examined. The level of derivatives-induced haemolysis was as obtained for the control RBC; however, derivative **27** was an exception due to its slight haemolytic activity (Table S1, [supplementary materials](#)). Examination of derivatives-induced RBC shape modification showed no impact in comparison with the control RBC; however, derivatives **16, 24**, and **25–27** were the exceptions. Namely, **16** and **24** induced echinocytosis, **25–27** induced stomatocytosis, what are the result of incorporation of molecules into the RBC. According to the bilayer-couple hypothesis (Lim et al. 2002), echinocytes are the result of molecules incorporation into the exoplasmic layer of the RBC membrane (**16,24**). On the other hand, stomatocytes are created as an effect of compound (**25–27**) accumulation in the endoplasmic layer. However, no changes in the RBC shape are not clear evidence of a lack of membrane-partitioning activity of compound tested (Manaargadoo-Catin et al. 2016). As has been shown in Figure S5 ([supplementary materials](#)) the high cytoprotective properties against free radicals induced oxidative haemolysis was reported for compounds **8,15,17,24** and **26**. The data obtained

show a strong correlation between the chemical structure of the derivatives and their cytoprotective activity. Structurally, the compounds can be divided into diindole derivatives and derivatives in which the triazole ring is present in two different gamine positions. As shown from the data in Fig. S5, for each group of compounds an essential element of the structure is the alkyl linker length. In the case of di-indole compounds, only compound **8** (propyl linker) has a high cytoprotective activity while dimeric derivatives with pentyl or octyl linker, exhibit a low activity. Among the triazole derivatives, activity show compounds with propyl and octyl linker, whereas for derivatives with a pentyl or dodecyl linker, the RBC protection properties are very low (compounds **16** and **18**) or none (compounds **25** and **27**). Moreover, compounds containing phthalimide rings with a propyl (**24**) and octyl (**26**) linker are more effective than the derivatives with 4-phenyltriazole ring connected with gamine nitrogen atom by propyl and octyl linker (compounds **15** and **17**, respectively). Particularly noteworthy is derivative **24**, whose cytoprotective activity is almost twice as high as obtained for derivative **15**. It should also be noted that the most cytoprotective derivatives caused RBC shape transformation, namely echinocytosis (**24**) or stomatocytosis (**26**). Therefore, the high efficiency of **24** and **26** against RBC oxidative haemolysis can be explained as a result of their specific RBC membrane-partitioning activity. Based on the data contained in the paper, we can state that the protective activity of gamine derivatives is influenced by all structural elements: the length of the alkyl linker, the place of introducing the triazole group into the parent molecule and the presence of additional functional groups (phenyl ring, phthalimide group). In order to clearly state which structural factor is the most important, additional experimentation is necessary.

### 2.3. Theoretical calculations

The molecular geometry, energy, and dipole moments of new compounds were calculated by DFT methods. Semiempirical calculations were made to determine the influence of spatial structure on the properties of compounds. The lowest values of energy are observed for compounds **10**, **18**, and **27** (Table S2, [supplementary materials](#)). Energy decreases from a shorter to longer hydrocarbon chain, which is related to symmetry and convertible position of long hydrocarbon chains of molecules. Compounds with longer hydrocarbon chains are also much more thermodynamically stable. We suppose that specific folded molecular structure of **24** and **26** may also influence its RBC membrane partitioning and high cytoprotective efficiency in oxidative stress conditions. Compounds **25** and **27** form a linear structure and have no cytoprotective effects on RBC at all. Calculated structures of compounds are in supplementary part (Figure S6).

## 3. Experimental

All experimental procedures are described in the [supplementary materials](#).



## 4. Conclusions

In summary, the results obtained in this study show that new gramine-triazole-phthali-mide conjugates with a propyl (**24**) and octyl linker (**26**) are active as cell membrane-partitioning and cytoprotective agents in oxidative stress conditions. Taking together, the structural features such as (i) the position of gramine modification, (ii) the type of group connected to the triazole ring, (iii) the length of the hydrocarbon chain, and (iv) the spatial arrangement of the molecule, seems to be crucial for the favorable biological activity of new gramine derivatives under the oxidative stress conditions. Further studies should help to find more detailed structure–activity relationships.

## Disclosure statement

No potent conflict of interest was reported by the author.

## Funding

This work was financially supported by the funds of Faculty of Chemistry, Adam Mickiewicz University in Poznań, and within the Research Subsidy at the Faculty of Biology of the Adam Mickiewicz University in Poznań.

## References

- Chiou C-T, Chen GS, Chen M-L, Li H, Shi L, Huang X-H, Dai W-M, Chern J-W. 2010. Synthesis of anti-microtubule N-(2-Arylindol-7-yl)benzenesulfonamide derivatives and their antitumor mechanisms. *ChemMedChem*. 5(9):1489–1497.
- de la Harpe KM, Kondiah PPD, Choonara YE, Marimuthu T, Du Toit LC, Pillay V. 2019. The hemocompatibility of nanoparticles: a review of cell–nanoparticle interactions and hemostasis. *Cells*. 8(10):1209.
- Farag MR, Alagawany M. 2018. Erythrocytes as a biological model for screening of xenobiotics toxicity. *Chem Biol Interact*. 279:73–83.
- Garg V, Maurya RK, Thanikachalam PV, Bansal G, Monga V. 2019. An insight into the medicinal perspective of synthetic analogs of indole: a review. *Eur J Med Chem*. 180:562–612.
- Herraiz T, Galisteo J. 2004. Endogenous and dietary indoles: a class of antioxidants and radical scavengers in the ABTS assay. *Free Radic Res*. 38(3):323–331.
- Hong Y, Hu H-Y, Xie X, Sakoda A, Sagehashi M, Li F-M. 2009. Gramine-induced growth inhibition, oxidative damage and antioxidant responses in freshwater cyanobacterium *Microcystis aeruginosa*. *Aquat Toxicol*. 91(3):262–269.
- Kozanecka-Okupnik W, Jasiewicz B, Pospieszny T, Jastrzab R, Skrobańska M, Mrówczyńska L. 2018. Spectroscopy, molecular modeling and anti-oxidant activity studies on novel conjugates containing indole and uracil moiety. *J Mol Struct*. 1169:130–137.
- Kozanecka-Okupnik W, Jasiewicz B, Pospieszny T, Matuszak M, Mrówczyńska L. 2017. Haemolytic activity of formyl- and acetyl-derivatives of bile acids and their gramine salts. *Steroids*. 126: 50–56.
- Lee Y-J, Han Y-R, Park W, Nam S-H, Oh K-B, Lee H-S. 2010. Synthetic analogs of indole-containing natural products as inhibitors of sortase A and isocitrate lyase. *Bioorg Med Chem Lett*. 20(23):6882–6885.
- Li X, Yu L, Xiaohui J, Xia S, Zhao H. 2009. Synthesis, algal inhibition activities and QSAR studies of novel gramine compounds containing ester functional groups. *Chin J Ocean Limnol*. 27(2): 309–316.

- Lim HWG, Wortis M, Mukhopadhyay R. 2002. Stomatocyte-discocyte-echinocyte sequence of the human red blood cell: evidence for the bilayer-couple hypothesis from membrane mechanics. *Proc Natl Acad Sci USA*. 99(26):16766–16769.
- Malczewska-Jaskóła K, Jasiewicz B, Mrówczyńska L. 2016. Nicotine alkaloids as antioxidant and potential protective agents against in vitro oxidative haemolysis. *Chem Biol Interact*. 243: 62–71.
- Manaargadoo-Catin M, Ali-Cherif A, Pougna JL, Perrin C. 2016. Hemolysis by surfactants-a review. *Adv Colloid Interface Sci*. 228:1–16.
- Minvielle MJ, Bunders CA, Melander C. 2013. Indole/triazole conjugates are selective inhibitors and inducers of bacterial biofilms. *Medchemcomm*. 4(6):916–919.
- Pawar K, Yadav A, Prasher P, Mishra S, Singh B, Singh P, Komath SS. 2015. Identification of an indole-triazole-amino acid conjugate as a highly effective antifungal agent. *Med Chem Commun*. 6(7):1352–1359.
- Rao VK, Chhikara BS, Shirazi AN, Tiwari R, Parang K, Kumar A. 2011. 3-substituted indoles: one-pot synthesis and evaluation of anticancer and Src kinase inhibitory activities. *Bioorg Med Chem Lett*. 21(12):3511–3514.
- Survase DN, Karhale SS, Khedkar VM, Helavi VB. 2019. Synthesis, characterization, and biological evaluation of indole aldehydes containing N-benzyl moiety. *Synth Commun*. 49(24): 3486–3497.
- Suzen S, Cihaner SS, Coban T. 2012. Synthesis and comparison of antioxidant properties of indole-based melatonin analogue indole amino acid derivatives. *Chem Biol Drug Des*. 79(1): 76–83.

## **New triazole-bearing gramine derivatives – synthesis, structural analysis and protective effect against oxidative haemolysis**

Weronika Kozanecka-Okupnik, Arleta Sierakowska, Natalia Berdzik, Iwona Kowalczyk,  
Lucyna Mrówczyńska, and Beata Jasiewicz

The new series of triazole-bearing gramine derivatives were synthesized through a CuAAC procedure. The structures of all newly obtained compounds were confirmed by spectroscopic analysis and DFT methods. The obtained derivatives were screened for their protective potency against oxidative haemolysis induced by free radicals generated from 2,2'-azobis(2-methylpropionamidine) dihydrochloride (AAPH). Our work demonstrates that derivatives with propyl or octyl linker and phthalimide group associated with indole-triazole moiety, which have a folded structure, effectively protect human erythrocytes against oxidative stress-induced haemolysis.

## Supplementary Material

General Methods.....	S1
Exemplary <sup>1</sup> H NMR and EI-MS spectra .....	S7
Biological assay.....	S10
Table S1. Effects of compounds on RBCs membrane permeability and RBC shape.....	S12
Figure S5. Protective activity of derivatives and Trolox against AAPH-induced haemolysis.....	S13
Statistical analysis.....	S13
Calculation.....	S14
Table S2. Selected parameters of investigated compounds estimated by calculations.....	S14
Structures of compounds calculated by the theoretical method.....	S15
References.....	S18

### General Methods:

The melting points (mp) were obtained with a Büchi SMP-20 apparatus. <sup>1</sup>H NMR spectra were recorded on a Varian 300/400 spectrometer with CDCl<sub>3</sub> or DMSO-*d*<sub>6</sub> as the solvent and TMS as the internal standard. Chemical shifts are reported in δ (parts per million) values. EI mass spectra were recorded on Bruker 320MS/450 GC mass spectrometer. FT-IR spectra were recorded on Nicolet iS 5 (KBr pellets). TLC analysis was performed using Sigma-Aldrich silica gel 60 plates with a fluorescent indicator (254 nm). All chemicals or reagents used for syntheses were commercially available.

### Synthesis of indole derivatives

*N,O*-diacetyl-indole-3-carbinol (**2**). A solution of gramine (522 mg, 3 mmol) in fresh distilled acetic anhydride (8 mL) was heated at the reflux temperature for 5 h (TLC: MeOH-(CH<sub>3</sub>)<sub>2</sub>CO-NH<sub>4</sub>OH 10:10:1). The reaction mixture was then cooled to 0-5 °C. Then 30 mL of ice-cooled water was added, and the solution was stirred at 0-5 °C temperature for 3 h. The obtained brown solid was washed with water and crystallized from *n*-hexane. Compound **2** was obtained as a white powder. Mp 89-90 °C, yield 70%. <sup>1</sup>H NMR (300 MHz, CDCl<sub>3</sub>, TMS,

*ppm*):  $\delta_{\text{H}} = 8.45\text{-}8.42$  (d, 1H, 7-H), 7.63-7.60 (d, 1H, 4-H), 7.48 (s, 1H, 2-H), 7.42-7.36 (t, 1H, 5-H/6-H), 7.35-7.29 (t, 1H, 5-H/6-H), 5.27 (s, 2H, -CH<sub>2</sub>O-), 2.63 (s, 3H, CH<sub>3</sub>CO-), 2.09 (s, 3H, CH<sub>3</sub>COO-). EI-MS (*m/z*, % int.): 231 (M<sup>+</sup>, 100). FT-IR (KBr)  $\nu_{\text{max}}$ : 3115, 1732, 1705, 1607, 1457, 1342, 1331, 1249.

*3-Ethoxy-indole-3-carbinol (3)*. Compound **2** (50 mg, 0,2 mmol) was dissolved in 1 mL ethanol, 0,5 ml 10% NaOH was added. The mixture was stirred for 24h at room temperature (TLC: (C<sub>6</sub>H<sub>5</sub>)CH<sub>3</sub>-AcOEt 5:1). The mixture was cooled in an ice/water bath, added dropwise 35 mL of cold water, and put in a refrigerator overnight. The resulting white precipitate was infiltrated and crystallized from *n*-hexane.

Yellow oil, yield 70%. <sup>1</sup>H NMR (300 MHz, DMSO-*d*<sub>6</sub>, TMS, *ppm*):  $\delta_{\text{H}} = 9.93$  (s, 1H, NH), 7.58-6.97 (5H, indole ring), 4.72 (s, 2H, indole ring-CH<sub>2</sub>O-), 3.58 (q, 2H, -O-CH<sub>2</sub>-), 1.24 (t, 3H, -CH<sub>3</sub>). EI-MS (*m/z*, % int.): 175 (M<sup>+</sup>, 63). FT-IR (KBr)  $\nu_{\text{max}}$ : 3402-2862, 1457, 1338, 1079.

*General procedure for the preparation of N-(n-bromoalkane)-3-ethoxy-indole-3-carbinol (4-7) and dimers (8-10)*.

Compound **3** (200 mg, 1.14 mmol) was dissolved in 3 mL toluene. To a stirred mixture, an aqueous solution of NaOH (50% w/w) (1 g) and after 15 min (120 mg, 0.4 mmol) Bu<sub>4</sub>NBr (tetrabutylammonium bromide) were added, followed by appropriate dibromoalkane (0.4 mmol). The solution was stirred at room temperature overnight, monitored by TLC, and then was poured onto crushed ice and extracted with diethyl ether (3 x 30 mL). The extract was washed with water (3 x 50 mL), brine (100 mL), and dried over anhydrous Na<sub>2</sub>SO<sub>4</sub>. The solvent was evaporated under reduced pressure to afford a residue that was purified over silica gel ((C<sub>6</sub>H<sub>5</sub>)CH<sub>3</sub>/AcOEt, 5:1).

*N-(3-bromopropane)-3-ethoxy-indole-3-carbinol (4)*. Yellow oil, yield 56 %. <sup>1</sup>H NMR (403 MHz, CDCl<sub>3</sub>, TMS, *ppm*):  $\delta_{\text{H}} = 7.71$  (d, 1H, 7-H), 7.35 (d, 1H, 4-H), 7.22 (t, 1H, 6-H), 7.15-7.12 (m, 2H, 5-H, 2-H), 4.69 (bs, 2H, indole ring-CH<sub>2</sub>O-), 4.27 (t, 2H, -CH<sub>2</sub>-indole ring), 3.59-3.54 (q, 2H, -O-CH<sub>2</sub>-), 3.29 (t, 2H, -CH<sub>2</sub>-Br), 2.34-2.28 (m, 2H, -CH<sub>2</sub>-), 1.25-1.21 (t, 3H, -CH<sub>3</sub>). EI-MS (*m/z*, % int.): 297 (M<sup>+</sup>, 100).

*N-(5-bromopentane)-3-ethoxy-indole-3-carbinol (5)*. Yellow oil, yield 70 %. <sup>1</sup>H NMR (403 MHz, CDCl<sub>3</sub>, TMS, *ppm*):  $\delta_{\text{H}} = 7.72$  (d, 1H, 7-H), 7.32 (d, 1H, 4-H), 7.28-7.16 (m, 2H, 5-H, 6-H), 7.12 (s, 1H, 2-H), 4.73 (s, 2H, -CH<sub>2</sub>O-), 4.13 (t, 2H, -CH<sub>2</sub>-indole ring), 3.64-3.57 (q,

2H, -O-CH<sub>2</sub>-), 3.46-3.37 (m, 2H, -CH<sub>2</sub>-Br), 1.94-1.83 (m, 4H, -CH<sub>2</sub>-), 1.55-1.45 (m, 2H, -CH<sub>2</sub>-), 1.27 (t, 3H, -CH<sub>3</sub>). EI-MS (*m/z*, % int.): 325 (M<sup>+</sup>, 65).

*N*-(8-bromooctane)-3-ethoxy-indole-3-carbinol (**6**). Yellow oil, yield 50 %. <sup>1</sup>H NMR (300 MHz, CDCl<sub>3</sub>, TMS, ppm): δ<sub>H</sub> = 7.71 (d, 1H, 7-H), 7.32 (d, 1H, 4-H), 7.28-7.14 (m, 2H, 5-H, 6-H), 7.12 (s, 1H, 2-H), 4.73 (s, 2H, -CH<sub>2</sub>O-), 4.10 (t, 2H, -CH<sub>2</sub>-indole ring), 3.63-3.51 (q, 2H, -O-CH<sub>2</sub>-), 3.41 (t, 2H, -CH<sub>2</sub>-Br), 1.90-1.80 (m, 4H, -CH<sub>2</sub>-), 1.45-1.40 (m, 4H, -CH<sub>2</sub>-), 1.34 (bs, 4H, -CH<sub>2</sub>-), 1.26 (t, 3H, -CH<sub>3</sub>). EI-MS (*m/z*, % int.): 365 (M<sup>+</sup>, 60).

*N*-(12-bromododecane)-3-ethoxy-indole-3-carbinol (**7**). Yellow oil, yield 20 %. <sup>1</sup>H NMR (300 MHz, CDCl<sub>3</sub>, TMS, ppm): δ<sub>H</sub> = 7.68 (d, 1H, 7-H), 7.29 (d, 1H, 4-H), 7.21-7.09 (m, 3H, 2-H, 5-H, 6-H), 4.70 (s, 2H, -CH<sub>2</sub>O-), 4.06 (t, 2H, -CH<sub>2</sub>-indole ring), 3.60-3.44 (q, 2H, -O-CH<sub>2</sub>-), 3.40 (t, 2H, -CH<sub>2</sub>-Br), 1.89-1.79 (m, 4H, -CH<sub>2</sub>-), 1.43-1.38 (m, 2H, -CH<sub>2</sub>-), 1.25 (t, 3H, -CH<sub>3</sub>), 1.24-1.21 (m, 14H, -CH<sub>2</sub>-). EI-MS (*m/z*, % int.): 421 (M<sup>+</sup>, 50).

*N,N'*-propanedi-(3-ethoxy-indole-3-carbinol) (**8**). Yellow oil, yield 32 %. <sup>1</sup>H NMR (300 MHz, CDCl<sub>3</sub>, TMS, ppm): δ<sub>H</sub> = 7.73 (d, 2H, 7-H), 7.21-7.11 (m, 6H, 4-H, 5-H, 6-H), 7.03 (s, 2H, 2-H), 4.69 (s, 4H, -CH<sub>2</sub>O-), 4.06 (t, 4H, -CH<sub>2</sub>-indole ring), 3.61-3.54 (q, 4H, -O-CH<sub>2</sub>-), 2.43-2.34 (m, 2H, -CH<sub>2</sub>-), 1.24 (t, 6H, -CH<sub>3</sub>). EI-MS (*m/z*, % int.): 390 (M<sup>+</sup>, 50). FT-IR (KBr) ν<sub>max</sub>: 3433, 3047, 2970, 2925, 2858, 1662, 1467.

*N,N'*-pentanedi-(3-ethoxy-indole-3-carbinol) (**9**). Yellow oil, yield 10 %. <sup>1</sup>H NMR (300 MHz, CDCl<sub>3</sub>, TMS, ppm): δ<sub>H</sub> = 7.72 (d, 2H, 7-H), 7.35-7.12 (m, 6H, 4-H, 5-H, 6-H), 7.06 (s, 2H, 2-H), 4.72 (s, 4H, -CH<sub>2</sub>O-), 4.06 (t, 4H, -CH<sub>2</sub>-indole ring), 3.64-3.57 (q, 4H, -O-CH<sub>2</sub>-), 1.88-1.83 (m, 6H, -CH<sub>2</sub>-), 1.27 (t, 6H, -CH<sub>3</sub>). EI-MS (*m/z*, % int.): 418 (M<sup>+</sup>, 50). FT-IR (KBr) ν<sub>max</sub>: 3431, 3048, 2927, 2856, 1660, 1467.

*N,N'*-octanedi-(3-ethoxy-indole-3-carbinol) (**10**). Yellow oil, yield 13 %. <sup>1</sup>H NMR (300 MHz, CDCl<sub>3</sub>, TMS, ppm): δ<sub>H</sub> = 7.90 (d, 2H, 7-H), 7.71 (d, 2H, 4-H), 7.39-7.10 (m, 6H, 2-H, 5-H, 6-H), 4.72 (s, 4H, -CH<sub>2</sub>O-), 4.07 (t, 4H, -CH<sub>2</sub>-indole ring), 3.66-3.56 (q, 4H, -O-CH<sub>2</sub>-), 2.07 (s, 2H, -CH<sub>2</sub>-), 1.82 (bs, 6H, -CH<sub>2</sub>-), 1.71 (s, 2H, -CH<sub>2</sub>-), 1.30 (bs, 2H, -CH<sub>2</sub>-), 1.26 (t, 6H, -CH<sub>3</sub>). EI-MS (*m/z*, % int.): 460 (M<sup>+</sup>, 70). FT-IR (KBr) ν<sub>max</sub>: 3400, 3052, 2928, 2855, 1716, 1663, 1612, 1467, 1363.

*General procedure for the preparation of azides 11-14.* To a stirred solution of appropriate *N*-(*n*-bromoalkane)-3-ethoxy-indole-3-carbinol (**4-7**) (1 eq) in 3 mL, acetone was added the sodium azide (1.3 eq) dissolved in water (3 mL). The solution was stirred at room temperature overnight, monitored by TLC, and then was poured onto crushed ice and extracted with diethyl ether (3 x 30 mL). The extract was washed with water (3 x 50 mL), brine (100 mL),

and dried over anhydrous Na<sub>2</sub>SO<sub>4</sub>. The solvent was evaporated under reduced pressure to afford azides **11-14** with good yield (80%). The products were characterized by FT-IR spectra (KBr).

*General procedure for the preparation of compounds 15-18.* An appropriate azide (1 eq) was dissolved in a mixture of dichloromethane and water (5 mL, 1:1), phenylacetylene (1.2 eq) was added, the mixture was stirred for 15 min. To the homogenous solution, CuSO<sub>4</sub>·5H<sub>2</sub>O (5 mg, catalytic amount) and sodium ascorbate (10 mg, catalytic amount) in water 1 mL were added. The solution was stirred at room temperature overnight, monitored by TLC, and then was poured onto crushed ice and extracted with dichloromethane (3 x 30 mL). The extract was washed with water (3 x 50 mL), brine (100 mL), and dried over anhydrous Na<sub>2</sub>SO<sub>4</sub>. The solvent was evaporated under reduced pressure to afford a residue that was purified over silica gel ((C<sub>6</sub>H<sub>5</sub>)CH<sub>3</sub>/AcOEt, 5:1).

*3-(ethoxymethyl)-1-(3-(4-phenyl-1H-1,2,3-triazol-1-yl)propyl)-1H-indole (15).* Yellow oil, yield 36 %. <sup>1</sup>H NMR (300 MHz, CDCl<sub>3</sub>, TMS, ppm): δ<sub>H</sub> = 7.82 (d, 1H, 7-H), 7.73 (d, 1H, 4-H), 7.63 (s, 1H, triazole ring), 7.48-7.34 (m, 3H, 2-H, 5-H, 6-H), 7.28-7.18 (m, 5H, Ar-H), 4.71 (s, 2H, -CH<sub>2</sub>O-), 4.34 (t, 2H, -CH<sub>2</sub>-triazole ring), 4.23 (t, 2H, -CH<sub>2</sub>-indole ring), 3.64-3.57 (q, 2H, -O-CH<sub>2</sub>-), 2.58-2.49 (m, 2H, -CH<sub>2</sub>-), 1.29-1.24 (t, 3H, -CH<sub>3</sub>). EI-MS (*m/z*, % int.): 332.3 [M<sup>+</sup>, 8]. FT-IR (KBr) ν<sub>max</sub>: 3132, 3048, 2927, 2854, 1659, 1611, 1464, 1334.

*3-(ethoxymethyl)-1-(5-(4-phenyl-1H-1,2,3-triazol-1-yl)pentyl)-1H-indole (16).* Yellow oil, yield 80 %. <sup>1</sup>H NMR (300 MHz, CDCl<sub>3</sub>, TMS, ppm): δ<sub>H</sub> = 7.78 (d, 1H, 7-H), 7.68 (d, 1H, 4-H), 7.58 (s, 1H, triazole ring), 7.41 (t, 2H, 5-H, 6-H), 7.34-7.09 (m, 5H, Ar-H), 7.03 (s, 1H, 2-H), 4.65 (s, 2H, -CH<sub>2</sub>O-), 4.27 (t, 2H, -CH<sub>2</sub>-triazole ring), 4.04 (t, 2H, -CH<sub>2</sub>-indole ring), 3.58-3.51 (q, 2H, -O-CH<sub>2</sub>-), 1.92-1.79 (m, 4H, -CH<sub>2</sub>-), 1.26-1.19 (t, 3H, -CH<sub>3</sub>), 0.88-0.83 (m, 2H, -CH<sub>2</sub>-). EI-MS (*m/z*, % int.): 360.4 [M<sup>+</sup>, 9]. FT-IR (KBr) ν<sub>max</sub>: 3439, 3129, 3054, 2929, 2856, 1611, 1551, 1464.

*3-(ethoxymethyl)-1-(8-(4-phenyl-1H-1,2,3-triazol-1-yl)octyl)-1H-indole (17).* Yellow oil, yield 50 %. <sup>1</sup>H NMR (300 MHz, CDCl<sub>3</sub>, TMS, ppm): δ<sub>H</sub> = 7.71 (d, 1H, 7-H), 7.68 (bs, 1H, triazole ring), 7.48-7.42 (m, 1H, 4-H), 7.31-7.29 (m, 2H, 5-H, 6-H), 7.24-7.08 (m, 5H, Ar-H), 6.95 (s, 1H, 2-H), 4.69 (s, 2H, -CH<sub>2</sub>O-), 4.06 (t, 2H, -CH<sub>2</sub>-triazole ring), 3.62-3.52 (q, 2H, -O-CH<sub>2</sub>-), 3.40 (t, 2H, -CH<sub>2</sub>-indole ring), 1.87-1.80 (m, 4H, -CH<sub>2</sub>-), 1.43 (bs, 4H, -CH<sub>2</sub>-), 1.32 (bs, 4H, -CH<sub>2</sub>-), 1.23 (t, 3H, -CH<sub>3</sub>). EI-MS (*m/z*, % int.): 402.5 [M<sup>+</sup>, 5]. FT-IR (KBr) ν<sub>max</sub>: 3357, 3055, 2934, 2854, 1614, 1553, 1467.

*3-(ethoxymethyl)-1-(12-(4-phenyl-1H-1,2,3-triazol-1-yl)dodecyl)-1H-indole (18)*. Oil, yield 58 %. <sup>1</sup>H NMR (300 MHz, CDCl<sub>3</sub>, TMS, ppm): δ<sub>H</sub> = 7.71 (d, 1H, 7-H), 7.68 (bs, 1H, triazole ring), 7.48-7.42 (d, 1H, 4-H), 7.31-7.29 (m, 2H, 5-H, 6-H), 7.23-7.08 (m, 5H, Ar-H), 6.95 (s, 1H, 2-H), 4.69 (s, 2H, -CH<sub>2</sub>O-), 4.05 (t, 2H, -CH<sub>2</sub>-triazole ring), 3.64-3.49 (q, 2H, -O-CH<sub>2</sub>-), 3.49 (t, 2H, -CH<sub>2</sub>-indole ring), 1.88-1.79 (m, 4H, -CH<sub>2</sub>-), 1.43-1.21 (m, 19H, -CH<sub>2</sub>-, -CH<sub>3</sub>). EI-MS (*m/z*, % int.): 458.6 [M<sup>+</sup>, 4]. FT-IR (KBr) ν<sub>max</sub>: 3355, 3054, 2928, 2857, 1614, 1553, 1481.

*3-propargyloxy-indole-3-carbinol (19)*. Compound **2** (200 mg, 0,86 mmol) was dissolved in 1 mL propargyl alcohol, 0,5 mL 10% NaOH was added. The mixture was stirred for 24h at room temperature (TLC: (C<sub>6</sub>H<sub>5</sub>)CH<sub>3</sub>/AcOEt, 5:1). The reaction mixture was then poured onto crushed ice and extracted with diethyl ether (3 x 30 mL). The extract was washed with water (3 x 50 mL), brine (100 mL), and dried over KOH (pellets). The solvent was evaporated under reduced pressure to afford the crude product, which was purified over silica gel ((C<sub>6</sub>H<sub>5</sub>)CH<sub>3</sub>/AcOEt, 5:1).

Yellow oil, yield 75%. <sup>1</sup>H NMR (300 MHz, CDCl<sub>3</sub>, TMS, ppm): δ<sub>H</sub> = 8.13 (s, 1H, NH), 7.75 (d, 1H, 7-H), 7.32 (d, 1H, 4-H), 7.21-7.12 (m, 2H, 5-H, 6-H), 7.17 (s, 1H, 2-H), 4.84 (s, 2H, -CH<sub>2</sub>O-), 4.16 (s, 2H, -CH<sub>2</sub>-CCH), 2.47 (s, 1H, -C≡CH). EI-MS (*m/z*, % int.): 185 (M<sup>+</sup>, 40). FT-IR (KBr) ν<sub>max</sub>: 3396, 3052, 2922, 2854, 2095, 1720, 1455.

Azides **20-23** were obtained according to (Krchová et al. 2013).

*General procedure for the preparation of compounds 24-27*. Compound **19** was dissolved in CH<sub>2</sub>Cl<sub>2</sub>:H<sub>2</sub>O (10 mL, 1:1) and was stirred for 24 h. After that, to the mixture, an appropriate azide **20-23** (1.3 mmol for **20** and **21**; 1.5 mmol for **22** and **23**), CuSO<sub>4</sub>·5H<sub>2</sub>O (5 mg, catalytic amount), and sodium ascorbate (13 mg, catalytic amount) in 1 mL water were added. The solution was stirred at room temperature for seven days and monitored by TLC. The mixture was washed by diethyl ether (3 x 15 mL) and extracted with dichloromethane (3 x 15 mL). The extract was washed by water (3 x 50 mL), brine (100 mL), and dried over anhydrous Na<sub>2</sub>SO<sub>4</sub>. The solvent was evaporated under reduced pressure to obtain brown oils.

*2-(3-(4-(((1H-indol-3-yl)methyl)-1H-1,2,3-triazol-1-yl)propyl)isoindoline-1,3-dione (24)*.

Brown oil, yield 35 %. <sup>1</sup>H NMR (400 MHz, CDCl<sub>3</sub>, TMS, ppm): δ<sub>H</sub> = 10.11 (s, 1H, NH), 8.00 (s, 1H, triazole ring), 7.84-7.82 (d, 4H, ArH phthalimide), 7.75-7.71 (d, 4H, 4-H, 7-H), 7.21 (s, 1H, 2-H), 5.29 (s, 2H, triazole ring-CH<sub>2</sub>-O-), 4.75 (s, 2H, -O-CH<sub>2</sub>-indole ring), 4.37 (t, 2H,

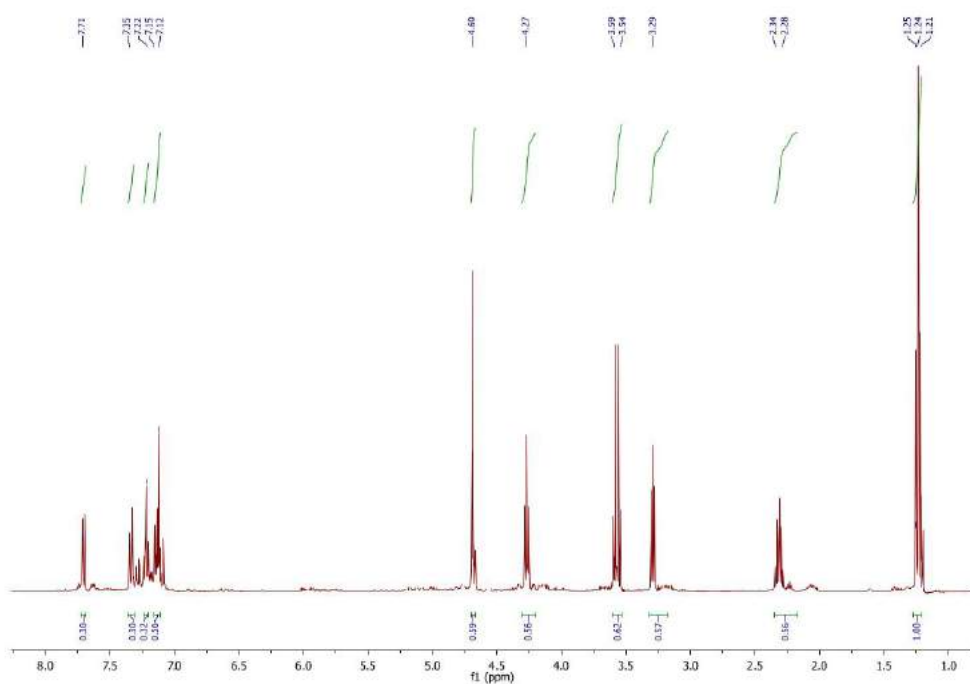


$N_{\text{phthalimid-CH}_2-}$ ), 3.72 (t, 2H,  $-\text{CH}_2\text{-N}_{\text{triazol}}$ ), 2.30 (m, 2H,  $-\text{CH}_2-$ ). EI-MS ( $m/z$ , % int.): 414.7 [ $\text{M}^+$ , 2]. FT-IR (KBr)  $\nu_{\text{max}}$ : 3402, 2880, 2818, 1770, 1709, 1613, 1460, 1399, 1365, 1189.

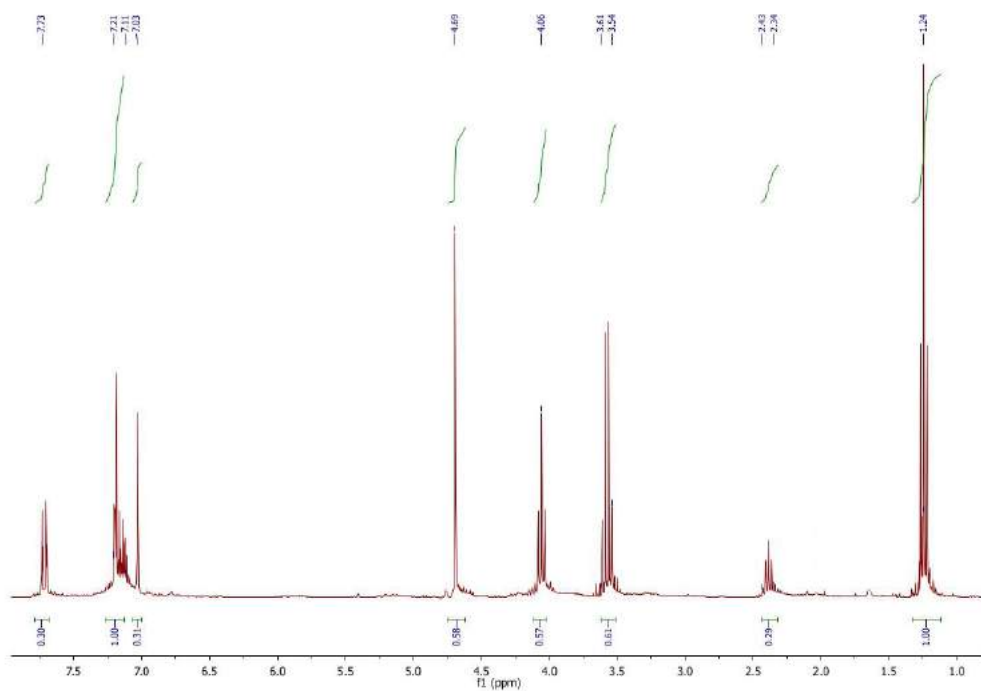
*2-(5-(4-(((1H-indol-3-yl)metoxy)methyl)-1H-1,2,3-triazol-1-yl)pentyl)isoindoline-1,3-dione* (**25**). Brown oil, yield 21 %.  $^1\text{H}$  NMR (400 MHz,  $\text{CDCl}_3$ , TMS, ppm):  $\delta_{\text{H}}$  = 10.08 (s, 1H, NH), 8.02 (s, 1H, triazole ring), 7.83-7.80 (d, 4H, ArH phthalimide), 7.71-7.67 (d, 4H, 4-H, 7-H), 7.18 (s, 1H, 2-H), 5.29 (s, 2H, triazole ring- $\text{CH}_2\text{-O-}$ ), 4.65 (s, 2H,  $-\text{O-CH}_2\text{-indole ring}$ ), 4.29 (t, 2H,  $N_{\text{phthalimid-CH}_2-}$ ), 3.65 (t, 2H,  $-\text{CH}_2\text{-N}_{\text{triazol}}$ ), 2.17 (m, 2H,  $-\text{CH}_2-$ ), 1.90 (m, 2H,  $-\text{CH}_2-$ ), 1.25 (m, 2H,  $-\text{CH}_2-$ ). EI-MS ( $m/z$ , % int.): 441.2 [ $\text{M}^+$ , 4]. FT-IR (KBr)  $\nu_{\text{max}}$ : 3272, 2946, 2866, 1770, 1706, 1609, 1458, 1437, 1398, 1187.

*2-(8-(4-(((1H-indol-3-yl)metoxy)methyl)-1H-1,2,3-triazol-1-yl)octyl)isoindoline-1,3-dione* (**26**). Brown oil, yield 15 %.  $^1\text{H}$  NMR (400 MHz,  $\text{DMSO-}d_6$ , TMS, ppm):  $\delta_{\text{H}}$  = 9.94 (s, 1H, NH), 8.04 (s, 1H, triazole ring), 7.86-7.83 (d, 4H, ArH phthalimide), 7.59-7.50 (d, 4H, 4-H, 7-H), 7.06 (s, 1H, 2-H), 4.97 (s, 2H, triazole ring- $\text{CH}_2\text{-O-}$ ), 4.52 (s, 2H,  $-\text{O-CH}_2\text{-indole ring}$ ), 4.32 (t, 2H,  $N_{\text{phthalimid-CH}_2-}$ ), 3.56 (t, 2H,  $-\text{CH}_2\text{-N}_{\text{triazol}}$ ), 3.37 (m, 2H,  $-\text{CH}_2-$ ), 2.98 (m, 2H,  $-\text{CH}_2-$ ), 1.70 (m, 2H,  $-\text{CH}_2-$ ), 1.60 (m, 2H,  $-\text{CH}_2-$ ), 1.36 (m, 2H,  $-\text{CH}_2-$ ), 1.26 (m, 2H,  $-\text{CH}_2-$ ). EI-MS ( $m/z$ , % int.): 484.4 [ $\text{M}^+$ , 6]. FT-IR (KBr)  $\nu_{\text{max}}$ : 3413, 2933, 2857, 1770, 1708, 1613, 1462, 1397, 1328, 1244.

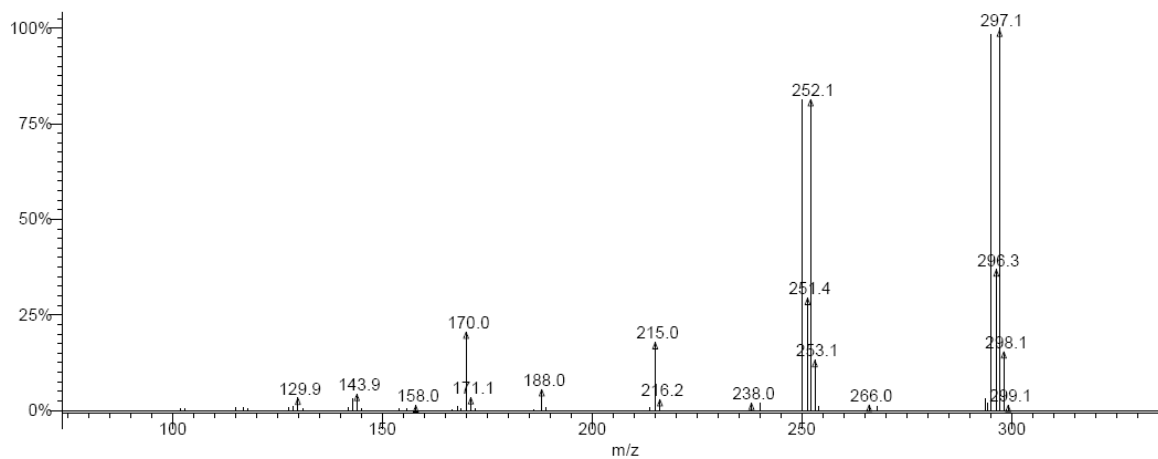
*(12-(4-(((1H-indol-3-yl)metoxy)methyl)-1H-1,2,3-triazol-1-yl)dodecyl)isoindoline-1,3-dione* (**27**). Brown oil, yield 5 %.  $^1\text{H}$  NMR (400 MHz,  $\text{CDCl}_3$ , TMS, ppm):  $\delta_{\text{H}}$  = 10.11 (s, 1H, NH), 8.05 (s, 1H, triazole ring), 7.84-7.81 (d, 4H, ArH phthalimide), 7.71-7.69 (d, 4H, 4-H, 7-H), 7.07 (s, 1H, 2-H), 5.30 (s, 2H, triazole ring- $\text{CH}_2\text{-O-}$ ), 4.79 (s, 2H,  $-\text{O-CH}_2\text{-indole ring}$ ), 4.32 (t, 2H,  $N_{\text{phthalimid-CH}_2-}$ ), 3.53 (t, 2H,  $-\text{CH}_2\text{-N}_{\text{triazol}}$ ), 3.40 (m, 2H,  $-\text{CH}_2-$ ), 3.25 (m, 2H,  $-\text{CH}_2-$ ), 1.86 (m, 2H,  $-\text{CH}_2-$ ), 1.76 (m, 2H,  $-\text{CH}_2-$ ), 1.65 (m, 2H,  $-\text{CH}_2-$ ), 1.49 (m, 2H,  $-\text{CH}_2-$ ), 1.41 (m, 8H,  $-\text{CH}_2-$ ). EI-MS ( $m/z$ , % int.): 527.5 [ $\text{M}^+ - \text{CH}_2$ , 2]. FT-IR (KBr)  $\nu_{\text{max}}$ : 3419, 2929, 2843, 1769, 1707, 1613, 1459, 1397, 1337, 1189.



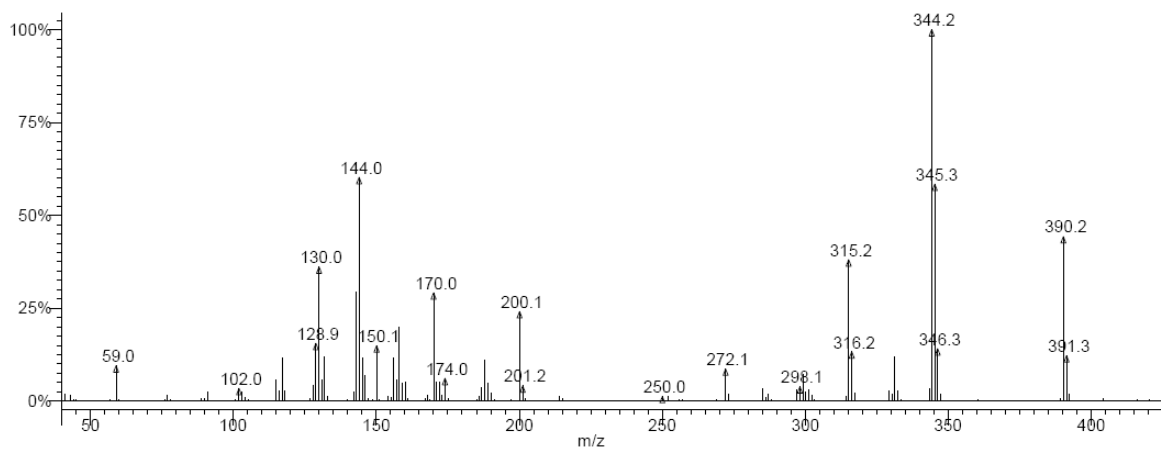
**Figure S1.  $^1\text{H}$  NMR spectrum of compound 4.**



**Figure S2.  $^1\text{H}$  NMR spectrum of dimeric compound 8.**



**Figure S3a. EI-MS spectrum of compound 4.**



**Figure S3b. EI-MS spectrum of dimeric compound 8.**

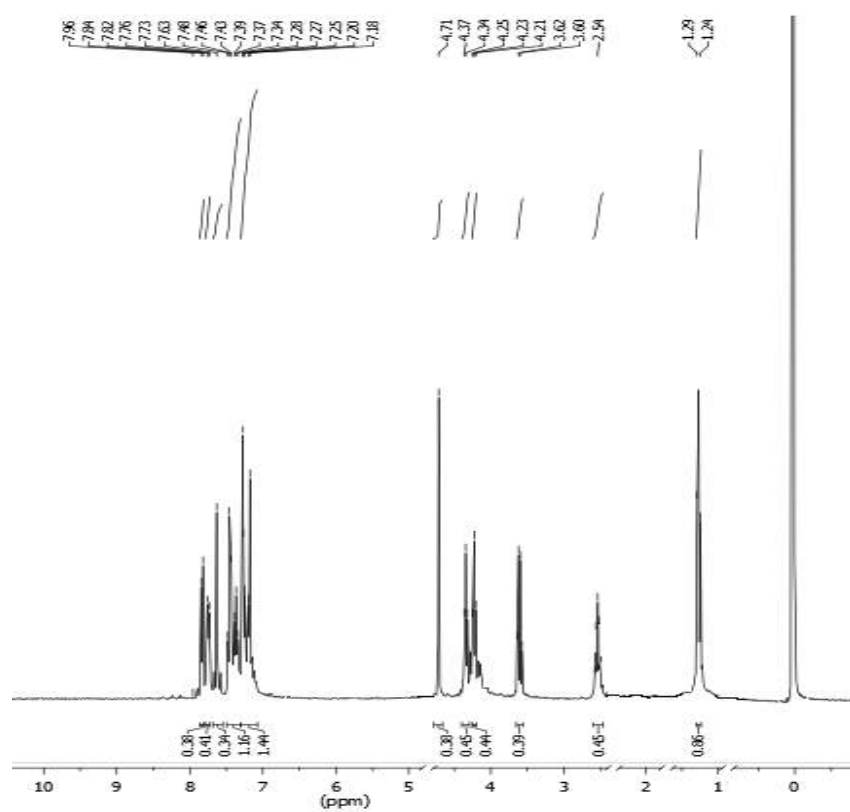


Figure S4.  $^1\text{H}$  NMR spectrum of compound 15.

### ***Biological assay***

#### ***Human red blood cells (RBC)***

Fresh human RBC suspensions were purchased from the blood bank in Poznan according to the bilateral agreement no. ZP/907/1002/18. The cells were washed three times (3000 rpm, 10 min, 4 °C) in 7.4 pH phosphate-buffered saline (PBS - 137 mM NaCl, 2.7 mM KCl, 10 mM Na<sub>2</sub>HPO<sub>4</sub>, 1.76mM KH<sub>2</sub>PO<sub>4</sub>) supplemented with 10 mM glucose. After washing, RBC were suspended in the PBS buffer at 1.65 x 10<sup>9</sup> cells/mL, stored at 4 °C, and used within 5 h.

#### ***Haemolysis assay***

RBC (1.65 x 10<sup>8</sup> cells/mL, ~1.5% haematocrit) were incubated in PBS (7.4 pH) supplemented with 10 mM glucose and containing derivatives tested at concentration equal to 0.1 mg/mL for 60 min at 37°C in a in a thermo-shaker. Samples with RBC incubated in PBS without compounds tested were taken as the controls. Each sample was repeated three times, and the experiments were repeated three times using RBC from different donors. After incubation, the RBC suspensions were centrifuged (3000 rpm, 10 min, 4°C), and the degree of haemolysis was estimated by measuring the absorbance of the supernatant at 540 nm. The results were expressed as the percentage (%) of haemolysis, which was determined using the following formula:

$$\text{haemolysis (\%)} = (\text{sample Ab} - \text{negative control Ab}) / (\text{positive control Ab} - \text{negative control Ab}) \times 100$$

where the negative control means samples with RBC in PBS, the positive control means samples with PBS replaced by ice-cold distilled water.

#### ***Erythrocyte shape determination***

The following incubation, as above, RBC were fixed in 5% paraformaldehyde (PFA) plus 0.01% glutaraldehyde (GA) for 1 h at room temperature. The fixed cells were washed by exchanging the supernatant with PBS buffer, settled on poly-L-lysine-treated (0.1 mg/mL, 10 min, room temperature) cover glasses, and mounted on 80% glycerol. The coverslips were sealed with nail polish. A large number of cells in several separate experimental samples were studied using a RED-233 MOTIC microscope (63 x objective, 10 x ocular). Images were acquired using a Motica 3.0 MP microscopic camera and the program Motic Images Plus 3.0. The shapes of RBC in every sample were estimated according to the Bessis classification (Bessis et al. 1973).

#### ***Inhibition of oxidative-haemolysis***

RBC (1.65 x 10<sup>8</sup> cells/mL, ~1.5% haematocrit) were pre-incubated in PBS buffer (pH 7.4) supplemented with 10 mM glucose, and containing derivatives at the concentration equal to

0.1 mg/mL for 20 minutes at 37 °C in a shaking water bath. After pre-incubation, the standard free radicals inducer 2,2'-azobis(2-methylpropionamidine)dihydrochloride (AAPH) were added to get the final concentration equal to 60 mM. Samples were incubated for the next 4 hours at 37 °C in a thermo-shaker. RBC incubated in PBS only and in the presence of AAPH, were taken as a control. After incubation, the RBC suspensions were centrifuged (3000 rpm, 10 min, 4 °C), and the degree of haemolysis was determined by measuring the absorbance values (Ab) of the supernatants at 540 nm. The percentage of oxidative haemolysis inhibition was calculated using the following equation:

$$\text{Inhibition of haemolysis(\%)} = 100 - [(Ab_{\text{sample}} - Ab_{\text{blank}} / Ab_{\text{control}} - Ab_{\text{blank}})] \times 100$$

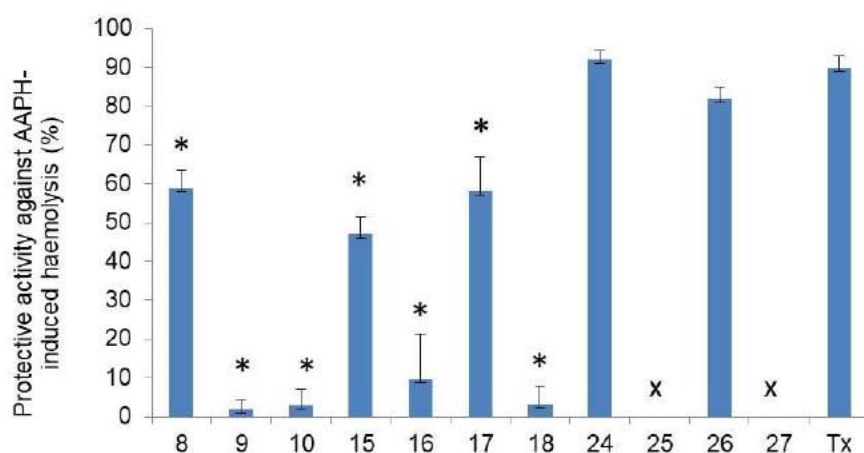
where  $Ab_{\text{sample}}$  is the absorbance value of supernatant obtained from samples incubated with compounds tested,  $Ab_{\text{blank}}$  is the absorbance of the supernatant obtained from samples without compounds tested and without AAPH, and  $Ab_{\text{control}}$  is the absorbance of the supernatant obtained from samples with AAPH and in the absence of compound tested.

Each sample was repeated three times, and the experiments were repeated three times using RBC from different donors.

**Table S1.** Effects of compounds on RBCs membrane permeability (haemolysis) and RBC shape. Incubation conditions: 0.1 mg/mL, 60 min, 37° C

Compound	Haemolysis (%) 60 min	RBCs dominated shape
<b>control (PBS)</b>	1.52±1.30	D,DE
<b>8</b>	2.08±1.29	D,DE
<b>9</b>	2.47±1.65	D,DE
<b>10</b>	1.80±1.32	D,DE
<b>15</b>	2.12±1.76	D,DE
<b>16</b>	1.79±0.94	DE,E
<b>17</b>	2.50±1.68	D,DE
<b>18</b>	2.82±2.03	D,DE
<b>24</b>	1.02±0.56	DE,E
<b>25</b>	1.38±0.70	S
<b>26</b>	1.26±0.35	S
<b>27</b>	6.40±2.40	S
<b>Trolox (Tx)</b>	1.09±0.41	D,DE

Haemolysis values lower than 5% means no haemolytic activity of compounds; abbreviations of dominated RBCs shape: D-discocytes, DE-discoechinocytes, E-echinocytes, S-stomatocytes



**Figure S5.** Protective activity of derivatives and standard antioxidant Trolox (Tx) against AAPH-induced haemolysis. Incubation conditions: pre-incubation with compounds at 0.1 mg/mL for 20 min at 37° C, incubation with 60 mM AAPH for 240 min at 37° C; means values  $\pm$  SD are presented (n=9). X - no cytoprotective activity; \* - the significant difference as compared to Trolox ( $p < 0.05$ ).

### *Statistical analysis*

Data presented are shown as mean values  $\pm$  standard deviation (SD) (n = 9). Statistically significant differences were assessed by applying a paired Student's *t*-test and were considered statistically significant at  $p < 0.05$ .

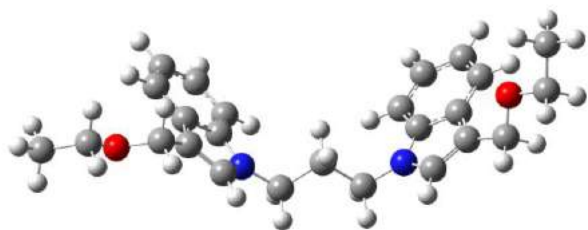


### *Calculation*

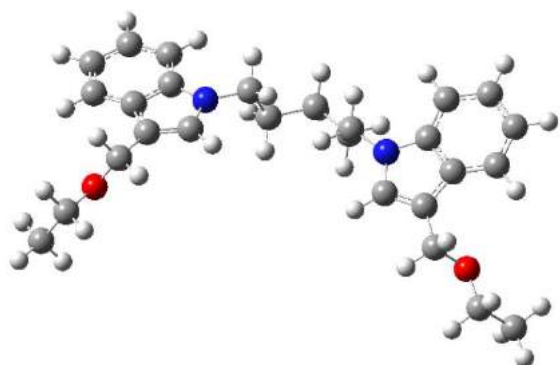
The DFT calculations were performed using the Gaussian 09 program package (Frisch et al. 2009). The calculations employed the B3LYP exchange-correlation functional, which combines the hybrid functional of Becke (Becke et al. 1997). with the gradient-correlation function of Lee (Lee et al. 1988) and the split-valence polarized 6-311G(d,p) basis set (Hehre et al. 1989).

**Table S2.** Selected parameters of investigated compounds **8-10**, **15-18**, and **24-27** estimated by B3LYP/6-311G(d,p) calculations.

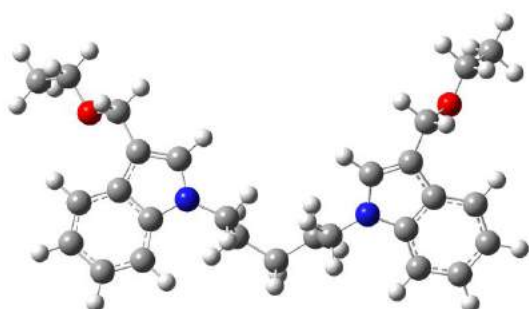
<b>Compound</b>	<b>Parameters</b>	
	<b>Energy (a.u)</b>	<b>Dipol moment (Debye)</b>
<b>8</b>	-1230.713714	3.4925
<b>9</b>	-1309.343263	1.0518
<b>10</b>	-1427.298480	3.2879
<b>15</b>	-1147.028173	2.2068
<b>16</b>	-1225.661378	5.3643
<b>17</b>	-1343.583298	6.5947
<b>18</b>	-1500.869152	3.8216
<b>24</b>	-1388.550507	6.0594
<b>25</b>	-1506.496486	7.1761
<b>26</b>	-1585.129722	6.8779
<b>27</b>	-1742.392641	5.4308



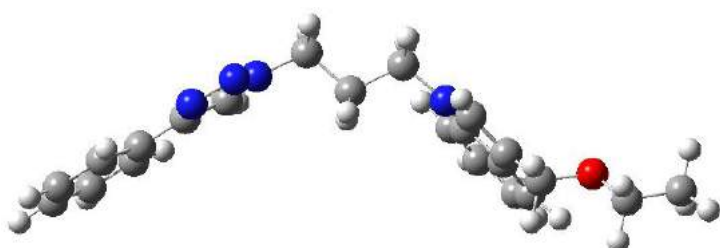
**Compound 8**



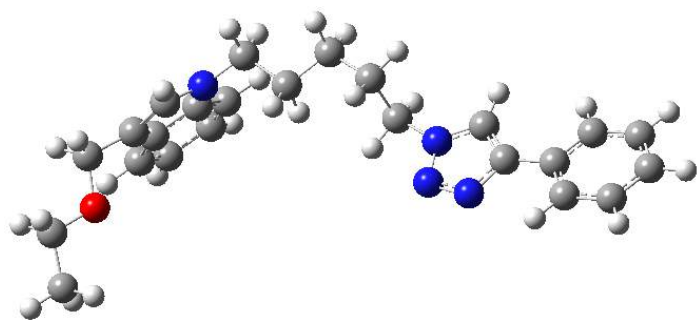
**Compound 9**



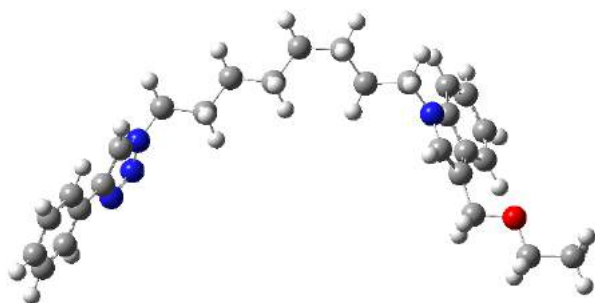
**Compound 10**



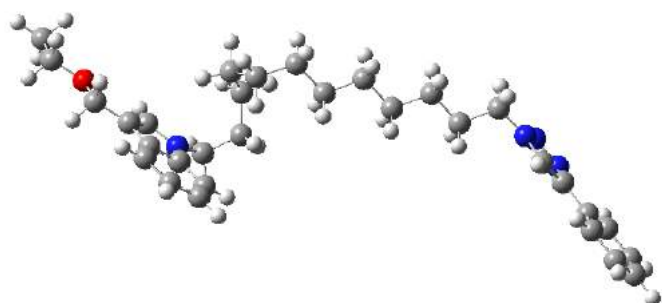
**Compound 15**



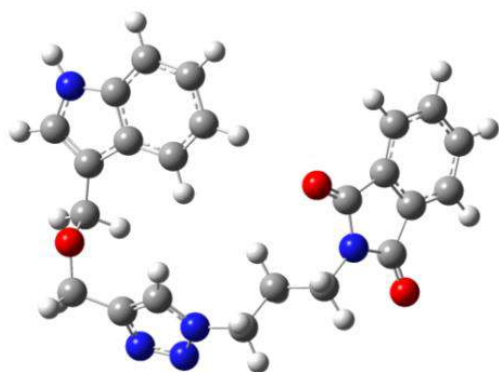
**Compound 16**



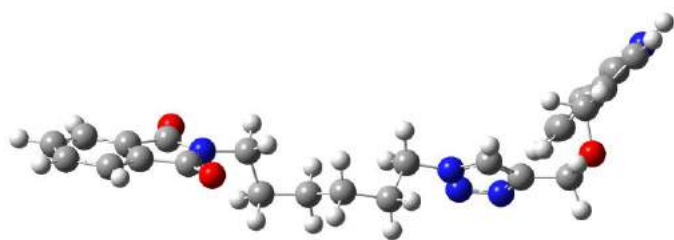
**Compound 17**



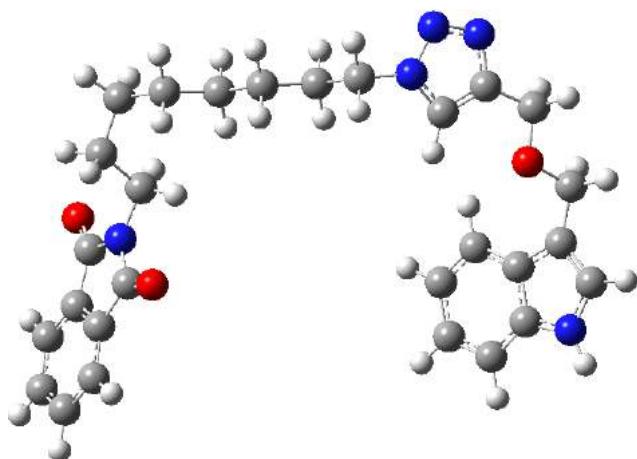
**Compound 18**



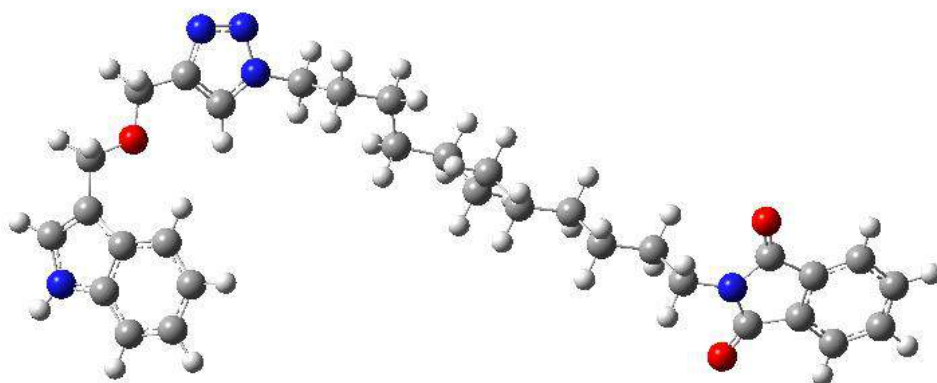
**Compound 24**



**Compound 25**



**Compound 26**

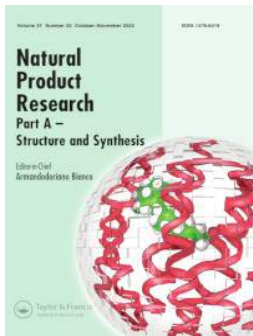


**Compound 27**

**Figure S6. Structures of compounds calculated by the B3LYP/6-311G (d,p) method.**

## References

- Becke ADJ. 1997. Density-functional thermochemistry. V. Systematic optimization of exchange-correlation functional. *J Chem Phys.* 107(20):8554-8560 (and ref. cited therein)
- Bessis M, Weed RI, Lablond PF. 1973. Red cell shape. In: *Physiology, Pathology, Ultrastructure.* Springer-Verlag New York, Heidelberg, Berlin.
- Frisch M, Trucks GW, Schlegel HB, Scuseria GE, Robb MA, Cheeseman JR, Scalmani G, Barone V, Mennucci B, Petersson GA, Nakatsuji H, Caricato M, Li X, Hratchian HP, Izmaylov AF, Bloino J, Zheng G, Sonnenberg JL, Hada M, Ehara M, Toyota K, Fukuda R, Hasegawa J, Ishida M, Nakajima T, Honda Y, Kitao O, Nakai H, Vreven T, Montgomery Jr JA, Peralta JE, Ogliaro F, Bearpark M, Heyd JJ, Brothers E, Kudin KN, Staroverov VN, Kobayashi R, Normand J, Raghavachari K, Rendell A, Burant JC, Iyengar SS, Tomasi J, Cossi M, Rega N, Millam JM, Klene M, Knox JE, Cross JB, Bakken V, Adamo C, Jaramillo J, Gomperts R, Stratmann RE, Yazyev O, Austin AJ, Cammi R, Pomelli C, Ochterski JW, Martin RL, Morokuma K, Zakrzewski VG, Voth GA, Salvador P, Dannenberg JJ, Dapprich S, Daniels AD, Farkas O, Foresman JB, Ortiz JV, Cioslowski J, Fox DJ. 2009. Gaussian 09, Revision D.01, Gaussian, Inc., Wallingford CT.
- Hehre WJ, Random L, Schleyer PVR, Pople JA. 1989. *Ab Initio Molecular Orbital Theory,* Wiley, New York
- Krchová T, Kotek J, Jiráček D, Havlíčková J, Cisařová I, Hermann P. 2013. Lanthanide(III) complexes of aminoethyl-DO3A as PARACEST contrast agents based on decoordination of the weakly bound amino group. *Dalton Trans.* 42:15735-15747.
- Lee C, Yang W, Parr RG. 1988. Development of the Colle-Salvetti correlation-energy formula into a functional of the electron density. *Phys Rev. B* 37(2):785-789.



# Natural Product Research

Formerly Natural Product Letters

ISSN: (Print) (Online) Journal homepage: <https://www.tandfonline.com/loi/gnpl20>


## Novel gramine-based bioconjugates obtained by click chemistry as cytoprotective compounds and potent antibacterial and antifungal agents

Natalia Berdzik, Beata Jasiewicz, Kamil Ostrowski, Arleta Sierakowska, Milda Szlaużys, Damian Nowak & Lucyna Mrówczyńska


To cite this article: Natalia Berdzik, Beata Jasiewicz, Kamil Ostrowski, Arleta Sierakowska, Milda Szlaużys, Damian Nowak & Lucyna Mrówczyńska (26 Sep 2023): Novel gramine-based bioconjugates obtained by click chemistry as cytoprotective compounds and potent antibacterial and antifungal agents, Natural Product Research, DOI: [10.1080/14786419.2023.2261139](https://doi.org/10.1080/14786419.2023.2261139)

To link to this article: <https://doi.org/10.1080/14786419.2023.2261139>

 View supplementary material 

 Published online: 26 Sep 2023.

 Submit your article to this journal 

 View related articles 

 View Crossmark data 



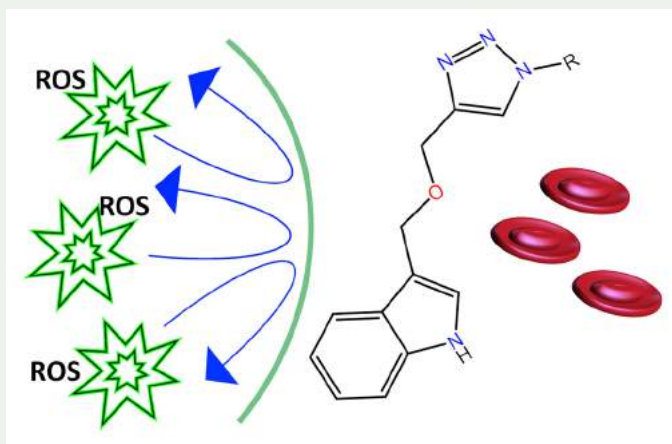
## Novel gramine-based bioconjugates obtained by click chemistry as cytoprotective compounds and potent antibacterial and antifungal agents

Natalia Berdzik<sup>a</sup>, Beata Jasiewicz<sup>a</sup>, Kamil Ostrowski<sup>a</sup>, Arleta Sierakowska<sup>a</sup>, Milda Szlauzys<sup>a</sup>, Damian Nowak<sup>b</sup> and Lucyna Mrówczyńska<sup>c</sup>

<sup>a</sup>Department of Bioactive Compounds, Adam Mickiewicz University, Poznań, Poland; <sup>b</sup>Department of Quantum Chemistry, Adam Mickiewicz University, Poznań, Poland; <sup>c</sup>Department of Cell Biology, Adam Mickiewicz University, Poznań, Poland

### ABSTRACT

A series of indole-1,4-disubstituted-1,2,3-triazole conjugates were synthesised by click chemistry. The haemolytic properties and cytoprotective activity of all the newly synthesised indole-triazole conjugates were tested *in vitro*. In addition, molecular docking was performed *in silico* for the selected conjugates to determine their antibacterial and antifungal properties. The results indicate that indole-triazole derivatives effectively protect human erythrocytes against free radical-induced haemolysis in a structure-dependent manner and that bis-indole-bis-triazole derivatives with alkyl linkers are excellent cytoprotective agents against oxidative haemolysis. The tested series of indole-1,4-disubstituted-1,2,3-triazole conjugates may have an affinity for the active sites of specific protein domains (PDB IDs: 2Q85 and 5V5Z) according to molecular docking studies.





### ARTICLE HISTORY

Received 31 May 2023  
Accepted 13 September 2023

### KEYWORDS

Gramine; indole-triazole conjugate; human erythrocytes; oxidative stress; cytoprotective activity; molecular docking

**CONTACT** Beata Jasiewicz  [beatakoz@amu.edu.pl](mailto:beatakoz@amu.edu.pl)

 Supplemental data for this article can be accessed online at <https://doi.org/10.1080/14786419.2023.2261139>.

© 2023 Informa UK Limited, trading as Taylor & Francis Group

## 1. Introduction

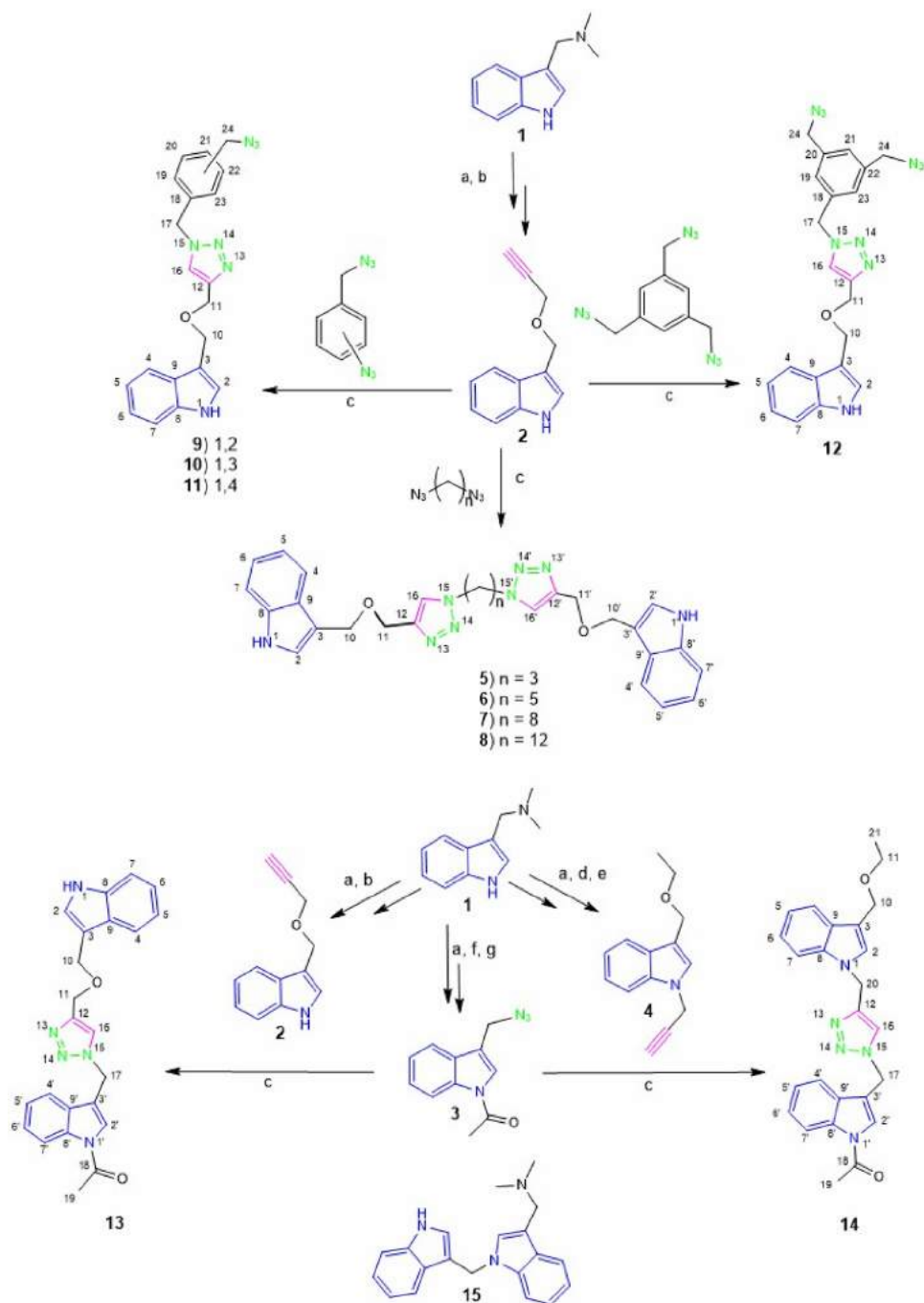
Reactive oxygen species (ROS) are products of the incomplete reduction of oxygen molecules (Hajam et al. 2022) and are involved in many cellular processes (Parcheta et al. 2021). Chronic oxidative stress induced by high levels of ROS may contribute to the induction of lifestyle diseases (Hajam et al. 2022). Despite the wide range of natural and endogenous antioxidants, there is a growing interest in the synthesis of new bioactive compounds with antioxidant properties. *N*-heterocyclic compounds such as indoles and triazoles play an important role in the pharmaceutical industry. Synthetic indole derivatives with remarkable antioxidant properties include indole hydrazones (Demurtas et al. 2019) and indole-3-acetamides (Kanwal et al. 2021). Antioxidant properties are also found in triazole analogues (Alam 2022). The combination of indole and triazole pharmacophores in a single molecule is a promising strategy for the development of new compounds with improved biological efficacy (Danne et al. 2018). As shown in our previous work (Kozanecka-Okupnik et al. 2022; Jasiewicz et al. 2023) selected C-3 substituted indole compounds effectively protect against AAPH (2,2'-azobis (amidinopropane dihydrochloride)-induced oxidative haemolysis of human erythrocytes. Human erythrocytes (red blood cells, RBC) are an excellent model to study free radical-induced oxidative damage in the cell membrane and to evaluate the antioxidant activity of new compounds. The action of free radicals on the RBC membrane results in peroxidation of membrane proteins and lipids and an increase in membrane permeability, leading to ROS-dependent oxidative haemolysis (Srouf et al. 2000). In our previous work (Kozanecka-Okupnik et al. 2022), we showed that the protective activity of triazole-based gamine derivatives is influenced by the length of the alkyl linker, the position of the triazole group in the indole moiety and additional functional groups. In order to determine which structural factor is most important, we synthesised a series of novel indole-triazole derivatives containing at least one triazole ring and one or more indole moieties and evaluated their protective properties against oxidative haemolysis. In addition, docking studies were performed to determine their potential antibacterial and antifungal properties. By combining *in vitro* and *in silico* studies, we characterise the multilevel biological activity of a new series of indole-1,4-disubstituted-1,2,3-triazole conjugates.

## 2. Results and discussion

### 2.1. Chemistry

Compound **2** was synthesised from gamine (**1**) according to reported procedures (Kozanecka-Okupnik et al. 2022). *N*-Acetyl-3-azidemethylindole (**3**) was synthesised in a reaction of *N*-acetyl-3-hydroxy-methylindole with DPPA, while compound **4** was obtained in a reaction of 3-etoxyindole-3-carbinol with propargyl bromide. Bioconjugates **5-14** were synthesised using Cu(I)-catalysed alkyne/azide cycloadditions (Scheme 1). The azide substrates were prepared from appropriate dibromoalkanes, dibromoxylenes, or 1,3,5-tris(bromomethyl)benzene by reaction with sodium azide. The reaction of alkyl azides with compound **2** afforded compounds **5-8** containing two indole moieties and two triazole rings linked by an alkyl linker. The reaction of aryl azides with





**Scheme 1.** Synthesis of indole derivatives **2-15**.

compound **2**, regardless of the molar ratio of substrates (1:1, 2:1 or 3:1), gave derivatives with one triazole ring and one indole group (compounds **9-12**). The combination of propargyl derivatives **2** or **4** with azide derivative **3** gave bis-indole compounds **13** and **14**. Compound **15** was obtained by the published method (Thesing 1954).

The structures of the new compounds were confirmed by spectral data (Figures S1–S10 in the Supplementary). In the  $^1\text{H}$  NMR spectra of compounds **5–14**, signals at 8.40 to 6.95 ppm correspond to protons from the indole moiety, triazole ring and benzene ring (compounds **9–12**). Conjugates with triazole ring (compounds **5–13**) show characteristic proton signals (NH) at about 11 ppm. The  $\text{CH}_3$  groups give singlet signals at 2.60 ppm for compound **13** and 2.51 ppm for compound **14**. The  $^{13}\text{C}$  NMR spectra of compounds **5–14** show characteristic signals in the range 146.05–109.50 which are assigned to carbon atoms from the indole and triazole rings. The carbon atoms of the carbonyl groups (for compounds **13** and **14**) are observed at 168.41 ppm and 168.37 ppm, respectively. The appearance of absorption bands at  $3050\text{ cm}^{-1}$  is attributed to  $=\text{CH}$  (triazole) stretching frequencies. Absorption bands at  $2100\text{ cm}^{-1}$  (compounds **9–12**) and  $1700\text{ cm}^{-1}$  (compounds **13** and **14**) confirmed the presence of  $-\text{N}_3$  and  $-\text{C}=\text{O}$  groups in the structure of the synthesised compounds.

## 2.2. Biological activity

Assessing the haemolytic activity of new compounds is one of the most important methods for evaluating their haemobiocompatibility (Jasiewicz et al. 2021). Haemolysis of red blood cells is explained by the incorporation of various molecules into the lipid bilayer of the red blood cell membrane, resulting in an increase in membrane permeability to ions. Compounds that induce haemolysis of 5% or more of the RBC in the sample at a given concentration are not haemobiocompatible (Farag and Alagawany 2018). The haemolytic activity of the derivatives was evaluated at a concentration of 0.1 mg/mL. No haemolytic activity was confirmed for compounds with the alkyl linker, namely compounds **5**, **7** and **8** (from  $2.89\% \pm 1.02$  to  $3.13\% \pm 0.91$ , respectively), and compounds with the benzene ring, namely compounds **10** and **11** ( $2.13\% \pm 0.80$  and  $2.95\% \pm 1.25$ , respectively). Compounds **13** and **14**, are also haemocompatible at the concentration used ( $4.98\% \pm 1.97$  and  $4.2\% \pm 1.52$ , respectively). On the other hand, compounds **6** ( $5.94\% \pm 2.25$ ), **9** ( $6.17\% \pm 2.89$  SD), and **12** ( $8.84\% \pm 3.47$  SD), were not haemobiocompatible in this study. Interestingly, the haemolytic activity of gramine dimer **15** ( $37.75\% \pm 2.54$  SD) was significantly higher than that of gramine ( $2.92\% \pm 1.02$ ). Our previous work (Kozanecka-Okupnik et al. 2022) showed that selected indole-triazole conjugates at concentrations of 0.1 mg/mL did not induce significant structural modification in the RBC membrane and protect RBC against free radical-induced haemolysis. In order to compare the cytoprotective properties of our new compounds with the previous ones, the same concentration (0.1 mg/mL) was used to assess their cytoprotective activity. As shown in Figure S11, all new indole-triazole conjugates (**5–14**) exhibit higher cytoprotective activity (ranging from  $47.81\% \pm 10.56$  to  $84.06\% \pm 3.17$ ) than the parent gramine ( $30\% \pm 2.00$ ) (Jasiewicz et al. 2021). Bis-indole-bis-triazole derivatives with an alkyl linker (**5–7**) are the most effective cytoprotective agents with activity ranging from  $80.60\% \pm 12.56$  to  $84.06\% \pm 3.17$ , assuming the highest values ( $>80\%$ ) for compounds with a propyl (**5**), pentyl (**6**), and octyl (**7**) linker. The results indicate that compounds **5–7** protect RBC against free radical-induced haemolysis as effectively ( $p > 0.05$ ) as the standard Trolox ( $83.42\% \pm 2.87$ ). The cytoprotective activity of compounds with a benzene ring (**9–12**) is lower

(in the range from  $63.93\% \pm 13.88$  to  $73.19\% \pm 7.04$ ) and decreases in the following order **9** > **10** = **11** > **12**. A comparison of the bis-indole triazole compounds **13** and **14** shows differences in their cytoprotective properties ( $69.66\% \pm 13.88$  versus  $47.81\% \pm 10.58$ ). The antiradical activity of indole derivatives is related to aromatic indole systems with an NH group. Free radicals are neutralised when the indole rings initially transfer hydrogen or electrons to free radicals (HAT and SET mechanisms, respectively), forming a resonance-stabilised indolyl radical (Silveira et al. 2013). As shown in our previous work (Jasiewicz et al. 2023), an essential element of the structure of indole derivatives that significantly affects their cytoprotective efficacy is the nature of the functional groups present at the C-3 position. The electron-rich triazole ring, linked to the indole system by an electron-donating ether group at the C-3 position, makes derivatives **5-13** effective cytoprotective compounds under oxidative stress. Furthermore, compounds **5-13** can become resonance-stabilised radicals as a result of the loss of a hydrogen atom from the  $-\text{CH}_2-\text{O}-\text{CH}_2-$  groups. Such loss of a hydrogen atom from the methylene group has been previously described for other C-3 substituted indoles (Jasiewicz et al. 2021). In addition, compounds **5-13** can interact with the hydrophobic and/or hydrophilic domain of cell membrane components through hydrogen bonding. Since the NH group is the active redox centre of indole, the substitution of the nitrogen atoms of the indole rings may be responsible for the lower cytoprotective activity of compound **14**. Furthermore, unlike **13**, derivative **14** does not have an ether group in its structure. Gramine dimer **15** has no cytoprotective activity due to its very high haemolytic activity ( $37.74\% \pm 2.54$ ) at a concentration of 0.1 mg/mL.

### 2.3. ADME analysis

The SwissADME web server was used to determine the ADME (absorption, distribution, metabolism and excretion) profile of compounds **5-14**. As shown in Table S1 (Supplementary part), most of the compounds fulfil Lipinski's rule of five: molecular weight  $\leq 500$ , number of hydrogen bond donors  $\leq 5$ , number of hydrogen bond acceptors  $\leq 10$  and LogP values  $\leq 5$ . Of all the compounds tested, compound **8** is the most lipophilic (log P 5.96). The log *p* value of the other derivatives range from 1.83 to 4.57, indicating that they can interact with the lipid bilayer of the cell membrane.

### 2.4. Docking study

The potential antibacterial and antifungal activity of compounds **5**, **7**, **10**, **11**, and **13** was determined in a docking study. Molecular docking studies reveal potential interactions between a ligand and a macromolecular target and estimate the ligand-receptor binding energy. At lower energy levels, the ligand-receptor binding is more stable (Morris and Lim-Wilby 2008; Nowak et al. 2023). Figures S12(a-f) (Supplementary part) show the probable binding mechanisms of the ligands to the 2Q85 and 5V5Z protein domains (PDB IDs). The binding energies are comparable to one another (Table S2, Supplementary part). These statistics indicate that the affinity for the selected protein domain is significant.

The synthesis, biological experiments and molecular docking study are described in the [supplementary material](#).

### 3. Conclusions

In conclusion, bis-indole-bis-triazole compounds with a propyl (**5**), pentyl (**6**) and octyl (**7**) linkers showed significant cytoprotective activity *in vitro* by inhibiting oxidative haemolysis of human erythrocytes. The haemocompatible compound **5** with propyl linker and a molecular weight of <500 is the best candidate for future research as a potential new antioxidant. Molecular docking studies show affinity of compounds **5**, **7**, **10**, **11** and **13** to the macromolecular targets. The affinity to 2Q85 and 5V5Z receptors implies that the compounds **5**, **7**, **10**, **11** and **13** have potent antibacterial and antifungal properties.

### Disclosure statement

No potent conflict of interest was reported by the author.

### Funding

This work was financially supported by the funds of Faculty of Chemistry, Adam Mickiewicz University in Poznań, and within the Research Subsidy at the Faculty of Biology of the Adam Mickiewicz University in Poznań.

### References

- Alam MM. 2022. 1,2,3-Triazole hybrids as anticancer agents: review. Arch Pharm (Weinheim). 355(1):e2100158. doi:10.1002/ardp.202100158.
- Danne AB, Choudhari AS, Chakraborty S, Sarkar D, Khedkar VM, Shingate BB. 2018. Triazole-diindolylmethane conjugates as new antitubercular agents: synthesis, bioevaluation and molecular docking. Medchemcomm. 9(7):1114–1130. doi:10.1039/c8md00055g.
- Demurtas M, Baldisserotto A, Lampronti I, Moi D, Balboni G, Pacifico S, Vertuani S, Manfredini S, Onnis V. 2019. Indole derivatives as multifunctional drugs: synthesis and evaluation of antioxidant, photoprotective and antiproliferative activity of indole hydrazones. Bioorg Chem. 85:568–576. doi:10.1016/j.bioorg.2019.02.007.
- Farag MR, Alagawany M. 2018. Erythrocytes as a biological model for screening of xenobiotics toxicity. Chem Biol Interact. 279:73–83. doi:10.1016/j.cbi.2017.11.007.
- Hajam YA, Rani R, Ganie SY, Sheikh TA, Javaid D, Qadri SS, Pramodh S, Alsulimani A, Alkhanani MF, Harakeh S, et al. 2022. Oxidative stress in human pathology and aging: molecular mechanisms and perspectives. Cells. 11(3):552. doi:10.3390/cells11030552.
- Jasiewicz B, Babijczuk K, Warżajtis B, Rychlewska U, Starzyk J, Cofta G, Mrówczyńska L. 2023. Indole derivatives bearing imidazole, benzothiazole-2-thione or benzoxazole-2-thione moieties—synthesis, structure and evaluation of their cytoprotective, antioxidant, antibacterial and fungicidal activities. Molecules. 28(2):708. doi:10.3390/molecules28020708.
- Jasiewicz B, Kozanecka-Okupnik W, Przygodzki M, Warżajtis B, Rychlewska U, Pospieszny T, Mrówczyńska L. 2021. Synthesis, antioxidant and cytoprotective activity evaluation of C-3 substituted indole derivatives. Sci Rep. 11(1):15425. doi:10.1038/s41598-021-94904-z.
- Kanwal, Khan, KM, Chigurupati, S, Ali, F, Younus, M, Aldubayan, M, Wadood, A, Khan, H, Taha, M, Perveen, S. 2021. Perveen, indole-3-acetamides: as potential antihyperglycemic and

- antioxidant agents; synthesis, in vitro  $\alpha$ -amylase inhibitory activity, structure-activity relationship, and in silico studies. *ACS Omega*. 6(3): 2264–2275. doi:[10.1021/acsomega.0c05581](https://doi.org/10.1021/acsomega.0c05581).
- Kozanecka-Okupnik W, Sierakowska A, Berdzik N, Kowalczyk I, Mrówczyńska L, Jasiewicz B. 2022. New triazole-bearing gramine derivatives—synthesis, structural analysis and protective effect against oxidative haemolysis. *Nat Prod Res*. 33:3413–3419.
- Morris GM, Lim-Wilby M. 2008. Molecular docking. *Methods Mol Biol*. 443:365–382. doi:[10.1007/978-1-59745-177-2\\_19](https://doi.org/10.1007/978-1-59745-177-2_19).
- Nowak D, Bachorz RA, Hoffmann M. 2023. Neural networks in the design of molecules with affinity to selected protein domains. *Int J Mol Sci*. 24(2):1762. doi:[10.3390/ijms24021762](https://doi.org/10.3390/ijms24021762).
- Parcheta M, Świsłocka R, Orzechowska S, Akimowicz M, Choińska R, Lewandowski W. 2021. Recent developments in effective antioxidants: the structure and antioxidant properties. *Materials*. 14(8):1984. doi:[10.3390/ma14081984](https://doi.org/10.3390/ma14081984).
- Silveira CC, Mendes SR, Soares JR, Victoria FN, Martinez DM, Savegnago L. 2013. Synthesis and antioxidant activity of new C-3 sulphenyl indoles. *Tetrahedron Lett*. 54(36):4926–4929. doi:[10.1016/j.tetlet.2013.07.004](https://doi.org/10.1016/j.tetlet.2013.07.004).
- Srouf MA, Bilto YY, Juma M, Irhimeh MR. 2000. Exposure of human erythrocytes to oxygen radicals causes loss of deformability, increased osmotic fragility, lipid peroxidation and protein degradation. *Clin Hemorheol Microcirc*. 23:13–21.
- Thesing J. 1954. Beitrage zur Chemie des Indols, 111. Mitteil.: Uber die einwirkung von alkali auf quartare salze des gramins. *Chem Ber*. 87(5):692–699. doi:[10.1002/cber.19540870513](https://doi.org/10.1002/cber.19540870513).

## **Novel gramine-based bioconjugates obtained by click chemistry as cytoprotective compounds and potent antibacterial and antifungal agents**

Natalia Berdzik<sup>a</sup>, Beata Jasiewicz<sup>a\*</sup>, Kamil Ostrowski<sup>a</sup>, Arleta Sierakowska<sup>a</sup>, Milda Szlauzys<sup>a</sup>, Damian Nowak<sup>b</sup> and Lucyna Mrówczyńska<sup>c</sup>

A series of indole-1,4-disubstituted-1,2,3-triazole conjugates were synthesised by click chemistry. The haemolytic properties and cytoprotective activity of all the newly synthesised indole-triazole conjugates were tested *in vitro*. In addition, molecular docking was performed *in silico* for the selected conjugates to determine their antibacterial and antifungal properties. The results indicate that indole-triazole derivatives effectively protect human erythrocytes against free radical-induced haemolysis in a structure-dependent manner and that bis-indole-bis-triazole derivatives with alkyl linkers are excellent cytoprotective agents against oxidative haemolysis. The tested series of indole-1,4-disubstituted-1,2,3-triazole conjugates may have an affinity for the active sites of specific protein domains (PDB IDs: 2Q85 and 5V5Z), according to molecular docking studies.

## Supplementary Material

Chemistry - general experimental information	S2
Synthesis of compound <b>3</b>	S3
Synthesis of compound <b>4</b>	S3
General procedure for the preparation of compounds <b>5-8</b>	S4
General procedure for the preparation of compounds <b>9-12</b>	S5
Synthesis of compound <b>13</b>	S7
Synthesis of compound <b>14</b>	S7
<sup>1</sup> H and <sup>13</sup> C NMR spectra of compound <b>5</b>	S9
<sup>1</sup> H and <sup>13</sup> C NMR spectra of compound <b>6</b>	S10
<sup>1</sup> H and <sup>13</sup> C NMR spectra of compound <b>7</b>	S11
<sup>1</sup> H and <sup>13</sup> C NMR spectra of compound <b>8</b>	S12
<sup>1</sup> H and <sup>13</sup> C NMR spectra of compound <b>9</b>	S13
<sup>1</sup> H and <sup>13</sup> C NMR spectra of compound <b>10</b>	S14
<sup>1</sup> H and <sup>13</sup> C NMR spectra of compound <b>11</b>	S15
<sup>1</sup> H and <sup>13</sup> C NMR spectra of compound <b>12</b>	S16
<sup>1</sup> H and <sup>13</sup> C NMR spectra of compound <b>13</b>	S17
<sup>1</sup> H and <sup>13</sup> C NMR spectra of compound <b>14</b>	S18
Biological activity	S19
Statistical analysis	S20
Cytoprotective activity of compounds - Figure <b>S11</b>	S21
Docking study	S22
The probable binding mechanisms of the ligands (Figs. <b>S12a-f</b> ) to the 2Q85 and 5V5Z protein domains (PDB IDs)	S23
Tables S1 and S2	S26
Reference	S26

### 1. Chemistry - general experimental information

All synthesis reagents were purchased from Sigma-Aldrich. The solvents chloroform, dichloromethane, toluene, dimethylformamide, dimethylsulfoxide, tetrahydrofuran, ethyl acetate and methanol were purchased from commercial sources (Merck, Fisher) and used without purification. IR spectra: FT/IR Nicolet iS5 (KBr pellet, cm<sup>-1</sup>) <sup>1</sup>H and <sup>13</sup>C NMR

spectra: Bruker Avance 600 MHz, Varian VNMR-S 400 MHz. Elemental analysis was carried out on an Elemental Analyzer Vario EL III apparatus to determine the percentage content of nitrogen, carbon and hydrogen.

### Synthesis of compound 3

*N*-acetyl-3-hydroxymethylindole (0.54 mmol) was dissolved in dimethylformamide (2 mL). DPPA in dimethylformamide (1 mL) was then added. The reaction mixture was cooled to 0°C and DBU was added dropwise. The mixture was stirred at 0°C for 2 hours. The reaction was monitored by TLC (PhMe:EtOAc 5:1). Distilled water (5 mL) was added and the reaction mixture was extracted with ethyl acetate, washed with distilled water and brine and dried (anh. Na<sub>2</sub>SO<sub>4</sub>). The organic layer was evaporated to dryness under reduced pressure. The crude was purified by column chromatography (PhMe: EtOAc 50:1).

#### *N*-Acetyl-3-azidemethylindole (3)

Yellow oil, yield 59%. <sup>1</sup>H NMR (400 MHz, CDCl<sub>3</sub>): δ<sub>H</sub> = 8.44 (d, *J* = 8.2 Hz, 1H), 7.59 (d, *J* = 8.2 Hz, 1H), 7.44 (bs, 1H), 7.40–7.30 (m, 2H), 4.49 (d, *J* = 1.0 Hz, 2H, -CH<sub>2</sub>-N<sub>3</sub>), 2.64 (s, 3H, COCH<sub>3</sub>). <sup>13</sup>C NMR (101 MHz, CDCl<sub>3</sub>): δ<sub>C</sub> = 168.36, 136.00, 129.80, 125.83, 123.88, 118.87, 116.77, 46.08, 23.92. FT-IR (KBr, cm<sup>-1</sup>) ν<sub>max</sub>: 3120, 3049, 2928, 2871, 2107, 1706. EI-MS (*m/z*, % int.): 214 (M<sup>+</sup>, 25%).

### Synthesis of compound 4

Crushed KOH (1 mmol) was added to 3-ethoxymethylindole (0.7 mmol), dissolved in dimethylformamide (2 mL). The mixture was stirred for 10 min at room temperature. Propargyl bromide (0.9 mmol) was then added dropwise. The reaction mixture was stirred for 24 hours at room temperature. The reaction was monitored by TLC (PhMe: EtOAc 5:1). The crude product was purified by column chromatography (PhMe: EtOAc 50:1).

#### *3*-(ethoxymethyl)-1-(prop-2-yn-1-yl)-1*H*-indole (4)

Yellow oil, yield 60%. <sup>1</sup>H NMR (400 MHz, CDCl<sub>3</sub>): δ<sub>H</sub> = 7.71 (d, *J* = 7.9 Hz, 1H), 7.38 (d, *J* = 8.2 Hz, 1H), 7.28 – 7.24 (m, 1H), 7.22 (s, 1H), 7.17 (ddd, *J* = 8.0, 7.1, 1.0 Hz, 1H), 4.85 (d, *J* = 2.6 Hz, 2H, -N-CH<sub>2</sub>-), 4.70 (d, *J* = 0.6 Hz, 2H, -CH<sub>2</sub>-O-), 3.58 (q, *J* = 7.0 Hz, 2H, -O-CH<sub>2</sub>-), 2.39 (t, *J* = 2.6 Hz, 1H, -C≡CH), 1.23 (d, *J* = 7.0 Hz, 3H, -CH<sub>2</sub>-CH<sub>3</sub>). FT-IR (KBr, cm<sup>-1</sup>) ν<sub>max</sub>: 3285, 3053, 2972, 2926, 2855, 2122. EI-MS (*m/z*, % int.): 213 (M<sup>+</sup>, 100).



## General procedure for the preparation of compounds 5-8

3-Propalgyloxymethylindole (1 mmol) was dissolved in THF (2 mL). A suitable azide (0.5 mmol) was then added.  $\text{CuSO}_4 \cdot 5\text{H}_2\text{O}$  (5 mg, 0.00002 mmol) and sodium ascorbate (13 mg, 0.00007 mmol) were added in 1 mL of distilled water. The mixture was stirred at room temperature. Subsequent portions of the catalyst were added until the aqueous layer of the reaction mixture turned bluish-green. The reaction was monitored by TLC (PhMe: EtOAc 5:1). A brown solid precipitated when the reaction mixture was stirred. The precipitate was filtered off under reduced pressure, then washed with distilled water and diethyl ether. The precipitate was dried at room temperature.

### *1,3-bis(4-(((1H-indol-3-yl)methoxy)methyl)-1H-1,2,3-triazol-1-yl)propane (5)*

Brown solid, yield 36%, mp 100-105°C.  $^1\text{H}$  NMR (600 MHz,  $\text{DMSO}-d_6$ ):  $\delta_{\text{H}} = 11.02$  (s, 2H, NH), 8.15 (s, 2H, triazole rings), 7.56 (d,  $J=7.9$  Hz, 2H, indole rings), 7.38-7.36 (m, 4H, indole rings), 7.10-7.07 (m, 2H, indole rings) 7.01-6.98 (m, 2H, indole rings), 4.68 (s, 4H), 4.53 (s, 4H,  $-\text{O}-\underline{\text{CH}_2}-$ ), 4.44-4.23 (m, 4H), 1.79-1.72 (m, 2H).  $^{13}\text{C}$  NMR (600 MHz,  $\text{DMSO}-d_6$ ):  $\delta_{\text{C}} = 145.01, 136.25, 126.92, 125.12, 124.18, 121.12, 118.66, 118.60, 111.38, 111.18, 63.41, 61.93, 46.59, 30.05$ . FT-IR (KBr)  $\nu_{\text{max}}$ : 3262, 3138, 3055, 2925, 2858, 1728, 1456. Anal. Calcd for  $\text{C}_{27}\text{H}_{28}\text{N}_8\text{O}_2$  (MW = 496.23): C 65.31, H 5.68, N 22.57; Found: C 65.82, H 5.49, N 22.53%.

### *1,5-bis(4-(((1H-indol-3-yl)methoxy)methyl)-1H-1,2,3-triazol-1-yl)pentane (6)*

Brown solid, yield 39 %, mp 100-105°C.  $^1\text{H}$  NMR (400 MHz,  $\text{DMSO}-d_6$ ):  $\delta_{\text{H}} = 11.03$  (s, 2H, NH), 8.09 (s, 2H, triazole rings), 7.54 (d,  $J=7.9$  Hz, 2H, indole rings), 7.38-7.36 (m, 4H, indole rings), 7.11-7.07 (m, 2H, indole rings) 7.01-6.97 (m, 2H, indole rings), 4.66 (d,  $J=4.0$  Hz, 4H,  $-\underline{\text{CH}_2}-\text{O}-$ ), 4.53 (d,  $J=5.3$  Hz, 4H,  $-\text{O}-\underline{\text{CH}_2}-$ ), 4-36-4.23 (m, 4H), 1-77-1.74 (m, 6H).  $^{13}\text{C}$  NMR (400 MHz,  $\text{DMSO}-d_6$ ):  $\delta_{\text{C}} = 144.66, 136.30, 126.97, 125.21, 123.88, 122.72, 121.19, 118.72, 111.45, 111.20, 63.46, 61.97, 49.08, 34.85, 31.51$ . FT-IR (KBr)  $\nu_{\text{max}}$ : 3395, 3057, 2926, 2859, 1788, 1457. Anal. Calcd. for  $\text{C}_{29}\text{H}_{32}\text{N}_8\text{O}_2$  (MW = 524.26): C 66.39, H 6.15, N 21.36; Found: C 66.18, H 6.24, N 21.28%.

### *1,8-bis(4-(((1H-indol-3-yl)methoxy)methyl)-1H-1,2,3-triazol-1-yl)octane (7)*

Brown solid, yield 19%, mp 90-92°C.  $^1\text{H}$  NMR (600 MHz,  $\text{DMSO}-d_6$ ):  $\delta_{\text{H}} = 11.03$  (s, 2H, NH), 8.12 (s, 2H, triazole rings), 7.53 (d,  $J=7.9$  Hz, 2H, indole rings), 7.38-7.33 (m, 4H, indole rings), 7.10-7.07 (m, 2H, indole rings) 7.00-6.97 (m, 2H, indole rings), 4.66 (d,  $J=2.5$

Hz, 4H,  $-\underline{\text{CH}_2}\text{-O-}$ ), 4.53 (s, 4H,  $-\text{O-}\underline{\text{CH}_2}\text{-}$ ), 4.34-4.28 (m, 8H), 1.77-1.74 (m, 8H).  $^{13}\text{C}$  NMR (600 MHz, DMSO- $d_6$ ):  $\delta_{\text{C}} = 144.69, 136.27, 126.92, 125.10, 123.95, 121.12, 118.64, 118.57, 111.39, 111.18, 63.41, 61.95, 49.29, 29.42, 27.97, 25.51$ . FT-IR (KBr)  $\nu_{\text{max}}$ : 3140, 3055, 2927, 2855, 1800, 1457. Anal. Calcd for  $\text{C}_{32}\text{H}_{38}\text{N}_8\text{O}_2$  (MW = 566.31): C 67.82, H 6.76, N 19.77; Found: C 67.74, H 6.59, N 19.52%.

*1,12-bis(4-(((1H-indol-3-yl)methoxy)methyl)-1H-1,2,3-triazol-1-yl)dodecane (8)*

Brown solid, yield 49 %, mp 100-105°C.  $^1\text{H}$  NMR (400 MHz, DMSO- $d_6$ ):  $\delta_{\text{H}} = 11.03$  (s, 2H, NH), 8.11 (s, 2H, triazole rings), 7.53 (d,  $J=8.2$  Hz, 2H, indole rings), 7.38-7.36 (m, 4H, indole rings), 7.11-7.07 (m, 2H, indole rings) 7.00-6.97 (m, 2H, indole rings), 4.66 (s, 4H,  $-\underline{\text{CH}_2}\text{-O-}$ ), 4.52 (s, 4H,  $-\text{O-}\underline{\text{CH}_2}\text{-}$ ), 4.30 (d,  $J=6.8$  Hz, 8H), 1.77-1.74 (m, 8H) 1.11-1.07 (m, 8H).  $^{13}\text{C}$  NMR (400 MHz, DMSO- $d_6$ ):  $\delta_{\text{C}} = 144.47, 136.35, 125.23, 123.85, 122.99, 121.20, 118.72, 118.66, 111.49, 111.24, 63.46, 61.98, 49.42, 29.61, 28.79, 28.32, 25.76, 25.13$ . FT-IR (KBr)  $\nu_{\text{max}}$ : 3250, 2923, 2851, 1794, 1457. Anal. Calcd. for  $\text{C}_{36}\text{H}_{46}\text{N}_8\text{O}_2$  (MW = 622.37): C 69.43, H 7.44, N 17.99; Found: C 69.26, H 7.28, N 18.08%.

**General procedure for the preparation of compounds 9-12**

3-Propalgyloxymethylindole (1 mmol) was dissolved in DMSO (3 mL). A suitable azide (0.5 mmol) was then added.  $\text{CuSO}_4 \cdot 5\text{H}_2\text{O}$  (5 mg, 0.00002 mmol) and sodium ascorbate (13 mg, 0.00007 mmol) were added in 1 mL of distilled water. The mixture was stirred at room temperature. Further portions of the catalyst were added until the aqueous layer of the reaction mixture turned bluish-green. The reaction was monitored by TLC (PhMe: EtOAc 5:1). A brownish-yellow solid precipitated when the reaction mixture was stirred. The precipitate was filtered under reduced pressure, then washed with distilled water and diethyl ether. The precipitate was dried at room temperature.

*3-(((1-(2-(azidomethyl)benzyl)-1H-1,2,3-triazol-4-yl)methoxy)methyl)-1H-indole (9)*

Brown solid, yield 18%, mp 78-82°C.  $^1\text{H}$  NMR (400 MHz, DMSO- $d_6$ ):  $\delta_{\text{H}} = 11.03$  (s, 1H, NH), 8.12 (s, 1H, triazole ring), 7.53 (d,  $J=8.8$  Hz, 1H, indole ring), 7.37 (s, 1H, indole ring) 7.36 (d,  $J=2.8$  Hz, 1H, indole ring) 7.34-7.32 (m, 2H), 7.12-7.07 (m, 3H), 6.99-6.97 (m, 2H, indole ring), 5.81 (s, 2H), 4.67 (s, 2H,  $-\text{O-}\underline{\text{CH}_2}\text{-}$ ), 4.53 (s, 2H,  $-\underline{\text{CH}_2}\text{-O-}$ ), 2.50 (s, 2H).  $^{13}\text{C}$  NMR (400 MHz, DMSO- $d_6$ ):  $\delta_{\text{C}} = 145.19, 136.81, 134.69, 130.41, 129.48, 129.26, 129.04, 127.48, 125.67, 124.66, 123.56, 121.68, 119.22, 119.13, 111.94, 111.73, 63.97, 62.42, 51.50, 50.28$ . FT-IR (KBr)  $\nu_{\text{max}}$ : 3251, 3056, 2913, 2859, 2098, 1618, 1433. Anal. Calcd. for

C<sub>20</sub>H<sub>19</sub>N<sub>7</sub>O (MW = 373.17): C 64.33, H 5.13, N 26.26; Found: C 64.48, H 5.21, N 26.33%.

*3-(((1-(3-(azidomethyl)benzyl)-1H-1,2,3-triazol-4-yl)methoxy)methyl)-1H-indole (10)*

Brown solid, yield 50 %, mp 110-114°C. <sup>1</sup>H NMR (400 MHz, DMSO-*d*<sub>6</sub>): δ<sub>H</sub> = 11.05 (s, 1H, NH), 8.17 (s, 1H, triazole ring), 8.03 (s, 1H), 7.55 (s, 1H, indole ring), 7.46-7.42 (m, 4H), 7.36 (d, *J*=1.2 Hz, 1H), 7.12-7.09 (m, 1H, indole ring), 7.01-6.98 (m, 1H, indole ring), 5.62 (s, 2H), 4.68 (s, 2H, -O-CH<sub>2</sub>-), 4.54 (s, 2H, -CH<sub>2</sub>-O-), 2.55 (s, 2H). <sup>13</sup>C NMR (400 MHz, DMSO-*d*<sub>6</sub>): δ<sub>C</sub> = 144.64, 136.63, 136.32, 136.18, 129.10, 128.25, 128.12, 127.70, 126.99, 125.18, 123.96, 122.83, 121.19, 118.65, 111.46, 111.24, 63.46, 61.96, 55.03, 53.34. FT-IR (KBr) ν<sub>max</sub>: 3400, 3058, 2929, 2873, 2099, 1611, 1488. Anal. Calcd. for C<sub>20</sub>H<sub>19</sub>N<sub>7</sub>O (MW = 373.17): C 64.33, H 5.13, N 26.26; Found: C 64.30, H 5.28, N 26.22%.

*3-(((1-(4-(azidomethyl)benzyl)-1H-1,2,3-triazol-4-yl)methoxy)methyl)-1H-indole (11)*

Brown solid, yield 40 %, mp 104-106°C. <sup>1</sup>H NMR (400 MHz, DMSO-*d*<sub>6</sub>): δ<sub>H</sub> = 11.03 (s, 1H, -NH), 8.13 (s, 1H, triazole ring), 7.52 (d, *J*=7.8 Hz, 1H, indole ring), 7.38-7.29 (m, 6H), 7.10-7.07 (m, 1H, indole ring), 6.99-6.95 (m, 1H, indole ring), 5.56 (s, 2H), 4.65 (s, 2H, -O-CH<sub>2</sub>-), 4.50 (s, 2H, -CH<sub>2</sub>-O-), 2.50 (s, 2H). <sup>13</sup>C NMR (400 MHz, DMSO-*d*<sub>6</sub>): δ<sub>C</sub> = 144.75, 136.31, 136.00, 135.54, 128.78, 128.29, 126.98, 125.21, 124.02, 121.21, 118.74, 118.65, 111.47, 111.22, 63.47, 61.92, 55.01, 52.38. FT-IR (KBr) ν<sub>max</sub>: 3394, 3244, 3054, 2914, 2858, 2097, 1617, 1457. Anal. Calcd. for C<sub>20</sub>H<sub>19</sub>N<sub>7</sub>O (MW = 373.17): C 64.33, H 5.13, N 26.26; Found: C 64.29, H 5.20, N 26.19%.

*3-(((1-(3,5-bis(azidomethyl)benzyl)-1H-1,2,3-triazol-4-yl)methoxy)methyl)-1H-indole (12)*

Brown solid, yield 12 %, mp 105-110°C. <sup>1</sup>H NMR (400 MHz, DMSO-*d*<sub>6</sub>): δ<sub>H</sub> = 11.02 (s, 1H, NH), 8.12 (d, *J*=7.0 Hz, 1H, triazole ring), 7.53 (d, *J*=7.9 Hz, indole ring) 7.41-7.23 (m, 5H), 7.10-7.07 (m, 1H, indole ring), 7.00-6.96 (m, 1H, indole ring), 5.54 (s, 2H), 4.64 (s, 2H, -O-CH<sub>2</sub>-), 4.50 (s, 2H, -CH<sub>2</sub>-O-), 3.35 (s, 4H). <sup>13</sup>C NMR (400 MHz, DMSO-*d*<sub>6</sub>): δ<sub>C</sub> = 144.72, 137.15, 136.32, 127.35, 126.98, 125.24, 124.12, 121.21, 118.75, 118.66, 111.47, 111.17, 63.52, 61.91, 54.95, 52.33. FT-IR (KBr) ν<sub>max</sub>: 3394, 3241, 3054, 3006, 2861, 2100, 1611, 1457. Anal. Calcd. for C<sub>21</sub>H<sub>20</sub>N<sub>10</sub>O (MW = 428.18): C 58.87, H 4.71, N 32.69; Found: C 58.92, H 4.74, N 32.73%.

### Synthesis of compound 13

*N*-acetyl-3-azidomethylindole (0.3 mmol) and 3-propargyloxymethylindole (0.4 mmol) were dissolved in dichloromethane (5 mL). CuSO<sub>4</sub>·5H<sub>2</sub>O (5 mg, 0.00002 mmol) and sodium ascorbate (13 mg, 0.00007 mmol) were added in 1 mL of distilled water. The mixture was stirred at room temperature. Further portions of the catalyst were added until the aqueous layer of the reaction mixture turned bluish-green. The reaction was monitored by TLC (PhMe: EtOAc 1:1). An orange solid precipitated when the reaction mixture was stirred. The reaction mixture was extracted with ethyl acetate and washed with water and brine. The organic layer was dried (anh.Na<sub>2</sub>SO<sub>4</sub>) and evaporated under reduced pressure. The crude product was purified by column chromatography (gradient elution PhMe: EtOAc 5:1 – PhMe: EtOAc 1:1).

*1-(3-((4-(((1*H*-indol-3-yl)methoxy)methyl)-1*H*-1,2,3-triazol-1-yl)methyl)-1*H*-indol-1-yl)ethanone (13)*

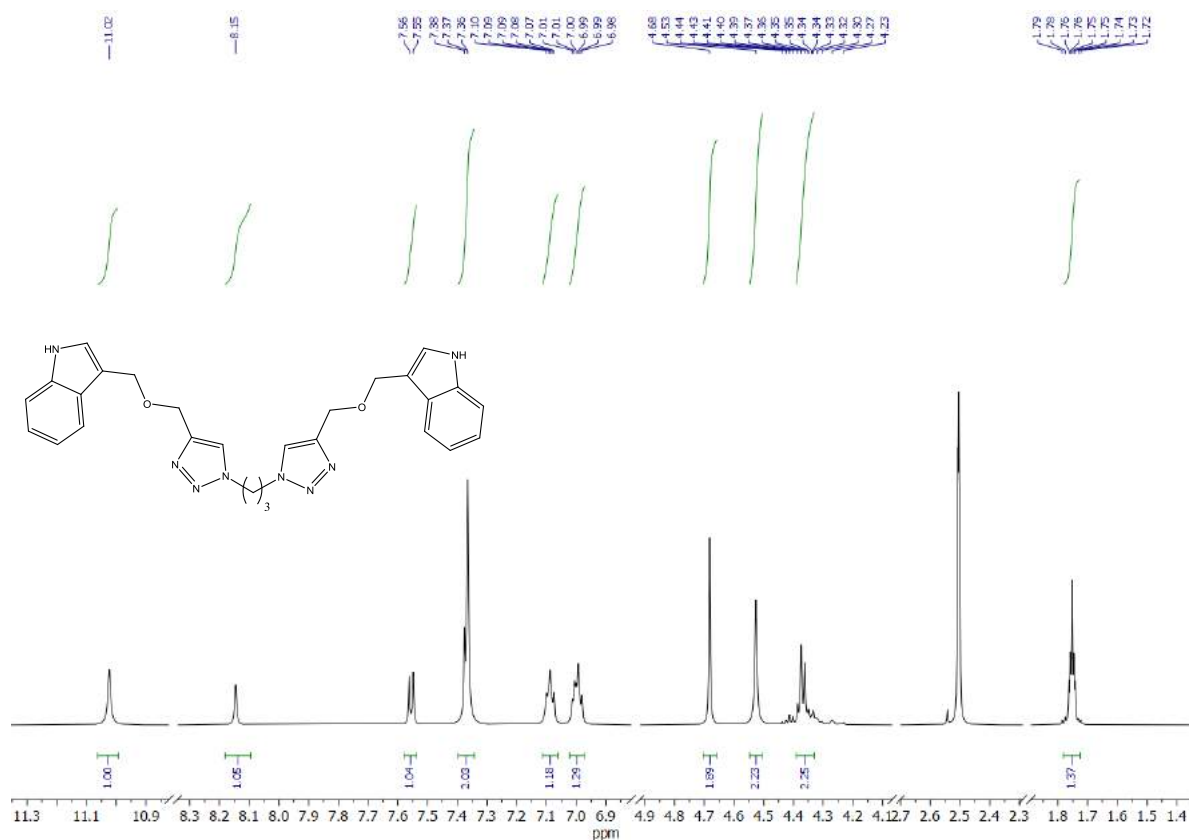
Yellow, thick oil, yield 74%. <sup>1</sup>H NMR (400 MHz, CDCl<sub>3</sub>): δ<sub>H</sub> = 11.01 (s, 1H, NH), δ 8.42 (d, *J* = 8.4 Hz, 2H, indole rings), 8.28 (s, 1H), 7.61-7.06 (m, 10H, indole rings), 5.60 (s, 2H, triazole ring), 4.74 (s, 2H), 4.63 (s, 2H), 2.60 (s, 3H, -CH<sub>3</sub>). <sup>13</sup>C NMR (400 MHz, CDCl<sub>3</sub>): δ<sub>C</sub> = 168.42, 146.05, 136.31, 135.92, 128.43, 127.00, 126.03, 124.75, 124.15, 122.30, 122.23, 119.78, 119.05, 118.65, 116.79, 115.73, 112.48, 111.18, 64.42, 62.92, 45.29, 29.62. FT-IR (KBr) ν<sub>max</sub>: 3401, 3114, 3052, 2924, 2854, 1710. Anal. Calcd. for C<sub>23</sub>H<sub>21</sub>N<sub>5</sub>O<sub>2</sub> (MW = 399.17): C 69.16, H 5.30, N 17.53; Found: C 68.99, H 5.34, N 17.48%.

### Synthesis of compound 14

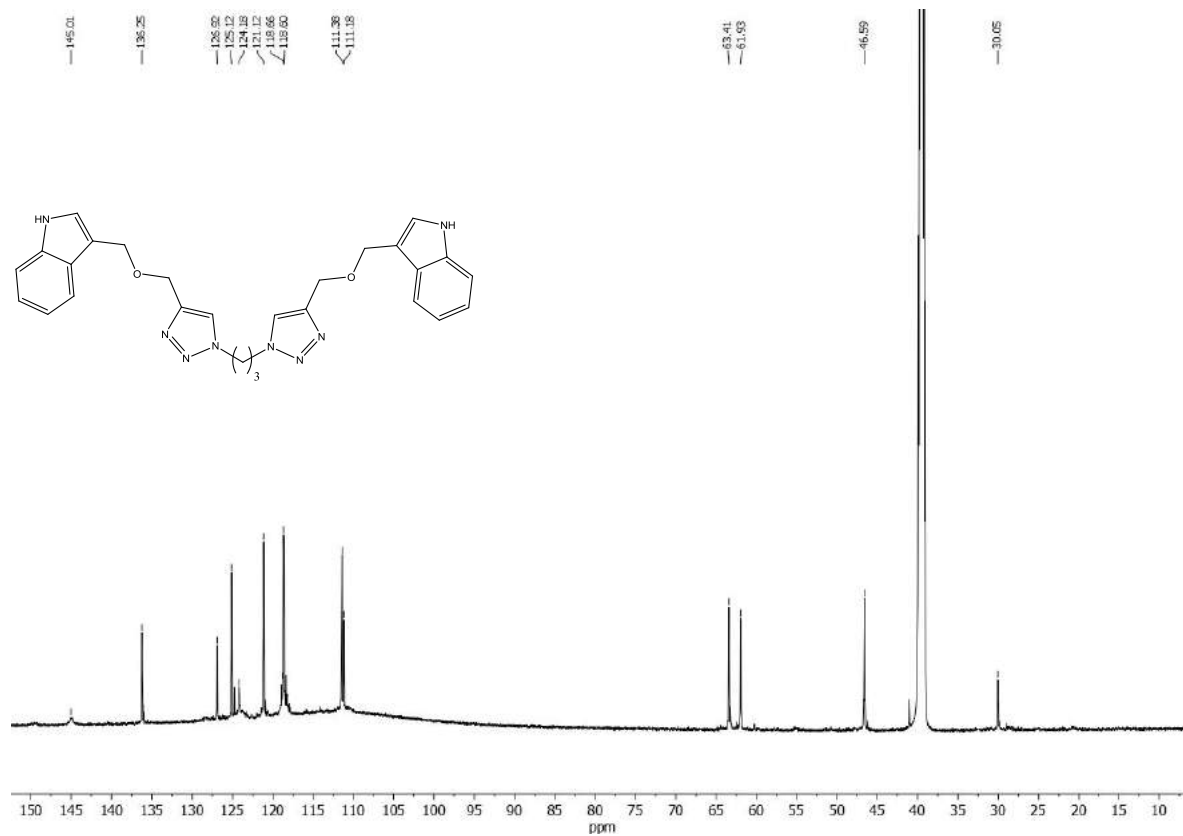
*N*-acetyl-3-azidomethylindole (0.3 mmol) and *N*-propargil-3-etoxyethylindole (0.4 mmol) were dissolved in dichloromethane (5 mL). CuSO<sub>4</sub>·5H<sub>2</sub>O (5 mg, 0.00004 mmol) and sodium ascorbate (13 mg, 0.00007 mmol) were added in 1 mL of distilled water. The mixture was stirred at room temperature. Further portions of the catalyst were added until the aqueous layer of the reaction mixture turned bluish-green. The reaction was monitored by TLC (PhMe: EtOAc 1:1). The reaction mixture was extracted with ethyl acetate and washed with water and brine. The organic layer was dried (anh. Na<sub>2</sub>SO<sub>4</sub>) and evaporated under reduced pressure. The crude product was purified by column chromatography (gradient elution CHCl<sub>3</sub>: EtOAc 5:1 – CHCl<sub>3</sub>: EtOAc 1:1).

*1-(3-((4-((3-(ethoxymethyl)-1H-indol-1-yl)methyl)-1H-1,2,3-triazol-1-yl)methyl)-1H-indol-1-yl)ethanone (14)*

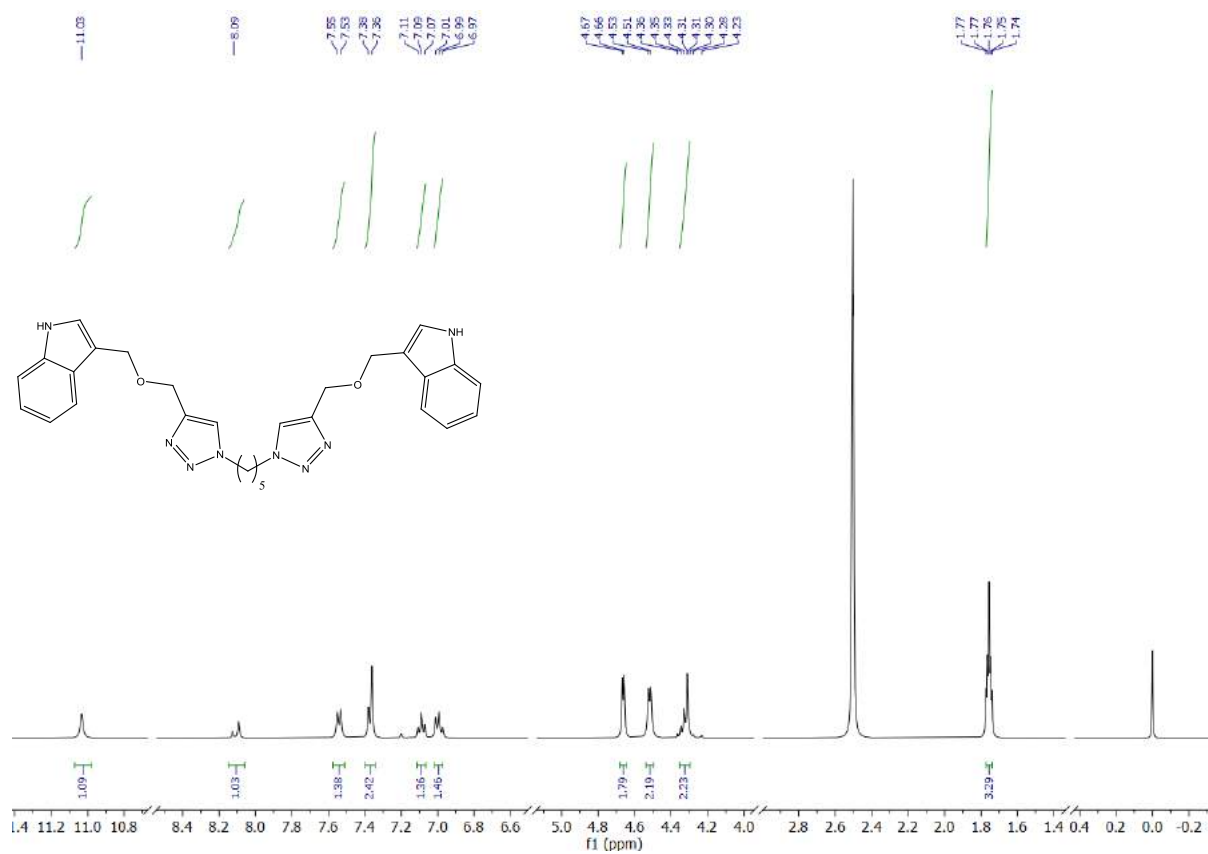
Brown, thick oil, yield 21%. <sup>1</sup>H NMR (400 MHz, CDCl<sub>3</sub>): δ 8.41-8.38 (m, 2H, indole rings), 8.34 (s, 1H), 7.41-7.11 (m, 10H, indole rings), 5.56 (s, 2H), 5.36 (s, 2H), 4.64 (s, 2H), 3.75-3.67 (m, 2H), 2.58 (s, 3H), 2.54-2.52 (s, 3H). <sup>13</sup>C NMR (400 MHz, CDCl<sub>3</sub>): δ<sub>C</sub> = 168.37, 145.13, 136.30, 135.96, 130.90, 128.30, 127.10, 126.10, 124.74, 124.17, 122.18, 121.65, 119.77, 119.55, 118.65, 116.84, 115.50, 113.01, 109.50, 65.46, 64.47, 45.58, 42.06, 29.70, 15.30. FT-IR (KBr) ν<sub>max</sub>: 3435, 3119, 3049, 2955, 1709. Anal. Calcd. for C<sub>25</sub>H<sub>25</sub>N<sub>5</sub>O<sub>2</sub> (MW = 427.20): C 70.24, H 5.89, N 16.38; Found: C 70.32, H 5.92, N 16.41%.



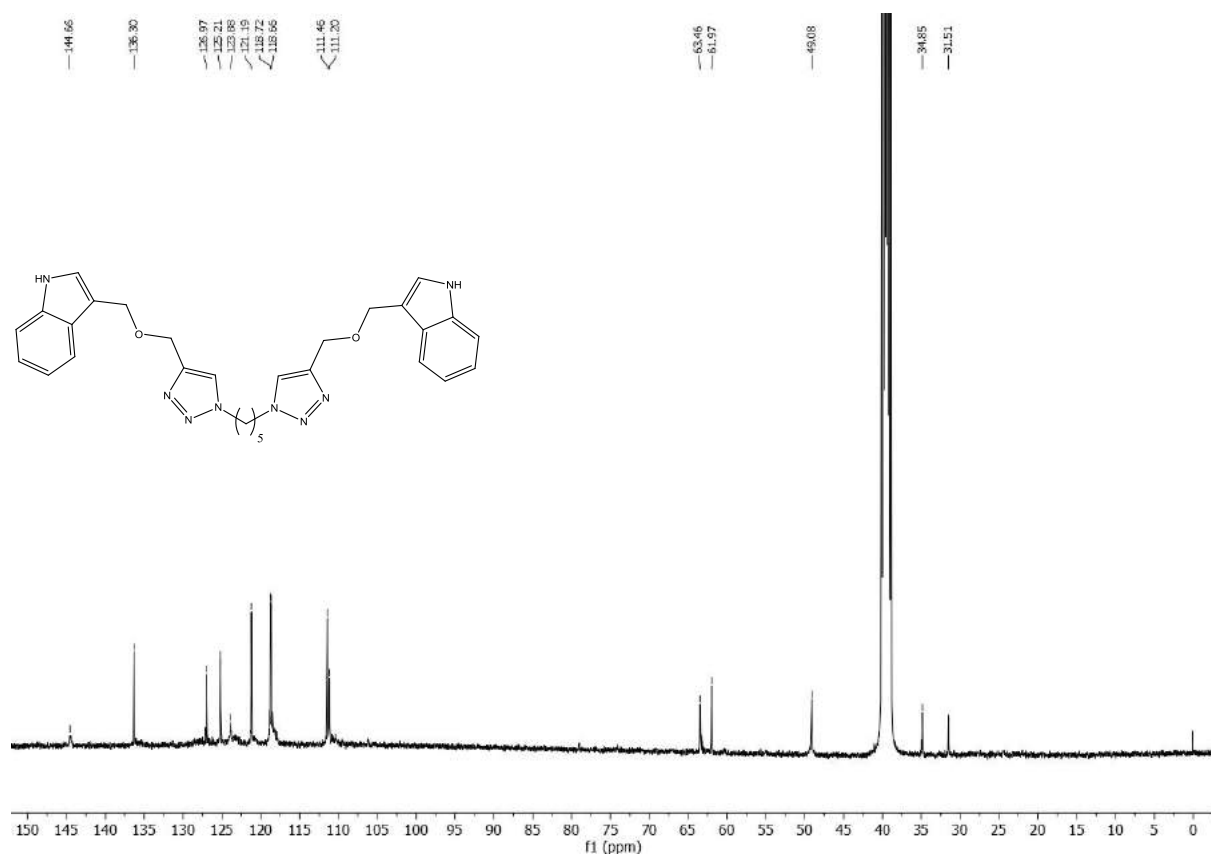
**Fig. S1a.** <sup>1</sup>H NMR spectrum of compound 5



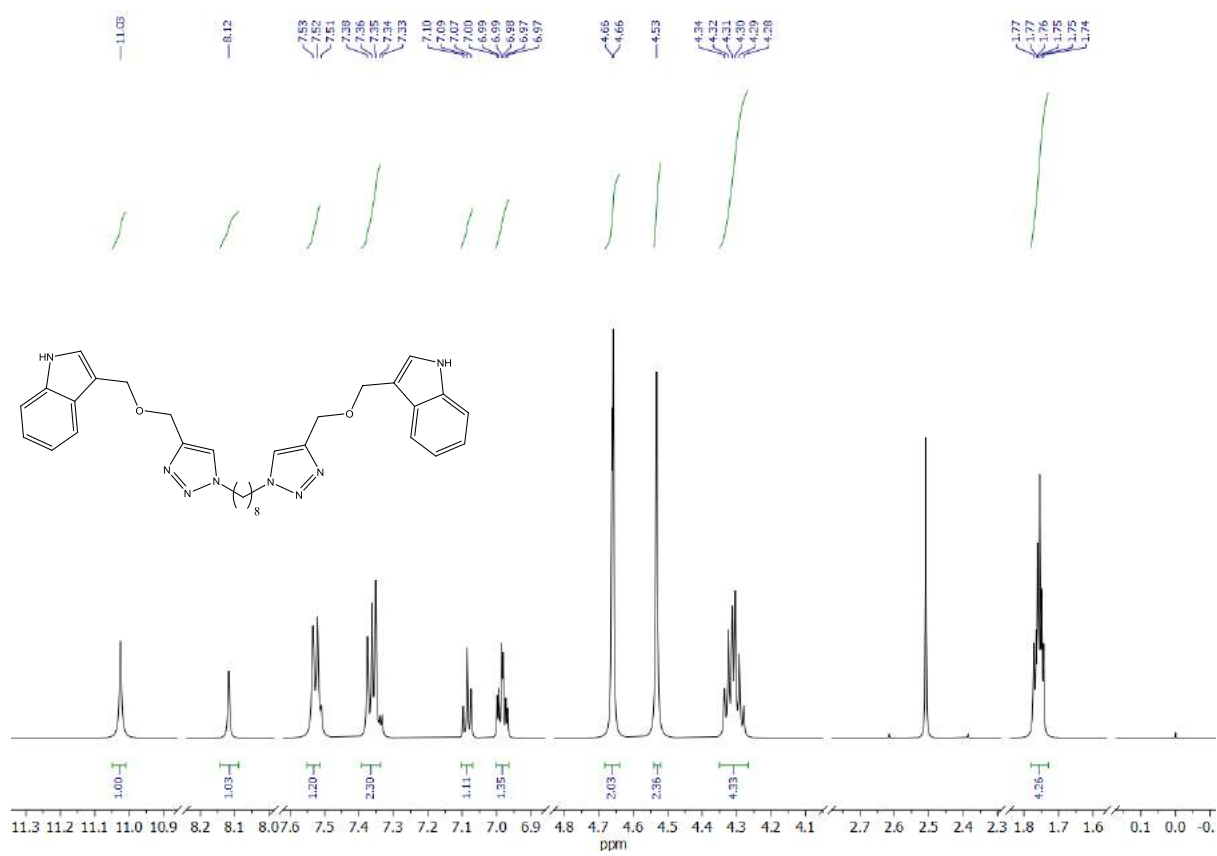
**Fig. S1b.** <sup>13</sup>C NMR spectrum of compound 5



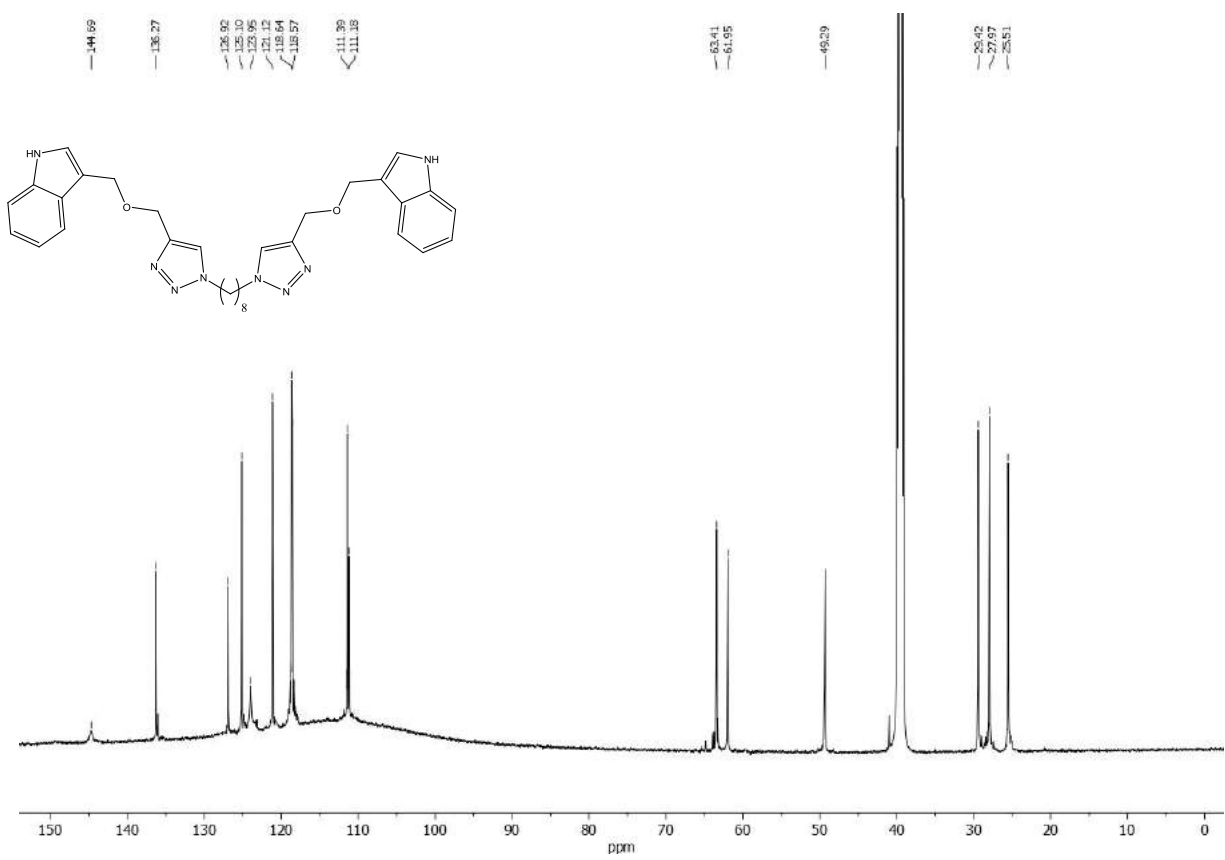
**Fig. S2a.** <sup>1</sup>H NMR spectrum of compound **6**



**Fig. S2b.** <sup>13</sup>C NMR spectrum of compound **6**

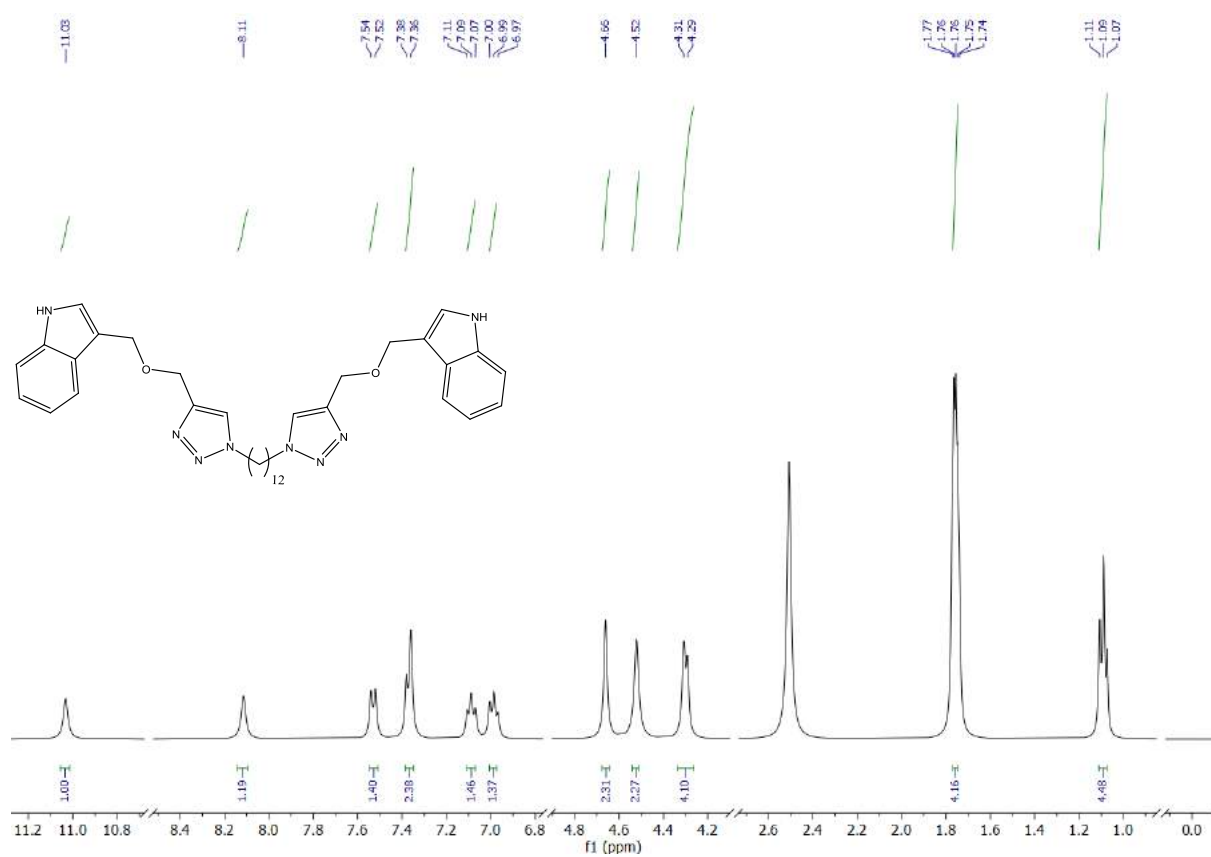


**Fig. S3a.**  $^1\text{H}$  NMR spectrum of compound 7

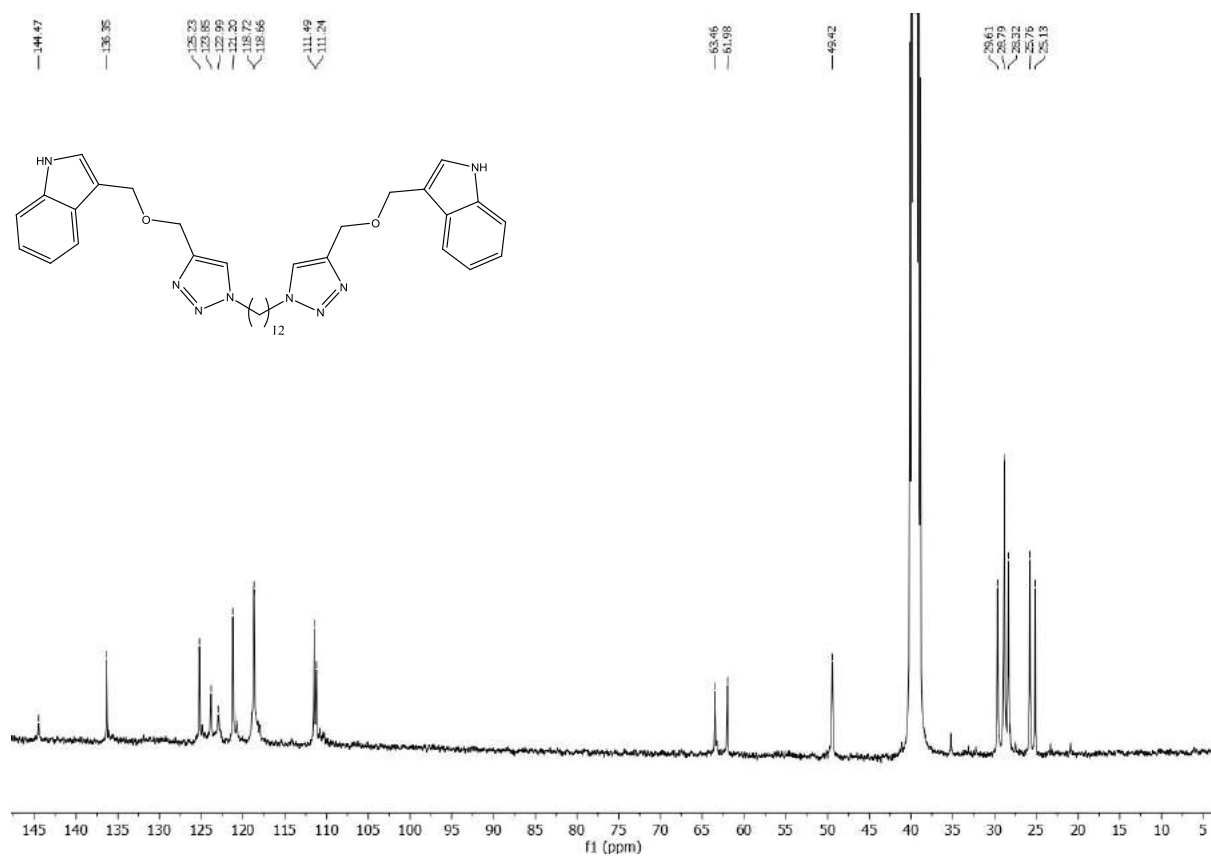


**Fig. S3b.**  $^{13}\text{C}$  NMR spectrum of compound 7

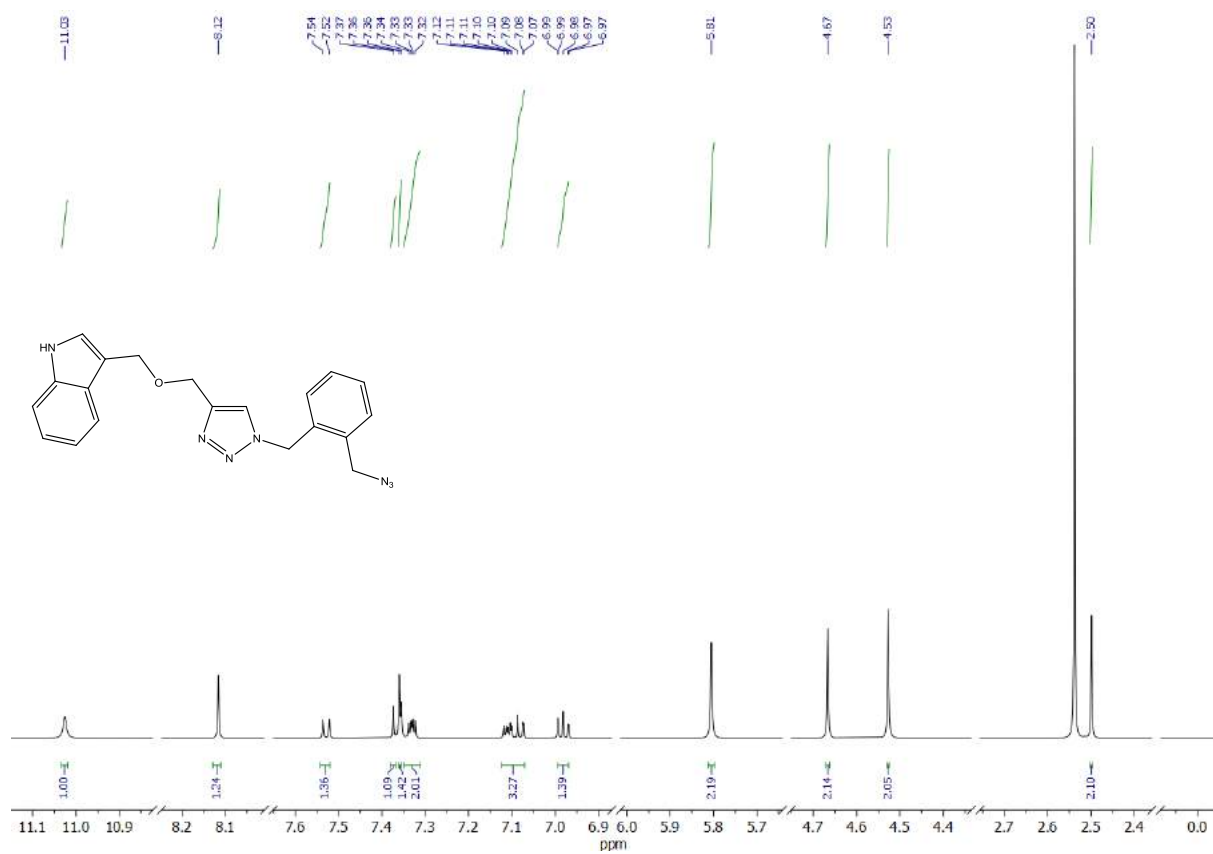




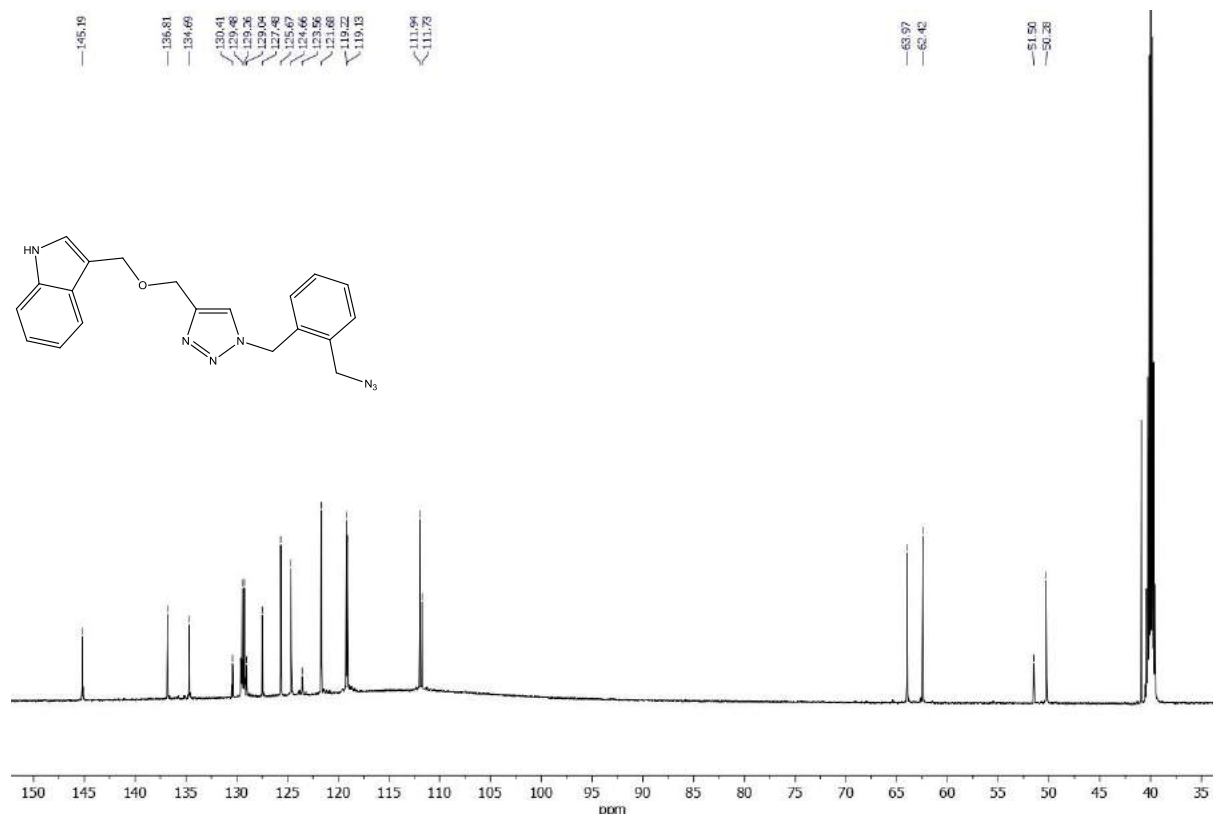
**Fig. S4a.** <sup>1</sup>H NMR spectrum of compound **8**



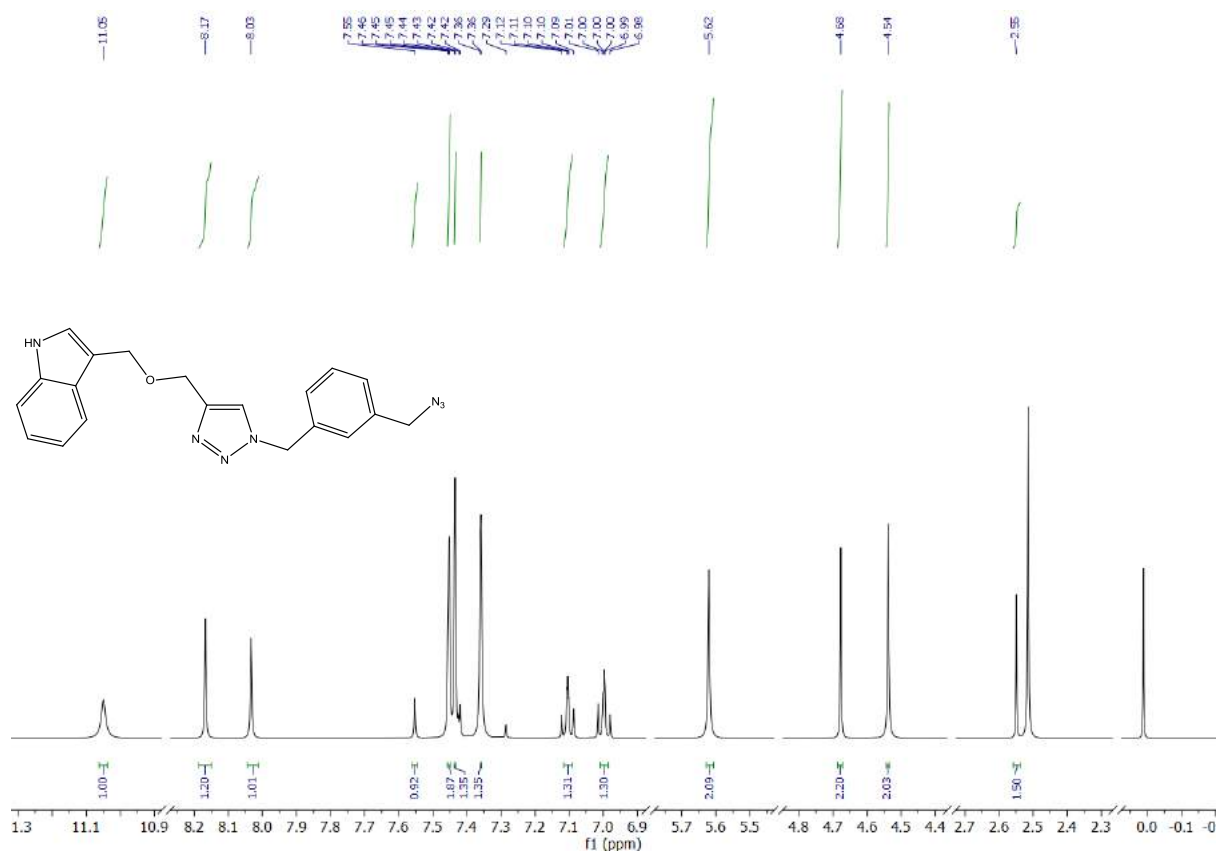
**Fig. S4b.** <sup>13</sup>C NMR spectrum of compound **8**



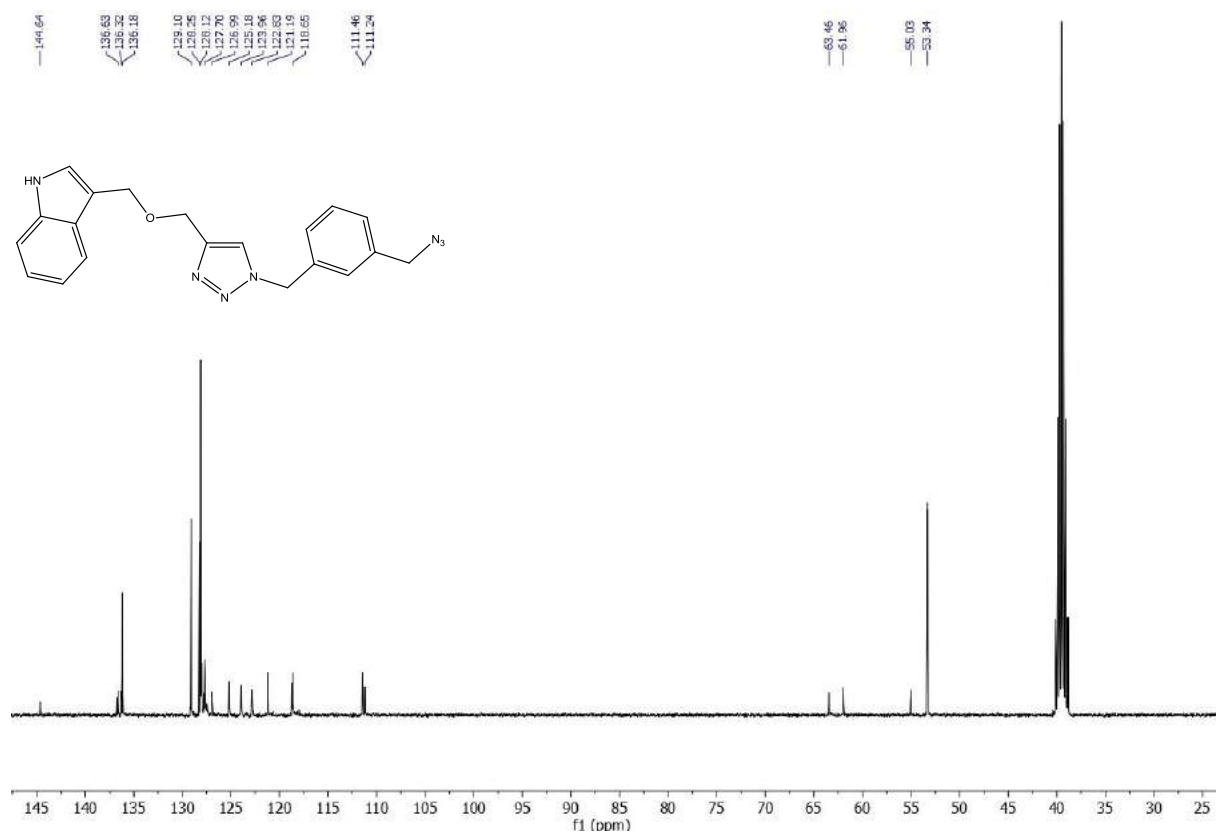
**Fig. S5a.** <sup>1</sup>H NMR spectrum of compound **9**



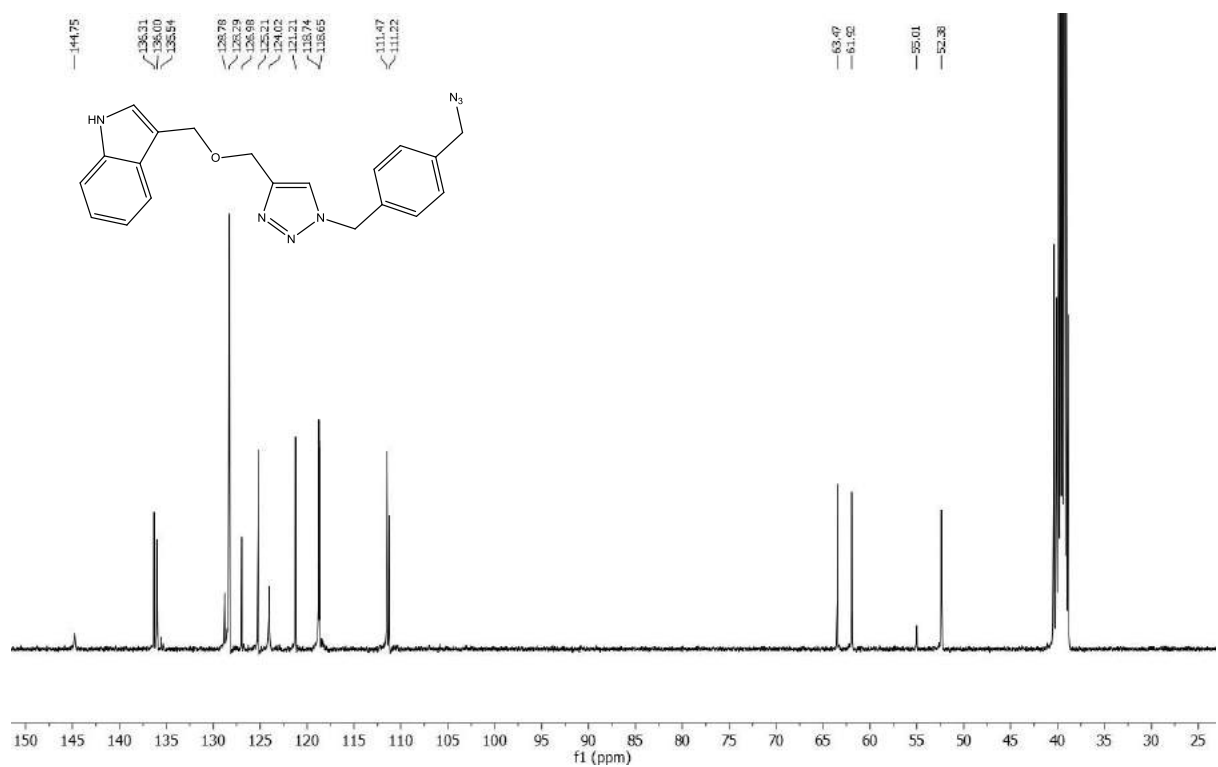
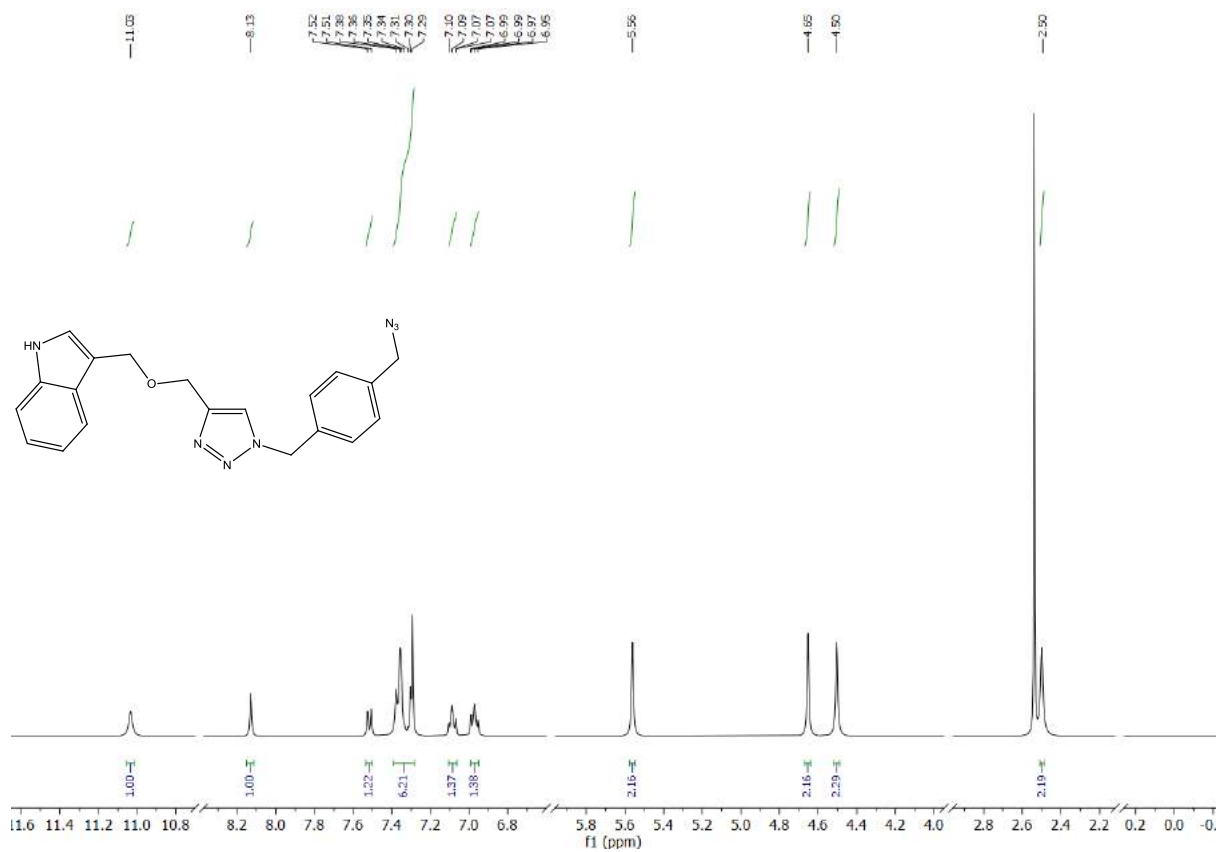
**Fig. S5b.** <sup>13</sup>C NMR spectrum of compound **9**

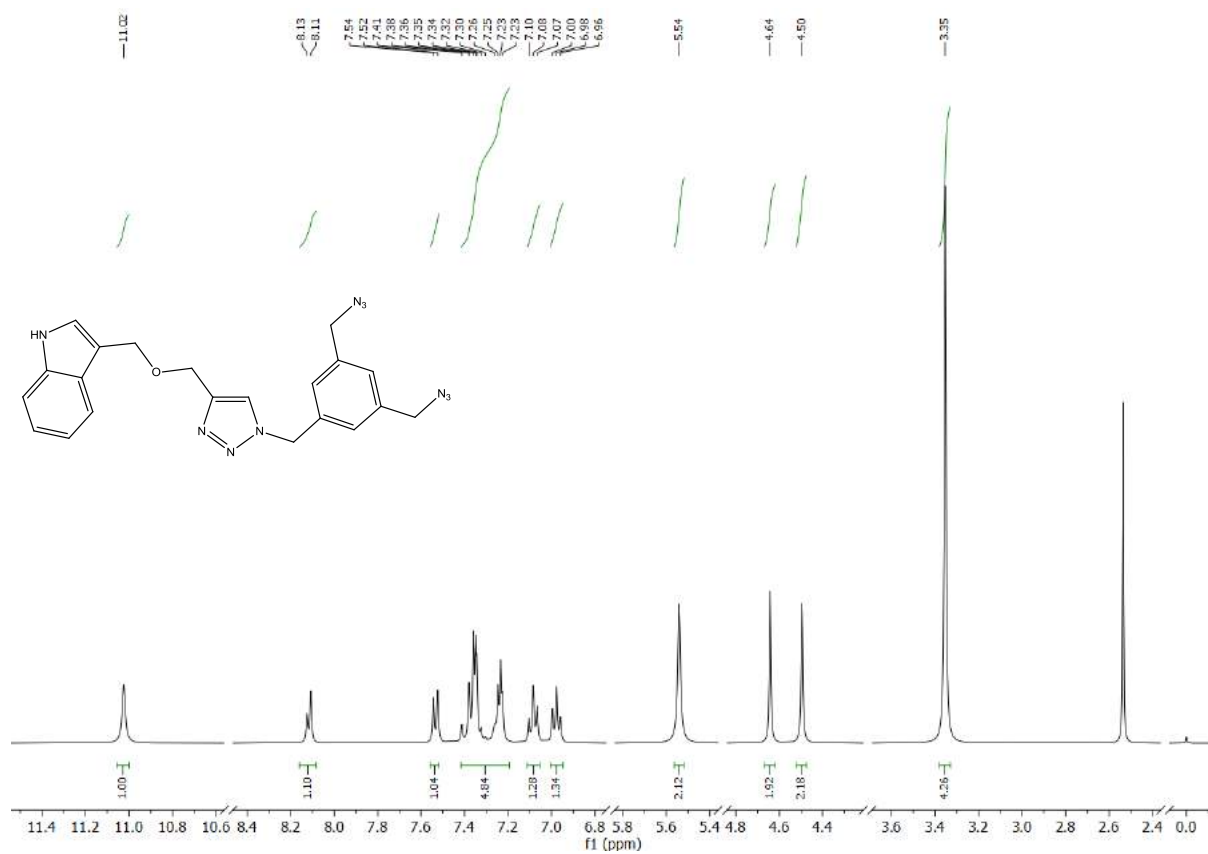


**Fig. S6a.** <sup>1</sup>H NMR spectrum of compound 10

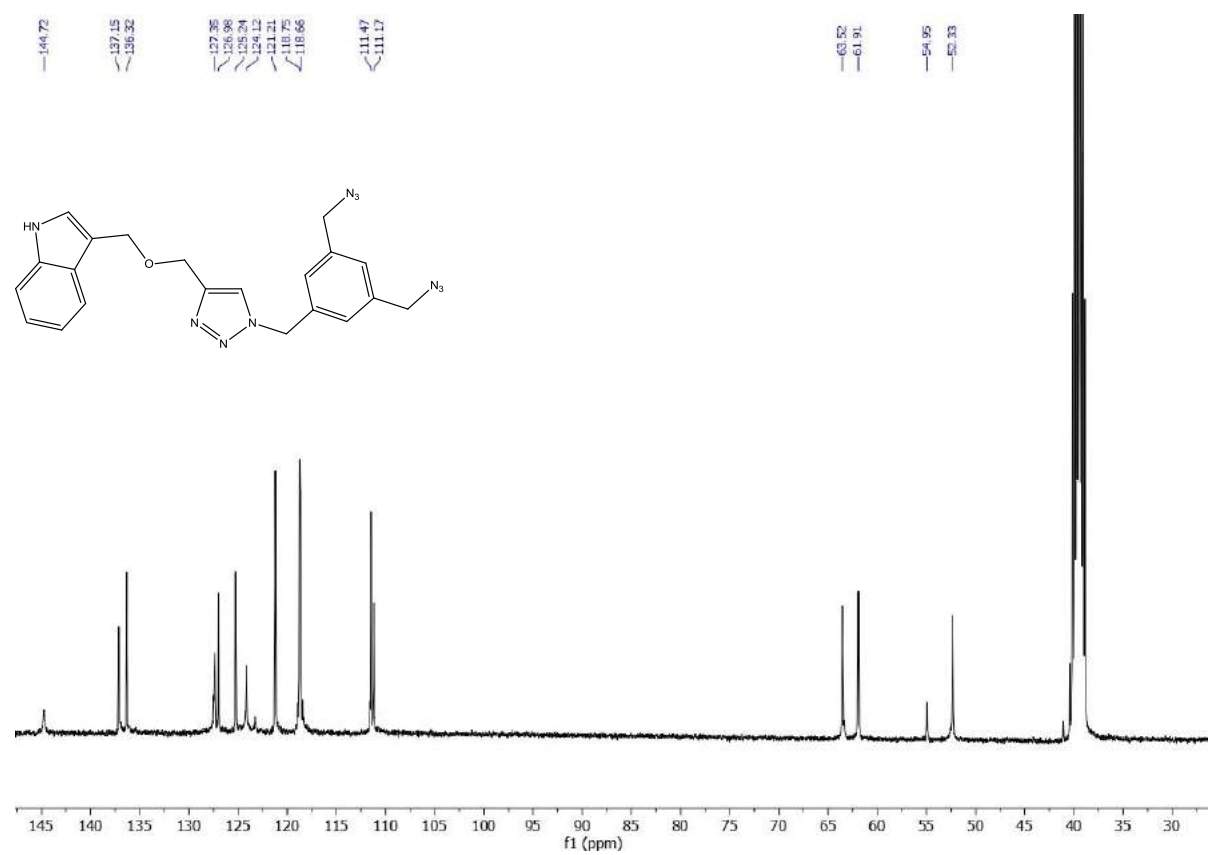


**Fig. S6b.** <sup>13</sup>C NMR spectrum of compound 10

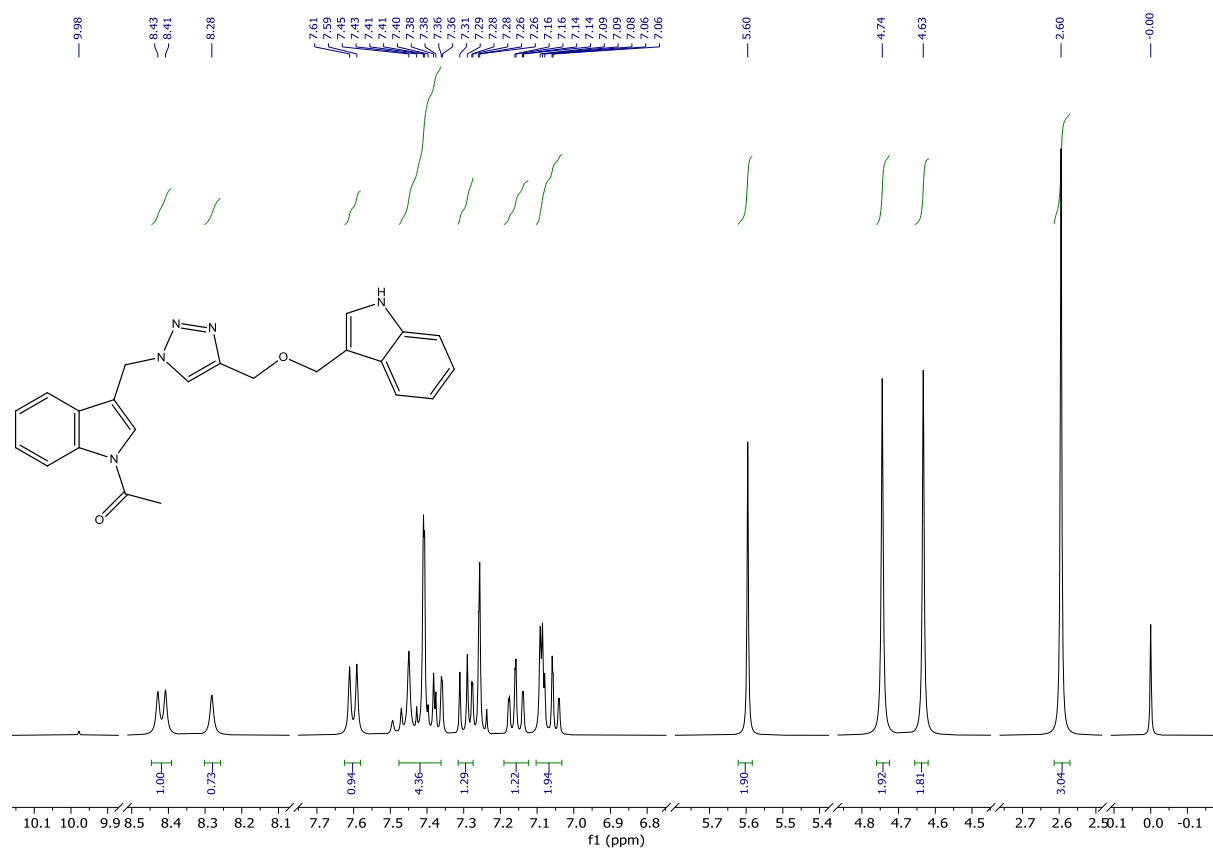




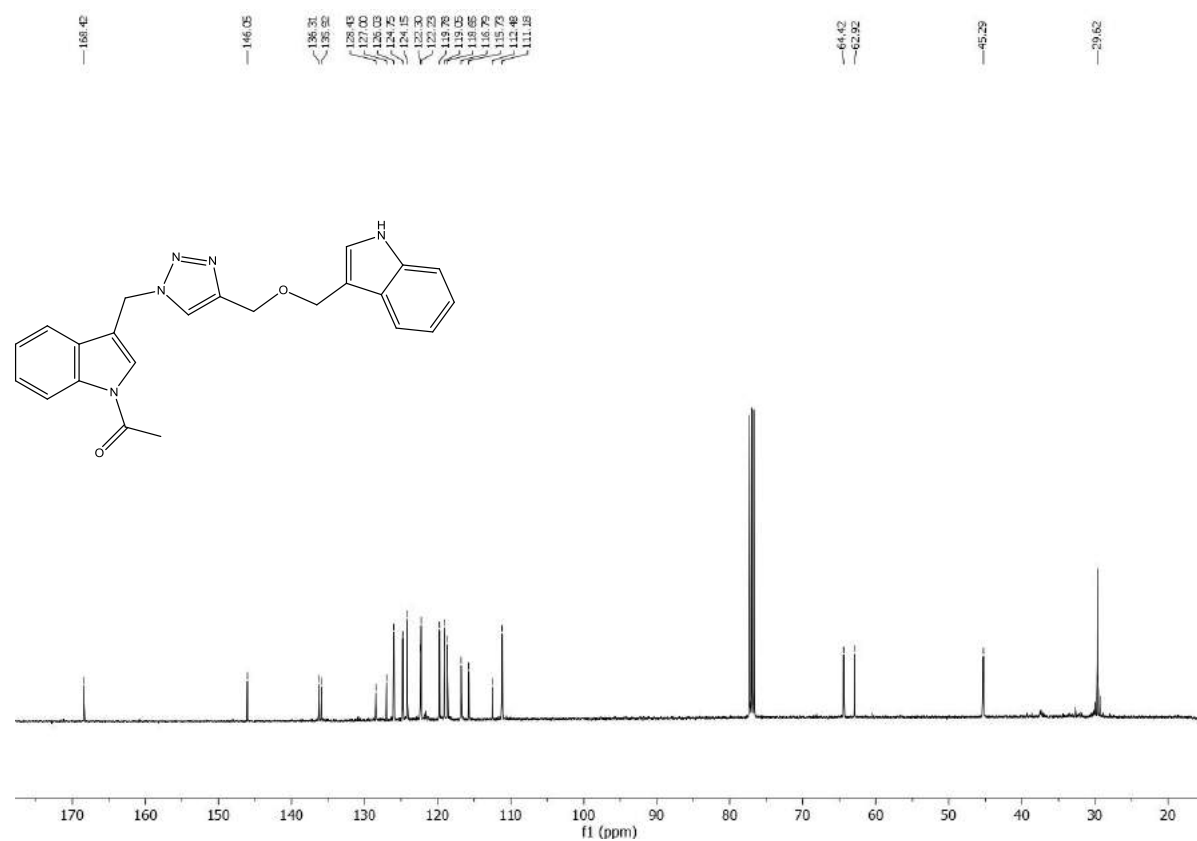
**Fig. S8a.** <sup>1</sup>H NMR spectrum of compound 12



**Fig. S8b.** <sup>13</sup>C NMR spectrum of compound 12



**Fig. S9a.** <sup>1</sup>H NMR spectrum of compound **13**



**Fig. S9b.** <sup>13</sup>C NMR spectrum of compound **13**



## Biological activity

### *Human red blood cells preparation*

All methods were carried out in accordance with the relevant guidelines and regulations, and the Bioethics Committee approved all experimental protocols for Scientific Research at the Medical University of Poznań (agreement no. ZP/907/1002/18). Human red blood cell concentrates were purchased from Blood Bank in Poznań without any contact with blood donors. Informed consent was obtained from all blood donors. Freshly human RBC suspensions (hematocrit 65%) were washed three times (3000 rpm, 10 min, +4°C) in 7.4 pH phosphate buffered saline (PBS – 137 mM NaCl, 2.7 mM KCl, 10 mM Na<sub>2</sub>HPO<sub>4</sub>, 1.76 mM KH<sub>2</sub>PO<sub>4</sub>) supplemented with 10 mM glucose. After washing, cells were suspended in PBS buffer at 1.65x10<sup>9</sup> cells/mL (hematocrit 15%), stored at 4°C, and used within 5 h.

### *Haemolytic assay*

RBC (1.65 x 10<sup>8</sup> cells/mL, ~1.5% hematocrit) were incubated in PBS (7.4 pH) supplemented with 10 mM glucose and containing derivatives tested at a concentration equal to 0.1 mg/mL for 60 min at 37 °C in a thermo-shaker. RBC incubated in PBS without compounds tested were taken as the negative controls, RBC incubated in ice-cold deionized water were taken as the positive controls. Each sample was prepared in triplicate, and the experiments were repeated three times (n=9). After incubation, the RBC suspensions were centrifuged (3000 rpm, 10 min, 4 °C), and the absorbance of the supernatants at 540 nm was measured. The results were expressed as a percentage (%) of haemolysis which was calculated using the following formula:

$$\text{haemolysis (\%)} = (\text{sample Ab/positive control Ab}) \times 100$$

where *sample Ab* is the absorbance value of the supernatant of RBC incubated with compounds tested and *positive control AB* is an absorbance value of supernatant of RBC incubated in ice-cold deionized water. Each sample was prepared in triplicate, and the results are presented as a mean value (±SD) of three independent experiments (n=9). Haemolysis degree <5% indicates no haemolytic activity of a compound.

### *Inhibition of oxidative stress-induced haemolysis*

The cytoprotective activity of derivatives was evaluated according to the previously described method (Jasiewicz et al 2021). Briefly, RBC (1.65x10<sup>8</sup> cells/mL, 1.5% hematocrit) were preincubated in PBS (pH 7.4) supplemented with 10 mM glucose, containing compound tested or Trolox used as the standard antioxidant at a concentration of 0.1 mg/mL for 20 min



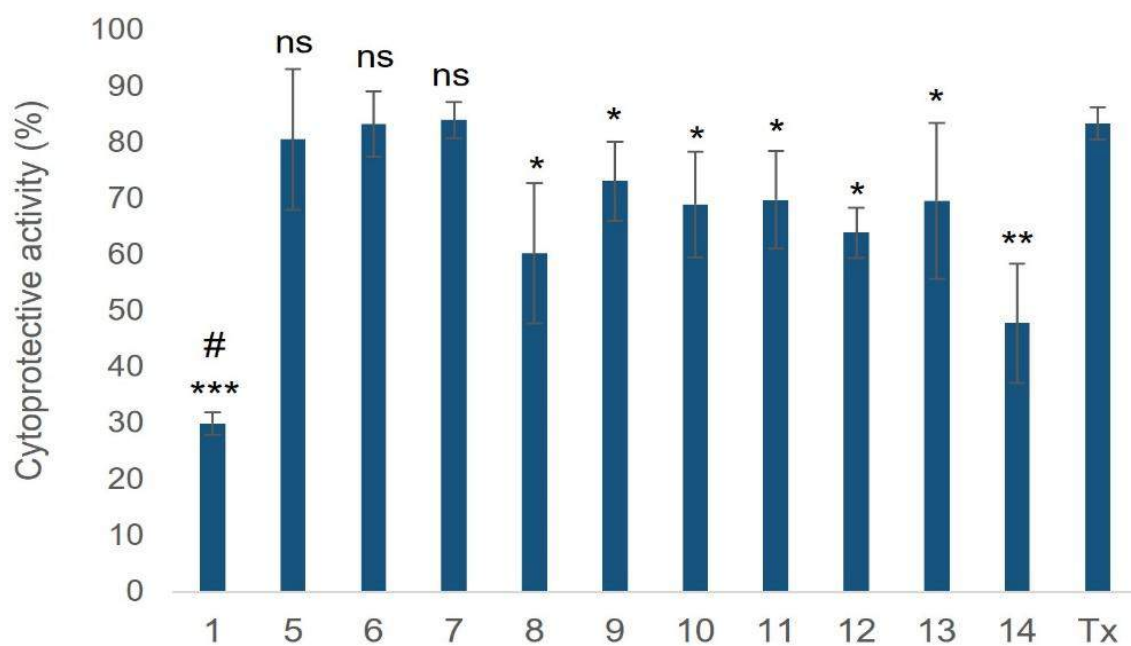
at 37°C in the shaking incubator. After pre-incubation, 2,2'-azobis(2-methylpropionamide) dihydrochloride (AAPH) was added at a final concentration of 60 mM, and samples were incubated for the next four hours. Erythrocytes incubated in PBS, and incubated with AAPH, were taken as the negative and positive controls, respectively. After incubation, the RBC suspensions were centrifuged (3000 rpm, 5 min, +4° C), and the degree of haemolysis was determined by measuring the absorbance (Abs) of the supernatant at  $\lambda=540$  nm in BioMate™ 160 UV-Vis spectrophotometer. The percentage of ROS-induced haemolysis inhibition was calculated using the following equation:

$$\text{Inhibition of haemolysis (\%)} = 100 - [(Abs_{\text{comp}} - Abs_{\text{PBS}} / Abs_{\text{AAPH}} - Abs_{\text{PBS}}) \times 100\%]$$

where  $Abs_{\text{comp}}$  is the absorbance value of supernatant obtained from samples incubated with a compound tested in the presence of AAPH,  $Abs_{\text{PBS}}$  is the absorbance of the supernatant obtained from negative control, and  $Abs_{\text{AAPH}}$  is the absorbance of the supernatant obtained from positive control, respectively. Each sample was made in triplicate, and the results are presented as a mean value ( $\pm$ SD) of three independent experiments with RBC obtained from different donors.

### **Statistical analysis**

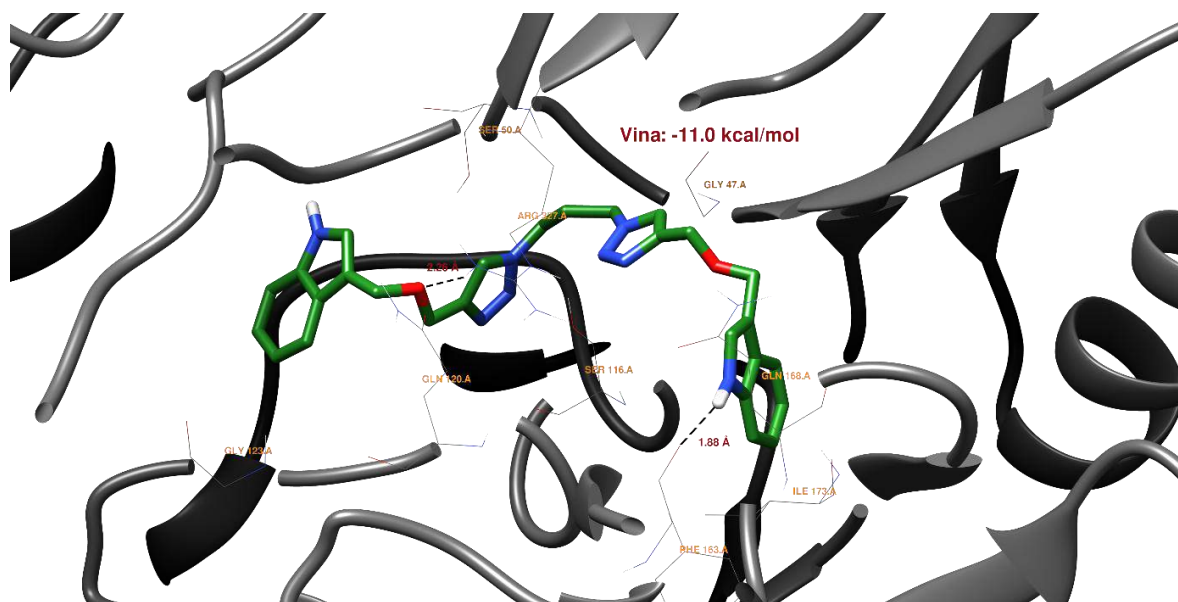
For haemolytic activity, data were plotted as the arithmetic mean  $\pm$  standard deviation (SD) of the results of three independent experiments, with every sample (test samples and positive controls) in triplicate (n = 9).



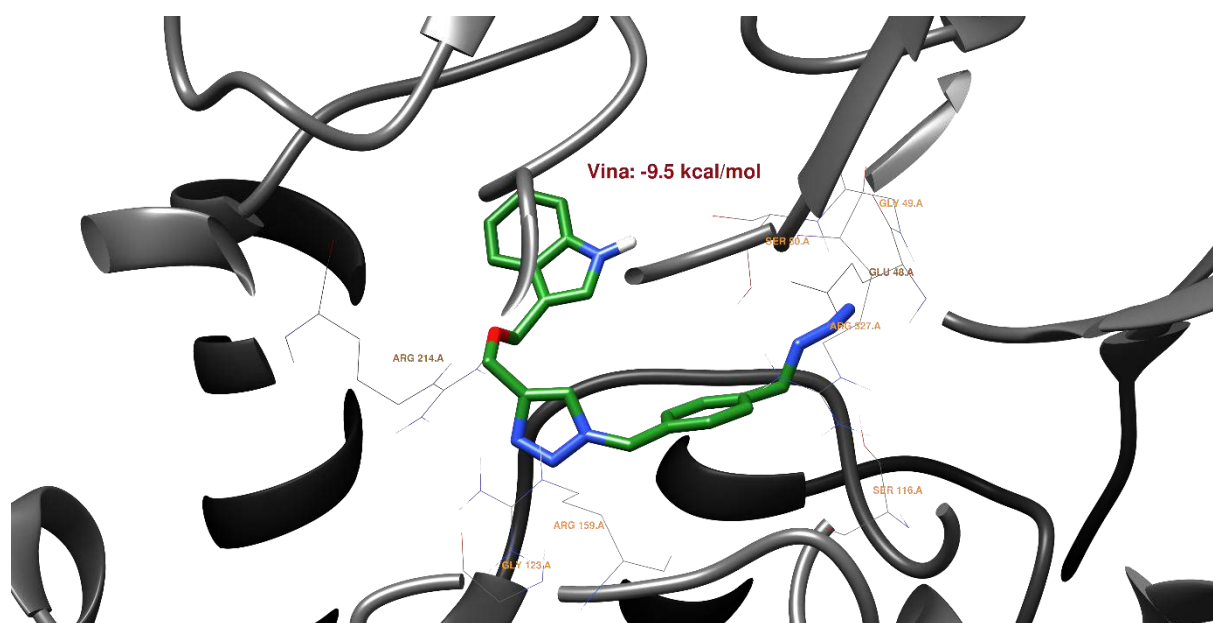
**Figure S11.** Cytoprotective activity of gramine (**1**), compounds **5–14** and the standard antioxidant Trolox (Tx) at the concentration of 0.1 mg/mL against oxidative haemolysis induced by AAPH (60 mM, 37°C, 4 hours). The results are presented as the mean value  $\pm$  standard deviation in comparison with Tx activity (\* $p$  < 0.05, \*\* $p$  < 0.01, \*\*\* $p$  < 0.001). Non statistically significant difference is indicated as ns. # - data adopted from (Jasiewicz et al. 2021).

## Molecular docking

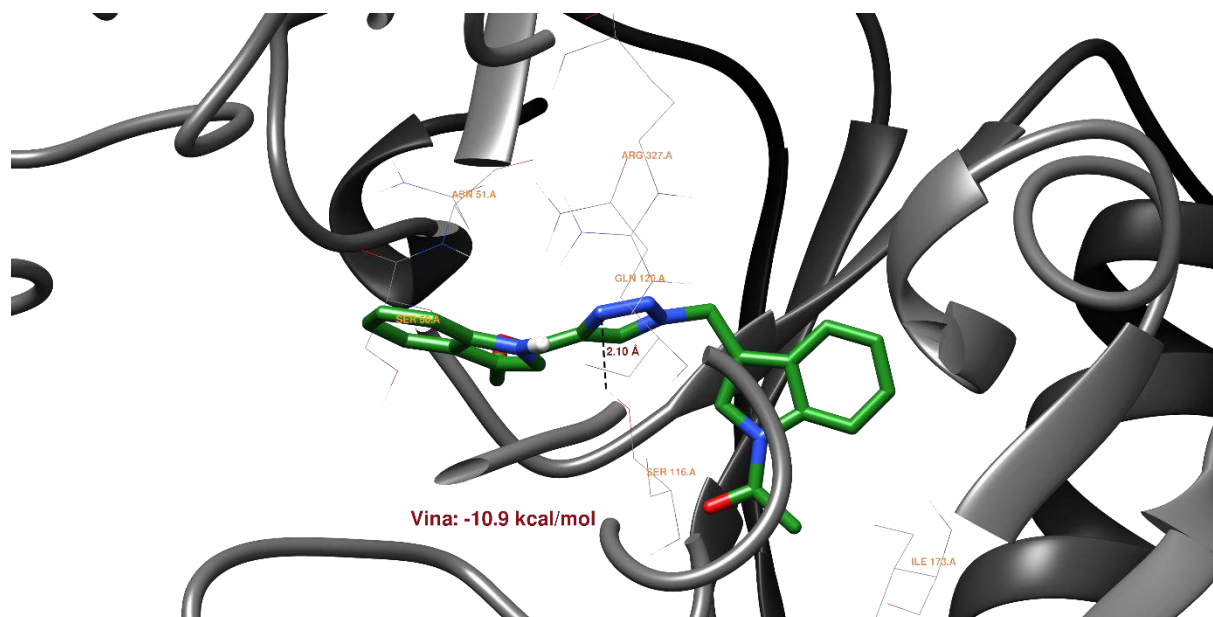
The chosen 2Q85 and 5V5Z receptors can be found in the Protein Data Bank (PDB) (RCBS Protein DATA BANK). The 2Q85 receptor is thought to have antibacterial activity (*E. coli* MurB) (Zoeiby et al. 2003), whereas the 5V5Z receptor is thought to have antifungal activity (CYP51 Ca) (Hargrove et al. 2017). Docked structures are examined in the same active site of the protein domains as co-crystallized ligands. 2Q85's search parameters were as follows: centre (x, y, z): 13.853, 0.000, 0.000, and size (x, y, z) (80\*80\*80) Å<sup>3</sup>. The centre (x, y, z) of 5V5Z was -41.500, -11.400, 23.547, and the size (x, y, z) was (70\*100\*60) Å<sup>3</sup>. It helped us test if chosen structures can bind to selected active sites of the 2Q85 and 5V5Z proteins' domains. The molecular docking technique was carried out with the help of the rdkit tool (Landrum 2016), which enables the creation of 3D structures using SMILES representations of structures. The 3D structures were saved in \*.pdb format and subsequently translated to the AutoDock Vina algorithm's needed \*.pdbqt format (Trott and Olson 2010). The files were converted using the OpenBabel application (O'Boyle et al 2011; The Open Babel Package 2023). The receptors were created using AutoDock Tools 1.5.7 (Sanner 1996; Morris et al 2009). The AutoDock Vina multiple CPU methodology (Trott and Olson 2010) was used to perform the molecular docking process. The Chimera tool (1.16) was used to visualize the highest-scoring ligand postures in molecular docking as well as probable H-bond formation (Pettersen et al 2004).



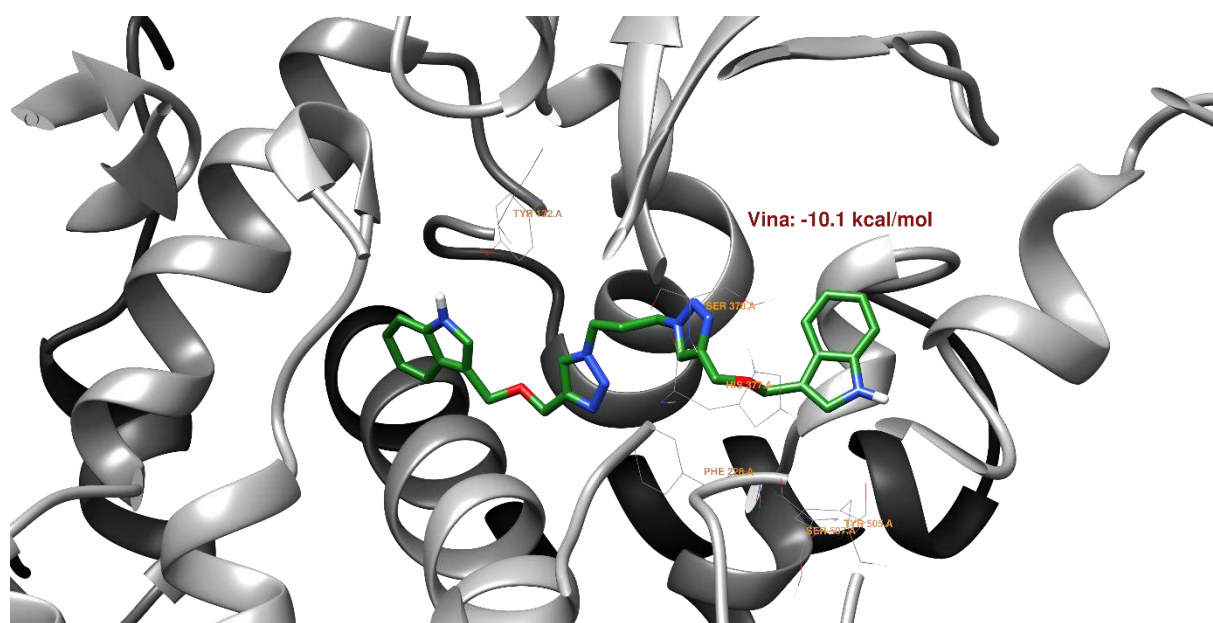
**Fig. S12a.** The structure 5<sup>th</sup> inside the active site of the 2Q85 protein domain with black marked possible H-bonds.



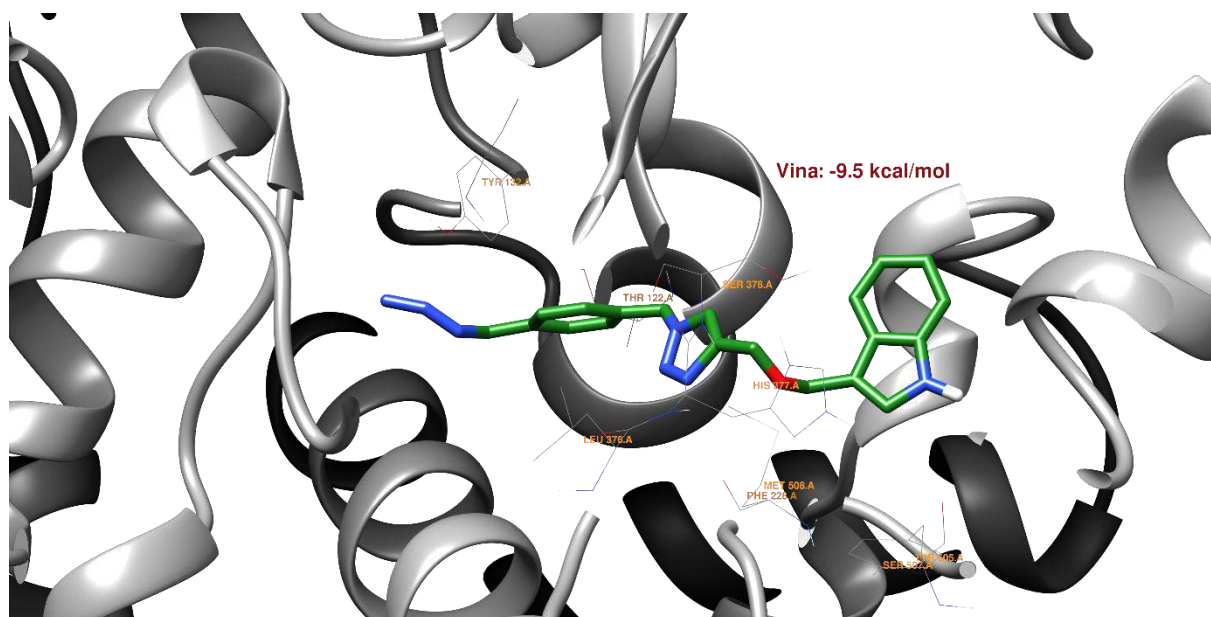
**Fig. S12b.** The structure 11<sup>th</sup> inside the active site of the 2Q85 protein domain.



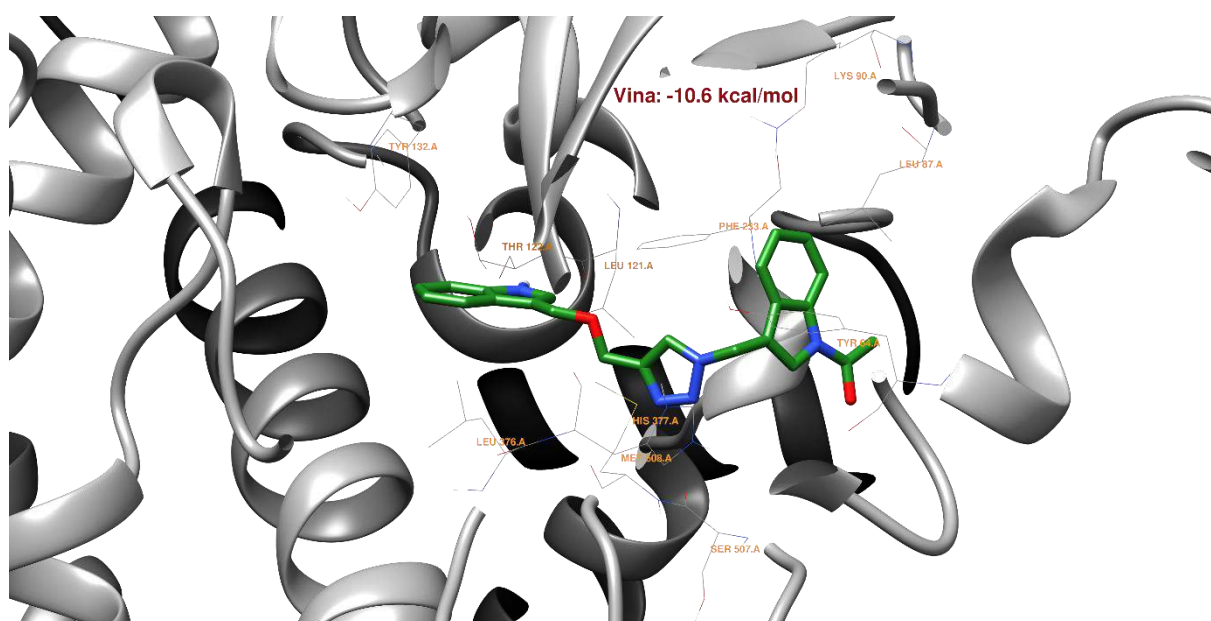
**Fig. S12c.** The structure 13<sup>th</sup> inside the active site of the 2Q85 protein domain with a black-marked possible H-bond.



**Fig. S12d.** The structure 5<sup>th</sup> inside the active site of the 5V5Z protein domain.



**Fig. S12e.** The structure **11<sup>th</sup>** inside the active site of the 5V5Z protein domain.



**Fig. S12f.** The structure **13<sup>th</sup>** inside the active site of the 5V5Z protein domain.

**Table S1.** Physicochemical properties of compounds **5–14**.

Compound	HBA	HBD	log $P_{o/w}$	M [g/mol]
<b>5</b>	6	2	2.87	496.56
<b>6</b>	6	2	3.56	524.62
<b>7</b>	6	2	4.57	566.70
<b>8</b>	6	2	5.96	622.80
<b>9</b>	6	1	2.07	373.41
<b>10</b>	6	1	2.07	373.41
<b>11</b>	6	1	2.07	373.41
<b>12</b>	9	1	1.83	428.45
<b>13</b>	4	0	3.37	427.50
<b>14</b>	4	1	3.03	399.45

**Table S2.** Binding energies (kcal/mol) for structures **5, 7, 10, 11, 13**.

Compound	Binding energy – 2Q85 (kcal/mol)	Binding energy – 5V5Z (kcal/mol)
<b>5</b>	-11.0	-10.1
<b>7</b>	-10.2	-8.0
<b>10</b>	-9.6	-9.4
<b>11</b>	-9.5	-9.5
<b>13</b>	-10.9	-10.6

## Reference

- Hargrove TH, Friggeri L, Wawrzak Z, Qi A, Hoekstra WJ, Schotzinger RJ, York JD, Guengerich FP, Lepesheva GI. 2017. Structural analyses of *Candida Albicans* sterol 14 $\alpha$ -demethylase complexed with azole drugs address the molecular basis of azole-mediated inhibition of fungal sterol biosynthesis. *J Biol Chem.* 292: 6728–6743.
- Jasiewicz B, Kozanecka-Okupnik W, Przygodzki M, Warżajtis B, Rychlewska U, Pospieszny T, Mrówczyńska L. 2021. Synthesis, antioxidant and cytoprotective activity evaluation of C-3 substituted indole derivatives. *Sci Rep.* 11: 15425. doi:10.1038/s41598-021-94904-z.
- Landrum G. 2016. RDKit: Open-Source Cheminformatics Software. doi:10.5281/zenodo.7415128.

- Morris GM, Huey R, Lindstrom W, Sanner MF, Belew RK, Goodsell DS, Olson AJ. 2009. Autodock4 and AutoDockTools4: automated docking with selective receptor flexibility. *J Comput Chem.* 16: 2785-2791.
- O'Boyle NM, Banck M, James CA, Morley C, Vandermeersch T, Hutchison GR. 2011. Open Babel: An open chemical toolbox. *J Cheminform.* 3: 3-33.
- Pettersen EF, Goddard TD, Huang CC, Couch GS, Greenblatt DM, Meng EC, Ferrin TE. 2004. UCSF Chimera-a visualization system for exploratory research and analysis. *J Comput Chem.* 25: 1605-1612.
- RCBS Protein DATA BANK [accessed 2023 Feb 16]. <https://www.rcsb.org>.
- Sanner MF. 1999. Python: A Programming Language for Software Integration and Development. *J Mol Graph Model.* 17: 57-61.
- The Open Babel Package, version 3.1.1 <http://openbabel.org> (accessed 08.02.2023)
- Trott O, Olson AJ. 2010. AutoDock Vina: Improving the Speed and Accuracy of Docking with a New Scoring Function, Efficient Optimization, and Multithreading. *J Comput Chem.* 31: 455-461.
- Zoeiby AE, Sanschagrin F, Levesque RC. 2003. Structure and function of the Mur enzymes: development of novel inhibitors. *Mol Microbiol.* 47: 1-12.



# Synthesis and Hemolytic Activity of Bile Acid-Indole Bioconjugates Linked by Triazole

Natalia Berdzik, Hanna Koenig, Lucyna Mrówczyńska, Damian Nowak, Beata Jasiewicz,\* and Tomasz Pospieszny\*



Cite This: *J. Org. Chem.* 2023, 88, 16719–16734



Read Online

ACCESS |



Metrics & More

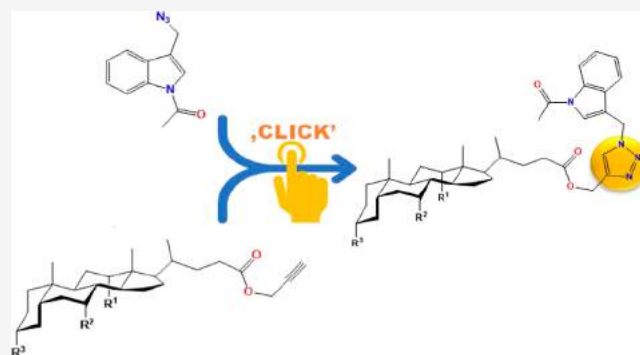


Article Recommendations



Supporting Information

**ABSTRACT:** New formyl and acetyl derivatives of bile acid propargyl esters and their bioconjugates with modified gramine molecules have been obtained using the click chemistry method to study their hemolytic potency. The structures of all compounds were confirmed by spectral ( $^1\text{H}$ - and  $^{13}\text{C}$  NMR and FT-IR) analysis and mass spectrometry (ESI-MS) as well as PM5 semiempirical methods. According to the results, the structural modification of formyl and acetyl bile acid derivatives, leading to the formation of new propargyl esters and indole bioconjugates, reduces their hemolytic activity. According to molecular docking studies, the tested ligands are highly likely to exhibit a similar affinity, as native ligands, for the active sites of specific protein domains (PDB IDs: 2Q85 and 5V5Z). The obtained results may be helpful for the development of selective bile acid bioconjugates



as effective antibacterial, antifungal, or antioxidant agents.

## 1. INTRODUCTION

Natural products represent many chemical compounds synthesized by living organisms that play a significant role in different physiological processes. Steroids and alkaloids are important natural products.<sup>1</sup> Among steroids, cholesterol is a crucial component of the animal cell membrane<sup>2–8</sup> and a substrate for synthesizing vitamin D, bile acid, and steroid hormones.<sup>1–4</sup> Steroids vary in the presence of different functional groups. Due to their biological significance and chemical properties, steroids and their derivatives are widely used in biomimetic chemistry, host–guest chemistry, and pharmacology.<sup>9,10</sup> As structural building blocks, bile acids are used in constructing molecular receptors, and their dimers are employed in developing macrocyclic artificial receptors that exhibit good organogellation properties.<sup>11–14</sup>

Among the alkaloids, the group that gained much interest is indole alkaloids. Reserpine is known for its antipsychotic and antihypertensive activity. Vincristine and vinblastine are used for cancer treatment. Harmine, Harman, and harmaline exhibit antidepressant, antiplatelet, and spasmolytic activity.<sup>15–18</sup> Gramine, [1-(1*H*-indol-3-yl)-*N,N*-dimethylmethanamine], the best-known indole alkaloid, is often used as an initial compound in synthesizing various biologically active substituted indoles. This tertiary amine and its derivatives have broad biological activities such as antiviral, antibacterial, antioxidant, and anticancer. They also play an essential role in amino acid metabolism and affect redox processes.<sup>19–21</sup>

Bioconjugates are compounds containing at least one biomolecule. Among the most known steroid-polyamine bioconjugates is squalamine, an amino sterol antibiotic.<sup>22,23</sup> Squalamine has been isolated from liver cells of spiny dogfish (*Squalus acanthias*),<sup>24</sup> and its activity against Gram-positive and Gram-negative bacteria, protozoa, fungi, and viruses, including HIV, has been confirmed.<sup>22</sup>

Bioconjugates of indole, such as indole-phthalimide or indole-uracil, exhibit high cytoprotective effects against AAPH-induced oxidative hemolysis.<sup>25,26</sup> Some indole-containing pyrazole analogs showed significant activity against leukemia, whereas substituted-3-(4,5-diphenyl-1*H*-imidazol-2-yl)-1*H*-indole derivatives act as an antibacterial agent.<sup>27,28</sup>

In recent years, compounds containing a triazole ring have gained more attention. Triazoles are attractive pharmacophores because they resist oxidation, reduction, and hydrolysis.<sup>29–32</sup> The 1,2,3-triazole five-membered heterocyclic ring can form inter- or intramolecular hydrogen bonds and dipole–dipole interactions, increasing product solubility and ability to bind other molecules.<sup>33</sup>

**Received:** April 13, 2023

**Revised:** November 16, 2023

**Accepted:** November 22, 2023

**Published:** December 7, 2023



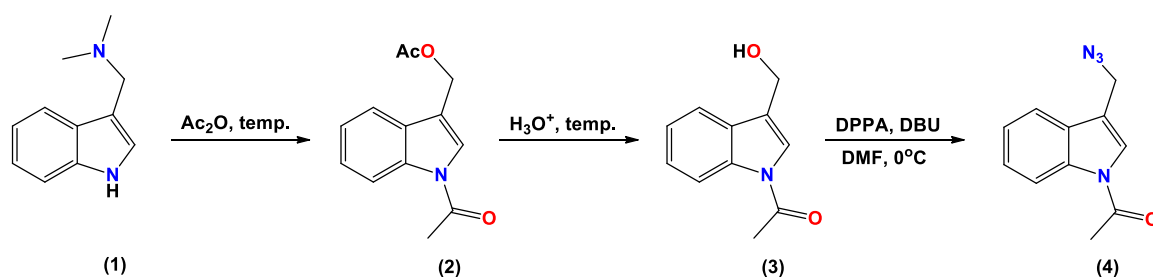


Figure 1. Synthesis of *N*-acetyl-3-azidemethylindole (4).

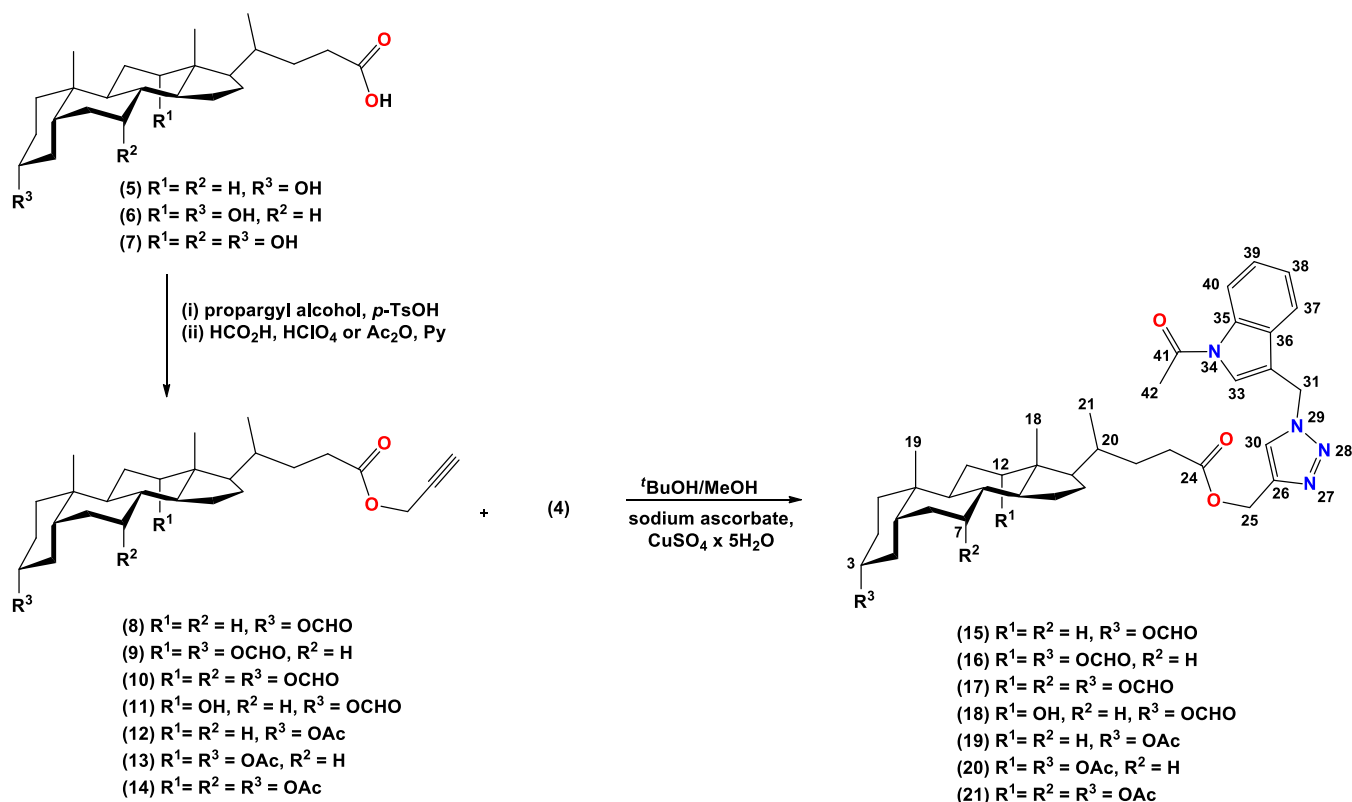


Figure 2. Synthesis of bile-acids propargyl esters (8–14) and new 1,2,3-triazole ring bioconjugates (15–21) of bile acid derivatives and gramine derivative.

Owing to the importance of both the indole compounds and bile acids and as a continuation of our interest in alkaloid and steroid modification, in this work, we report the synthesis and structural analysis of bile acids-indole conjugates linked by triazole ring.

It is well-known that bile acids as amphiphilic molecules possess hemolytic potency dependent on their chemical structure and concentration. The molecular mechanism of interaction between bile acids molecules and the cell membrane, as well as the hemolysis type, is dependent on the protonation of the anionic group of bile acids.<sup>34,35</sup>

Based on the fact that the hemolytic activity of bile acids and their formyl and acetyl derivatives can be reduced or eliminated by the introduction of gramine,<sup>36</sup> the newly synthesized compounds have also been evaluated for their hemolytic potency.

Considering that both bile acid derivatives and indole compounds could be efficient antibacterial and fungicidal agents, we studied their potent antimicrobial activity with a molecular docking methodology. Molecular docking can

inform us whether our ligand will fit the protein's active site and what the binding energy might be. The lower the energy level, the more stable the ligand–receptor complex.<sup>37,38</sup> Moreover, molecular docking studies can reveal possible interactions between a tiny molecule, the ligand, and a macromolecular target, in this instance, a protein domain.

## 2. RESULTS AND DISCUSSION

### 2.1. Synthesis and Spectroscopic Characterization.

The synthesis of *N*-acetyl-3-azidomethylindole (4) is shown in Figure 1. Compound (4) was synthesized in good yield from gramine (1) by three successive reactions: acylation, hydrolysis, and nucleophilic substitution. In the final experiment, *N*-acetyl-3-hydroxymethylindole and diphenylphosphoryl azide (DPPA) was dissolved in DMF with a catalytic amount of DBU at 0 °C. A mixture of crude bioconjugates was obtained and then separated by column chromatography. The bile acid propargyl esters were obtained by reaction of propargyl bile acids with  $\text{HCO}_2\text{H}$  (8–10) or  $\text{Ac}_2\text{O}$  (12–

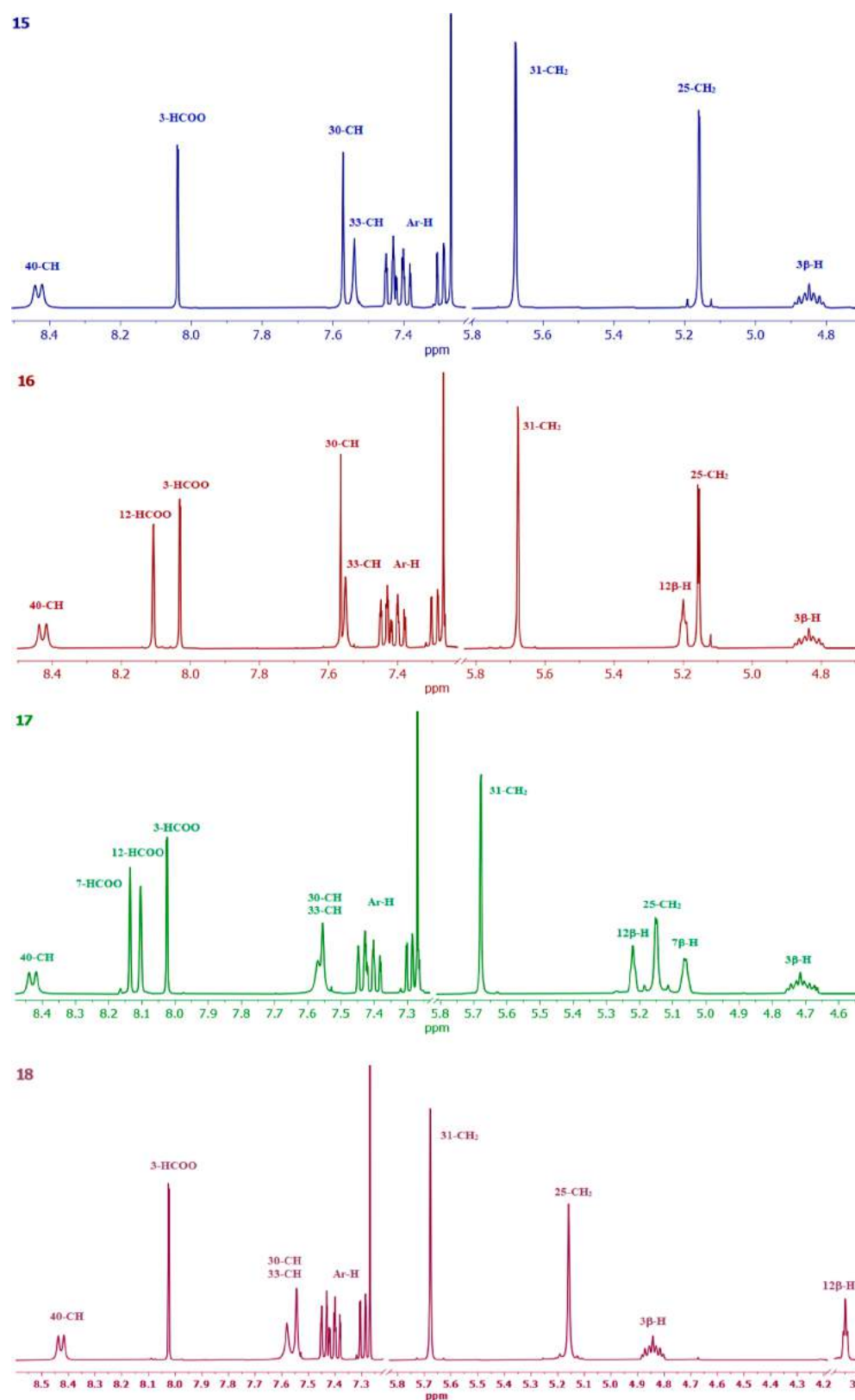


Figure 3.  $^1\text{H}$  NMR Spectra in the region of 3.90–8.50 ppm for the most characteristic signals of compounds (15–18).

14) with satisfactory yields except for compound (11), a byproduct with extremely low efficiency.

The synthesis of new bioconjugates of bile acids (lithocholic, LCA; deoxycholic, DCA; cholic, CA) and gramine is presented in Figure 2. The reaction of propargyl esters of bile acid formyl

derivatives (8–14) and the azide derivative of gramine (4) in the presence of  $\text{CuSO}_4 \cdot 5\text{H}_2\text{O}$  and sodium ascorbate in *t*-BuOH/MeOH (5:1) gave products (15–21) in good yields.

The most characteristic signals of representative compounds (15–18) in the range of 3.90–8.50 ppm in the  $^1\text{H}$  NMR

spectra are shown in Figure 3. In the  $^1\text{H}$  NMR spectrum of propargyl  $3\alpha$ -formyl- $5\beta$ -cholan-24-oate (8), propargyl  $3\alpha,12\alpha$ -diformyl- $5\beta$ -cholan-24-oate (9), propargyl  $3\alpha,7\alpha,12\alpha$ -triformyl- $5\beta$ -cholan-24-oate (10), propargyl  $3\alpha$ -formyl- $12\alpha$ -hydroxy- $5\beta$ -cholan-24-oate (11), and  $3\alpha$ -acetyl- $5\beta$ -cholan-24-oate (12), characteristic two hydrogen singlets in the range 0.76–0.64 and 0.95–0.93 ppm and a doublet at 0.98–0.83 ppm assigned to  $\text{CH}_3$ -18,  $\text{CH}_3$ -19, and  $\text{CH}_3$ -21, respectively, are present. The protons of the  $3\alpha$ -OCHO group gave signals in the range 8.04–8.02 ppm for all bioconjugates (8–11) and additionally 8.11 ppm for the  $7\alpha$ -OCHO group in compound (10), and the  $12\alpha$ -OCHO group gave signals in the range of 8.16–8.14 ppm for compounds (9) and (10). For compound (12), the signal at 2.03 ppm corresponds to the protons of the  $3\alpha$ -OCOCH<sub>3</sub> group. All compounds show characteristic multiplets associated with the axial positions of the C $3\beta$ -H protons in the steroid skeleton in the range of 4.94–4.67 ppm. In the spectrum of compounds (10) and (11), additional signals correspond to the C $12\beta$ -H proton at 5.27 and 3.99 ppm, respectively. For compound 10, the C $7\beta$ -H protons appear at 5.07 ppm. All bile acids–indole conjugates with 1,2,3-triazole ring (15–21) in CDCl<sub>3</sub> show diagnostic proton signals C $30$ -H at 7.58–7.57 ppm. The formyl derivatives (15–18) show additional signals at 8.11–8.02 assigned to the proton of the formyloxy groups. Signals diagnostic for the aromatic ring of the indole moiety appear at the range of 8.43–7.28 ppm for all new bioconjugates. The protons of the methylene groups C $25$ -H and C $31$ -H linked directly to the triazole ring give signals at about 5.16–5.15 ppm and 5.69–5.68 ppm, respectively. The diagnostic protons CH<sub>3</sub> from the acetyl groups of compounds (19–21) and the *N*-acetoxy group of all new bioconjugates are found at 2.12–2.03 and 2.66 ppm, respectively.  $^1\text{H}$  NMR spectra of bioconjugates (15–21) show characteristic multiplets of protons of C $3\beta$ -H from the bile acid skeleton, ranging from 4.89 to 4.53 ppm. The characteristic signals of C $12\beta$ -H protons are observed at 5.22–5.04 ppm for compounds (16, 17, 20, 21) and 3.95 ppm for compound (18). Signals assigned to the C $7\beta$ -H protons of the bile acid skeleton occur as doublets at 5.06 and 4.90 ppm for bioconjugates (17) and (21), respectively. In the bile acids skeleton, two hydrogen singlets ranking from 0.69 to 0.59 and 0.94–0.90 ppm and a characteristic doublet at 0.90–0.74 ppm were assigned to  $\text{CH}_3$ -18,  $\text{CH}_3$ -19, and  $\text{CH}_3$ -21, respectively.

The  $^{13}\text{C}$  NMR spectra of substrates (8–14) and bioconjugates (15–21) show characteristic signals at 12.71–11.94, 23.07–20.78, and 18.24–17.23 ppm, which are assigned to  $\text{CH}_3$ -18,  $\text{CH}_3$ -19, and  $\text{CH}_3$ -21, respectively. For all newly obtained acetyl derivatives (12) and (19–21), signals from the C=O carbon atom occur at 170.66–170.52 ppm ( $3\alpha$ -OCOCH<sub>3</sub>), 170.48–170.44 ppm ( $12\alpha$ -OCOCH<sub>3</sub>), and 170.36 ppm ( $7\alpha$ -OCOCH<sub>3</sub>). However, for the new formyl derivatives (15–18), carbon atoms in positions  $3\alpha$  of formyloxy groups resonate at 160.82–160.46 ppm. The carbon atoms of the C(12)=O steroid skeleton gave signals in the range of 160.67–160.47 ppm, whereas the carbon atoms of C(7)=O were detected at 160.55–160.53 ppm. Alternatively, carbon atoms of the C(24)=O and C(41)=O groups of all new bioconjugates gave signals in the range of 174.11–173.06 ppm and 168.32–168.29 ppm, respectively. The diagnostics signal for C(26) as well as C(30) atoms in the 1,2,3-triazole ring in compounds (15–21) are observed in the range of 143.40–143.25 ppm and 123.59–123.53 ppm. Additionally, signals originating from the indole ring carbon atoms are

observed in the 135.96–115.56 ppm range. The carbon atoms of the HC≡C–CH<sub>2</sub> group in substrates (8–12) are observed in the range 74.76–74.70 ppm, 77.80–77.72 ppm, 51.79–51.76 ppm, and 77.80–74.70, respectively.

**2.2. PM5 Calculations.** The molecular models of all bioconjugates are shown in Figure 4. The final heats of formation (HOF) for the bioconjugates (15–21) are presented in Table 1.

The lowest values of HOF for bioconjugates of bile acids and gramine (15–21) are observed for cholic acids and their conjugates (17) and (21). The number of hydroxyl groups in the bile acid skeleton lowers the value of the determinant of the HOF. The same relationship was observed for blocked hydroxyl groups by formyl and acetate groups. The OAc and OAc groups facilitate the formation of intramolecular H-bonds and stable host–guest complexes. These complexes may be stabilized by H-bonding or electrostatic interactions arising from the bile acid molecule's OCHO and OAc groups. The HOF value decreases with increasing numbers of OCHO and OAc groups in the bile acids skeleton.

Bioconjugates with hydroxyl groups blocked with formyl groups (15–17) also have higher HOF values than derivatives with acetic groups. This fact can be explained by their smaller steric hindrance and lower electron density, which are not conducive to creating interactions with other molecules. In contrast, comparing the HOF values of bioconjugates of deoxycholic acid (16) and (18), in which one or two hydroxyl groups have been blocked, the bioconjugate with the unblocked hydroxyl group at C(12) has a higher HOF value than the one with all blocked groups.

**2.3. Hemolytic Activity.** The effect of structural modifications of bile acid molecules on their ability to incorporate into cell membranes was investigated using red blood cells (RBCs) as a model.<sup>34,35</sup> Our previous study has shown that at a concentration of 0.1 mg/mL, the formyl modification of bile acids increases their hemolytic activity, especially in the case of noncytotoxic cholic acid. The hemolytic activity of acetyl-LCA and DCA was significantly higher than their native forms, whereas the acetyl-CA was not active as membrane perturbing agents at the same concentration.<sup>36</sup>

As shown in Figure 5, the hemolytic activity (%) of all synthesized formyl derivatives of bile acids propargyl esters (8–11) and their bioconjugates with modified gramine molecules linked with 1,2,3-triazole ring (15–18), is significantly decreased (in the range of 2.36–13.87%) in comparison with formyl derivatives (F-LCA, F-DCA, and F-CA in the range of 94–99%). Similarly, acetyl derivatives of bile acid propargyl esters (12–13) and their triazole bioconjugates (19–20) are less cytotoxic (3.36–8.26%) than acetylated bile acids (Ac-LCA, Ac-DCA—97–98%). A notable exception is cholic acid derivatives, where the hemolytic activity has not changed significantly (Figure 6).

As mentioned before, as amphiphilic compounds, bile acids interact easily with the lipid bilayer of RBC and modify RBC shape from dysocytic to echinocytic or stomatocytic, depending on their chemical structure and concentration used.<sup>36</sup> As shown in Figure 7, after incubation with derivatives 10 and 17, the RBC shape is dysocytic. Therefore, structural modification of bile acid formyl derivatives by introducing indole and 1,2,3-triazole moieties modifies their interaction with the RBC membrane and consequently does not affect the discocytic

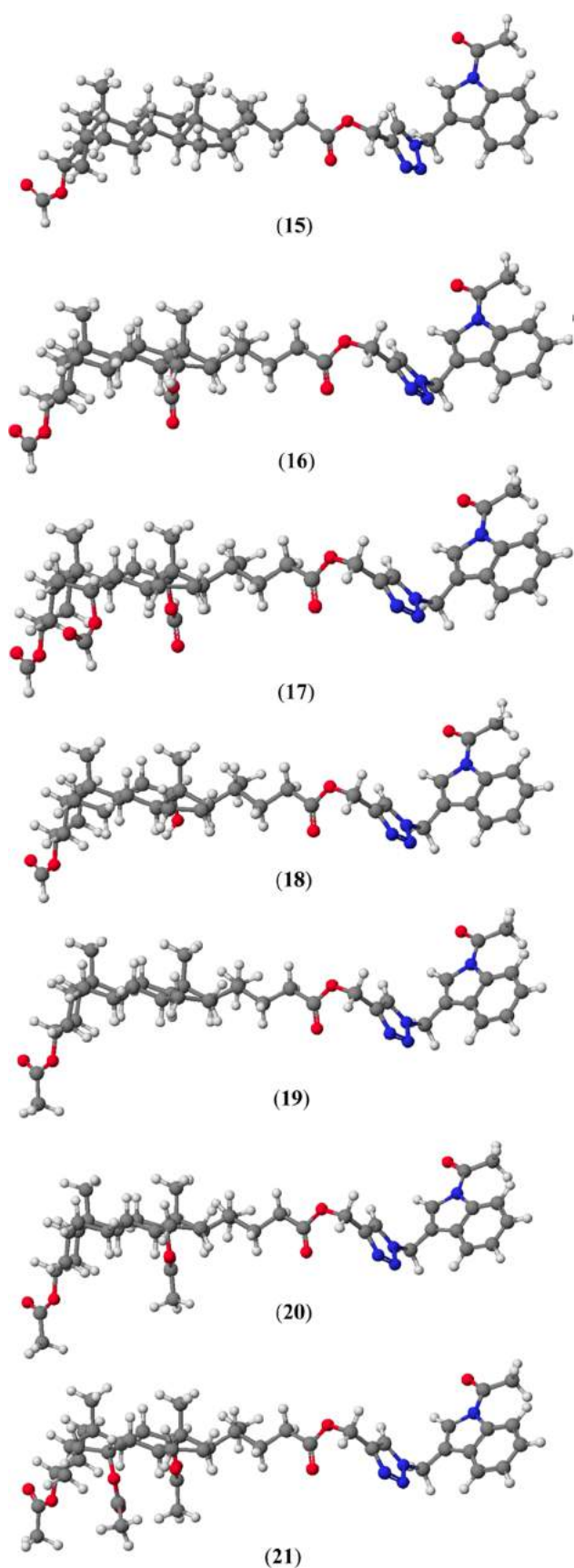


Figure 4. Molecular models of bioconjugates (15–21) calculated by the PMS method.

Table 1. Heat of Formation (HOF) [kcal/mol] Bioconjugates (15–21)

compound	HOF [kcal/mol]
15	−187.4677
16	−277.1396
17	−362.3263
18	−229.9797
19	−196.5772
20	−282.5585
21	−376.1200

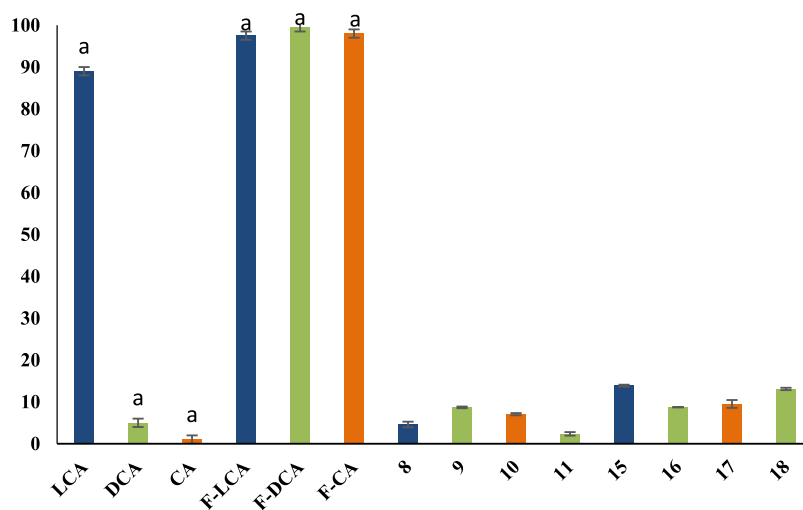
RBC shape. A similar result is observed in the acetyl derivatives.

**2.4. Molecular Docking.** The PDB IDs for the studied macromolecular structures were 2Q85 and 5V5Z. The possible interactions between the analyzed structures and the protein domains are presented below. The graphical representations reflect the “best” ligand pose in each of the protein domains. It is the pose with the lowest binding energy.

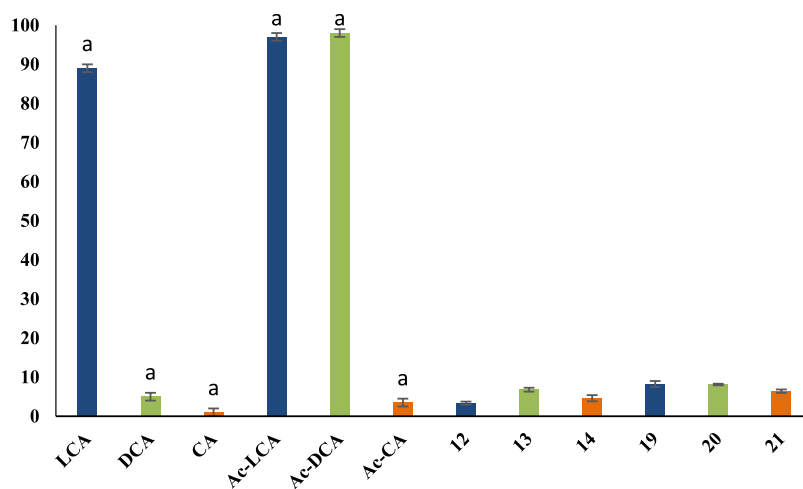
Figures 8–13 show how the best poses of the 16th, 18th, and 20th structures interact with the 2Q85 protein domain. For compound 16, six hydrogen bonds (Figure 8) could be formed between the ligand and the protein domain. The weakest hydrogen bond could occur between the ligand’s oxygen and the protein’s LYS-262 amino acid due to the longest distance. The strongest hydrogen bond could occur between the ligand’s oxygen atom and the TYR-158 residue. Figure 9 indicates the possibility of a cation–pi interaction. For 18, one hydrogen bond could occur between the ligand and the GLN-120 or ARG-327 residues. Both are strong and comparable (Figure 10). Figure 11 shows the possibility of two hydrogen bond formations along with cation–pi interaction. For derivative 20, two hydrogen bonds could form between the ligand and the protein domain. Both with comparable strength. Because of the shorter length (2.11 Å), a hydrogen bond between the ligand’s oxygen and the ARG-327 residue is more likely to form. Figure 13 suggests that two additional hydrogen bonds can be formed between the ligand and SER-229 and TYR-190.

Figure 14 shows that no hydrogen bonds can form between the best pose of the 16thth structure and the 5V5Z protein domain. Figure 15 indicates that the 16th structure can be additionally stabilized by the pi–pi interaction. Figure 16 indicates that one hydrogen bond could form between the 18th structure’s best pose and SER-378 or HIS-377 residues in the 5V5Z protein domain. Figure 17 shows one additional hydrogen bond between the ligand and the TYR-132 amino acid. Figure 18 displays no hydrogen bonds between the 20th structure’s best pose and that of the 5V5Z protein domain. Figure 19 shows the additional stabilization due to pi–pi interactions.

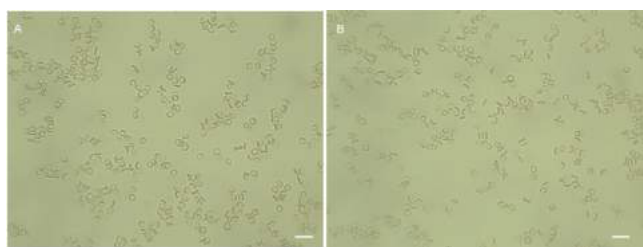
The docked molecules possess a non-negligible affinity to the 2Q85 protein domain, implying that they could be suitable inhibitors. Each figure (Figures 8, 10, 12, 14, 16, and 18) shows binding energies with a specified kcal/mol unit. Despite forming a lower number of possible hydrogen bonds, the affinities of structures 16, 18, and 20 (Figure 4) for the 5V5Z protein domain are even a little stronger than those of the 2Q85 domain. Figures 9, 11, 13, 15, 17, and 19 explain the interaction between the ligands and the protein domains.



**Figure 5.** Hemolytic activity of bile acids (LCA, DCA, and CA), their formyl derivatives (F-LCA, F-DCA, and F-CA), new esters (8–11), and bioconjugates with gramine (15–18). The bile acid derivatives are marked with a different pattern. The compounds were tested at a concentration of 0.1 mg/mL. <sup>a</sup>Data are published in ref 36.



**Figure 6.** Hemolytic activity of bile acids (LCA, DCA, and CA), their acetyl derivatives (Ac-LCA, Ac-DCA, and Ac-CA), new esters (12–14), and bioconjugates with gramine (19–21). The bile acid derivatives are marked with different pattern. The compounds were tested at a concentration of 0.1 mg/mL. <sup>a</sup>Data are published in ref 36.



**Figure 7.** Effect of derivatives 10 (A) and 17 (B) (0.1 mg/mL) on RBC shape as observed in light microscopy (60 min, 37 °C) at 63× magnification. Scale bar—10 μm.

### 3. CONCLUSIONS

In summary, this study presents the synthesis and chemical characterization of new formyl and acetyl derivatives of bile acid propargyl esters and their bioconjugates with modified gramine molecules linked with a 1,2,3-triazole ring. The results obtained in this study confirm that structural modification of

formyl and acetyl derivatives of bile acids results in alterations of their cell membrane interactions and decreases their hemolytic activity. The molecular docking investigations reveal that the selected compounds have an affinity for the protein targets of interest (2Q85 and 5VSZ), which are associated with antibacterial and antifungal activity, respectively. Therefore, they are likely to be biologically active compounds.

### 4. EXPERIMENTAL SECTION

**4.1. Chemistry.** **4.1.1. Synthesis of *N*-Acetyl-3-azidemethylindole (4).** *N*-Acetyl-3-hydroxymethylindole (3) (0.54 mmol, 102 mg) was dissolved in dimethylformamide (2 mL). Then diphenylphosphoryl azide (DPPA) (1 mmol, 275 mg) diluted in dimethylformamide (1 mL) was added. The reaction mixture was cooled to 0 °C, and then 1,8-diazabicyclo[5.4.0]undec-7-ene (DBU) (1 mmol, 152 mg) was added dropwise. The mixture was stirred at 0 °C for 2 h. The reaction was monitored by TLC (PhMe/EtOAc 5:1). The distilled water was added (5 mL), and the reaction mixture was extracted with ethyl acetate, washed with distilled water and brine, then dried over anhydrous Na<sub>2</sub>SO<sub>4</sub>. The organic layer was evaporated under reduced pressure. The crude product was purified by column chromatography (PhMe/EtOAc 50:1).

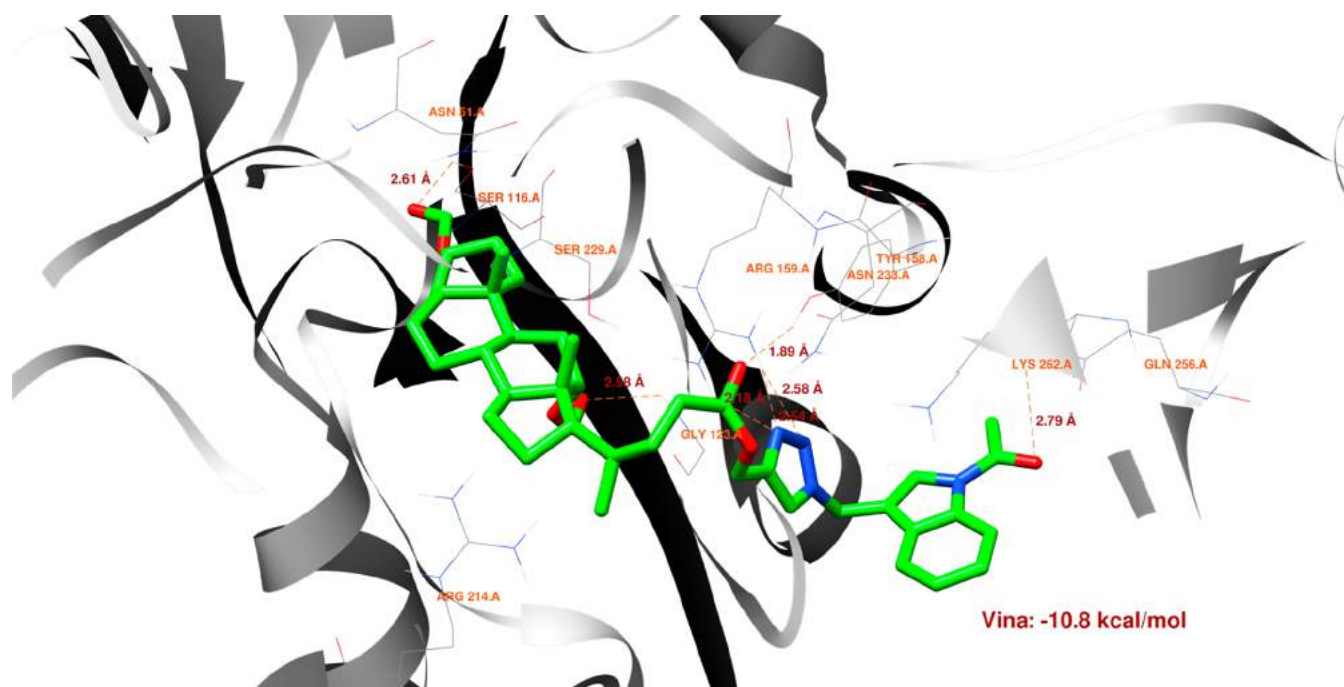


Figure 8. Structure of bioconjugate 16 (Figure 4) inside the active site of the 2Q85 protein domain with yellow marked possible H-bonds.

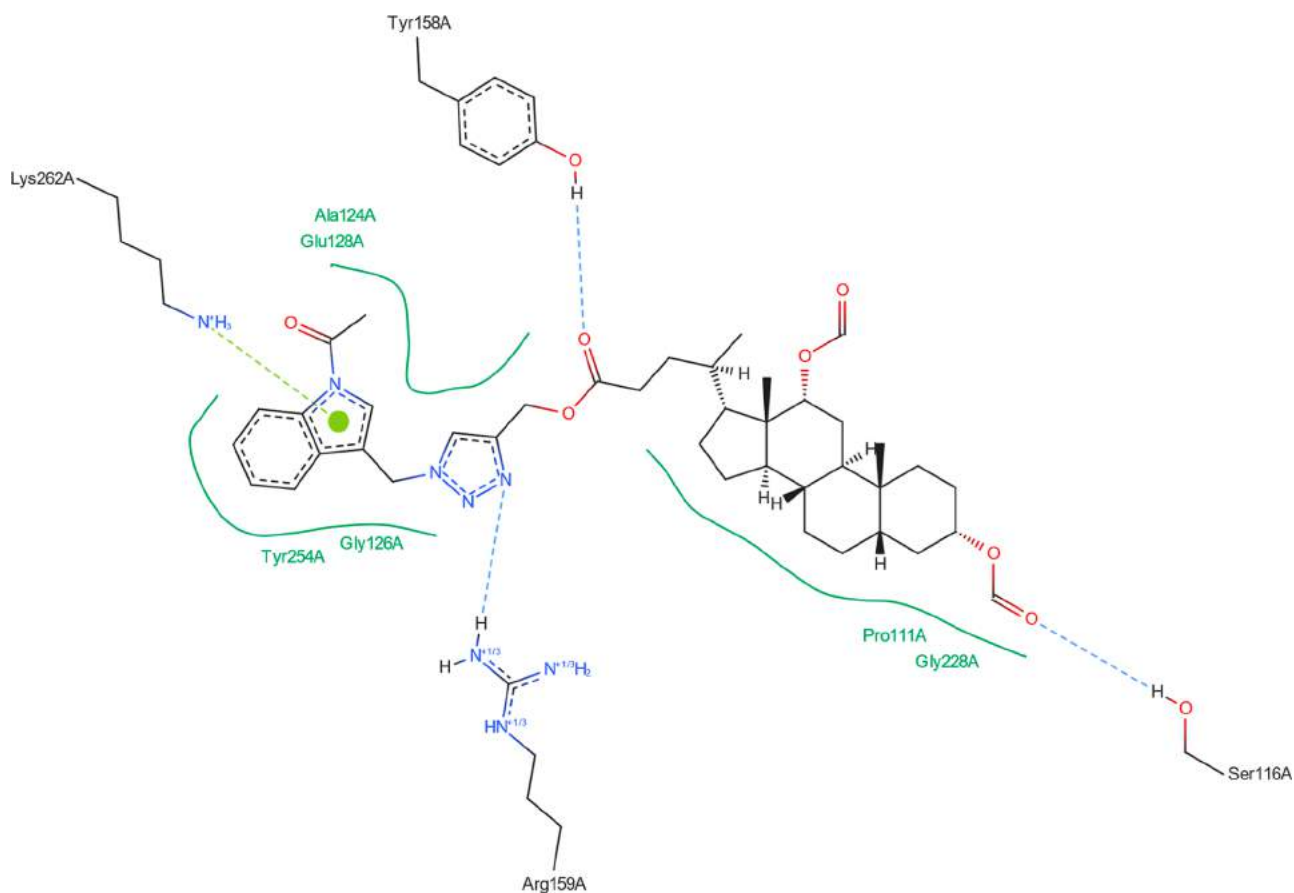
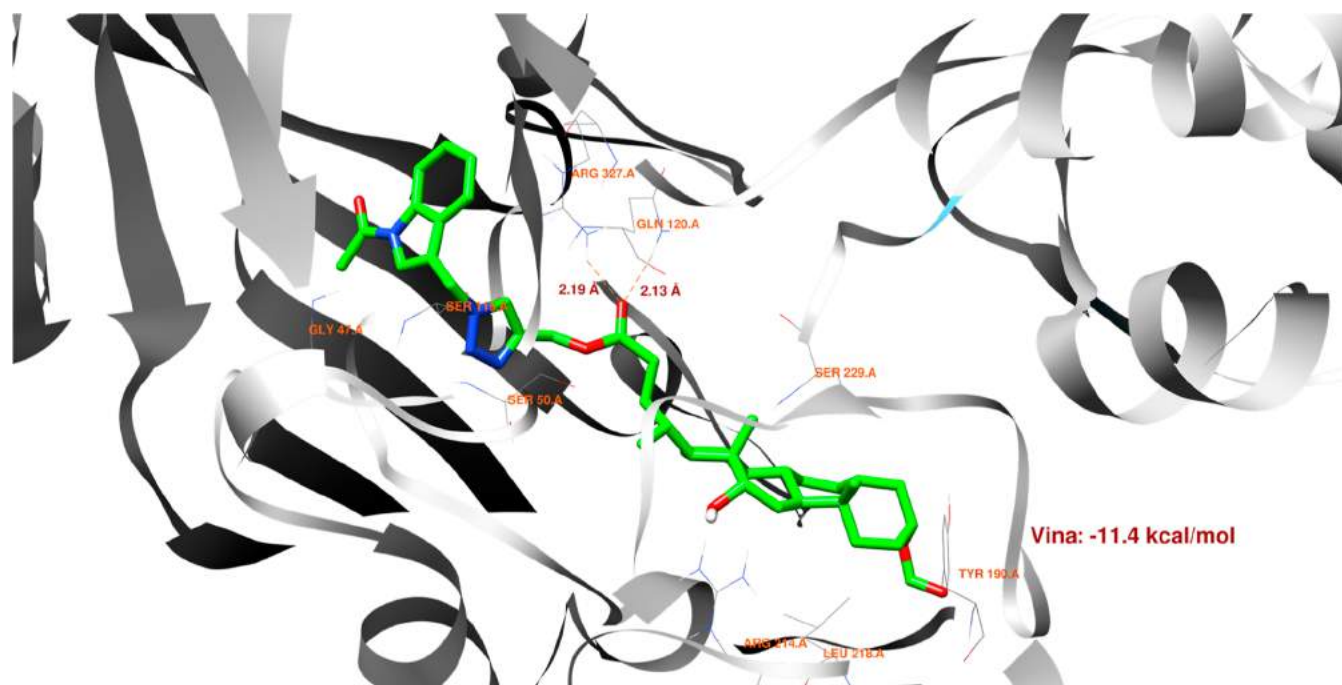


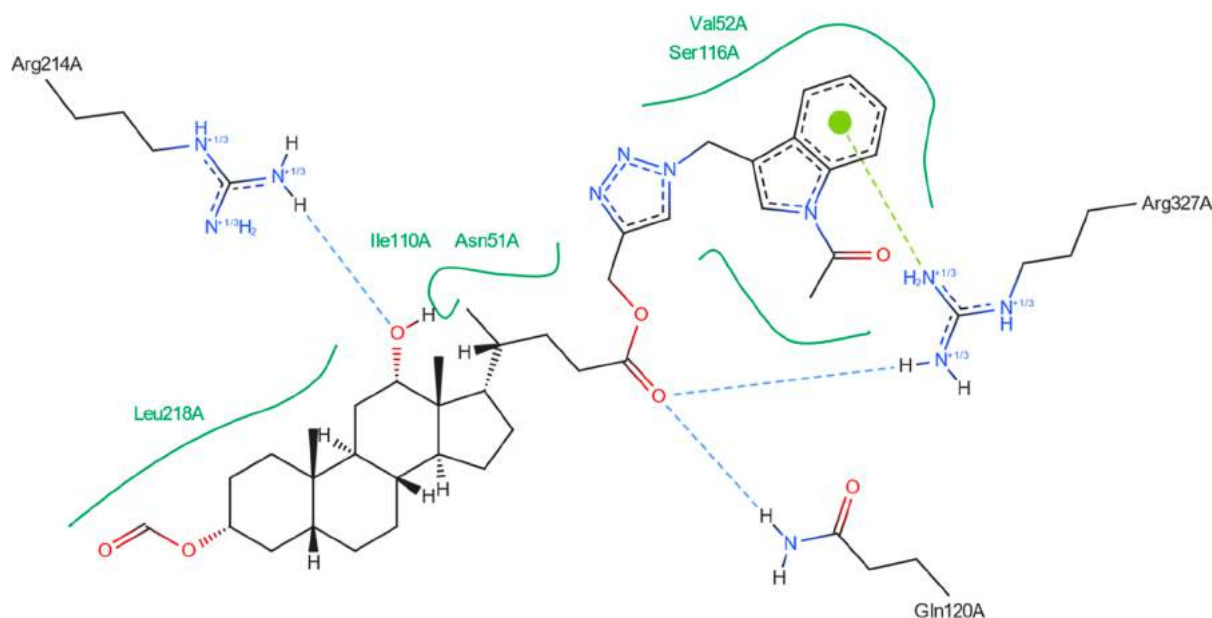
Figure 9. Structure of bioconjugate 16 (Figure 4) inside the active site of the 2Q85 protein domain with marked following interactions: green solid lines—hydrophobic contact, light-blue—hydrogen bond, and light-green—cation- $\pi$  interaction.

Yellow oil, yield: 68 mg, 59%,  $^1\text{H}$  NMR (400 MHz,  $\text{CDCl}_3$ ):  $\delta$  8.44 (d,  $J$  = 8.2 Hz, 1H, 40 H), 7.59 (d,  $J$  = 8.2 Hz, 1H, 37 H), 7.44 (s, 1H, 33 H), 7.40–7.30 (m, 2H, 38 H, 39 H), 4.49 (d,  $J$  = 1.0 Hz, 2H, 31-

$\text{CH}_2\text{-N}_3$ ), 2.64 (s, 3H, 42- $\text{CH}_3$ ).  $^{13}\text{C}\{^1\text{H}\}$  NMR (101 MHz,  $\text{CDCl}_3$ ):  $\delta$  168.4 (C-41), 136.0, 129.8, 128.8, 125.8, 123.9, 120.1, 118.9, 116.8, 46.1 (31- $\text{CH}_2\text{-N}_3$ ), 23.9 (42- $\text{CH}_3$ ). FT-IR (KBr,  $\text{cm}^{-1}$ )  $\nu_{\text{max}}$ : 3120



**Figure 10.** Structure of bioconjugate 18 (Figure 4) inside the active site of the 2Q85 protein domain with yellow marked possible H-bonds.



**Figure 11.** Structure of bioconjugate 18 (Figure 4) inside the active site of the 2Q85 protein domain with marked following interactions: green solid lines—hydrophobic contact, light-blue—hydrogen bond, and light-green—cation- $\pi$  interaction.

(=C–H), 3049 (=C–H), 2928 (C–H), 2871 (C–H), 2107 (–N<sub>3</sub>), 1706 (C=O). EI-MS ( $m/z$ ): 214 (25%). Anal. Calcd for C<sub>11</sub>H<sub>10</sub>N<sub>4</sub>O (MW = 214.09): C, 61.67; H, 4.71; N, 26.15; O, 7.47. Found: C, 61.69; H, 4.68; N, 26.17; O, 7.46.

**4.1.2. General Procedure for the Preparation of Compounds (8–11).** Propargyl lithocholate (or deoxycholate and cholate) (7.23 mmol, 1.0 equiv) was dissolved in 20 mL of HCOOH (90%) and heated at 60 °C in a water bath for 4 h. The reaction was monitored by TLC. The reaction mixture was cooled to room temperature and poured onto ice, and the white solid was washed with water. The crude product was obtained and purified by column chromatography (eluent CHCl<sub>3</sub>). The reaction yield was: (8) 3.0 g, 94%, (9) 3.3 g, 94%, (10) 3.72 g, 97%, and (11) 200 mg, 6% (product of nonexhaustive formylation), respectively.

**4.1.2.1. Propargyl 3 $\alpha$ -Formyl-5 $\beta$ -cholan-24-oate (8).** White oil, <sup>1</sup>H NMR (300 MHz, CDCl<sub>3</sub>):  $\delta$  8.04 (d,  $J$  = 1.0 Hz, 1H, 3 $\alpha$ -OCHO), 4.94–4.78 (m, 1H, 3 $\beta$ -H), 4.68 (d,  $J$  = 3.0 Hz, 2H, O–CH<sub>2</sub>), 2.47 (t,  $J$  = 2.5 Hz, 1H, –C $\equiv$ CH), 0.94 (s, 3H, CH<sub>3</sub>-19), 0.92 (d,  $J$  = 6.4 Hz, 3H, CH<sub>3</sub>-21), 0.64 (s, 3H, CH<sub>3</sub>-18). <sup>13</sup>C{<sup>1</sup>H}NMR (76 MHz, CDCl<sub>3</sub>):  $\delta$  173.4 (C-24), 160.8 (3-OCHO), 77.8 (–C $\equiv$ ), 74.7 ( $\equiv$ CH), 74.4 (C-3), 56.4, 55.9, 51.8 (OCH<sub>2</sub>), 42.7, 41.9, 40.4, 40.1, 35.8, 35.3, 34.9, 34.6, 32.2, 30.9, 30.8, 28.2, 27.0, 26.6, 26.3, 24.2, 23.3, 20.8 (C-19), 18.2 (C-21), 12.0 (C-18). FT-IR (KBr, cm<sup>–1</sup>)  $\nu_{\max}$ : 3302 (C $\equiv$ C–H), 2938 (C–H), 2867 (C–H), 1746 (C=O), 1714 (C=O), 1436 (C–H), 1376 (C–O), 1202 (C–O). ESI-MS  $m/z$ : 465 [M + Na]<sup>+</sup> (100%), 481 [M + K]<sup>+</sup> (10%). Anal. Calcd for C<sub>28</sub>H<sub>42</sub>O<sub>4</sub> (MW = 442.31): C, 75.98; H, 9.56; O, 14.46. Found: C, 75.95; H, 9.58; O, 14.47.



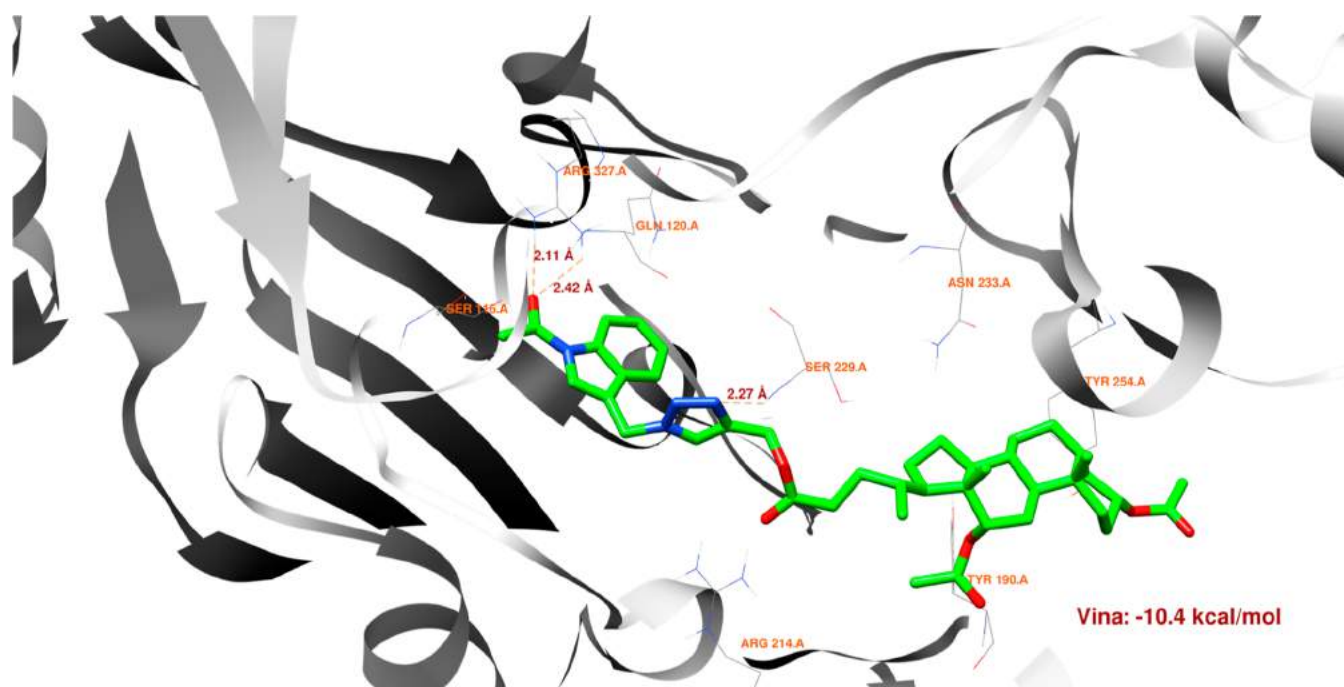


Figure 12. Structure of bioconjugate 20 (Figure 4) inside the active site of the 2Q85 protein domain with yellow marked possible H-bonds.

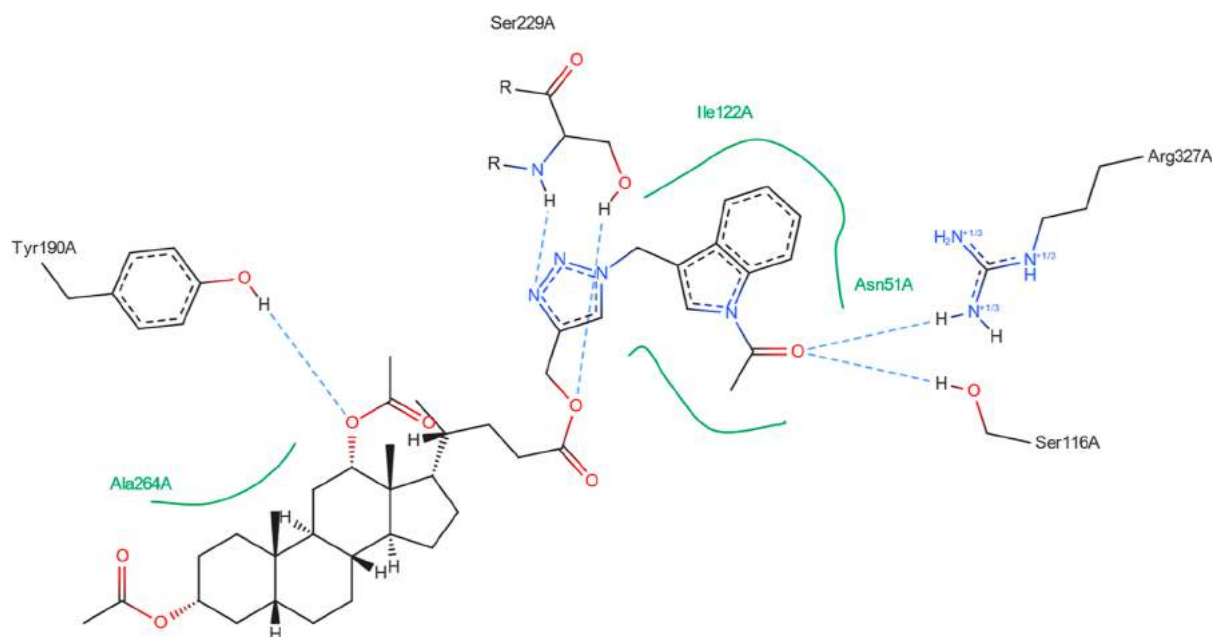


Figure 13. Structure of bioconjugate 20 (Figure 4) inside the active site of the 2Q85 protein domain with marked following interactions: green solid lines—hydrophobic contact and light-blue—hydrogen bond.

4.1.2.2. *Propargyl 3 $\alpha$ ,12 $\alpha$ -Diformyl-5 $\beta$ -cholan-24-oate (9)*. White oil,  $^1\text{H}$  NMR (300 MHz,  $\text{CDCl}_3$ ):  $\delta$  8.14 (s, 1H, 12 $\alpha$ -OCHO), 8.04 (d,  $J$  = 0.9 Hz, 1H, 3 $\alpha$ -OCHO), 5.25 (s, 1H, 12 $\beta$ -H), 4.89–4.79 (m, 1H, 3 $\beta$ -H), 4.68 (d,  $J$  = 3.0 Hz, 2H, O–CH<sub>2</sub>), 2.48 (t,  $J$  = 2.5 Hz, 1H, –C $\equiv$ CH), 0.93 (s, 3H, CH<sub>3</sub>-19), 0.83 (d,  $J$  = 6.3 Hz, 3H, CH<sub>3</sub>-21), 0.75 (s, 3H, CH<sub>3</sub>-18).  $^{13}\text{C}\{^1\text{H}\}$  NMR (76 MHz,  $\text{CDCl}_3$ ):  $\delta$  173.2 (C-24), 160.7 (12-OCHO), 160.6 (3-OCHO), 77.7 (C $\equiv$ ), 76.0 (C-12), 74.8 ( $\equiv$ CH), 74.1 (C-3), 51.8, 49.2, 47.3, 45.0, 41.7, 35.6, 34.8, 34.7, 34.2, 34.0, 32.1, 30.9, 30.5, 27.4, 26.8, 26.5, 25.9, 25.7, 23.4, 22.9 (C-19), 17.5 (C-21), 12.3 (C-18). FT-IR (KBr,  $\text{cm}^{-1}$ )  $\nu_{\text{max}}$ : 3249 (C $\equiv$  C–H), 2935 (C–H), 2867 (C–H), 1717 (C=O), 1450 (C–H), 1378 (C–O), 1251 (C–O), 1167 (C–H). ESI-MS  $m/z$ : 525 [ $\text{M} + \text{K}$ ]<sup>+</sup> (100%), 509 [ $\text{M} + \text{Na}$ ]<sup>+</sup> (50%). Anal. Calcd for C<sub>29</sub>H<sub>42</sub>O<sub>6</sub> (MW

= 486.30): C, 71.57; H, 8.70; O, 19.73. Found: C, 71.61; H, 8.68; O, 19.71.

4.1.2.3. *Propargyl 3 $\alpha$ ,7 $\alpha$ ,12 $\alpha$ -Triformyl-5 $\beta$ -cholan-24-oate (10)*. White oil,  $^1\text{H}$  NMR (300 MHz,  $\text{CDCl}_3$ ):  $\delta$  8.16 (s, 1H, 12 $\alpha$ -OCHO), 8.11 (s, 1H, 7 $\alpha$ -OCHO), 8.03 (d,  $J$  = 1.0 Hz, 1H, 3 $\alpha$ -OCHO), 5.27 (s, 1H, 12 $\beta$ -H), 5.07 (s, 1H, 7 $\beta$ -H), 4.76–4.69 (m, 1H, 3 $\beta$ -H), 4.67 (dd,  $J$  = 2.5 Hz, 2H, OCH<sub>2</sub>), 2.47 (t,  $J$  = 2.5 Hz, 1H, –C $\equiv$ CH), 0.95 (s, 3H, CH<sub>3</sub>-19), 0.84 (d,  $J$  = 6.4 Hz, 3H, CH<sub>3</sub>-21), 0.76 (s, 3H, CH<sub>3</sub>-18).  $^{13}\text{C}\{^1\text{H}\}$  NMR (76 MHz,  $\text{CDCl}_3$ ):  $\delta$  173.1 (C-24), 160.5 (12-OCHO), 160.5 (3-OCHO), 77.7 (–C $\equiv$ ), 75.2 (C-12), 74.7 ( $\equiv$  CH), 73.7 (C-3), 70.6 (C-7), 51.8 (O–CH<sub>2</sub>), 47.2, 45.0, 43.0, 40.8, 37.7, 34.7, 34.5, 34.4, 34.3, 31.3, 30.8, 30.5, 28.5, 27.1, 26.6, 25.5, 22.8, 22.3 (C-19), 17.4 (C-21), 12.1 (C-18). FT-IR (KBr,  $\text{cm}^{-1}$ )  $\nu_{\text{max}}$ :

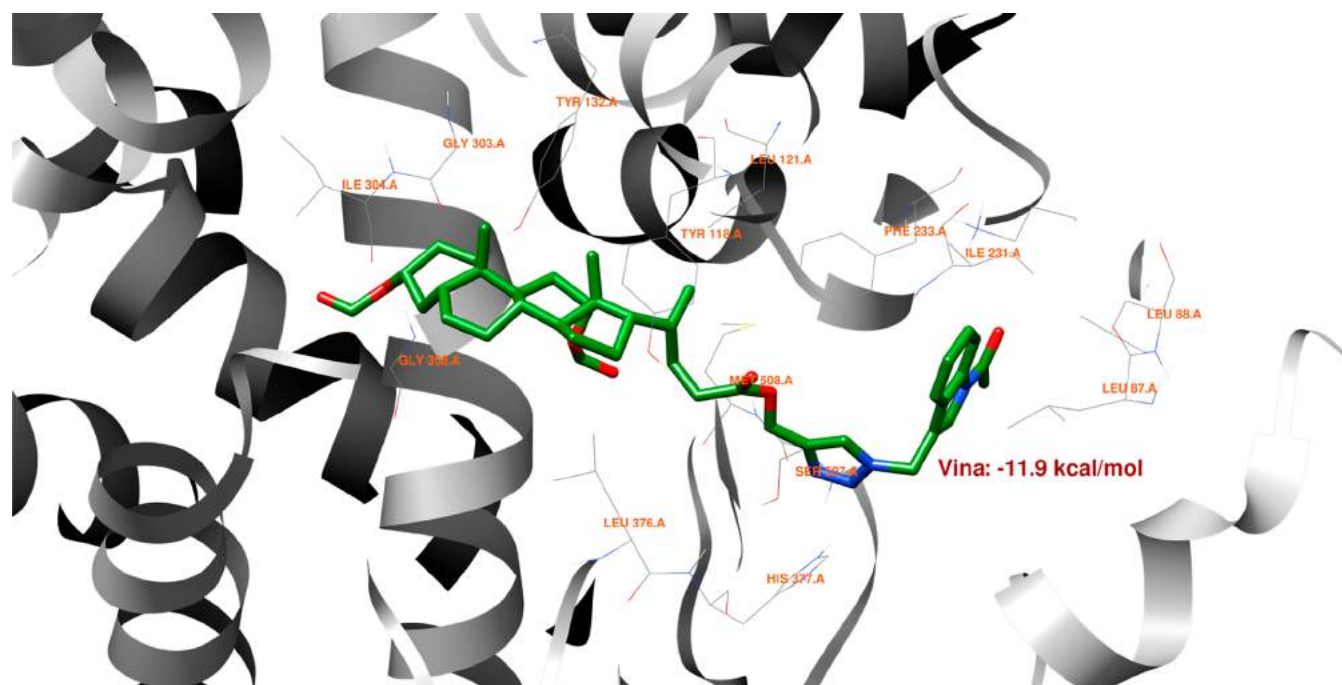


Figure 14. Structure of bioconjugate 16 (Figure 4) inside the active site of the SVSZ protein domain.

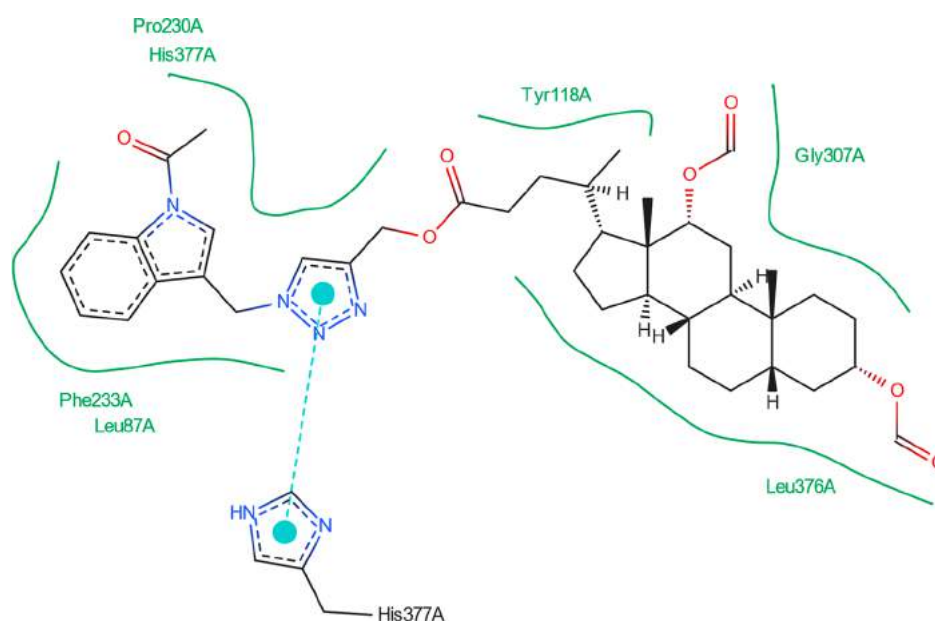


Figure 15. Structure of bioconjugate 16 (Figure 4) inside the active site of the SVSZ protein domain with marked following interactions: green solid lines—hydrophobic contact and cyan—pi–pi interaction.

3285 (C≡C–H), 2942 (C–H), 2872 (C–H), 1716 (C=O), 1468 (C–H), 1449 (C–H), 1381 (C–O), 1181 (C–O). ESI-MS  $m/z$ : 553 [M + Na]<sup>+</sup> (100%), 569 [M + K]<sup>+</sup> (10%). Anal. Calcd for C<sub>30</sub>H<sub>42</sub>O<sub>8</sub> (MW = 530.29): C, 67.90; H, 7.98; O, 24.12. Found: C, 67.91; H, 8.01; O, 24.08.

4.1.2.4. *Propargyl 3 $\alpha$ -Formyl-12 $\alpha$ -hydroxy-5 $\beta$ -cholan-24-oate (11)*. White oil, <sup>1</sup>H NMR (300 MHz, CDCl<sub>3</sub>):  $\delta$  8.03 (d,  $J$  = 1.0 Hz, 1H, 3 $\alpha$ -OCHO), 4.91–4.79 (m, 1H, 3 $\beta$ -H), 4.68 (dd,  $J_1$  = 2.5,  $J_2$  = 0.5 Hz, 2H, O–CH<sub>2</sub>), 3.99 (s, 1H, 12 $\beta$ -H), 2.47 (t,  $J$  = 2.5 Hz, 1H, –C≡CH), 0.98 (d,  $J$  = 6.3 Hz, 3H, CH<sub>3</sub>-21), 0.93 (s, 3H, CH<sub>3</sub>-19), 0.68 (s, 3H, CH<sub>3</sub>-18). <sup>13</sup>C{<sup>1</sup>H} NMR (76 MHz, CDCl<sub>3</sub>):  $\delta$  173.3 (C-24), 160.8 (3-OCHO), 77.8 (–C≡), 74.7 (≡CH), 74.2 (C-3), 73.1 (C-12), 51.8, 51.7, 48.2, 47.3, 46.5, 41.8, 35.9, 35.0, 34.8, 34.1, 34.0, 33.6, 32.1, 31.0, 30.7, 28.7, 27.4, 26.9, 26.5, 26.0, 23.6, 23.1 (C-19),

17.3 (C-21), 12.7 (C-18). FT-IR (KBr, cm<sup>–1</sup>)  $\nu_{\max}$ : 3510 (O–H), 3253 (C≡C–H), 2944 (C–H), 2866 (C–H), 2129 (C≡C), 1725 (C=O), 1466 (C–H), 1380 (C–O), 1194 (C–O). ESI-MS  $m/z$ : 481 [M + Na]<sup>+</sup> (100%), 497 [M + K]<sup>+</sup> (20%). Anal. Calcd for C<sub>28</sub>H<sub>42</sub>O<sub>5</sub> (MW = 458.30): C, 73.33; H, 9.23; O, 17.44. Found: C, 73.40; H, 9.19; O, 17.41.

4.1.2.5. *Synthesis of Propargyl 3 $\alpha$ -Acetyl-5 $\beta$ -cholan-24-oate (12)*. Propargyl lithocholate (5 mmol, 2 g) was dissolved in 2 mL of anhydrous pyridine, and 2 mL of acetic anhydride was placed in the round-bottom flask. The mixture was stirred at room temperature for 22 h. The reaction was monitored by TLC. The reaction mixture was poured onto ice, extracted with CHCl<sub>3</sub>, washed with 5% NaHCO<sub>3</sub> solution, water, and brine, and dried over anhydrous Na<sub>2</sub>SO<sub>4</sub>. 2.14 g of crude product (97%) was obtained as an oil and purified by column

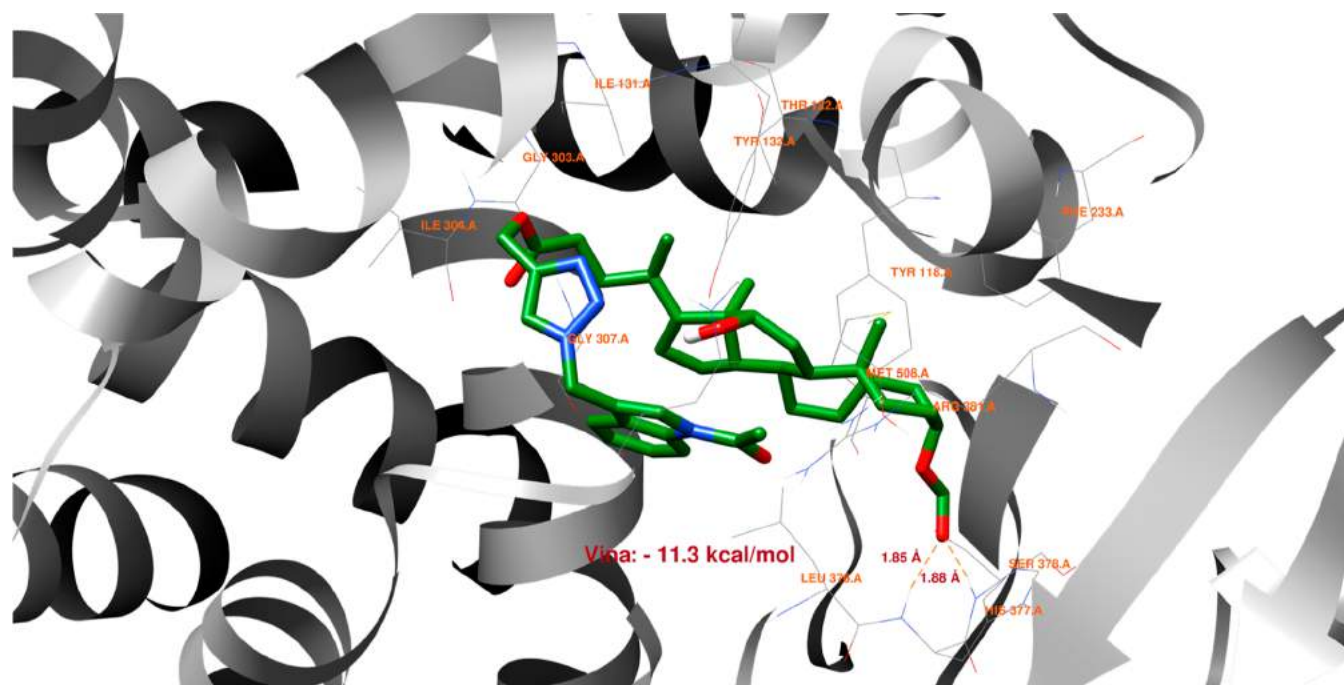


Figure 16. Structure of bioconjugate 18 (Figure 4) inside the active site of the SVSZ protein domain with yellow marked possible H-bonds.

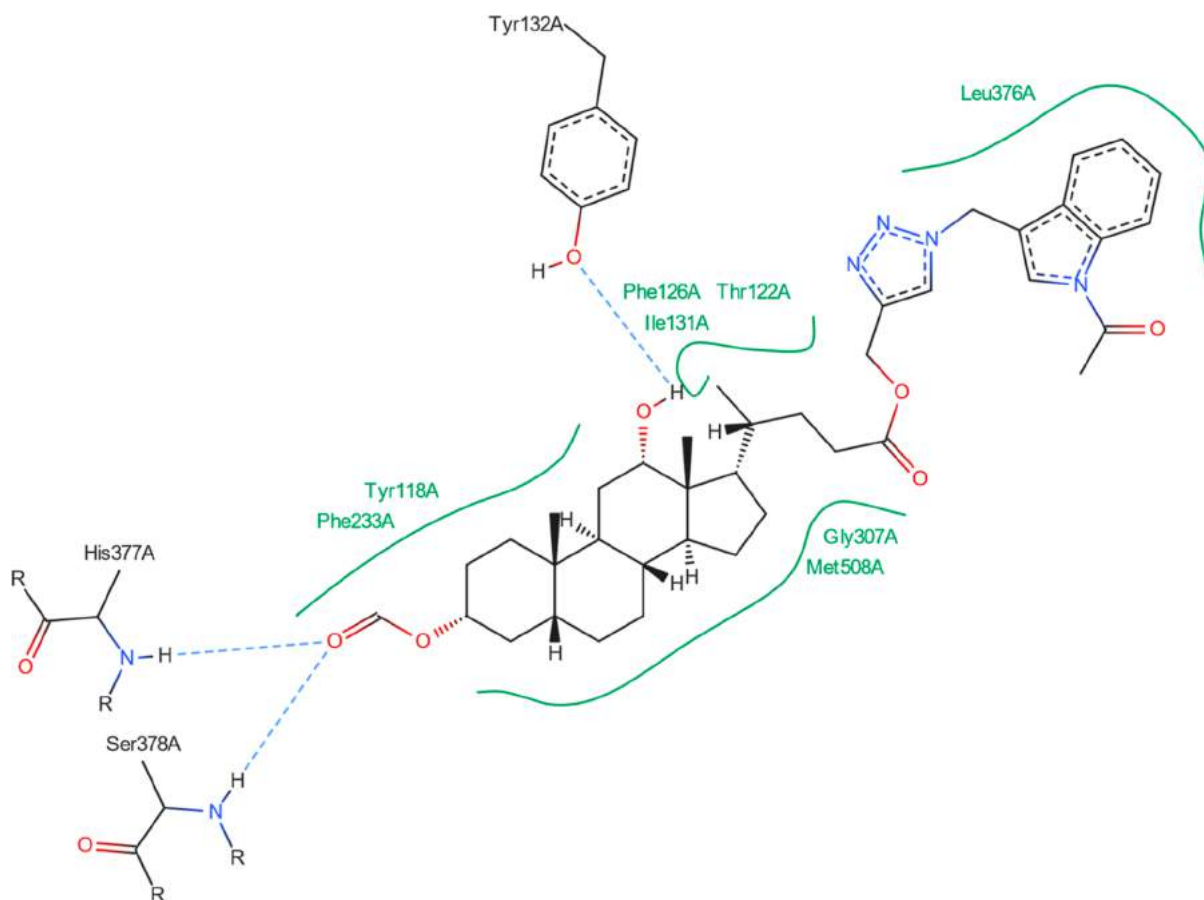


Figure 17. Structure of bioconjugate 18 (Figure 4) inside the active site of the SVSZ protein domain with marked following interactions: green solid lines—hydrophobic contact and light-blue—hydrogen bond.

chromatography (eluent  $\text{CHCl}_3$ : hexane fraction 10:1). 1.52 g portion of pure product (12) (71%) was obtained.

White oil,  $^1\text{H}$  NMR (300 MHz,  $\text{CDCl}_3$ ):  $\delta$  4.77–4.67 (m, 3H, 3 $\beta$ -H), 4.68 (dd,  $J_1 = 2.5$ ,  $J_2 = 0.5$  Hz, 2H, O–CH<sub>2</sub>) 2.46 (t,  $J = 6.8$  Hz, 1H, –C $\equiv$ CH), 2.03 (s, 3H, 3-OAc), 0.92 (s, 3H, CH<sub>3</sub>-19), 0.91 (d,  $J$

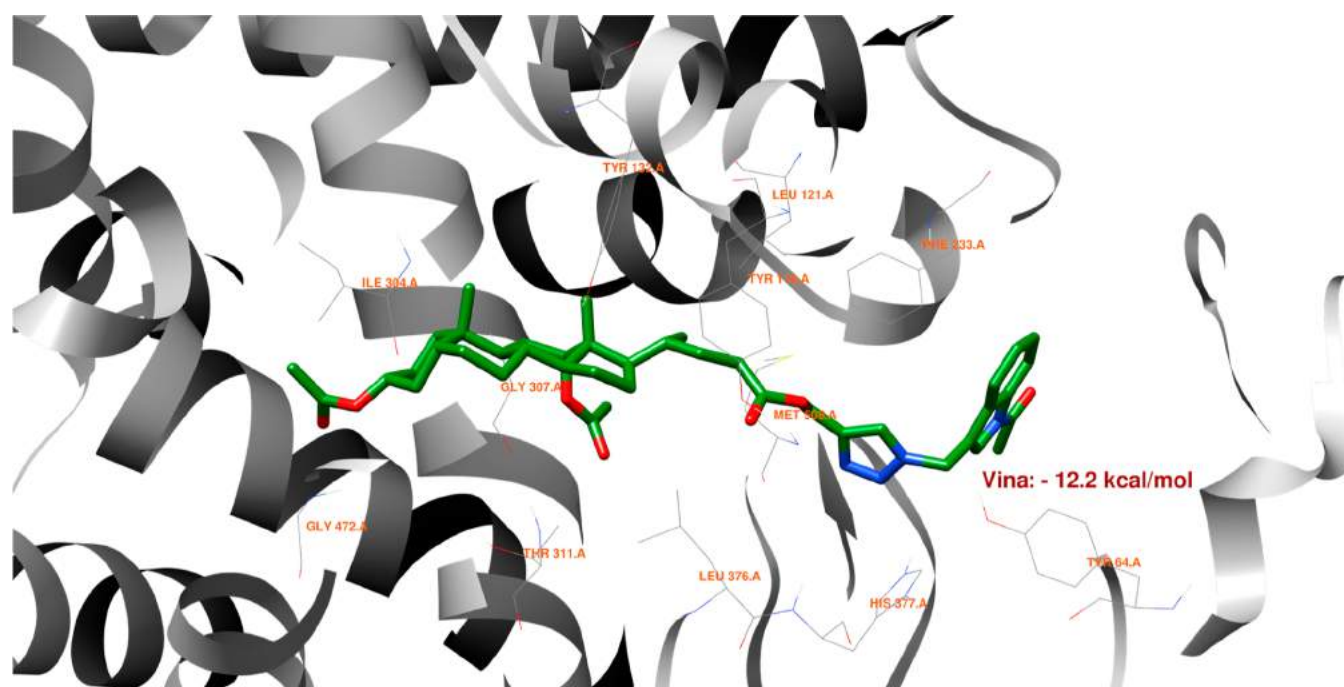


Figure 18. Structure of bioconjugate 20 (Figure 4) inside the active site of the SVSZ protein domain.

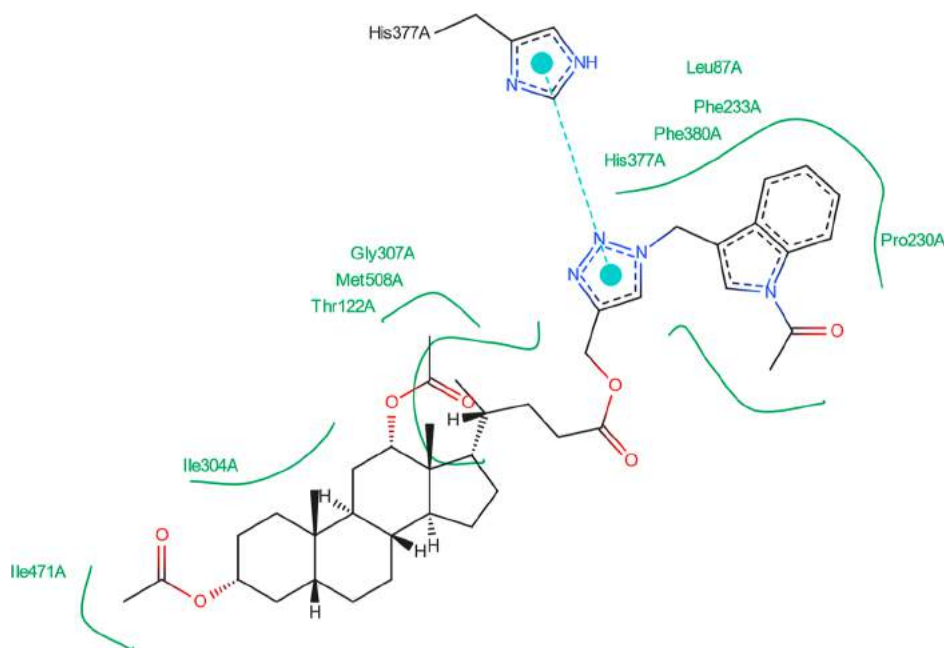


Figure 19. Structure of bioconjugate 20 (Figure 4) inside the active site of the SVSZ protein domain with marked following interactions: green solid lines—hydrophobic contact, cyan—pi-pi interaction.

= 6.1 Hz, 3H, CH<sub>3</sub>-21), 0.64 (s, 3H, CH<sub>3</sub>-18). <sup>13</sup>C{<sup>1</sup>H} NMR (76 MHz, CDCl<sub>3</sub>): δ 173.4 (C-24), 170.7 (3-AcO), 77.8 (C≡), 74.7 (≡CH), 74.4 (C-3), 56.5, 55.9, 53.2, 51.8, 42.7, 41.9, 40.4, 40.1, 35.8, 35.3, 35.0, 34.6, 32.2, 31.0, 30.8, 28.2, 27.0, 26.6, 26.3, 24.2, 23.3, 21.5, 20.8 (C-19), 18.2 (C-21), 12.0 (C-18). FT-IR (KBr, cm<sup>-1</sup>) ν<sub>max</sub>: 3253 (C≡C-H), 2925 (C-H), 2863 (C-H), 1719 (C=O), 1452 (C-H), 1376 (C-H), 1249 (C-O), 1162 (C-O), 1022 (C-O). ESI-MS *m/z*: 479 [M + Na]<sup>+</sup> (100%), 495 [M + K]<sup>+</sup> (10%). Anal. Calcd for C<sub>29</sub>H<sub>44</sub>O<sub>4</sub> (MW = 456.32): C, 76.27; H, 9.71; O, 14.01. Found: C, 76.29; H, 9.67; O, 14.04.

Compounds 13 and 14 were synthesized according to literature data.<sup>39,40</sup>

**4.1.3. General Procedure for the Preparation of Compounds (15–21).** An appropriate bile acid derivative (8–14) (0.2 mmol, 1.0 equiv) was dissolved in *t*-BuOH/MeOH (5:1), (4 mL) at 60 °C using a water bath. Then an *N*-acetyl-3-azidomethylindole (4) (0.2 mmol, 1.0 equiv) was dissolved in *t*-BuOH/MeOH (5:1) (2 mL) was added. CuSO<sub>4</sub>·5H<sub>2</sub>O (0.00002 mmol, 0.0001 equiv) and sodium ascorbate (0.00007 mmol, 0.0004 equiv) in 1 mL of distilled water were added. The mixture was stirred on a magnetic stirrer and heated in a water bath at 60 °C. Subsequent portions of the catalyst were added until the aqueous layer of the reaction mixture turned bluish-green. The reaction was monitored by TLC (PhMe/EtOAc 1:1). An orange solid precipitated as the reaction mixture was stirred. The reaction mixture was extracted with chloroform. The organic layer was evaporated

under reduced pressure. The crude product was purified over column chromatography (gradient elution, starting from  $\text{CHCl}_3/\text{EtOAc}$  5:1).

**4.1.3.1.** *{1-[(N-Acetyl-methylindole)-3-methylene]-1H-1,2,3-triazole-4-yl} Methyl 3 $\alpha$ -Formyloxy-cholan-24-oate (15)*. White oil, yield: 108 mg, 82%,  $^1\text{H}$  NMR (400 MHz,  $\text{CDCl}_3$ ):  $\delta$  8.43 (d,  $J = 7.9$  Hz, 1H, 40 H), 8.04 (d,  $J = 0.9$  Hz, 1H, 3-HCOO), 7.57 (s, 1H, 30 H), 7.54 (br s, 1H, 33-H<sub>indole</sub>), 7.45–7.38 (m, 2H, 38 H, 39 H), 7.31–7.29 (m, 1H, 37 H), 5.68 (d,  $J = 1.0$  Hz, 2H,  $\text{CH}_2$ -31), 5.16 (d,  $J = 1.4$  Hz, 2H,  $\text{CH}_2$ -25), 4.89–4.81 (m, 1H, 3 $\beta$ -H), 2.66 (s, 3H,  $\text{CH}_3$ -42), 0.93 (s, 3H,  $\text{CH}_3$ -19), 0.85 (d,  $J = 6.4$  Hz, 3H,  $\text{CH}_3$ -21), 0.60 (s, 3H,  $\text{CH}_3$ -18).  $^{13}\text{C}\{^1\text{H}\}$  NMR (101 MHz,  $\text{CDCl}_3$ ):  $\delta$  174.1 (C-24), 168.3 (C-41), 160.8 (3-OCHO), 143.4 (C-26), 136.0, 128.4, 126.1, 124.6, 124.2, 123.6 (C-30), 118.6, 116.8, 115.6, 74.4 (C-3), 57.4, 56.4, 55.8, 45.5, 42.7, 41.9, 40.4, 40.0, 35.7, 35.2, 34.9, 34.5, 32.2, 31.0, 30.8, 29.7, 28.1, 26.9, 26.6, 26.3, 24.1, 23.3, 20.9 (C-19), 18.9 (C-21), 12.0 (C-18). FT-IR (KBr,  $\text{cm}^{-1}$ )  $\nu_{\text{max}}$ : 3434 (C–H), 3140 (=C–H), 2927 (C–H), 2865 (C–H), 1717 (C=O). ESI-MS ( $m/z$ ): 679 [M + Na]<sup>+</sup> (100%), 695 [M + K]<sup>+</sup> (20%), 692 [M + Cl]<sup>−</sup>. Anal. Calcd for  $\text{C}_{39}\text{H}_{52}\text{N}_4\text{O}_6$  (MW = 656.39): C, 71.31; H, 7.98; N, 8.53; O, 12.18. Found: C, 71.28; H, 7.87; N, 8.76; O, 12.09.

**4.1.3.2.** *{1-[(N-Acetyl-methylindole)-3-methylene]-1H-1,2,3-triazole-4-yl} Methyl 3 $\alpha$ ,12 $\alpha$ -Diformyloxy-cholan-24-oate (16)*. White oil, yield: 97 mg, 69%,  $^1\text{H}$  NMR (400 MHz,  $\text{CDCl}_3$ ):  $\delta$  8.43 (d,  $J = 8.3$  Hz, 1H, 40 H), 8.11 (s, 1H, 12-HCOO), 8.03 (d,  $J = 0.9$  Hz, 1H, 3-HCOO), 7.57 (s, 1H, 30 H), 7.55 (br s, 1H, 33 H), 7.45–7.38 (m, 2H, 38 H, 39 H), 7.30–7.29 (m, 1H, 37 H), 5.68 (d,  $J = 0.8$  Hz, 2H,  $\text{CH}_2$ -31), 5.20 (d,  $J = 3.3$  Hz, 1H, 12 $\beta$ -H), 5.15 (d,  $J = 2.0$  Hz, 2H,  $\text{CH}_2$ -25), 4.87–4.80 (m, 1H, 3 $\beta$ -H), 2.66 (s, 3H,  $\text{CH}_3$ -42), 0.92 (s, 3H,  $\text{CH}_3$ -19), 0.76 (d,  $J = 6.4$  Hz, 3H,  $\text{CH}_3$ -21), 0.69 (s, 3H,  $\text{CH}_3$ -18).  $^{13}\text{C}\{^1\text{H}\}$  NMR (101 MHz,  $\text{CDCl}_3$ ):  $\delta$  173.9 (C-24), 168.3 (C-41), 160.6 (3-OCHO), 160.5 (12-OCHO), 143.3 (C-26), 135.9, 128.3, 126.1, 124.8, 124.2, 123.5 (C-30), 118.6, 116.8, 115.6, 75.9 (C-12), 74.1 (C-3), 57.4, 49.2, 47.2, 45.4, 44.9, 41.7, 35.5, 34.7, 34.6, 34.1, 34.0, 32.0, 30.9, 30.5, 27.3, 26.7, 26.4, 25.9, 24.0, 23.4, 22.9 (C-19), 17.4 (C-21), 12.2 (C-18). FT-IR (KBr,  $\text{cm}^{-1}$ )  $\nu_{\text{max}}$ : 3143 (C–H), 2941 (C–H), 2872 (C–H), 1716 (C=O). ESI-MS ( $m/z$ ): 723 [M + Na]<sup>+</sup> (100%), 739 [M + K]<sup>+</sup> (12%), 701 [M + H]<sup>+</sup> (10%), 799 [M + ClO<sub>4</sub>]<sup>−</sup>, 735 [M + Cl]<sup>−</sup>. Anal. Calcd for  $\text{C}_{40}\text{H}_{52}\text{N}_4\text{O}_7$  (MW = 700.38): C, 68.55; H, 7.48; N, 7.99; O, 15.98. Found: C, 68.54; H, 7.46; N, 8.01; O, 15.99.

**4.1.3.3.** *{1-[(N-Acetyl-methylindole)-3-methylene]-1H-1,2,3-triazole-4-yl} Methyl 3 $\alpha$ ,7 $\alpha$ ,12 $\alpha$ -Triformyloxy-cholan-24-oate (17)*. White oil, yield: 103 mg, 69%,  $^1\text{H}$  NMR (400 MHz,  $\text{CDCl}_3$ ):  $\delta$  8.43 (d,  $J = 8.5$  Hz, 1H, 40 H), 8.14 (s, 1H, 7-HCOO), 8.10 (s, 1H, 12-HCOO), 8.02 (d,  $J = 0.9$  Hz, 1H, 3-HCOO), 7.57 (br s, 1H, 30 H), 7.45–7.38 (m, 2H, 38 H, 39 H), 7.30–7.28 (m, 1H, 37 H), 5.68 (d,  $J = 0.9$  Hz, 2H,  $\text{CH}_2$ -31), 5.22 (t,  $J = 3.0$  Hz, 1H, 12 $\beta$ -H), 5.15 (d,  $J = 2.7$  Hz, 2H,  $\text{CH}_2$ -25), 5.06 (d,  $J = 3.5$  Hz, 1H, 7 $\beta$ -H), 4.75–4.69 (m, 1H, 3 $\beta$ -H), 2.66 (s, 3H,  $\text{CH}_3$ -42), 0.94 (s, 3H,  $\text{CH}_3$ -19), 0.76 (d,  $J = 6.5$  Hz, 3H,  $\text{CH}_3$ -21), 0.70 (s, 3H,  $\text{CH}_3$ -18).  $^{13}\text{C}\{^1\text{H}\}$  NMR (101 MHz,  $\text{CDCl}_3$ ):  $\delta$  173.8 (C-24), 168.3 (C-41), 160.6 (3-OCHO), 160.5 (12-OCHO), 160.5 (7-OCHO), 143.3 (C-26), 134.0, 128.4, 126.1, 124.8, 124.2, 123.5 (C-30), 118.6, 116.8, 115.6, 75.2 (C-12), 73.7 (C-3), 70.6 (C-7), 57.4, 47.0, 45.5, 44.9, 42.9, 40.8, 37.6, 34.6, 34.5, 34.2, 31.3, 30.8, 30.4, 28.5, 27.1, 26.5, 25.5, 24.0, 22.7, 22.3 (C-19), 17.4 (C-21), 12.0 (C-18). FT-IR (KBr,  $\text{cm}^{-1}$ )  $\nu_{\text{max}}$ : 3143 (C–H), 2941 (C–H), 2869 (C–H), 1715 (C=O). ESI-MS ( $m/z$ ): 767 [M + Na]<sup>+</sup> (100%), 783 [M + K]<sup>+</sup> (60%), 745 [M + H]<sup>+</sup> (20%), 843 [M + ClO<sub>4</sub>]<sup>−</sup>, 823 [M + Br]<sup>−</sup>, 779 [M + Cl]<sup>−</sup>. Anal. Calcd for  $\text{C}_{41}\text{H}_{52}\text{N}_4\text{O}_9$  (MW = 744.37): C, 66.11; H, 7.04; N, 7.52; O, 19.33. Found: C, 66.14; H, 7.01; N, 7.54; O, 19.31.

**4.1.3.4.** *{1-[(N-Acetyl-methylindole)-3-methylene]-1H-1,2,3-triazole-4-yl} Methyl 3 $\alpha$ -Formyloxy-12 $\alpha$ -hydroxycholan-24-oate (18)*. White oil, yield: 91 mg, 68%,  $^1\text{H}$  NMR (400 MHz,  $\text{CDCl}_3$ ):  $\delta$  8.43 (d,  $J = 8.3$  Hz, 1H, 40 H), 8.02 (d,  $J = 0.9$  Hz, 1H, 3-HCOO), 7.58 (br s, 1H, 30 H), 7.56 (br s, 1H, 33 H), 7.45–7.38 (m, 2H, 38 H, 39 H), 7.31–7.28 (m, 1H, 37 H), 5.68 (d,  $J = 0.8$  Hz, 2H,  $\text{CH}_2$ -31), 5.16 (s, 2H,  $\text{CH}_2$ -25), 4.88–4.80 (m, 1H, 3 $\beta$ -H), 3.95 (t,  $J = 2.9$  Hz, 1H, 12 $\beta$ -H), 2.66 (s, 3H,  $\text{CH}_3$ -42), 0.92 (s, 3H,  $\text{CH}_3$ -19), 0.90 (d,  $J = 6.3$  Hz, 3H,  $\text{CH}_3$ -21), 0.63 (s, 3H,  $\text{CH}_3$ -18).  $^{13}\text{C}\{^1\text{H}\}$  NMR (101 MHz,

$\text{CDCl}_3$ ):  $\delta$  174.0 (C-24), 168.3 (C-41), 160.8 (3-OCHO), 143.4 (C-26), 136.0, 128.4, 126.1, 124.8, 124.2, 123.6 (C-30), 118.6, 116.8, 115.6, 74.2, 73.0, 57.4, 48.2, 47.2, 46.4, 45.5, 41.8, 35.9, 35.0, 34.8, 34.1, 33.6, 32.1, 31.0, 30.7, 28.7, 27.4, 26.9, 26.5, 26.0, 24.0, 23.5, 23.1 (C-19), 17.2 (C-21), 12.6 (C-18). FT-IR (KBr,  $\text{cm}^{-1}$ )  $\nu_{\text{max}}$ : 3435 (O–H), 3144 (=C–H), 2936 (C–H), 2868 (C–H), 1716 (C=O). ESI-MS ( $m/z$ ): 695 [M + Na]<sup>+</sup> (100%), 673 [M + H]<sup>+</sup> (15%), 753 [M + Br]<sup>−</sup>, 707 [M + Cl]<sup>−</sup>. Anal. Calcd for  $\text{C}_{39}\text{H}_{52}\text{N}_4\text{O}_6$  (MW = 672.39): C, 69.62; H, 7.79; N, 8.33; O, 14.27. Found: C, 69.59; H, 7.80; N, 8.31; O, 14.30.

**4.1.3.5.** *{1-[(N-Acetyl-methylindole)-3-methylene]-1H-1,2,3-triazole-4-yl} Methyl 3 $\alpha$ -Acetoxy-cholan-24-oate (19)*. White oil, yield: 80 mg, 60%,  $^1\text{H}$  NMR (400 MHz,  $\text{CDCl}_3$ ):  $\delta$  8.43 (d,  $J = 7.9$  Hz, 1H, 40 H), 7.57 (s, 1H, 30 H), 7.54 (bs, 1H, 33 H), 7.45–7.39 (m, 2H, 38 H, 39 H), 7.31–7.28 (m, 1H, 37 H), 5.68 (d,  $J = 0.9$  Hz, 2H,  $\text{CH}_2$ -31), 5.16 (d,  $J = 1.6$  Hz, 2H,  $\text{CH}_2$ -25), 4.76–4.68 (m, 1H, 3 $\beta$ -H), 2.66 (s, 3H,  $\text{CH}_3$ -42), 2.03 (s, 3H, 3-OCOCH<sub>3</sub>), 0.92 (s, 3H,  $\text{CH}_3$ -19), 0.85 (d,  $J = 6.4$  Hz, 3H,  $\text{CH}_3$ -21), 0.59 (s, 3H,  $\text{CH}_3$ -18).  $^{13}\text{C}\{^1\text{H}\}$  NMR (101 MHz,  $\text{CDCl}_3$ ):  $\delta$  174.1 (C-24), 170.6 (3-COCH<sub>3</sub>), 168.3 (C-41), 143.4 (C-26), 135.9, 128.3, 126.1, 124.7, 124.2, 123.6 (C-30), 118.6, 116.8, 115.6, 74.4 (C-3), 57.3, 56.4, 55.9, 45.5, 42.7, 41.8, 40.3, 40.1, 35.7, 35.2, 35.0, 34.5, 32.2, 31.0, 30.8, 28.1, 27.0, 26.6, 26.3, 24.1, 24.0, 23.3, 21.5, 20.8 (C-19), 18.2 (C-21), 11.9 (C-18). FT-IR (KBr,  $\text{cm}^{-1}$ )  $\nu_{\text{max}}$ : 3147 (=C–H), 2930 (C–H), 2865 (C–H), 1734 (C=O). ESI-MS ( $m/z$ ): 693 [M + Na]<sup>+</sup> (100%), 710 [M + K]<sup>+</sup> (50%), 671 [M + H]<sup>+</sup> (10%), 705 [M + Cl]<sup>−</sup>. Anal. Calcd for  $\text{C}_{40}\text{H}_{54}\text{N}_4\text{O}_5$  (MW = 670.41): C, 71.61; H, 8.11; N, 8.35; O, 11.92. Found: C, 71.64; H, 8.12; N, 8.37; O, 11.87.

**4.1.3.6.** *{1-[(N-Acetyl-methylindole)-3-methylene]-1H-1,2,3-triazole-4-yl} Methyl 3 $\alpha$ ,12 $\alpha$ -Diacetoxy-cholan-24-oate (20)*. White oil, yield: 124 mg, 85%,  $^1\text{H}$  NMR (400 MHz,  $\text{CDCl}_3$ ):  $\delta$  8.43 (d,  $J = 8.2$  Hz, 1H, 40 H), 7.57 (d,  $J = 7.7$  Hz, 2H, 30 H, 33 H), 7.45–7.38 (m, 2H, 38 H, 39 H), 7.30–29 (m, 1H, 37 H), 5.69 (s, 2H,  $\text{CH}_2$ -31), 5.16 (s, 2H,  $\text{CH}_2$ -25), 5.04 (t,  $J = 2.9$  Hz, 1H, 12 $\beta$ -H), 4.74–4.66 (m, 1H, 3 $\beta$ -H), 2.66 (s, 3H,  $\text{CH}_3$ -42), 2.08 (s, 3H, 12-OCOCH<sub>3</sub>), 2.04 (s, 3H, 3-OCOCH<sub>3</sub>), 0.90 (s, 3H,  $\text{CH}_3$ -19), 0.73 (d,  $J = 6.4$  Hz, 3H,  $\text{CH}_3$ -21), 0.67 (s, 3H,  $\text{CH}_3$ -18).  $^{13}\text{C}\{^1\text{H}\}$  NMR (101 MHz,  $\text{CDCl}_3$ ):  $\delta$  173.9 (C-24), 170.6 (3-COCH<sub>3</sub>), 170.4 (12-COCH<sub>3</sub>), 168.3 (C-41), 143.3 (C-26), 135.9, 128.4, 126.1, 124.8, 124.2, 123.6 (C-30), 118.6, 116.8, 115.6, 75.8 (C-3), 74.2 (C-12), 57.4, 49.3, 47.4, 45.5, 44.9, 41.8, 35.6, 34.7, 34.5, 34.3, 34.0, 32.2, 30.9, 30.6, 27.2, 26.8, 26.6, 25.6, 25.6, 24.0, 23.3, 23.0, 21.4, 21.4 (C-19), 17.4 (C-21), 12.3 (C-18). FT-IR (KBr,  $\text{cm}^{-1}$ )  $\nu_{\text{max}}$ : 3121 (=C–H), 2930 (C–H), 2868 (C–H), 1735 (C=O). ESI-MS ( $m/z$ ): 751 [M + Na]<sup>+</sup> (100%), 767 [M + K]<sup>+</sup> (10%), 808 [M + Br]<sup>−</sup>, 763 [M + Cl]<sup>−</sup>. Anal. Calcd for  $\text{C}_{42}\text{H}_{56}\text{N}_4\text{O}_7$  (MW = 728.41): C, 69.21; H, 7.74; N, 7.69; O, 15.36. Found: C, 69.17; H, 7.73; N, 7.72; O, 15.38.

**4.1.3.7.** *{1-[(N-Acetyl-methylindole)-3-methylene]-1H-1,2,3-triazole-4-yl} Methyl 3 $\alpha$ ,7 $\alpha$ ,12 $\alpha$ -Triacetoxycholan-24-oate (21)*. White oil, yield: 138 mg, 88%,  $^1\text{H}$  NMR (400 MHz,  $\text{CDCl}_3$ ):  $\delta$  8.43 (d,  $J = 8.6$  Hz, 1H, 40 H), 7.58 (br s, 1H, 30 H), 7.56 (bs, 1H, 33 H), 7.45–7.38 (m, 2H, 38 H, 39 H), 7.30–7.29 (m, 1H, 37 H), 5.68 (s, 2H,  $\text{CH}_2$ -31), 5.15 (s, 2H,  $\text{CH}_2$ -25), 5.04 (t,  $J = 3.0$  Hz, 1H, 12 $\beta$ -H), 4.90 (d,  $J = 9.5$  Hz, 1H, 7 $\beta$ -H), 4.61–4.53 (m, 1H, 3 $\beta$ -H), 2.66 (s, 3H,  $\text{CH}_3$ -42), 2.12 (s, 3H, 7-OCOCH<sub>3</sub>), 2.09 (s, 3H, 12-OCOCH<sub>3</sub>), 2.05 (s, 3H, 3-OCOCH<sub>3</sub>), 0.91 (s, 3H,  $\text{CH}_3$ -19), 0.74 (d,  $J = 6.4$  Hz, 3H,  $\text{CH}_3$ -21), 0.68 (s, 3H,  $\text{CH}_3$ -18);  $^{13}\text{C}\{^1\text{H}\}$  NMR (101 MHz,  $\text{CDCl}_3$ ):  $\delta$  173.9 (C-24), 170.5 (3-COCH<sub>3</sub>), 170.5 (12-COCH<sub>3</sub>), 170.4 (7-COCH<sub>3</sub>), 168.3 (C-41), 143.3 (C-26), 136.0, 128.4, 126.1, 124.8, 124.2, 123.5 (C-30), 118.6, 116.8, 115.6, 75.3 (C-3), 74.1 (C-12), 70.6 (C-7), 57.3, 47.2, 45.5, 43.3, 40.9, 37.7, 34.7, 34.6, 34.4, 34.3, 31.2, 30.8, 30.5, 28.8, 27.1, 26.9, 25.5, 24.0, 22.7, 22.5, 21.6, 21.5, 21.4 (C-19), 17.4 (C-21), 12.1 (C-18). FT-IR (KBr,  $\text{cm}^{-1}$ )  $\nu_{\text{max}}$ : 3141 (=C–H), 2961 (C–H), 2871 (C–H), 1732 (C=O). ESI-MS ( $m/z$ ): 809 [M + Na]<sup>+</sup> (100%), 825 [M + K]<sup>+</sup> (50%), 787 [M + H]<sup>+</sup> (20%), 866 [M + Br]<sup>−</sup>, 821 [M + Cl]<sup>−</sup>. Anal. Calcd for  $\text{C}_{44}\text{H}_{58}\text{N}_4\text{O}_9$  (MW = 786.42): C, 67.15; H, 7.43; N, 7.12; O, 18.30. Found: C, 67.17; H, 7.40; N, 7.14; O, 18.29.

Synthesis of {1-[(*N*-acetyl-methylindole)-3-methylene]-1*H*-1,2,3-triazole-4-yl} methyl 3 $\alpha$ ,7 $\alpha$ ,12 $\alpha$ -triacetoxycholan-24-oate (21)—The experiment was carried out on a larger scale.

**4.1.3.8. Propargyl 3 $\alpha$ ,7 $\alpha$ ,12 $\alpha$ -triacetyl-5 $\beta$ -cholan-24-oate (14).** 2 mmol (1.11 g) was dissolved in *t*-BuOH/MeOH (5:1), (40 mL) at 60 °C using a water bath. Then, *N*-acetyl-3-azidomethylindole (4) (2 mmol, 428 mg) was dissolved in *t*-BuOH/MeOH (5:1) (20 mL). CuSO<sub>4</sub>·5H<sub>2</sub>O (0.0002 mmol, 50 mg) and sodium ascorbate (0.0007 mmol, 139 mg) in 10 mL of distilled water were added. The mixture was stirred on a magnetic stirrer and heated in a water bath at 60 °C. Subsequent portions of the catalyst were added until the aqueous layer of the reaction mixture turned bluish-green. The reaction was monitored by TLC (PhMe/EtOAc 1:1). An orange solid precipitated as the reaction mixture was stirred. The reaction mixture was extracted with chloroform. The organic layer was evaporated under reduced pressure. The crude product was purified over column chromatography (gradient elution, starting from CHCl<sub>3</sub>/EtOAc 5:1). 944 mg portion of pure product (60%) was obtained as a white oil.

**4.2. PM5 Calculations.** PMS semiempirical calculations were performed by using the WinMopac 2003 program.

**4.3. Biological Activity.** **4.3.1. Human Red Blood Cells.** Freshly human RBC suspensions were purchased from the blood bank in Pozna according to the bilateral agreement between Adam Mickiewicz University and blood bank no. ZP/2867/D/21 without any contact with blood donors. RBCs were washed three times (3000 rpm, 10 min, 4 °C) in 7.4 pH phosphate buffered saline (PBS—137 mM NaCl, 2.7 mM KCl, 10 mM Na<sub>2</sub>HPO<sub>4</sub>, 1.76 mM KH<sub>2</sub>PO<sub>4</sub>) supplemented with 10 mM glucose. After washing, RBC was suspended in the PBS buffer at 1.65 × 10<sup>9</sup> cells/mL, stored at 4 °C, and used within 5 h.

**4.3.2. Hemolysis Assay.** RBCs (1.65 × 10<sup>8</sup> cells/mL, ~1.5% hematocrit) were incubated in PBS (7.4 pH) supplemented with 10 mM glucose and containing derivatives tested at a 0.1 mg/mL concentration for 60 min at 37 °C in a thermo-shaker. RBCs incubated in PBS without compounds tested were taken as the negative controls, and RBCs incubated in ice-cold deionized water were taken as the positive controls. Each sample was prepared in triplicate, and the experiments were repeated three times (*n* = 9). After incubation, the RBC suspensions were centrifuged (3000 rpm, 10 min, 4 °C) and the absorbance of the supernatants at 540 nm was measured. The results were expressed as a percentage (%) of hemolysis, which was calculated using the following formula

$$\text{hemolysis (\%)} = (\text{sample Ab}/\text{positive control Ab}) \times 100$$

where sample Ab is the absorbance value of the supernatant of RBC incubated with compounds tested, and positive control, AB is an absorbance value of the supernatant of RBC incubated in ice-cold deionized water. Each sample was prepared in triplicate, and the results are presented as a mean value ( $\pm$ SD) of three independent experiments (*n* = 9).

**4.3.3. Erythrocyte Shape Evaluation.** The incubation was carried out as follows: RBC was fixed in the mixture of 5% paraformaldehyde (PFA) and 0.01% glutaraldehyde (GA) for 60 min at room temperature. After fixation, cells were washed by exchanging the supernatant with PBS buffer, settled on poly-L-lysine-treated (0.1 mg/mL, 10 min, room temperature) cover glasses (15 min, room temperature), and mounted 80% glycerol. The coverslips were sealed with nail polish. Many cells in several separate experimental samples were studied using a RED-233 MOTIC microscope (63 $\times$  objective, 10 $\times$  ocular). Images were acquired using a Motica 3.0 MP microscopic camera and the program Motica Images Plus 3.0. The shapes of RBC in every sample were estimated according to the Bessis classification.<sup>41</sup>

**4.3.4. Statistical Analysis.** For hemolytic activity, data were plotted as the arithmetic mean  $\pm$  standard deviation (SD) of the results of three independent experiments, with every sample (test samples and positive controls) in triplicate (*n* = 9).

**4.4. Molecular Docking.** The molecular docking procedure was carried out using the rdkit tool,<sup>42</sup> which allows for the construction of 3D structures from SMILES representations of structures. The 3D

structures were saved in \*.pdb format and then converted to the \*.pdbqt format required by the AutoDock Vina algorithm.<sup>43</sup> The OpenBabel program was used to convert the files.<sup>44,45</sup> The receptors were prepared with the help of AutoDock Tools 1.5.7.<sup>46,47</sup> The molecular docking method was carried out using the AutoDock Vina multiple CPU technique.<sup>43</sup> The visualizations of the molecular docking's best ligand's poses along with the possible H-bond formation have been done with the Chimera tool (1.16).<sup>48</sup> The 2D ligand–protein domain interactions graphs have been prepared with the application of ProteinsPlus.<sup>49–54</sup>

2Q85 and 5V5Z (PDB IDs) were chosen as receptors for the molecular docking of structures 16, 18, and 20 (see Figure 4). These are obtained from the Protein Data Bank (PDB).<sup>55</sup> The former is attributed to antibacterial action (*Escherichia coli* MurB),<sup>56</sup> whereas the latter is attributed to antifungal activity (CYP51<sub>ca</sub>).<sup>57</sup>

Docked structures share the same active site of the protein domain as cocrystallized ligands. The search parameters for 2Q85's search parameters were center (*x*, *y*, *z*): 13.853, 0.000, 0.000, and size (*x*, *y*, *z*) (80 × 80 × 80) Å<sup>3</sup>. 5V5Z had the center (*x*, *y*, *z*) of –41.500, –11.400, 23.547, and the size (*x*, *y*, *z*) of (70 × 100 × 60) Å<sup>3</sup>.

## ■ ASSOCIATED CONTENT

### Data Availability Statement

The data underlying this study are available in the published article and its Supporting Information.

### Supporting Information

The Supporting Information is available free of charge at <https://pubs.acs.org/doi/10.1021/acs.joc.3c00815>.

General information and copies of ESI-MS and <sup>1</sup>H and <sup>13</sup>C NMR spectra (PDF)

## ■ AUTHOR INFORMATION

### Corresponding Authors

**Beata Jasiewicz** – Department of Bioactive Products, Faculty of Chemistry, Adam Mickiewicz University, 61-614 Poznań, Poland; Email: [beata.jasiewicz@amu.edu.pl](mailto:beata.jasiewicz@amu.edu.pl)

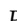
**Tomasz Pospieszny** – Department of Bioactive Products, Faculty of Chemistry, Adam Mickiewicz University, 61-614 Poznań, Poland;  [orcid.org/0000-0001-5071-7016](https://orcid.org/0000-0001-5071-7016); Email: [tposp@amu.edu.pl](mailto:tposp@amu.edu.pl)

### Authors

**Natalia Berdzik** – Department of Bioactive Products, Faculty of Chemistry, Adam Mickiewicz University, 61-614 Poznań, Poland

**Hanna Koenig** – Department of Bioactive Products, Faculty of Chemistry, Adam Mickiewicz University, 61-614 Poznań, Poland

**Lucyna Mrówczyńska** – Department of Cell Biology, Faculty of Biology, Adam Mickiewicz University, 61-614 Poznań, Poland

**Damian Nowak** – Department of Quantum Chemistry, Faculty of Chemistry, Adam Mickiewicz University in Poznań, 61-614 Poznań, Poland;  [orcid.org/0000-0003-3739-3306](https://orcid.org/0000-0003-3739-3306)

Complete contact information is available at:

<https://pubs.acs.org/doi/10.1021/acs.joc.3c00815>

### Funding

This work was financially supported within the Research Subsidy at the Faculty of Chemistry of the Adam Mickiewicz University in Poznań and within the Research Subsidy at the Faculty of Biology of the Adam Mickiewicz University in Poznań.

## Notes

The authors declare no competing financial interest.

## REFERENCES

- (1) Dewick, P. M. *Steroids, in Medicinal Natural Products A Biosynthetic Approach*, 3rd ed.; John Wiley & Sons Ltd: Chichester, UK, 2009; 275–298 & 366–395.
- (2) Savić, M. P.; Sakač, M. N.; Kuzminac, I. Z.; Ajduković, J. J. Structural diversity of bioactive steroid compounds isolated from soft corals in the period 2015–2020. *J. Steroid Biochem. Mol. Biol.* **2022**, *218*, 106061.
- (3) Lee, M. S.; Bensinger, S. J. Reprogramming cholesterol metabolism in macrophages and its role in host defense against cholesterol-dependent cytolysins. *Cell. Mol. Immunol.* **2022**, *19*, 327–336.
- (4) Bloch, K. Sterol molecule: Structure, biosynthesis, and function. *Steroids* **1992**, *57*, 378–383.
- (5) Ridlon, J. M. Special Issue: Microbial Impact on Cholesterol and Bile Acid Metabolism. *Microorganisms* **2022**, *10* (2), 477.
- (6) Risley, M. Cholesterol biosynthesis: lanosterol to cholesterol. *J. Chem. Educ.* **2002**, *79*, 377–384.
- (7) Hanukoglu, I. Steroidogenic enzymes: Structure, function, and role in regulation of steroid hormone biosynthesis. *J. Steroid Biochem. Mol. Biol.* **1992**, *43*, 779–804.
- (8) Nagrady, T.; Weaver, D. F. Steroid hormones: cholesterol as a biosynthetic precursor, *Medicinal Chemistry. A Molecular and Biochemical Approach*, 3rd ed.; Oxford University Press: New York, NY, USA, 2005; pp 316–320.
- (9) Santiago-Sampedro, G. I.; Aguilar-Granda, A.; Torres-Huerta, A.; Flores-Álamo, M.; Maldonado-Domínguez, M.; Rodríguez-Molina, B.; Iglesias-Arteaga, M. A Self-Assembly of an Amphiphilic Bile Acid Dimer: A Combined Experimental and Theoretical Study of Its Medium-Responsive Fluorescence. *J. Org. Chem.* **2022**, *87* (5), 2225–2266.
- (10) Patel, S.; Bariya, D.; Mishra, R.; Mishra, S. Bile acid-based receptors and their applications in recognition. *Steroids* **2022**, *179*, 108981.
- (11) Jain, M.; Nowak, B. P.; Ravoo, B. J. Supramolecular Hydrogels Based on Cyclodextrins: Progress and Perspectives. *Chem. Nanomater.* **2022**, *8*, No. e202200077.
- (12) Kovacevic, B.; Jones, M.; Ionesc, C.; Walker, D.; Wagle, S.; Chester, J.; Foster, T.; Brown, D.; Mikov, M.; Mooranian, A.; Al-Salami, H. The emerging role of bile acids as critical components in nanotechnology and bioengineering: Pharmacology, formulation optimizes and hydrogel-biomaterial applications. *Biomaterials* **2022**, *28*, 121459.
- (13) Gao, H.; Dias, J. R. Synthesis and characterization of dimeric bile acid ester derivatives. *Prakt. Chem.* **1997**, *339* (1), 187–190.
- (14) Pospieszny, T. Molecular Pockets, Umbrellas and Quasi Podands from Steroids: Synthesis, Structure and Applications. *Org. Chem.* **2015**, *12*, 258–270.
- (15) Omar, F.; Tareq, A. M.; Alqahtani, A. M.; Dhama, K.; Sayeed, M. A.; Emran, T. B.; Simal-Gandara, J. Plant-Based Indole Alkaloids: A Comprehensive Overview from a Pharmacological Perspective. *Molecules* **2021**, *26*, 2297.
- (16) Debnath, B.; Singh, W. S.; Das, M.; Goswami, S.; Singh, M. K.; Maiti, D.; Manna, K. Role of plant alkaloids on human health: A review of biological activities. *Mater. Today Chem.* **2018**, *9*, 56–72.
- (17) Roberts, M. F. *Alkaloids: Biochemistry, Ecology, and Medicinal Applications*; Springer Science & Business Media, 2013; pp 340–347.
- (18) Kerzarea, D. R.; Khedekar, P. B. Indole Derivatives acting on Central Nervous System – Review Indole Derivatives acting on Central Nervous System – Review. *J. Pharm. Sci. Bio-Sci. Res.* **2016**, *6* (1), 144–156.
- (19) Jasiewicz, B.; Kozanecka-Okupnik, W.; Przygodzki, M.; Warzajtis, B.; Rychlewska, U.; Pospieszny, T.; Mrówczyńska, L. Synthesis, antioxidant and cytoprotective activity evaluation of C-3 substituted indole derivatives. *Sci. Rep.* **2021**, *11* (1), 15425.
- (20) Ke, S.; Shi, L.; Cao, X.; Yang, Q.; Liang, Y.; Yang, Z. Heterocycle-functional gramine analogues: Solvent- and catalyst-free synthesis and their inhibition activities against cell proliferation. *Eur. J. Med. Chem.* **2012**, *54*, 248–254.
- (21) Froidi, G.; Silvestrin, B.; Dorigo, P.; Caparrotta, L. Gramine: A vasorelaxing alkaloid acting on 5-HT<sub>2A</sub> receptors. *Planta Med.* **2004**, *70* (4), 373–375.
- (22) Moore, K. S.; Wehrli, S.; Roder, H.; Rogers, M.; Forrest, J. N.; McCrimmon, D.; Zasloff, M. Squalamine: an aminosterol antibiotic from the shark. *Proc. Natl. Acad. Sci. U.S.A.* **1993**, *90*, 1354–1358.
- (23) Wehrli, S. L.; Moore, K. S.; Roder, H. S.; Durell, S.; Zasloff, M. Structure of the novel steroidal antibiotic squalamine determined by two-dimensional NMR spectroscopy. *Steroids* **1993**, *58*, 370–378.
- (24) Zasloff, M.; Adams, A. P.; Beckerman, B.; Campbell, A.; Han, Z.; Luijten, E.; Meza, L.; Julander, J.; Mishra, A.; Qu, W.; Taylor, J. M.; Weaver, S. C.; Wong, G. C. L. Squalamine as a broad-spectrum systemic antiviral agent with therapeutic potential. *Proc. Natl. Acad. Sci. U.S.A.* **2011**, *108*, 15978–15983.
- (25) Kozanecka-Okupnik, W.; Sierakowska, A.; Berdzik, N.; Kowalczyk, I.; Mrówczyńska, L.; Jasiewicz, B. New triazole-bearing gramine derivatives—synthesis, structural analysis and protective effect against oxidative haemolysis. *Nat. Prod. Res.* **2022**, *36* (3), 3413–3419.
- (26) Kozanecka-Okupnik, W.; Jasiewicz, B.; Pospieszny, T.; Jastrzab, R.; Skrobańska, M.; Mrówczyńska, L. Spectroscopy, molecular modeling and anti-oxidant activity studies on novel conjugates containing indole and uracil moiety. *J. Mol. Struct.* **2018**, *1169*, 130–137.
- (27) Iacopetta, D.; Catalano, A.; Ceramella, J.; Barbarossa, A.; Carocci, A.; Fazio, A.; La Torre, C.; Caruso, A.; Ponassi, M.; Rosano, C.; Franchini, C.; Sinicropi, M. S. Synthesis, anticancer and antioxidant properties of new indole and pyranindole derivatives. *Bioorg. Chem.* **2020**, *105*, 104440.
- (28) Mounika, K.; Anupama, B.; Pragathi, J.; Gyanakumari, C. Synthesis Characterization and Biological Activity of a Schiff Base Derived from 3-Ethoxy Salicylaldehyde and 2-Amino Benzoic acid and its Transition Metal Complexes. *J. Sci. Res.* **2010**, *2*, 513–524.
- (29) Zhang, L.; Chen, X.; Xue, P.; Sun, H. H. Y.; Williams, I. D.; Sharpless, K. B.; Fokin, V. V.; Jia, G. Ruthenium-catalyzed cycloaddition of alkynes and organic azides. *J. Am. Chem. Soc.* **2005**, *127* (46), 15998–15999.
- (30) Meldal, M.; Diness, F. Recent Fascinating Aspects of the CuAAC Click Reaction. *Trends Chem.* **2020**, *2* (6), 569–584.
- (31) Castro, V.; Rodríguez, H.; Albericio, F. CuAAC: An Efficient Click Chemistry Reaction on Solid Phase. *ACS Comb. Sci.* **2016**, *18* (1), 1–14.
- (32) Haldón, E.; Nicasio, M. C.; Pérez, P. J. Copper-catalysed azide-alkyne cycloadditions (CuAAC): An update. *Org. Biomol. Chem.* **2015**, *13* (37), 9528–9550.
- (33) Latyshev, G. V.; Baranov, M. S.; Kazantsev, A. V.; Averin, A. D.; Lukashov, N. V.; Beletskaya, I. P. Copper-catalyzed [1,3]-dipolar cycloaddition for the synthesis of macrocycles containing acyclic, aromatic and steroidal moieties. *Synthesis* **2009**, *2009*, 2605–2615.
- (34) Mrówczyńska, L.; Bielawski, J. The mechanism of bile salt-induced hemolysis. *Cell. Mol. Biol. Lett.* **2001**, *6* (4), 881–895.
- (35) Mrówczyńska, L.; Bobrowska-Hägerstrand, M.; Wróbel, A.; Söderström, T.; Hägerstrand, H. Inhibition of MRP1-mediated efflux in human erythrocytes by mono-anionic bile salts. *Anticancer Res.* **2005**, *25* (5), 3173–3178.
- (36) Kozanecka-Okupnik, W.; Jasiewicz, B.; Pospieszny, T.; Matuszak, M.; Mrówczyńska, L. Haemolytic activity of formyl- and acetyl-derivatives of bile acids and their gramine salts. *Steroids* **2017**, *126*, 50–56.
- (37) Nowak, D.; Bachorz, R. A.; Hoffmann, M. Neural Networks in the Design of Molecules with Affinity to Selected Protein Domains. *Int. J. Mol. Sci.* **2023**, *24*, 1762.
- (38) Garrett, Z. M.; Morris; Lim-Wilby, M. Molecular Docking. In *Molecular Modeling of Proteins*; Kukul, A., Ed.; *Methods in Molecular Biology*, 2008; Vol. 443, pp 365–382.

- (39) Anandkumar, D.; Rajakumar, P. Synthesis and anticancer activity of bile acid dendrimers with triazole as bridging unit through click chemistry. *Steroids* **2017**, *125*, 37–46.
- (40) Mądrzak-Litwa, L.; Wojciechowska, A.; Paryzek, Z. Synthesis of Isomeric Dimers of Deoxycholic Acid Derivatives Linked by 1,2,3-Triazole. *Synth. Commun.* **2015**, *45*, 1222–1230.
- (41) Bessis, M.; Weed, R. I.; Lablond, P. F. Red cell shape. *Physiology, Pathology, Ultrastructure*; Springer-Verlag New York: Heidelberg, Berlin, 1973.
- (42) Landrum, G. *RDKit: Open-Source Cheminformatics Software*, 2016.
- (43) Trott, O.; Olson, A. J. AutoDock Vina: Improving the Speed and Accuracy of Docking with a New Scoring Function, Efficient Optimization, and Multithreading. *J. Comput. Chem.* **2010**, *31* (2), 455–461.
- (44) O’Boyle, N. M.; Banck, M.; James, C. A.; Morley, C.; Vandermeersch, T.; Hutchison, G. R. Open Babel: An Open Chemical Toolbox. *J. Cheminf.* **2011**, *3* (1), 33.
- (45) *The Open Babel Package*, version 3.1.1. <https://github.com/openbabel/releases> (accessed 08/02/2023).
- (46) Sanner, M. F. Python: A Programming Language for Software Integration and Development. *J. Mol. Graphics Modell.* **1999**, *17*, 57–61.
- (47) Morris, G. M.; Huey, R.; Lindstrom, W.; Sanner, M. F.; Belew, R. K.; Goodsell, D. S.; Olson, A. J. Autodock4 and AutoDockTools4: automated docking with selective receptor flexibility. *J. Comput. Chem.* **2009**, *30*, 2785–2791.
- (48) Pettersen, E. F.; Goddard, T. D.; Huang, C. C.; Couch, G. S.; Greenblatt, D. M.; Meng, E. C.; Ferrin, T. E. UCSF Chimera—a visualization system for exploratory research and analysis. *J. Comput. Chem.* **2004**, *25* (13), 1605–1612.
- (49) ProteinsPlus. <https://proteins.plus> (accessed 03.10.2023).
- (50) Stierand, K.; Rarey, M. Drawing the PDB - Protein-Ligand Complexes in two Dimensions. *ACS Med. Chem. Lett.* **2010**, *1* (9), 540–545.
- (51) Stierand, K.; Rarey, M. From Modeling to Medicinal Chemistry: Automatic Generation of Two-Dimensional Complex Diagrams. *ChemMedChem* **2007**, *2* (6), 853–860.
- (52) Stierand, K.; Maaß, P. C.; Rarey, M. Molecular complexes at a glance: automated generation of two-dimensional complex diagrams. *Bioinformatics* **2006**, *22* (14), 1710–1716.
- (53) Fricker, P. C.; Gastreich, M.; Rarey, M. Automated drawing of structural molecular formulas under constraints. *J. Chem. Inf. Comput. Sci.* **2004**, *44* (3), 1065–1078.
- (54) Diedrich, K.; Krause, B.; Berg, O.; Rarey, M. PoseEdit: enhanced ligand binding mode communication by interactive 2D diagrams. *J. Comput. Aided Mol. Des.* **2023**, *37* (10), 491–503.
- (55) RCBS Protein DATA BANK. <https://www.rcsb.org> (accessed 16.02.2023).
- (56) El Zoeiby, A.; Sanschagrin, F.; Levesque, R. C. Structure and Function of the Mur Enzymes: Development of Novel Inhibitors. *Mol. Microbiol.* **2003**, *47* (1), 1–12.
- (57) Hargrove, T. Y.; Friggeri, L.; Wawrzak, Z.; Qi, A.; Hoekstra, W. J.; Schotzinger, R. J.; York, J. D.; Guengerich, F. P.; Lepesheva, G. I. Structural analyses of *Candida albicans* sterol 14 $\alpha$ -demethylase complexed with azole drugs address the molecular basis of azole-mediated inhibition of fungal sterol biosynthesis. *J. Biol. Chem.* **2017**, *292* (16), 6728–6743.



*Supporting information*

**Synthesis and hemolytic activity of bile acids-indole bioconjugates linked  
by triazole**

**Natalia Berdzik<sup>a</sup>, Hanna Koenig<sup>a</sup>, Lucyna Mrówczyńska<sup>b</sup>, Damian Nowak<sup>c</sup>,  
Beata Jasiewicz<sup>a\*</sup> and Tomasz Pospieszny<sup>a\*</sup>**

<sup>a</sup>*Department of Bioactive Products, Faculty of Chemistry, Adam Mickiewicz University, Uniwersytetu  
Poznańskiego 8, 61-614 Poznań, Poland*

<sup>b</sup>*Department of Cell Biology, Faculty of Biology, Adam Mickiewicz University, Uniwersytetu Poznańskiego 6,  
61-614 Poznań, Poland*

<sup>c</sup>*Department of Quantum Chemistry, Faculty of Chemistry, Adam Mickiewicz University in Poznan,  
Uniwersytetu Poznańskiego 8, 61-614 Poznan, Poland*

\*Corresponding Authors: [beata.jasiewicz@amu.edu.pl](mailto:beata.jasiewicz@amu.edu.pl) and [tposp@amu.edu.pl](mailto:tposp@amu.edu.pl)

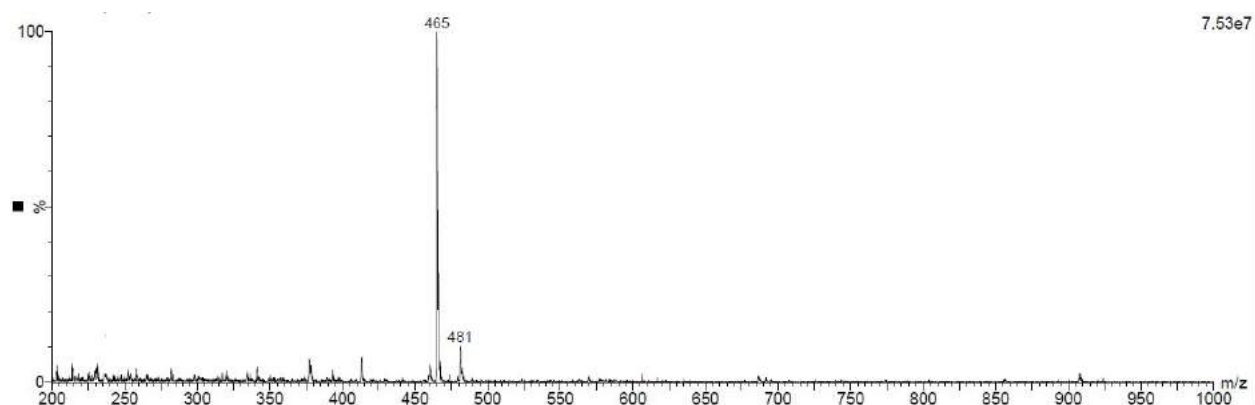
**Table of Contents**

1. General information	S2
2. Copies of ESI-MS spectra	S2–S6
3. Copies of NMR spectra	S6-S19

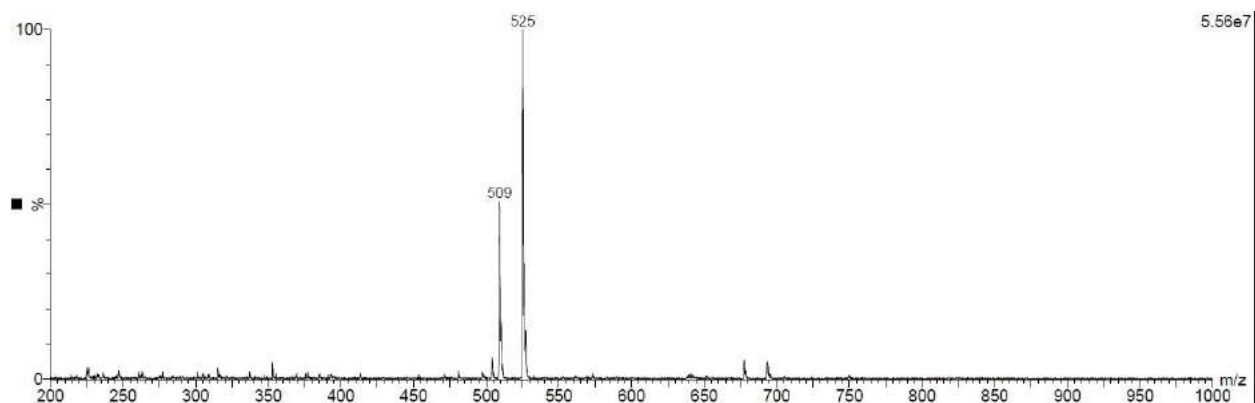
## 1. General Information

All of the synthesis reagents were purchased from Sigma-Aldrich. Solvents chloroform, dichloromethane, toluene, dimethylformamide, dimethylsulfoxide, tetrahydrofuran, ethyl acetate, and methanol were obtained from commercial sources (Merck, Fisher) and used without purification. IR Spectra: FT/IR Nicolet iS5 (KBr pellet,  $\text{cm}^{-1}$ )  $^1\text{H}$  and  $^{13}\text{C}$  NMR spectra: Bruker Avance 600 MHz, Varian VNMR-S 400 MHz and Varian Mercury 300 MHz spectrometer (Oxford, UK). EI-MS spectra: AMD Intectra Mass AMD 402 spectrometer ESI-MS spectra: Waters HPLC/MS chromatograph. The elemental analysis was performed on the Elemental Analyzer Vario EL III apparatus, examining the percentage content of nitrogen, carbon and hydrogen.

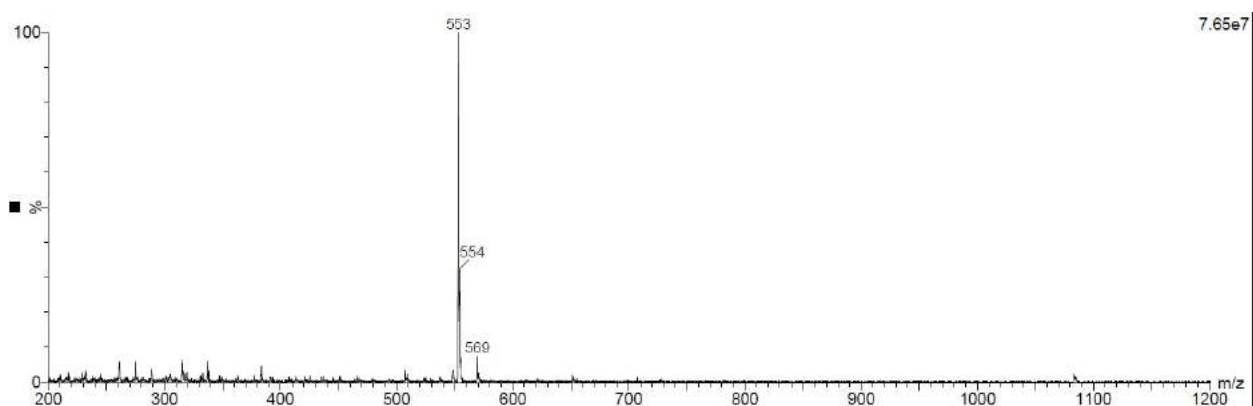
## 2. Copies of ESI-MS spectra



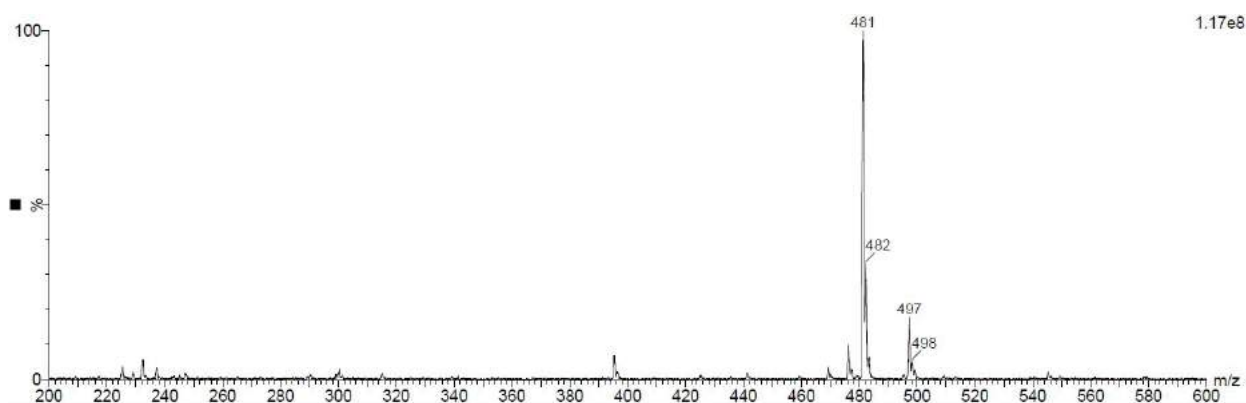
ESI-MS spectra of compound **8**



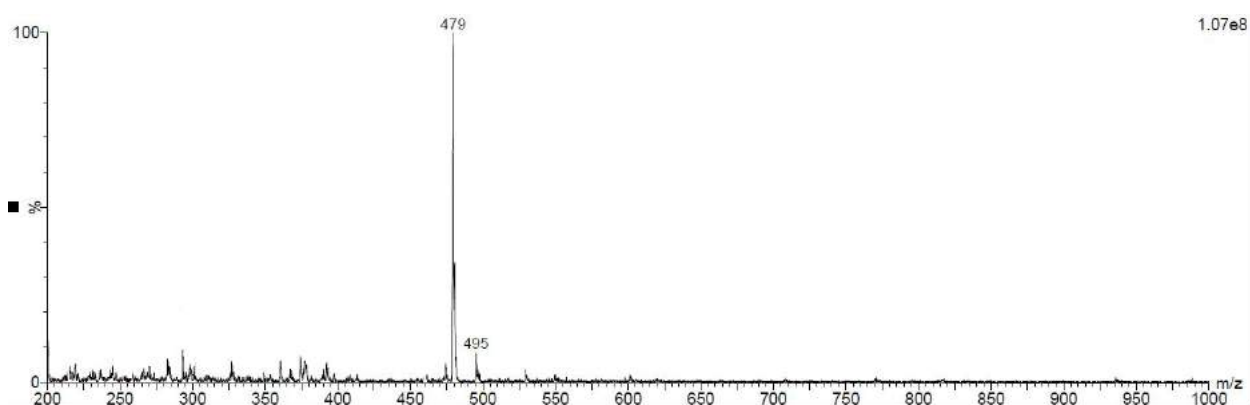
ESI-MS spectra of compound **9**



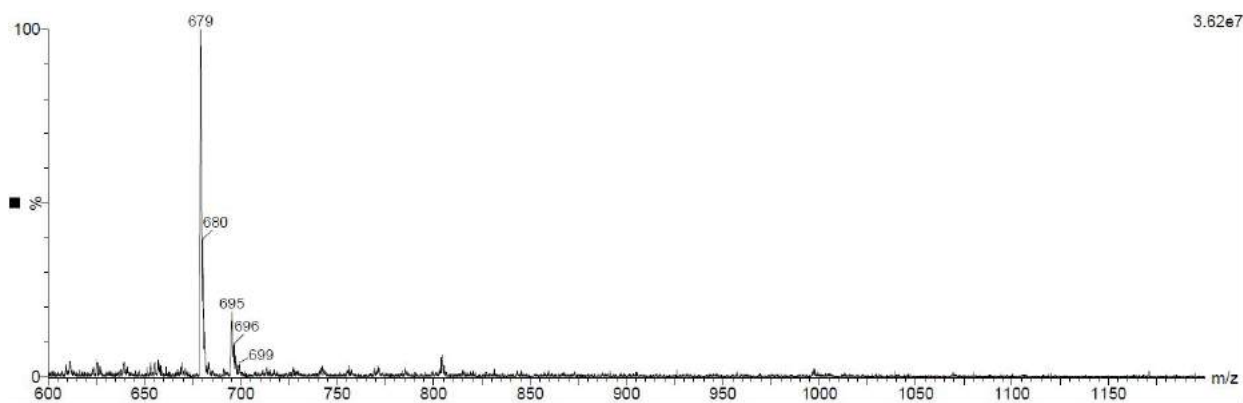
ESI-MS spectra of compound 10



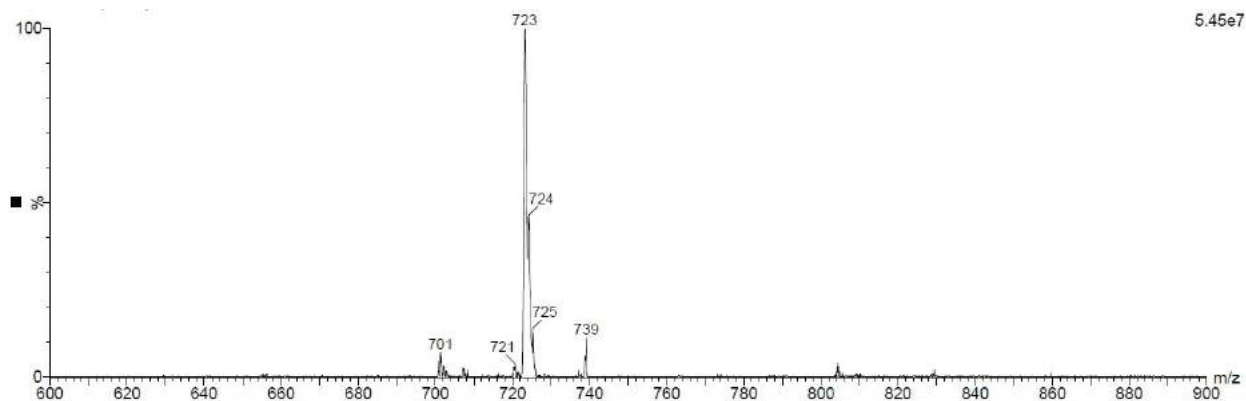
ESI-MS spectra of compound 11



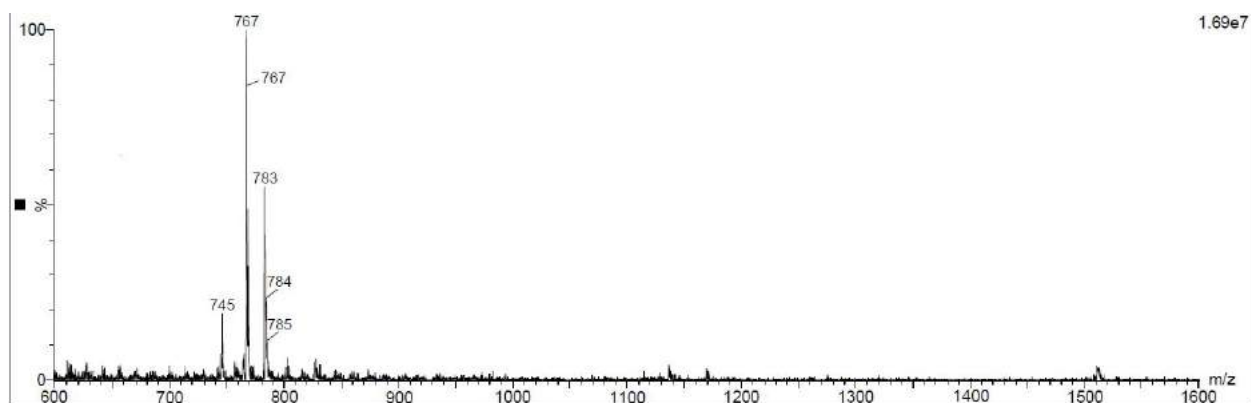
ESI-MS spectra of compound 12



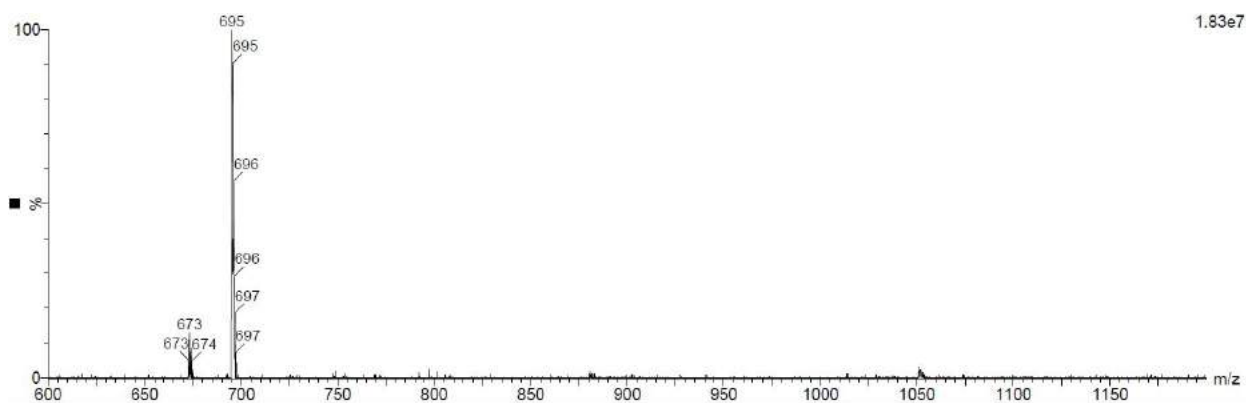
ESI-MS spectra of compound **15**



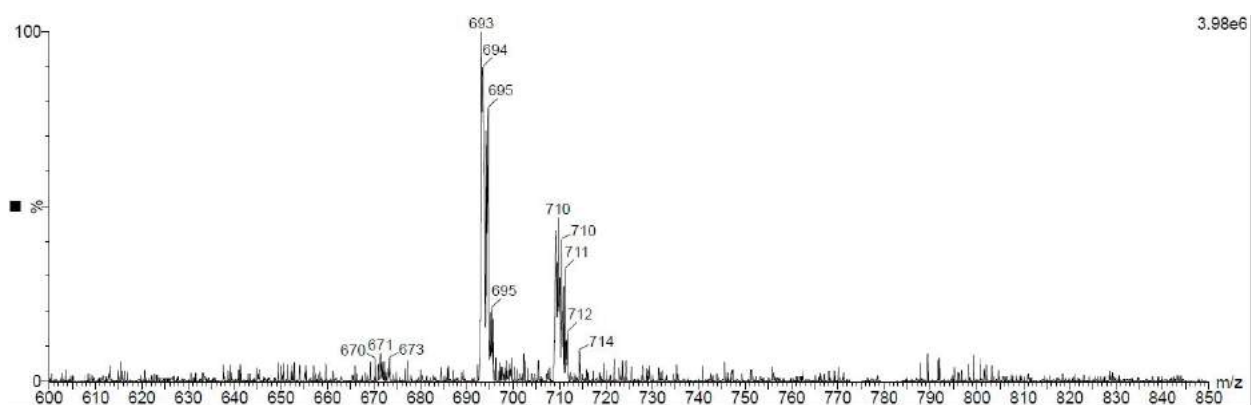
ESI-MS spectra of compound **16**



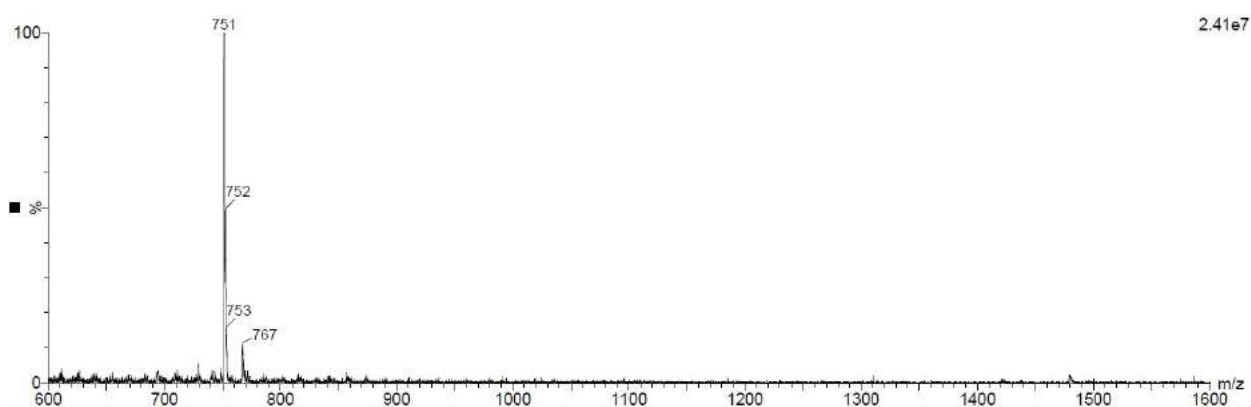
ESI-MS spectra of compound **17**



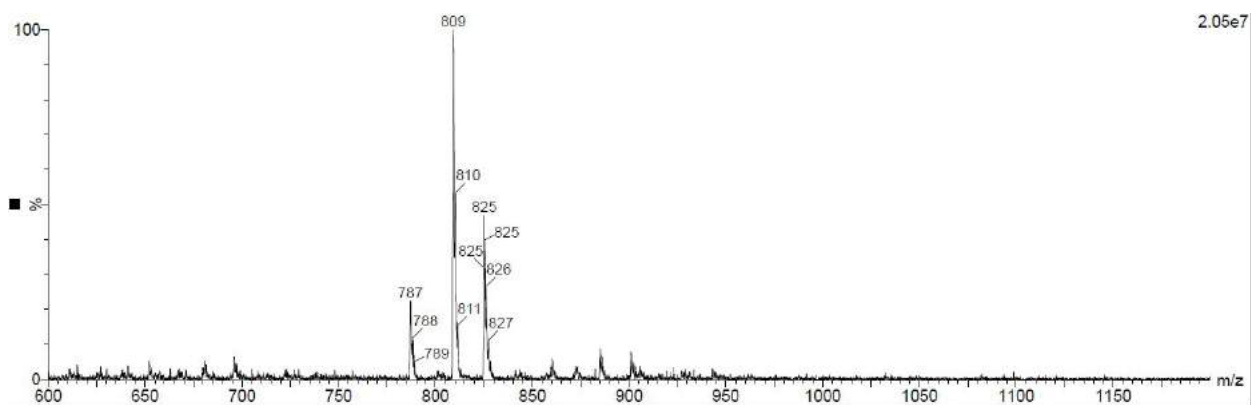
ESI-MS spectra of compound **18**



ESI-MS spectra of compound **19**

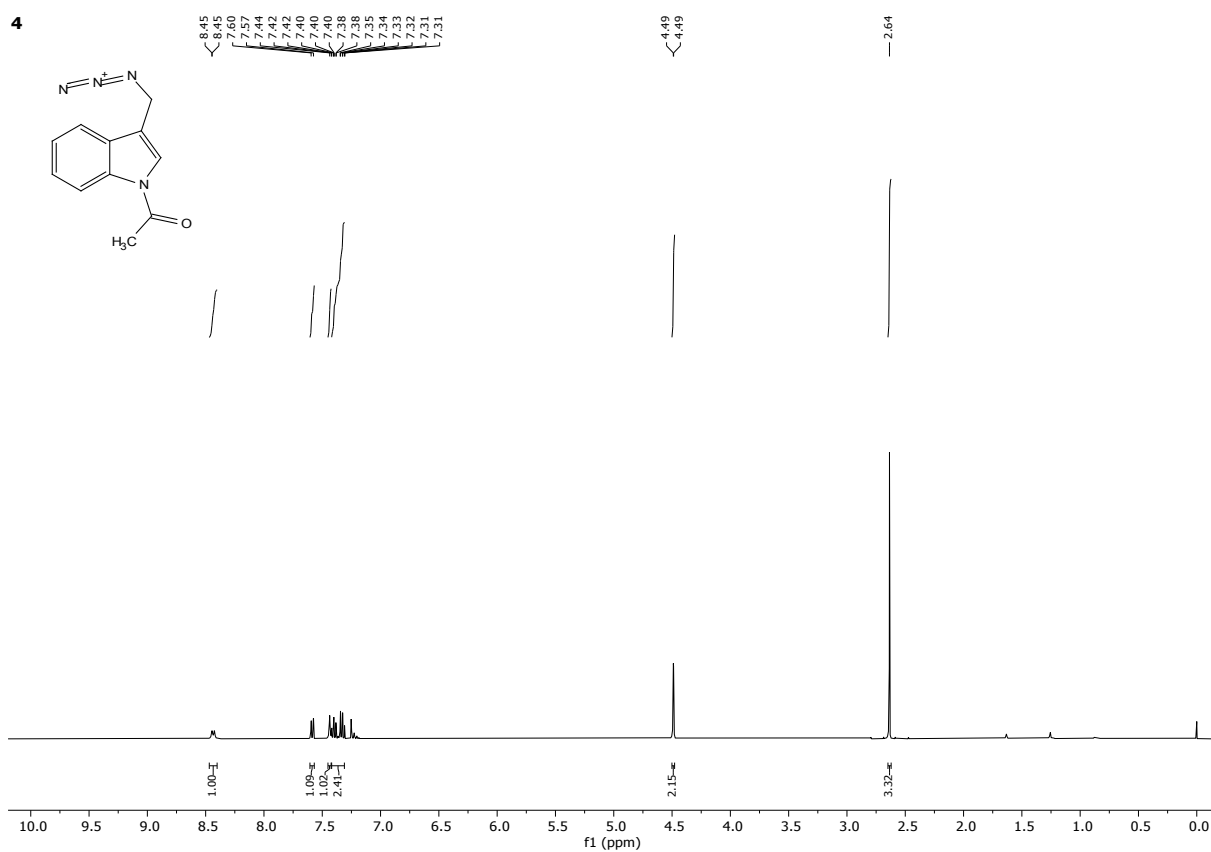


ESI-MS spectra of compound **20**

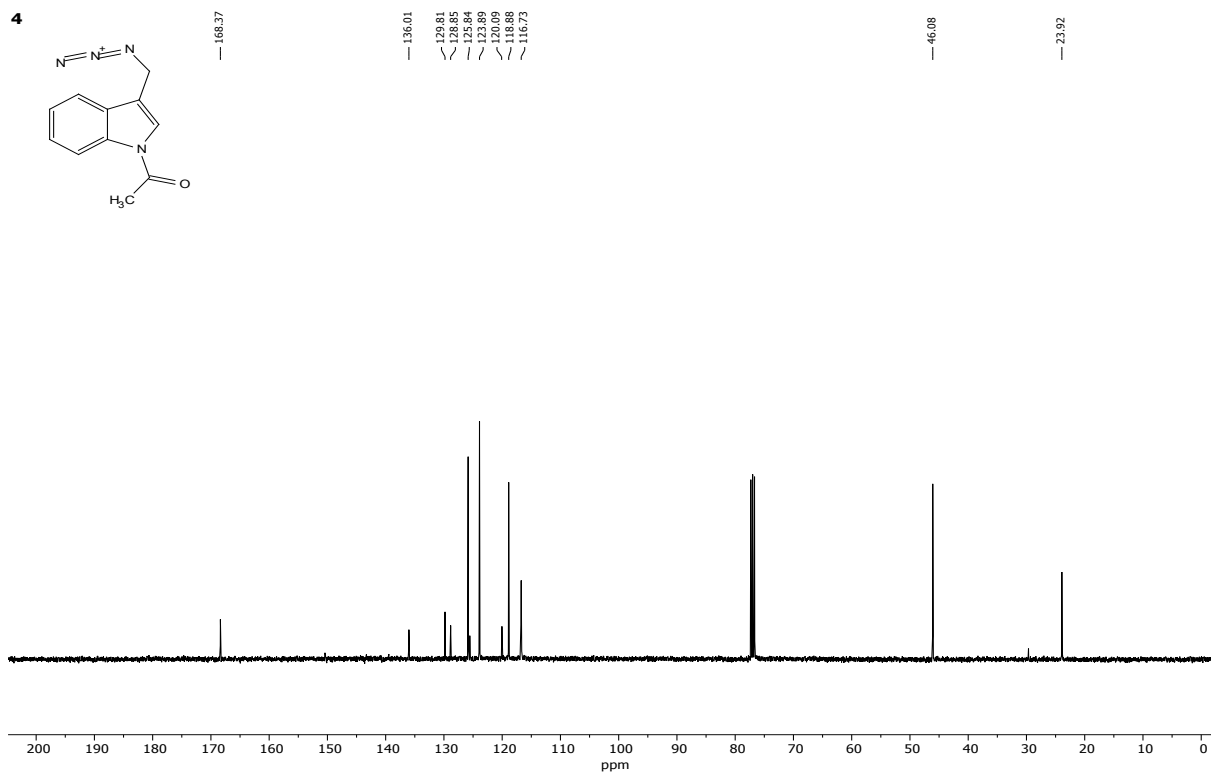


ESI-MS spectra of compound **21**

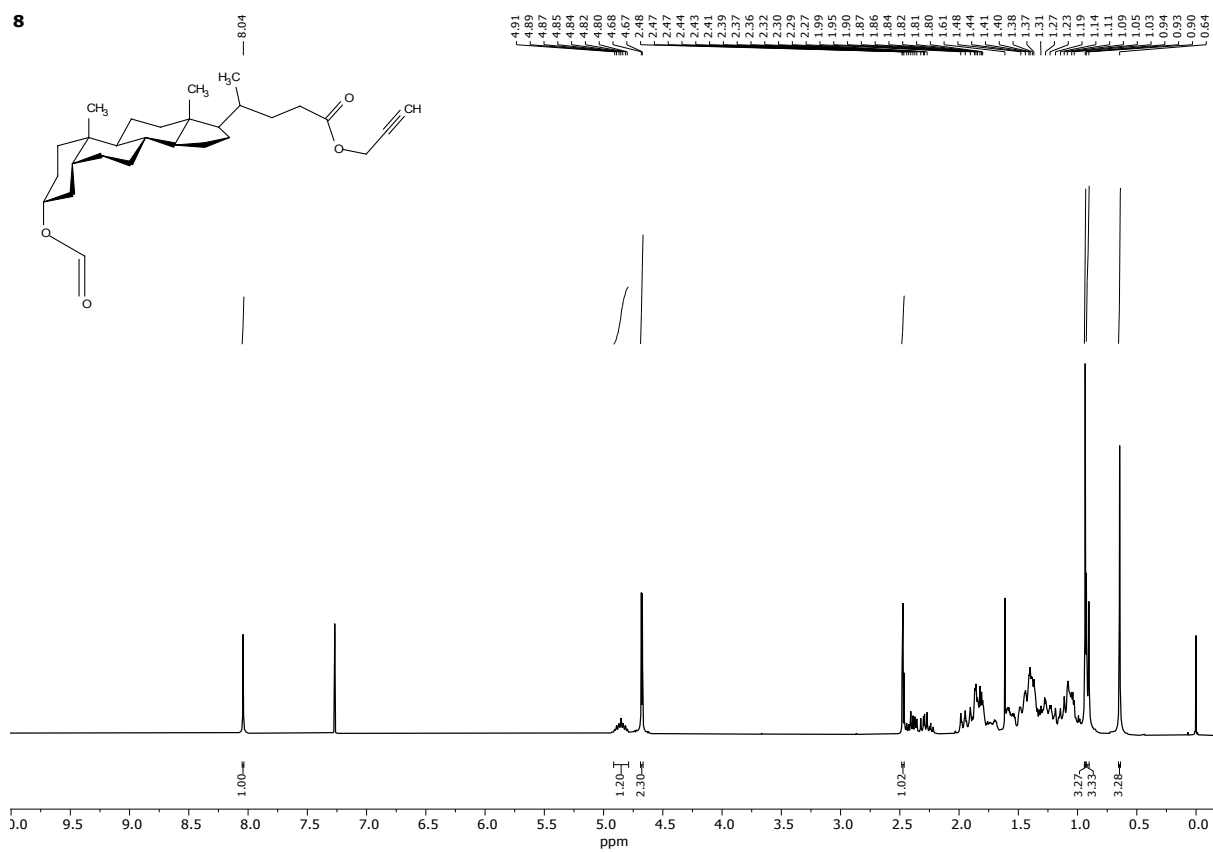
#### 4. Copies of NMR spectra



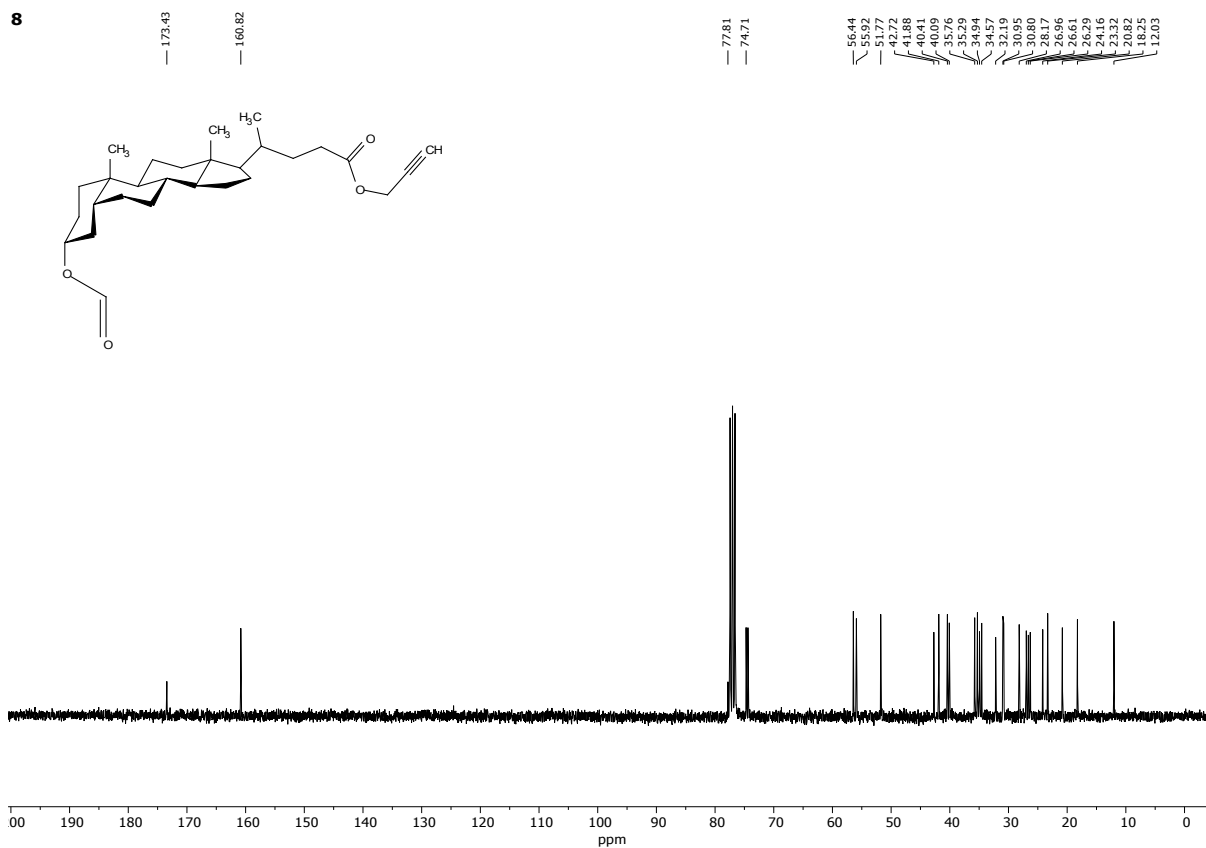
<sup>1</sup>H NMR (400 MHz, CDCl<sub>3</sub>) spectra of compound **4**



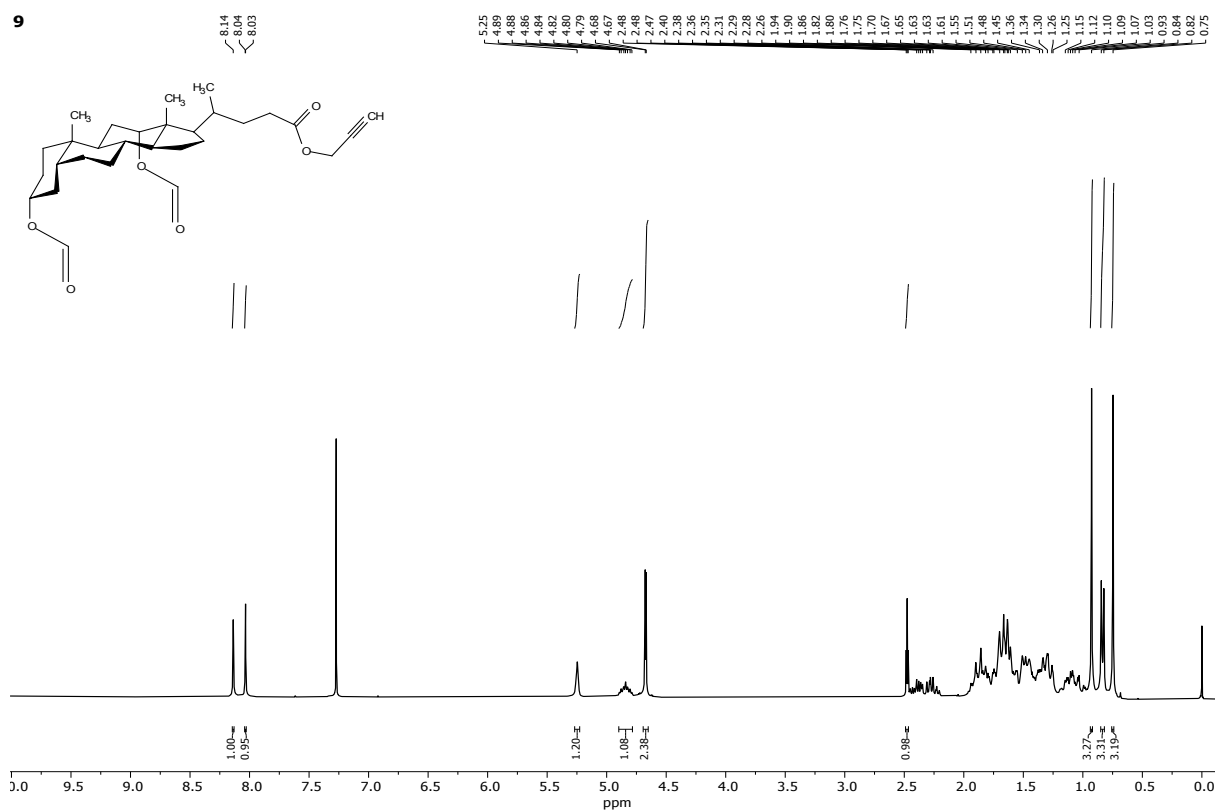
$^{13}\text{C}\{^1\text{H}\}$  NMR (101 MHz,  $\text{CDCl}_3$ ) spectra of compound **4**



$^1\text{H}$  NMR (300 MHz,  $\text{CDCl}_3$ ) spectra of compound **8**

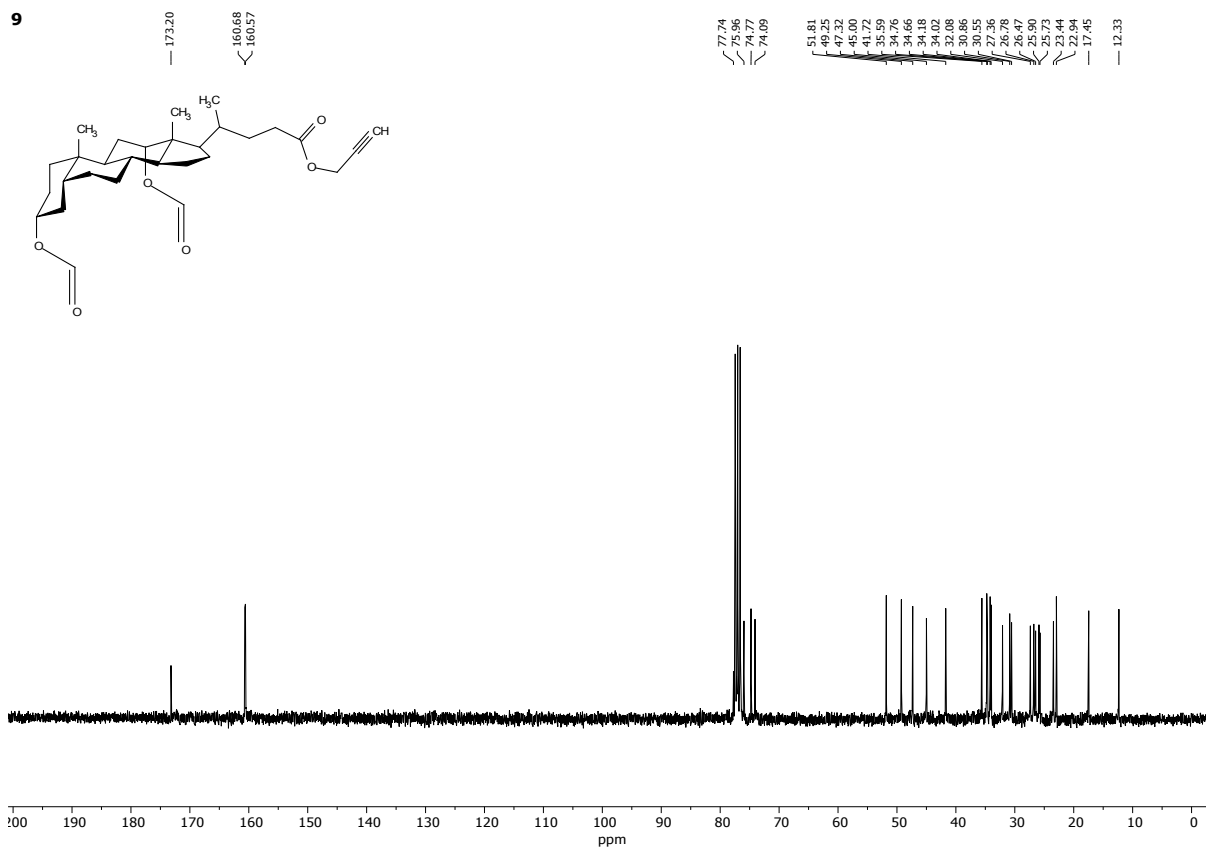


$^{13}\text{C}\{^1\text{H}\}$  NMR (76 MHz,  $\text{CDCl}_3$ ) spectra of compound **8**

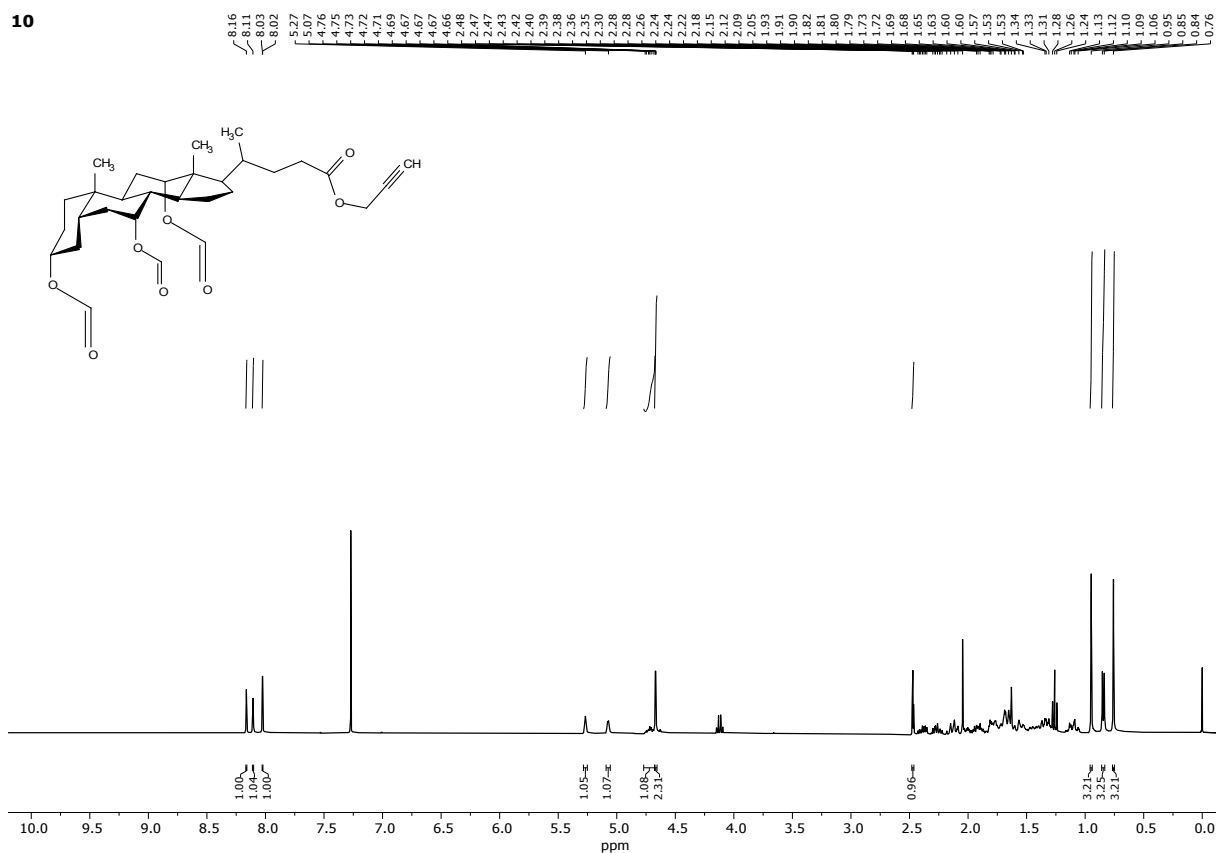


$^1\text{H}$  NMR (300 MHz,  $\text{CDCl}_3$ ) spectra of compound **9**

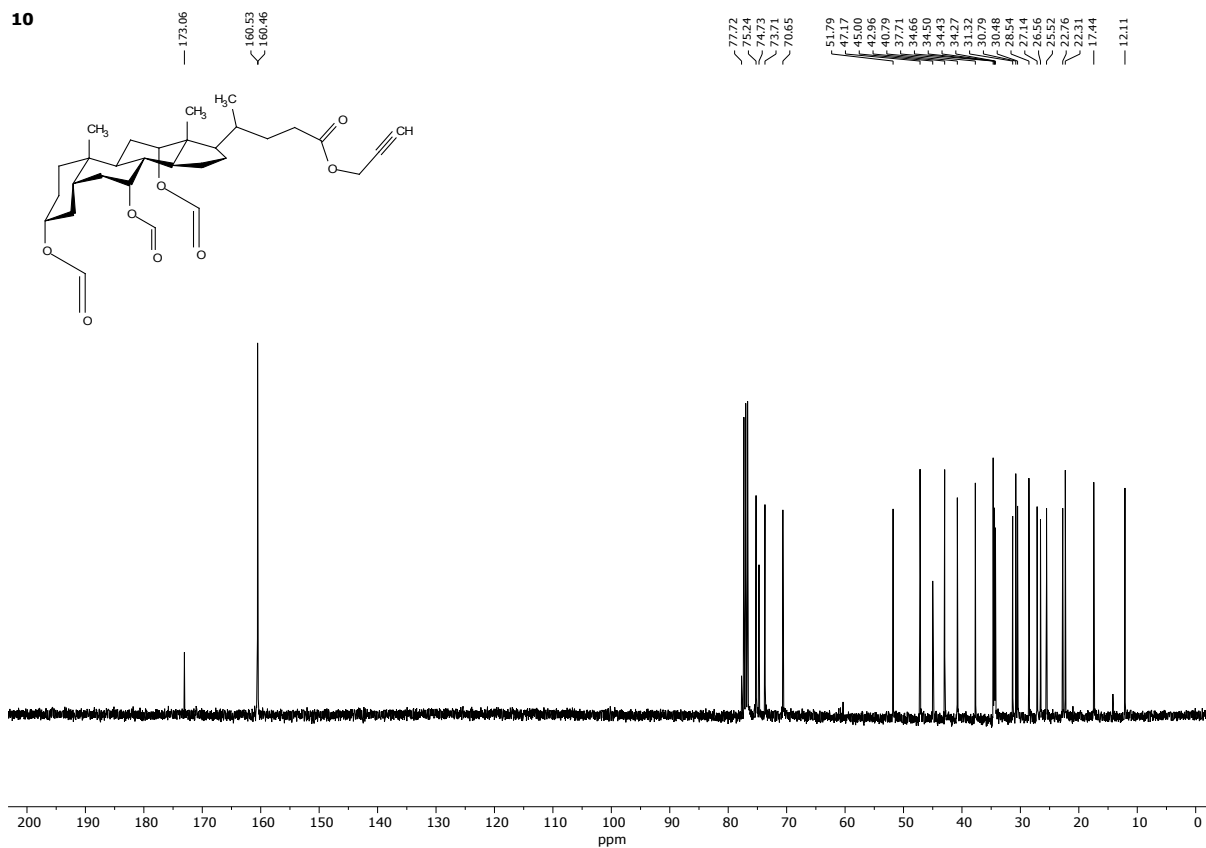




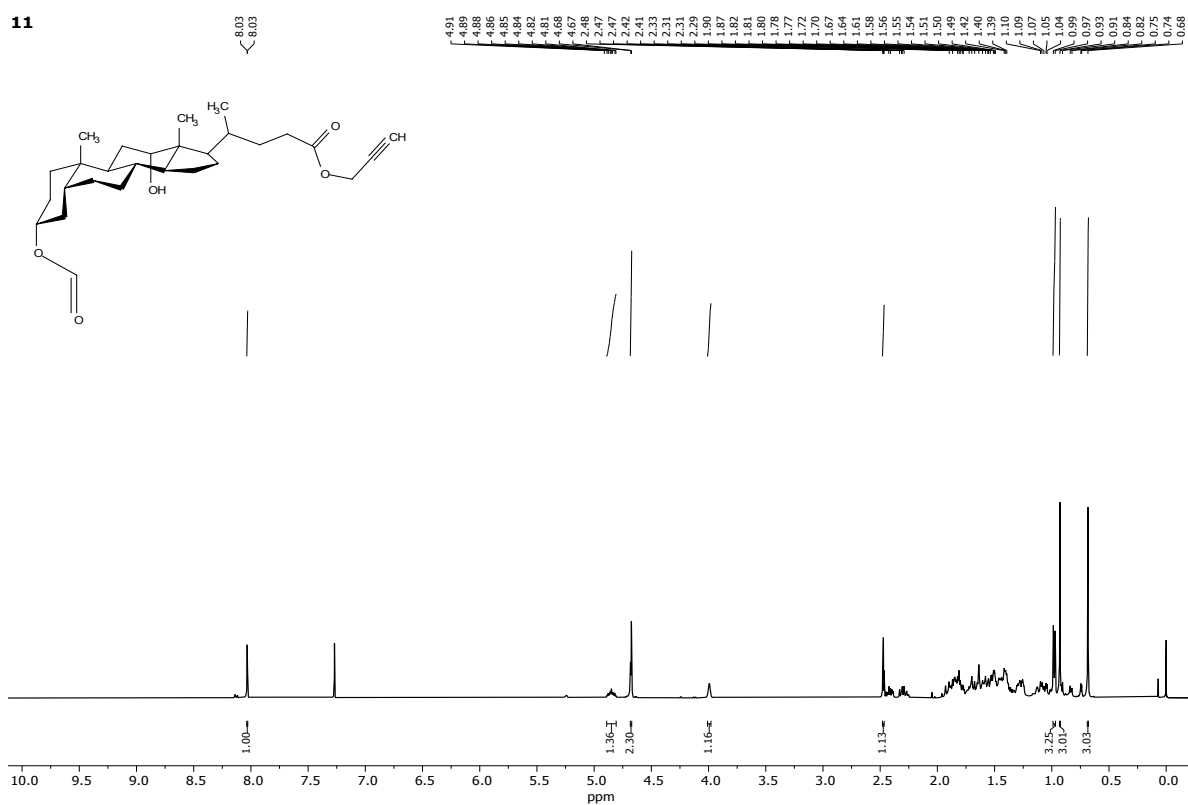
$^{13}\text{C}\{^1\text{H}\}$  NMR (76 MHz,  $\text{CDCl}_3$ ) spectra of compound **9**



$^1\text{H}$  NMR (300 MHz,  $\text{CDCl}_3$ ) spectra of compound **10**

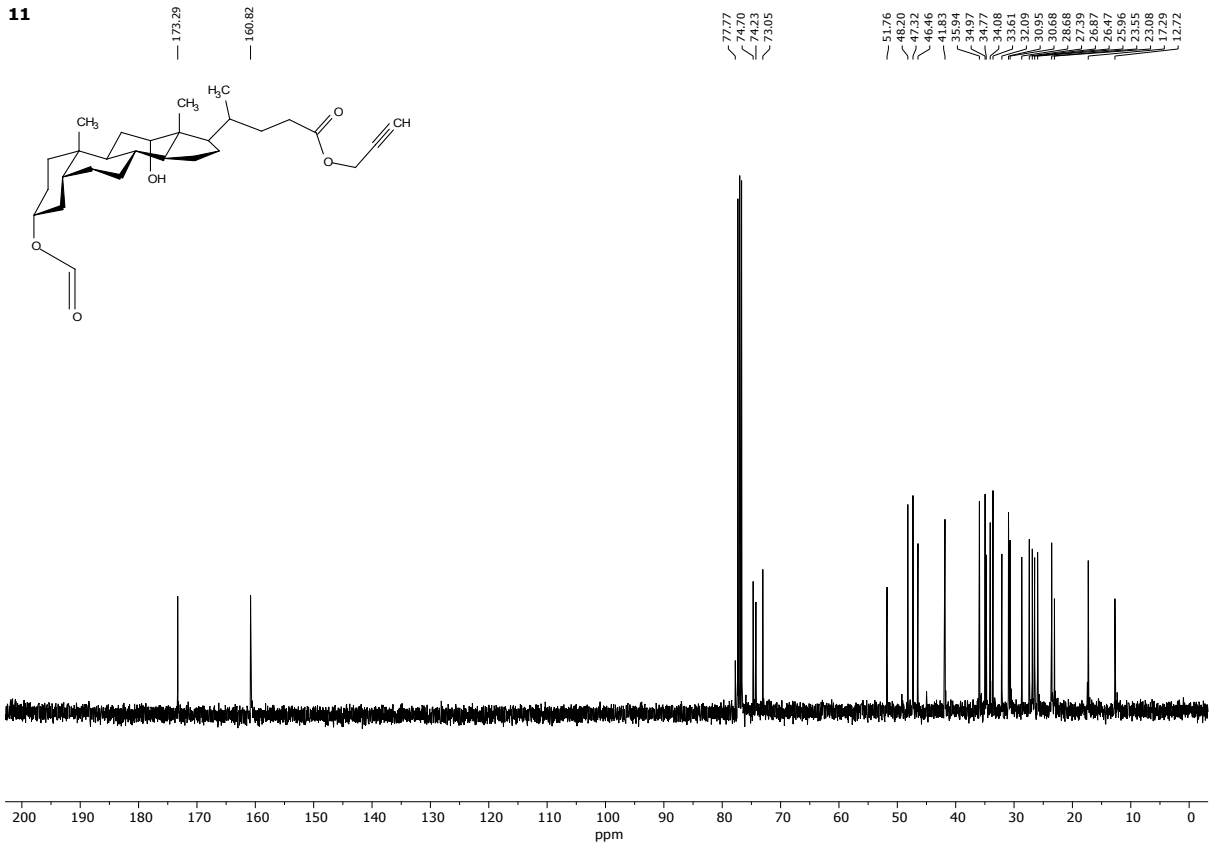


$^{13}\text{C}\{^1\text{H}\}$  NMR (76 MHz,  $\text{CDCl}_3$ ) spectra of compound **10**



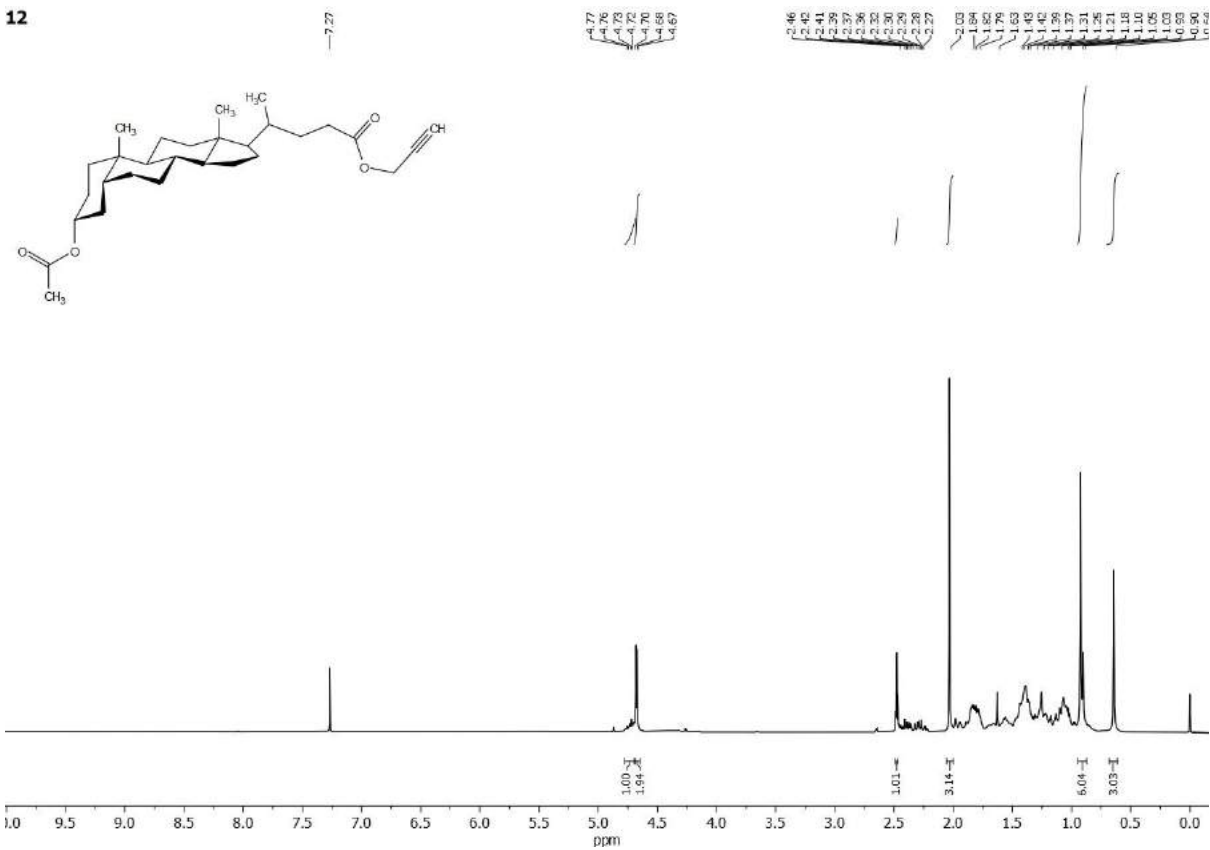
$^1\text{H}$  NMR (300 MHz,  $\text{CDCl}_3$ ) spectra of compound **11**

11



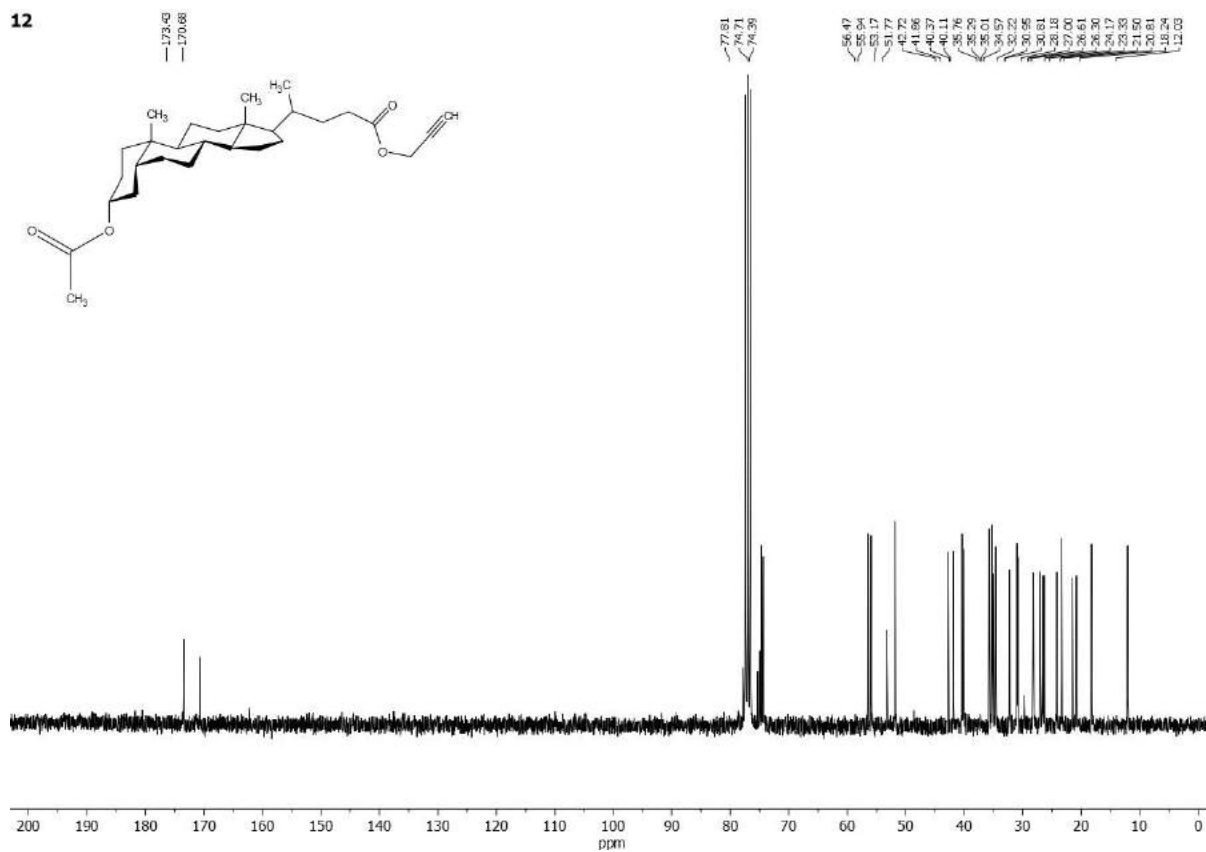
<sup>13</sup>C {<sup>1</sup>H} NMR (76 MHz, CDCl<sub>3</sub>) spectra of compound 11

12



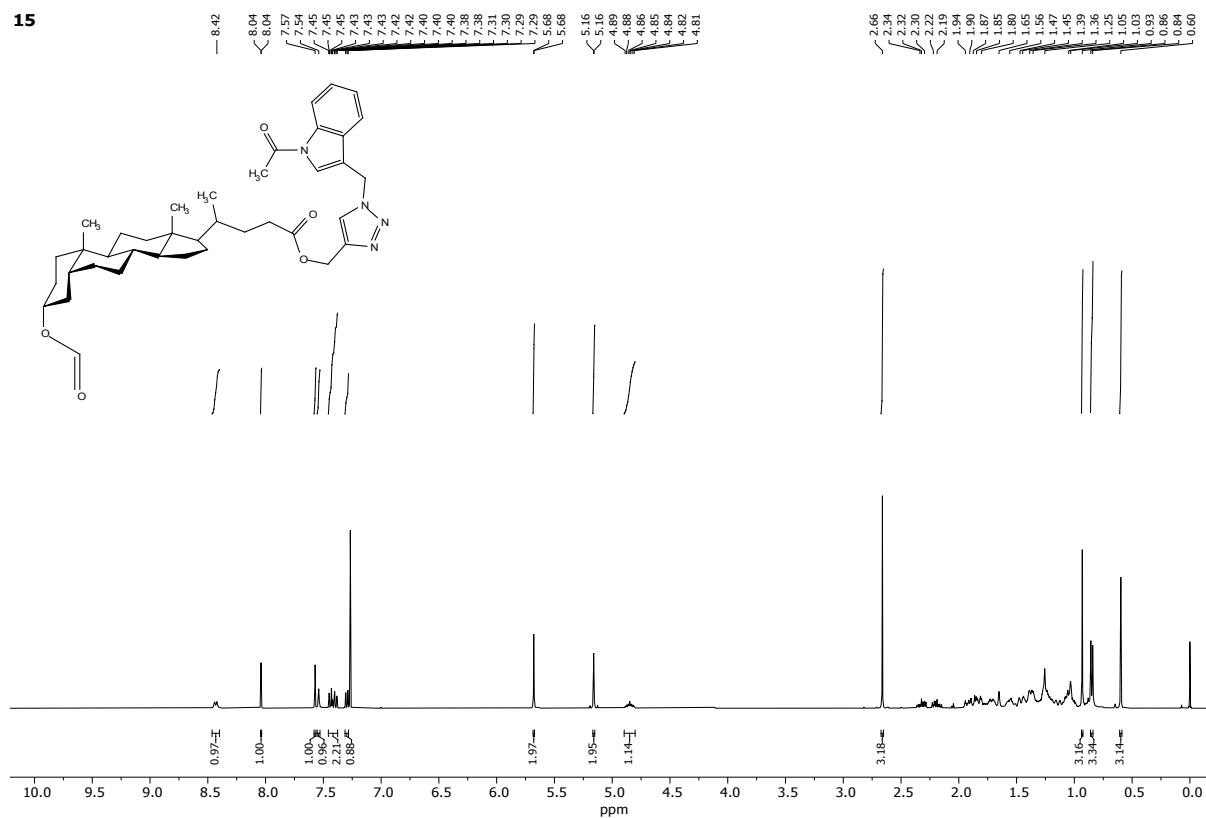
<sup>1</sup>H NMR (300 MHz, CDCl<sub>3</sub>) spectra of compound 12

12



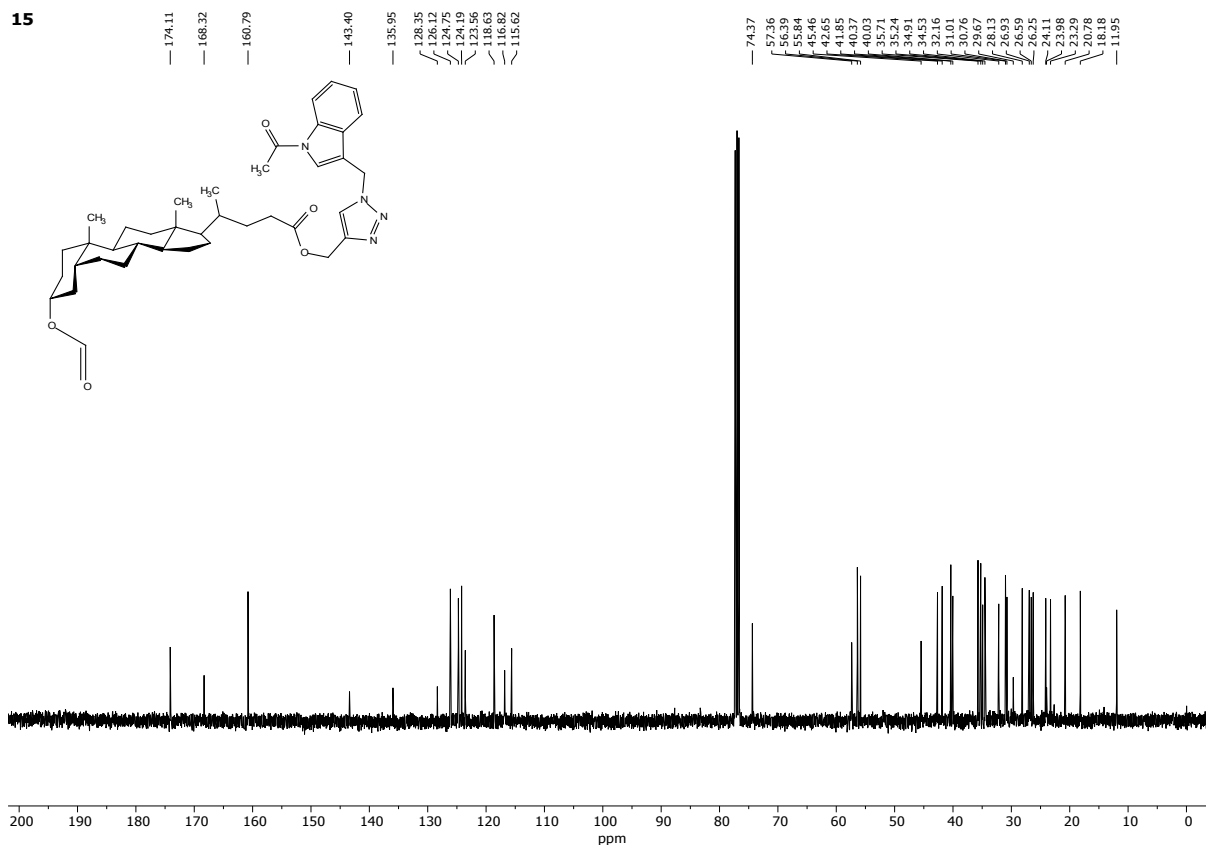
$^{13}\text{C}\{^1\text{H}\}$  NMR (76 MHz,  $\text{CDCl}_3$ ) spectra of compound 12

15



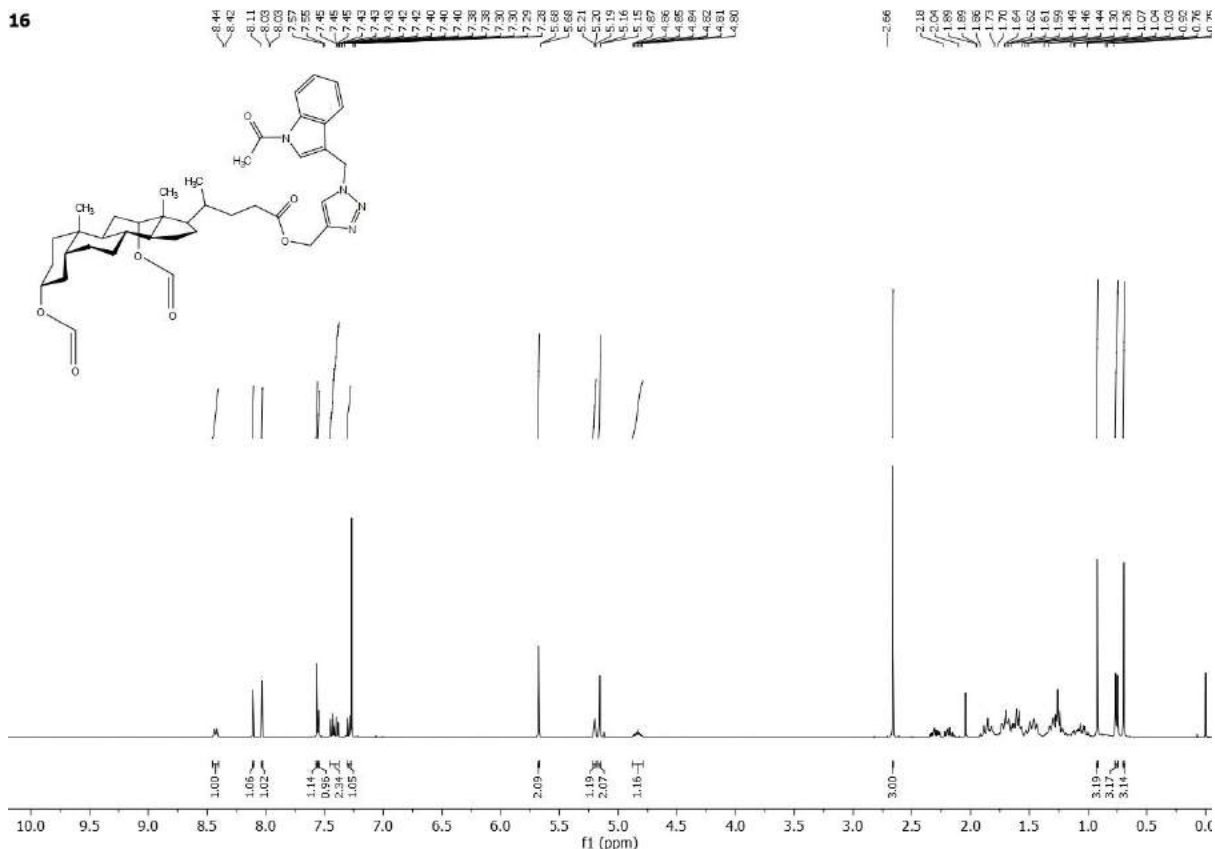
$^1\text{H}$  NMR (400 MHz,  $\text{CDCl}_3$ ) spectra of compound 15

15



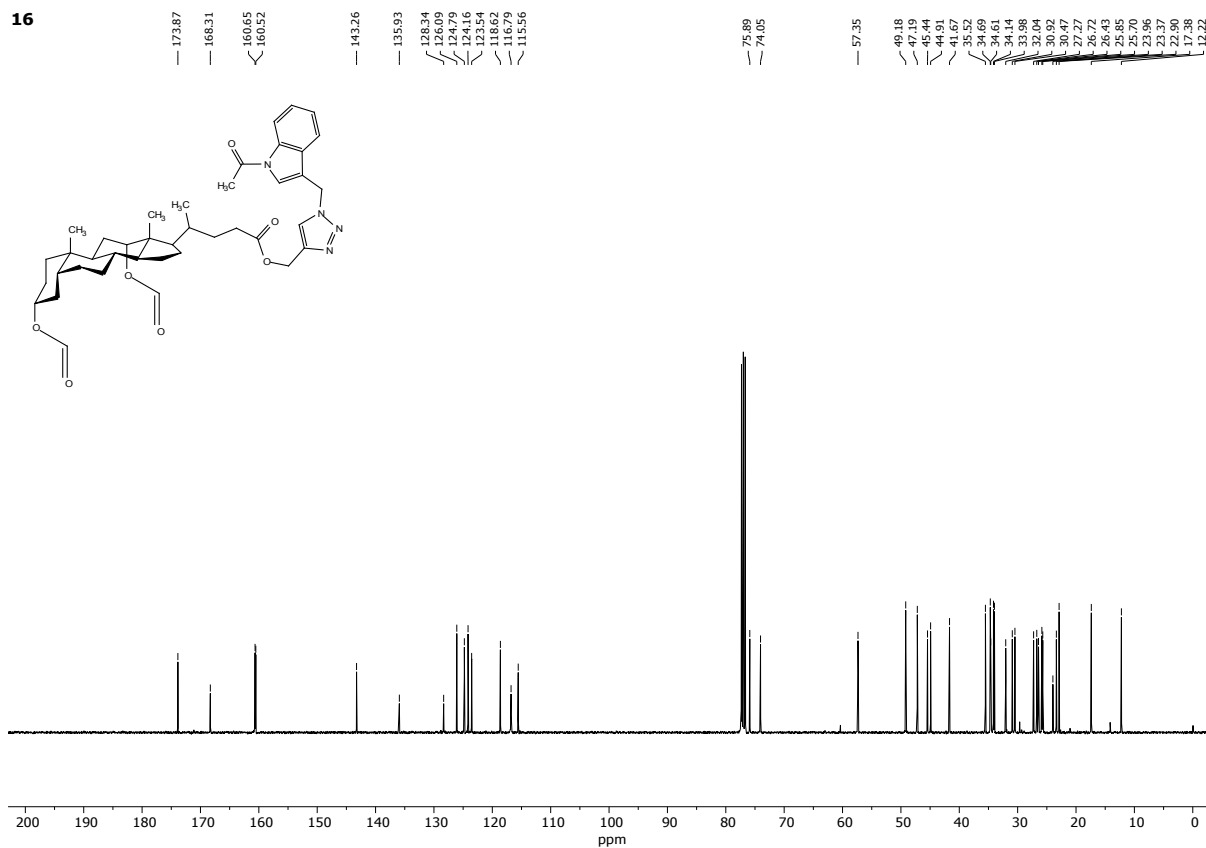
$^{13}\text{C}\{^1\text{H}\}$  NMR (101 MHz,  $\text{CDCl}_3$ ) spectra of compound 15

16



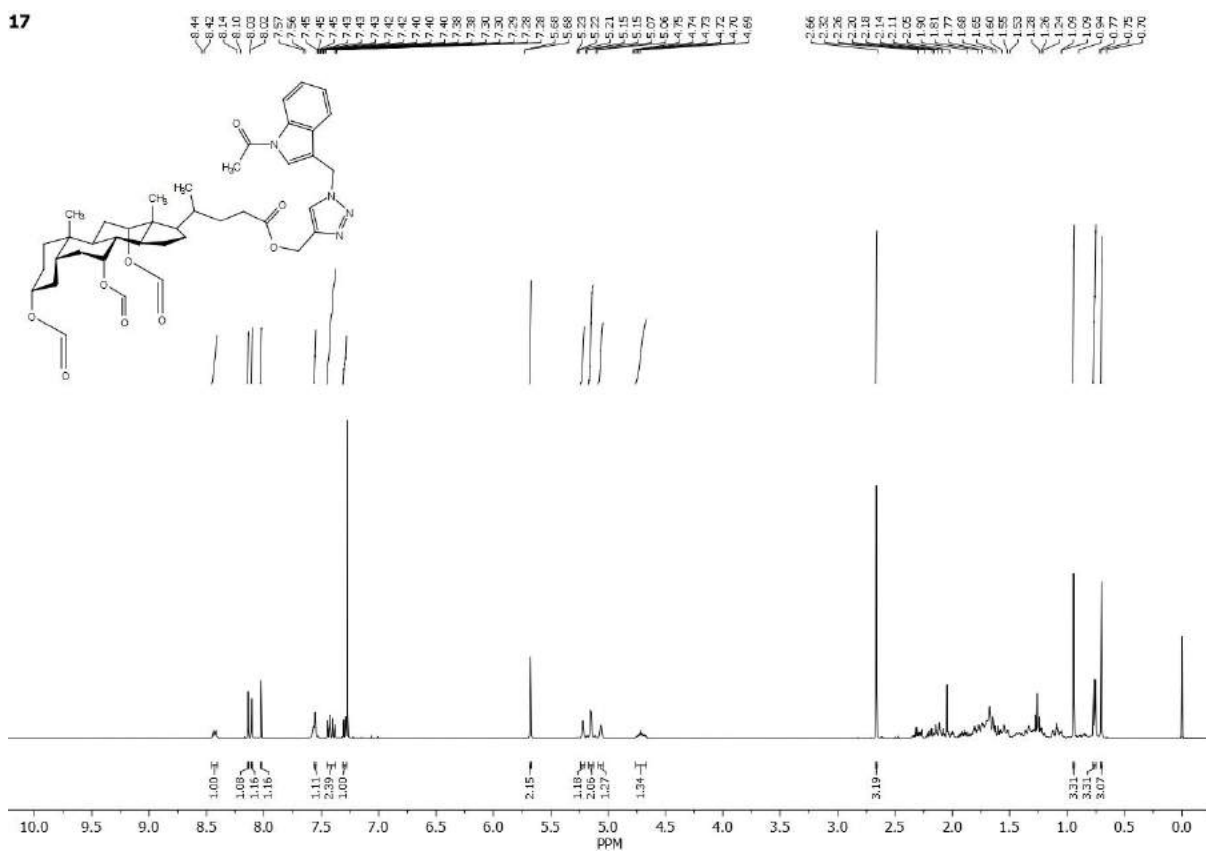
$^1\text{H}$  NMR (400 MHz,  $\text{CDCl}_3$ ) spectra of compound 16

16

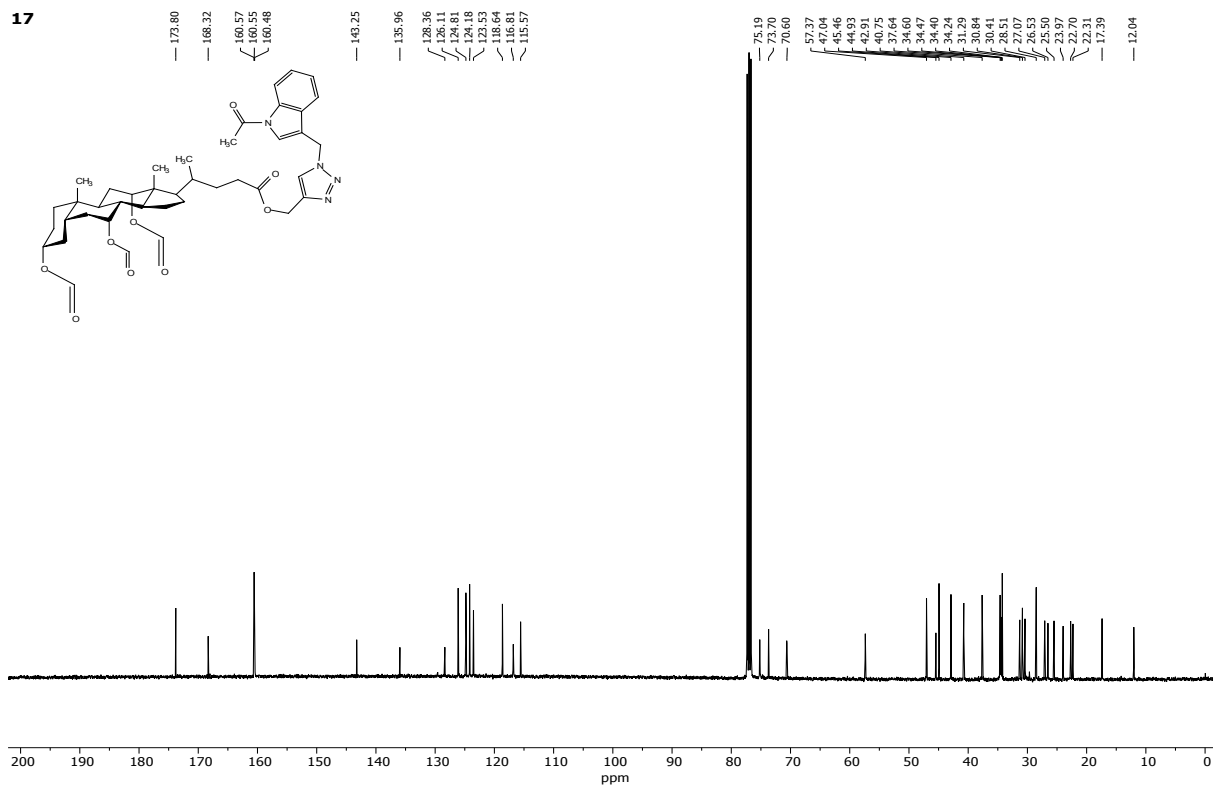


$^{13}\text{C}\{^1\text{H}\}$  NMR (101 MHz,  $\text{CDCl}_3$ ) spectra of compound 16

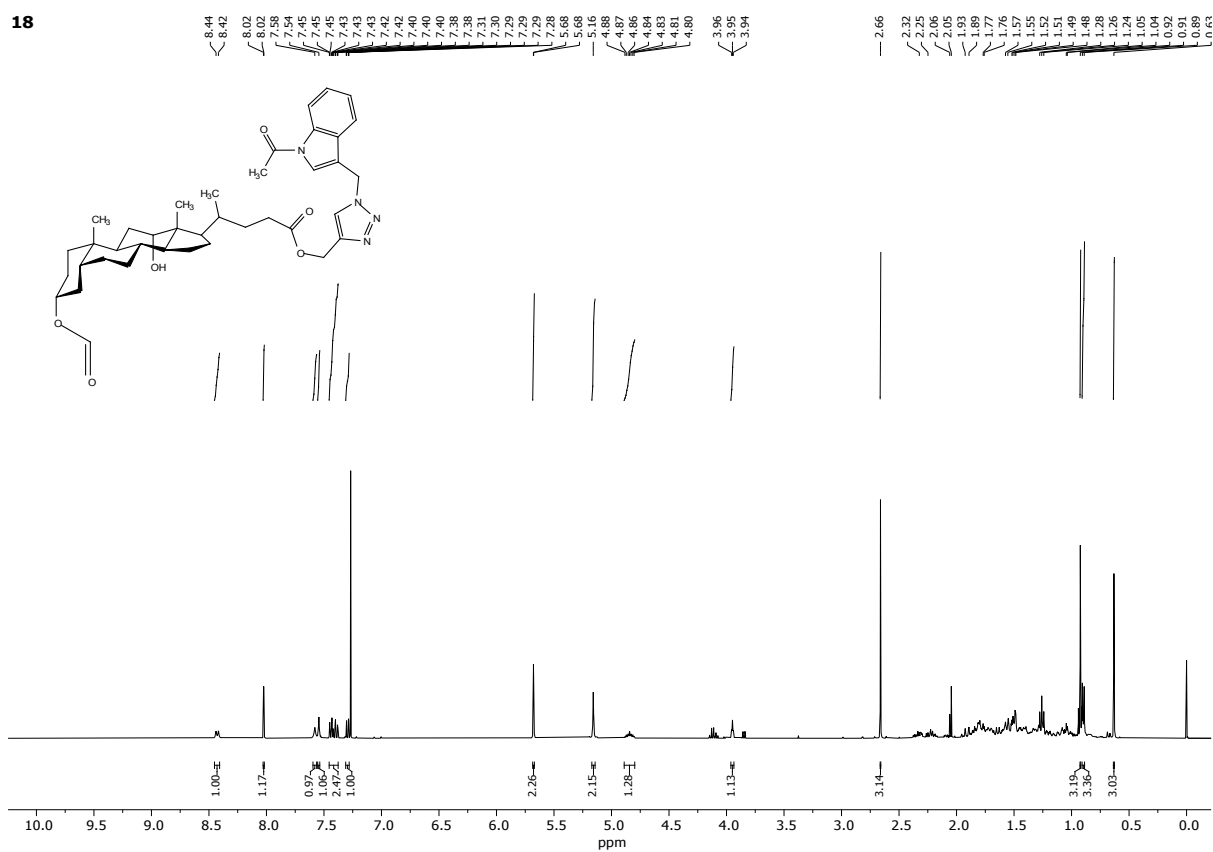
17



$^1\text{H}$  NMR (400 MHz,  $\text{CDCl}_3$ ) spectra of compound 17

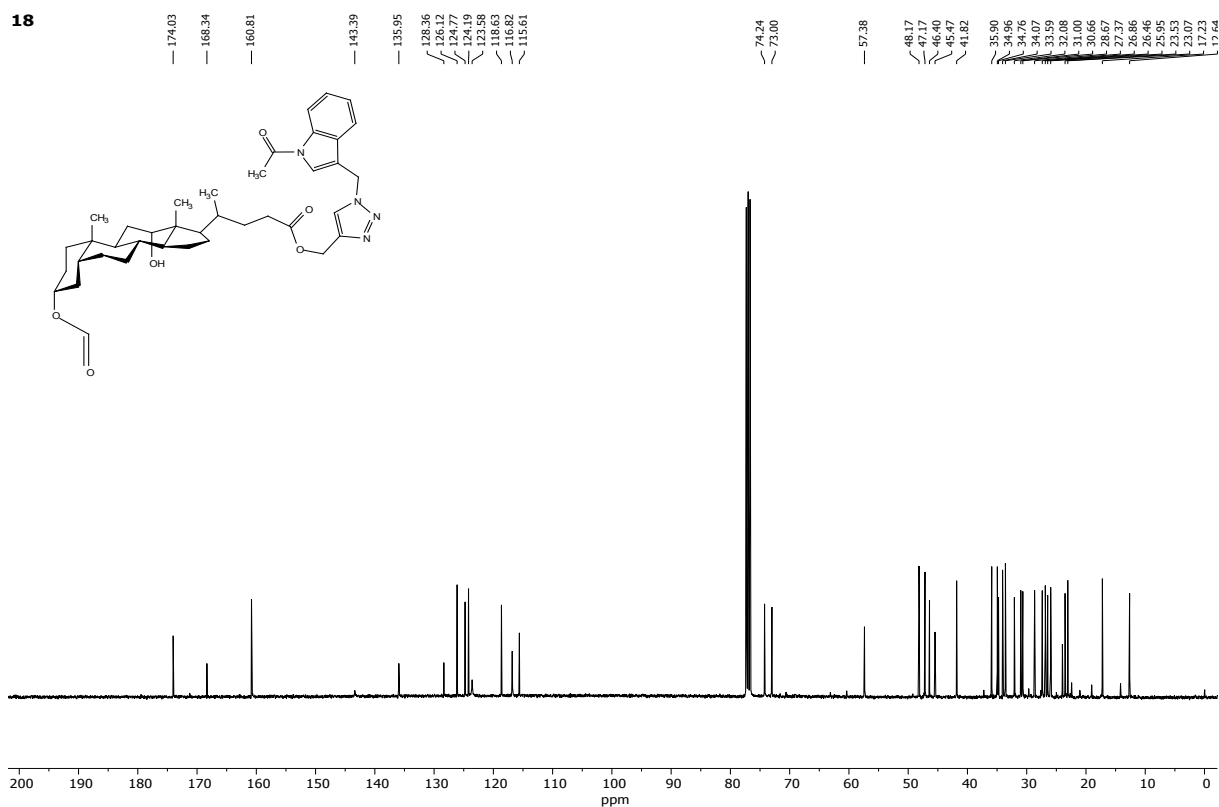


$^{13}\text{C}$   $\{^1\text{H}\}$  NMR (101 MHz,  $\text{CDCl}_3$ ) spectra of compound 17



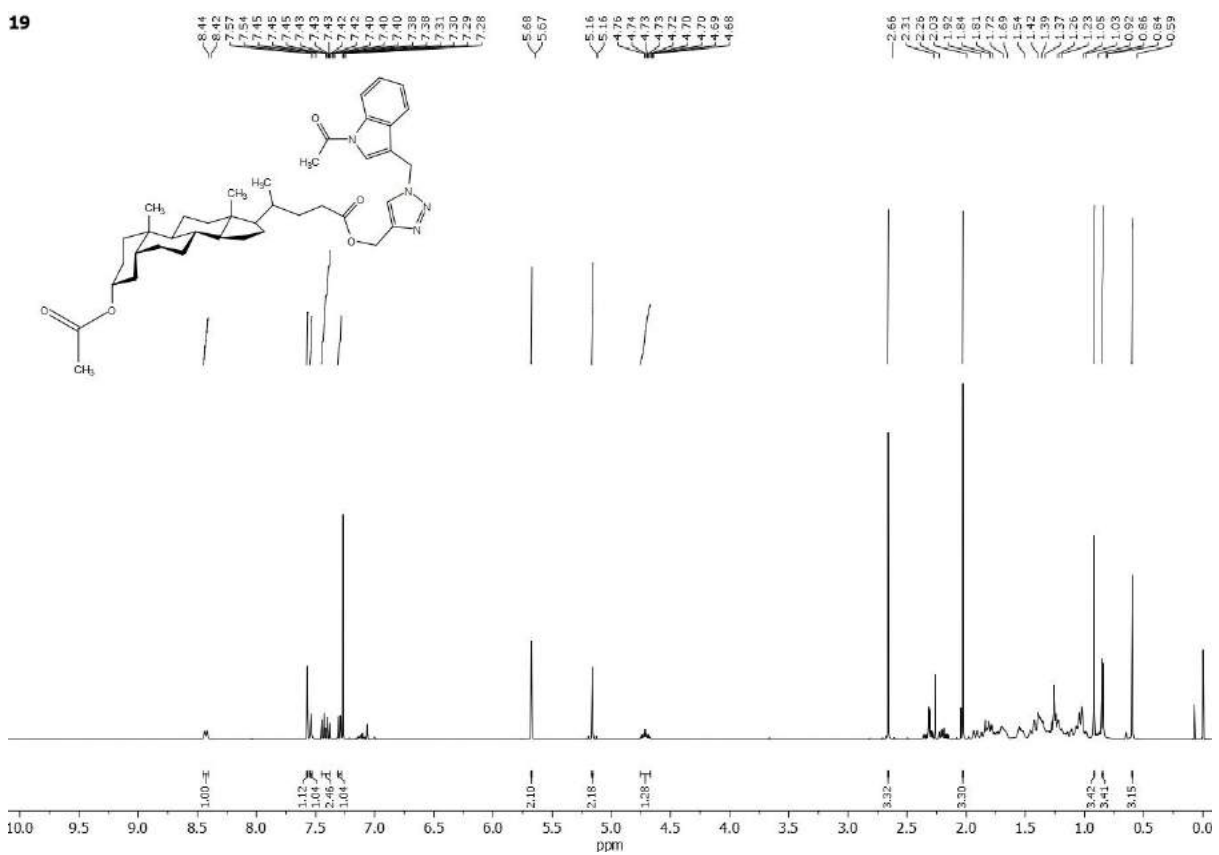
$^1\text{H}$  NMR (400 MHz,  $\text{CDCl}_3$ ) spectra of compound 18

18



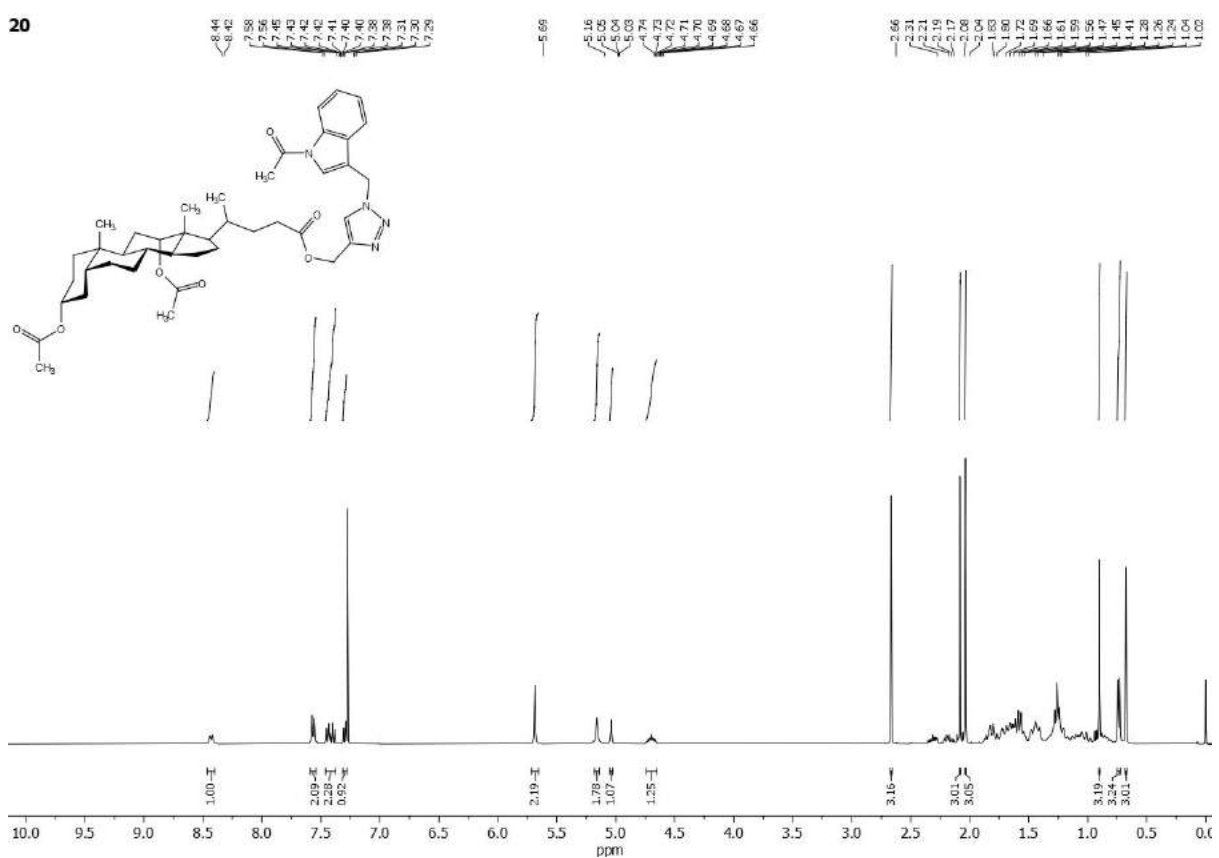
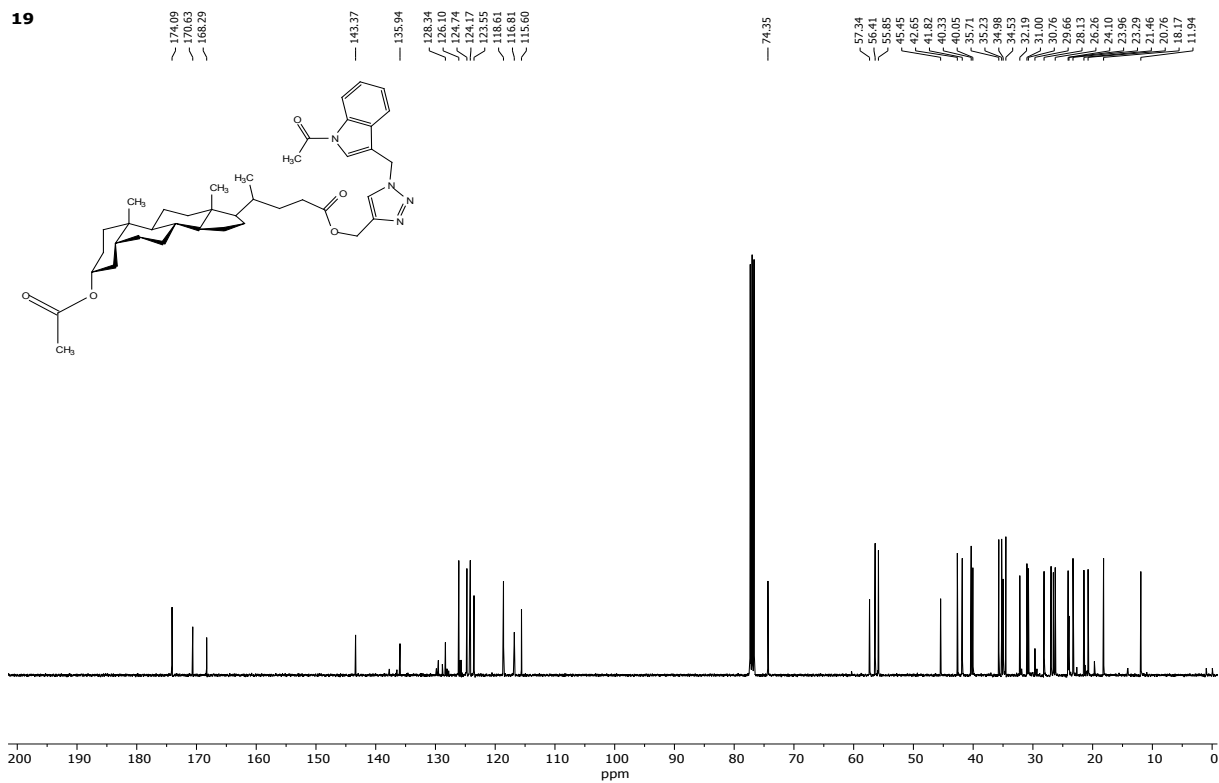
$^{13}\text{C}\{^1\text{H}\}$  NMR (101 MHz,  $\text{CDCl}_3$ ) spectra of compound 18

19

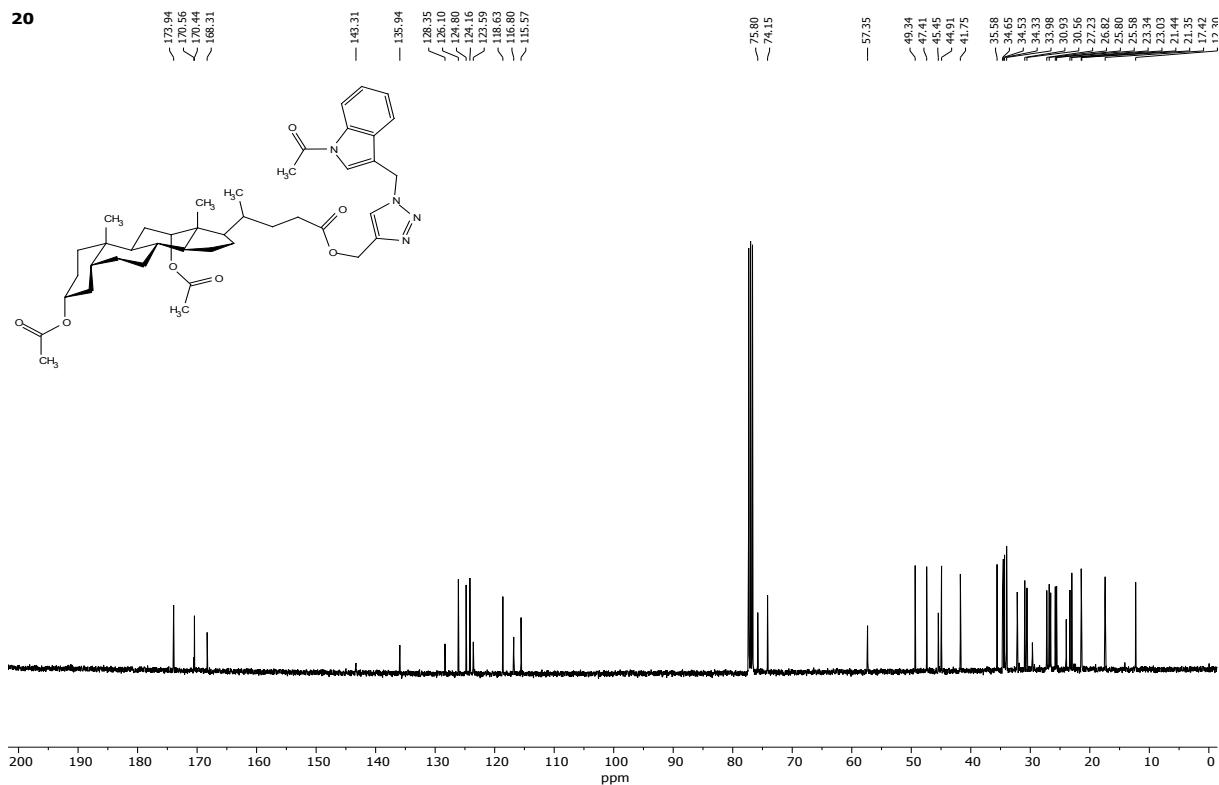


$^1\text{H}$  NMR (400 MHz,  $\text{CDCl}_3$ ) spectra of compound 19



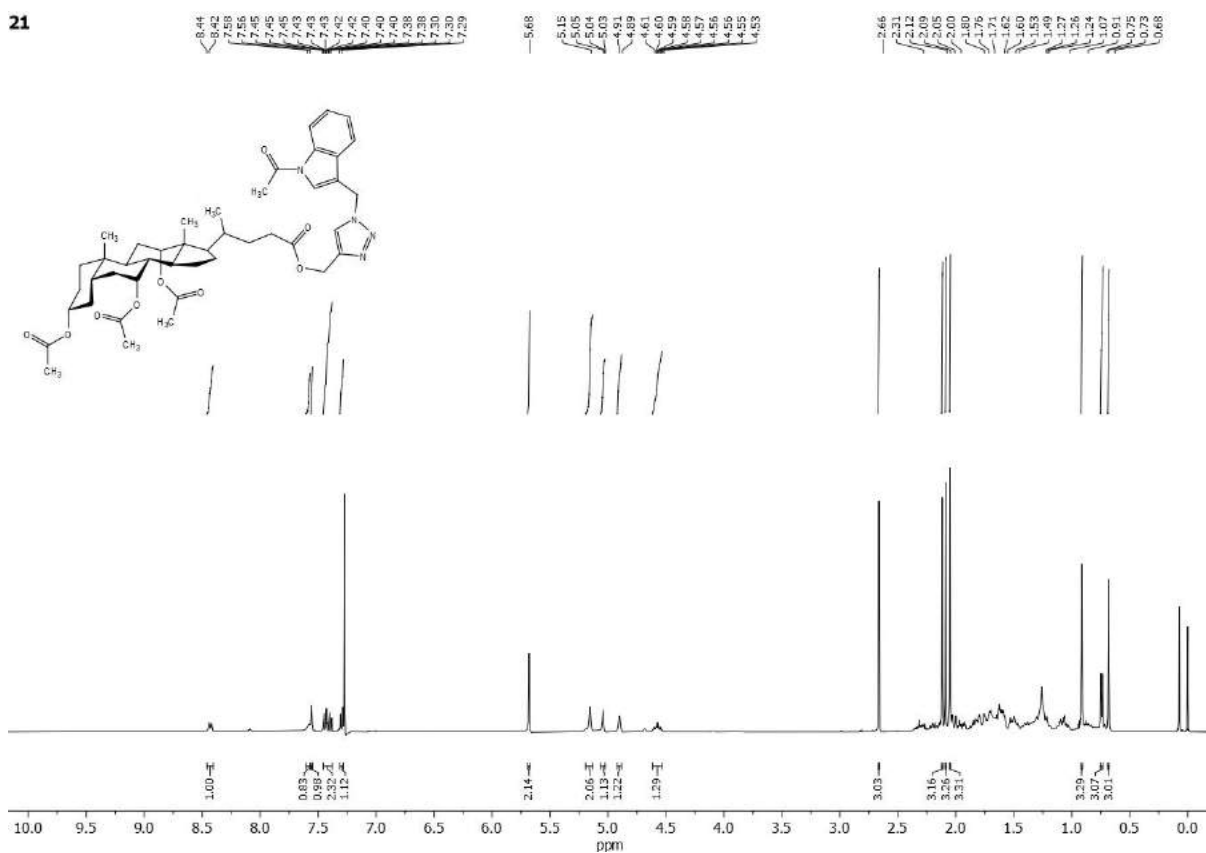


20



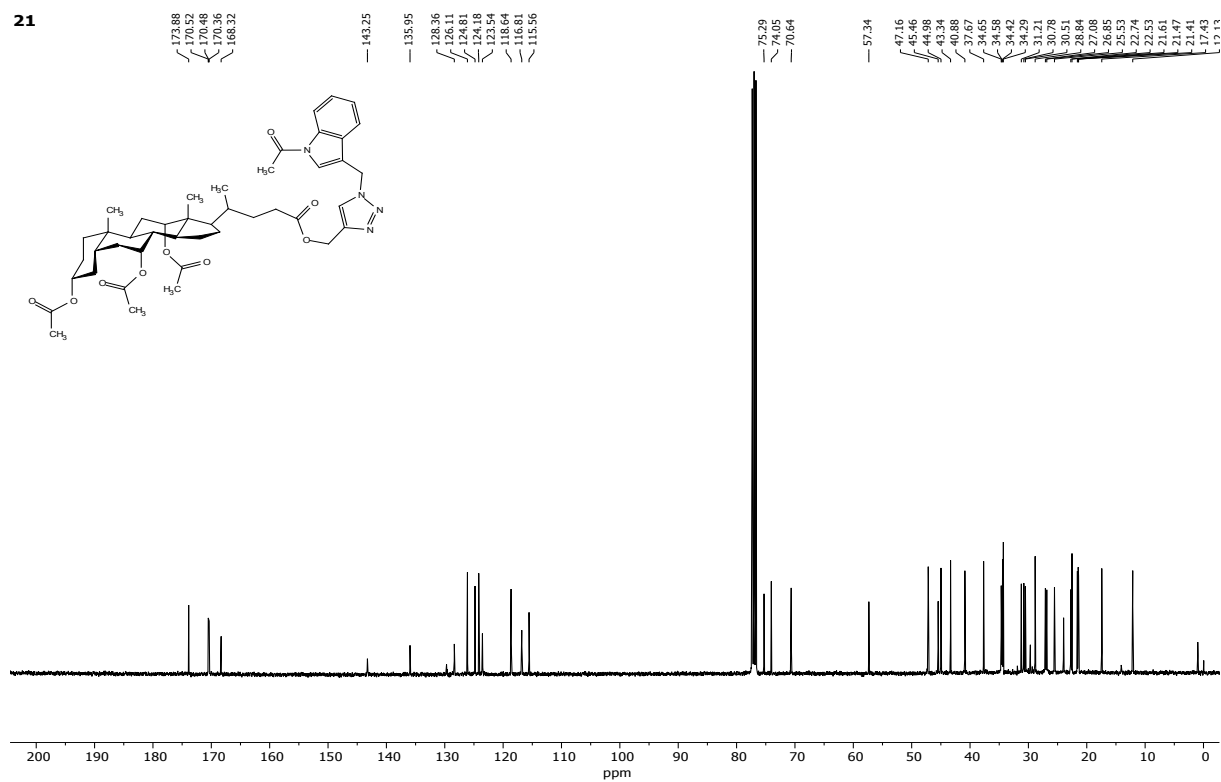
$^{13}\text{C}\{^1\text{H}\}$  NMR (101 MHz,  $\text{CDCl}_3$ ) spectra of compound 20

21



$^1\text{H}$  NMR (400 MHz,  $\text{CDCl}_3$ ) spectra of compound 21

21



$^{13}\text{C}\{^1\text{H}\}$  NMR (101 MHz,  $\text{CDCl}_3$ ) spectra of compound **21**



Article

# Novel C3-Methylene-Bridged Indole Derivatives with and without Substituents at N1: The Influence of Substituents on Their Hemolytic, Cytoprotective, and Antimicrobial Activity

Karolina Babijczuk <sup>1</sup>, Natalia Berdzik <sup>1</sup>, Damian Nowak <sup>2</sup>, Beata Warzajtis <sup>3</sup>, Urszula Rychlewska <sup>3</sup>, Justyna Starzyk <sup>4</sup>, Lucyna Mrówczyńska <sup>5</sup> and Beata Jasiewicz <sup>1,\*</sup>

- <sup>1</sup> Department of Bioactive Products, Faculty of Chemistry, Adam Mickiewicz University, Uniwersytetu Poznańskiego 8, 61-614 Poznań, Poland; babijczukk@gmail.com (K.B.); natalia.berdzik@amu.edu.pl (N.B.)
- <sup>2</sup> Department of Quantum Chemistry, Faculty of Chemistry, Adam Mickiewicz University, Uniwersytetu Poznańskiego 8, 61-614 Poznań, Poland; damian.nowak@amu.edu.pl
- <sup>3</sup> Department of Crystallography, Faculty of Chemistry, Adam Mickiewicz University, Uniwersytetu Poznańskiego 8, 61-614 Poznań, Poland; beata.warzajtis@amu.edu.pl (B.W.); urszula.rychlewska@amu.edu.pl (U.R.)
- <sup>4</sup> Department of Soil Science and Microbiology, Faculty of Agronomy, Horticulture, and Bioengineering, University of Life Science, Szydlowska 50, 60-656 Poznań, Poland; justyna.starzyk@up.poznan.pl
- <sup>5</sup> Department of Cell Biology, Faculty of Biology, Adam Mickiewicz University, Uniwersytetu Poznańskiego 6, 61-614 Poznań, Poland; lumro@amu.edu.pl
- \* Correspondence: beatakoz@amu.edu.pl

**Abstract:** Alkaloids are natural compounds useful as scaffolds for discovering new bioactive molecules. This study utilized alkaloid gramine to synthesize two groups of C3-substituted indole derivatives, which were either functionalized at N1 or not. The compounds were characterized by spectroscopic methods. The protective effects of the new compounds against in vitro oxidative hemolysis induced by standard oxidant 2,2'-azobis(2-amidinopropane dihydro chloride (AAPH) on human erythrocytes as a cell model were investigated. Additionally, the compounds were screened for antimicrobial activity. The results indicated that most of the indole derivatives devoid of the N1 substitution exhibited strong cytoprotective properties. The docking studies supported the affinities of selected indole-based ligands as potential antioxidants. Furthermore, the derivatives obtained exhibited potent fungicidal properties. The structures of the eight derivatives possessing indole moiety bridged to the imidazole-, benzimidazole-, thiazole-, benzothiazole-, and 5-methylbenzothiazoline-2-thiones were determined by X-ray diffraction. The C=S bond lengths in the thioamide fragment pointed to the involvement of zwitterionic structures of varying contribution. The predominance of zwitterionic mesomers may explain the lack of cytoprotective properties, while steric effects, which limit multiple the hydrogen-bond acceptor properties of a thione sulfur, seem to be responsible for the high hemolytic activity.

**Keywords:** gramine; indole derivatives; thione derivatives; anti-oxidant properties; oxidative hemolysis; docking study; crystal structures



**Citation:** Babijczuk, K.; Berdzik, N.; Nowak, D.; Warzajtis, B.; Rychlewska, U.; Starzyk, J.; Mrówczyńska, L.; Jasiewicz, B. Novel C3-Methylene-Bridged Indole Derivatives with and without Substituents at N1: The Influence of Substituents on Their Hemolytic, Cytoprotective, and Antimicrobial Activity. *Int. J. Mol. Sci.* **2024**, *25*, 5364. <https://doi.org/10.3390/ijms25105364>

Academic Editor: Ylenia Zambito

Received: 15 April 2024

Revised: 9 May 2024

Accepted: 10 May 2024

Published: 14 May 2024



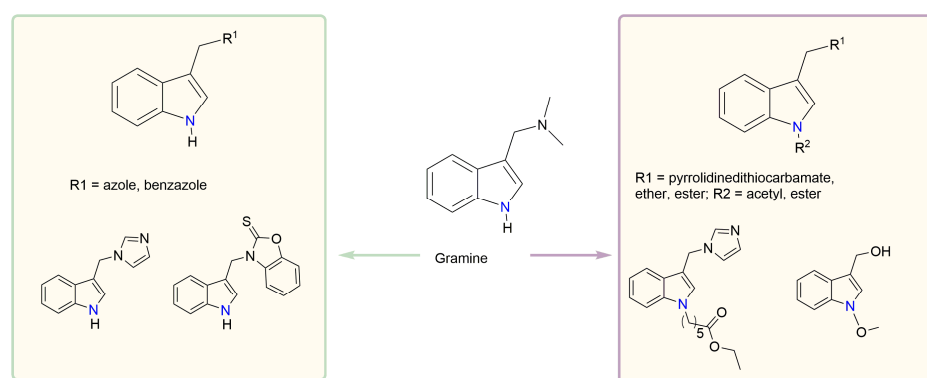
**Copyright:** © 2024 by the authors. Licensee MDPI, Basel, Switzerland. This article is an open access article distributed under the terms and conditions of the Creative Commons Attribution (CC BY) license (<https://creativecommons.org/licenses/by/4.0/>).

## 1. Introduction

Alkaloids are a large group of naturally occurring compounds used as precursors for synthesizing new drugs [1–4]. Among them, the indole alkaloids, such as vinca alkaloids (vincristine and vinblastine), reserpine, or ergot alkaloids, are of significant pharmacological interest [5–10]. Another indole alkaloid that has been constantly receiving increasing attention in sustainable chemistry is gramine. This earth-abundant natural compound is used as a pharmaceutical lead scaffold for synthesizing indole-based compounds with

different biological activities [11–16]. The dimethylamine group at the C3 position of the indole ring in gramine can undergo substitution reactions [17,18]. Therefore, functionalizing this position is convenient for obtaining more intricate structures or starting materials for further functionalization and reactions. Many C3-substituted indole analogs are effective as anticancer, antitubercular, antimicrobial, and antioxidant agents [5,9,19,20]. Another modification in the structure of gramine involves substituting the nitrogen atom in the indole group. *N*-substituted indole derivatives have shown anti-inflammatory, antimicrobial, antipsychotic, antifungal, and antioxidant effects [14,21–24]. Indole derivatives with tertiary amino and phenyl groups at the N1 nitrogen atom exhibit significant activity against the *Staphylococcus aureus* pathogen [24].

We synthesized two groups of new indole-based derivatives based on the literature data (Figure 1) to evaluate their selected biological activity. One group of molecules consisted of indole derivatives, featuring substituents at both the C3 and N1 positions. Another group of gramine derivatives contained indole moieties attached by a methylene linker at the C3 position to azoles or benzazoles.



**Figure 1.** Design of the new gramine derivatives. Examples of bioactive indole derivatives substituted at the C3 position (left) or at the C3 and N1 positions (right).

Azole-based compounds are essential building blocks in many pharmaceutical agents, and they have various effects, including antimicrobial properties [25–29]. Their activities are explained by the existence of a tautomeric equilibrium. Tautomers differ in their molecular shapes and proton donor–acceptor properties; therefore, depending on the tautomeric form, they can be involved in different molecular interactions between themselves or with other targets. In the investigated series that comprise the azole-2-thione moieties, the molecules can theoretically exist in two tautomeric forms, viz., thione and thiol. The thione form provides the only ‘classical’ hydrogen bond acceptor site, the other possibility being the engagement as a hydrogen bond acceptor site of  $\pi$ -electron systems or solvation.

In the studies of membrane-active compounds for any biomedical application, human red blood cells (RBCs) are commonly used as a cell model [30–32]. Due to their availability and lack of organelles, they are used to evaluate the cytotoxicity of newly synthesized compounds.

RBCs are an excellent model cell for antioxidant studies due to their membrane, which has a high polyunsaturated fatty acid content. Furthermore, RBCs with hemoglobin containing heme iron are continuously exposed to oxidation during oxygen transport [33,34]. ROS (reactive oxygen species) are both radical (superoxide  $O_2^{\bullet-}$ , hydroxyl  $OH^{\bullet}$ , peroxy  $RO_2^{\bullet}$ , hydroperoxyl  $HO_2^{\bullet}$ ) and nonradical (hydrogen peroxide  $H_2O_2$ , hypochlorous acid  $HOCl$ , and ozone  $O_3$ ) forms of oxygen. They are formed through enzymatic and non-enzymatic processes, and they can be acquired from external sources, such as food, UV radiation, or environmental pollution [35]. Although ROS play a significant role in signal transduction [36], excess can lead to an oxidative stress that causes cancer, diabetes, and neurodegenerative diseases [37,38].

Exposure of RBCs to oxidative stress can consequently result in changes in the molecular structure of their cell membrane, thus leading to hemolysis. Therefore, one of the main criteria limiting the *in vitro* use of new bioactive compounds is the evaluation of their hemocompatibility. Compounds considered hemocompatible [32] are not toxic to all cells.

Cells have developed a series of antioxidant defense systems to scavenge or minimize the formation of oxygen-derived radicals, thereby protecting themselves from oxidative damage. These antioxidant systems include dietary antioxidants and endogenous enzymatic and non-enzymatic constituents. Enzymatic antioxidants, which act as catalysts, are responsible for removing ROS from biological systems. Superoxide dismutase catalyzes the conversion of  $O_2^{\bullet-}$  to  $H_2O_2$ , while  $H_2O_2$  can be reduced to water by catalase or glutathione peroxidase through two distinct mechanisms. Hydroxyl radicals are generated in the Fenton reaction from hydrogen peroxide in the presence of Fe (II) or Cu (I), and they are neutralized by glutathione peroxidase [38,39]. The most common dietary antioxidants include vitamins A, C, and E, as well as flavonoids and alkaloids [40,41].

This study aimed to utilize alkaloid gramine in the synthesis of two new groups of indole derivatives with altering substituents at C3 and N1, determine their structures and spectroscopic characteristics, and *in vitro* evaluate their hemocompatibility and cytoprotective activity under oxidative stress conditions. In addition, an *in silico* docking study was conducted to estimate the affinity of the obtained compounds for three protein domains: myeloperoxidase (MPO), xanthine dehydrogenase, and cyclooxygenase-2 (COX-2). These enzymes are involved in generating ROS and contributing to oxidative stress [42–47]. Since gramine and its derivatives have demonstrated the potential to inhibit the growth of certain bacterial and fungal species [12], the compounds obtained were also preliminarily screened for *in vitro* antimicrobial activity.

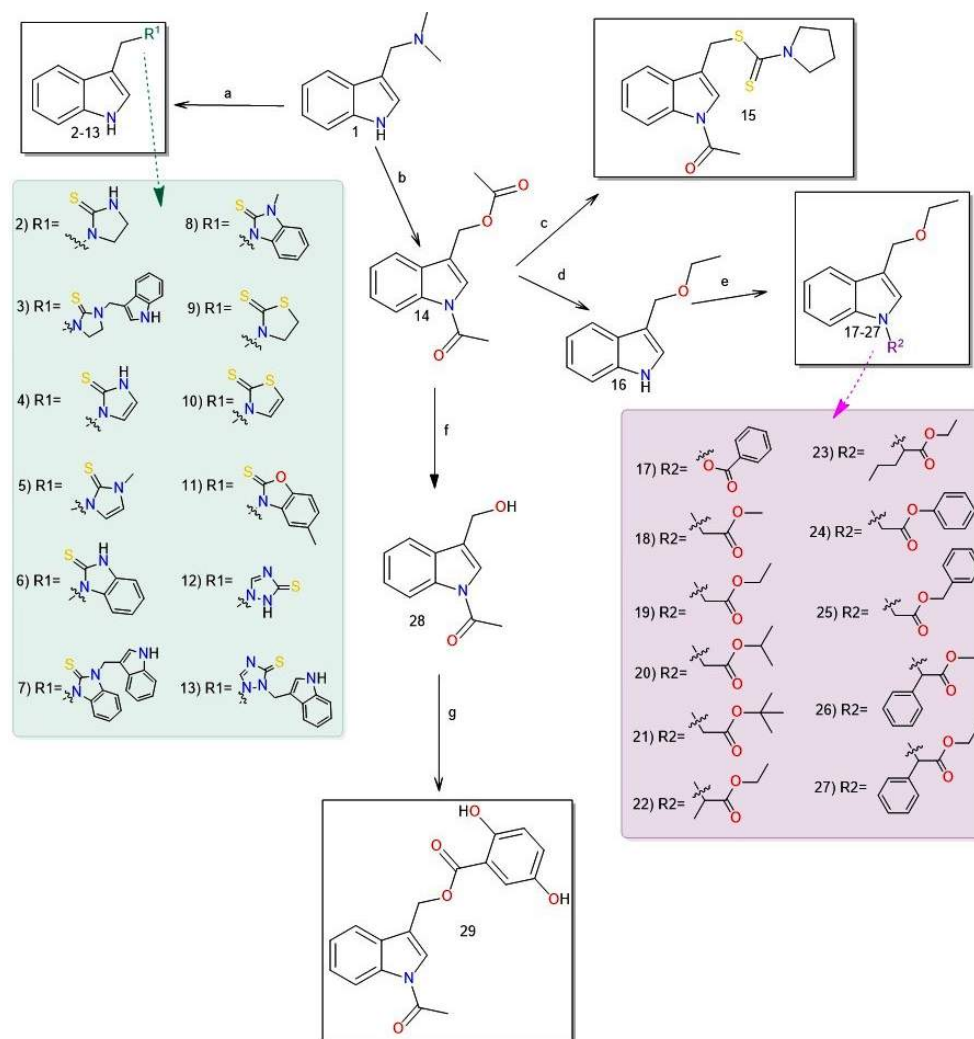
## 2. Results and Discussion

### 2.1. Synthesis and Spectroscopic Characterization of New Indole Derivatives

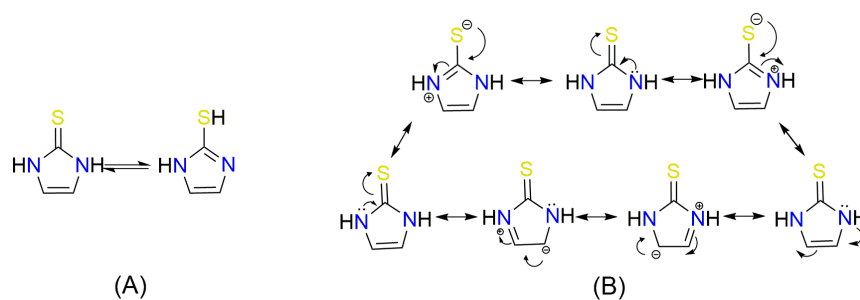
Gramine (**1**), a commercial indole alkaloid, was used as the substrate for the synthetic routes, as shown in Figure 2.

Compounds **2–13** were synthesized by heating gramine with the corresponding substrate in ethanol. Derivatives **2–9** were synthesized in an alkaline medium, which was achieved by adding NaOH to the substrate in ethanol before adding gramine and heating. Dimers **3** and **7** crystallized first, and, after adding water to the filtrate, Monomers **2** and **6** appeared as solids, which were then filtered. In the reaction with 1,2-dihydro-1,2,4-triazole-3-thione (i.e., a synthesis of **12** and **13**), column chromatography was necessary to separate the dimer and monomer forms. Heating gramine in acetic anhydride produced *N*-acetyl-3-acetoxymethylindole (**14**), which can be converted to Compound **15**. Compound **14** was reacted with anhydrous ethyl alcohol in an alkaline medium to produce 3-ethoxymethylindole (**16**). The resulting ether derivative (**16**) was then treated with benzoic acid to yield Compound **17**. Compounds **18–27** were obtained by reaction of Derivative **16** with a series of bromoesters. Derivative **29** was synthesized through a two-step process involving the hydrolysis of *N*-acetyl-3-acetoxymethylindole (**14**), which was followed by a reaction with 2,5-dihydroxybenzoic acid.

A crucial structural feature of azoles and benzazoles is the existence of tautomeric forms. Figure 3 shows the following: (A) two tautomeric forms of imidazole-2-thiones (thione and thiol) and (B) their mesomeric effect. According to the literature data, the thione form is predominant in polar solvents and the solid state [16,48–55].



**Figure 2.** Synthesis of Compounds 2–29: (a) H-R<sup>1</sup>, EtOH, NaOH, reflux (2–9) or H-R<sup>1</sup>, EtOH, and reflux (10–13); (b) Ac<sub>2</sub>O and reflux; (c) sodium pyrrolidinedithiocarbamate, H<sub>2</sub>O, and reflux; (d) EtOH, base, and r.t.; (e) CHCl<sub>2</sub>, benzoic acid, PPh<sub>3</sub>, NBS, Et<sub>3</sub>N, and 0 °C; (17) Br-R<sup>2</sup>, DMF, base, and 0 °C (18–27); (f) H<sub>2</sub>O and reflux; or (g) THF, 2,5-dihydroxybenzoic acid, DCC, and r.t.



**Figure 3.** (A) The tautomeric forms of imidazole-2-thione. (B) The mesomeric effect in imidazole-2-thione.

The NMR spectra analysis confirmed the presence of the thione forms of the newly obtained gramine derivatives (2, 4, 6, 12, and 13) in the DMSO-*d*<sub>6</sub> solution.

The newly synthesized compounds (2–13, 15, 17–27, and 29) exhibited characteristic signals for the aromatic indole system in the 8.50–6.20 ppm range, as observed in their <sup>1</sup>H NMR spectra. Additionally, the signals from theazole rings and phenyl (17, 24–27, and 29) substituents were visible in the aromatic region (7.00–8.50 ppm). The singlets at 11–14 ppm were assigned to the NH protons of the gramine moiety (2–13) and the

imidazole-, benzimidazole-2-thione or triazole-3-thione rings (4, 6, 12). The protons of the  $-C(10)H_2-$  groups of all the new compounds showed singlets in the range of about 4.65–5.80 ppm. The singlets from the  $-CH_3$  group present at the nitrogen atoms in 5 and 8 were at 3.48 and 3.75 ppm, respectively. The singlet from the methyl group at position C5 in 11 was at 2.33 ppm. A singlet near 2.60 ppm was observed for three protons from the acetyl group (15, 29).

The  $^{13}C$  NMR spectra of the new compounds showed signals from the carbon atoms of the indole rings at 109–162 ppm. Compounds 17, 24–27, and 29 also exhibited signals in the 109–158 ppm range, which originated from the phenyl substituents. Additionally, the spectra of Compounds 17–27 displayed signals from the carbonyl carbon atoms at about 166–171 ppm. The acetyl group signal for Compounds 15 and 29 was observed at approximately 168 ppm. The thione group signal was located at approximately 160 ppm (4–8, 12, and 13) or 180–195 ppm (2, 3, and 9–11). Additionally, the signals from the azole (4, 5, 10, 12, and 13) and benzazole (6–8 and 11) rings were present in the range of 111–152 ppm. The signals corresponding to the carbon atoms at the C10 position of all compounds occurred in the 33–69 ppm region. The carbon signal from the methyl group was connected to the nitrogen atom in 5 and 8, and was approximately 33 ppm, while the signal from the methyl group in Position C5 in 11 was at 20.92 ppm. The carbon signal from the  $-CH_3$  in the acetyl group (15 and 29) was present at 24.23 ppm and 29.92 ppm, respectively.

The structures of all the new indole derivatives were also confirmed by EI-MS and IR spectroscopy, as well as elemental analysis.

The FT-IR spectra of all the compounds in the KBr tablets exhibited characteristic absorption bands of 3050–2800  $cm^{-1}$ , which corresponded to the C-H bonds of the aromatic rings. Furthermore, in the spectra of Compounds 2–13, a wide band at 3500–3200  $cm^{-1}$  was present, thereby corresponding to the stretching vibrations of N-H in the indole ring. The carbonyl group exhibited an intense stretching vibration peak at approximately 1700  $cm^{-1}$  (15, 17–27, and 29). Stretching vibrations of C=S were observed from 1000  $cm^{-1}$  to 1300  $cm^{-1}$ . The FT-IR spectrum of Compound 29 showed a broad absorption band with a maximum of 3215  $cm^{-1}$ , thereby indicating the O-H bond vibrations of the hydroxyl groups.

The EI-MS spectra of all the newly synthesized compounds showed signals corresponding to molecular ions, with relative abundances ranging from 2 to 100%. For derivatives 2–13 and 15, ions with an intensity of 100% were identified at  $m/z = 130$  ( $C_9H_8N$ )<sup>+</sup>.

The NMR ( $^1H$  and  $^{13}C$ ), EI-MS, and FT-IR spectra of the investigated compounds are provided in the Supplementary Materials (Figures S1–S25).

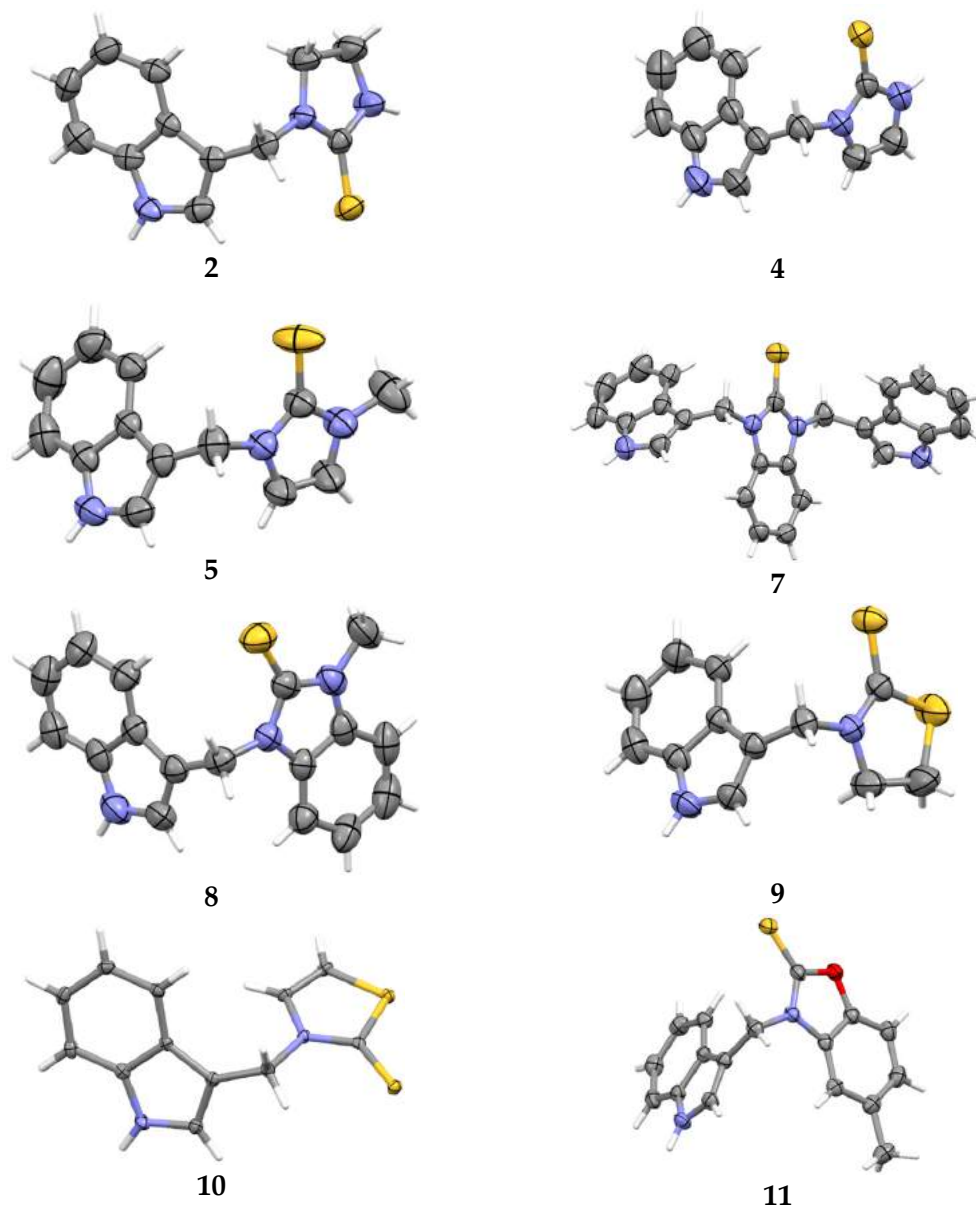
## 2.2. X-ray Analysis

We investigated, by X-ray diffraction, a series of eight compounds (2, 4–5, and 7–11), in which indole moiety was bridged by the  $-CH_2-$  group to the five-membered heterocyclic fragments containing altered imidazole-, benzimidazole-, thiazole-, benzothiazole-, and 5-methylbenzothiazoline-2-thiones (Figure 2). The structures of the molecules, as seen in the crystals, are presented in Figure 4. The hydrogen bond geometrical parameters with intramolecular interactions are presented in Table S1. The crystal data, together with the experimental and refinement details, are shown in Table S2.

The molecules in all of the investigated crystals appeared in a thione form. The C=S bonds in the thioamide fragment in Compounds 2, 4, 5, 7, and 8 measured at room temperature varied from 1.679(3) to 1.697(2) Å, with the mean value of 1.685(7) Å. The value was between that which is typical for single and double bonds. This was rationalized in terms of a substantial involvement of zwitterionic structures, as presented in Figure 3B [55]. In particular, the thione tautomer in 4 had a more significant contribution of the zwitterionic forms that involve single  $C^+-S^-$  covalent bonds than any other structure. The main skeleton can be described as consisting of two methylene-bridged subunits, each containing aromatic rings, which are inclined with respect to each other at angles varying from 66.6 to 87.9°. One of the fragments was always a C3-substituted planar indole moiety, while the others



were N-substituted 2-thione derivatives of imidazole (2, 4, and 5), benzimidazole (7 and 8), thiazole (9 and 10), and 5-methylbenzoxazole (11). A description of the molecular conformation was provided by a pair of torsion angles ( $\varphi_1$  and  $\varphi_2$ ) measured along the C-C-C-N and C-C-N-C methylene bonds, which are listed in Table 1.



**Figure 4.** Perspective views of the molecules as present in the crystals of Compounds 2, 4, 5, 7–9 (room temperature structures), and 10, 11 (100 and 130 K structures, respectively). The thermal ellipsoids were all drawn at the 50% probability level; hence, they are smaller for the Low-Temperature structures 10 and 11, and the H-atoms are represented as sticks.

To enable an easier comparison, Table 1 also provides chemical diagrams and a capped stick representation of the molecules, all of which were seen in the same orientation, i.e., along the indole plane. This allowed us to combine the values of the torsion angles with a particular molecular shape.

**Table 1.** Torsion angles ( $\circ$ ) describing the rotation around the methylene C-C and C-N bonds in the molecules present in crystals. Molecular diagrams and perspective views of the molecules are provided to relate the metrical values to a particular molecular shape.

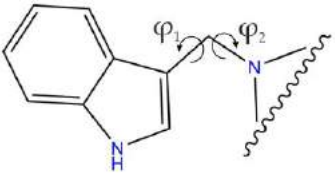

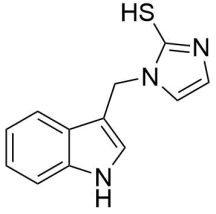

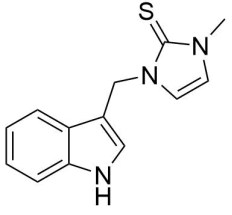

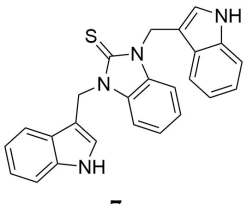

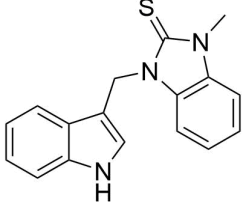
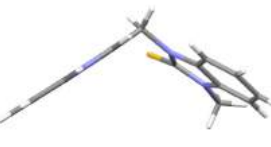
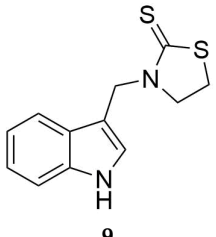

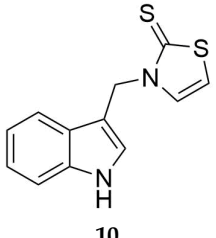
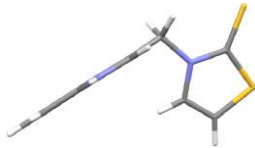
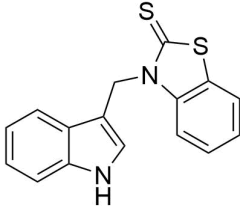
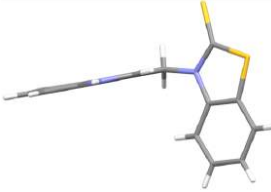
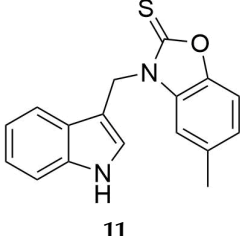

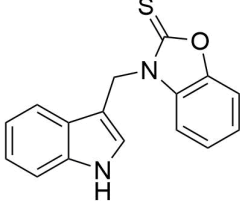

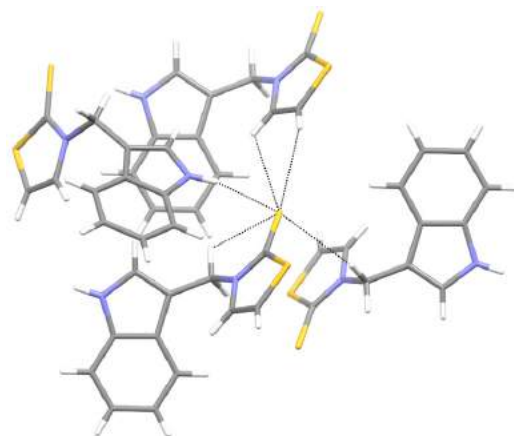
	$\varphi_1$	$\varphi_2$	
 2	-77.7(5)	89.6(5)	
 4	-74.6(2)	-57.9(2)	
 5	-79.2(3)	-58.3(3)	
 7	-69.1(3)–67.9(3)	-63.6(2)–66.6(2)	
 8	-84.3(3)	-74.8(3)	

Table 1. Cont.

	$\varphi_1$	$\varphi_2$	
 <p><b>9</b></p>	−79.1(2)	−62.0(2)	
 <p><b>10</b></p>	−83.23(19)	34.4(2)	
 <p><b>10, from ref. [16]</b></p>	−165.4(2)	76.1(3)	
 <p><b>11</b></p>	−51.6(2)	−63.64(19)	
 <p><b>11, from ref. [16]</b></p>	−88.96(16)	−80.65(16)	

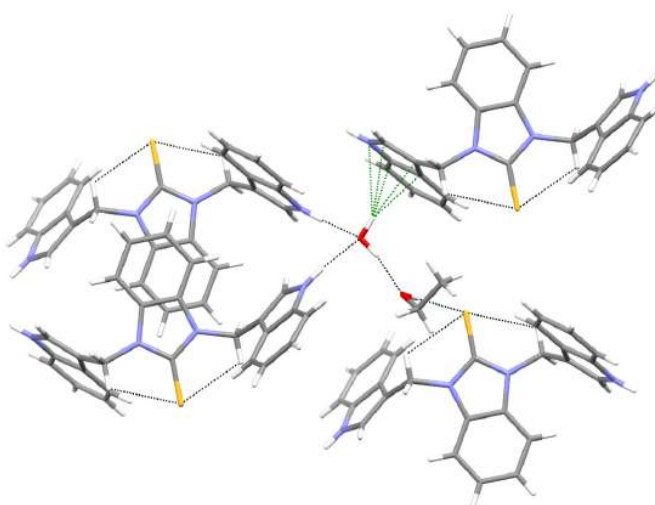
Except for **10**, the investigated molecules adopted similar, propeller-shaped conformation. The exceptional conformation of **10** could be due to the involvement of its thiocarbonyl group as a quintuple hydrogen bond acceptor (Figure 5, Table S1). The ability of the sulfur atom to simultaneously engage in a greater number of interactions than conventional acceptors such as O and N was evidenced by Bogdanovic and colleagues [56].



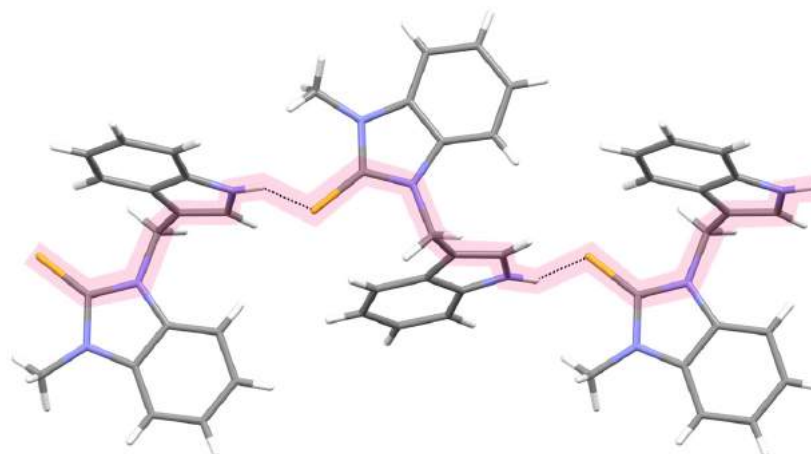
**Figure 5.** An example from the thiocarbonyl group acting as a quintupole hydrogen-bond acceptor in the crystal structure of **10**. The formed supramolecular motifs extended in three dimensions.

Moreover, a comparison of **10** with its benzothiazole analog [16] revealed that the latter analog totally excluded the C=S group from its involvement in intermolecular interactions. Although the alteration took place in the crystals, we were tempted to combine it with the finding that the compound with the benzothiazole-2-thione moiety neither displayed a cytoprotective or chelating ability, nor did it protect the RBCs from the oxidative stress-induced hemolysis [16]. Meanwhile, its homolog, **10**, with the thiazole-2-thione scaffold, showed significant cytoprotective activity and was hemocompatible (*vide infra*).

Unlike the thiazole-2-thione derivatives, the imidazole-2-thiones were less prone to the structural changes caused by chemical modifications. The isostructuralism of **5** and **9** (Table S2) indicated that the N-methyl group and sulfur atom are structural isosters, supposedly because neither of these fragments are involved in hydrogen bonding. Molecules **2**, **4**, and **7**, which contained two N-H hydrogen-bond donor groups, formed three-dimensional associates, either by taking advantage of the relatively easy approach of these groups to the thione sulfur (**2** and **4**), or by including solvent molecules to overcome the steric hindrance in an approach to the sulfur acceptor (**7**, Figure 6). The remaining derivatives (**5**, **8**, **9**, and **11**), having only one N-H donor group, associated into 1D chains or tapes (Figure 7). A detailed description of the molecular conformation and intermolecular interactions in the crystals of Compounds **2**, **4–5**, and **7–11** (Figures S26 and S27) is provided in the Supplementary Materials.



**Figure 6.** The whole palette of intermolecular interactions in the solvated crystals of **7**.



**Figure 7.** The helical arrangement of the hydrogen-bonded molecules of **8**. The bulky methyl groups and benzene rings were directed away from the HB-chain. The hydrogen bond was significantly bent due to steric hindrance (Table S1).

### 2.3. Biological Activity

#### 2.3.1. Antibacterial and Fungicidal Activity

A preliminary screening of the *in vitro* antimicrobial activity of gramine and its derivatives against pathogens microorganisms was studied using the well diffusion technique. Analysis of the interactions of the selected bacterial species with the tested compounds showed no antagonistic effects in most cases, except for Compounds **13** and **15**. Compound **13** exhibited antagonistic effects, as evidenced by the growth inhibition zones of *M. luteus* (7.3 mm), *B. subtilis* (9.4 mm), and *P. fluorescens* (10.5 mm). Derivative **15** was the most potent in inhibiting the growth of *M. luteus* and *E. coli*, thereby resulting in a zone of inhibition of 11 and 7.7 mm, respectively (see Table S3).

An analysis of the effect of gramine and its derivatives on the development of the tested mold species revealed that Compound **10** exhibited the strongest antagonistic reaction toward *B. cinerea*, with a growth inhibition zone of 23 mm (Table 2). This fungal species was also effectively inhibited by gramine and Compounds 3, 11–13, 21, 24, and 25, thus resulting in growth inhibition zones ranging from 11 to 19 mm.

**Table 2.** Fungicidal activities of Compounds 1–29. Growth inhibition zones: <9 mm—low active compounds; 10–15 mm—medium active compounds; and >15 mm—active compounds.

Compound	Zone of Growth Inhibition [mm]				
	<i>Alternaria alternata</i>	<i>Fusarium culmorum</i>	<i>Trichoderma harzianum</i>	<i>Trichoderma atroviride</i>	<i>Botrytis cinerea</i>
Gramine ( <b>1</b> )	10.0	3.5	0	13.0	11.2
<b>2</b>	2.3	2.8	8.0	2.5	3.5
<b>3</b>	9	1	4	11	16
<b>4</b>	2.0	3.5	7.5	1.5	4.3
<b>5</b>	13.0	4.5	7.0	4.0	4.5
<b>6</b>	2.3	7.8	13.0	22.0	3.3
<b>7</b>	4.8	5.5	2.8	13.5	2.3
<b>8</b>	2.3	4.0	9.0	12.0	5.0
<b>9</b>	2.0	2.5	3.7	3.0	4.0
<b>10</b>	9	2.1	8	5	23
<b>11</b>	9	1	3.5	0	17
<b>12</b>	10	1	8.4	6.6	19
<b>13</b>	18	13.2	4.5	7	16.5
<b>17</b>	1.3	3.8	5.0	20.0	4.0
<b>18</b>	0	3.0	7.5	10.0	3.8

Table 2. Cont.

Compound	Zone of Growth Inhibition [mm]				
	<i>Alternaria alternata</i>	<i>Fusarium culmorum</i>	<i>Trichoderma harzianum</i>	<i>Trichoderma atroviride</i>	<i>Botrytis cinerea</i>
19	8.0	4.5	6.5	11.5	3.5
20	0	5.0	8.0	10.5	3.5
21	10.0	1.5	0	3.0	18.0
22	3.5	4.5	8.5	11.0	4.5
23	1.5	3.8	9.5	10.0	4.5
24	7.0	1.5	2.0	0	11.0
25	6.0	2.0	0	8.0	15.0
26	2.8	5.0	20.0	20.0	4.0
27	0	4.0	9.0	2.0	3.8
29	8.5	3.8	6.0	15.0	5.3

Most of the analyzed compounds (1, 3, 6–8, 17–20, 22, 23, 26, and 29) significantly inhibited the growth of *T. atroviride*. The most-effective compounds were 6, 17, and 26, with growth inhibition zones of  $\geq 20$  mm. Derivatives 6 and 26 also had a clear impact on the growth of *Trichoderma* fungi, thus causing growth inhibition zones of 13 and 20 mm in *T. harzianum*, respectively. Compounds 5, 12, 13, and 21 significantly limited the growth of *A. alternata*, with at least 10 mm inhibition zones. Compound 13 was also important in inhibiting the growth of *F. culmorum*, thereby causing the formation of a 13.2 mm growth inhibition zone.

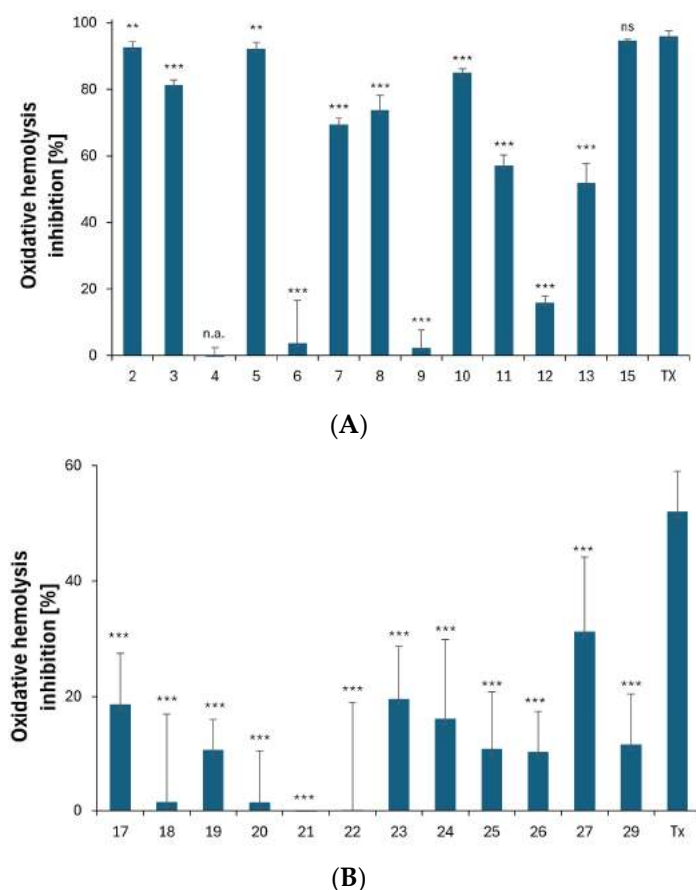
### 2.3.2. Cytoprotective Activity against Free Radicals

The ability of all compounds to inhibit 2,2'-azobis(2-amidinopropane dihydrochloride (AAPH)-induced oxidative hemolysis was used to determine their cytoprotective activity. AAPH was widely used as a standard free radical inducer. During a temperature-dependent homolysis of AAPH, peroxy and alkoxy radicals were generated [57], thus leading to lipid peroxidation in the cell membranes [58]. In an AAPH assay, Trolox (TX), a water-soluble vitamin E, was used as a standard antioxidant [59].

As shown in Figure 8A, most derivatives containing azole, benzazole, or pyrrolidine rings (2–13, 16), in a concentration of 0.1 mg/mL, exhibited cytoprotective activities against oxidative stress in the range of  $57.0\% \pm 3.20$ – $94.7\% \pm 0.4$ . The most-effective derivatives were 2, 5, and 15, with activity values of  $92.7\% \pm 1.6$ ,  $92.2\% \pm 1.8$ , and  $94.7\% \pm 0.4$ , respectively. These values are comparable to the standard antioxidant Trolox ( $96.0\% \pm 1.5$ ). Compounds 2 and 5 were found to be hydrophilic, with logP values of 1.80 and 1.94, respectively. They contained polar substituents in Position C3 of the indole ring, resulting in a “polar head-non-polar tail” structure, which enhanced the stability of the RBC membrane by interacting in the lipid bilayer of the cell membrane [14,60]. The high cytoprotective activity also characterized Derivative 10 ( $84.9\% \pm 1.3$ ), especially in comparison to its benzothiazole analog [16].

Derivatives 2–3, 5, 7–8, and 10–11 had a substituent at the C3 position, which stabilized the resulting indolyl radical. Additionally, these compounds had an unsubstituted nitrogen atom N1, which further promoted the radical stabilization and enhanced their cytoprotective activity. However, Compound 15 showed high cytoprotective activity despite having a substituted N1 nitrogen atom. This result was likely due to the pyrrolidinedithiocarbamate moiety at the C3 position.

Only four compounds showed a cytoprotective activity lower than 20%: 4, 6, 9, and 12. It was suggested that Derivatives 4, 6, and 12, like 4-mercaptoimidazole [61], are predominantly in the zwitterionic form at a physiological pH, with a thiolate group that converts to a thiyl radical ( $RS^{\bullet}$ ) in the presence of the free radicals generated by AAPH.



**Figure 8.** (A) Cytoprotective activity of Compounds 2–15 and the standard antioxidant Trolox at a concentration of 0.1 mg/mL against the oxidative hemolysis induced by free radicals generated from AAPH. The results ( $n = 9$ ) are presented as the mean value  $\pm$  standard deviation (\*\* $p < 0.01$ , \*\*\*  $p < 0.001$ ) in comparison with the standard antioxidant Trolox. The non statistically significant difference ( $p > 0.05$ ) is indicated as ns. Inactive compounds are indicated as n.a. (B) Cytoprotective activity of Compounds 17–29 and the standard antioxidant Trolox at a concentration of 0.01 mg/mL against the oxidative hemolysis induced by free radicals generated from AAPH. The results ( $n = 10$ ) are presented as the mean value  $\pm$  standard deviation (\*\* $p < 0.01$ , \*\*\*  $p < 0.001$ ) in comparison with the standard antioxidant Trolox. The non statistically significant difference ( $p > 0.05$ ) is indicated as ns.

Thiyl radicals can cause the excessive generation of oxidants in erythrocytes, thereby leading to an imbalance in pro- and antioxidant levels. In addition, the thiyl radical can interfere with the lipid bilayer of RBCs by a direct addition to the double bonds in unsaturated fatty acids or by initiating the lipid peroxidation process by removing hydrogen from lipids [62,63]. It is noteworthy that Derivative 9 showed low cytoprotective activity ( $2.4\% \pm 5.3$ ), which was attributed to the substituent in Position C3 of the indole ring. The thiazole-2-thione moiety cannot form resonance structures, which results in a lack of stabilization in the free radicals formed.

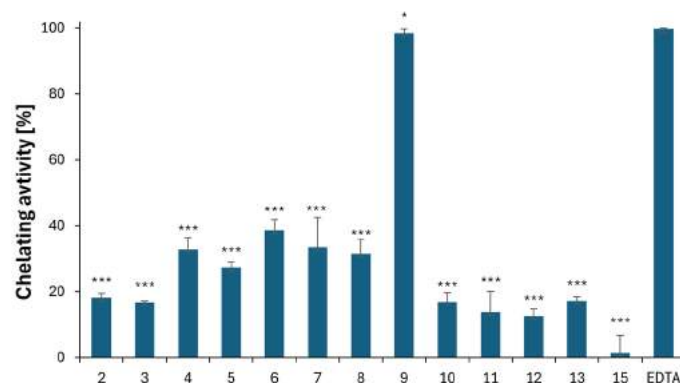
Since most of the derivatives in the second group (17–27 and 29) were hemolytic at 0.1 mg/mL, antioxidant studies were performed at a 10-fold lower concentration of 0.01 mg/mL. The results are shown in Figure 8B.

Among all the derivatives, Derivative 27, with a phenylacetate substituent in the N1 position, demonstrated the highest cytoprotective activity at  $31.3\% \pm 12.9$ . The cytoprotective activity of the standard Trolox (Tx) was  $52.1\% \pm 7.0$ . Compound 29 had an acetyl group in the N1 position and a dihydroxybenzoic substituent in the C3 position. Its cytoprotective activity value was surprisingly low at  $11.5\% \pm 8.9$ , despite the high antiradical activity exhibited by the derivatives of benzoic acid, particularly with respect to its hydroxy derivatives [64,65].

The HAT (Hydrogen Atom Transfer) mechanism is one of the primary antioxidant mechanisms of indoles. The key to this mechanism is the hydrogen atom located on the nitrogen atom of the pyrrole ring [66,67]. Derivatives 17–27 and 29, which have substitutions at the N1 position, may have low cytoprotective activity due their prevention of the formation of the indolyl radical.

### 2.3.3. Chelating Activity

The hydroxyl radical  $\bullet\text{OH}$  is considered the most harmful free radical and is primarily responsible for the cytotoxic effects on aerobic organisms. It is formed in the presence of iron by the Haber–Weiss and Fenton reactions, where ferrous ions ( $\text{Fe}^{2+}$ ) are oxidized to ferric ions ( $\text{Fe}^{3+}$ ). Therefore, the ability of compounds to chelate  $\text{Fe}^{2+}$  ions can be used to evaluate their antioxidant properties. Compounds 2–13 and 15, which contain heteroatoms with a lone electron pair (N and S), were investigated for their complexing activity. Figure 9 shows that most of the derivatives had ferrous chelating properties within the range of  $1.4\% \pm 5.4$  to  $38.6\% \pm 3.2$ . However, only Compound 9 ( $98.5\% \pm 1.5$ ) complexed  $\text{Fe}^{2+}$  ions more effectively than gramine, and it was found to be comparable to the standard chelator EDTA ( $99.7\% \pm 0.2$ ). This derivative differed from all others because the electrons in its thiazoline-2-thione moiety were not involved in resonance, as in 2 and 4, or in the aromatic system (as in Compound 10), thus allowing them to be used for ferrous ion complexation.



**Figure 9.** Ferrous ion chelating activity of the iron ions of Compounds 2–15 and the standard chelating agent EDTA. The results ( $n = 6$ ) are presented as the mean value  $\pm$  standard deviation (\*  $p < 0.05$ , \*\*\*  $p < 0.001$ ) in comparison with EDTA.

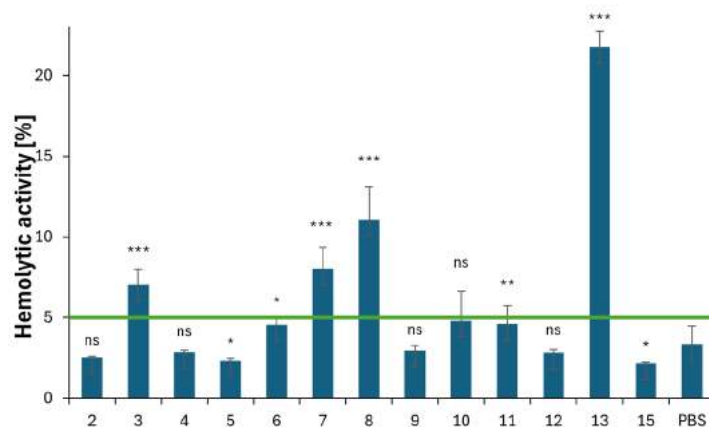
### 2.3.4. Hemolytic Properties

The hemolytic activity of all derivatives has been assessed in vitro using human RBCs as a cell model. In general, a bioactive compound is considered hemolytic at a given concentration if it causes hemolysis of 5% or more of RBCs in a given sample [14–16]. Bioactive compounds that do not induce hemolysis of more than 5% of exposed RBCs are considered hemocompatible [68].

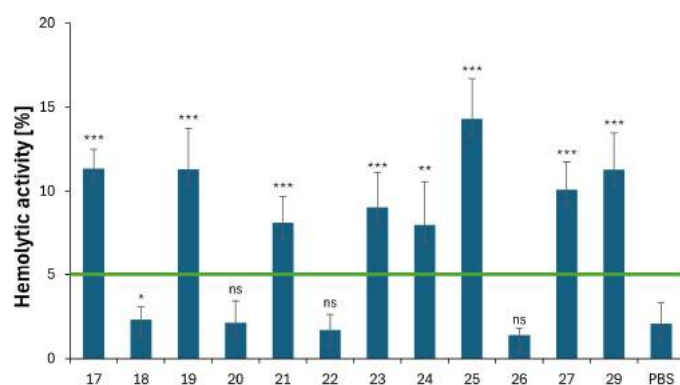
As shown in Figure 10A, the majority of derivatives with anazole or benzazole substituent at the C3 position of the indole ring are not hemolytic (hemolysis from  $2.1\% \pm 0.1$  to  $4.8\% \pm 0.1$ ). Compound 15, which contains a pyrrolidinedithiocarbamate moiety, is also hemocompatible ( $2.1\% \pm 0.1$ ). Compounds 3, 7, 8, and 13 demonstrated high hemolytic activity, with values of  $7.0\% \pm 0.9$ ,  $8.0\% \pm 1.3$ ,  $11.1\% \pm 2.0$ , and  $21.8\% \pm 1.0$ , respectively. The high hemolytic activity of these compounds may be attributed to steric reasons, particularly the presence of two indole moieties. The impact of having two indole groups on the increase in hemolytic activity is evident when comparing the hemolytic activity values for Compounds 2 ( $2.5\% \pm 0.1$ ) versus 3 ( $7.0\% \pm 0.9$ ), 6 ( $4.6\% \pm 0.4$ ) versus 7 ( $8.0\% \pm 1.3$ ), and—especially for triazole derivatives—12 ( $2.8\% \pm 0.1$ ) and 13 ( $21.8\% \pm 1.0$ ). The hemolytic activity of Derivative 8, which contains an *N*-methylated benzimidazole ring, increased from  $4.6\% \pm 0.4$  in the parent Molecule 6 to  $11.1\% \pm 2.0$ . The increase in hemolytic activity can be attributed to changes in the molecular conformation of Compound



8 compared to Compound 6, which resulted in different interactions with the lipid bilayer of the RBCs. No significant effects were observed when comparing the hemolytic activity values of Derivative 11 with those of the parent molecule (non-methylated at C5) [16], as well as the non-methylated Compound 4 with the N-methylated Compound 5. In both cases, the hemolytic activity values were similar.



(A)



(B)

**Figure 10.** (A) Hemolytic activity of Compounds 2–15 at a concentration of 0.1 mg/mL. Results ( $n = 9$ ) are presented as the mean value  $\pm$  standard deviation (\*  $p < 0.05$ , \*\*  $p < 0.01$ , and \*\*\*  $p < 0.001$ ) in comparison with the standard buffer PBS. Non statistically significant difference ( $p > 0.05$ ) is indicated as ns. The green line indicates a hemolysis threshold of 5%. (B) Hemolytic activity of Compounds 17–29 at a concentration of 0.1 mg/mL. Results ( $n = 9$ ) are presented as the mean value  $\pm$  standard deviation. (\*  $p < 0.05$ , \*\*  $p < 0.01$ , and \*\*\*  $p < 0.001$ ) in comparison with the standard buffer PBS. Non statistically significant difference ( $p > 0.05$ ) is indicated as ns. The green line indicates a hemolysis threshold of 5%.

The hemolytic activity of Compounds 18–27 (Figure 10B) was dependent on the hydrophobicity of the ester substituents at the N1 position. It can be stated that the presence of these substituents enables incorporation into the phospholipid bilayer of RBCs. Among all the ester derivatives examined, Compounds 18, 20, 22, and 26 exhibited no hemolytic activity (ranging from  $1.4\% \pm 0.4$  to  $2.3\% \pm 0.7$ ) and demonstrated hemocompatibility at the tested concentration.

#### 2.4. In Silico Study

Lipinski's and Verber's rules provide criteria for determining whether new derivatives meet the requirements for a drug. According to Lipinski [69], a drug-like compound should have a molecular mass (MW) of less than 500 g/mol, an octanol/water partition coefficient ( $\log P$ ) of under 5, no more than 5 hydrogen bond donors (HBD), and 10 hydrogen bond

acceptors (HBA). Veber's rule [70] considers rotatable bonds (RTB) to be less than 10, and a polar surface area (TPSA) should not be greater than  $140\text{\AA}^2$ . In addition to the drug-likeness parameters mentioned above, it is important to consider water solubility, gastrointestinal absorption (GI absorption), and blood–brain barrier penetration (BBB permeability). The physicochemical properties of the derivatives were evaluated using the SwissADME website [70]. Table 3 shows that all the derivatives met Lipinski's and Veber's rules and had high gastrointestinal absorption. Most could penetrate the blood–brain barrier (except for Compounds 3, 10, 12, 15, and 29), which means they may act in the central nervous system. All compounds, except Compound 7, were either soluble or moderately soluble in water. The low solubility of Compound 7 was due to its high lipophilicity, as indicated by its logP value of 4.78, the highest among all the compounds studied.

**Table 3.** The physicochemical, pharmacokinetic, and drug-likeness properties of the indole derivatives. LogS in the table is the average value of the logS calculated using three different methods. \* Solubility class—logS scale: insoluble < −10, poorly < −6, moderately < −4, soluble < −2, and very < 0.

Compound	MW [g/mol]	logP	HBD	HBA	RTB	TPSA [ $\text{\AA}^2$ ]	GI Absorption	BBB Permeant	LogS	Solubility *
2	231.32	1.80	2	0	2	63.15	High	Yes	−3.01	Soluble
3	360.48	3.39	2	0	4	70.15	High	No	−5.32	Moderately
4	229.30	2.17	1	1	2	72.41	High	Yes	−3.63	Soluble
5	245.34	1.94	1	0	2	61.07	High	Yes	−3.32	Soluble
6	279.36	3.25	1	1	2	72.41	High	Yes	−5.08	Moderately
7	408.52	4.78	2	0	4	73.53	High	Yes	−6.91	Poorly
8	293.39	3.43	1	0	2	57.74	High	Yes	−4.58	Moderately
9	248.37	2.63	1	0	2	76.42	High	Yes	−3.77	Soluble
10	246.35	3.03	1	0	2	70.15	High	No	−3.99	Soluble
11	294.37	3.90	1	1	2	65.95	High	Yes	−5.34	Moderately
12	230.29	1.85	1	2	2	85.30	High	No	−5.47	Moderately
13	359.45	3.38	2	1	4	86.42	High	Yes	−2.90	Soluble
15	318.46	3.27	0	1	5	82.63	High	No	−5.47	Moderately
17	295.33	3.43	0	3	6	40.46	High	Yes	−4.74	Moderately
18	247.29	2.14	0	3	6	40.46	High	Yes	−3.01	Soluble
19	261.32	2.49	0	3	7	40.46	High	Yes	−3.35	Soluble
20	275.34	2.80	0	3	7	40.46	High	Yes	−3.62	Soluble
21	289.37	3.03	0	3	7	40.46	High	Yes	−3.87	Soluble
22	275.34	2.81	0	3	7	40.46	High	Yes	−3.61	Soluble
23	303.40	3.50	0	3	9	40.46	High	Yes	−4.36	Moderately
24	309.36	3.32	0	3	7	40.46	High	Yes	−4.73	Moderately
25	323.39	3.41	0	3	8	40.46	High	Yes	−4.82	Moderately
26	323.39	3.47	0	3	7	40.46	High	Yes	−4.83	Moderately
27	337.41	3.75	0	3	8	40.46	High	Yes	−5.17	Moderately
29	325.32	2.54	2	5	5	88.76	High	No	−4.25	Moderately

### 2.5. Molecular Docking

Compounds 2, 5, and 15 were selected for molecular docking due to their cytoprotective activity above 90%. These compounds were found to be non-hemolytic. The selection of protein domains was guided by their specific biological functions within the physiological system. The chosen proteins, Myeloperoxidase (MPO), Xanthine dehydrogenase, and Cyclooxygenase-2 (COX-2), play crucial roles in cellular processes, and targeting them can have significant implications for modulating oxidative stress. These proteins can generate reactive oxygen species (ROS) as part of the body's defense mechanism against pathogens, or as a by-product of their enzymatic activity. Inhibition of their activity may reduce the generation of ROS associated with their function, thereby reducing oxidative stress [42–47].

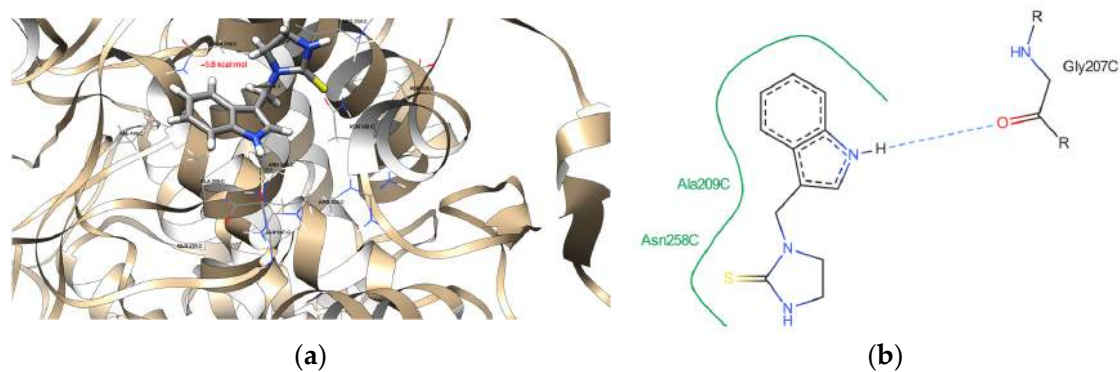
The molecular docking data revealed that the newly acquired indole-based derivatives indeed exhibited affinity for the investigated protein domains. In Table 4, their affinity to

the 1DNU protein domain is notably comparable to the reference ligand, melatonin. The ProteinsPlus algorithms, namely PoseView [71,72] and PoseEdit [71,73], were unable to produce 2D maps of the interactions. The following error was raised: “No interactions found by the PoseView interaction model”. This indicated that Compounds **15** did not have 2D depictions of the interactions between the protein domain and them. This raised the issue of whether it can be connected with the different settings and then used in UCSF Chimera 1.16 software [74]. Moving on to the 1N5X protein domain, the affinity of the indole-based derivatives was similar to the reference ligand, febuxostat. However, their affinity remained quite similar, indicating comparable binding tendencies. Similarly, for the 4COX protein domain, the affinity of the indole-based derivatives was slightly lower than that of the native ligand, indomethacin. Nevertheless, this disparity still suggests promising opportunities for its binding to the protein domain.

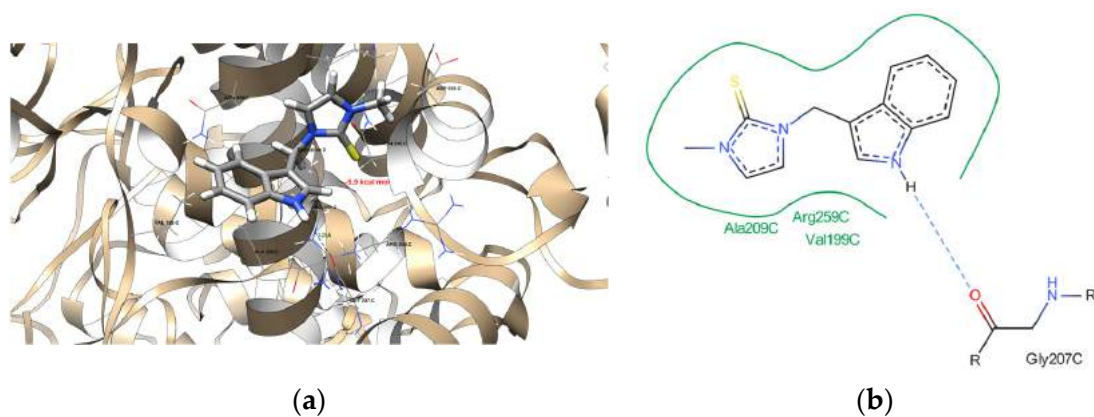
**Table 4.** The results of molecular docking to the 1DNU, 1N5X, and 4COX protein domains of all the compounds analyzed. Melatonin, febuxostat, and indomethacin were used as reference molecules.

PDB ID	Compound	Average Binding Energy [kcal/mol]	Standard Deviation of Binding Energy [kcal/mol]
1DNU	Melatonin	−5.3	0.15
	<b>2</b>	−5.4	0.21
	<b>5</b>	−5.5	0.25
	<b>15</b>	−5.2	0.15
1N5X	Febuxostat	−7.0	0.32
	<b>2</b>	−7.9	0.41
	<b>5</b>	−7.8	0.61
	<b>15</b>	−7.5	0.45
4COX	Indomethacin	−8.0	0.82
	<b>2</b>	−7.4	0.39
	<b>5</b>	−7.3	0.61
	<b>15</b>	−7.2	0.15

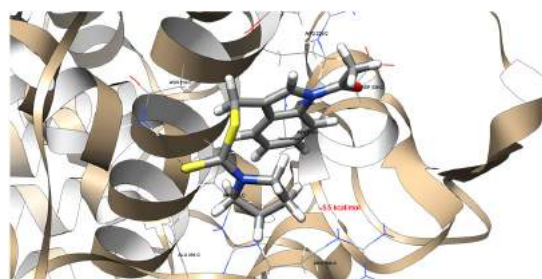
Figures 11–14 provide visual representations of the interactions between the indole-based derivatives and the 1DNU protein domain (PDB ID). Correspondingly, Figures S28–S31 (Supplementary part) depict the interactions between indole-based derivatives and the 1N5X protein domain (PDB ID). It is noteworthy that the recreation of the native ligand’s initial pose in the latter case has an acceptable accuracy, with a Root Mean Square Deviation (RMSD) of 2.635 Å [75]. Figures S32–S35 (Supplementary Materials), illustrate the interactions between indole-based derivatives and the 4COX protein domain (PDB ID). In this case, the recreation of the native ligand’s initial pose exhibits good accuracy, with an RMSD of 0.953 Å, which is considered satisfactory in the recreation of the initial pose [75]. These visualizations provide insights into the intricate molecular interactions underlying the binding of indole-based derivatives to the respective protein domains, thus reinforcing their potential as candidates for further exploration and development. All the molecular docking results are stored in Table 4.



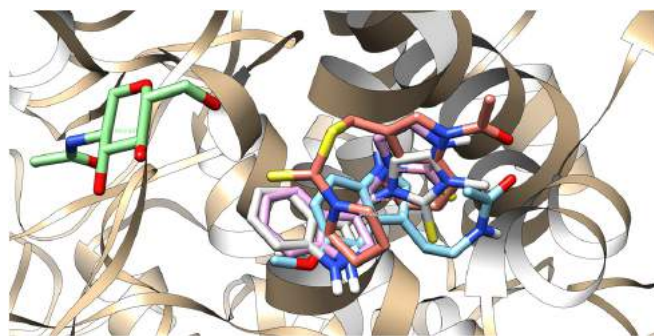
**Figure 11.** (a) The interactions between Derivative 2 and the 1DNU protein domain. The dark green dashed line suggests a potential hydrogen bond formation between the GLY 207 C residue and one of the hydrogen atoms bonded to the pyrrolic nitrogen atom of the ligand, with a length of 2.59 Å. (b) A detailed view of the interactions proposed by the molecular docking between the 1DNU protein domain's binding site and Derivative 2. One hydrogen bond was expected (blue dashed line), and the hydrophobic contacts are indicated by the green solid lines.



**Figure 12.** (a) The interactions between Derivative 5 and the 1DNU protein domain. The dark green dashed line suggests a potential hydrogen bond formation between the GLY 207 C residue and the pyrrolic hydrogen atom of the ligand, with a length of 2.29 Å. (b) A detailed view of the interactions proposed by the molecular docking between the 1DNU protein domain's binding site and Derivative 5. One hydrogen bond was expected (blue dashed line), and the hydrophobic contacts are indicated by the green solid lines.



**Figure 13.** The interactions between Derivative 15 and the 1DNU protein domain. A dark green dashed line indicates a potential hydrogen bond formation between the protein residues ASN 258 C (3.29 Å length) and the sulfur of the ligand.



**Figure 14.** The binding site of the 1DNU protein domain features the reference ligand (melatonin), the native ligand (NAG620), and the investigated Compounds **2**, **5**, and **15** simultaneously.

The conducted studies indicate that the analyzed indole-based ligands exhibited affinity profiles comparable to the reference ligands (melatonin for 1DNU and febuxostat for 1N5X), thus suggesting a similar strength of binding to these domains. However, a notable distinction emerged concerning the 4COX protein domain. In this particular case, all of the ligands exhibited lower binding energies than the reference ligand (indomethacin), thus implying a lower affinity to this protein domain. Consequently, these ligands may potentially demonstrate inferior antioxidant properties compared to the reference ligand in the context of the 4COX domain.

### 3. Materials and Methods

#### 3.1. Instrumentation and Chemicals

The synthesis reagents and solvents used in this study were commercially available. The IR spectra were obtained using FT/IR Nicolet iS5 (Thermo Scientific, Waltham, MA, USA) (KBr pellet,  $\text{cm}^{-1}$ ). The  $^1\text{H}$  and  $^{13}\text{C}$  NMR spectra were obtained using Varian (Palo Alto, CA, USA) VNMR-S 400 MHz (DMSO- $d_6$  as the solvent and TMS as the internal standard). The melting points were measured using the SMP-20 apparatus (Büchi Labortechnik AG, Flawil, Switzerland). The EI mass spectra were obtained using the 320MS/450GC mass spectrometer (Bruker, Billerica, MA, USA). The nitrogen, carbon, hydrogen, and sulfur percentage content was determined through elemental analysis using the Elemental Analyzer Vario EL III apparatus (Shimadzu, Kyoto, Japan). TLC analysis was conducted using silica gel 60 plates with a fluorescent indicator (254 nm) and was then visualized under UV light (Sigma-Aldrich, Poznan, Poland).

#### 3.2. Synthesis of Gramine Derivatives

A typical procedure for the synthesis of Compounds **2–9**

We used 2 mmol of the appropriate azole or benzazole (1,5-Dihydro-2*H*-imidazole-2-thione for **2** and **3**; imidazole-2-thione for **4**; 1-methyl-1*H*-imidazole-2-thione for **5**; 1,2-dihydro-2*H*-1,3-benzimidazole-2-thione for **6** and **7**; 3-methyl-1*H*-benzimidazole-2-thione for **8**; and 1,3-thiazolidine-2-thione for **9**). These were then diluted in 10 mL of EtOH and cooled to 0–5 °C. Then, a solution of NaOH (1.5 mmol) in 4 mL of H<sub>2</sub>O was added, and the mixture was stirred for 1 hour. After that, a solution of gramine (1 mmol) in 4 mL of EtOH was added, and the mixture was heated under reflux for 3–12 hours. The products obtained were filtered under a reduced pressure and washed with distilled water. Compounds **4**, **5**, and **9** were recrystallized from H<sub>2</sub>O (**4**) or toluene (**5**, **9**).

1-((1*H*-indol-3-yl)methyl)imidazolidine-2-thione (**2**)

White solid (99 mg, 43%); m.p 144–147 °C;  $^1\text{H}$  NMR (400 MHz, DMSO- $d_6$ ):  $\delta$  11.02 (s, 1H), 8.06 (s, 1H), 7.76 (d,  $J = 7.9$  Hz, 1H), 7.40–7.31 (m, 2H), 7.09 (ddd,  $J = 8.1, 6.9, 1.2$  Hz, 1H), 6.98 (ddd,  $J = 8.0, 7.0, 1.1$  Hz, 1H), 4.84 (s, 2H), 3.39 (ddd,  $J = 9.2, 6.8, 2.2$  Hz, 2H), and 3.37–3.27 (m, 2H);  $^{13}\text{C}$  NMR (101 MHz, DMSO- $d_6$ ):  $\delta$  181.83, 136.36, 126.62, 124.99, 121.28, 119.21, 118.68, 111.47, 109.71, 47.00, 41.35, and 40.58; IR (KBr,  $\text{cm}^{-1}$ )  $\nu_{\text{max}}$ : 3317, 3210, 2887, 1502, 1454, 1251, 1225, 1071, 753, 644, and 599; and EI-MS ( $m/z$ , % int.): 231 (34). Analysis

was calculated for  $C_{12}H_{13}N_3S$  (MW = 231.32) with the following: C, 62.31; H, 5.66; N, 18.17; and S, 13.86; and found: C, 62.02; H, 5.67; N, 18.12; and S, 13.54.

1,3-bis((1H-indol-3-yl)methyl)imidazolidine-2-thione (3)

White solid (14 mg, 6%); m.p 157–160 °C;  $^1H$  NMR (400 MHz, DMSO- $d_6$ ):  $\delta$  11.00 (d,  $J$  = 2.5 Hz, 2H), 7.78 (d,  $J$  = 7.9 Hz, 2H), 7.34 (dd,  $J$  = 5.4, 2.9 Hz, 4H), 7.07 (ddd,  $J$  = 8.1, 6.9, 1.2 Hz, 2H), 7.03–6.91 (m, 2H), 4.95 (s, 4H), and 3.22 (s, 4H);  $^{13}C$  NMR (101 MHz, DMSO- $d_6$ ): 180.49, 136.36, 126.59, 125.00, 121.24, 119.26, 118.69, 111.42, 109.65, 44.56, and 42.44; IR (KBr,  $cm^{-1}$ )  $\nu_{max}$ : 3397, 3057, 2910, 2881, 1502, 1455, 1328, 1254, 1094, 753, 635, and 593; and EI-MS ( $m/z$ , % int.): 360 (2). Analysis was calculated for  $C_{21}H_{20}N_4S$  (MW = 360.48) with the following: C, 69.97; H, 5.59; N, 15.54; and S, 8.89; and found: C, 69.23; H, 5.55; N, 15.91; and S, 9.01.

1-((1H-indol-3-yl)methyl)-1,3-dihydro-2H-imidazole-2-thione (4)

Light brown crystals (124 mg, 54%); m.p 206–209 °C;  $^1H$  NMR (400 MHz, DMSO- $d_6$ ):  $\delta$  12.07 (s, 1H), 11.09 (d,  $J$  = 7.9 Hz, 1H), 7.79–7.71 (m, 1H), 7.50 (dd,  $J$  = 6.0, 2.5 Hz, 1H), 7.37 (dt,  $J$  = 8.1, 0.9 Hz, 1H), 7.08 (dtd,  $J$  = 7.7, 6.7, 1.2 Hz, 1H), 6.96 (dddd,  $J$  = 9.1, 8.0, 7.0, 1.1 Hz, 1H), 6.93–6.80 (m, 2H), and 5.26 (s, 2H);  $^{13}C$  NMR (101 MHz, DMSO- $d_6$ ):  $\delta$  160.40, 136.19, 126.20, 125.45, 121.41, 118.99, 118.85, 117.80, 114.35, 111.52, 110.24, and 40.96; IR (KBr,  $cm^{-1}$ )  $\nu_{max}$ : 3221, 3116, 3029, 2916, 2713, 1551, 1470, 1263, 1138, 747, 616, and 576; and EI-MS ( $m/z$ , % int.): 229 (10). Analysis was calculated for  $C_{12}H_{11}N_3S$  (MW = 229.30) with the following: C, 62.86; H, 4.84; N, 13.33; and S, 13.98; and found: C, 63.32; H, 5.12; N, 17.43; and S, 13.21.

1-((1H-indol-3-yl)methyl)-3-methyl-1,3-dihydro-2H-imidazole-2-thione (5)

White crystals (159 mg, 65%); m.p 166–168 °C;  $^1H$  NMR (400 MHz, DMSO- $d_6$ ):  $\delta$  11.13–11.08 (m, 1H), 7.76–7.69 (m, 1H), 7.51 (d,  $J$  = 2.4 Hz, 1H), 7.37 (dt,  $J$  = 8.1, 0.9 Hz, 1H), 7.08 (ddd,  $J$  = 8.2, 7.0, 1.2 Hz, 1H), 7.04 (d,  $J$  = 2.4 Hz, 1H), 7.00–6.95 (m, 2H), 5.31–5.27 (m, 2H), and 3.48 (s, 3H);  $^{13}C$  NMR (101 MHz, DMSO- $d_6$ ):  $\delta$  161.12, 136.17, 126.18, 125.59, 121.41, 118.91, 118.88, 118.39, 116.61, 111.54, 109.98, 42.09, and 34.38; IR (KBr,  $cm^{-1}$ )  $\nu_{max}$ : 3427, 3212, 3162, 3132, 2914, 1554, 1459, 1223, 1139, 756, 664, and 599; and EI-MS ( $m/z$ , % int.): 245 (8). Analysis was calculated for  $C_{13}H_{15}N_3S$  (MW = 245.34) with the following: C, 63.64; H, 6.16; N, 17.13; and S, 13.07; and found: C, 64.30; H, 6.18; N, 17.32; and S, 13.25.

1-((1H-indol-3-yl)methyl)-1,3-dihydro-2H-benzo[d]imidazole-2-thione (6)

Beige crystals (142 mg, 51%); m.p 244–242 °C;  $^1H$  NMR (400 MHz, DMSO- $d_6$ ):  $\delta$  12.81 (s, 1H), 11.09 (d,  $J$  = 2.6 Hz, 1H), 7.95 (dd,  $J$  = 8.0, 1.1 Hz, 1H), 7.65 (d,  $J$  = 2.5 Hz, 1H), 7.46–7.37 (m, 1H), 7.33 (dt,  $J$  = 8.2, 1.0 Hz, 1H), 7.20–7.01 (m, 4H), 6.94 (ddd,  $J$  = 8.0, 7.0, 1.1 Hz, 1H), and 5.66 (s, 2H);  $^{13}C$  NMR (101 MHz, DMSO- $d_6$ ):  $\delta$  168.10, 136.21, 132.26, 130.79, 126.11, 125.79, 122.74, 121.95, 121.36, 119.37, 118.77, 111.52, 110.31, 109.58, and 109.37; IR (KBr,  $cm^{-1}$ )  $\nu_{max}$ : 3374, 3183, 3056, 1623, 1556, 1456, 1370, 1130, 737, 615, and 593; and EI-MS ( $m/z$ , % int.): 279 (39). Analysis was calculated for  $C_{16}H_{13}N_3S$  (MW = 279.36) with the following: C, 68.79; H, 4.69; N, 15.04; and S, 11.48; and found: C, 68.62; H, 4.32; N, 15.91; and S, 10.57.

1,3-bis((1H-indol-3-yl)methyl)-1,3-dihydro-2H-benzo[d]imidazole-2-thione (7)

White crystals (53 mg, 13%); m.p 232–235 °C;  $^1H$  NMR (400 MHz, DMSO- $d_6$ ):  $\delta$  11.10–11.05 (m, 2H), 7.98 (d,  $J$  = 8.0 Hz, 2H), 7.66 (d,  $J$  = 2.5 Hz, 2H), 7.43 (dq,  $J$  = 7.0, 4.0 Hz, 2H), 7.30 (d,  $J$  = 8.2 Hz, 2H), 7.04 (ddd,  $J$  = 11.2, 7.0, 2.3 Hz, 4H), 6.92 (ddd,  $J$  = 8.0, 7.0, 1.0 Hz, 2H), and 5.80 (s, 4H);  $^{13}C$  NMR (101 MHz, DMSO- $d_6$ ):  $\delta$  168.43, 136.24, 131.39, 126.02, 125.79, 122.36, 121.35, 119.51, 118.81, 111.46, 110.33, 109.38, and 40.66; IR (KBr,  $cm^{-1}$ )  $\nu_{max}$ : 3569, 3409, 2972, 2931, 1647, 1556, 1409, 1370, 1046, 777, 622, and 582; and EI-MS ( $m/z$ , % int.): 408 (4). Analysis was calculated for  $C_{25}H_{20}N_4S$  (MW = 408.52) with the following: C, 73.50; H, 4.93; N, 13.71; and S, 7.85; and found: C, 73.90; H, 4.34; N, 13.55; and S, 7.64.

1-((1H-indol-3-yl)methyl)-3-methyl-1,3-dihydro-2H-benzo[d]imidazole-2-thione (8)

Beige crystals (132 mg, 50%); m.p 180–182 °C;  $^1H$  NMR (400 MHz, DMSO- $d_6$ ):  $\delta$  11.12–11.07 (m, 1H), 7.92 (ddt,  $J$  = 7.9, 1.4, 0.7 Hz, 1H), 7.65 (d,  $J$  = 2.5 Hz, 1H), 7.54–7.47 (m, 1H), 7.43–7.37 (m, 1H), 7.33 (dt,  $J$  = 8.2, 0.9 Hz, 1H), 7.17 (pd,  $J$  = 7.4, 1.4 Hz, 2H), 7.05 (ddd,  $J$  = 8.2, 7.0, 1.2 Hz, 1H), 6.94 (ddd,  $J$  = 8.0, 7.0, 1.1 Hz, 1H), 5.75–5.68 (m, 2H), and 3.75 (s, 3H);  $^{13}C$  NMR (101 MHz, DMSO- $d_6$ ):  $\delta$  168.83, 136.17, 132.15, 131.18, 126.10, 125.83,

122.65, 122.52, 121.35, 119.34, 118.79, 111.51, 110.22, 109.45, 109.34, 40.29, and 31.16; IR (KBr): IR (KBr,  $\text{cm}^{-1}$ )  $\nu_{\text{max}}$ : 3454, 3228, 3062, 2930, 1549, 1486, 1408, 1338, 1129, 741, 623, and 598; and EI-MS ( $m/z$ , % int.): 293 (50). Analysis was calculated for  $\text{C}_{17}\text{H}_{15}\text{N}_3\text{S}$  (MW = 293.39) with the following: C, 69.60; H, 5.15; N, 14.32; and S, 10.93; and found: C, 69.43; H, 5.16; N, 14.28; and S, 11.13.

#### 3-((1H-indol-3-yl)methyl)thiazolidine-2-thione (9)

White solid (112 mg, 45%); m.p > 360 °C;  $^1\text{H}$  NMR (400 MHz,  $\text{DMSO-}d_6$ ):  $\delta$  11.16 (s, 1H), 7.69 (dt,  $J = 7.9, 1.0$  Hz, 1H), 7.46 (s, 1H), 7.39 (dt,  $J = 8.1, 1.0$  Hz, 1H), 7.11 (ddd,  $J = 8.2, 7.0, 1.2$  Hz, 1H), 7.01 (ddd,  $J = 8.0, 7.0, 1.1$  Hz, 1H), 5.07 (s, 2H), 3.93 (dd,  $J = 8.5, 7.5$  Hz, 2H), and 3.20 (dd,  $J = 8.6, 7.6$  Hz, 2H);  $^{13}\text{C}$  NMR (101 MHz,  $\text{DMSO-}d_6$ ):  $\delta$  194.00, 136.26, 126.32, 125.79, 121.49, 119.04, 118.90, 111.66, 108.45, 55.71, 43.73, and 26.33; IR (KBr,  $\text{cm}^{-1}$ )  $\nu_{\text{max}}$ : 3257, 3113, 3040, 2918, 1550, 1490, 1429, 1313, 1216, 1125, 758, 679, 645, and 591; and EI-MS ( $m/z$ , % int.): 248 (36). Analysis was calculated for  $\text{C}_{12}\text{H}_{12}\text{N}_2\text{S}_2$  (MW = 248.36) with the following: C, 58.03; H, 4.87; N, 11.28; S, and 25.82; and found: C, 57.72; H, 4.76; N, 11.67; and S, 25.72.

#### A typical procedure for the synthesis of Compounds 10–13

The gramine solution (1 mmol) and the corresponding substrate (1,3-thiazolidine-2-thione for **10**; 5-methyl-3H-1,3-benzoxazole-2-thione for **11**; and 1,2-dihydro-1,2,4-triazole-3-thione for **12** and **13**) (1 mmol) were heated under reflux for 5–10 hours in 8–10 mL of EtOH. Compounds **10** and **11** were crystallized, while **12** and **13** required purification through column chromatography (using  $\text{CHCl}_3$ ).

#### 3-((1H-indol-3-yl)methyl)thiazole-2(3H)-thione (10)

Brown crystals (91 mg, 37%); m.p 149–151 °C;  $^1\text{H}$  NMR (400 MHz,  $\text{DMSO-}d_6$ ):  $\delta$  11.20 (s, 1H), 7.72 (dt,  $J = 7.9, 1.0$  Hz, 1H), 7.57 (d,  $J = 2.6$  Hz, 1H), 7.46 (d,  $J = 4.6$  Hz, 1H), 7.39 (dt,  $J = 8.1, 0.9$  Hz, 1H), 7.11 (ddd,  $J = 8.2, 7.0, 1.2$  Hz, 1H), 7.01 (ddd,  $J = 8.1, 7.0, 1.1$  Hz, 1H), 6.94 (d,  $J = 4.6$  Hz, 1H), and 5.48 (s, 2H);  $^{13}\text{C}$  NMR (101 MHz,  $\text{DMSO-}d_6$ ):  $\delta$  185.59, 136.15, 132.55, 126.18, 126.00, 121.57, 119.14, 118.69, 111.68, 111.53, 109.14, and 44.06; IR (KBr,  $\text{cm}^{-1}$ )  $\nu_{\text{max}}$ : 3260, 3132, 3103, 3058, 2917, 1543, 1456, 1258, 1193, 1128, 1042, 746, 631, and 580; and EI-MS ( $m/z$ , % int.): 246 (25). Analysis was calculated for  $\text{C}_{12}\text{H}_{10}\text{N}_2\text{S}_2$  (MW = 246.35): C, 58.51; H, 4.09; N, 11.37; and S, 26.03; and found: C, 58.69; H, 3.56; N, 11.46; and S, 26.30.

#### 3-((1H-indol-3-yl)methyl)-5-methylbenzo[d]oxazole-2(3H)-thione (11)

White crystals (227 mg, 77%); m.p 231–234 °C;  $^1\text{H}$  NMR (400 MHz,  $\text{DMSO-}d_6$ ):  $\delta$  11.22–11.16 (m, 1H), 7.85 (dq,  $J = 7.9, 0.9$  Hz, 1H), 7.75 (d,  $J = 2.6$  Hz, 1H), 7.43–7.31 (m, 3H), 7.12–7.04 (m, 2H), 6.99 (ddd,  $J = 8.0, 7.0, 1.1$  Hz, 1H), 5.61 (s, 2H), and 2.33 (s, 3H);  $^{13}\text{C}$  NMR (101 MHz,  $\text{DMSO-}d_6$ ):  $\delta$  179.16, 144.60, 136.24, 134.58, 131.16, 126.43, 125.91, 124.84, 121.53, 119.04, 118.99, 111.69, 111.33, 109.60, 107.56, 41.72, and 20.92; IR (KBr,  $\text{cm}^{-1}$ )  $\nu_{\text{max}}$ : 3316, 3057, 2926, 1556, 1407, 1357, 1219, 1131, 796, 620, and 597; and EI-MS ( $m/z$ , % int.): 294 (15). Analysis was calculated for  $\text{C}_{17}\text{H}_{14}\text{N}_2\text{OS}$  (MW = 294.37) with the following: C, 69.36; H, 4.79; N, 9.52; and S, 10.89; and found: C, 69.14; H, 4.46; N, 9.50; and S, 10.96.

#### 1-((1H-indol-3-yl)methyl)-1,2-dihydro-3H-1,2,4-triazole-3-thione (12)

Colorless oil (60 mg, 26%);  $^1\text{H}$  NMR (400 MHz,  $\text{DMSO-}d_6$ ):  $\delta$  12.13–11.70 (s, 1H), 11.18 (s, 1H), 8.37 (s, 1H), 7.76–7.71 (m, 1H), 7.54 (d,  $J = 2.6$  Hz, 1H), 7.39 (dt,  $J = 8.1, 0.9$  Hz, 1H), 7.14–7.08 (m, 1H), 7.01 (ddd,  $J = 8.0, 7.0, 1.1$  Hz, 1H), and 5.28 (s, 2H);  $^{13}\text{C}$  NMR (101 MHz,  $\text{DMSO-}d_6$ ):  $\delta$  165.67, 141.83, 136.20, 125.91, 121.58, 119.11, 118.58, 111.71, and 109.00; IR (KBr,  $\text{cm}^{-1}$ )  $\nu_{\text{max}}$ : 3406, 3127, 3009, 2925, 1548, 1481, 1458, 1341, 1210, 1096, 745, 665, and 580; and EI-MS ( $m/z$ , % int.): 230 (25). Analysis was calculated for  $\text{C}_{11}\text{H}_{10}\text{N}_4\text{S}$  (MW = 230.29) with the following: C, 57.37; H, 4.38; N, 24.33; and S, 13.92; and found: C, 57.39; H, 4.65; N, 24.42; and S, 13.72.

#### 1,2-bis((1H-indol-3-yl)methyl)-1,2-dihydro-3H-1,2,4-triazole-3-thione (13)

Brown oil (36 mg, 10%);  $^1\text{H}$  NMR (400 MHz,  $\text{DMSO-}d_6$ ):  $\delta$  11.15 (s, 1H), 11.08–11.04 (m, 1H), 8.36 (s, 1H), 7.75 (dt,  $J = 7.9, 0.9$  Hz, 1H), 7.71 (dq,  $J = 8.0, 0.8$  Hz, 1H), 7.51 (d,  $J = 2.5$  Hz, 1H), 7.43 (d,  $J = 2.5$  Hz, 1H), 7.36 (dt,  $J = 8.1, 0.9$  Hz, 1H), 7.33 (dt,  $J = 8.2, 0.9$  Hz, 1H), 7.07 (dddd,  $J = 15.1, 8.2, 7.0, 1.2$  Hz, 2H), 6.96 (dddd,  $J = 14.8, 7.9, 7.0, 1.0$  Hz, 2H), 5.46 (s, 2H), and 5.32 (s, 2H);  $^{13}\text{C}$  NMR (101 MHz,  $\text{DMSO-}d_6$ ):  $\delta$  164.36, 140.51, 136.17, 136.08, 126.19,

125.88, 125.84, 125.53, 121.51, 121.29, 119.07, 119.00, 118.81, 118.54, 111.64, 111.46, 109.19, 108.79, 79.15, 43.90, and 40.55.; IR (KBr,  $\text{cm}^{-1}$ )  $\nu_{\text{max}}$ : 3412, 2925, 1636, 1537, 1457, 1421, 1342, 1208, 1093, 746, and 578; and EI-MS ( $m/z$ , % int.): 359 (4). Analysis was calculated for  $\text{C}_{20}\text{H}_{17}\text{N}_5\text{S}$  (MW = 359.45) with the following: C, 66.83; H, 4.77; N, 19.48; and S, 8.92; and found: C, 66.86; H, 4.53; N, 19.97; and S, 8.63.

#### Synthesis of (1-acetyl-1H-indol-3-yl)methyl pyrrolidine-1-carbodithioate (15)

N-acetyl-3-acetoxymethylindole (0.5 mmol) and sodium pyrrolidinedithiocarbamate (1 mmol) were dissolved in water (10 mL) and heated under reflux for 6 h. The resulting mixture was then extracted with diethyl ether, washed with water and brine, dried over anhydrous KOH, and then evaporated to give a brown oil.

Brown oil (248 mg, 78%);  $^1\text{H}$  NMR (400 MHz,  $\text{CDCl}_3$ ):  $\delta$  7.69 (dd,  $J = 7.9, 1.2$  Hz, 1H), 7.37–7.33 (m, 1H), 7.29 (d,  $J = 2.4$  Hz, 1H), 7.20 (ddd,  $J = 8.2, 7.0, 1.3$  Hz, 1H), 7.14 (ddd,  $J = 8.1, 7.0, 1.2$  Hz, 1H), 4.78 (s, 2H), 3.95 (t,  $J = 6.8$  Hz, 2H), 3.58 (t,  $J = 6.7$  Hz, 2H), 2.60 (s, 3H), 2.03–2.00 (m, 2H), and 1.95 (td,  $J = 6.9, 1.6$  Hz, 2H);  $^{13}\text{C}$  NMR (101 MHz,  $\text{CDCl}_3$ ):  $\delta$  192.97, 168.50, 136.10, 126.88, 125.48, 123.86, 122.33, 119.71, 119.03, 111.23, 54.71, 50.43, 32.80, 25.97, and 24.23; IR (KBr,  $\text{cm}^{-1}$ )  $\nu_{\text{max}}$ : 3405, 2969, 2869, 1702, 1329, 1160, 1006, 954, and 743; and EI-MS ( $m/z$ , % int.): 318 (6). Analysis was calculated for  $\text{C}_{16}\text{H}_{18}\text{N}_2\text{OS}_2$  (MW = 318.45) with the following: C, 60.35; H, 5.70; N, 8.80; and S, 20.13; and found: C, 61.01; H, 5.62; N, 8.72; and S, 20.42.

#### Synthesis of 3-(ethoxymethyl)-1H-indol-1-yl benzoate (17)

A mixture of benzoic acid (0.5 mmol),  $\text{PPh}_3$  (0.75 mmol), and NBS (0.75 mmol) in  $\text{CH}_2\text{Cl}_2$  (2 mL) was prepared. The solution was stirred at 0 °C for 15 minutes and then warmed to room temperature. Next, 3-ethoxymethylindole (0.55 mmol) and  $\text{Et}_3\text{N}$  (0.55 mmol) were added, and the reaction mixture was stirred for one hour. The mixture was then diluted with EtOAc and washed with  $\text{NaHCO}_3$ . The aqueous layer was extracted with EtOAc. The organic layers were combined, dried with anhydrous  $\text{Na}_2\text{SO}_4$ , and evaporated. The crude product obtained was purified by column chromatography ( $\text{CHCl}_3$ : EtOAc 5:1).

Yellow oil (37 mg, 32%);  $^1\text{H}$  NMR (400 MHz,  $\text{CDCl}_3$ ):  $\delta$  8.18–8.13 (m, 1H), 8.05 (d,  $J = 7.1$  Hz, 1H), 7.69–7.64 (m, 1H), 7.56–7.49 (m, 4H), 7.46–7.40 (m, 1H), 4.68 (s, 2H), 4.38 (q,  $J = 7.1$  Hz, 2H), and 1.39 (t,  $J = 7.1$  Hz, 3H);  $^{13}\text{C}$  NMR (101 MHz,  $\text{CDCl}_3$ ):  $\delta$  166.65, 162.35, 134.53, 132.79, 130.54, 129.50, 128.85, 128.79, 128.28, 121.21, 119.35, 117.48, 110.65, 60.94, and 14.30; FT-IR (KBr,  $\text{cm}^{-1}$ )  $\nu_{\text{max}}$ : 3057, 2924, 1783, 1715, and 1618; and EI-MS ( $m/z$ , % int.): 295 (100%). Analysis was calculated for  $\text{C}_{18}\text{H}_{17}\text{NO}_3$  (MW = 295.12) with the following: C, 73.20; H, 5.80; N, 4.74; and O, 16.25; and found: C, 73.41; H, 6.12; N, 4.53; and O, 15.94%.

#### A typical procedure for the synthesis of Compounds 18–27

Next, to 5 mL of anhydrous DMF, which was cooled to 0 °C, NaH (60%, 1 mmol) was added. The resulting mixture was stirred at 0 °C for 15 minutes. Then, 3-ethoxymethylindole (1 mmol) that was dissolved in 1 mL of anhydrous DMF was added, and the mixture was stirred for 30 minutes at 0 °C. Finally, an appropriate bromoester (methyl bromoacetate, ethyl bromoacetate, isopropyl bromoacetate, *tert*-butyl bromoacetate, ethyl 2-bromopropionate, ethyl 2-bromovalerate, phenyl bromoacetate, benzyl bromoacetate, methyl  $\alpha$ -bromophenyl acetate, and ethyl  $\alpha$ -bromophenyl acetate) (1 mmol) were added dropwise and stirred for 24 h at room temperature. The resulting mixture was then extracted with EtOAc, washed with water and brine, dried over anhydrous  $\text{Na}_2\text{SO}_4$ , and evaporated. The resulting crude product was purified using column chromatography with gradient elution, starting from PhMe: EtOAc 50:1.

#### Methyl 2-(3-(ethoxymethyl)-1H-indol-1-yl)acetate (18)

Yellow oil (94 mg, 38%);  $^1\text{H}$  NMR (400 MHz,  $\text{CDCl}_3$ ):  $\delta$  7.71 (dt,  $J = 7.8, 1.0$  Hz, 1H), 7.22 (d,  $J = 1.7$  Hz, 1H), 7.17–7.15 (m, 2H), 7.08 (s, 1H), 4.81 (s, 2H), 4.71 (d,  $J = 0.7$  Hz, 2H), 3.73 (s, 3H), 3.57 (q,  $J = 7.0$  Hz, 2H), 1.23 (t,  $J = 7.0$  Hz, 3H);  $^{13}\text{C}$  NMR (101 MHz,  $\text{CDCl}_3$ ):  $\delta$  168.95, 136.93, 127.77, 127.63, 122.36, 119.89, 119.63, 113.50, 108.89, 65.17, 64.38, 52.50, 47.55, 15.27; FT-IR (KBr,  $\text{cm}^{-1}$ )  $\nu_{\text{max}}$ : 3050, 2952, 2866, 1743, 1661, 1614; and EI-MS ( $m/z$ , % int.): 246 (15). Analysis was calculated for  $\text{C}_{14}\text{H}_{17}\text{NO}_3$  (MW = 247.12) with the following: C, 68.00; H, 6.93; N, 5.66; and O, 19.41; and found: C, 67.71; H, 7.43; N, 5.82; and O, 19.04%.



**Ethyl 2-(3-(ethoxymethyl)-1H-indol-1-yl)acetate (19)**

Yellow oil (144 mg, 55%);  $^1\text{H NMR}$  (400 MHz,  $\text{CDCl}_3$ ):  $\delta$  7.71 (d,  $J = 7.8$  Hz, 1H), 7.23 (dd,  $J = 2.5, 1.0$  Hz, 1H), 7.22 (d,  $J = 1.0$  Hz, 1H), 7.17–7.13 (m, 1H), 7.09 (s, 1H), 4.79 (s, 2H), 4.71 (s, 2H), 4.20 (q,  $J = 7.2$  Hz, 2H), 3.55 (t,  $J = 7.0$  Hz, 2H), and 1.27–1.21 (m, 6H);  $^{13}\text{C NMR}$  (101 MHz,  $\text{CDCl}_3$ ):  $\delta$  168.45, 136.97, 127.78, 127.71, 122.29, 119.83, 119.60, 113.39, 108.93, 65.10, 64.39, 61.63, 47.72, 15.27, and 14.09; FT-IR (KBr,  $\text{cm}^{-1}$ )  $\nu_{\text{max}}$ : 3053, 2978, 2932, 2867, 1750, and 1614; and EI-MS ( $m/z$ , % int.): 261 (20). Analysis was calculated for  $\text{C}_{15}\text{H}_{19}\text{NO}_3$  (MW = 261.14) with the following: C, 68.94; H, 7.33; N, 5.36; and O, 18.37; and found: C, 69.00; H, 7.15; N, 5.41; and O, 18.41%.

**Isopropyl 2-(3-(ethoxymethyl)-1H-indol-1-yl)acetate (20)**

Yellow oil (165 mg, 60%);  $^1\text{H NMR}$  (400 MHz,  $\text{CDCl}_3$ ):  $\delta$  7.71 (dt,  $J = 7.8, 1.0$  Hz, 1H), 7.23 (dd,  $J = 3.0, 1.0$  Hz, 1H), 7.22 (d,  $J = 1.0$  Hz, 1H), 7.17–7.13 (m, 1H), 7.09 (s, 1H), 5.06 (hept,  $J = 6.3$  Hz, 1H), 4.76 (s, 2H), 4.71 (d,  $J = 0.7$  Hz, 2H), 3.56 (q,  $J = 7.0$  Hz, 2H), and 1.24–1.21 (m, 9H);  $^{13}\text{C NMR}$  (101 MHz,  $\text{CDCl}_3$ ):  $\delta$  167.98, 137.00, 127.81, 122.25, 122.14, 119.80, 119.59, 113.30, 108.96, 69.49, 65.04, 64.39, 47.95, 21.69, and 15.28; FT-IR (KBr,  $\text{cm}^{-1}$ )  $\nu_{\text{max}}$ : 3056, 2979, 2933, 2859, 1737, and 1615; and EI-MS ( $m/z$ , % int.): 275 (12,5). Analysis was calculated for  $\text{C}_{16}\text{H}_{21}\text{NO}_3$  (MW = 275.15) with the following: C, 69.79; H, 7.69; N, 5.09; and O, 17.43; and found: C, 70.00; H, 7.51; N, 5.18; and O, 17.31%.

***Tert*-butyl 2-(3-(ethoxymethyl)-1H-indol-1-yl)acetate (21)**

Yellow oil (191 mg, 66%);  $^1\text{H NMR}$  (400 MHz,  $\text{CDCl}_3$ ):  $\delta$  7.71 (dt,  $J = 7.9, 1.0$  Hz, 1H), 7.23–7.22 (m, 2H), 7.16–7.12 (m, 1H), 7.09 (t,  $J = 0.8$  Hz, 1H), 4.71 (d,  $J = 0.7$  Hz, 2H), 4.70 (s, 2H), 3.55 (q,  $J = 7.0$  Hz, 2H), 1.48 (s, 1H), 1.44 (s, 9H), and 1.22 (t,  $J = 7.0$  Hz, 3H);  $^{13}\text{C NMR}$  (101 MHz,  $\text{CDCl}_3$ ):  $\delta$  167.59, 137.00, 127.86, 127.81, 122.19, 119.73, 119.57, 113.16, 108.97, 82.51, 64.99, 64.40, 48.50, 27.95, and 15.28; FT-IR (KBr,  $\text{cm}^{-1}$ )  $\nu_{\text{max}}$ : 3054, 2979, 2933, 2873, 1745, and 1614; and EI-MS ( $m/z$ , % int.): 289 (23). Analysis was calculated for  $\text{C}_{17}\text{H}_{23}\text{NO}_3$  (MW = 289.17) with the following: C, 70.56; H, 8.01; N, 4.84; and O, 16.59; and found: C, 70.73; H, 7.94; N, 5.03; and O, 16.30%.

**Ethyl 2-(3-(ethoxymethyl)-1H-indol-1-yl)propanoate (22)**

Yellow oil (157 mg, 57%);  $^1\text{H NMR}$  (400 MHz,  $\text{CDCl}_3$ ):  $\delta$  7.71 (d,  $J = 8.3$  Hz, 1H), 7.31–7.27 (m, 2H), 7.24–7.20 (m, 1H), 7.16–7.13 (m, 1H), 5.10 (q,  $J = 7.3$  Hz, 1H), 4.71 (s, 2H), 4.15 (qd,  $J = 7.1, 1.0$  Hz, 2H), 3.57 (q,  $J = 7.0$  Hz, 2H), 1.79 (d,  $J = 7.3$  Hz, 3H), and 1.22 (dt,  $J = 13.2, 7.1$  Hz, 6H);  $^{13}\text{C NMR}$  (101 MHz,  $\text{CDCl}_3$ ):  $\delta$  171.21, 136.62, 127.81, 124.45, 122.05, 119.84, 119.58, 113.26, 109.15, 65.16, 64.58, 61.57, 53.50, 17.56, 15.28, and 14.04; FT-IR (KBr,  $\text{cm}^{-1}$ )  $\nu_{\text{max}}$ : 3051, 2977, 2936, 2860, 1739, and 1614; and EI-MS ( $m/z$ , % int.): 275 (50). Analysis was calculated for  $\text{C}_{16}\text{H}_{21}\text{NO}_3$  (MW = 275.15) with the following: C, 69.79; H, 7.69; N, 5.09; O, and 17.43; and found: C, 69.76; H, 7.99; N, 4.92; and O, 17.33%.

**Ethyl 2-(3-(ethoxymethyl)-1H-indol-1-yl)pentanoate (23)**

Yellow oil (222 mg, 73%);  $^1\text{H NMR}$  (400 MHz,  $\text{CDCl}_3$ ):  $\delta$  7.71 (d,  $J = 7.9$  Hz, 1H), 7.33 (d,  $J = 8.3$  Hz, 1H), 7.29 (s, 1H), 7.24–7.20 (m, 1H), 7.16–7.12 (m, 1H), 4.96 (dd,  $J = 9.3, 6.2$  Hz, 1H), 4.72 (d,  $J = 0.7$  Hz, 2H), 4.15 (qd,  $J = 7.1, 2.9$  Hz, 2H), 3.56 (q,  $J = 7.0$  Hz, 2H), 1.30 (t,  $J = 7.1$  Hz, 3H), 1.25–1.20 (m, 6H), and 0.97–0.91 (m, 4H);  $^{13}\text{C NMR}$  (101 MHz,  $\text{CDCl}_3$ ):  $\delta$  170.91, 137.01, 127.68, 124.81, 122.00, 119.77, 119.55, 113.30, 109.13, 65.07, 64.62, 61.46, 57.82, 34.04, 19.24, 15.28, 14.07, and 13.52; FT-IR (KBr,  $\text{cm}^{-1}$ )  $\nu_{\text{max}}$ : 3051, 2964, 2932, 2873, 1740, and 1614; and EI-MS ( $m/z$ , % int.): 303 (45). Analysis was calculated for  $\text{C}_{18}\text{H}_{25}\text{NO}_3$  (MW = 303.18) with the following: C, 71.26; H, 8.31; N, 4.62; and O, 15.82; and found: C, 70.98; H, 8.42; N, 4.60; and O, 16.00%.

**Phenyl 2-(3-(ethoxymethyl)-1H-indol-1-yl)acetate (24)**

Yellow oil (114 mg, 37%);  $^1\text{H NMR}$  (400 MHz,  $\text{CDCl}_3$ ):  $\delta$  8.44 (d,  $J = 8.1$  Hz, 1H), 7.63 (d,  $J = 7.0$  Hz, 1H), 7.54 (s, 1H), 7.40–7.36 (m, 1H), 7.34–7.29 (m, 3H), 7.03–6.99 (m, 3H), 5.15 (s, 2H), 4.66 (d,  $J = 1.1$  Hz, 2H), 3.61 (q,  $J = 7.0$  Hz, 2H), and 1.27 (t,  $J = 7.0$  Hz, 3H);  $^{13}\text{C NMR}$  (101 MHz,  $\text{CDCl}_3$ ):  $\delta$  166.17, 157.54, 136.18, 129.70, 129.25, 125.75, 124.22, 122.11, 121.83, 121.20, 119.46, 116.67, 114.69, 67.78, 66.03, 64.33, and 15.21; FT-IR (KBr,  $\text{cm}^{-1}$ )  $\nu_{\text{max}}$ : 3119, 3059, 2969, 2940, 2842, 1707, and 1600; and EI-MS ( $m/z$ , % int.): 309 (35). Analysis was

calculated for  $C_{19}H_{19}NO_3$  (MW = 309.14) with the following: C, 73.77; H, 6.19; N, 4.53; and O, 15.52; and found: C, 73.80; H, 6.27; N, 4.49; and O, 15.43%.

**Benzyl 2-(3-(ethoxymethyl)-1H-indol-1-yl)acetate (25)**

Yellow oil (243 mg, 75%);  $^1H$  NMR (400 MHz,  $CDCl_3$ ):  $\delta$  7.71 (d,  $J$  = 7.8 Hz, 1H), 7.34–7.32 (m, 3H), 7.27 (d,  $J$  = 4.0 Hz, 2H), 7.21 (dd,  $J$  = 6.2, 1.3 Hz, 2H), 7.17–7.13 (m, 1H), 7.08 (s, 1H), 5.16 (s, 2H), 4.84 (s, 2H), 4.70 (d,  $J$  = 0.7 Hz, 2H), 3.55 (q,  $J$  = 7.0 Hz, 2H), and 1.22 (t,  $J$  = 7.0 Hz, 3H);  $^{13}C$  NMR (101 MHz,  $CDCl_3$ ):  $\delta$  168.31, 136.98, 135.02, 128.57, 128.48, 128.27, 127.83, 127.68, 122.36, 119.90, 119.65, 113.55, 108.96, 67.23, 65.07, 64.37, 47.71, and 15.27; FT-IR (KBr,  $cm^{-1}$ )  $\nu_{max}$ : 3033, 2974, 2874, 2840, 1747, and 1683; and EI-MS ( $m/z$ , % int.): 323 (23). Analysis was calculated for  $C_{20}H_{21}NO_3$  (MW = 323.15) with the following: C, 74.28; H, 6.55; N, 4.33; and O, 14.84; and found: C, 74.27; H, 6.74; N, 3.99; and O, 15.00%.

**Methyl 2-(3-(ethoxymethyl)-1H-indol-1-yl)-2-phenylacetate (26)**

Yellow oil (133 mg, 41%);  $^1H$  NMR (400 MHz,  $CDCl_3$ ):  $\delta$  7.72 (d,  $J$  = 7.3 Hz, 1H), 7.38 (d,  $J$  = 2.3 Hz, 3H), 7.19–7.17 (m, 3H), 7.16–7.13 (m, 1H), 7.10 (s, 1H), 7.10–7.08 (m, 1H), 4.65 (t,  $J$  = 0.7 Hz, 2H), 3.83 (s, 3H), 3.81 (s, 1H), 3.56–3.50 (m, 3H), and 1.20 (t,  $J$  = 7.0 Hz, 3H);  $^{13}C$  NMR (101 MHz,  $CDCl_3$ ):  $\delta$  170.01, 138.70, 129.63, 129.06, 128.98, 128.11, 127.92, 127.73, 125.94, 122.24, 120.15, 119.75, 113.32, 109.00, 65.14, 64.57, 61.85, 52.71, and 15.25; FT-IR (KBr,  $cm^{-1}$ )  $\nu_{max}$ : 3033, 2952, 2873, 1734, and 1612; and EI-MS ( $m/z$ , % int.): 323 (5). Analysis was calculated for  $C_{20}H_{21}NO_3$  (MW = 323.15) with the following: C, 74.28; H, 6.55; N, 4.33; and O, 14.84; and found: C, 74.22; H, 6.69; N, 4.12; and O, 14.97%.

**Ethyl 2-(3-(ethoxymethyl)-1H-indol-1-yl)-2-phenylacetate (27)**

Yellow oil (109 mg, 32%);  $^1H$  NMR (400 MHz,  $CDCl_3$ ):  $\delta$  7.72 (d,  $J$  = 7.8 Hz, 1H), 7.38–7.34 (m, 4H), 7.23–7.21 (m, 1H), 7.18–7.14 (m, 3H), 7.11 (d,  $J$  = 4.0 Hz, 1H), 6.19 (s, 1H), 4.66 (s, 2H), 4.31–4.26 (m, 2H), 3.53 (qd,  $J$  = 7.0, 0.9 Hz, 2H), 1.26 (t,  $J$  = 7.1 Hz, 4H), and 1.20 (t,  $J$  = 7.0 Hz, 3H);  $^{13}C$  NMR (101 MHz,  $CDCl_3$ ):  $\delta$  169.50, 137.03, 134.57, 129.68, 129.02, 128.09, 127.53, 126.04, 122.17, 120.10, 119.73, 113.20, 109.05, 65.07, 64.57, 61.94, 15.24, 14.07, and 13.97; FT-IR (KBr,  $cm^{-1}$ )  $\nu_{max}$ : 3058, 2978, 2935, 2864, 1745, and 1613; and EI-MS ( $m/z$ , % int.): 337 (40). Analysis was calculated for  $C_{21}H_{23}NO_3$  (MW = 337.17) with the following: C, 74.75; H, 6.87; N, 4.15; and O, 14.23; and found: C, 74.93; H, 6.59; N, 4.32; and O, 14.16%.

**Synthesis of (1-acetyl-1H-indol-3-yl)methyl 2,5-dihydroxybenzoate (29)**

***N*-acetyl-3-hydroxymethylindole**

(0.72 mmol) and 2,5-dihydroxybenzoic acid (0.72 mmol) were dissolved in THF (5 mL), then DCC (0.72 mmol) was added, and the mixture was then stirred for 48 hours at room temperature. The resulting white precipitate was filtered, and the filtrate was evaporated so as to obtain a dark brown precipitate. The precipitate was then dissolved in EtOAc, washed with 5% citric acid, saturated with  $NaHCO_3$  and brine, and then dried over anhydrous  $Na_2SO_4$  and evaporated. The crude product was purified by column chromatography (PhMe: EtOAc 5:1).

Orange oil (87 mg, 37%);  $^1H$  NMR (400 MHz,  $CDCl_3$ ):  $\delta$  8.41 (d,  $J$  = 8.4 Hz, 1H), 7.65 (d,  $J$  = 7.1 Hz, 1H), 7.54 (s, 1H), 7.39–7.27 (m, 3H), 7.18–7.16 (m, 2H), 5.50 (s, 2H), and 2.64 (s, 3H);  $^{13}C$  NMR (101 MHz,  $CDCl_3$ ):  $\delta$  169.60, 168.88, 155.71, 148.06, 135.84, 129.00, 128.19, 125.78, 125.26, 124.40, 124.05, 119.04, 118.48, 116.78, 114.60, 111.90, 58.72, and 23.92; FT-IR (KBr,  $cm^{-1}$ )  $\nu_{max}$ : 3215, 2931, 2854, 1733, 1686, and 1620; and EI-MS ( $m/z$ , % int.): 325 (10). Analysis was calculated for  $C_{18}H_{15}NO_5$  (MW = 325.10) with the following: C, 66.46; H, 4.65; N, 4.31; and O, 24.59; and found: C, 66.51; H, 9.58; N, 4.43; and O, 24.89%.

### 3.3. X-ray Analysis

Single-crystal X-ray diffraction measurements were carried out with the monochromated  $CuK\alpha$  radiation on a SuperNova diffractometer (**4**, **5**, **7**, **8**, **9**, and **11**), or with  $MoK\alpha$  radiation on an Xcalibur diffractometer (**2** and **10**). Each dataset was measured with an omega scan. These data were processed with the CrysAlisPro 1.171.42 software [76]. The crystal structures were solved by direct methods with SHELXT [77] and refined by full-matrix least-squares calculations on  $F^2$  with SHELXL [78]. All non-H atoms were refined with anisotropic displacement parameters. Hydrogen atoms bonded to C and N atoms

were placed at calculated positions based on the environment and perceived hybridization of the atoms to which they were bonded. For room temperature structures, the methyl, methylene, and aromatic C-H distances were standardized to 0.96, 0.97, and 0.93 Å, respectively, and the N-H distance was 0.86 Å. For low-temperature structures, the corresponding values were 0.98 and 0.99 and 0.95 Å and 0.88 Å. The solvent hydrogen atoms were located on difference Fourier maps, and their O-H distances were standardized to the values of 0.82 and 0.85 Å for the ethanol and water molecules, respectively. All H-atoms were refined as 'riding' on their carriers. During the refinement, isotropic displacement parameters for H-atoms were assigned as 20% higher than the isotropic equivalent for the atom to which the H-atom was bonded. The crystals of **8** were inversion-twinned with a ratio of 0.70(3):0.30(3). Moreover, in the crystal of **9**, there were signs of disorder in the thiazolidine moiety. We modeled this disorder by taking into account two alternative positions for one of the two methylene groups for which the component occupancy factors were refined to 0.62(3) and 0.38(3). MERCURY [79] was used to prepare drawings. CCDC contains the supplementary crystallographic data for **2** (Deposition Number 2346551), **4** (Deposition Number 2346552), **5** (Deposition Number 2346553), **7** (Deposition Number 2346554), **8** (Deposition Number 2346555), **9** (Deposition Number 2346556), **10** (Deposition Number 2346557), and **11** (Deposition Number 2346558). These data can be obtained free of charge via <http://www.ccdc.cam.ac.uk/conts/retrieving.html> (accessed on 8 April 2024) (or from the CCDC, 12 Union Road, Cambridge CB2 1EZ, UK; Fax: +44 1223 336033; email: deposit@ccdc.cam.ac.uk).

### 3.4. Biological Study

#### 3.4.1. Antibacterial and Antifungal Activity Measurements

The antibacterial properties of the compounds were determined against selected bacteria: *Micrococcus luteus*, *Bacillus subtilis*, *Escherichia coli*, and *Pseudomonas fluorescens*. The antifungal activity of the compounds was determined against *Alternaria alternata*, *Fusarium culmorum*, *Trichoderma harzianum*, *Trichoderma reesei*, and *Botrytis cinerea*. All the cultures of microorganisms were obtained from the pure culture collection of the Microbiology Department of the Faculty of Soil Science and Microbiology of the Poznan University of Life Sciences.

The well diffusion method was used to evaluate the antimicrobial properties of the compounds. A broth medium was used for the bacterial tests, while potato dextrose agar (PDA) was used for mold cultivation. Next, 6 mL of each liquidized medium was poured into sterile Petri dishes and allowed to solidify. After this, two 0.5 cm-diameter sterile glass rings were placed on the surface of each plate. Then, 20 mL of each liquid medium containing suspensions of the tested microorganisms was added. The final bacterial suspension had a density of 107 cells/cm<sup>3</sup>, which was obtained from 48-hour cultures on broth slants, and the fungal suspension had a density of 108 spores/cm<sup>3</sup>, which was obtained from 5-day cultures on PDA slants. After the medium solidified, the glass rings were removed with a pencil, leaving two wells on each plate. Then, 0.1 mL of the compound dissolved in pure dimethyl sulfoxide was added to one well, and 0.1 mL of pure dimethyl sulfoxide was added to the other well, which served as a control. Each compound was tested in four replicates. Plates were incubated in a thermostat at 27 °C for *M. luteus*, *B. subtilis*, and *P. fluorescens* cultures, as well as at 37 °C for the *E. coli* culture for 48 hours. All fungal cultures were incubated in a thermostat at 24 °C for five days. At the end of the incubation, the growth inhibition diameters of the tested strains were measured using calipers.

#### 3.4.2. Human Red Blood Cell (RBC) Preparation

Human RBC suspensions (~65% hematocrit) were purchased from the Blood Bank in Poznań according to the bilateral agreement between the Adam Mickiewicz University and Blood Bank no. ZP/2867/D/21 without any contact with blood donors. The RBCs were washed three times (960× g, 10 min, 4 °C) in 7.4 pH phosphate-buffered saline (PBS\_137 mM of NaCl, 2.7 mM of KCl, 10 mM of Na<sub>2</sub>HPO<sub>4</sub>, and 1.76 mM of KH<sub>2</sub>PO<sub>4</sub>), which was

supplemented with 10 mM of glucose. After washing, the RBCs were suspended in the PBS buffer at  $1.65 \times 10^9$  cells/mL, stored at 4 °C, and used within 5 h.

#### 3.4.3. Inhibition of Free Radical-Induced Hemolysis

The cytoprotective activity of the derivatives was evaluated in accordance with a previously described method [14–16]. Briefly, human RBCs ( $1.65 \times 10^8$  cells/mL, 1.5% hematocrit) were preincubated in PBS (pH 7.4) supplemented with 10 mM of glucose, which contained the tested compound or Trolox used as a standard antioxidant at a concentration of 0.01 mg/mL for 20 min at 37 °C in a shaking incubator. After preincubation, 2,2'-azobis(2-methylpropionamidine) dihydrochloride (AAPH) was added to a final concentration of 60 mM, and samples were incubated for the next four hours at 37 °C. RBCs incubated in PBS and in PBS with AAPH were used as negative and positive controls, respectively. After incubation, the RBC suspensions were centrifuged ( $960 \times g$ , 5 min, + 4 °C), and the degree of hemolysis was determined by measuring the absorbance (Ab) of the supernatant at  $\lambda = 540$  nm in a BioMate™ 160 UV–Vis spectrophotometer. The percentage of free radical-induced hemolysis inhibition was calculated using the following equation:

$$\text{inhibition of hemolysis (\%)} = 100 - [(\text{Ab}_{\text{comp}} / \text{Ab}_{\text{AAPH}}) \times 100],$$

where  $\text{Ab}_{\text{comp}}$  is the absorbance value of the supernatants obtained from samples incubated with a compound tested in the presence of AAPH and  $\text{Ab}_{\text{AAPH}}$  is the absorbance of the supernatant obtained from the positive control, respectively. Each sample was prepared in triplicate and results were expressed as the mean  $\pm$ SD value from three independent experiments ( $n = 6$ ), using RBCs obtained from different donors.

#### 3.4.4. Ferrous Ion ( $\text{Fe}^{2+}$ ) Chelating Assay

The ferrous ions' chelating activity of the derivatives was evaluated in accordance with a previously described method [15]. The  $\text{Fe}^{2+}$ -chelating ability of the tested compounds was determined by the absorbance of the ferrous-ion-ferrozine complex at 562 nm at room temperature ( $\sim 22$  °C, RT). Briefly, 0.1 mg/mL of the concentration of the tested compounds in 0.2 mL of ethyl alcohol was added to a solution of 0.6 mM of  $\text{FeCl}_2$  (0.05 mL). EDTA was used as the standard metal chelator. The reaction was started by adding 5 mM of ferrozine (0.05 mL) in ethyl alcohol and then immediately shaking vigorously. The samples were stored for 10 min at room temperature. After incubation, the absorbance (Ab) of the solutions was measured at 562 nm in a BioMate™ 160 UV–Vis spectrophotometer. The percentage of inhibition of the ferrozine– $\text{Fe}^{2+}$  complex formation was calculated using the following equation:

$$\text{Fe}^{2+} \text{ chelating (\%)} = [1 - (\text{Ab1} / \text{Ab0})] \times 100,$$

where Ab1 is the absorbance in the presence of the compound tested or EDTA and Ab0 is the absorbance of the sample without the tested compound. Each sample was made in triplicate and three independent experiments were performed ( $n = 9$ ).

#### 3.4.5. Hemolysis Assay under Physiological Condition

The hemolytic activity was evaluated according to the previously described method [14–16]. Briefly, RBCs ( $1.65 \times 10^8$  cells/mL, 1.5% hematocrit) were incubated in a PBS (pH = 7.4) supplemented with 10 mM of glucose (Sigma Aldrich, Steinheim, Germany) and containing the tested compound at the concentration of 0.1 mg/mL for 60 min at 37 °C in a thermo shaker (BioSan Thermo-Shaker TS-100C, Biosan, Riga, Latvia). The negative control sample was a solution with RBCs incubated in PBS without the addition of the tested compounds. The positive control sample was a solution of the RBCs incubated in deionized water without the addition of the tested compounds. Each sample was prepared in triplicate, and the experiments were repeated three times with RBCs from different donors. After incubation, the RBC suspensions were centrifuged (Sigma

3–30 K Sartorius AG, Göttingen, Germany) ( $960 \times g$ , 10 min, 4 °C), and the degree of hemolysis was estimated by measuring the absorbance of the supernatant on a BioMate™ 160 UV-Vis spectrophotometer (Thermo Scientific, Waltham, MA, USA) at 540 nm. The results were expressed as the percentage (%) of hemolysis, which was calculated using the following formula:

$$\text{hemolysis (\%)} = (\text{sample Ab/positive control Ab}) \times 100,$$

where sample Ab is the absorbance value of the supernatant of RBCs incubated with the tested compounds and the negative control, and the positive control AB is an absorbance value of the supernatant of RBCs incubated in ice-cold deionized water. Each sample was prepared in triplicate, and the results are presented as a mean value ( $\pm$ SD) of the three independent experiments ( $n = 9$ ).

### 3.4.6. Statistical Analysis

For the antioxidant and cytoprotective properties, data were plotted as the mean value  $\pm$  standard deviation (SD) of the results of three independent experiments, with every sample taken in triplicate ( $n = 9$ ). A paired t-Student test was used to, respectively, compare the derivatives' activity with the activity of the standard Trolox or EDTA. Statistical significance was defined as  $p < 0.05$ . Inactive compounds were indicated as n.a. Non statistically significant difference is indicated as n.s.

### 3.5. In Silico Study

The physicochemical calculations were conducted using the SwissADME website: [www.swissadme.ch](http://www.swissadme.ch) (accessed on 2 February 2024).

### 3.6. Molecular Docking

The molecular docking process commenced by converting the SMILES representation of indole-based chemical structures into 3D structures, and this was accomplished through the application of OpenBabel tool version 3.1.1 [80,81]. Subsequently, the protein domains corresponding to PDB [82], IDs 1DNU [83], 1N5X [84], and 4COX [85] were prepared in accordance with the standard AutoDock tool 1.5.7 scheme [86]. Molecular dockings were then carried out using AutoDock Vina [87], with the specific parameters outlined in Table 5 for each docking search.

**Table 5.** The search spaces of the analyzed binding sites of the protein domains.

PDB ID	Search Space Center (x, y, z)	Size of the Search Space (x, y, z)
1DNU	39.637, −38.454, −5.011	24, 24, 26
1N5X	96.559, 55.159, 39.980	24, 22, 40
4COX	23.941, 21.867, 13.892	26, 26, 32

## 4. Conclusions

The newly synthesized indole derivatives with methylene-bridgedazole and benzazole substituents at C3 are compounds with a strong cytoprotective activity under oxidative stress conditions. The exceptions are derivatives appearing as zwitterions at a physiological pH, which occurred because of their ability to convert to harmful thiyl radicals. Of the two possible tautomeric forms, the molecules in crystals and those in a DMSO- $d_6$  solution appeared as the thione tautomers. The C=S group was found to be the primary site for H-bonding in the condensed media: it has the ability to form multicenter hydrogen bonds with N-H and C-H donors.

Compared to imidazoles and oxazoles, thiazoles are more prone toward conformational changes driven by hydrogen bond association. The steric effects witnessed in the

crystals of 7 and 8 (which are also supposedly present in Compounds 3 and 13) accounted for their high hemolytic activity.

Since the majority of the indole derivatives substituted solely at the C3 position are hemocompatible, and as all of them adhere to the Lipinski and Veber rules, they represent promising candidates for future research on designing new bioactive compounds and drugs. The results presented in this study may facilitate the development of novel indole-based molecules with antioxidant and cytoprotective activities.

**Supplementary Materials:** The following supporting information can be downloaded at: <https://www.mdpi.com/article/10.3390/ijms25105364/s1>.

**Author Contributions:** Conceptualization, B.J. and L.M.; methodology, B.J., L.M., B.W., D.N. and J.S.; software, D.N.; validation, B.W., U.R. and D.N.; formal analysis, D.N.; investigation, B.J.; resources, B.J.; data curation, B.W. and D.N.; writing—original draft preparation, K.B., N.B. and D.N.; writing—review and editing, B.J., L.M. and U.R.; visualization, B.W., K.B., N.B. and D.N.; supervision, B.J.; project administration, K.B. and N.B.; funding acquisition, B.J., L.M., K.B. and N.B. All authors have read and agreed to the published version of the manuscript.

**Funding:** This work was financially supported by ID-UB 054 grants: 054/12/SNŚ.0011 (KB) and 054/13/SNŚ/0008 (NB).

**Institutional Review Board Statement:** Not applicable.

**Informed Consent Statement:** Not applicable.

**Data Availability Statement:** Data are contained within the article and Supplementary Materials.

**Conflicts of Interest:** The authors declare no conflicts of interest.

## References

1. Gryniewicz, G.; Gadzikowska, M. Tropane Alkaloids as Medicinally Useful Natural Products and Their Synthetic Derivatives as New Drugs. *Pharmacol. Rep.* **2008**, *60*, 439–463. [PubMed]
2. Ehrenworth, A.M.; Peralta-Yahya, P. Accelerating the Semisynthesis of Alkaloid-Based Drugs through Metabolic Engineering. *Nat. Chem. Biol.* **2017**, *13*, 249–258. [CrossRef]
3. Olofinson, K.; Abrahamse, H.; George, B.P. Therapeutic Role of Alkaloids and Alkaloid Derivatives in Cancer Management. *Molecules* **2023**, *28*, 5578. [CrossRef] [PubMed]
4. Kittakoop, P.; Mahidol, C.; Ruchirawat, S. Alkaloids as Important Scaffolds in Therapeutic Drugs for the Treatments of Cancer, Tuberculosis, and Smoking Cessation. *Curr. Top. Med. Chem.* **2014**, *14*, 239–252. [CrossRef]
5. Kumari, A.; Singh, R.K. Medicinal Chemistry of Indole Derivatives: Current to Future Therapeutic Prospectives. *Biol. Chem.* **2019**, *89*, 103021. [CrossRef] [PubMed]
6. Jagadeesan, S.; Karpagam, S. Novel Series of *N*-Acyl Substituted Indole Based Piperazine, Thiazole and Tetrazoles as Potential Antibacterial, Antifungal, Antioxidant and Cytotoxic Agents, and Their Docking Investigation as Potential Mcl-1 Inhibitors. *J. Mol. Struct.* **2023**, *1271*, 134013. [CrossRef]
7. Iacopetta, D.; Catalano, A.; Ceramella, J.; Barbarossa, A.; Carocci, A.; Fazio, A.; La Torre, C.; Caruso, A.; Ponassi, M.; Rosano, C.; et al. Synthesis, Anticancer and Antioxidant Properties of New Indole and Pyranoindole Derivatives. *Bioorg. Chem.* **2020**, *105*, 104440. [CrossRef] [PubMed]
8. Kerzarea, D.R.; Khedekar, P.B. Indole Derivatives Acting on Central Nervous System—Review. *J. Pharm. Sci. Biosci. Rev.* **2016**, *6*, 144–156.
9. Singh, T.P.; Singh, O.M. Recent Progress in Biological Activities of Indole and Indole Alkaloids. *Mini Rev. Med. Chem.* **2018**, *18*, 9–25. [CrossRef]
10. Jastrzębski, M.K.; Kaczor, A.A.; Wróbel, T.M. Methods of Lysergic Acid Synthesis—The Key Ergot Alkaloid. *Molecules* **2022**, *27*, 7322. [CrossRef]
11. Wei, Y.; Shi, L.; Wang, K.; Liu, M.; Yang, Q.; Yang, Z.; Ke, S. Discovery of Gramine Derivatives That Inhibit the Early Stage of EV71 Replication in Vitro. *Molecules* **2014**, *19*, 8949–8964. [CrossRef] [PubMed]
12. Zhang, J.; Jia, Q.; Li, N.; Gu, L.; Dan, W.; Dai, J. Recent Developments of Gramine: Chemistry and Biological Activity. *Molecules* **2023**, *28*, 5695. [CrossRef] [PubMed]
13. Zhang, X.-H.; Guo, Q.; Wang, H.-Y.; Li, Y.-H.; Khamis, M.Y.; Ma, L.-Y.; Wang, B.; Liu, H.-M. Gramine-Based Structure Optimization to Enhance Anti-Gastric Cancer Activity. *Biol. Chem.* **2021**, *107*, 104549. [CrossRef] [PubMed]
14. Kozanecka-Okupnik, W.; Sierakowska, A.; Berdzik, N.; Kowalczyk, I.; Mrówczyńska, L.; Jasiewicz, B. New Triazole-Bearing Gramine Derivatives—Synthesis, Structural Analysis and Protective Effect against Oxidative Haemolysis. *Nat. Prod. Res.* **2022**, *36*, 3413–3419. [CrossRef] [PubMed]

15. Jasiewicz, B.; Kozanecka-Okupnik, W.; Przygodzki, M.; Warżajtis, B.; Rychlewska, U.; Pospieszny, T.; Mrówczyńska, L. Synthesis, Antioxidant and Cytoprotective Activity Evaluation of C-3 Substituted Indole Derivatives. *Sci. Rep.* **2021**, *11*, 15425. [[CrossRef](#)] [[PubMed](#)]
16. Jasiewicz, B.; Babijczuk, K.; Warżajtis, B.; Rychlewska, U.; Starzyk, J.; Cofta, G.; Mrówczyńska, L. Indole Derivatives Bearing Imidazole, Benzothiazole-2-Thione or Benzoxazole-2-Thione Moieties—Synthesis, Structure and Evaluation of Their Cytoprotective, Antioxidant, Antibacterial and Fungicidal Activities. *Molecules* **2023**, *28*, 708. [[CrossRef](#)]
17. Fujita, H.; Nishikawa, R.; Sasamoto, O.; Kitamura, M.; Kunishima, M. Substitution of the Dimethylamino Group in Gramines and One-Pot Cyclization to Tetrahydro- $\beta$ -Carbolines Using a Triazine-Based Activating Agent. *J. Org. Chem.* **2019**, *84*, 8380–8391. [[CrossRef](#)]
18. Ibrahim, M. Synthesis and Chemistry of 4-Amino-1,2,4-Triazin-5-Ones. *Heterocycles* **2010**, *81*, 1393–1418. [[CrossRef](#)]
19. Bajad, N.G.; Singh, S.K.; Singh, S.K.; Singh, T.D.; Singh, M. Indole: A Promising Scaffold for the Discovery and Development of Potential Anti-Tubercular Agents. *Curr. Res. Pharmacol. Drug Discov.* **2022**, *3*, 100119. [[CrossRef](#)]
20. Ramesh, D.; Joji, A.; Vijayakumar, B.G.; Sethumadhavan, A.; Mani, M.; Kannan, T. Indole Chalcones: Design, Synthesis, in Vitro and in Silico Evaluation against Mycobacterium Tuberculosis. *Eur. J. Med. Chem.* **2020**, *198*, 112358. [[CrossRef](#)]
21. Singh, P.; Kaur, S.; Sharma, A.; Kaur, G.; Bhatti, R. TNF- $\alpha$  and IL-6 Inhibitors: Conjugates of N-Substituted Indole and Aminophenylmorpholin-3-One as Anti-Inflammatory Agents. *Eur. J. Med. Chem.* **2017**, *140*, 92–103. [[CrossRef](#)] [[PubMed](#)]
22. Tiwari, S.; Kirar, S.; Banerjee, U.C.; Neerupudi, K.B.; Singh, S.; Wani, A.A.; Bharatam, P.V.; Singh, I.P. Synthesis of N-Substituted Indole Derivatives as Potential Antimicrobial and Antileishmanial Agents. *Biol. Chem.* **2020**, *99*, 103787. [[CrossRef](#)] [[PubMed](#)]
23. MahamadAlli Shaikh, T.; Debebe, H. Synthesis and Evaluation of Antimicrobial Activities of Novel N-Substituted Indole Derivatives. *J. Chem.* **2020**, *2020*, e4358453. [[CrossRef](#)]
24. Sumiya, T.; Ishigaki, M.; Oh, K. Synthesis of Imidazole and Indole Hybrid Molecules and Antifungal Activity against Rice Blast. *IJCEA* **2017**, *8*, 233–236. [[CrossRef](#)]
25. Colorado-Peralta, R.; Olivares-Romero, J.L.; Rosete-Luna, S.; García-Barradas, O.; Reyes-Márquez, V.; Hernández-Romero, D.; Morales-Morales, D. Copper-Coordinated Thiazoles and Benzothiazoles: A Perfect Alliance in the Search for Compounds with Antibacterial and Antifungal Activity. *Inorganics* **2023**, *11*, 185. [[CrossRef](#)]
26. Kumar Bhaumik, P.; Ghosh, K.; Chattopadhyay, S. Synthetic Strategies, Crystal Structures and Biological Activities of Metal Complexes with the Members of Azole Family: A Review. *Polyhedron* **2021**, *200*, 115093. [[CrossRef](#)]
27. Emami, L.; Faghih, Z.; Ataollahi, E.; Sadeghian, S.; Rezaei, Z.; Khabnadideh, S. Azole Derivatives: Recent Advances as Potent Antibacterial and Antifungal Agents. *Curr. Med. Chem.* **2023**, *30*, 220–249. [[CrossRef](#)] [[PubMed](#)]
28. Devasia, J.; Nizam, A.; Vasantha, V.L. Azole-Based Antibacterial Agents: A Review on Multistep Synthesis Strategies and Biology. *Polycycl. Aromat. Comp.* **2021**, *42*, 5474–5495. [[CrossRef](#)]
29. Aatif, M.; Raza, M.A.; Javed, K.; Nashre-ul-Islam, S.M.; Farhan, M.; Alam, M.W. Potential Nitrogen-Based Heterocyclic Compounds for Treating Infectious Diseases: A Literature Review. *Antibiotics* **2022**, *11*, 1750. [[CrossRef](#)]
30. Wadhwa, R.; Aggarwal, T.; Thapliyal, N.; Kumar, A.; Priya, Yadav, P.; Kumari, V.; Reddy, B.S.C.; Chandra, P.; Maurya, P.K. Red Blood Cells as an Efficient in Vitro Model for Evaluating the Efficacy of Metallic Nanoparticles. *3 Biotech* **2019**, *9*, 279. [[CrossRef](#)]
31. Fischer, D.; Li, Y.; Ahlemeyer, B.; Krieglstein, J.; Kissel, T. In Vitro Cytotoxicity Testing of Polycations: Influence of Polymer Structure on Cell Viability and Hemolysis. *Biomaterials* **2003**, *24*, 1121–1131. [[CrossRef](#)]
32. Podsiedlik, M.; Markowicz-Piasecka, M.; Sikora, J. Erythrocytes as Model Cells for Biocompatibility Assessment, Cytotoxicity Screening of Xenobiotics and Drug Delivery. *Chem. Biol. Interact.* **2020**, *332*, 109305. [[CrossRef](#)]
33. Carlsen, C.U.; Møller, J.K.S.; Skibsted, L.H. Heme-Iron in Lipid Oxidation. *Coord. Chem. Rev.* **2005**, *249*, 485–498. [[CrossRef](#)]
34. Fujii, J.; Homma, T.; Kobayashi, S.; Warang, P.; Madkaikar, M.; Mukherjee, M.B. Erythrocytes as a Preferential Target of Oxidative Stress in Blood. *Free Radic. Res.* **2021**, *55*, 781–799. [[CrossRef](#)]
35. Pisoschi, A.M.; Pop, A.; Iordache, F.; Stanca, L.; Predoi, G.; Serban, A.I. Oxidative Stress Mitigation by Antioxidants—An Overview on Their Chemistry and Influences on Health Status. *EJMECH* **2021**, *209*, 112891. [[CrossRef](#)]
36. Sies, H.; Belousov, V.V.; Chandel, N.S.; Davies, M.J.; Jones, D.P.; Mann, G.E.; Murphy, M.P.; Yamamoto, M.; Winterbourn, C. Defining Roles of Specific Reactive Oxygen Species (ROS) in Cell Biology and Physiology. *Nat. Rev. Mol. Cell. Biol.* **2022**, *23*, 499–515. [[CrossRef](#)]
37. Bayr, H. Reactive Oxygen Species. *Crit. Care Med.* **2005**, *33*, S498. [[CrossRef](#)] [[PubMed](#)]
38. Khan, F.; Garg, V.; Singh, A.; Tinku, T. Role of Free Radicals and Certain Antioxidants in the Management of Huntington’s Disease: A Review. *J. Anal. Pharm. Res.* **2018**, *7*. [[CrossRef](#)]
39. Adwas, A.A.; Elsayed, A.S.I.; Azab, A.E.; Quwaydir, F.A. Oxidative stress and antioxidant mechanisms in human body. *J. Appl. Biotechnol. Bioeng.* **2019**, *6*, 43–47.
40. Tsoi, B.; Yi, R.-N.; Cao, L.-F.; Li, S.-B.; Tan, R.-R.; Chen, M.; Li, X.-X.; Wang, C.; Li, Y.-F.; Kurihara, H.; et al. Comparing Antioxidant Capacity of Purine Alkaloids: A New, Efficient Trio for Screening and Discovering Potential Antioxidants in Vitro and in Vivo. *Food Chem.* **2015**, *176*, 411–419. [[CrossRef](#)]
41. Rehman, S.; Khan, H. Advances in Antioxidant Potential of Natural Alkaloids. *Curr. Bioact. Compd.* **2017**, *13*, 101–108. [[CrossRef](#)]
42. Kargapolova, Y.; Geißen, S.; Zheng, R.; Baldus, S.; Winkels, H.; Adam, M. The Enzymatic and Non-Enzymatic Function of Myeloperoxidase (MPO) in Inflammatory Communication. *Antioxidants* **2021**, *10*, 562. [[CrossRef](#)]

43. Parker, H.; Winterbourn, C.C. Reactive Oxidants and Myeloperoxidase and Their Involvement in Neutrophil Extracellular Traps. *Front. Immunol.* **2012**, *3*, 424. [[CrossRef](#)]
44. Chung, H.Y.; Baek, B.S.; Song, S.H.; Kim, M.S.; Huh, J.I.; Shim, K.H.; Kim, K.W.; Lee, K.H. Xanthine Dehydrogenase/Xanthine Oxidase and Oxidative Stress. *Age* **1997**, *20*, 127–140. [[CrossRef](#)]
45. Berry, C.E.; Hare, J.M. Xanthine Oxidoreductase and Cardiovascular Disease: Molecular Mechanisms and Pathophysiological Implications. *J. Physiol.* **2004**, *555*, 589–606. [[CrossRef](#)] [[PubMed](#)]
46. Laube, M.; Kniess, T.; Pietzsch, J. Development of Antioxidant COX-2 Inhibitors as Radioprotective Agents for Radiation Therapy—A Hypothesis-Driven Review. *Antioxidants* **2016**, *5*, 14. [[CrossRef](#)]
47. Desai, S.J.; Prickril, B.; Rasooly, A. Mechanisms of Phytonutrient Modulation of Cyclooxygenase-2 (COX-2) and Inflammation Related to Cancer. *Nutr. Cancer* **2018**, *70*, 350–375. [[CrossRef](#)] [[PubMed](#)]
48. Delaere, D.; Raspoet, G.; Nguyen, M.T. Thiol–Thione Tautomerism in Thioformic Acid: Importance of Specific Solvent Interactions. *J. Phys. Chem. A* **1999**, *103*, 171–177. [[CrossRef](#)]
49. García-Báez, E.V.; Padilla-Martínez, I.I.; Cruz, A.; Rosales-Hernández, M.C. <sup>13</sup>C-NMR Chemical Shifts in 1,3-Benzazoles as a Tautomeric Ratio Criterion. *Molecules* **2022**, *27*, 6268. [[CrossRef](#)]
50. Babijczuk, K.; Warzajtis, B.; Starzyk, J.; Mrówczyńska, L.; Jasiewicz, B.; Rychlewska, U. Synthesis, Structure and Biological Activity of Indole–Imidazole Complexes with ZnCl<sub>2</sub>: Can Coordination Enhance the Functionality of Bioactive Ligands? *Molecules* **2023**, *28*, 4132. [[CrossRef](#)]
51. Ravikumar, K.; Chandra Mohan, K.; Bidyasagar, M.; Swamy, G.Y.S.K. Crystal Structure of 2-Mercaptobenzimidazole and Bis [2-mercaptobenzimidazole]Dichlorocobalt(II). *J. Chem. Crystallogr.* **1995**, *25*, 325–329. [[CrossRef](#)]
52. Tomkowiak, H.; Katrusiak, A. High Pressure Effects on Zwitterionic and Thione Mesomeric Contributions in 2-Benzimidazole-2-Thione. *J. Phys. Chem. C* **2017**, *121*, 18830–18836. [[CrossRef](#)]
53. Form, G.R.; Raper, E.S.; Downie, T.C. The Crystal and Molecular Structure of 2-Mercaptobenzimidazole. *Acta Crystallogr. Sect. B Struct. Crystallogr. Cryst. Chem.* **1976**, *32*, 345–348. [[CrossRef](#)]
54. Rong, Y.; Al-Harbi, A.; Kriegel, B.; Parkin, G. Structural Characterization of 2-Imidazolones: Comparison with their Heavier Chalcogen Counterparts. *Inorg. Chem.* **2013**, *52*, 7172–7182. [[CrossRef](#)] [[PubMed](#)]
55. Owczarzak, A.; Dutkiewicz, Z.; Kurczab, R.; Pietruś, W.; Kubicki, M.; Grzeńkiewicz, A.M. Role of Staple Molecules in the Formation of S...S Contact in Thioamides: Experimental Charge Density and Theoretical Studies. *Cryst. Growth Des.* **2019**, *19*, 7324–7335. [[CrossRef](#)]
56. Francuski, B.M.; Novakovic, S.B.; Bogdanovic, G.A. Electronic features and hydrogen bonding capacity of the sulfur acceptor in thioureido-based compounds. Experimental charge density study of 4-methyl-3-thiosemicarbazide. *CrystEngComm* **2011**, *13*, 3580. [[CrossRef](#)]
57. Werber, J.; Wang, Y.J.; Milligan, M.; Li, X.; Ji, J.A. Analysis of 2,2'-Azobis (2-Amidinopropane) Dihydrochloride Degradation and Hydrolysis in Aqueous Solutions. *J. Pharm. Sci.* **2011**, *100*, 3307–3315. [[CrossRef](#)] [[PubMed](#)]
58. Garrec, J.; Monari, A.; Assfeld, X.; Mir, L.M.; Tarek, M. Lipid Peroxidation in Membranes: The Peroxyl Radical Does Not “Float”. *J. Phys. Chem. Lett.* **2014**, *5*, 1653–1658. [[CrossRef](#)] [[PubMed](#)]
59. Wu, T.-W.; Hashimoto, N.; Wu, J.; Carey, D.; Li, R.-K.; Mickle, D.A.G.; Weisel, R.D. The Cytoprotective Effect of Trolox Demonstrated with Three Types of Human Cells. *Biochem. Cell Biol.* **1990**, *68*, 1189–1194. [[CrossRef](#)] [[PubMed](#)]
60. Sierakowska, A.; Jasiewicz, B.; Piosik, Ł.; Mrówczyńska, L. New C8-Substituted Caffeine Derivatives as Promising Antioxidants and Cytoprotective Agents in Human Erythrocytes. *Sci. Rep.* **2023**, *13*, 1785. [[CrossRef](#)]
61. Vo, Q.V.; Hang, D.T.N.; Hoa, N.T.; Nam, P.C.; Duong, T.Q.; Mechler, A. The radical scavenging activity of 4-mercaptoimidazole: Theoretical insights into the mechanism, kinetics and solvent effects. *New J. Chem.* **2003**, *47*, 10381. [[CrossRef](#)]
62. Sprinz, H.; Schwinn, J.; Naumov, S.; Brede, O. Mechanism of Thiyl Radical-Catalyzed Isomerization of Unsaturated Fatty Acid Residues in Homogeneous Solution and in Liposomes. *Biochim. Biophys. Acta Mol. Cell Biol. Lipids* **2000**, *1483*, 91–100. [[CrossRef](#)]
63. Tartaro Bujak, I.; Mihaljević, B.; Ferreri, C.; Chatgililoglu, C. The Influence of Antioxidants in the Thiyl Radical Induced Lipid Peroxidation and Geometrical Isomerization in Micelles of Linoleic Acid. *Free Radic. Res.* **2016**, *50*, S18–S23. [[CrossRef](#)] [[PubMed](#)]
64. Velika, B.; Kron, I. Antioxidant Properties of Benzoic Acid Derivatives against Superoxide Radical. *Free Radic. Antioxid.* **2012**, *2*, 62–67. [[CrossRef](#)]
65. Milenković, D.; Đorović, J.; Jeremić, S.; Dimitrić Marković, J.M.; Avdović, E.H.; Marković, Z. Free Radical Scavenging Potency of Dihydroxybenzoic Acids. *J. Chem.* **2017**, *2017*, e5936239. [[CrossRef](#)]
66. Vo, Q.V.; Mechler, A. In Silico Study of the Radical Scavenging Activities of Natural Indole-3-Carbinols. *J. Chem. Inf. Model.* **2020**, *60*, 316–321. [[CrossRef](#)] [[PubMed](#)]
67. Bentz, E.N.; Lobayan, R.M.; Martínez, H.; Redondo, P.; Largo, A. Intrinsic Antioxidant Potential of the Aminoindole Structure: A Computational Kinetics Study of Tryptamine. *J. Phys. Chem. B* **2018**, *122*, 6386–6395. [[CrossRef](#)] [[PubMed](#)]
68. Kwiatek, D.; Mrówczyńska, L.; Stopikowska, N.; Runowski, M.; Lesicki, A.; Lis, S. Surface Modification of Luminescent LnIII Fluoride Core-Shell Nanoparticles with Acetylsalicylic acid (Aspirin): Synthesis, Spectroscopic and in vitro Hemocompatibility Studies. *ChemMedChem* **2020**, *15*, 1490–1496. [[CrossRef](#)] [[PubMed](#)]
69. Lipinski, C.A. Lead- and Drug-like Compounds: The Rule-of-Five Revolution. *Drug Discov. Today Technol.* **2004**, *1*, 337–341. [[CrossRef](#)]



70. Veber, D.F.; Johnson, S.R.; Cheng, H.-Y.; Smith, B.R.; Ward, K.W.; Kopple, K.D. Molecular Properties That Influence the Oral Bioavailability of Drug Candidates. *J. Med. Chem.* **2002**, *45*, 2615–2623. [CrossRef]
71. ProteinsPlus Development Team. ProteinsPlus. Available online: <https://proteins.plus> (accessed on 17 January 2024).
72. Stierand, K.; Maaß, P.C.; Rarey, M. Molecular Complexes at a Glance: Automated Generation of Two-Dimensional Complex Diagrams. *Bioinformatics* **2006**, *22*, 1710–1716. [CrossRef] [PubMed]
73. Diedrich, K.; Krause, B.; Berg, O.; Rarey, M. PoseEdit: Enhanced Ligand Binding Mode Communication by Interactive 2D Diagrams. *J. Comput. Aided Mol. Des.* **2023**, *37*, 491–503. [CrossRef] [PubMed]
74. Pettersen, E.F.; Goddard, T.D.; Huang, C.C.; Couch, G.S.; Greenblatt, D.M.; Meng, E.C.; Ferrin, T.E. UCSF Chimera—A Visualization System for Exploratory Research and Analysis. *J. Comput. Chem.* **2004**, *25*, 1605–1612. [CrossRef] [PubMed]
75. Ramírez, D.; Caballero, J. Is It Reliable to Take the Molecular Docking Top Scoring Position as the Best Solution without Considering Available Structural Data? *Molecules* **2018**, *23*, 1038. [CrossRef]
76. *CrysAlis: Rigaku OD. CrysAlis PRO 1.171.42*; Rigaku Oxford Diffraction: Yarnton, UK, 2022.
77. Sheldrick, G.M. SHELXT—Integrated space-group and crystal-structure determination. *Acta Crystallogr. Sect. A Found. Adv.* **2015**, *71*, 3–8. [CrossRef] [PubMed]
78. Sheldrick, G.M. Crystal structure refinement with SHELXL. *Acta Crystallogr. Sect. C Struct. Chem.* **2015**, *71*, 3–8. [CrossRef]
79. Bruno, I.J.; Cole, J.C.; Edgington, P.R.; Kessler, M.; Macrae, C.F.; McCabe, P.; Pearson, J.; Taylor, R. New software for searching the Cambridge Structural Database and visualizing crystal structures. *Acta Crystallogr. Sect. B Struct. Sci.* **2002**, *58*, 389–397. [CrossRef]
80. O’Boyle, N.M.; Banck, M.; James, C.A.; Morley, C.; Vandermeersch, T.; Hutchison, G.R. Open Babel: An Open Chemical Toolbox. *J. Cheminform.* **2011**, *3*, 33. [CrossRef]
81. Open Babel Development Team. Open Babel, Version: 3.1.1. 2020. Available online: [http://openbabel.org/wiki/Main\\_Page](http://openbabel.org/wiki/Main_Page) (accessed on 17 January 2024).
82. Berman, H.M.; Battistuz, T.; Bhat, T.N.; Bluhm, W.F.; Bourne, P.E.; Burkhardt, K.; Feng, Z.; Gilliland, G.L.; Iype, L.; Jain, S.; et al. The Protein Data Bank. *Acta Cryst. D* **2002**, *58*, 899–907. [CrossRef]
83. Blair-Johnson, M.; Fiedler, T.; Fenna, R. Human Myeloperoxidase: Structure of a Cyanide Complex and Its Interaction with Bromide and Thiocyanate Substrates at 1.9 Å Resolution. *Biochemistry* **2001**, *40*, 13990–13997. [CrossRef]
84. Okamoto, K.; Eger, B.T.; Nishino, T.; Kondo, S.; Pai, E.F.; Nishino, T. An Extremely Potent Inhibitor of Xanthine Oxidoreductase: Crystal structure of the enzyme-inhibitor complex and mechanism of inhibition. *J. Biol. Chem.* **2003**, *278*, 1848–1855. [CrossRef] [PubMed]
85. Kurumbail, R.G.; Stevens, A.M.; Gierse, J.K.; McDonald, J.J.; Stegeman, R.A.; Pak, J.Y.; Gildehaus, D.; Iyashiro, J.M.; Penning, T.D.; Seibert, K.; et al. Structural Basis for Selective Inhibition of Cyclooxygenase-2 by Anti-Inflammatory Agents. *Nature* **1996**, *384*, 644–648. [CrossRef] [PubMed]
86. Morris, G.M.; Huey, R.; Lindstrom, W.; Sanner, M.F.; Belew, R.K.; Goodsell, D.S.; Olson, A.J. AutoDock4 and AutoDockTools4: Automated Docking with Selective Receptor Flexibility. *J. Comput. Chem.* **2009**, *30*, 2785–2791. [CrossRef] [PubMed]
87. Trott, O.; Olson, A.J. AutoDock Vina: Improving the Speed and Accuracy of Docking with a New Scoring Function, Efficient Optimization, and Multithreading. *J. Comput. Chem.* **2010**, *31*, 455–461. [CrossRef] [PubMed]

**Disclaimer/Publisher’s Note:** The statements, opinions and data contained in all publications are solely those of the individual author(s) and contributor(s) and not of MDPI and/or the editor(s). MDPI and/or the editor(s) disclaim responsibility for any injury to people or property resulting from any ideas, methods, instructions or products referred to in the content.

## Supplementary data

### **Novel C3-methylene-bridged indole derivatives with and without substituents at N1: the influence of substituents on their hemolytic, cytoprotective and antimicrobial activity**

Karolina Babijczuk<sup>1</sup>, Natalia Berdzik<sup>1</sup>, Damian Nowak<sup>2</sup>, Beata Warżajtis<sup>3</sup>, Urszula Rychlewska<sup>3</sup>, Justyna Starzyk<sup>4</sup>, Lucyna Mrówczyńska<sup>5</sup>, and Beata Jasiewicz<sup>1,\*</sup>

<sup>1</sup> Department of Bioactive Products, Faculty of Chemistry, Adam Mickiewicz University, Uniwersytetu Poznańskiego 8, 61-614 Poznań, Poland

<sup>2</sup> Department of Quantum Chemistry, Faculty of Chemistry, Adam Mickiewicz University, Uniwersytetu Poznańskiego 8, 61-614 Poznań, Poland

<sup>3</sup> Department of Crystallography, Faculty of Chemistry, Adam Mickiewicz University, Uniwersytetu Poznańskiego 8, 61-614 Poznań, Poland

<sup>4</sup> Department of Soil Science and Microbiology, Faculty of Agronomy, Horticulture, and Bioengineering, University of Life Science, Szydlowska 50, 60-656 Poznań, Poland

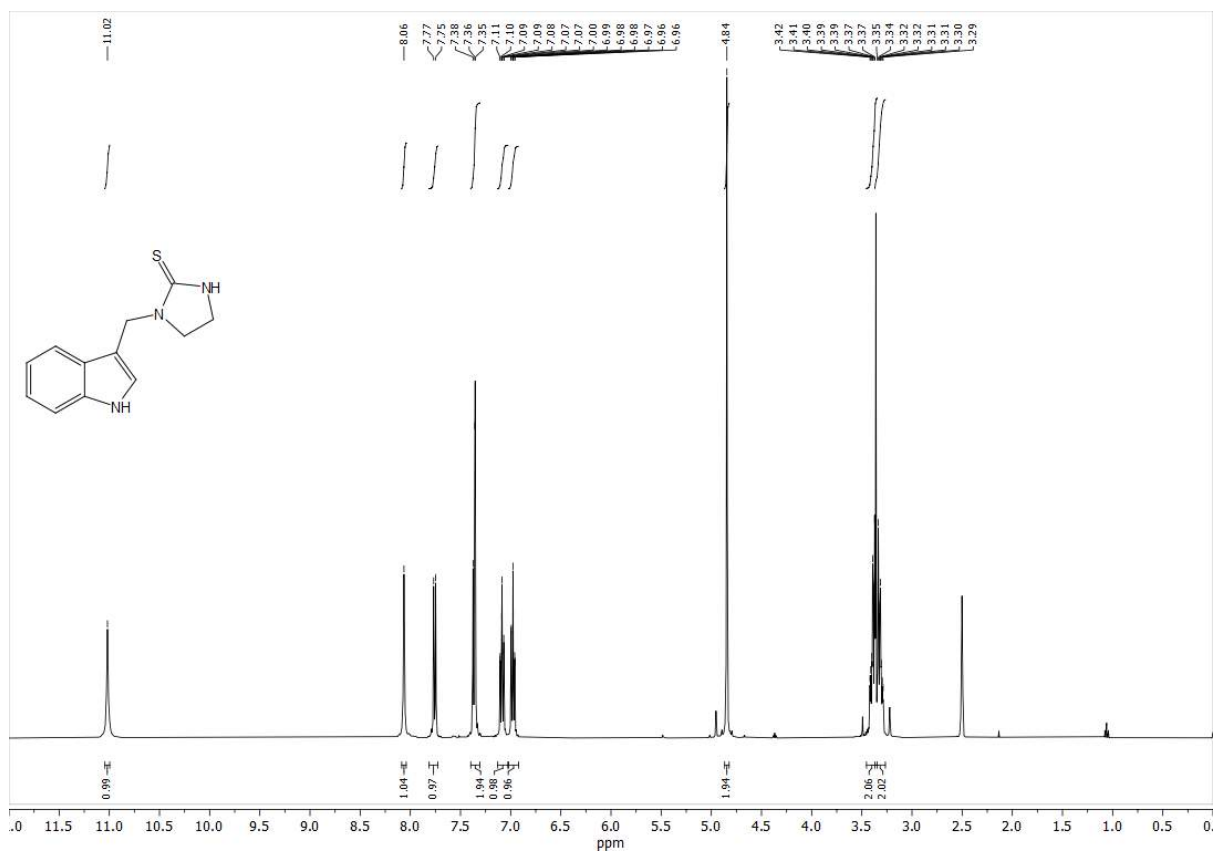
<sup>5</sup> Department of Cell Biology, Faculty of Biology, Adam Mickiewicz University, Uniwersytetu Poznańskiego 6, 61-614 Poznań, Poland

\* Correspondence: beatakoz@amu.edu.pl (B.J.)

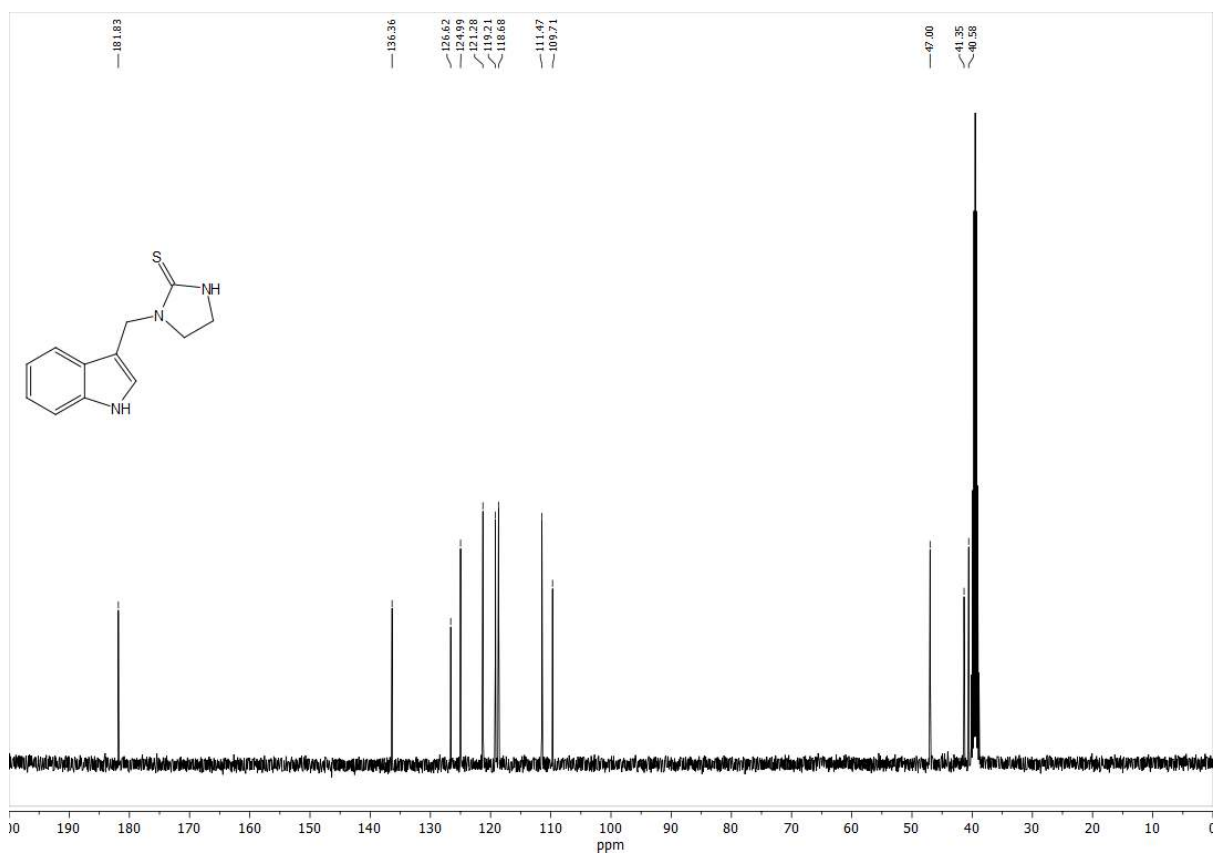
#### **TABLE OF CONTENTS**

<sup>1</sup> H and <sup>13</sup> C NMR spectra of compound <b>2</b> .....	S3
EI-MS and FIR spectra of compound <b>2</b> .....	S4
<sup>1</sup> H and <sup>13</sup> C NMR spectra of compound <b>3</b> .....	S5
EI-MS and IR spectra of compound <b>3</b> .....	S6
<sup>1</sup> H and <sup>13</sup> C NMR spectra of compound <b>4</b> .....	S7
EI-MS and IR spectra of compound <b>4</b> .....	S8
<sup>1</sup> H and <sup>13</sup> C NMR spectra of compound <b>5</b> .....	S9
EI-MS and IR spectra of compound <b>5</b> .....	S10
<sup>1</sup> H and <sup>13</sup> C NMR spectra of compound <b>6</b> .....	S11
EI-MS and IR spectra of compound <b>6</b> .....	S12
<sup>1</sup> H and <sup>13</sup> C NMR spectra of compound <b>7</b> .....	S13
EI-MS and IR spectra of compound <b>7</b> .....	S14
<sup>1</sup> H and <sup>13</sup> C NMR spectra of compound <b>8</b> .....	S15
EI-MS and IR spectra of compound <b>8</b> .....	S16
<sup>1</sup> H and <sup>13</sup> C NMR spectra of compound <b>9</b> .....	S17

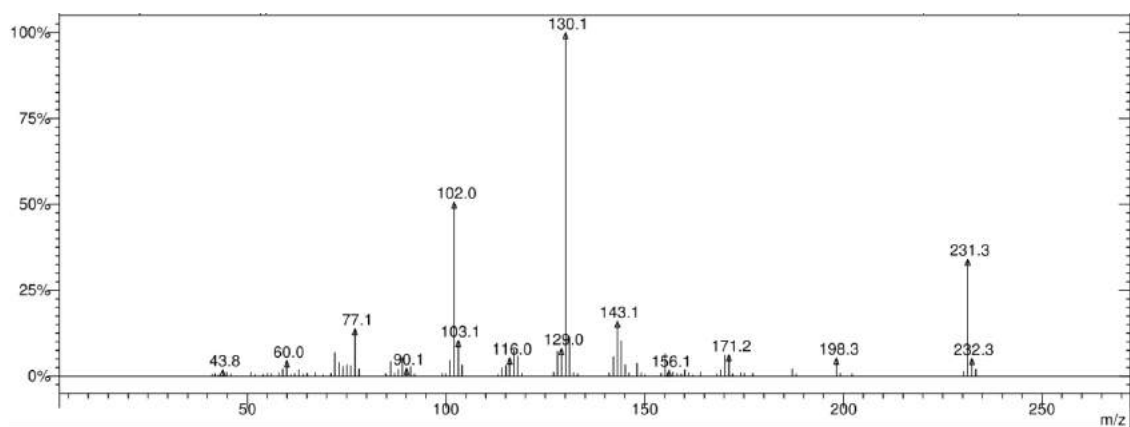
EI-MS and IR spectra of compound <b>9</b> .....	S18
<sup>1</sup> H and <sup>13</sup> C NMR spectra of compound <b>10</b> .....	S19
EI-MS and IR spectra of compound <b>10</b> .....	S20
<sup>1</sup> H and <sup>13</sup> C NMR spectra of compound <b>11</b> .....	S21
EI-MS and IR spectra of compound <b>11</b> .....	S22
<sup>1</sup> H and <sup>13</sup> C NMR spectra of compound <b>12</b> .....	S23
EI-MS and IR spectra of compound <b>12</b> .....	S24
<sup>1</sup> H and <sup>13</sup> C NMR spectra of compound <b>13</b> .....	S25
EI-MS and IR spectra of compound <b>13</b> .....	S26
<sup>1</sup> H and <sup>13</sup> C NMR spectra of compound <b>15</b> .....	S27
EI-MS and IR spectra of compound <b>15</b> .....	S28
<sup>1</sup> H and <sup>13</sup> C NMR spectra of compound <b>17</b> .....	S29
EI-MS and IR spectra of compound <b>17</b> .....	S30
<sup>1</sup> H and <sup>13</sup> C NMR spectra of compound <b>18</b> .....	S31
EI-MS and IR spectra of compound <b>18</b> .....	S32
<sup>1</sup> H and <sup>13</sup> C NMR spectra of compound <b>19</b> .....	S33
EI-MS and IR spectra of compound <b>19</b> .....	S34
<sup>1</sup> H and <sup>13</sup> C NMR spectra of compound <b>20</b> .....	S35
EI-MS and IR spectra of compound <b>20</b> .....	S36
<sup>1</sup> H and <sup>13</sup> C NMR spectra of compound <b>21</b> .....	S37
EI-MS and IR spectra of compound <b>21</b> .....	S38
<sup>1</sup> H and <sup>13</sup> C NMR spectra of compound <b>22</b> .....	S39
EI-MS and IR spectra of compound <b>22</b> .....	S40
<sup>1</sup> H and <sup>13</sup> C NMR spectra of compound <b>23</b> .....	S41
EI-MS and IR spectra of compound <b>23</b> .....	S42
<sup>1</sup> H and <sup>13</sup> C NMR spectra of compound <b>24</b> .....	S43
EI-MS and IR spectra of compound <b>24</b> .....	S44
<sup>1</sup> H and <sup>13</sup> C NMR spectra of compound <b>25</b> .....	S45
EI-MS and IR spectra of compound <b>25</b> .....	S46
<sup>1</sup> H and <sup>13</sup> C NMR spectra of compound <b>26</b> .....	S47
EI-MS and IR spectra of compound <b>26</b> .....	S48
<sup>1</sup> H and <sup>13</sup> C NMR spectra of compound <b>27</b> .....	S49
EI-MS and IR spectra of compound <b>27</b> .....	S50
<sup>1</sup> H and <sup>13</sup> C NMR spectra of compound <b>29</b> .....	S51
EI-MS and IR spectra of compound <b>29</b> .....	S52
Crystal data Description of the crystallographic results.....	S53
Table S1. Hydrogen bond geometrical parameters.....	S56
Table S2. Crystal data and structure refinement parameters for gramine derivatives.....	S58
Table S3. Antibacterial activities of compounds <b>1-29</b> .....	S59
Interactions between indole-based derivatives <b>2</b> , <b>5</b> , and <b>15</b> , and the 1N5X and the 4COX protein domains.....	S60



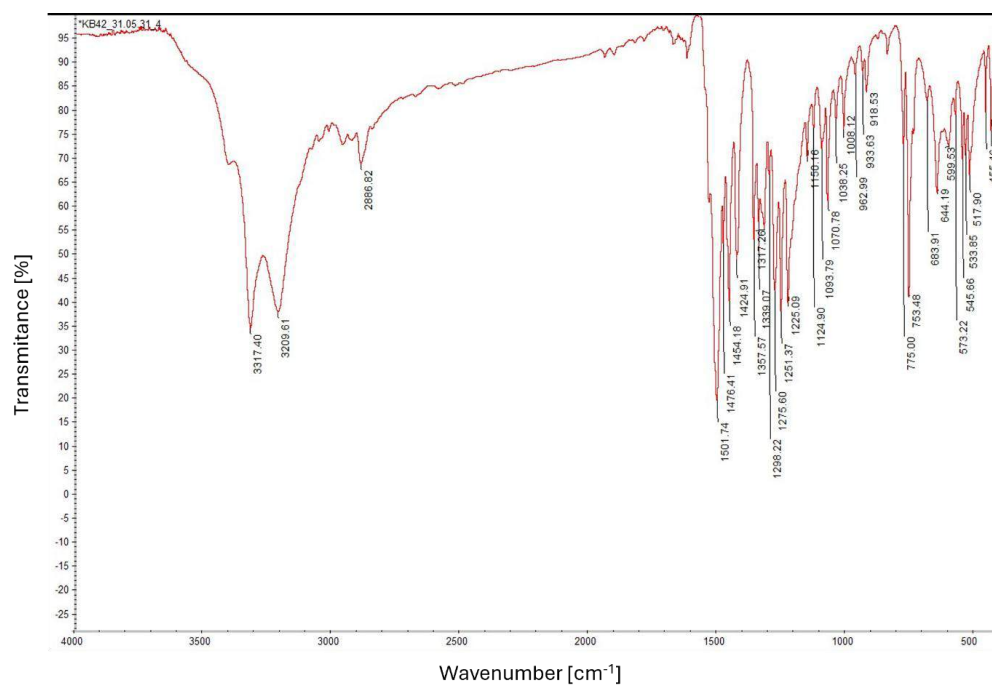
**Fig.S1a.**  $^1\text{H}$  NMR spectrum of compound 2



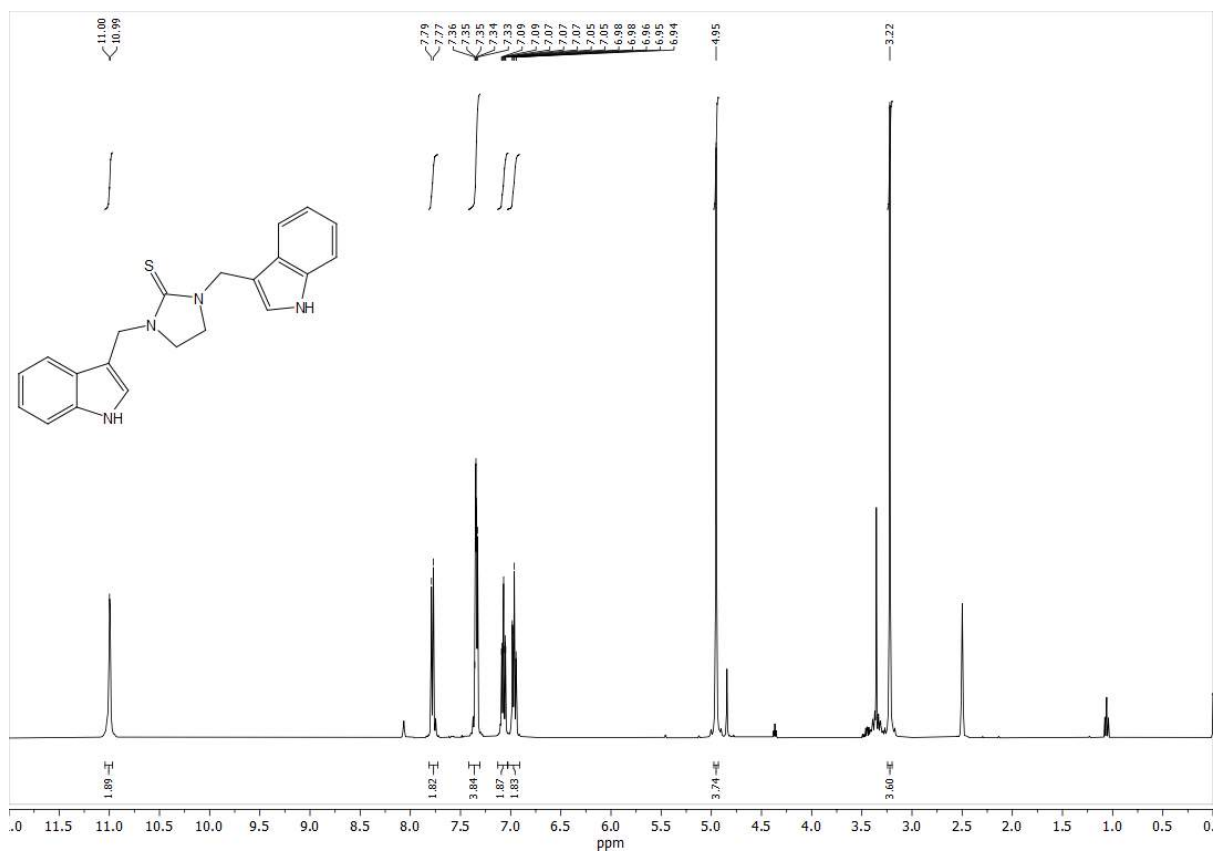
**Fig.S1b.**  $^{13}\text{C}$  NMR spectrum of compound 2



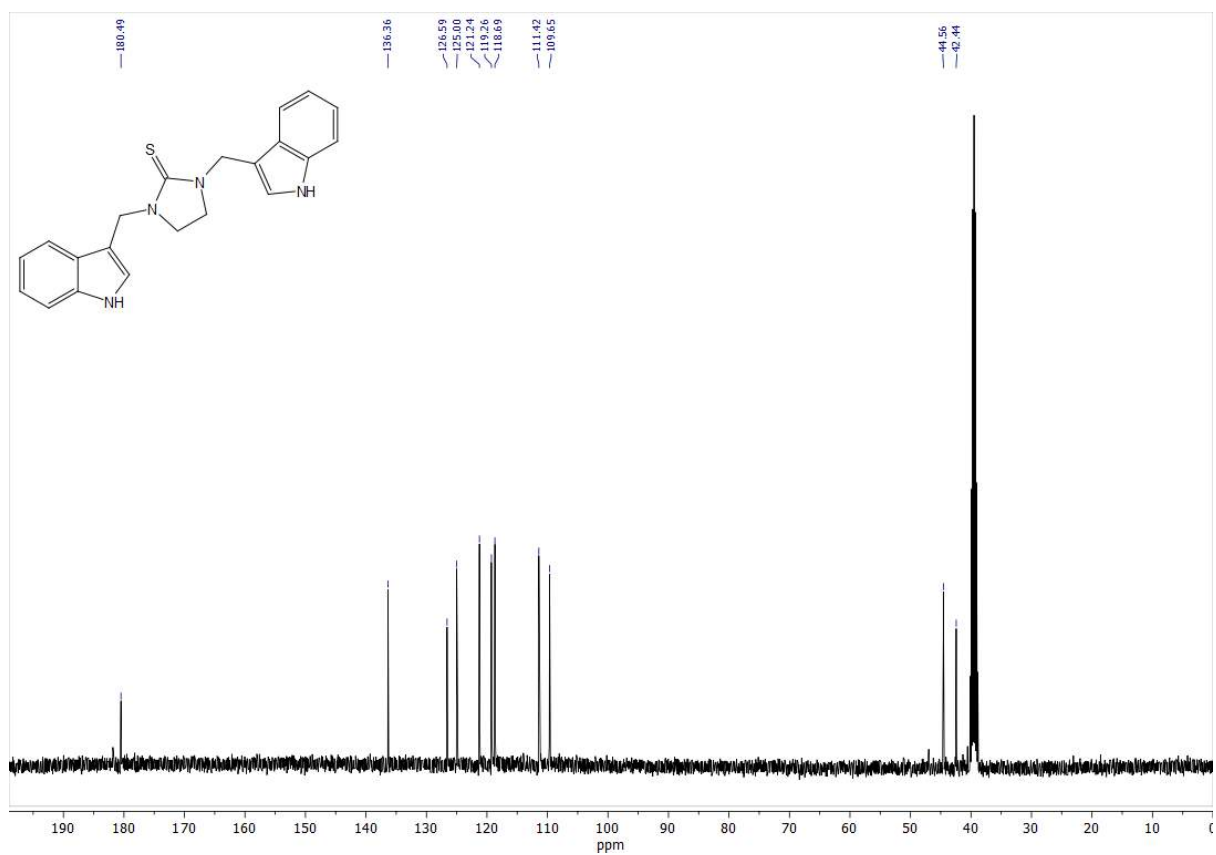
**Fig.S1c.** EI-MS spectrum of compound 2



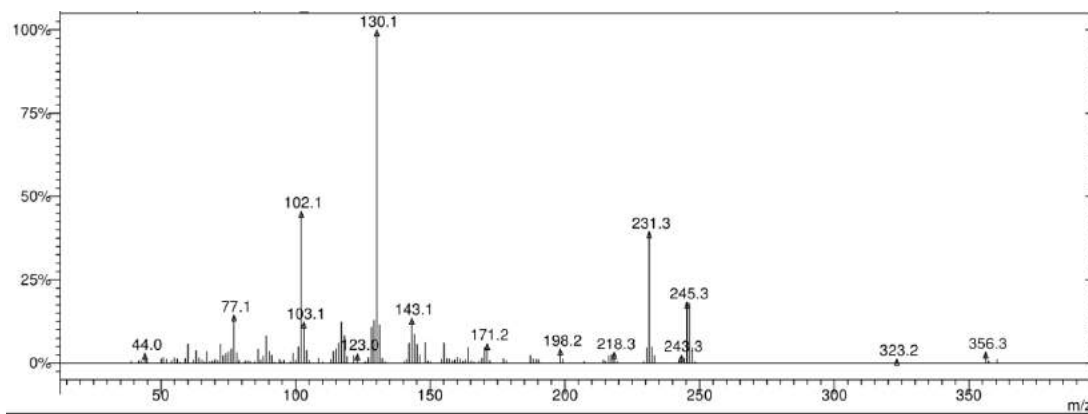
**Fig.S1d.** IR spectrum of compound 2



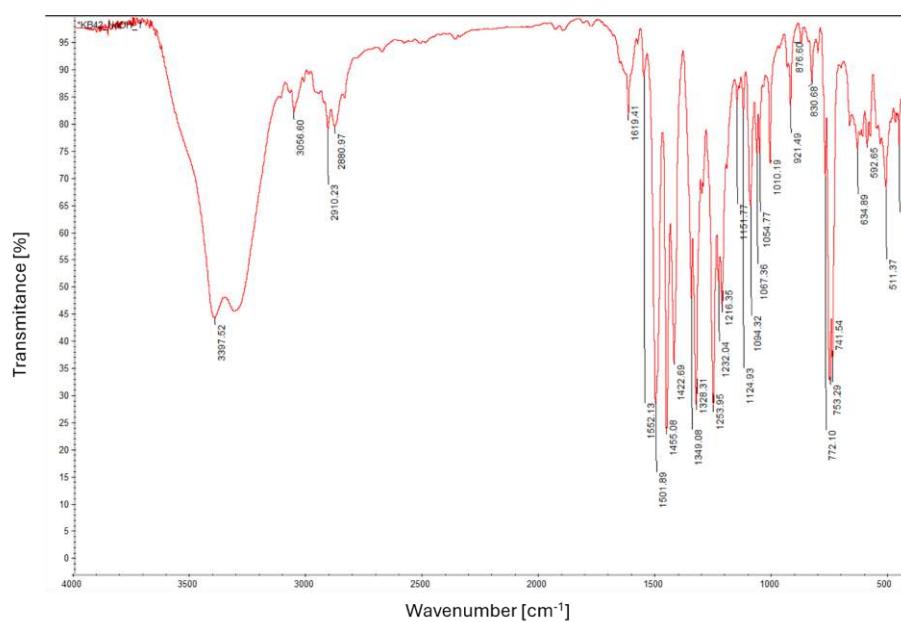
**Fig.S2a.**  $^1\text{H NMR}$  spectrum of compound 3



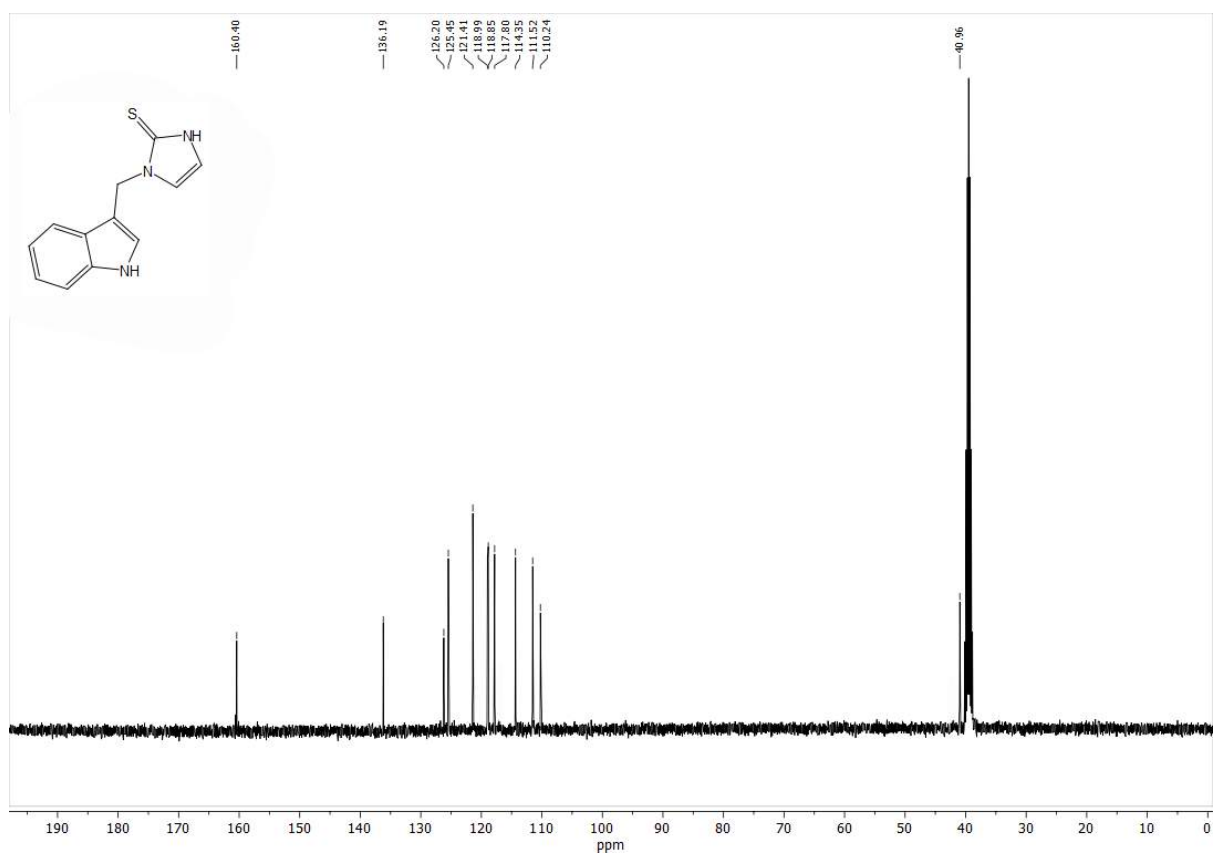
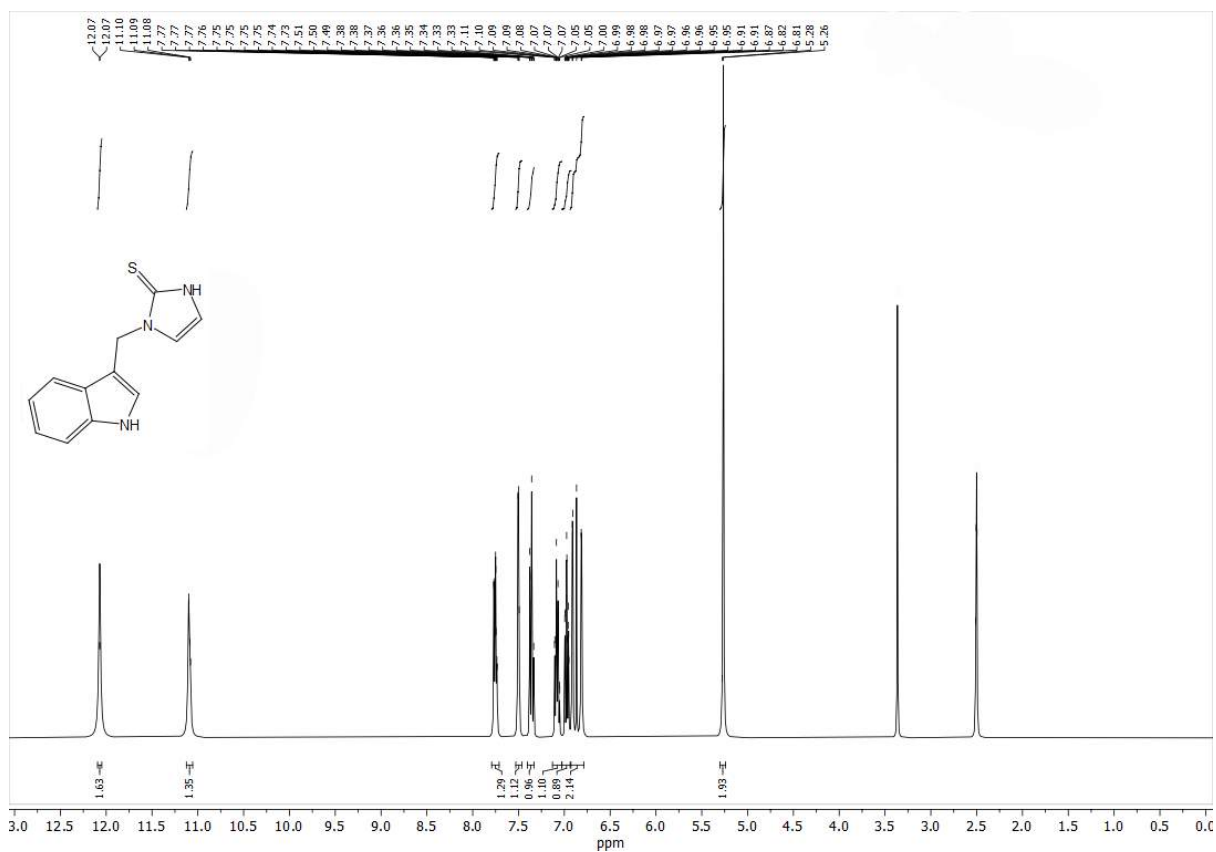
**Fig.S2b.**  $^{13}\text{C NMR}$  spectrum of compound 3



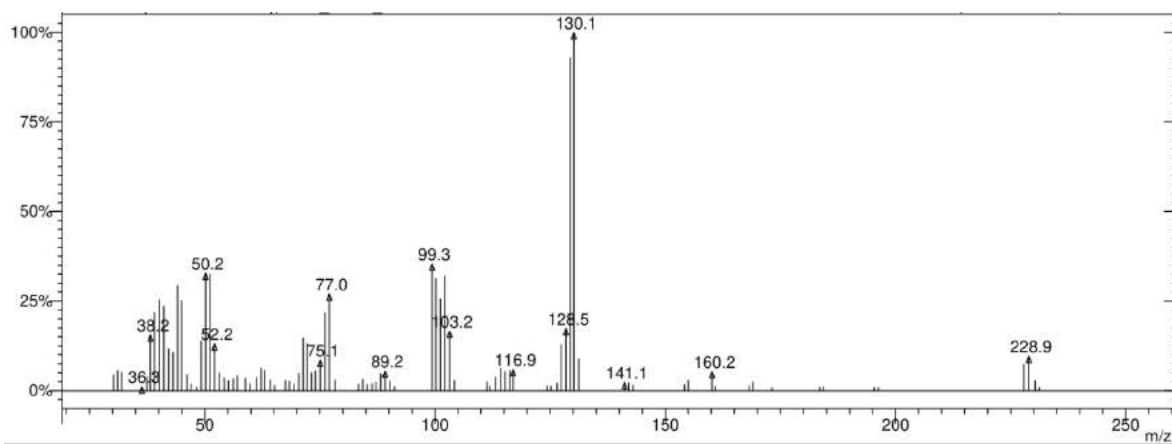
**Fig.S2c.** EI-MS spectrum of compound **3**



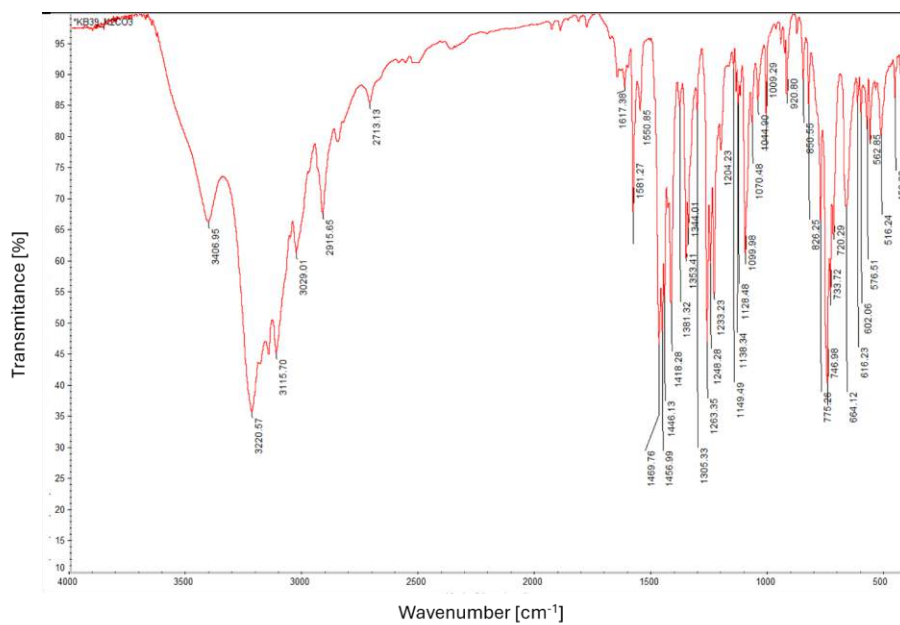
**Fig.S2d.** IR spectrum of compound **3**



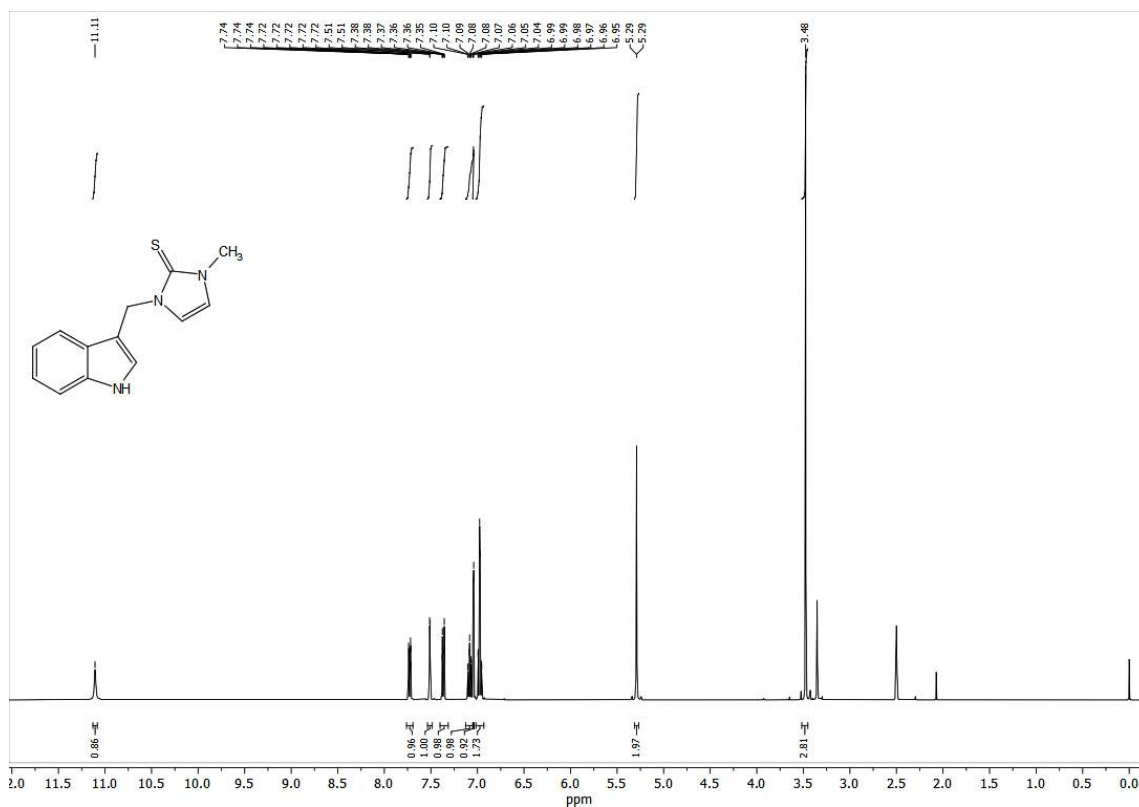




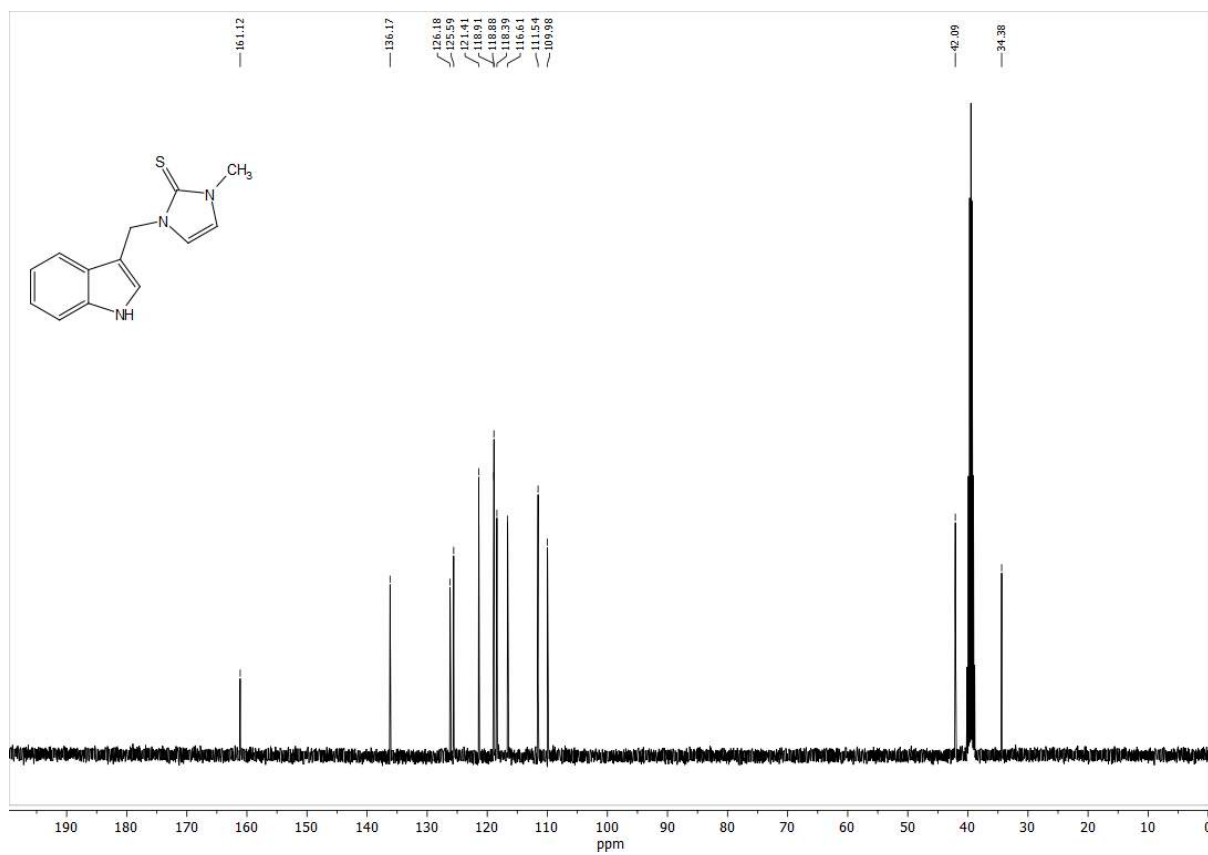
**Fig.S3c.** EI-MS spectrum of compound 4



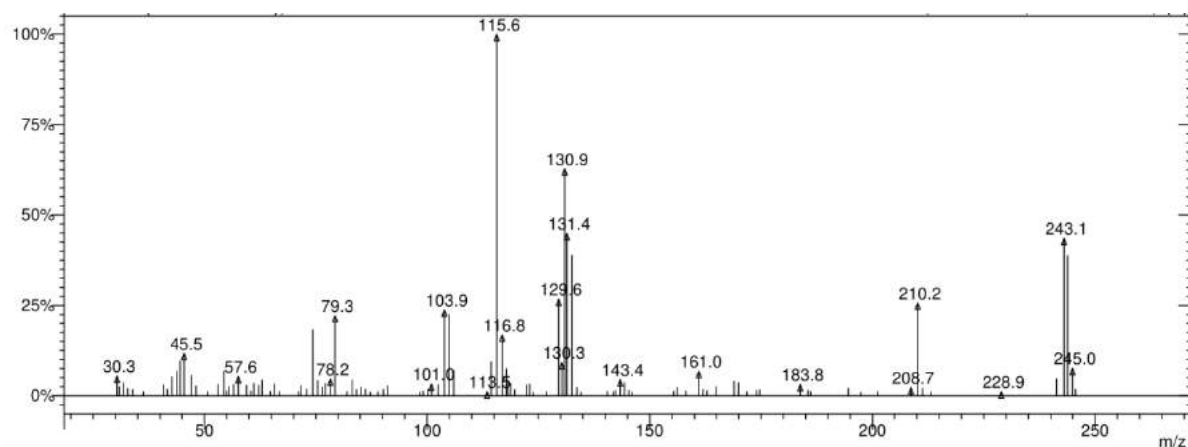
**Fig.S3d.** IR spectrum of compound 4



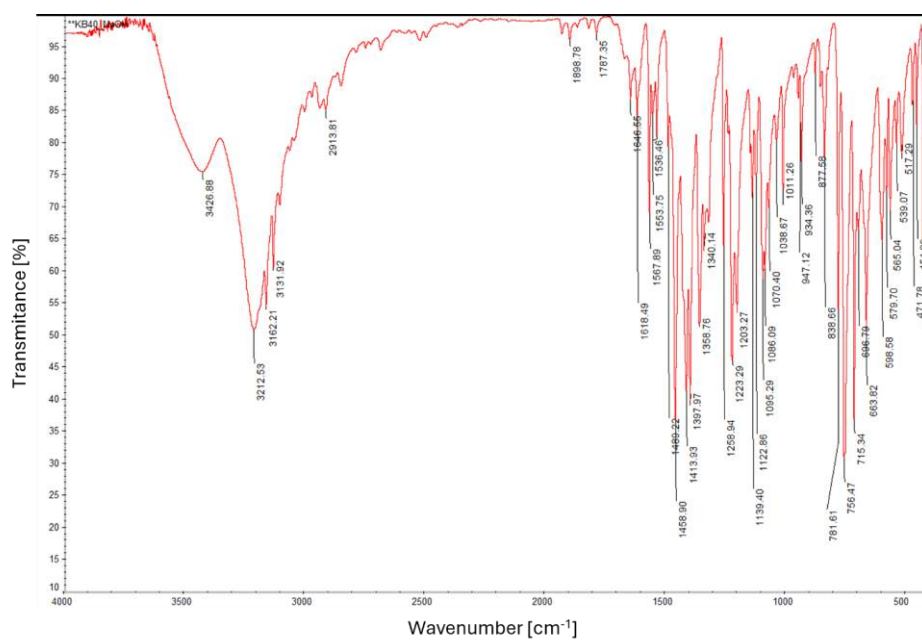
**Fig.S4a.**  $^1\text{H}$  NMR spectrum of compound **5**



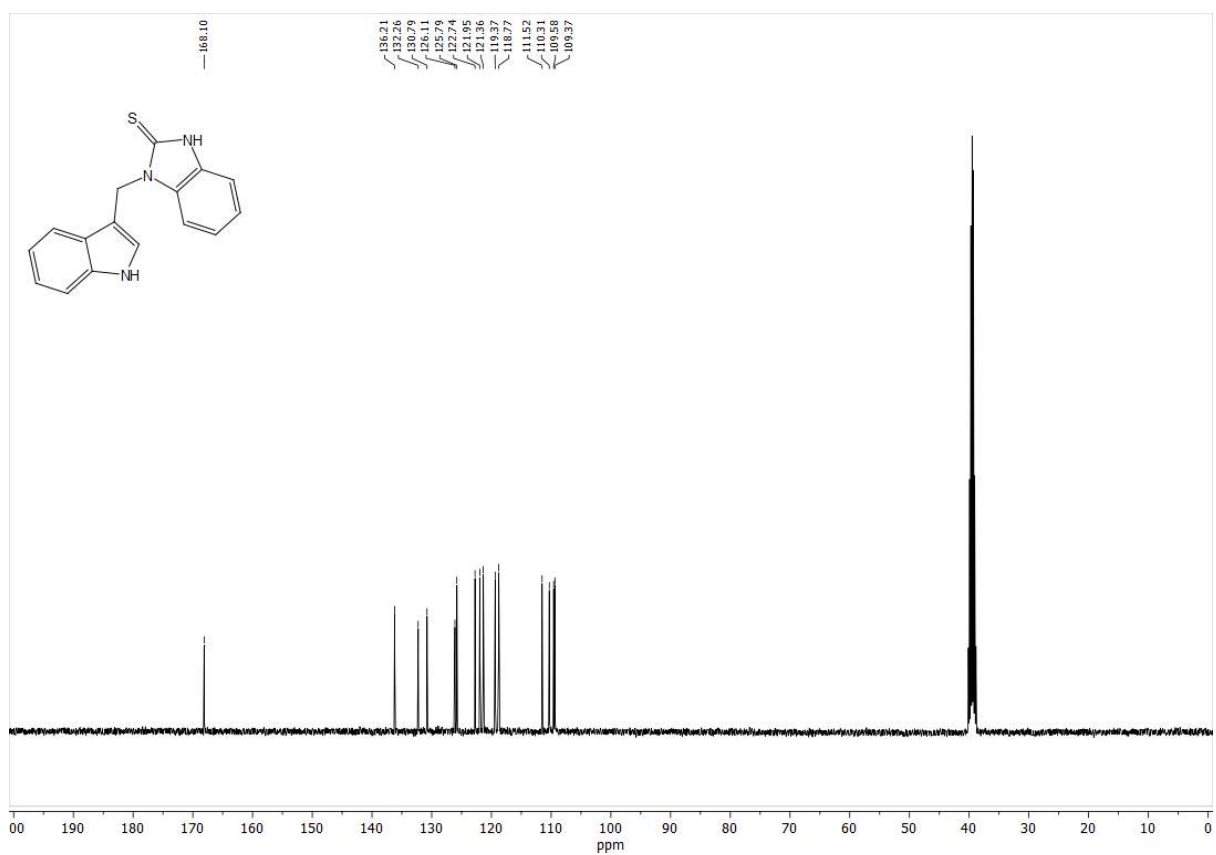
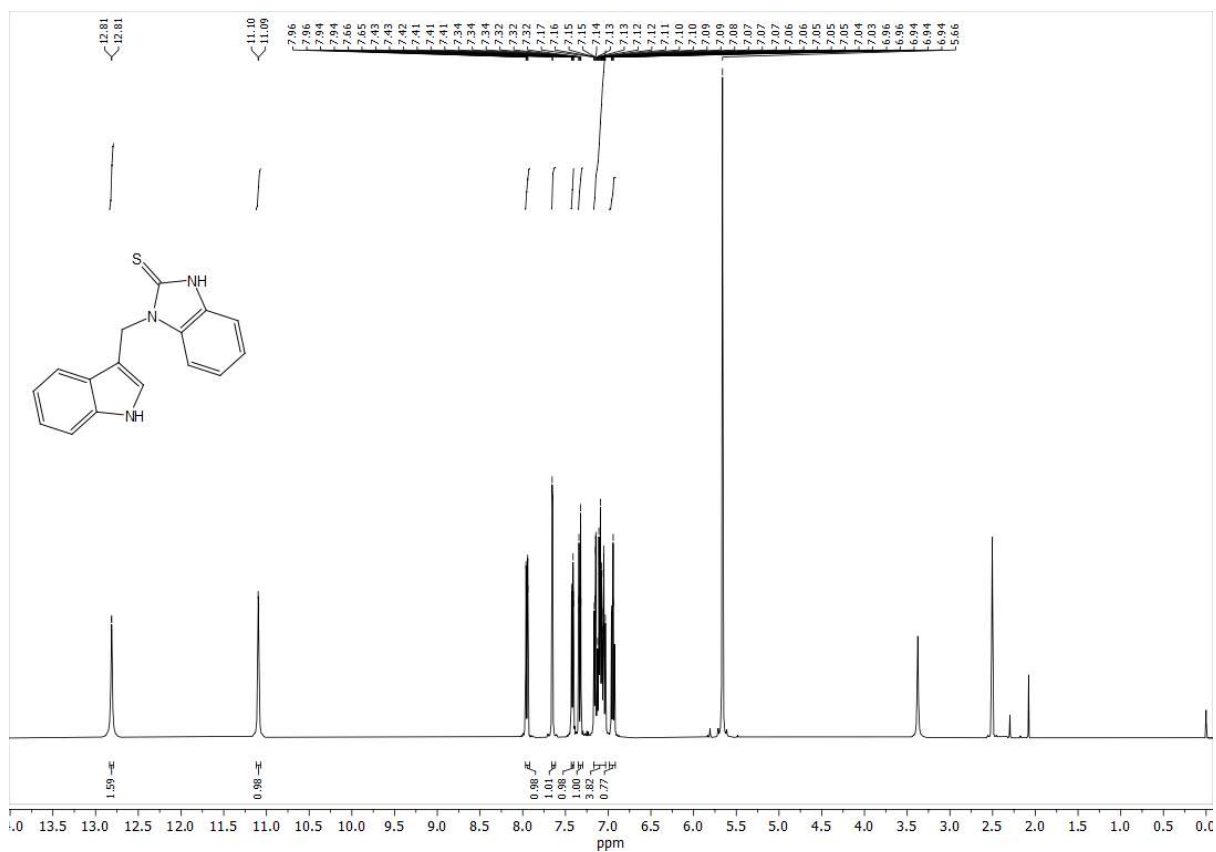
**Fig.S4b.**  $^{13}\text{C}$  NMR spectrum of compound **5**

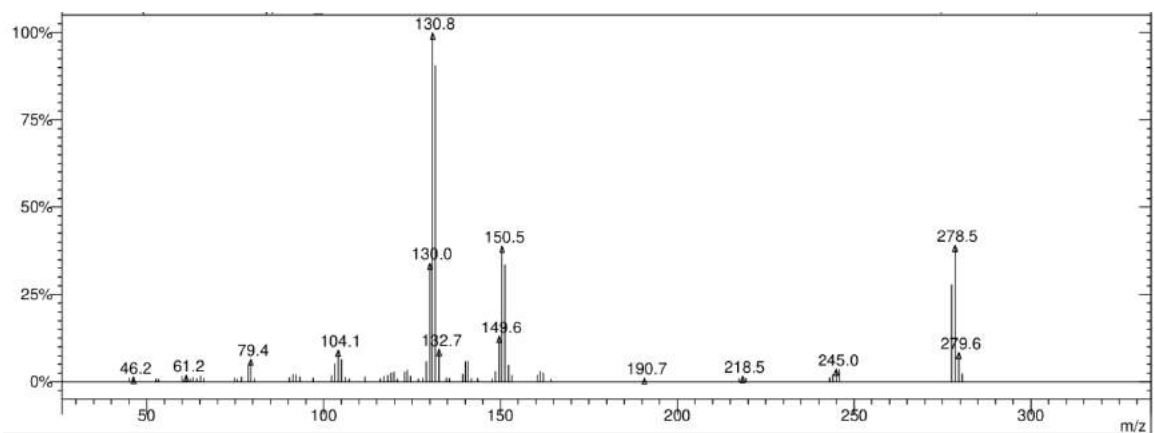


**Fig.S4c.** EI-MS spectrum of compound **5**

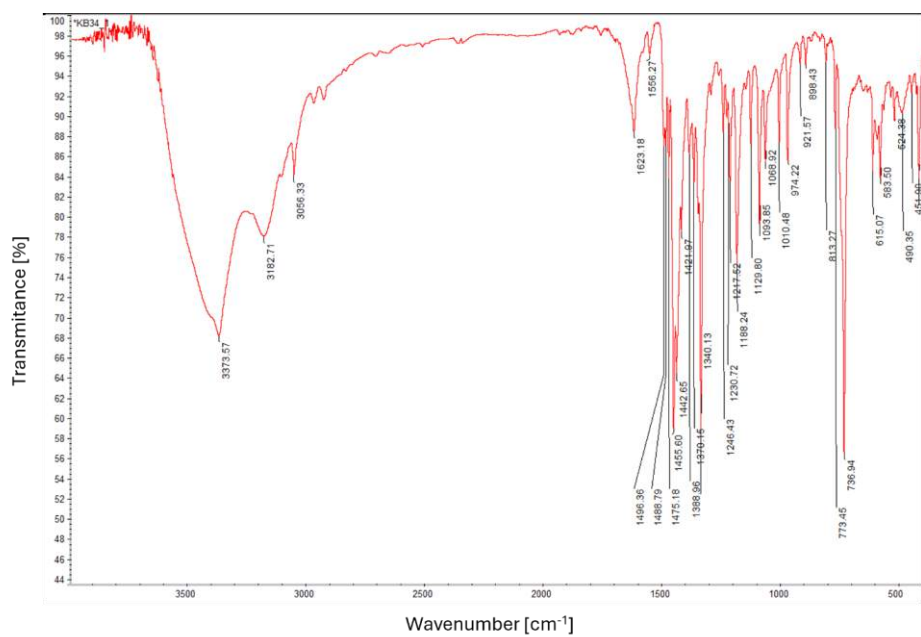


**Fig.S4d.** IR spectrum of compound **5**

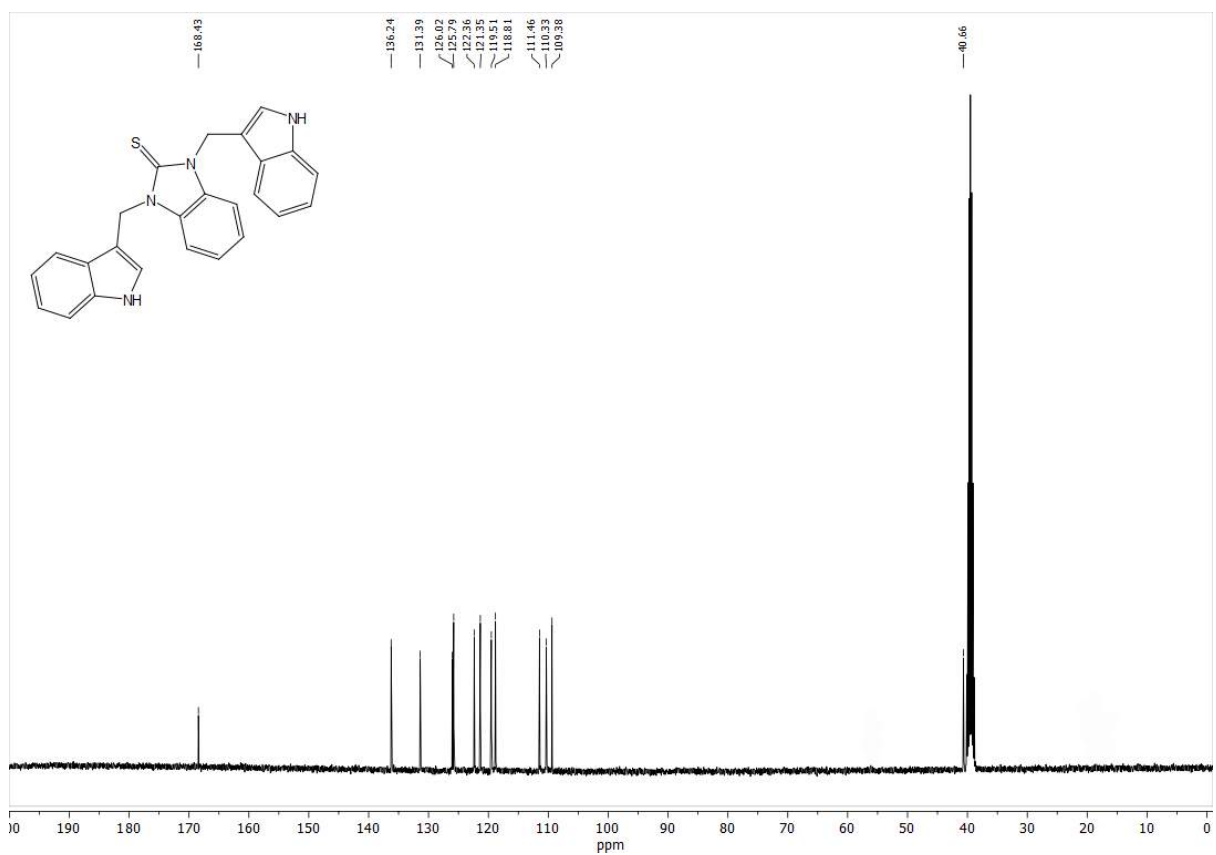
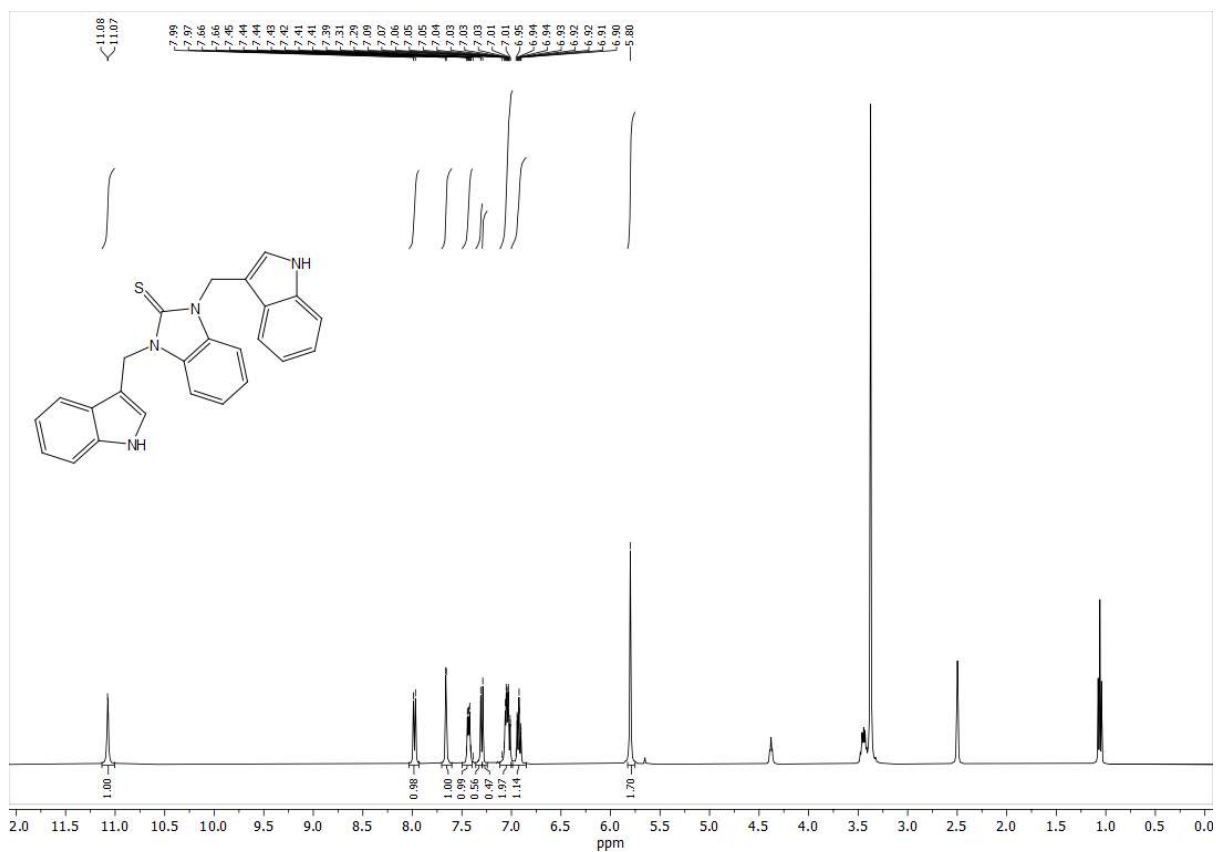


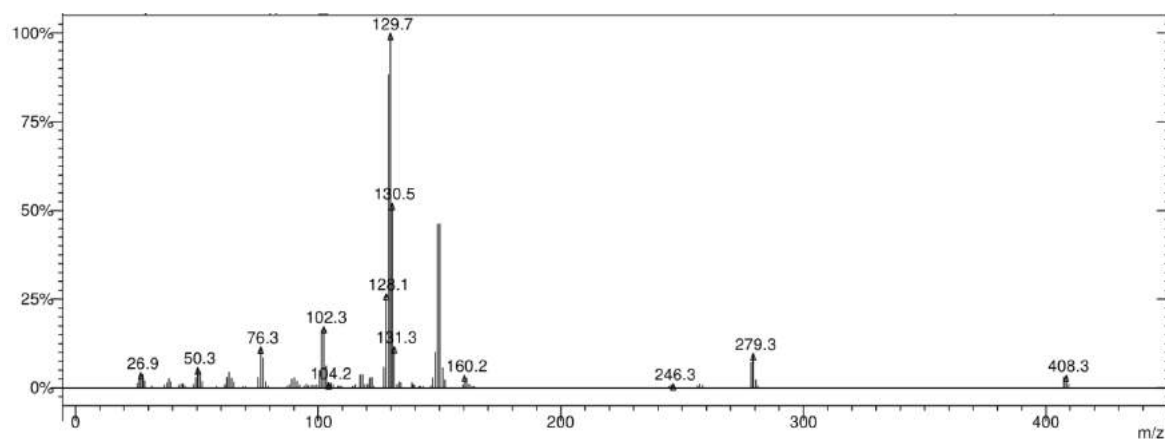


**Fig.S5c.** EI-MS spectrum of compound **6**

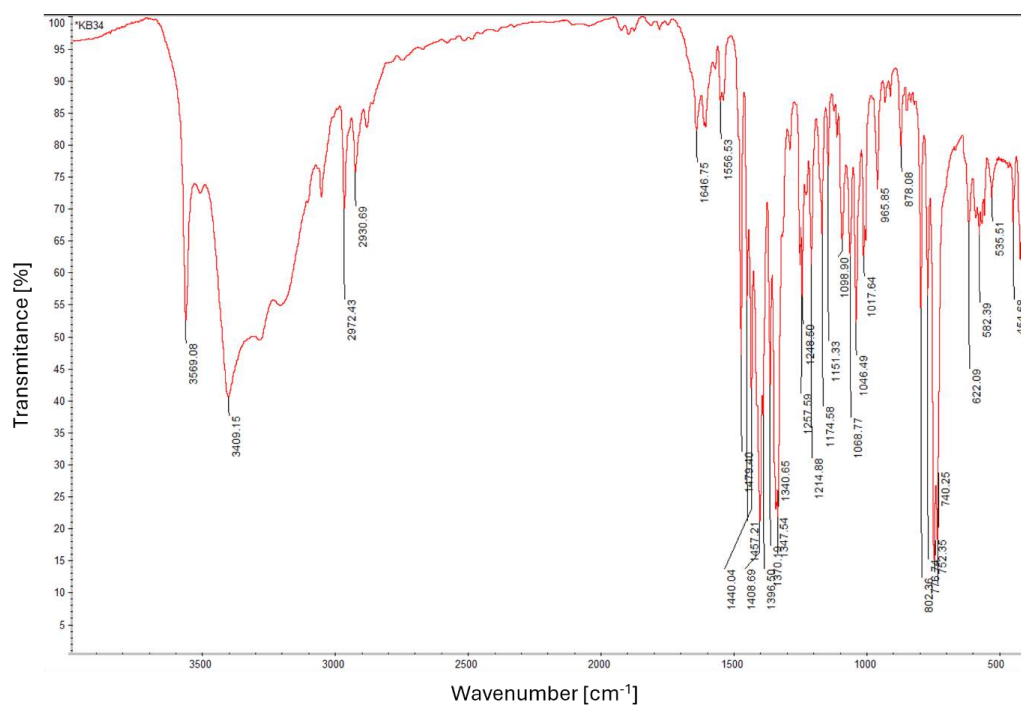


**Fig.S5d.** IR spectrum of compound **6**





**Fig.S6c.** EI-MS spectrum of compound **7**



**Fig.S6d.** IR spectrum of compound **7**

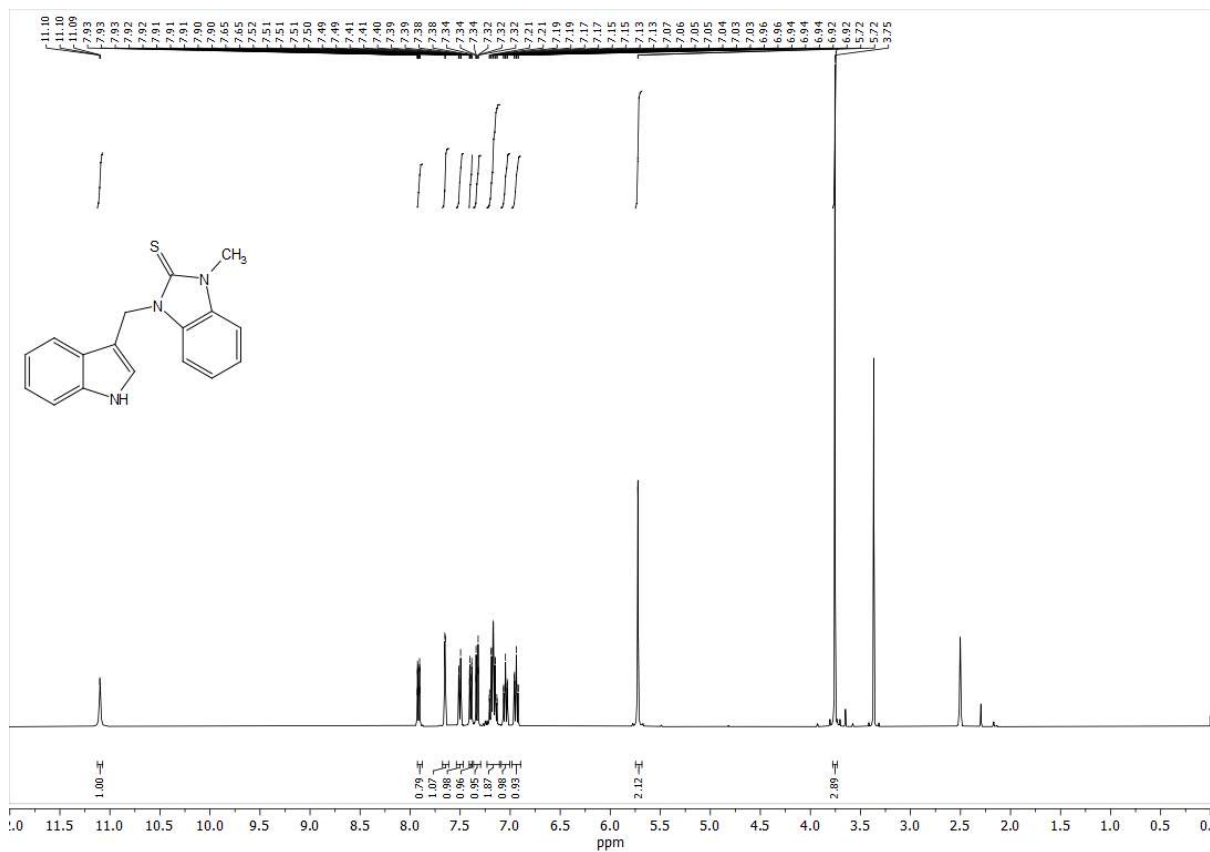


Fig.S7a. <sup>1</sup>H NMR spectrum of compound 8

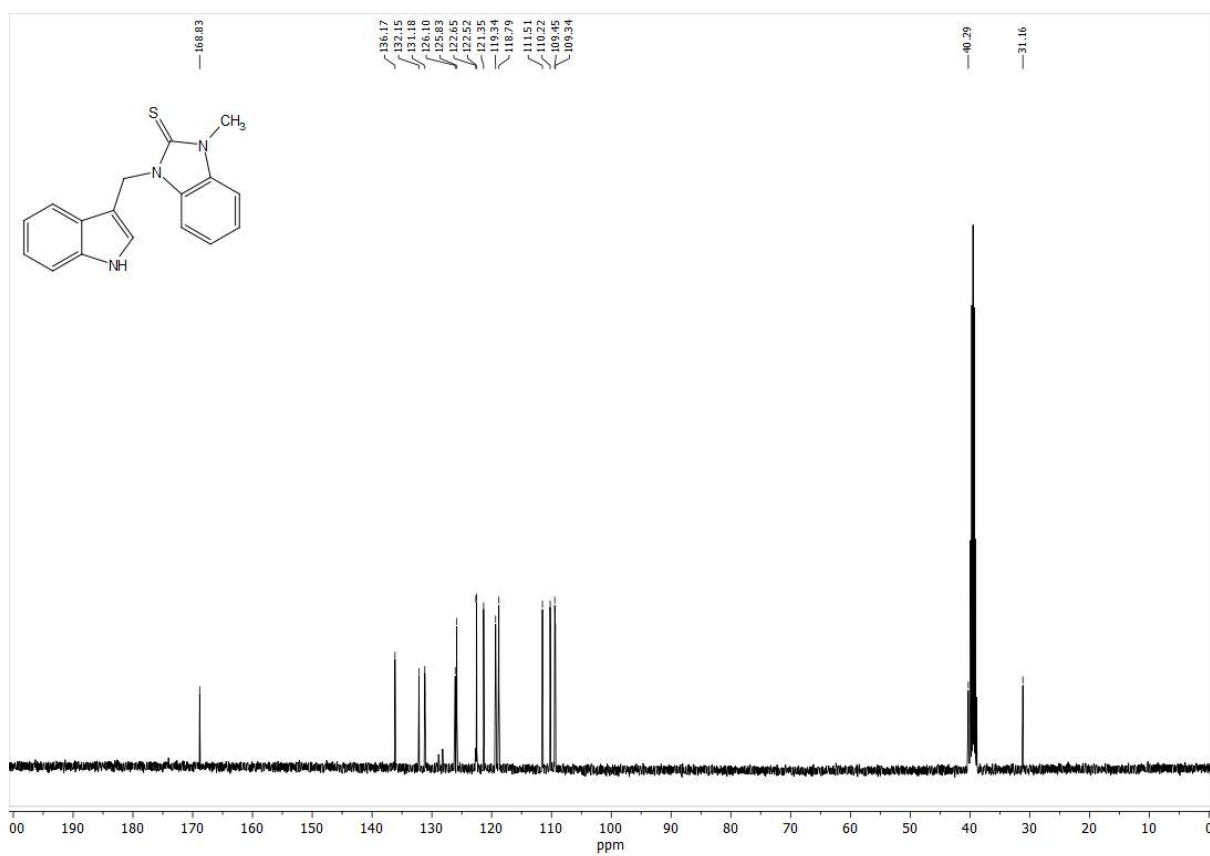
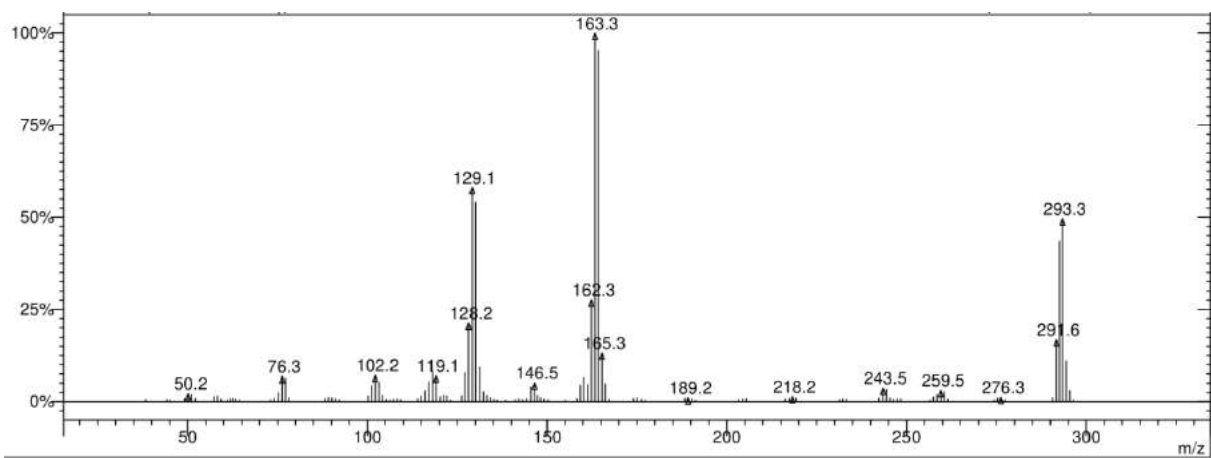
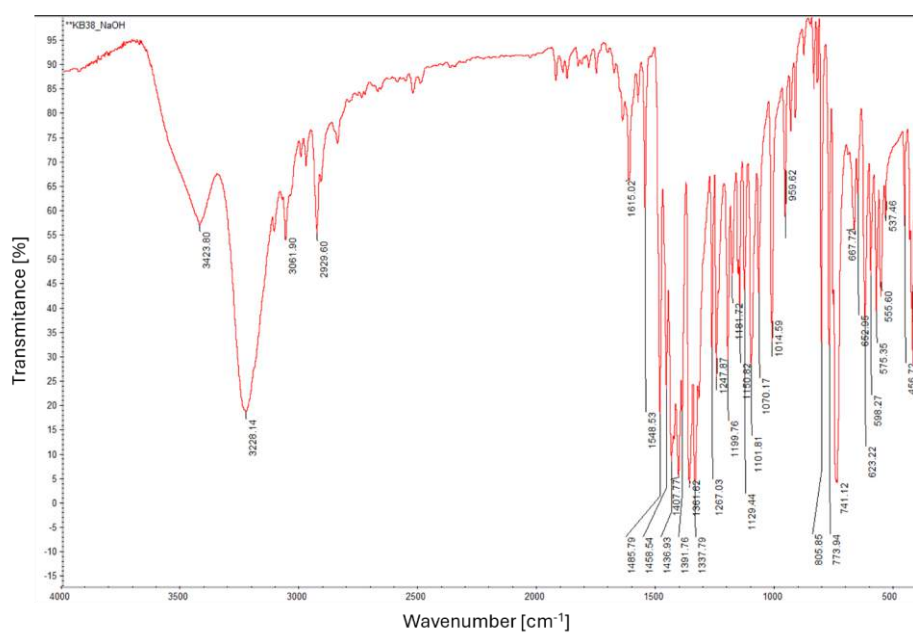


Fig.S7b. <sup>13</sup>C NMR spectrum of compound 8

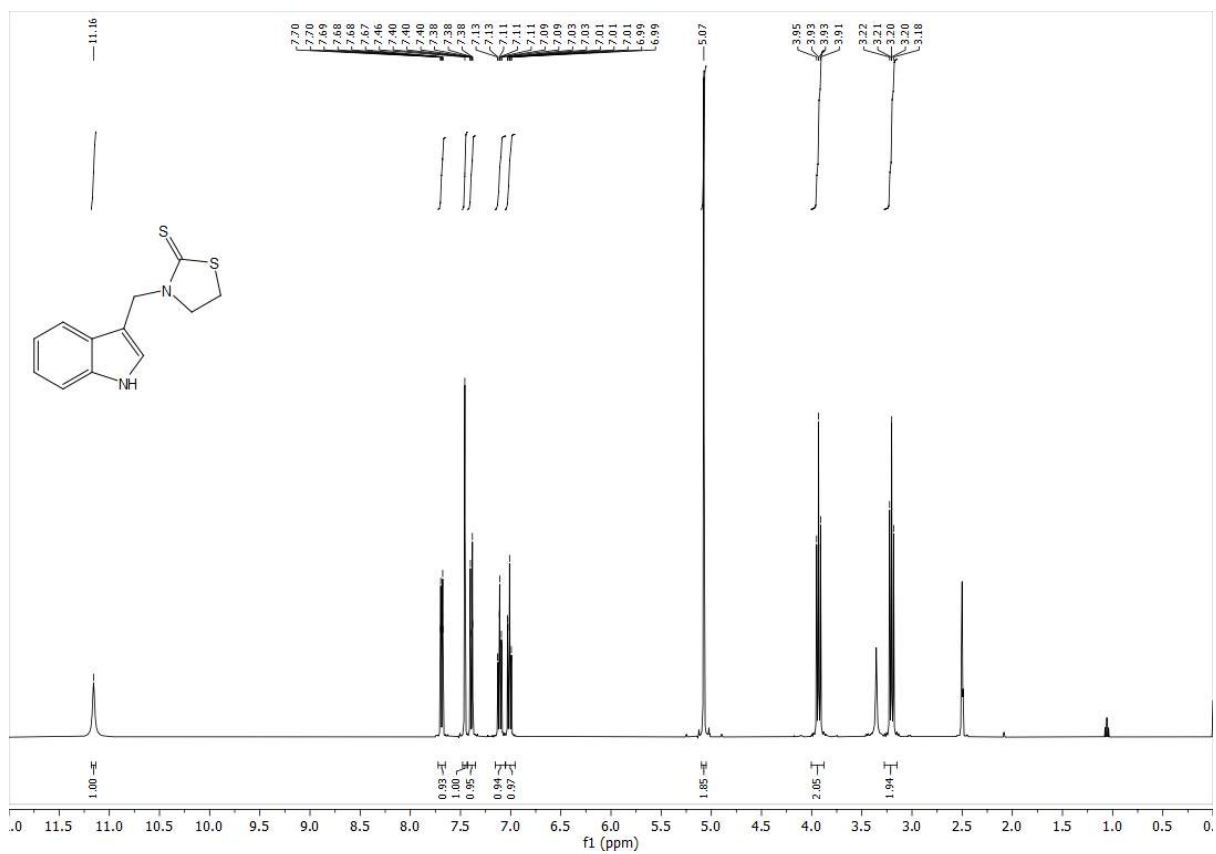




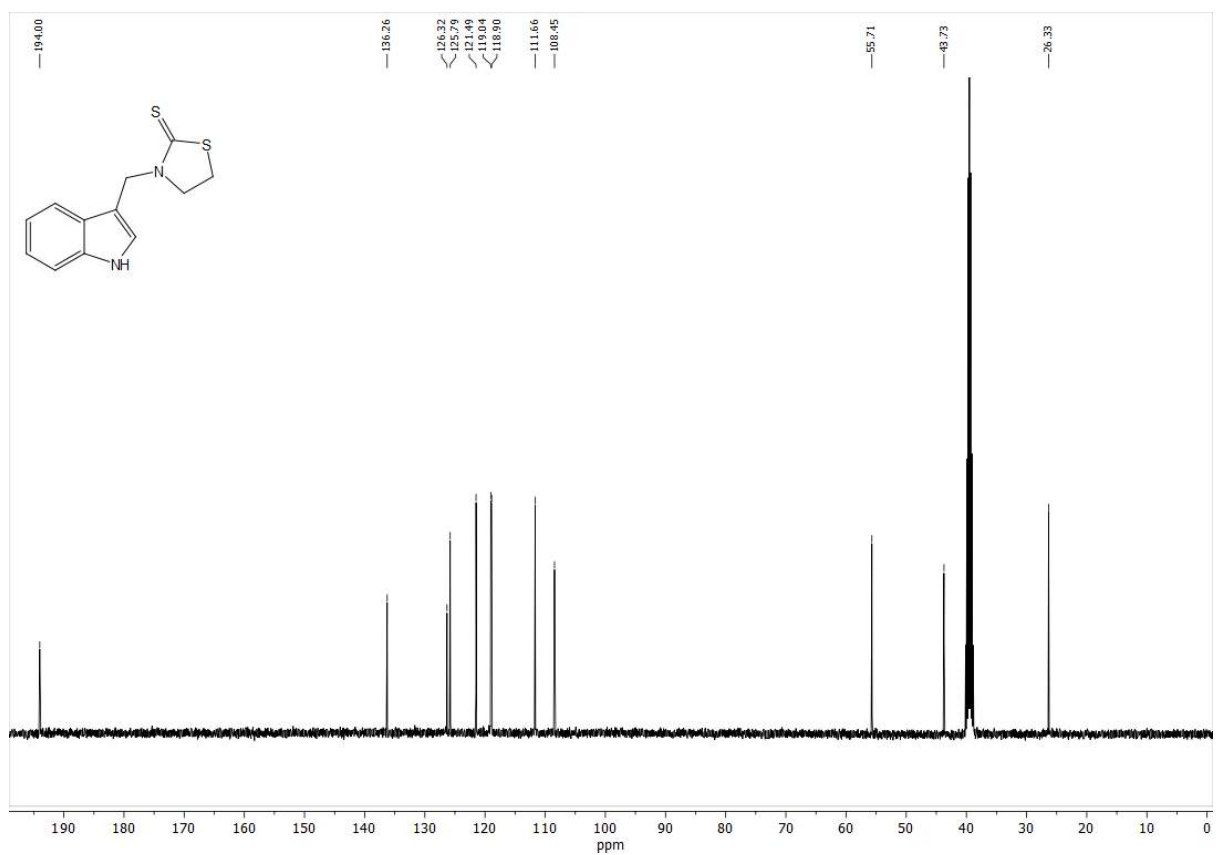
**Fig.S7c.** EI-MS spectrum of compound **8**



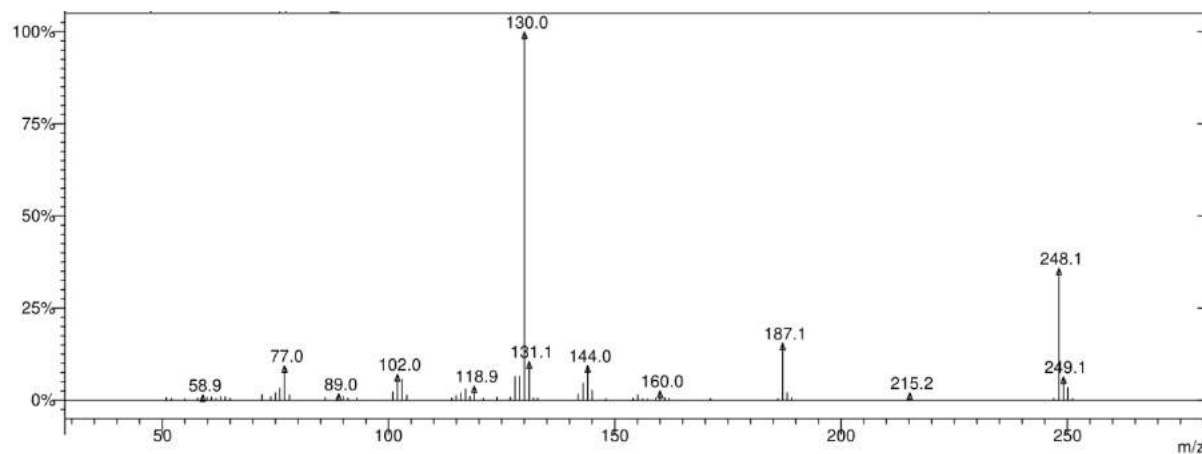
**Fig.S7d.** IR spectrum of compound **8**



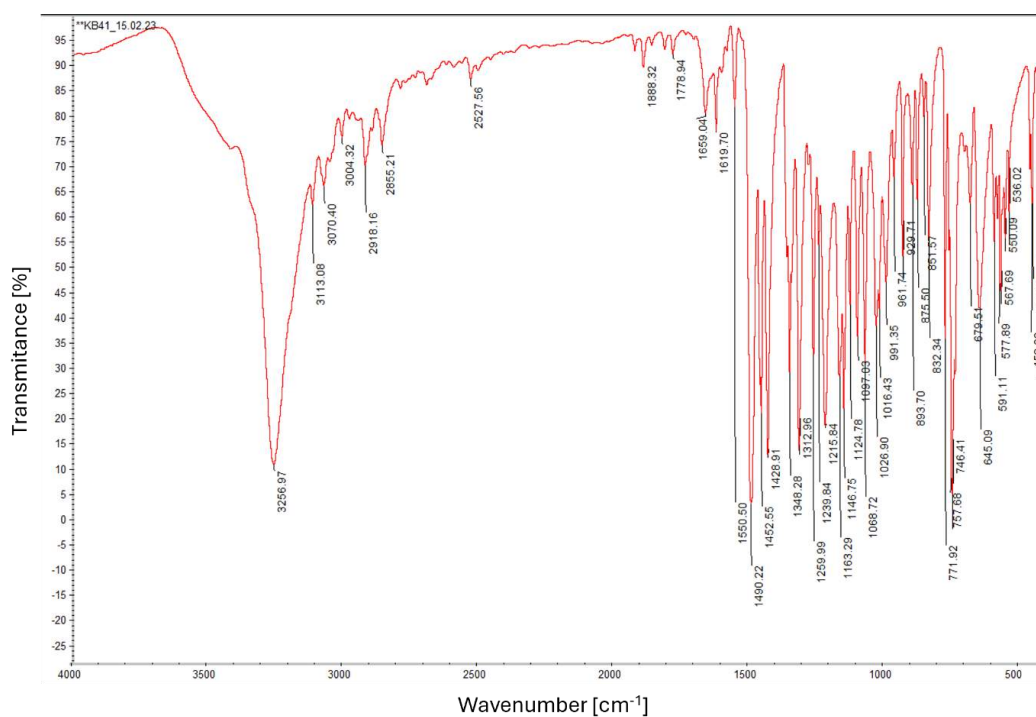
**Fig.S8a.**  $^1\text{H}$  NMR spectrum of compound **9**



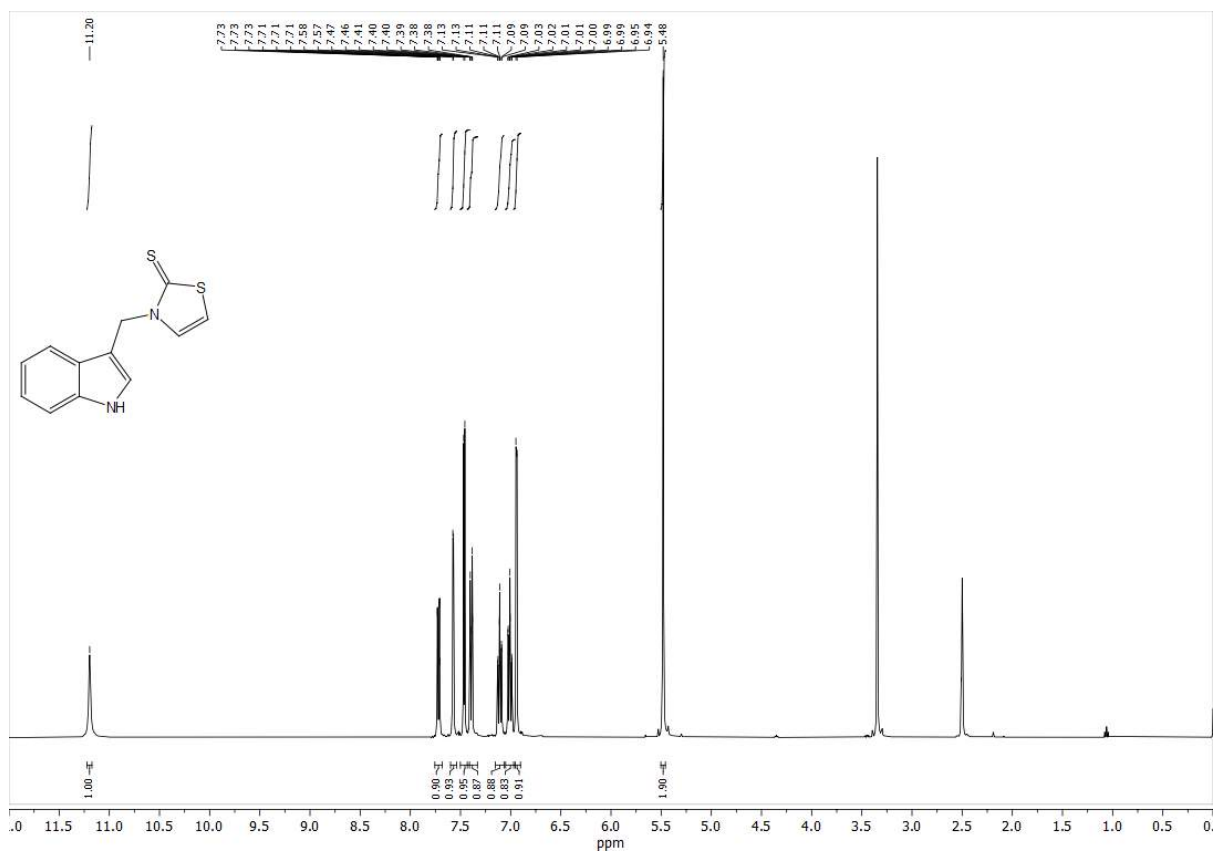
**Fig.S8b.**  $^{13}\text{C}$  NMR spectrum of compound **9**



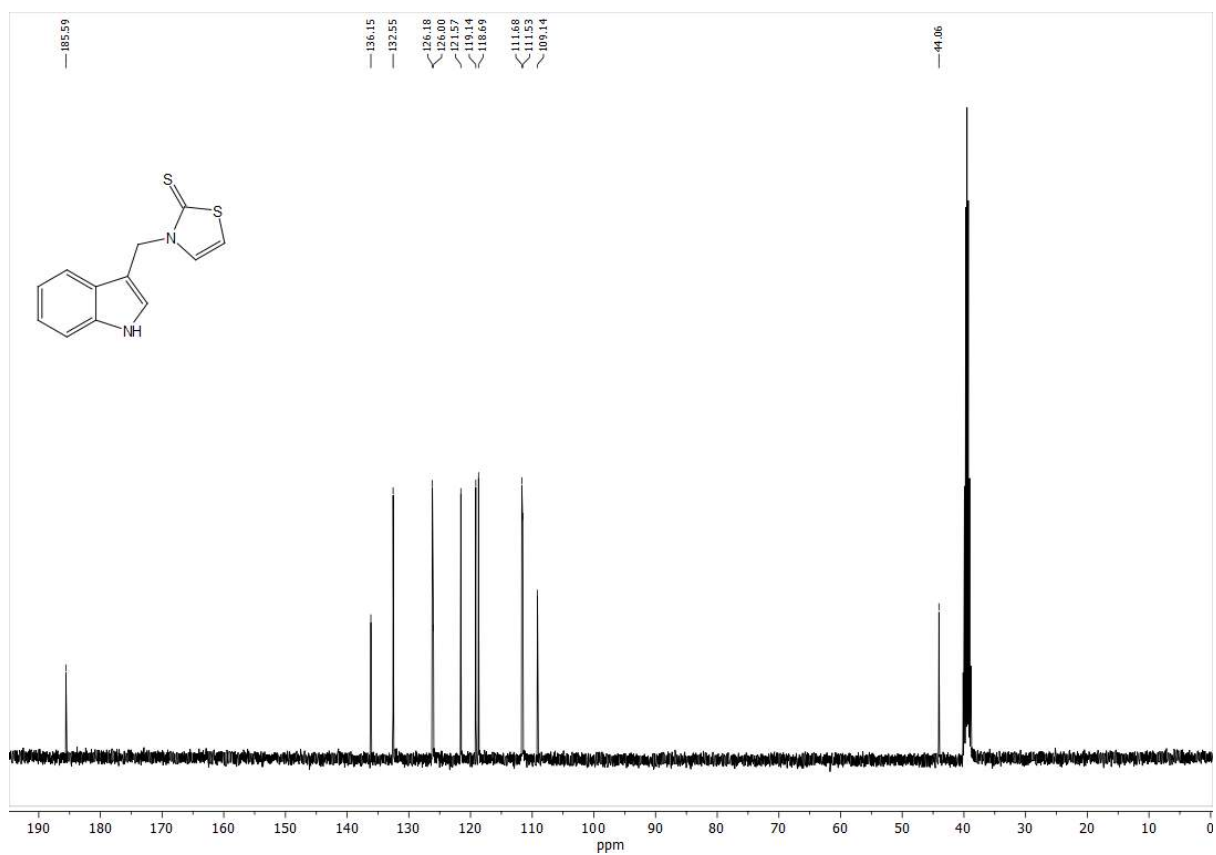
**Fig.S8c.** EI-MS spectrum of compound 9



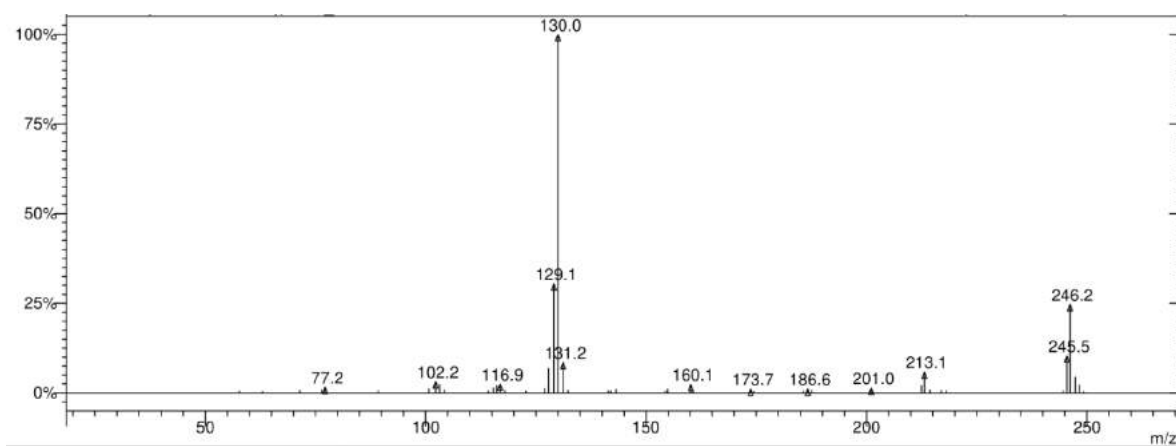
**Fig.S8d.** IR spectrum of compound 9



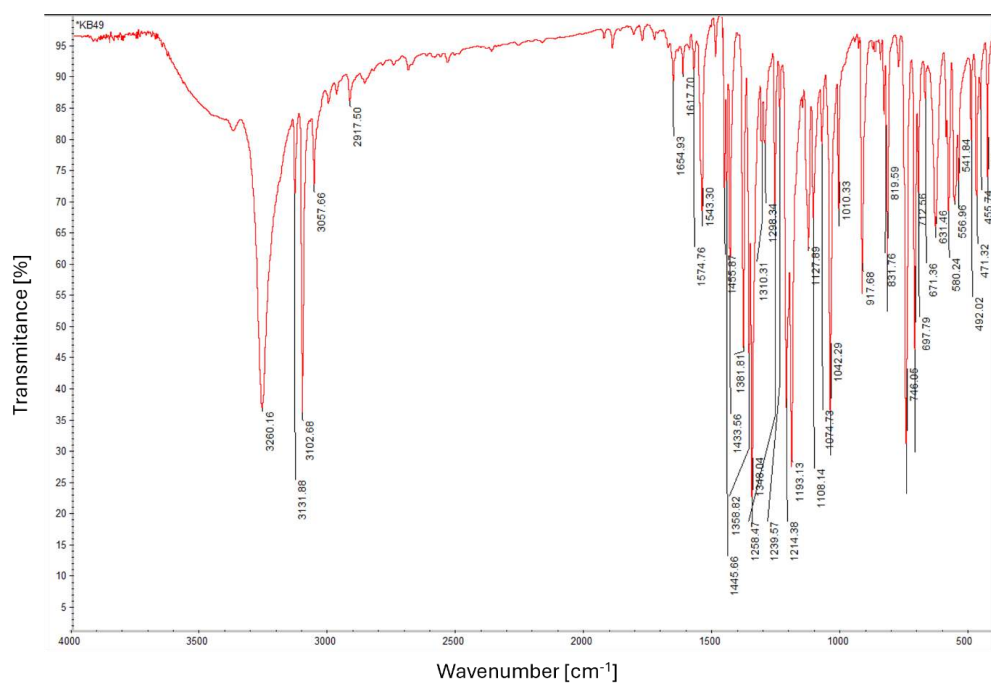
**Fig.S9a.**  $^1\text{H}$  NMR spectrum of compound 10



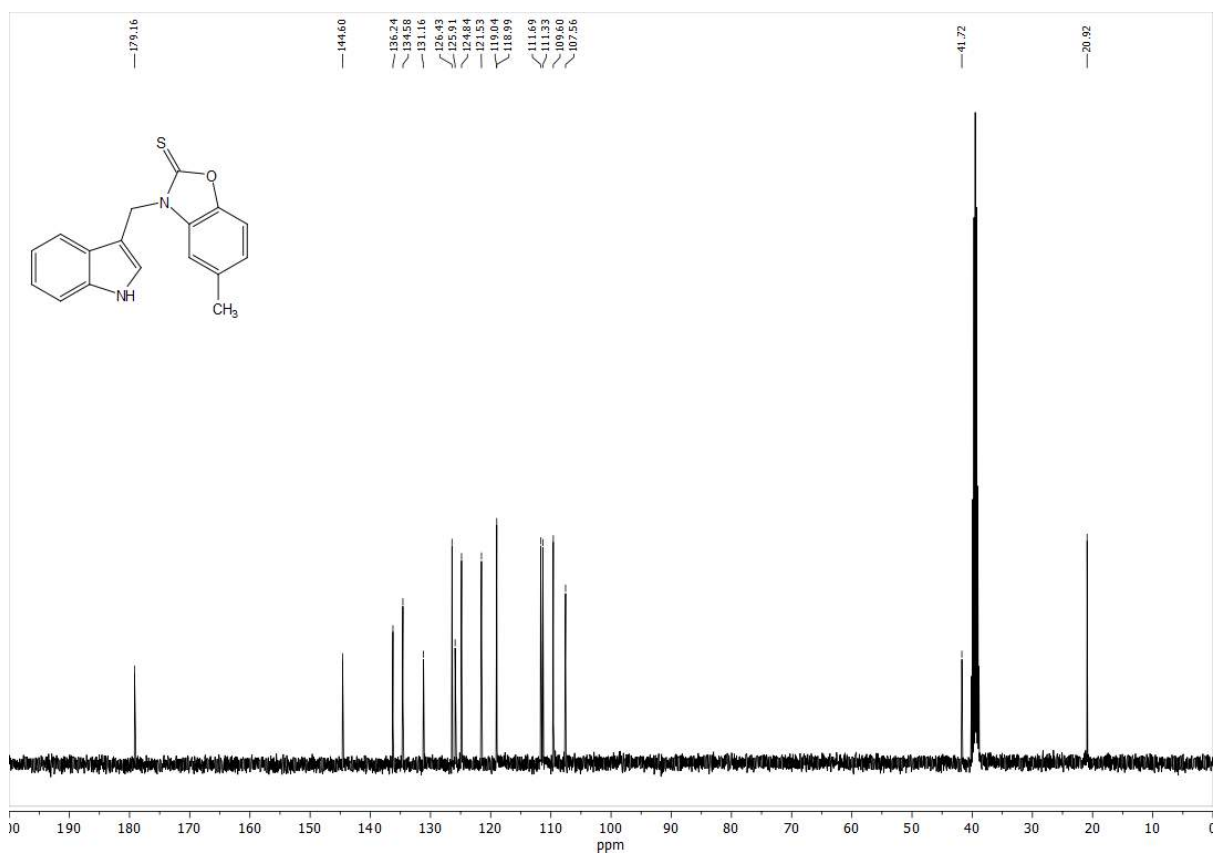
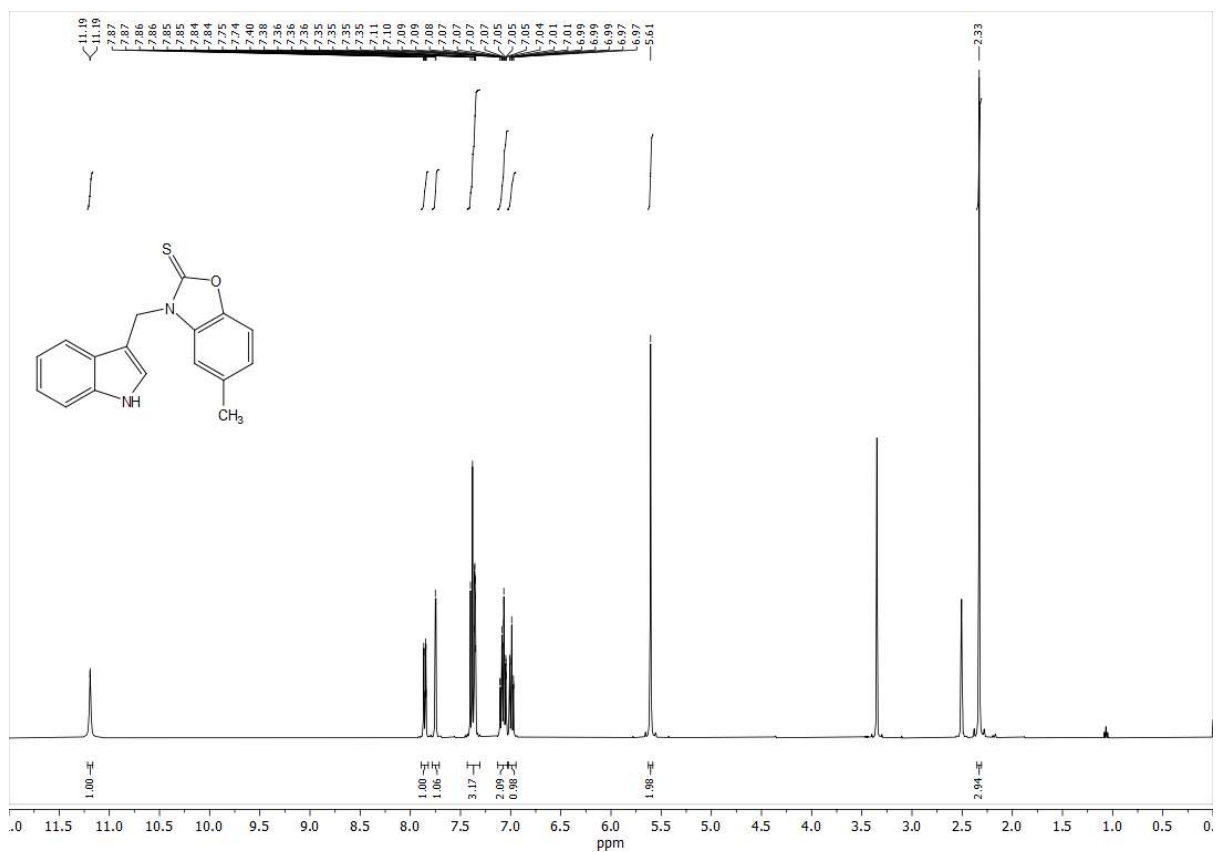
**Fig.S9b.**  $^{13}\text{C}$  NMR spectrum of compound 10

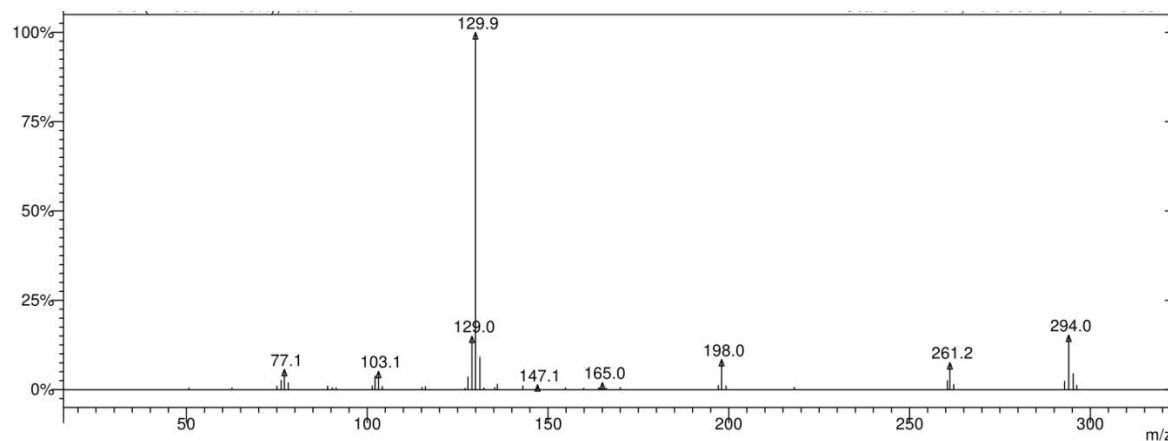


**Fig.S9c.** EI-MS spectrum of compound **10**

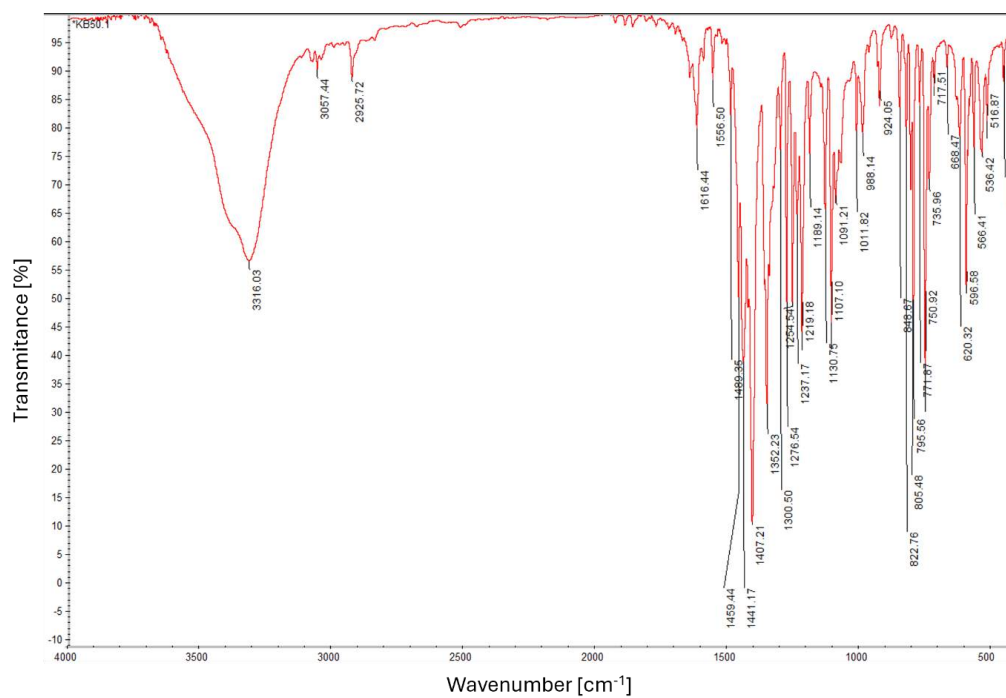


**Fig.S9d.** IR spectrum of compound **10**

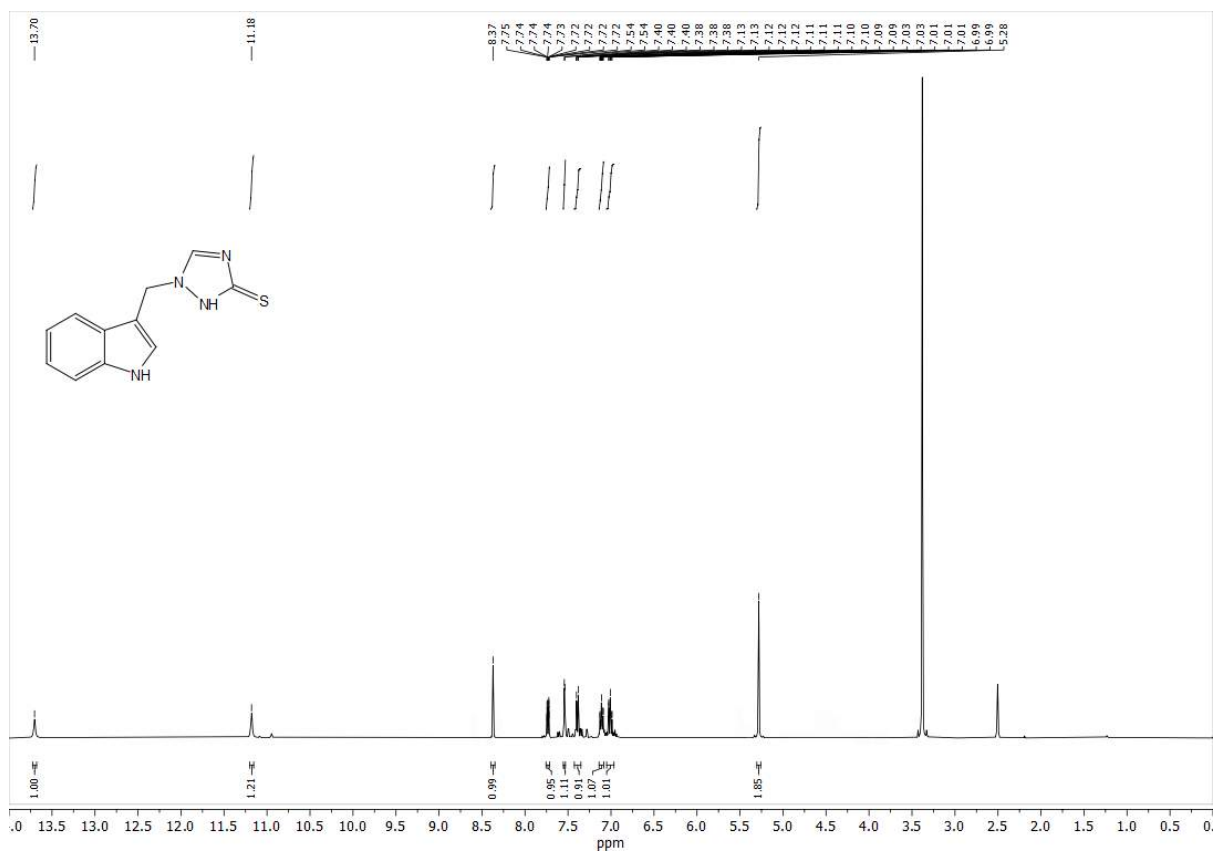




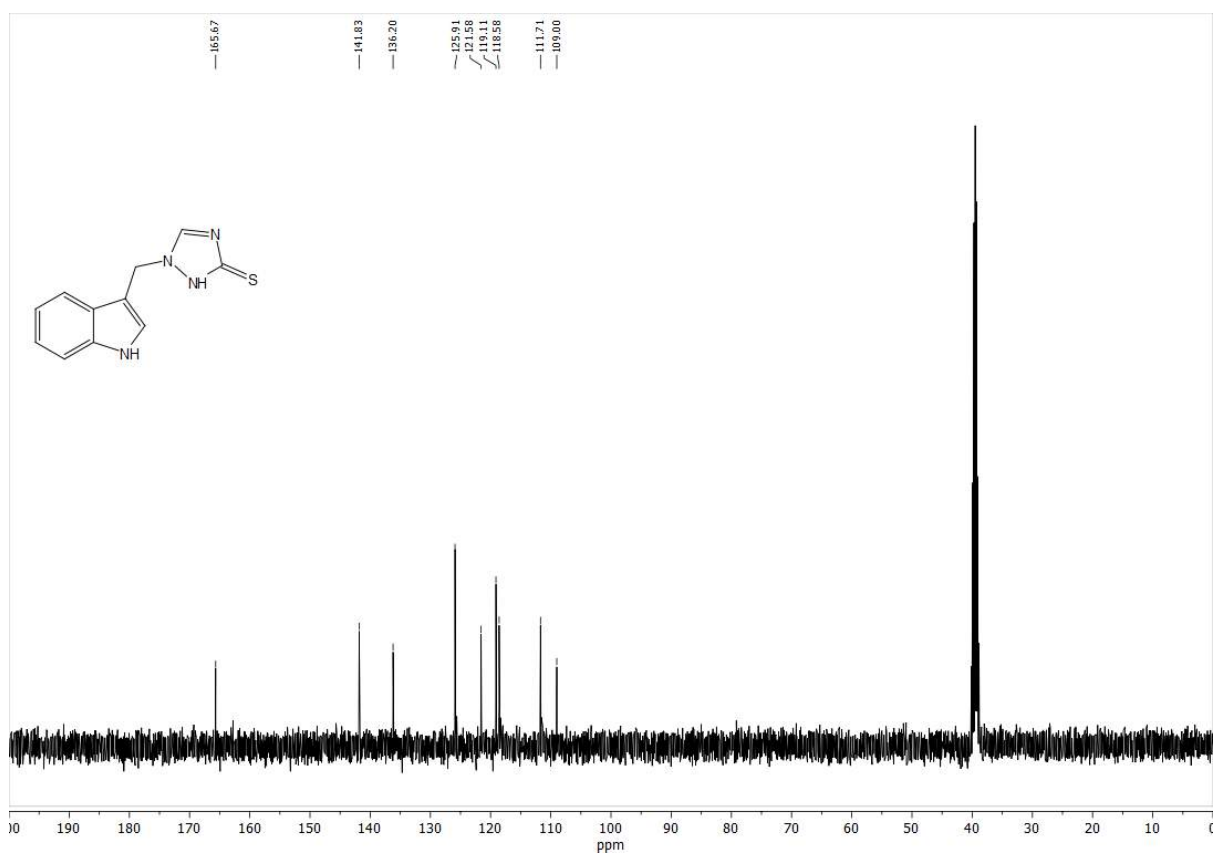
**Fig.S10c.** EI-MS spectrum of compound **11**



**Fig.S10d.** IR spectrum of compound **11**

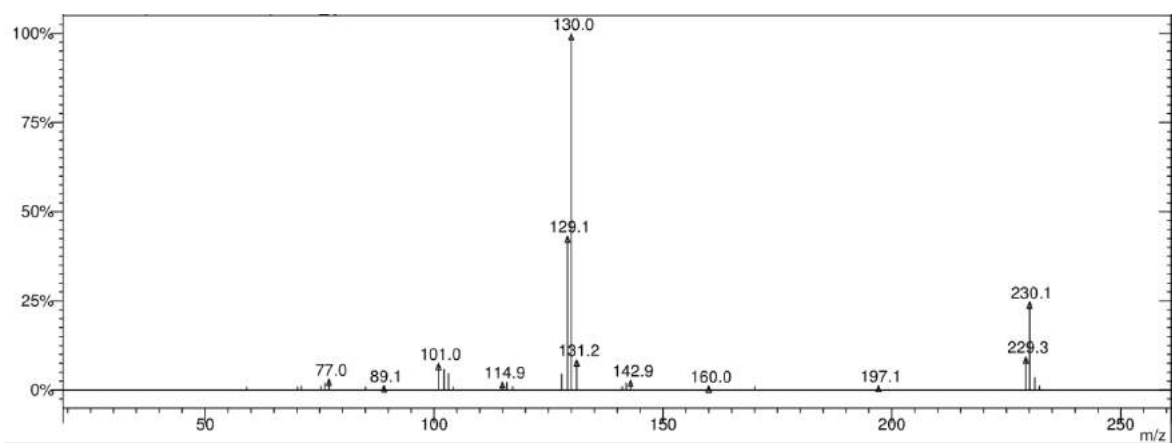


**Fig.S11a.**  $^1\text{H}$  NMR spectrum of compound 12

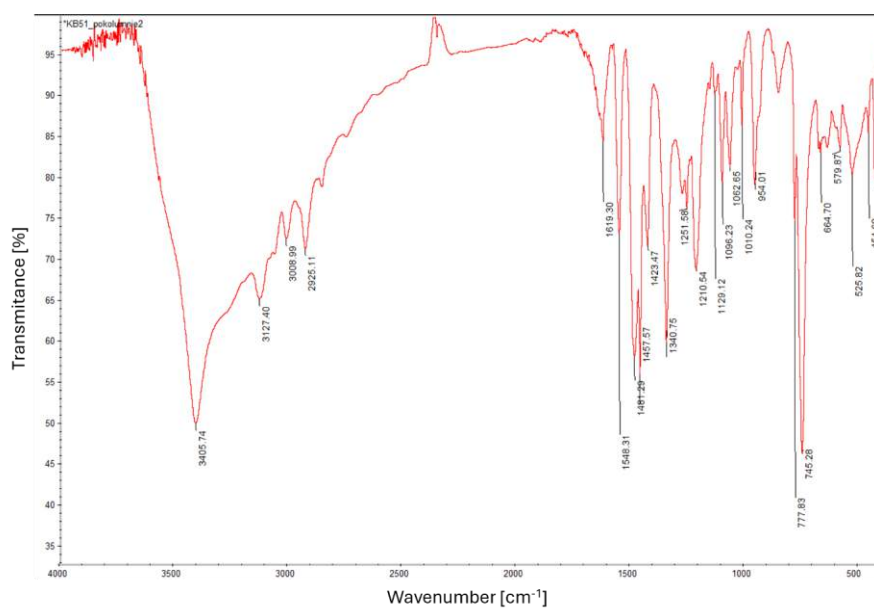


**Fig.S11b.**  $^{13}\text{C}$  NMR spectrum of compound 12





**Fig.S11c.** EI-MS spectrum of compound **12**



**Fig.S11d.** IR spectrum of compound **12**

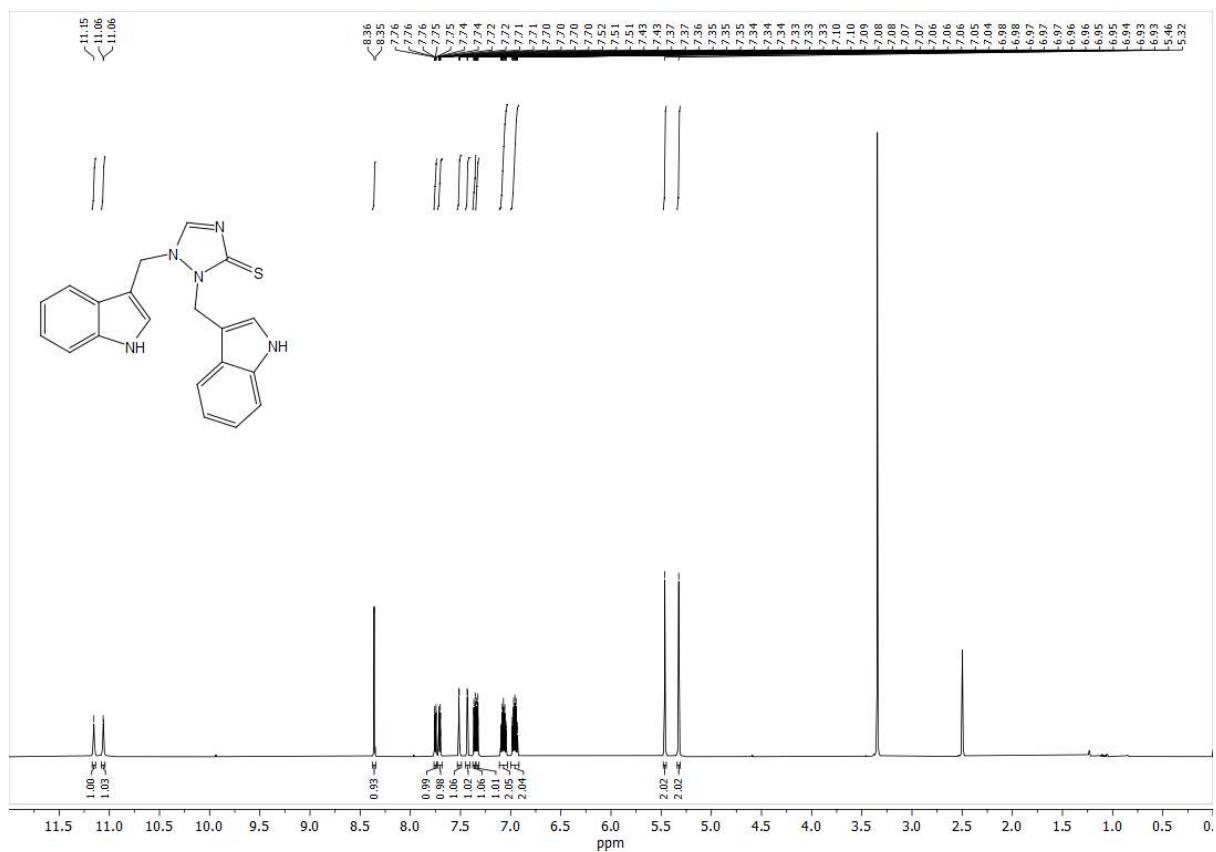


Fig.S12a. <sup>1</sup>H NMR spectrum of compound 13

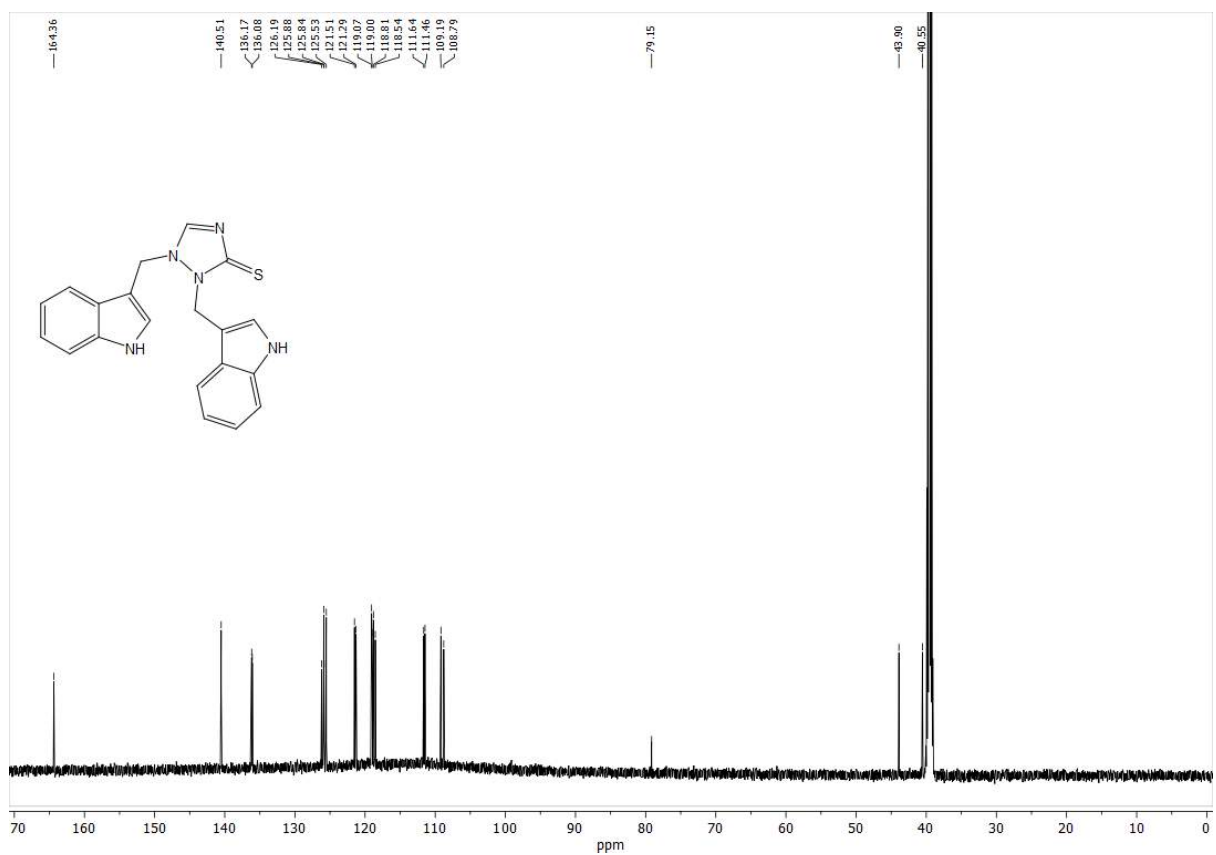
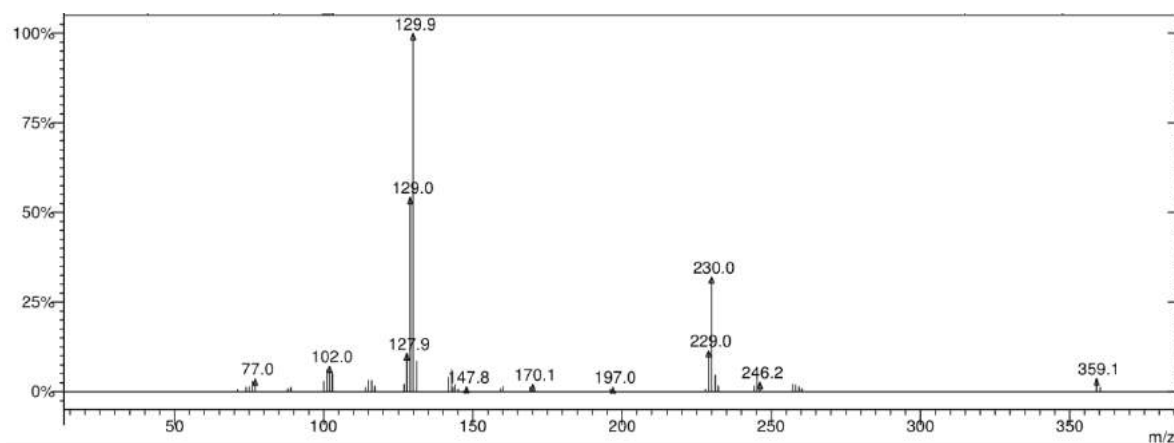
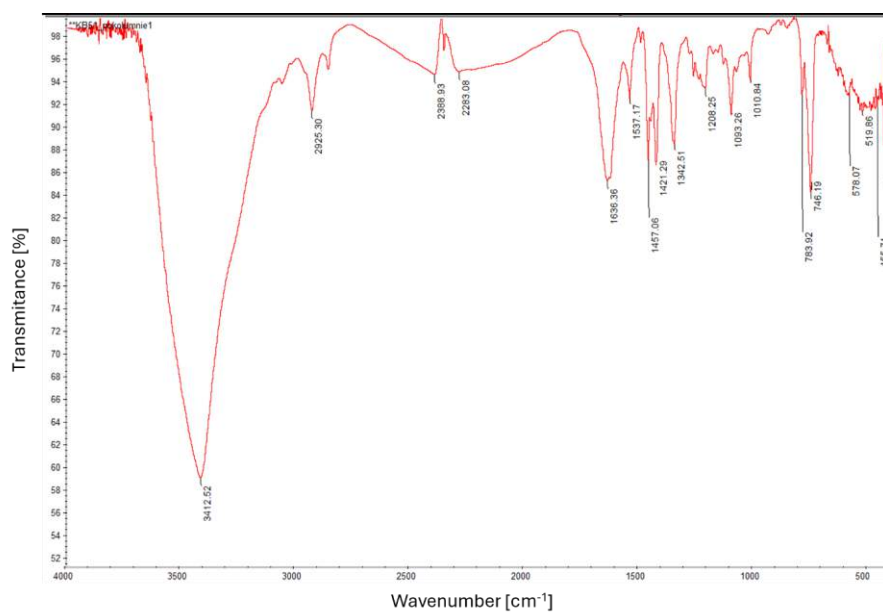


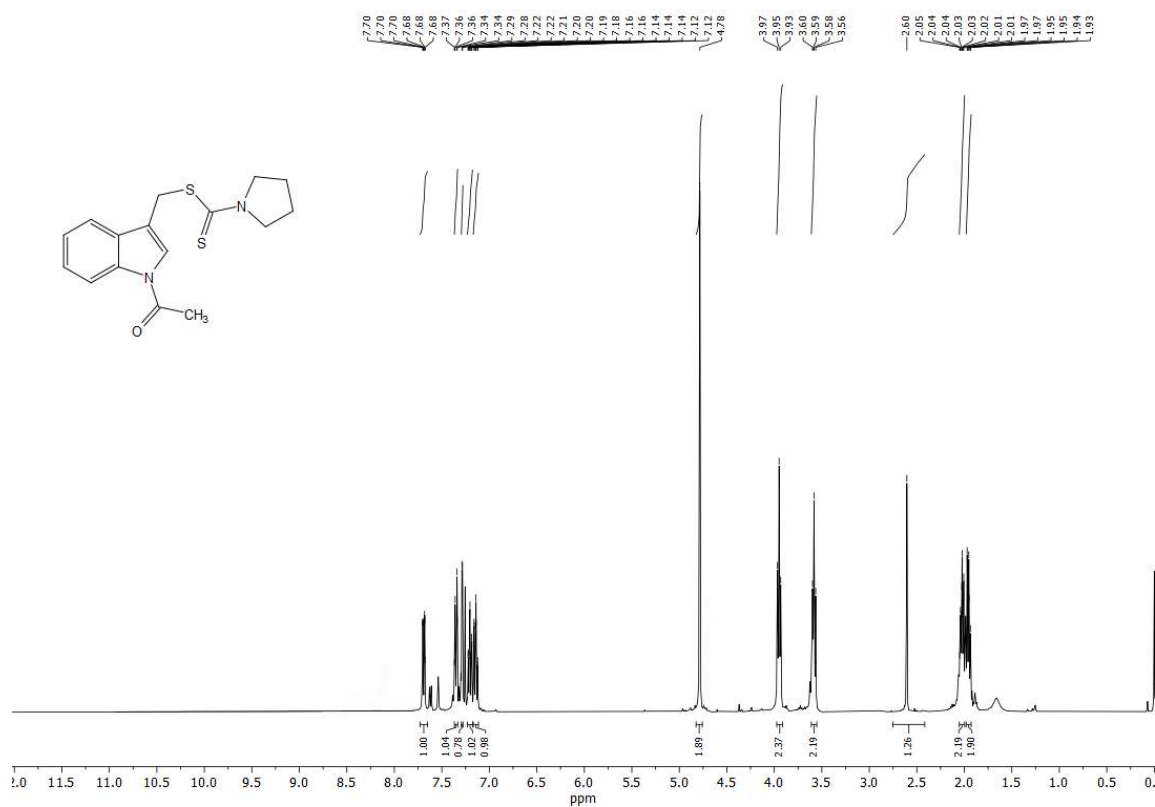
Fig.S12b. <sup>13</sup>C NMR spectrum of compound 13



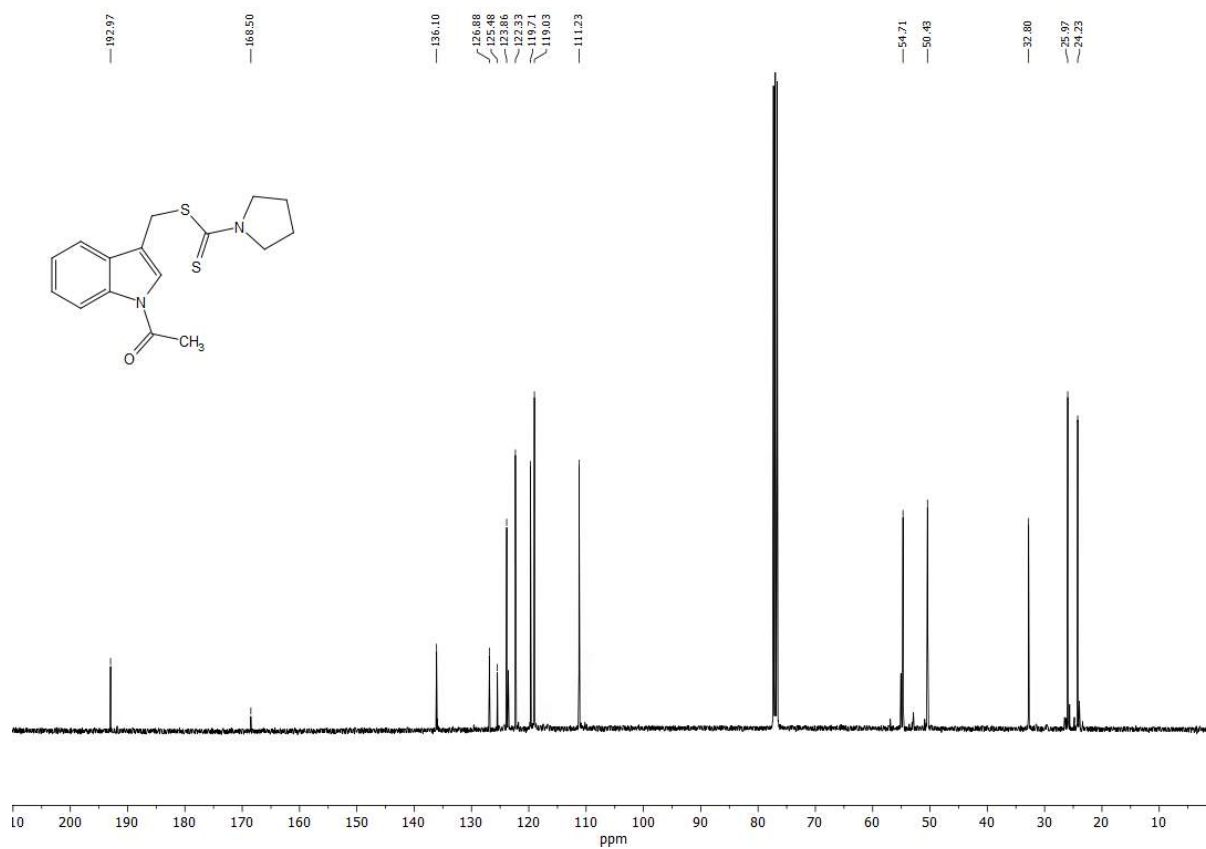
**Fig.S12c.** EI-MS spectrum of compound **13**



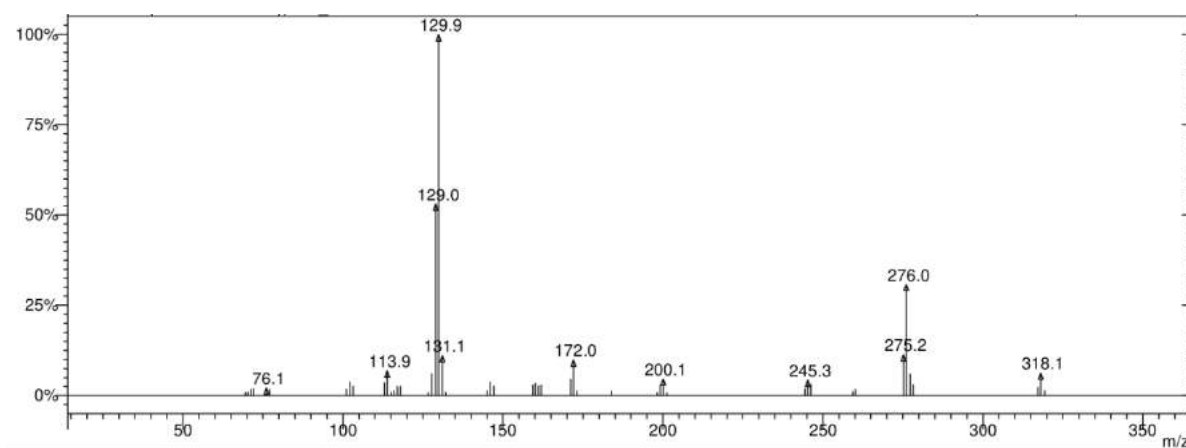
**Fig.S12d.** IR spectrum of compound **13**



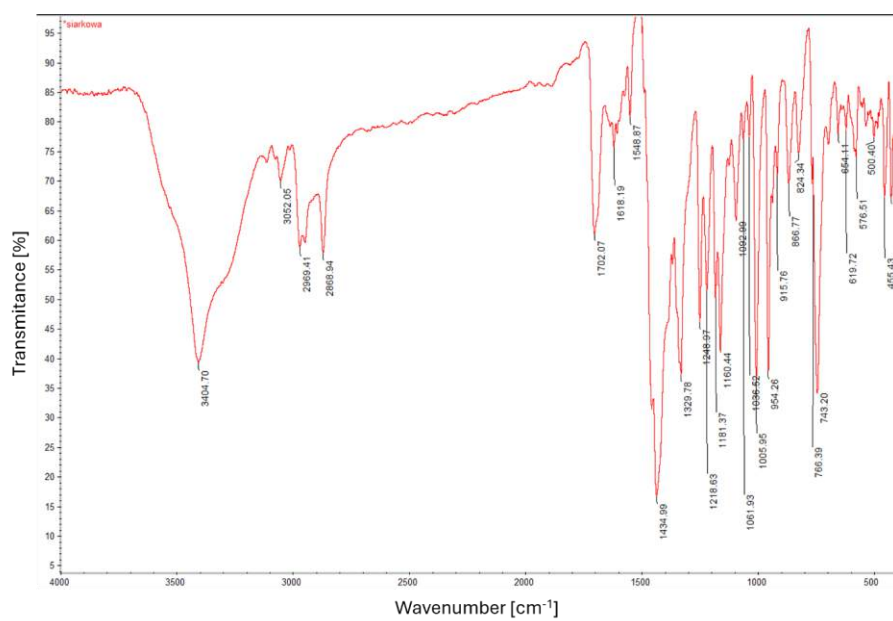
**Fig.S13a.** <sup>1</sup>H NMR spectrum of compound 15



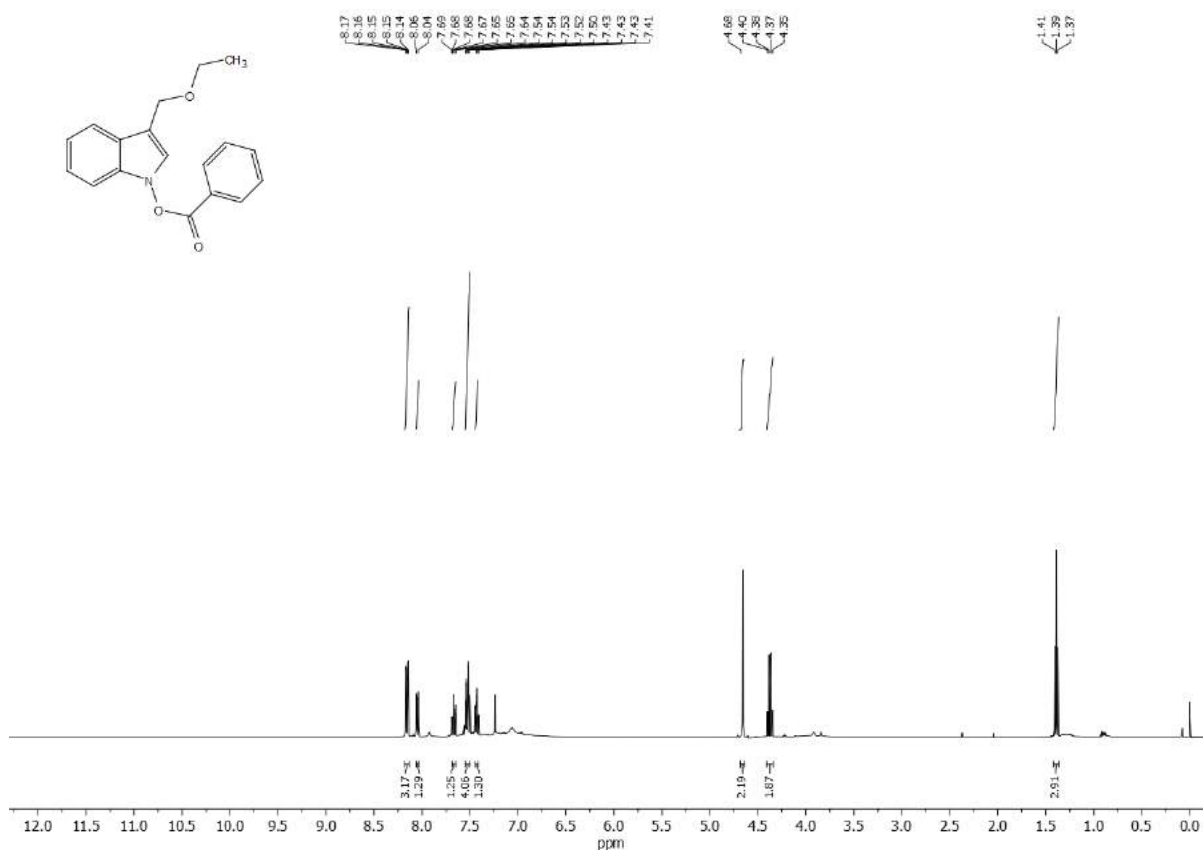
**Fig.S13b.** <sup>13</sup>C NMR spectrum of compound 15



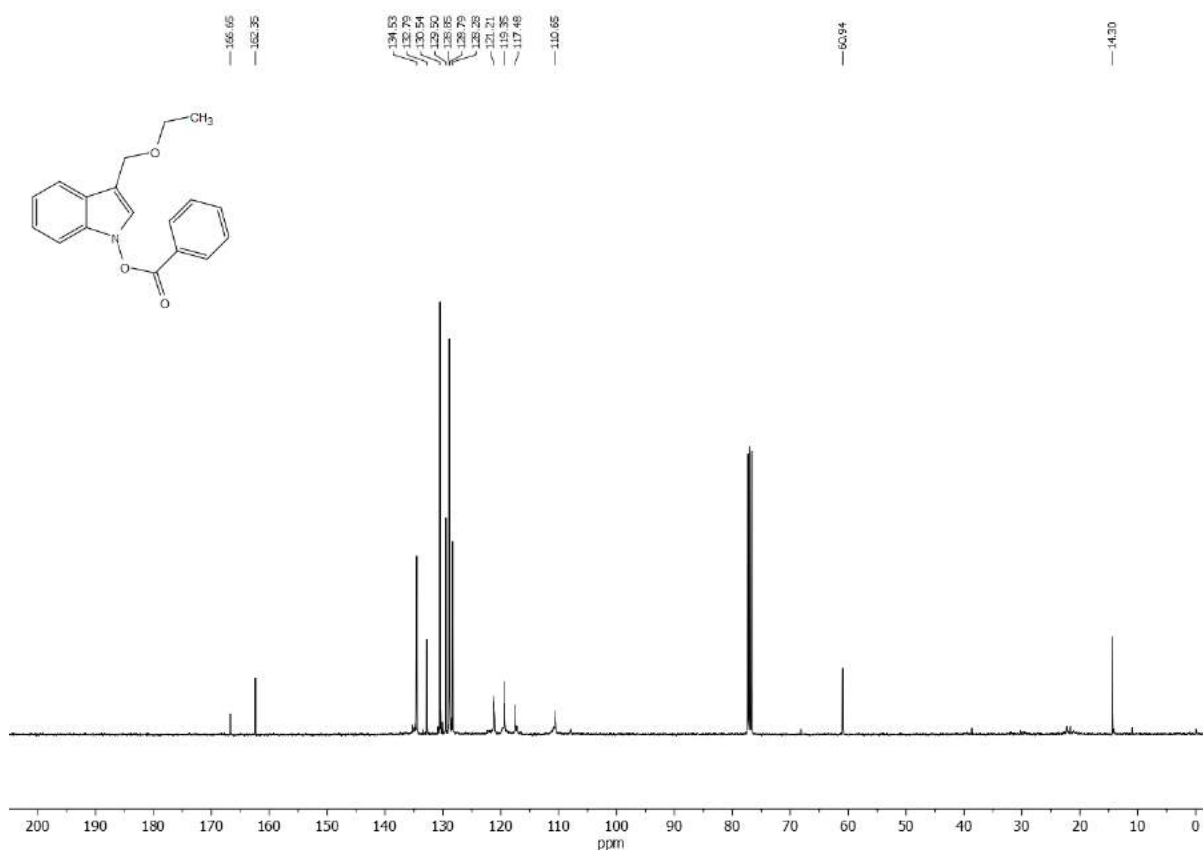
**Fig.S13c.** EI-MS spectrum of compound **15**



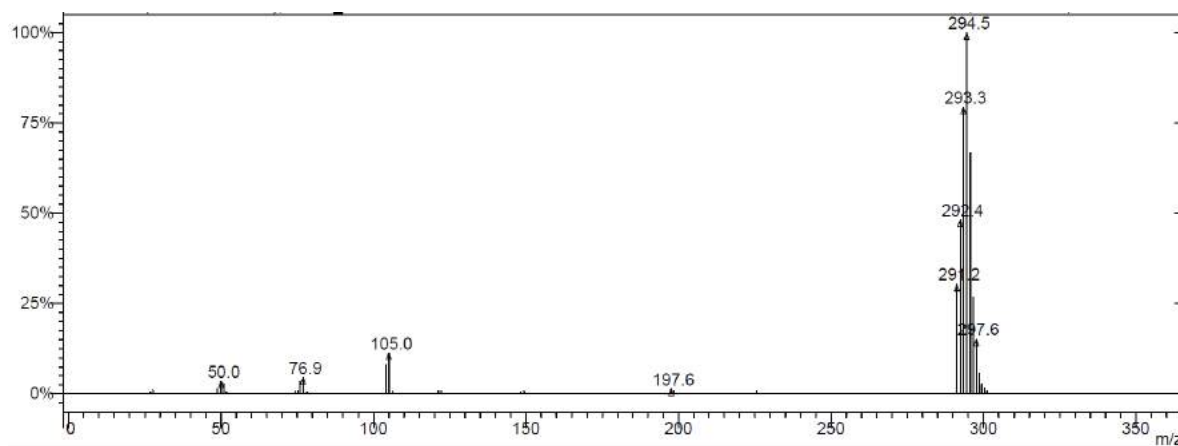
**Fig.S13d.** FT-IR spectrum of compound **15**



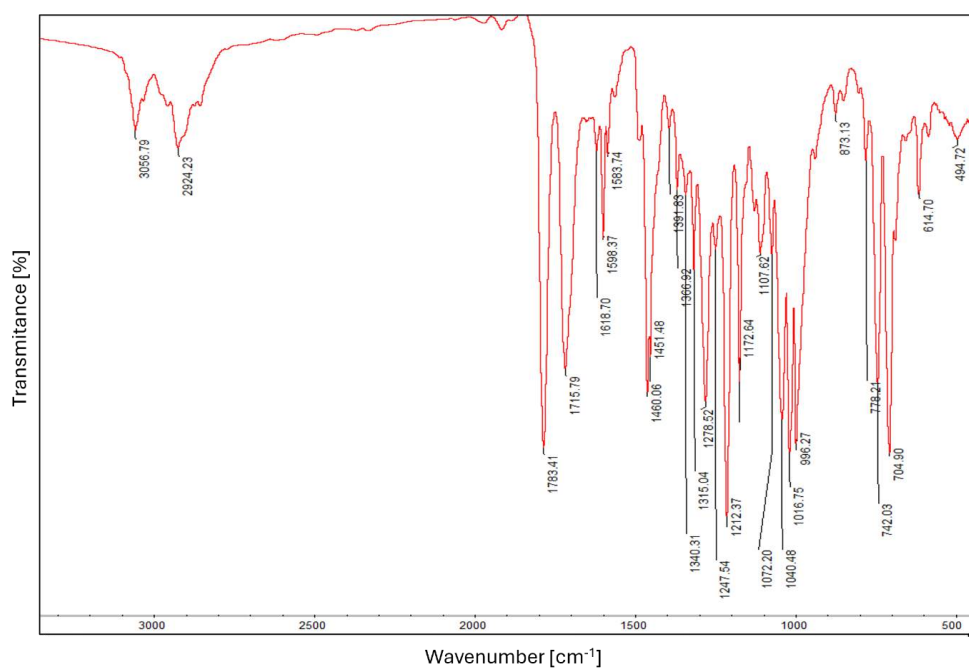
**Fig.S14a.** <sup>1</sup>H NMR spectrum of compound 17



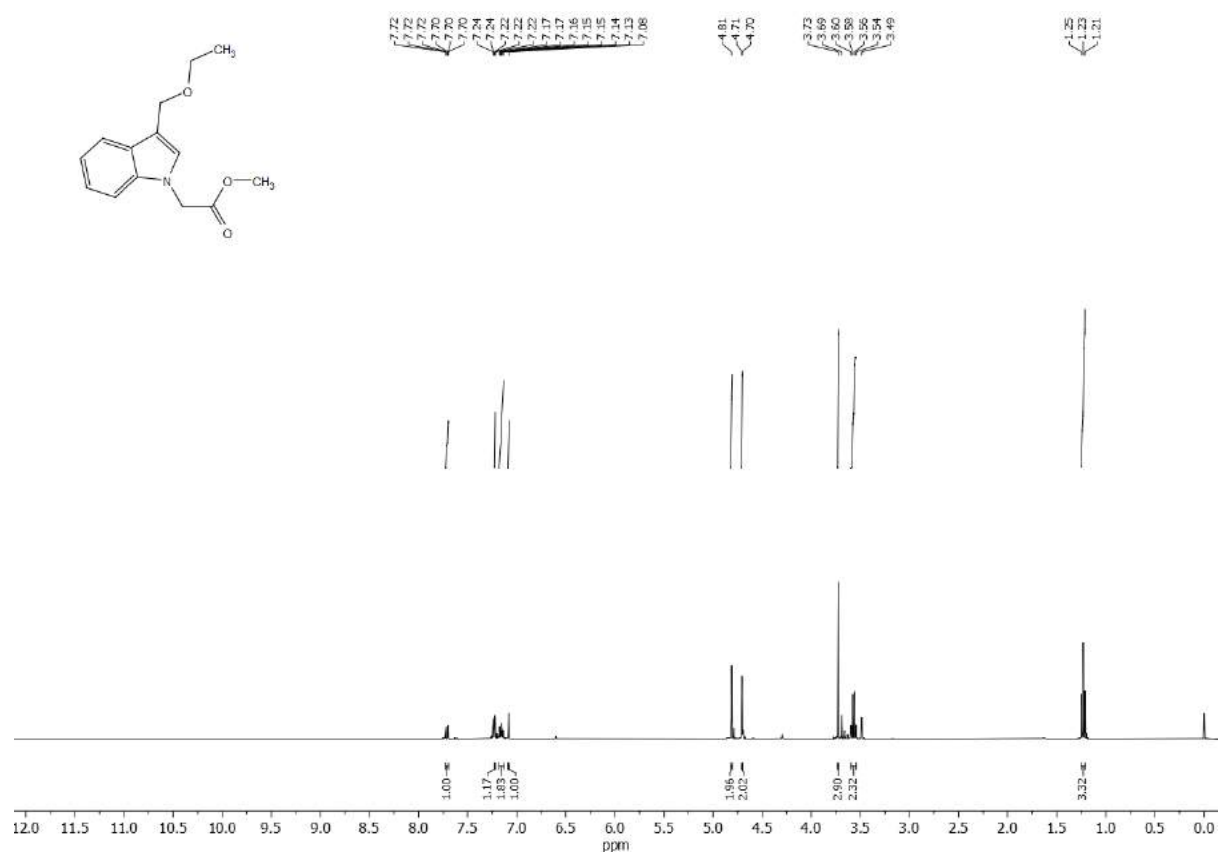
**Fig.S14b.** <sup>13</sup>C NMR spectrum of compound 17



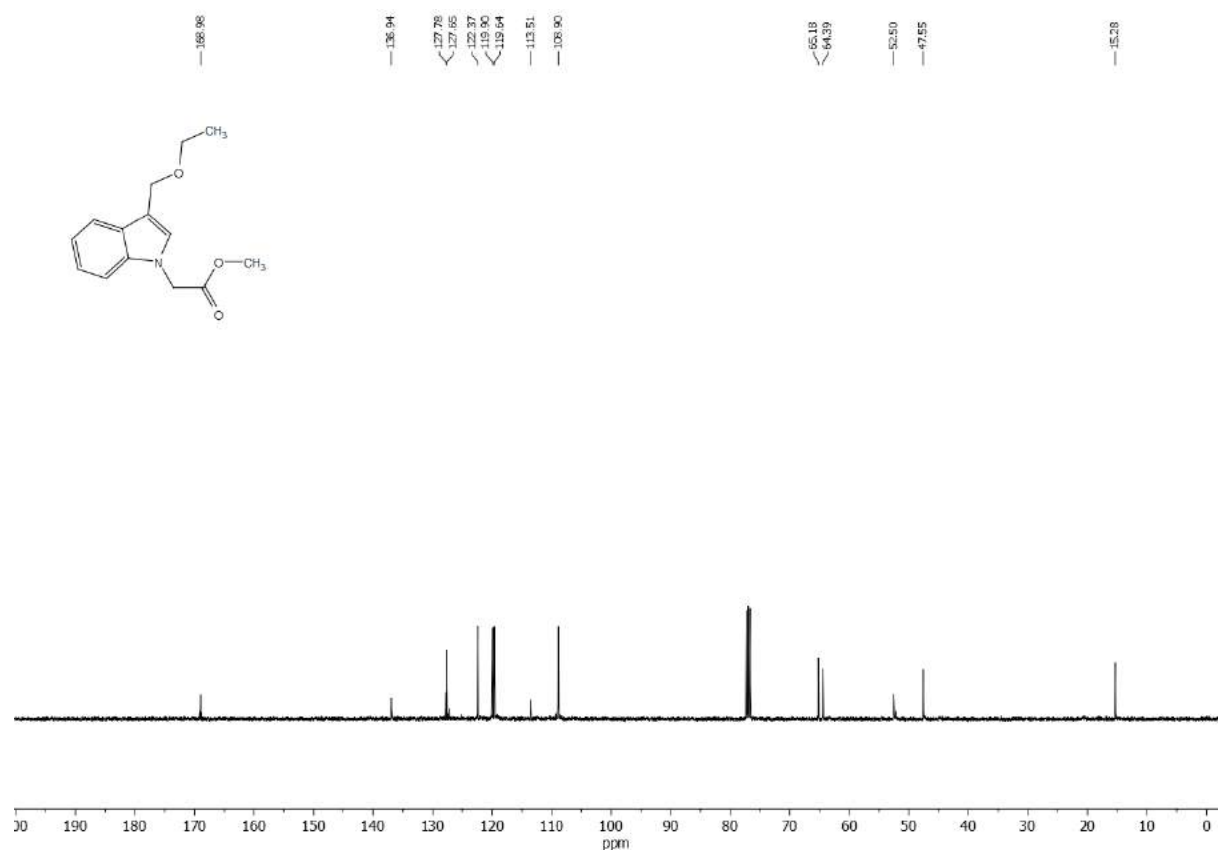
**Fig.S14c.** EI-MS spectrum of compound **17**



**Fig.S14d.** FT-IR spectrum of compound **17**

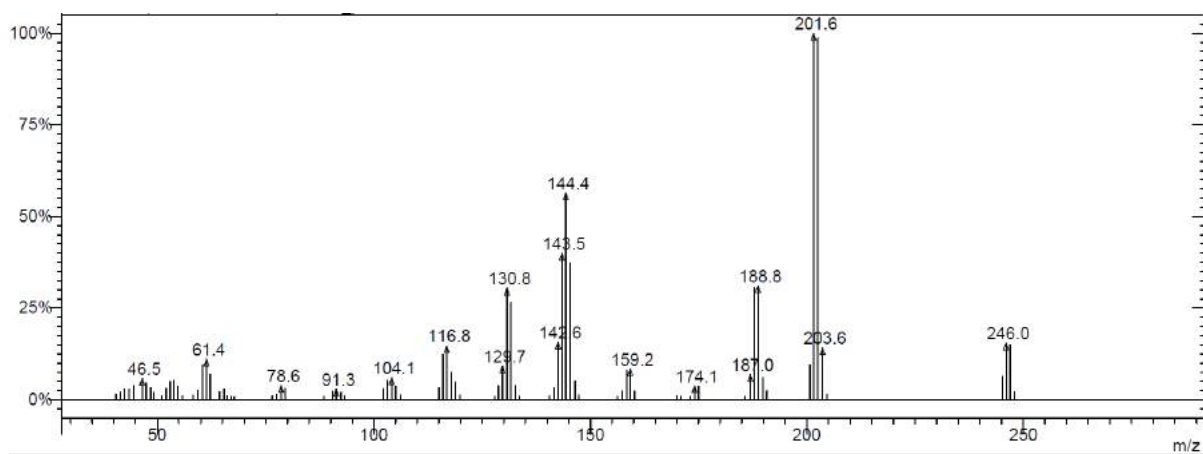


**Fig.S15a.** <sup>1</sup>H NMR spectrum of compound **18**

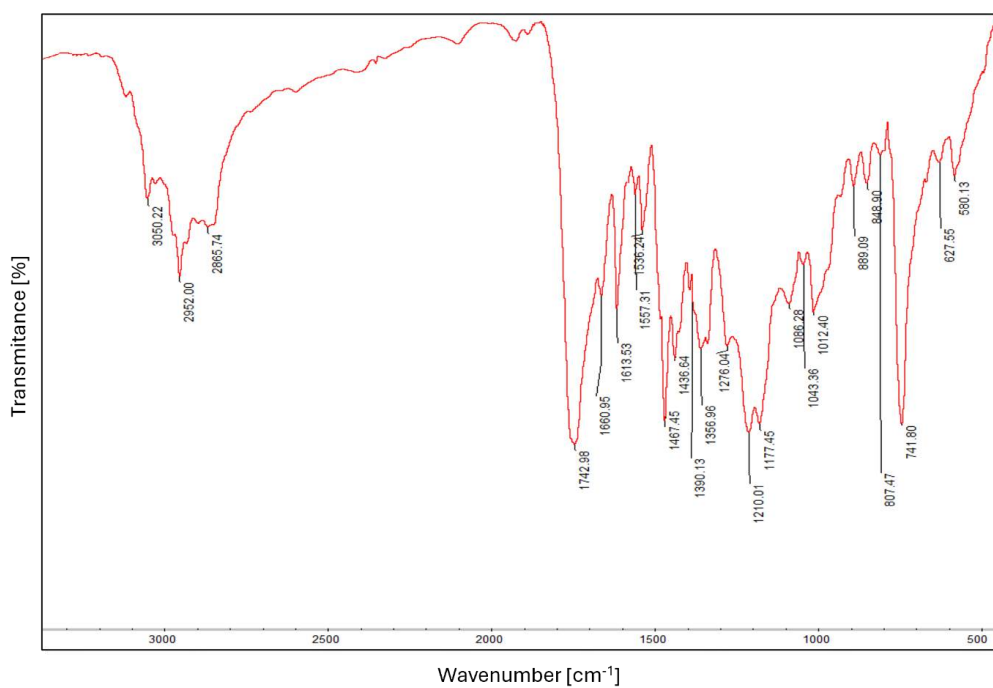


**Fig.S15b.** <sup>13</sup>C NMR spectrum of compound **18**

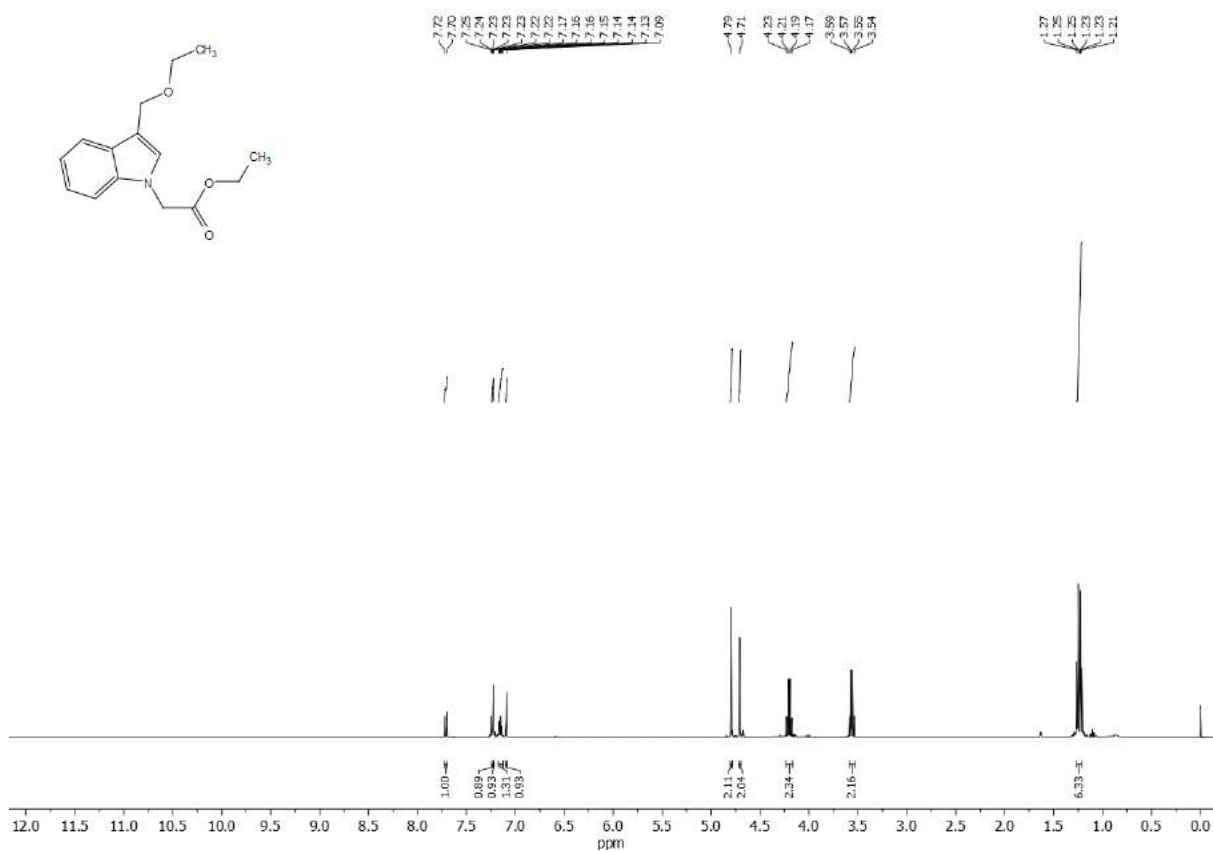




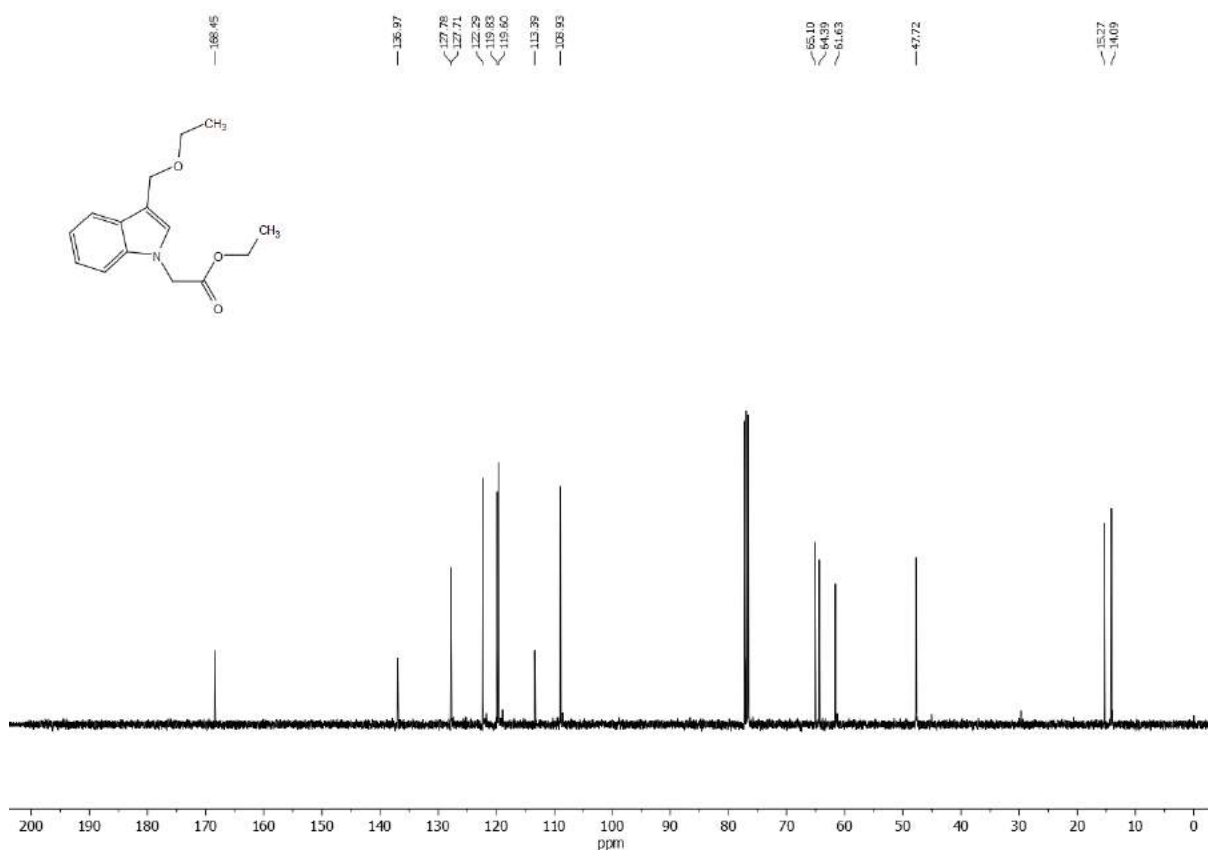
**Fig.S15c.** EI-MS spectrum of compound **18**



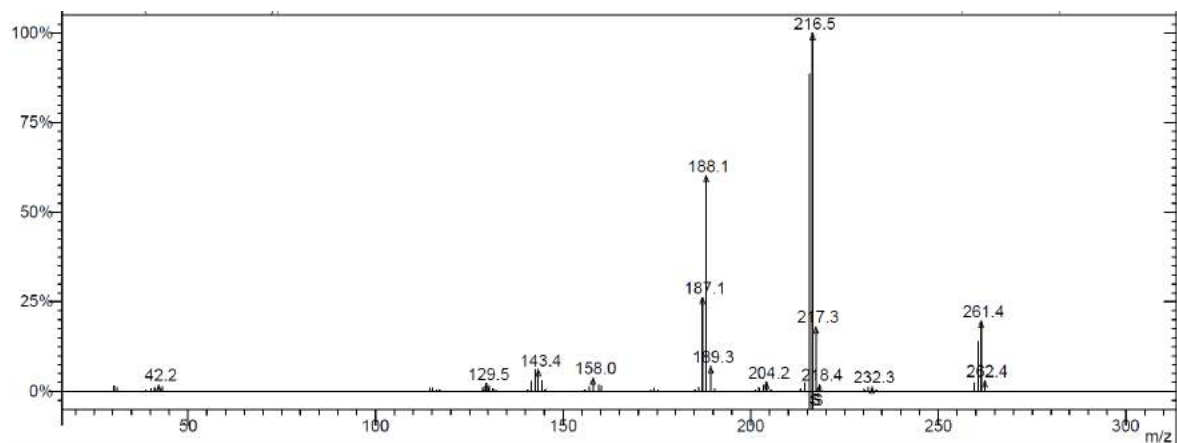
**Fig.S15d.** FT-IR spectrum of compound **18**



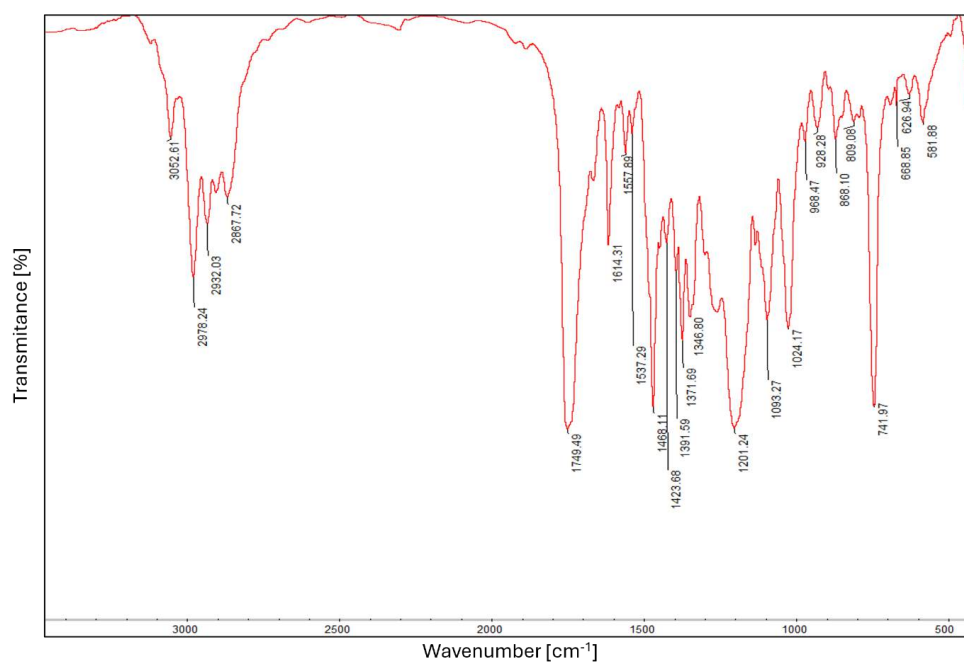
**Fig.S16a.** <sup>1</sup>H NMR spectrum of compound 19



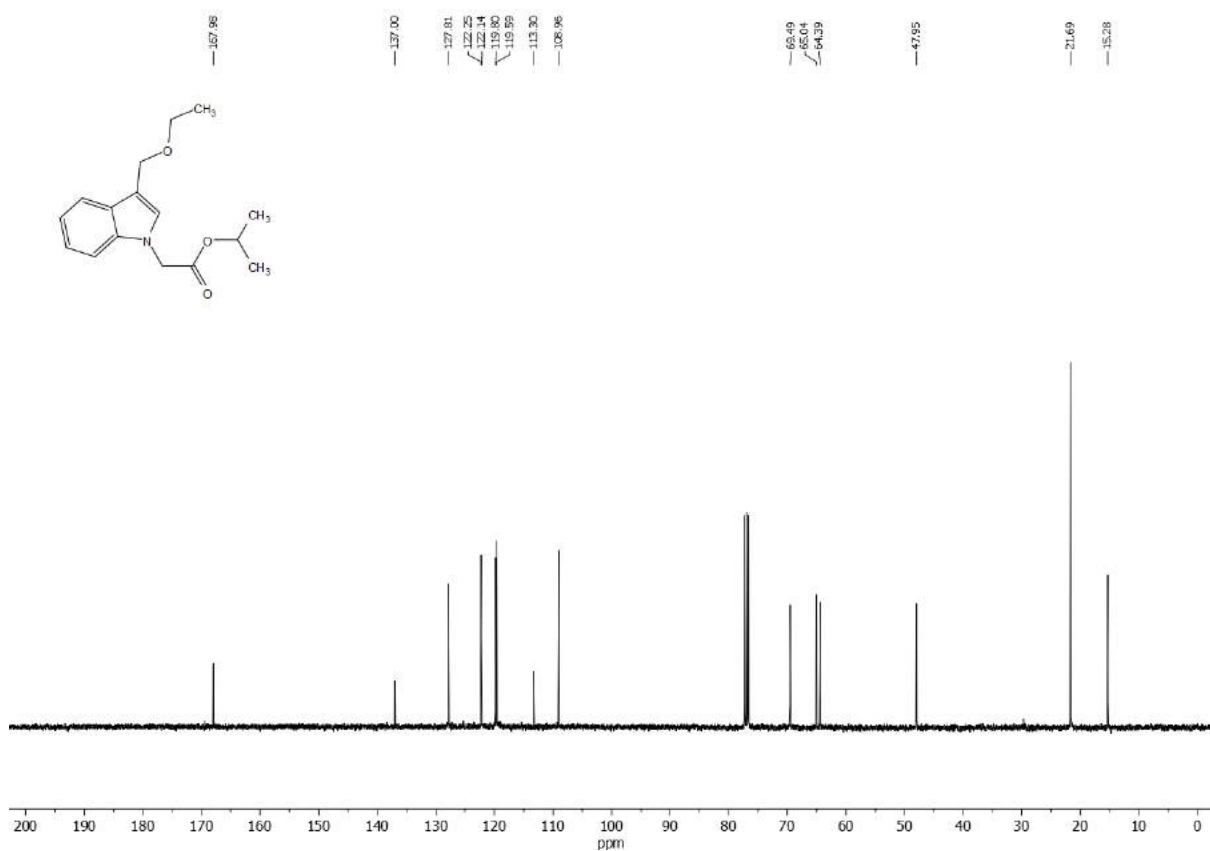
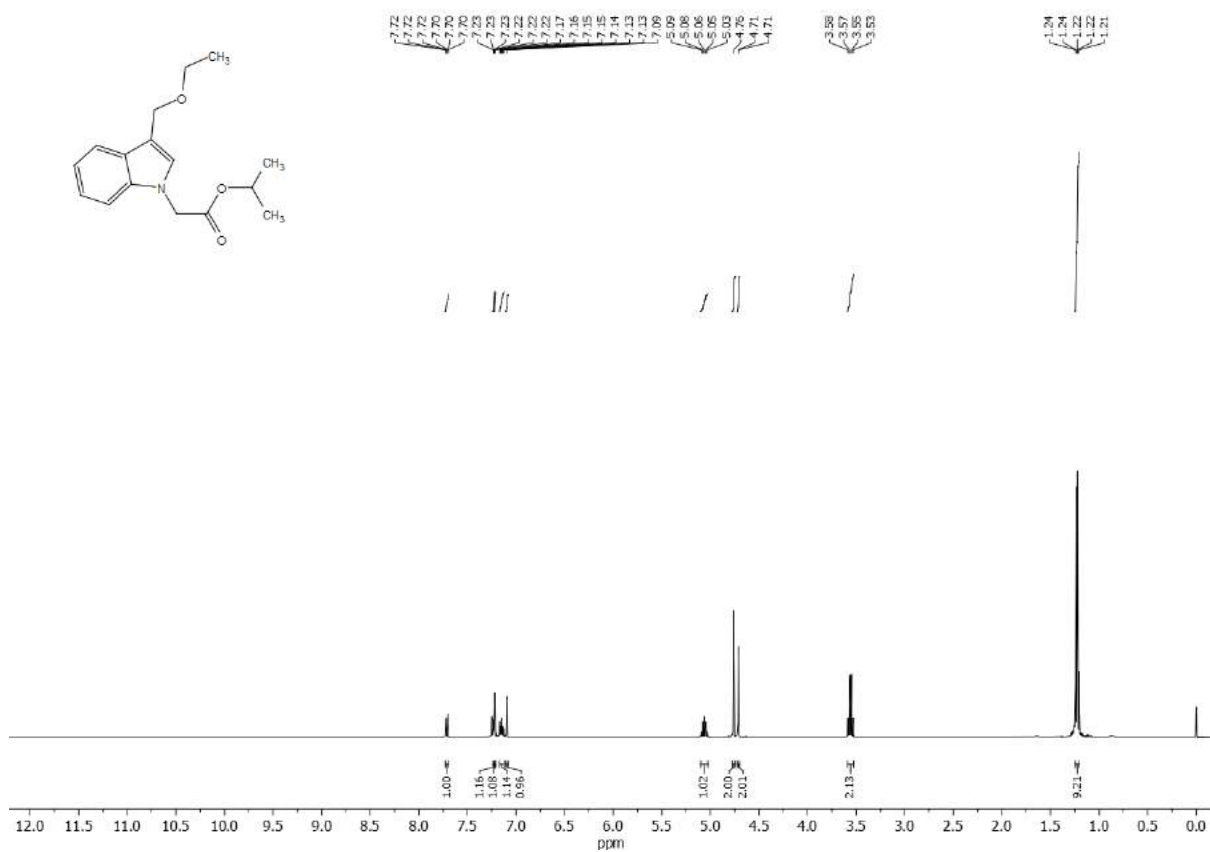
**Fig.S16b.** <sup>13</sup>C NMR spectrum of compound 19

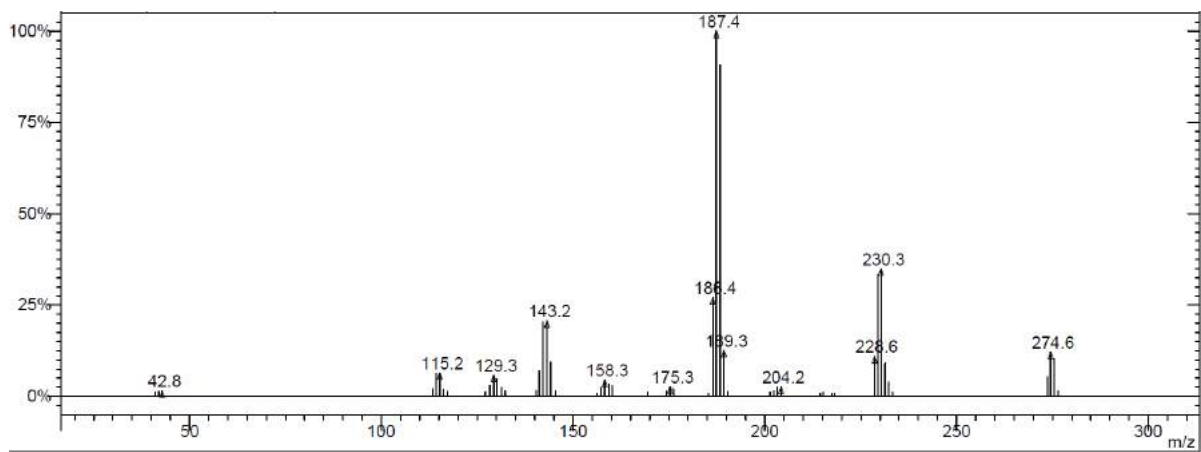


**Fig.S16c.** EI-MS spectrum of compound **19**

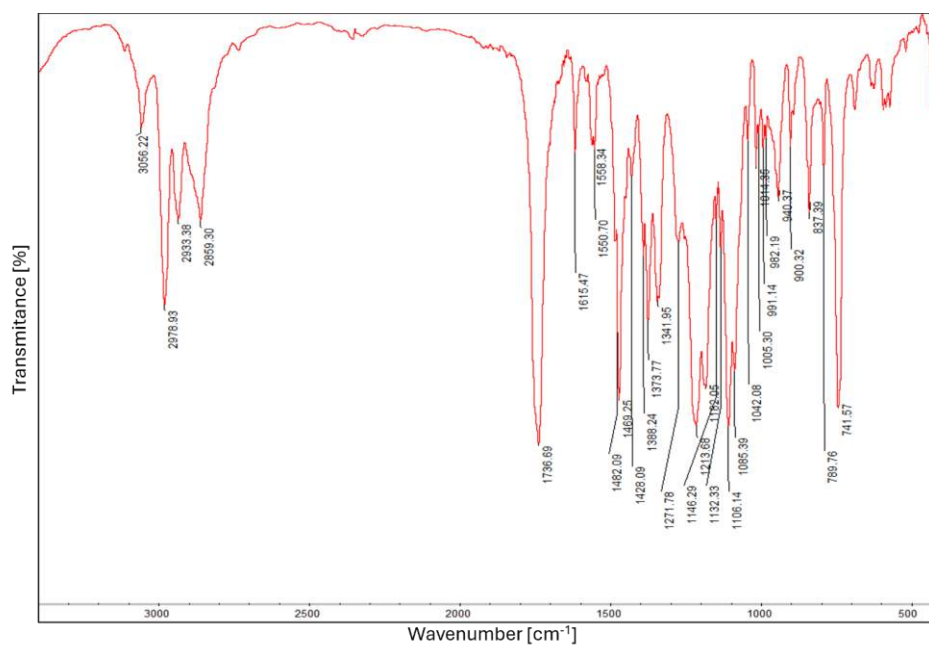


**Fig.S16d.** FT-IR spectrum of compound **19**



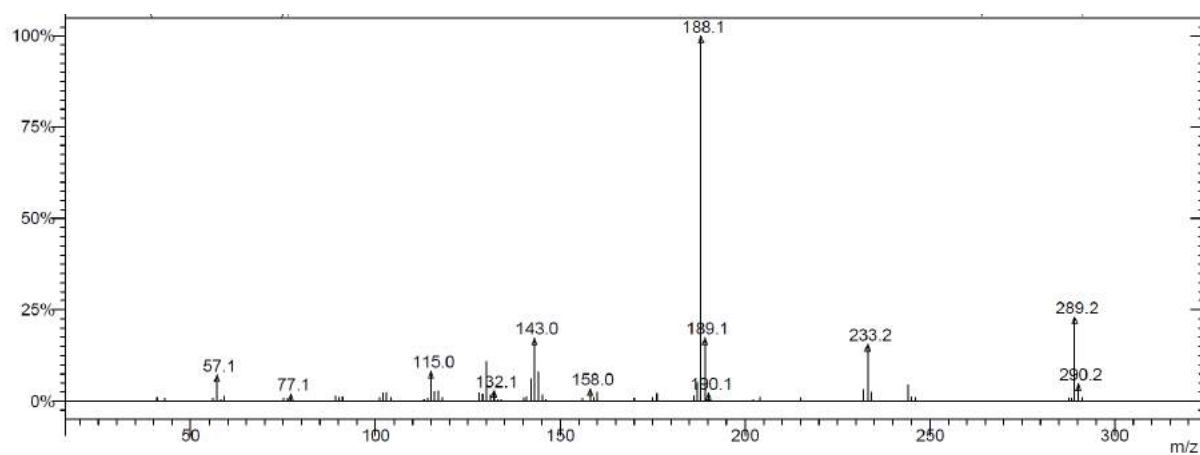


**Fig.S17c.** EI-MS spectrum of compound **20**

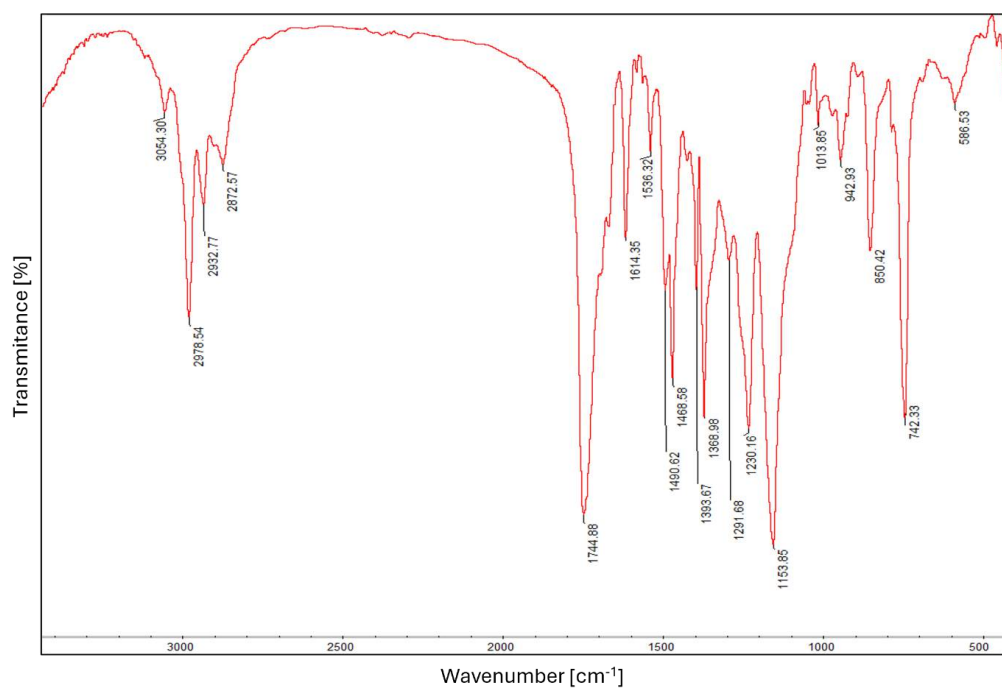


**Fig.S17d.** FT-IR spectrum of compound **20**

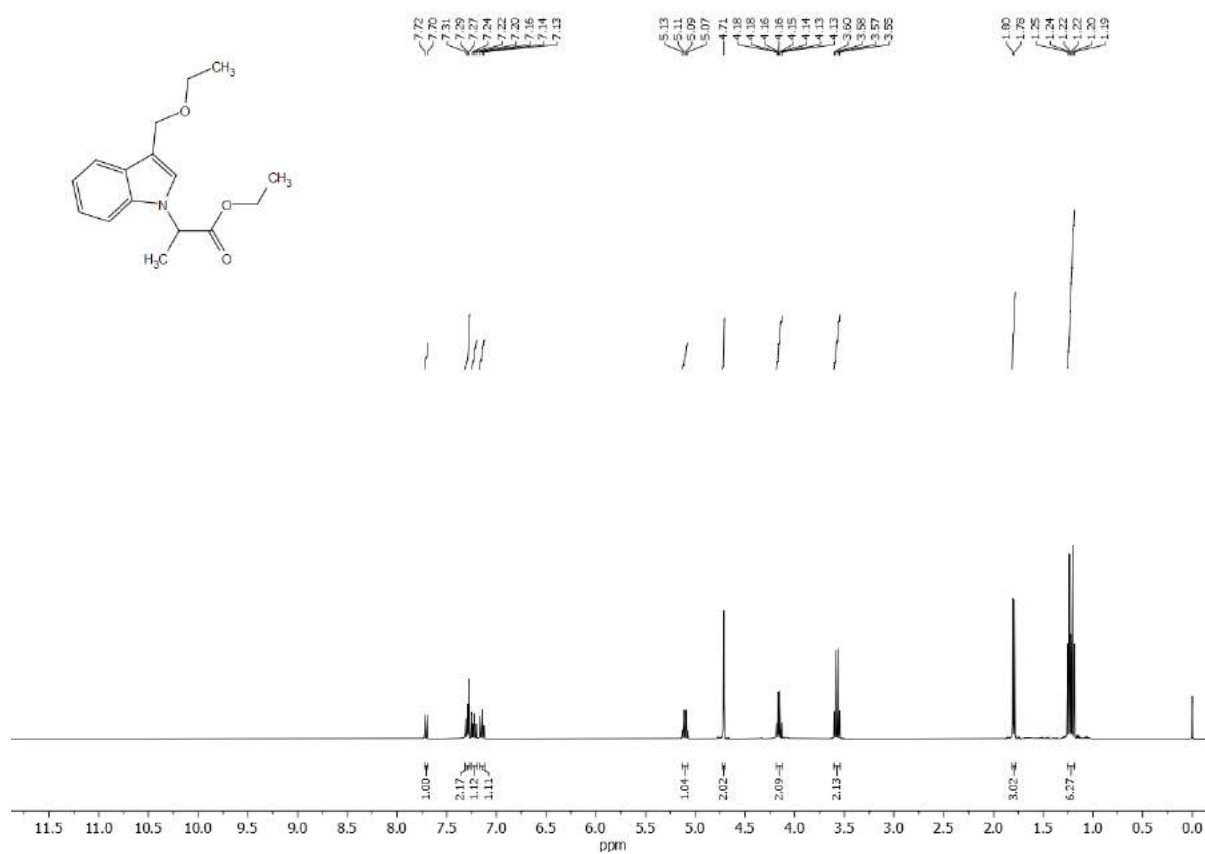




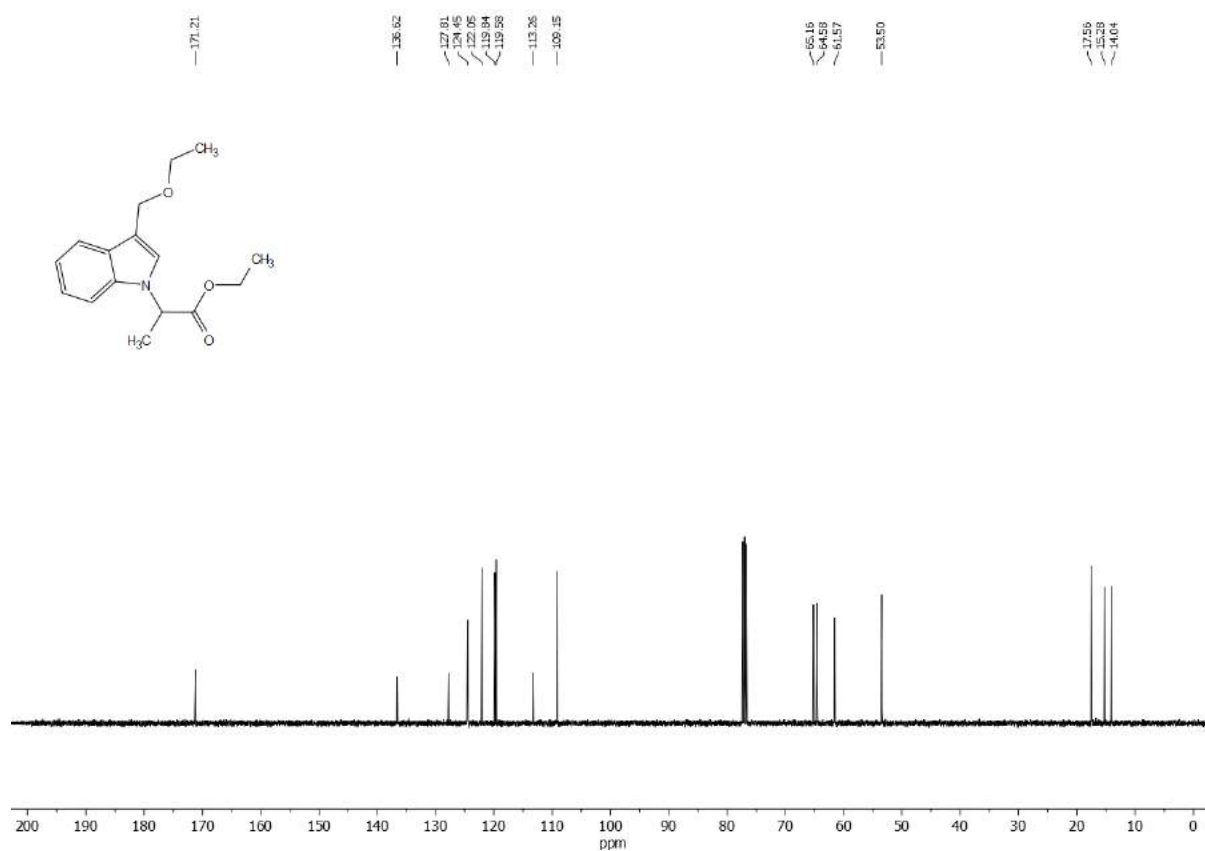
**Fig.S18c.** EI-MS spectrum of compound **21**



**Fig.S18d.** FT-IR spectrum of compound **21**

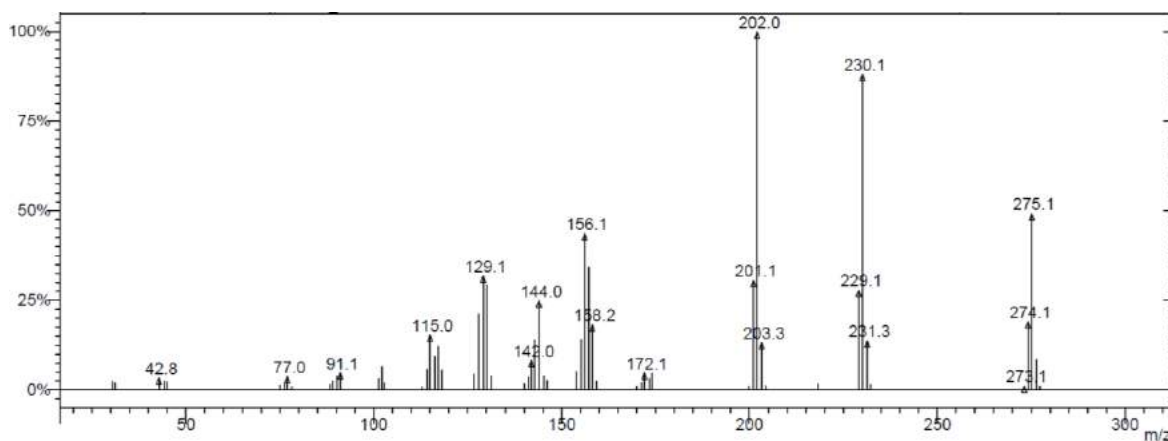


**Fig.S19a.** <sup>1</sup>H NMR spectrum of compound 22

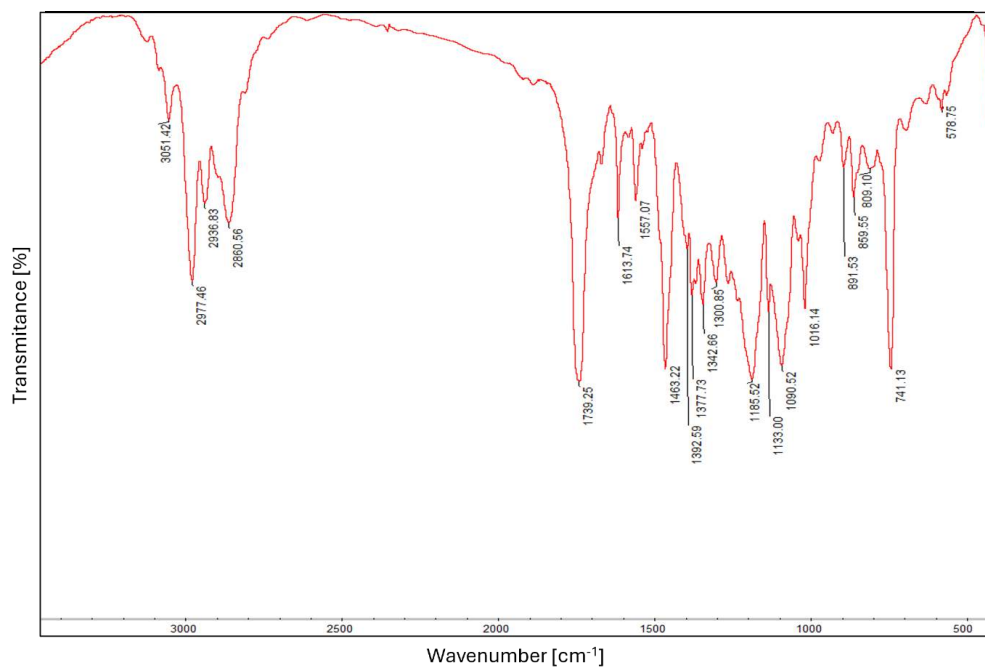


**Fig.S19b.** <sup>13</sup>C NMR spectrum of compound 22

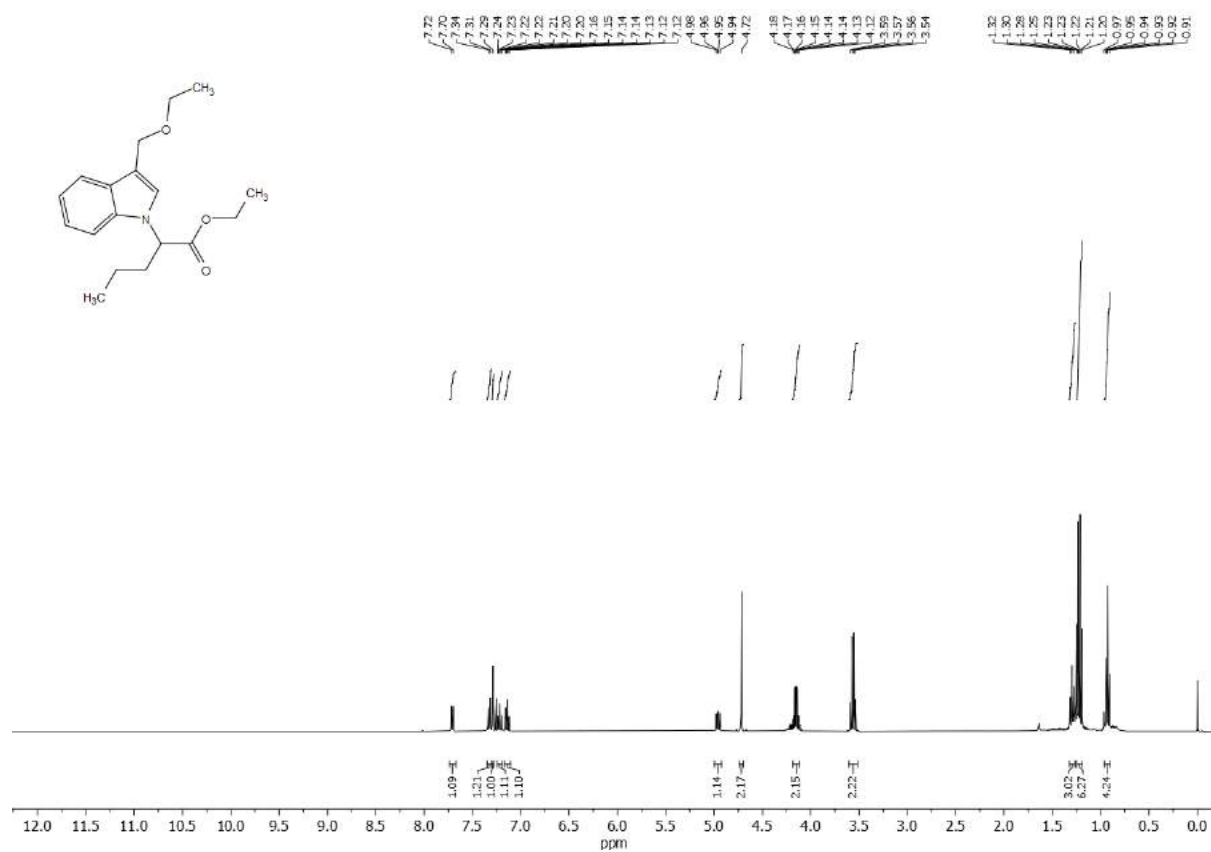




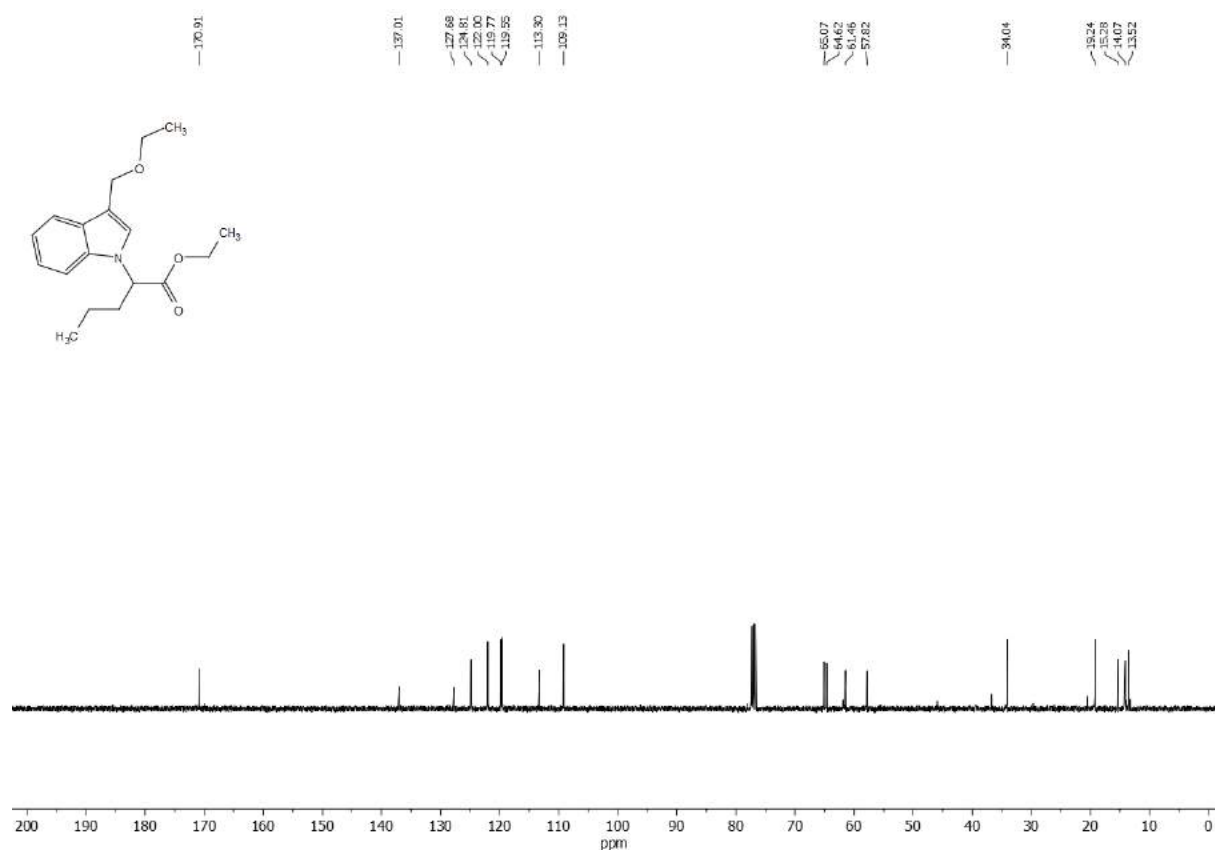
**Fig.S19c.** EI-MS spectrum of compound **22**



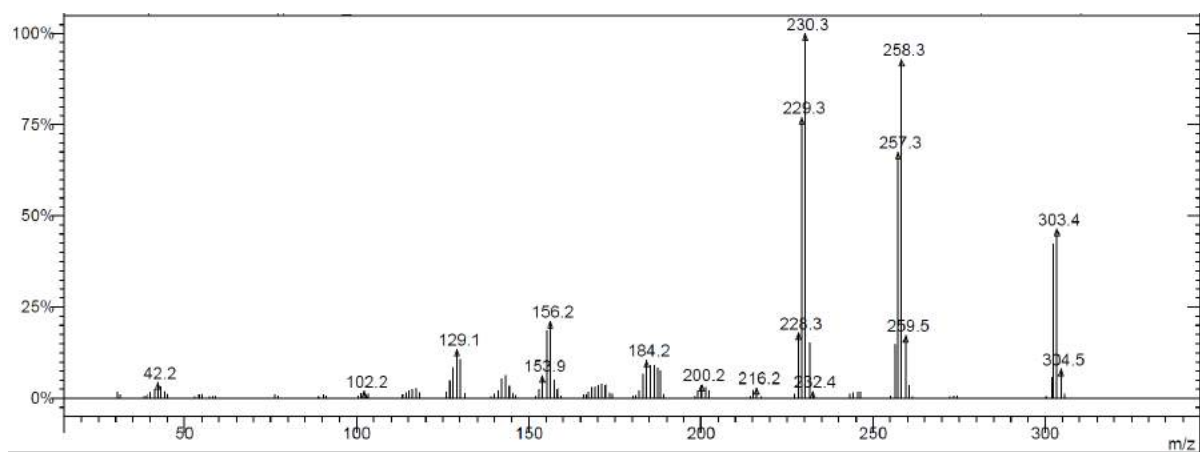
**Fig.S19d.** FT-IR spectrum of compound **22**



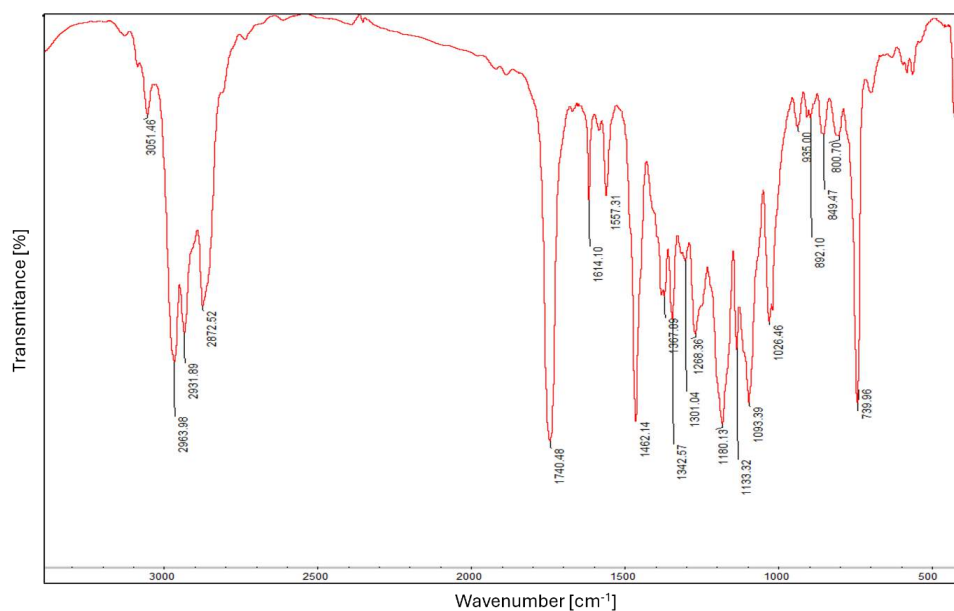
**Fig.S20a.** <sup>1</sup>H NMR spectrum of compound 23



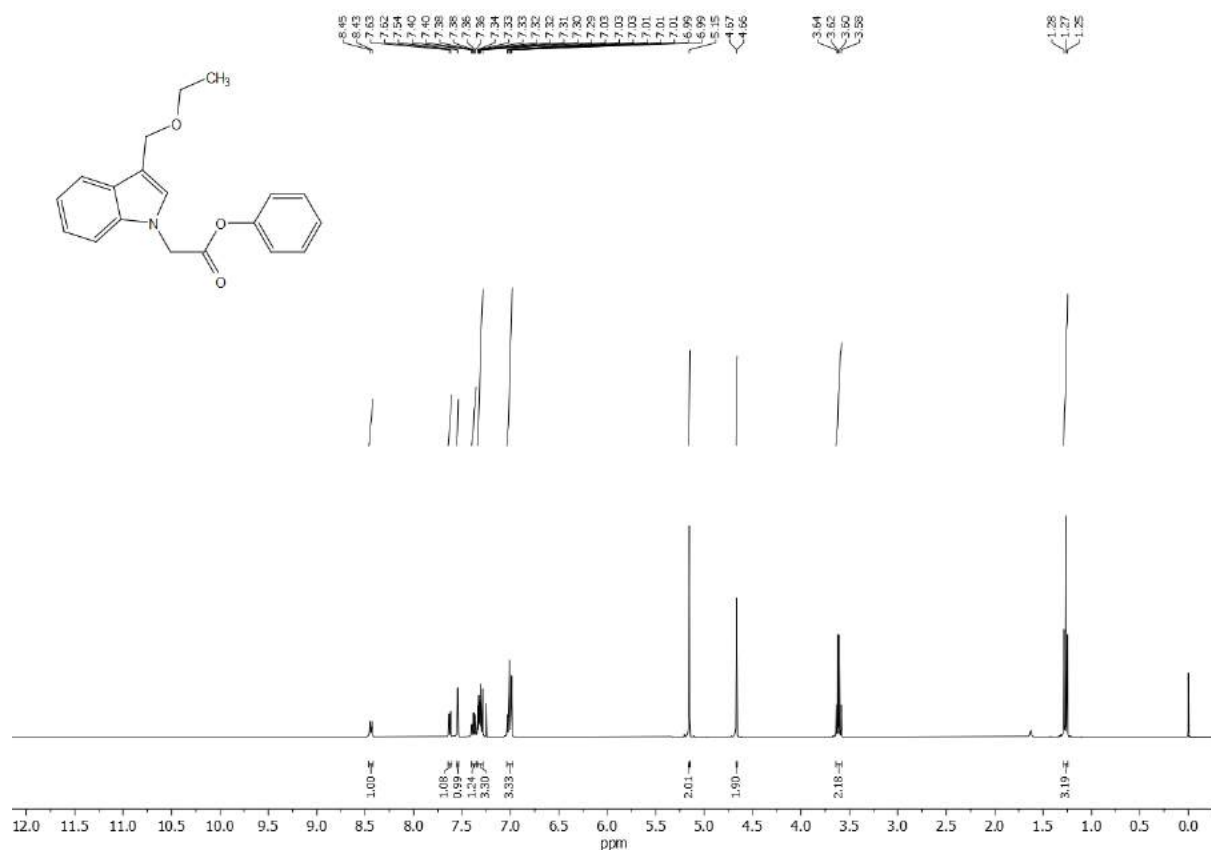
**Fig.S20b.** <sup>13</sup>C NMR spectrum of compound 23



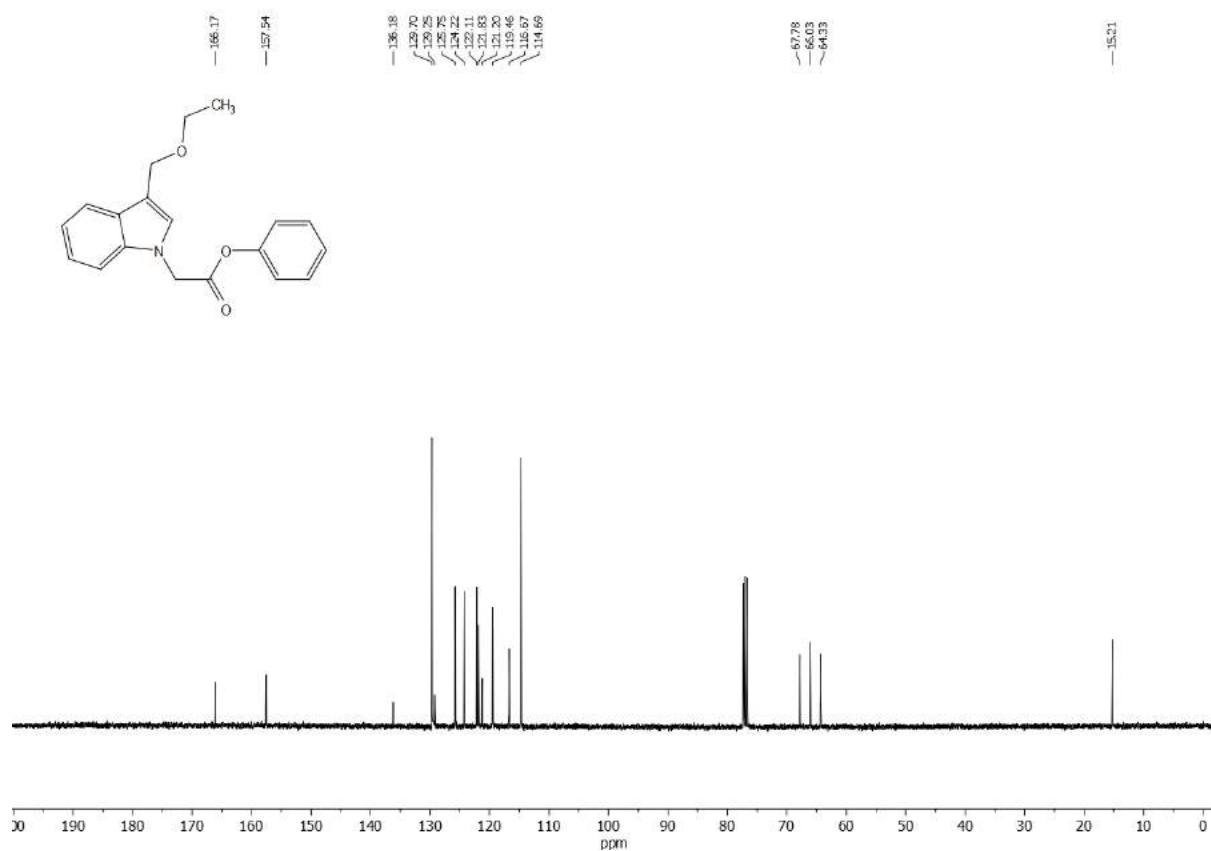
**Fig.S20c.** EI-MS spectrum of compound **23**



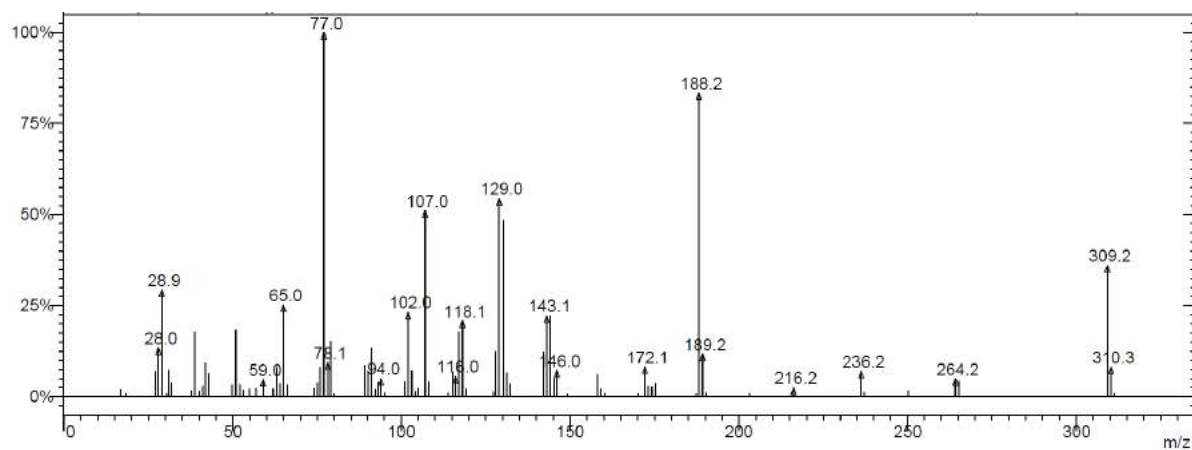
**Fig.S20d.** FT-IR spectrum of compound **23**



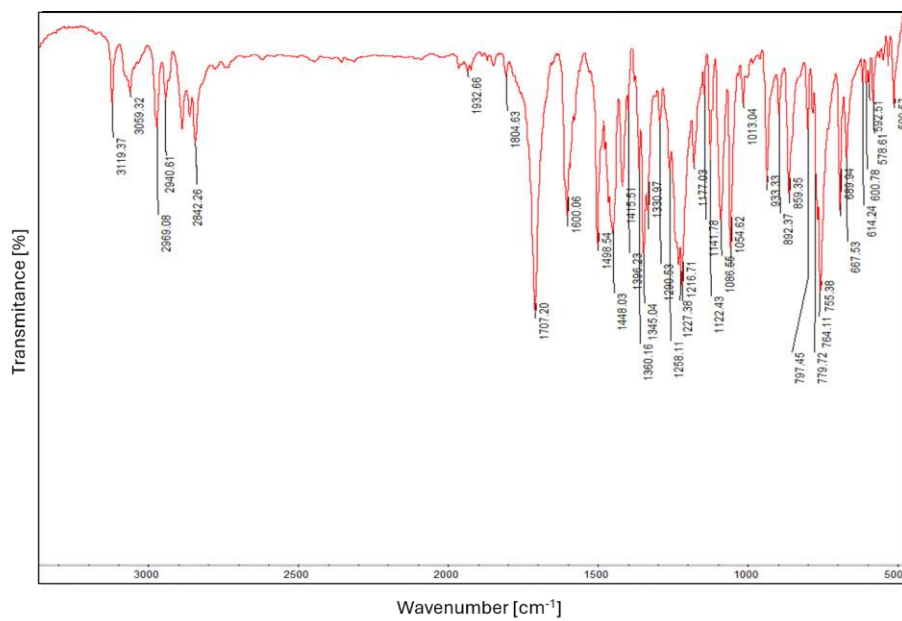
**Fig.S21a.** <sup>1</sup>H NMR spectrum of compound 24



**Fig.S21b.** <sup>13</sup>C NMR spectrum of compound 24

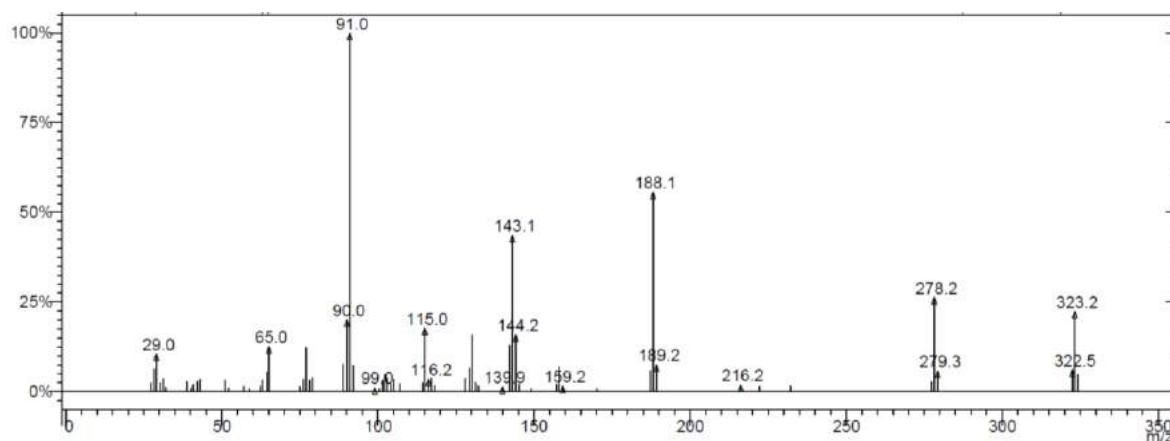


**Fig.S21c.** EI-MS spectrum of compound **24**

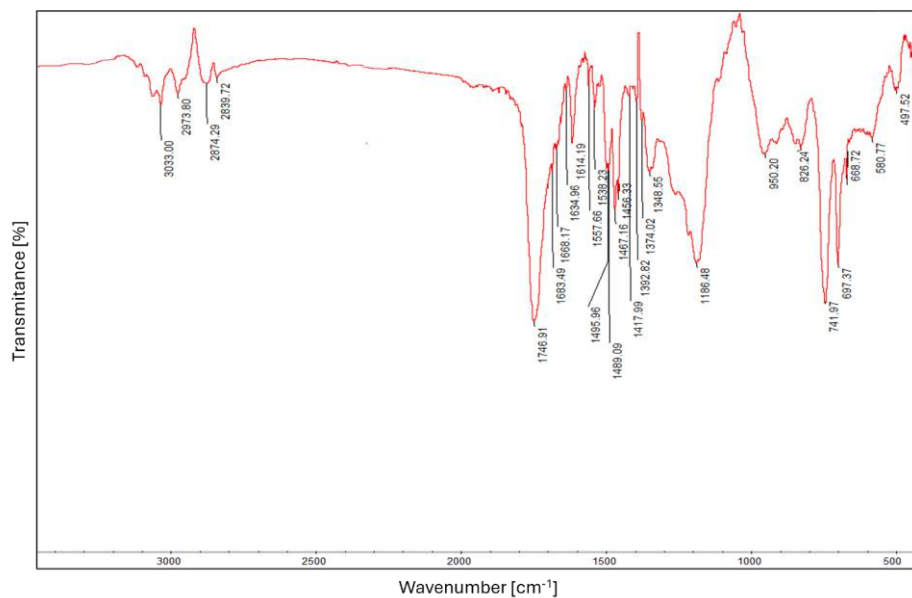


**Fig.S21d.** FT-IR spectrum of compound **24**





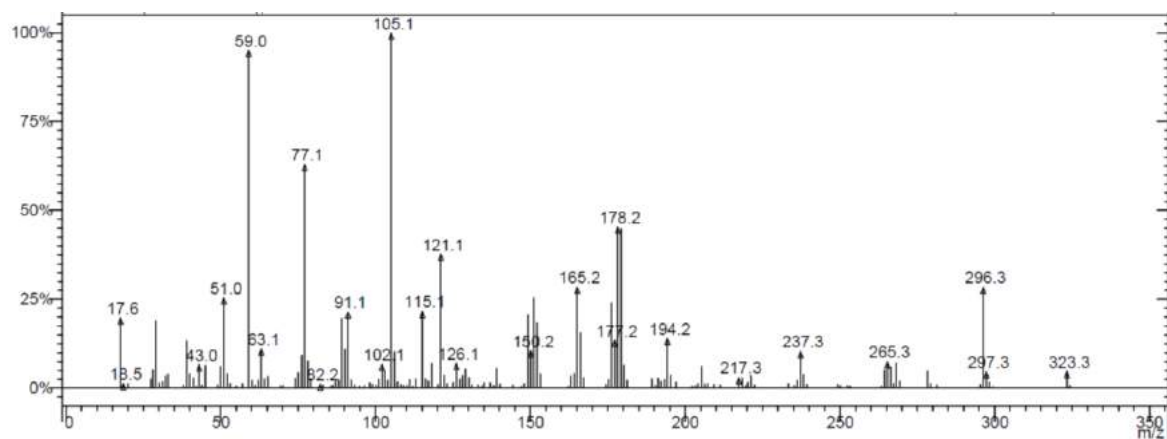
**Fig.S22c.** EI-MS spectrum of compound **25**



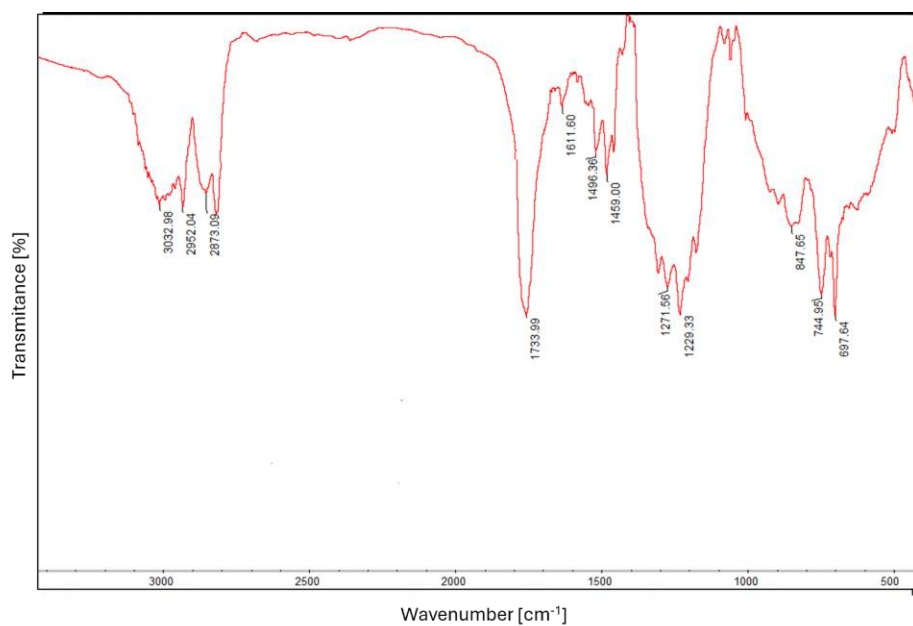
**Fig.S22d.** FT-IR spectrum of compound **25**



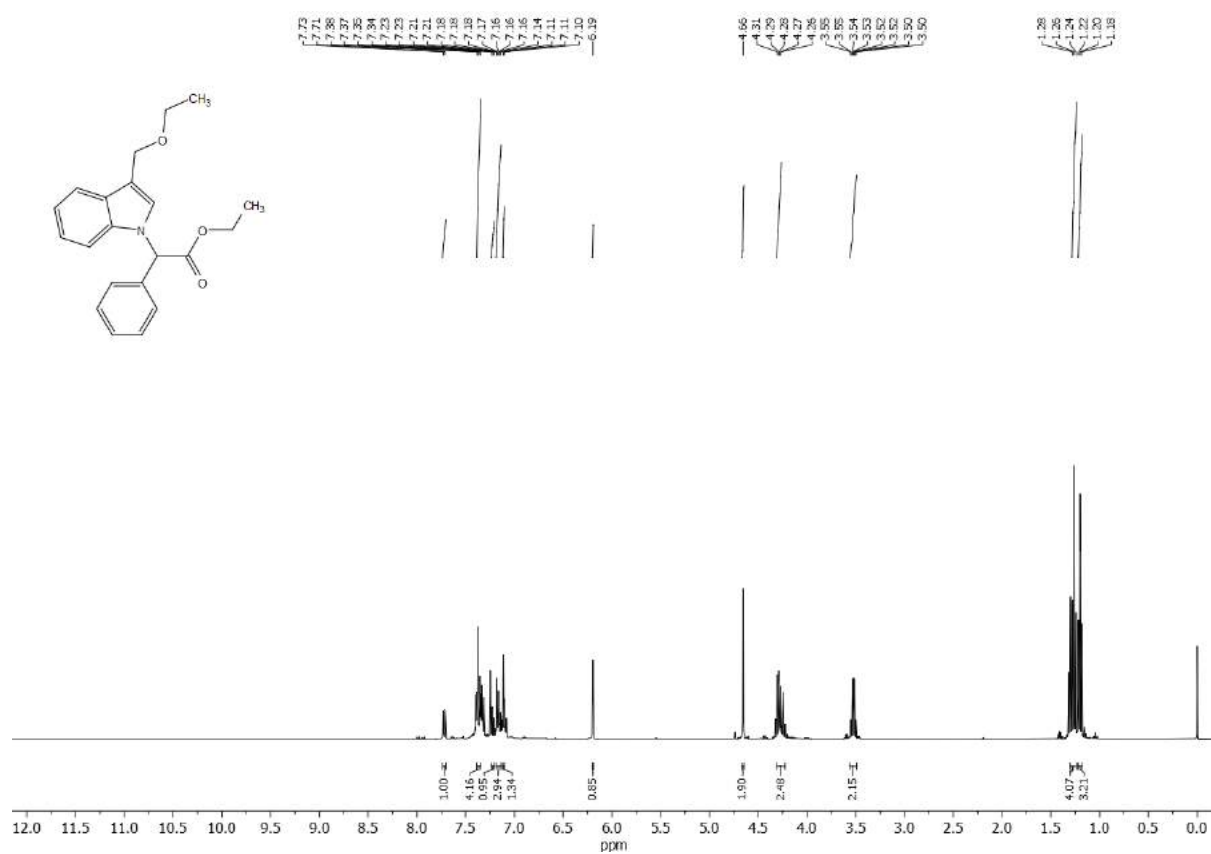




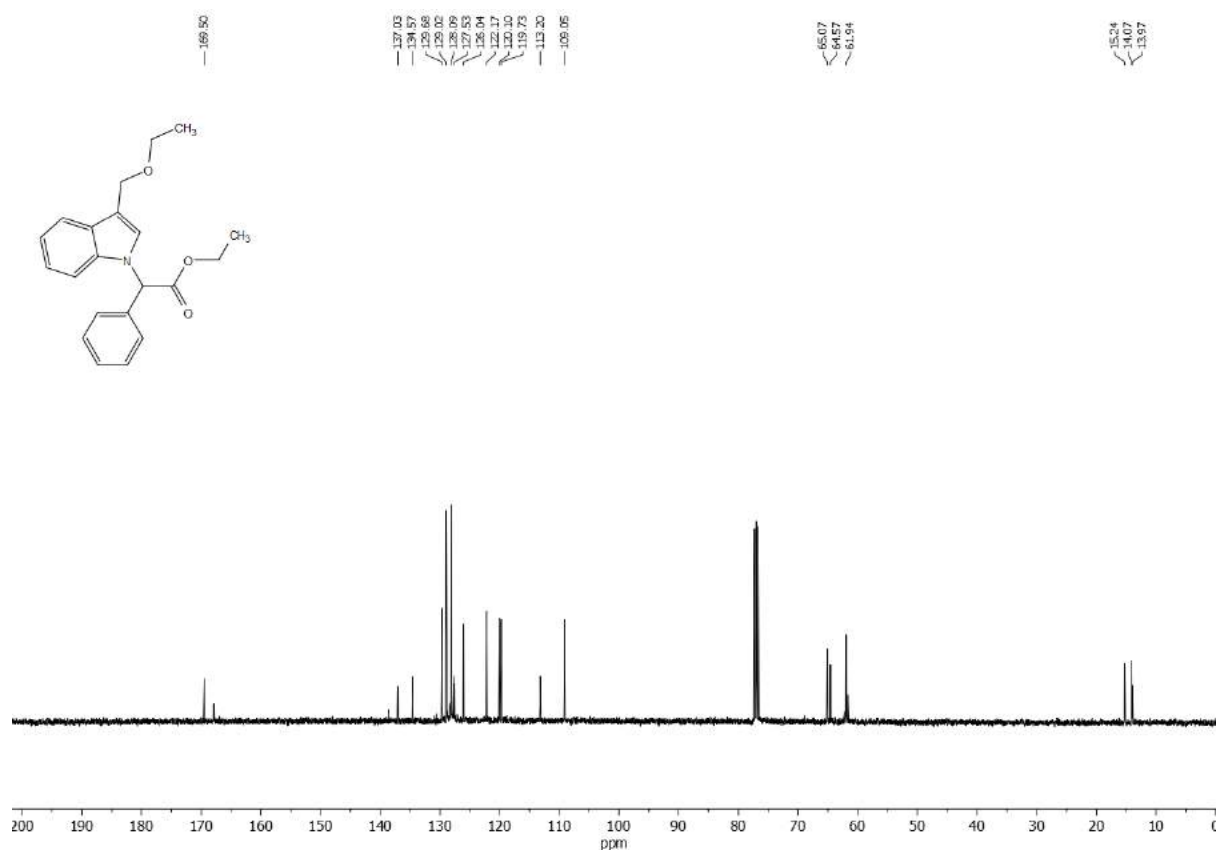
**Fig.S23c.** EI-MS spectrum of compound **26**



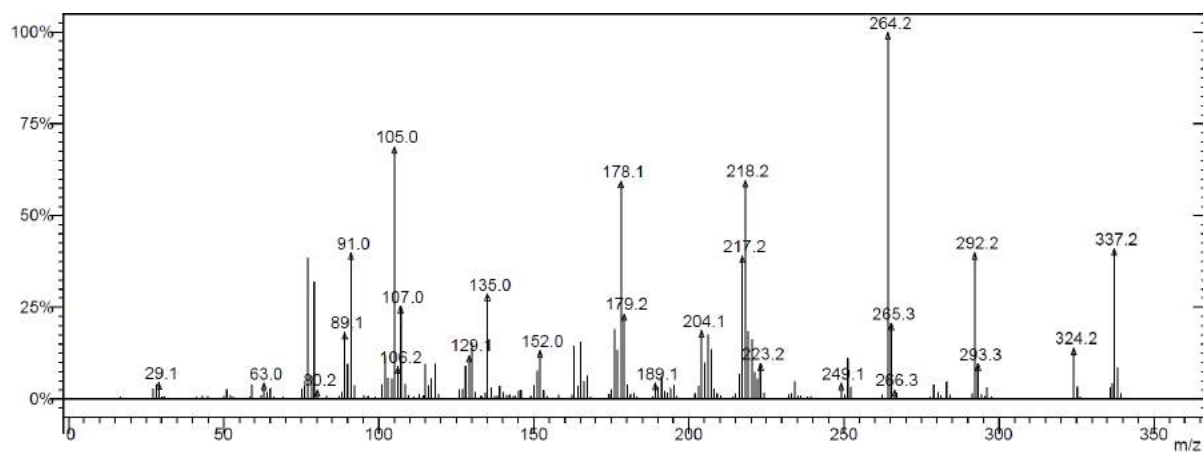
**Fig.S23d.** FT-IR spectrum of compound **26**



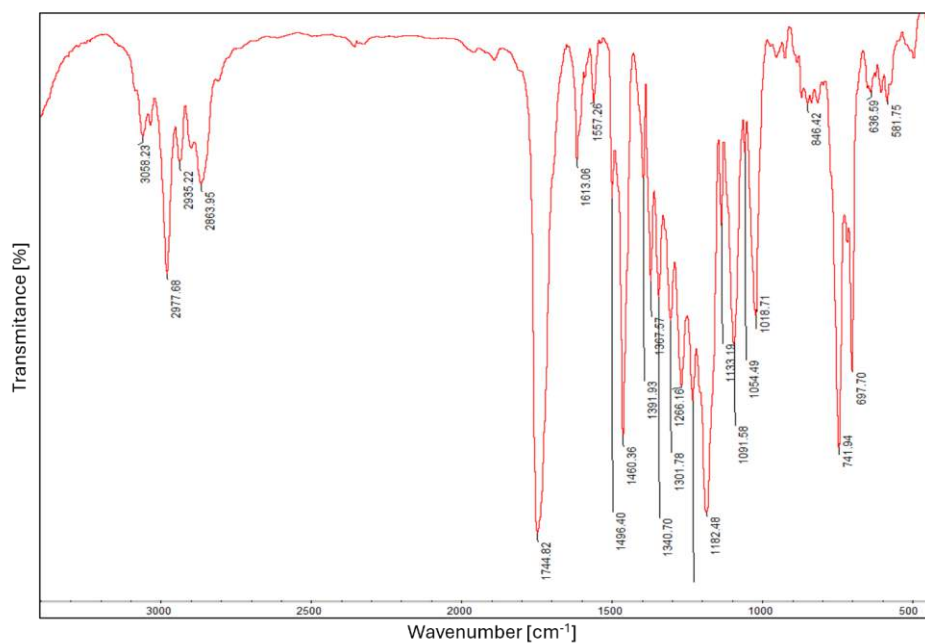
**Fig.S24a.** <sup>1</sup>H NMR spectrum of compound 27



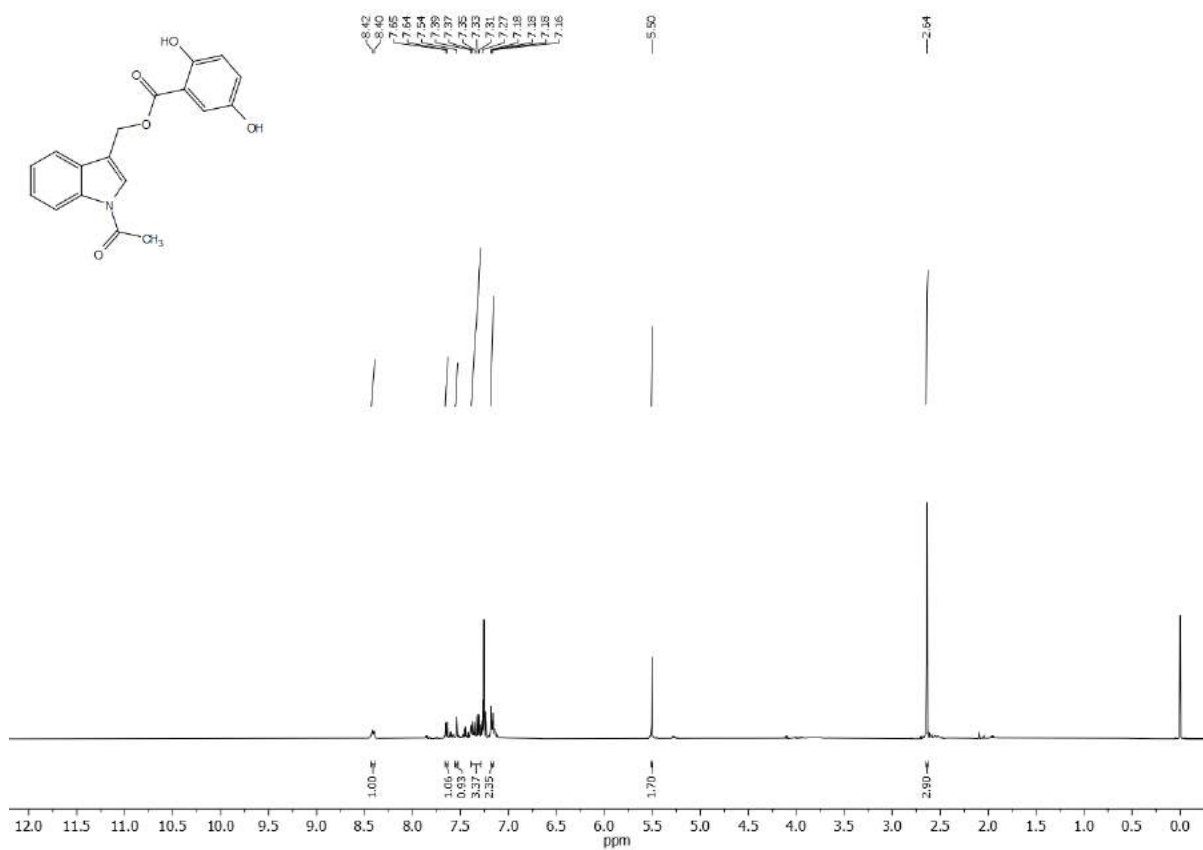
**Fig.S24b.** <sup>13</sup>C NMR spectrum of compound 27



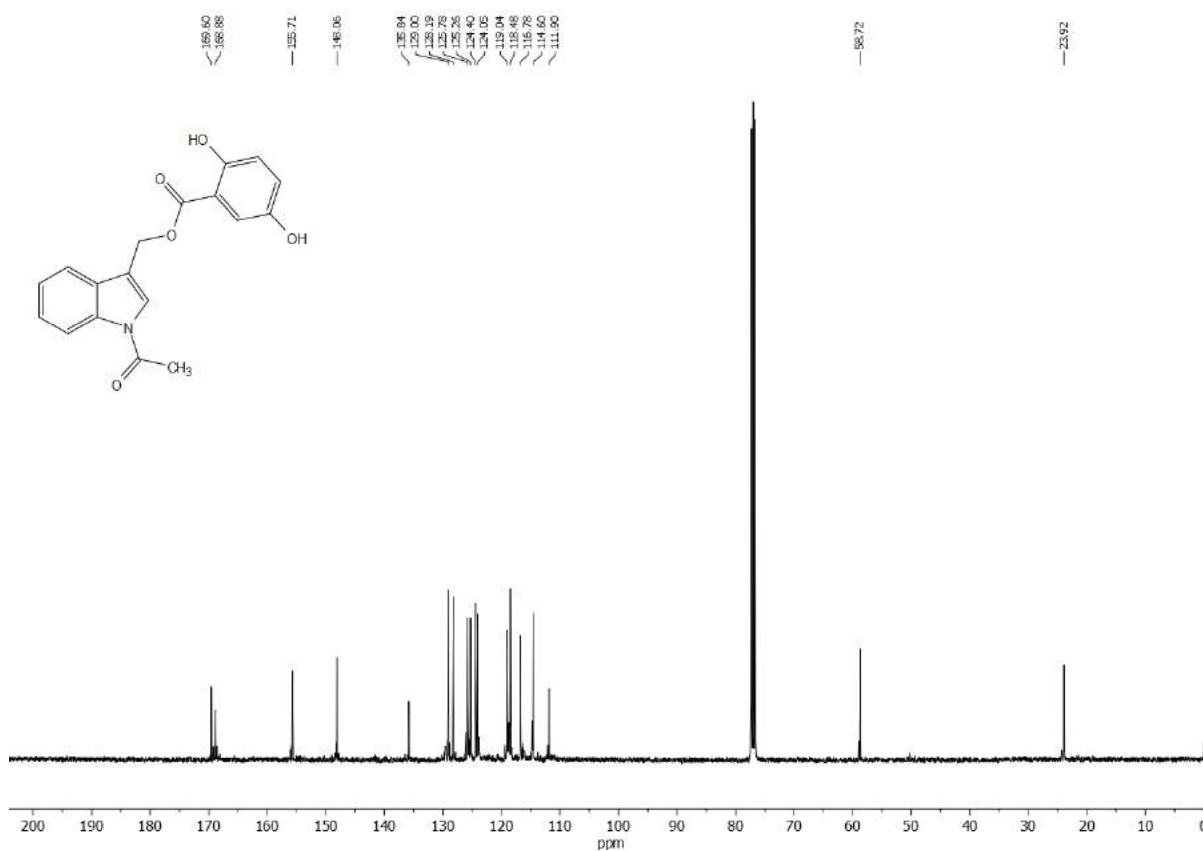
**Fig.S24c.** EI-MS spectrum of compound **27**



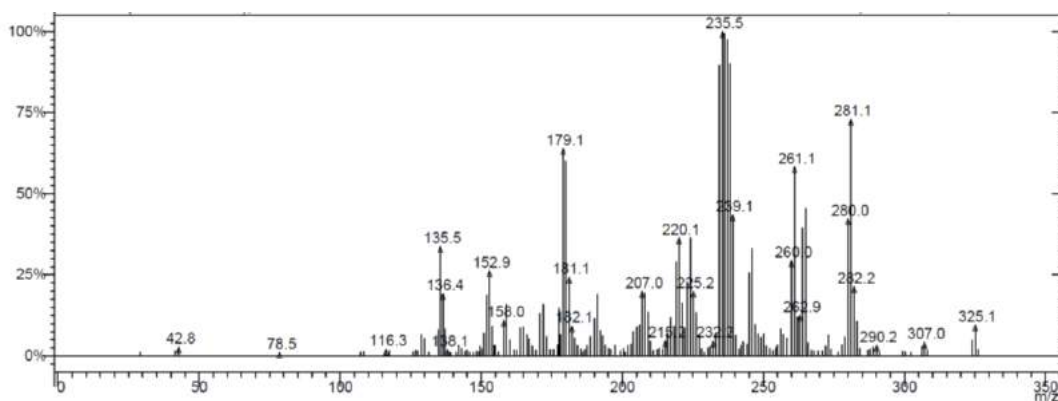
**Fig.S24d.** FT-IR spectrum of compound **27**



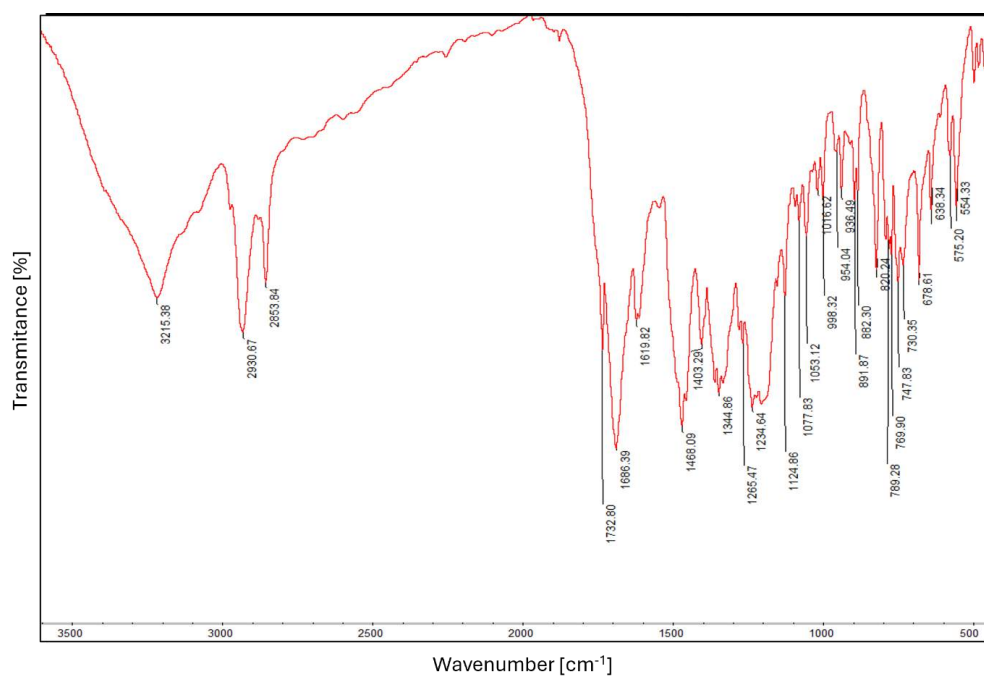
**Fig.S25a.** <sup>1</sup>H NMR spectrum of compound **29**



**Fig.S25b.** <sup>13</sup>C NMR spectrum of compound **29**



**Fig.S25c.** EI-MS spectrum of compound **29**



**Fig.S25d.** FT-IR spectrum of compound **29**

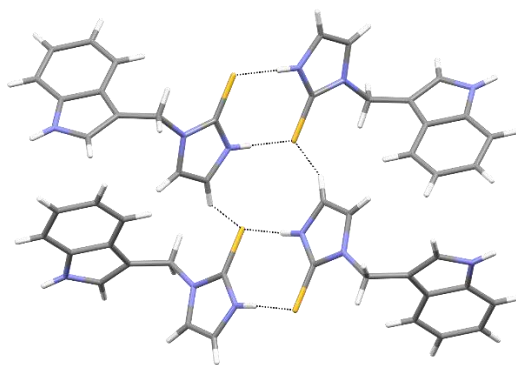
## Crystal data Description of the crystallographic results

With only one real exception of molecule **10**, the molecules **2**, **4**, **5**, **7**, **8**, **9** and **11** display in crystals a similar conformation. Chemical alterations such as hydrogenation or annelation with benzene ring have more significant effect on the structure of thiazole than imidazole derivatives on both the molecular and supramolecular levels. Based on the collected structural data we may follow structural changes caused by i) hydrogenation, (ii) methyl substitution, (iii) annelation with benzene ring and (iv) isosteric substitution.

The effect of N-H/N-CH<sub>3</sub> substitution can be tackled by comparing the structures **4** and **5**. As can be seen from Table 1, the molecular conformations are nearly identical but, as could be expected, the number of intermolecular hydrogen bonds has been reduced upon *N*-methylation (Table S1). Analogously, a consequence of annelation with benzene ring can be chased by comparing molecules **5** and **8**. While the lengths of the bonds in the condensed imidazole ring are greater than in the free imidazole system, the two molecules adopt similar conformation in crystals. Both utilize N-H<sub>indole</sub>⋯S hydrogen bond to form chains of molecules related either by a glide plane (**5**) or a two-fold screw axis (**8**). The arrangement of the latter molecules around a two-fold screw axis allows to overcome the steric hindrance by directing outwards the bulky methyl substituents and benzene rings (Figure 7). As a result, the hydrogen bond in **8** is the least linear of all the reported N-H⋯S hydrogen bonds (Table S1).

Although hydrogenation of imidazole (**4**) into imidazolidine (**2**) changes the bond lengths, diminishes the propeller feature of **4** (Table 1), and modifies the overall hydrogen-bonding pattern, in both crystals the molecules utilize the same set of two N-H and one C-H donor groups to the thione acceptor to connect molecules into three dimensions. The H-bond parameters that are listed in Table S1 are more adequate for **4** than **2**. Sulphur atom acts as a quadruple acceptor, again illustrating its capacity to simultaneously engage in a greater number of interactions than conventional acceptors. The C=S bond in molecules **2** and **4** amounts to 1.682(4) and 1.697(2) Å, respectively, which seems to indicate that the thione tautomer in **4** has more significant contribution of the zwitterionic structures that involve single C<sup>+</sup>-S<sup>-</sup> covalent bond (Figure 3B). While searching for possible explanation of this phenomenon we have noticed the existence of a short S⋯S contact (3.5694(8) Å) in **4** suggestive of the presence of S⋯S interactions. The two C=S⋯S angles are equal in value and amount to 171.56(5)° and the C=S⋯S=C torsion angle measures -142.0(7)°. Based on these geometrical parameters we were tempted to assume that the C=S bond in **4** elongates as

a result of the formation of the of chalcogen bond. However, the attractive character of such interaction has been questioned by Owczarzak *et al.* on the bases of experimental charge density studies and theoretical calculations carried out for selected thioamides [S1]. The authors postulate that the short S···S contacts in thioamides originate from the presence of the so called “staple molecules”. By forming strong hydrogen bonds, these molecules bring two sulphur atoms into close contact, which by nature is rather repulsive than attractive. In our case, the close S···S contact is reinforced by the imidazole H-N-C-H fragments, acting as “staples” (Figure S26). The stapling imidazole moieties can stabilize the zwitterionic mesomers in **4**, which in turn can account for the elongation of the C=S bond. The imidazolidine moiety in the crystals of **2** does not display such stapling capability.

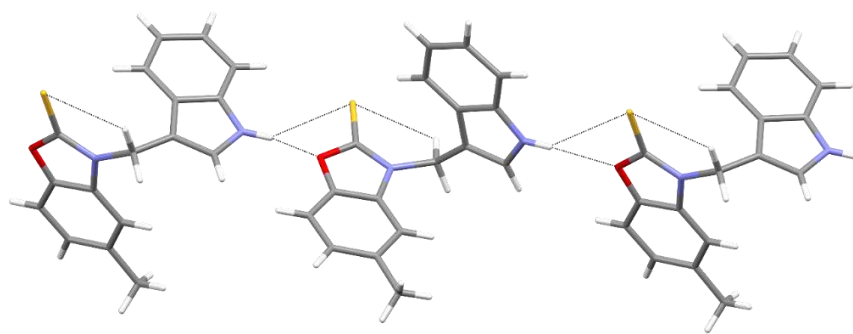


**Fig.S26.** Hydrogen-bonded tape motif present crystals of **4**. Resonance-assisted N-H···S hydrogen-bond dimers (formed around symmetry centres) are fused with a tetramer formed around two-fold symmetry axis, in which the sulphur atoms are stapled by two H-C-N-H imidazole fragments.

Like molecules **2** and **4**, the molecule **7** also contains two N-H hydrogen bond donor groups (although both come from the indole moieties) and a thione acceptor. However, most likely due to the steric hindrance, the molecules of **7** incorporate to their crystal lattice ethanol and water solvent molecules. The system becomes particularly rich in hydrogen bond functionalities thus leading to the formation of a whole palette of hydrogen bonds. All types of molecules utilize fully their potential in hydrogen bonding. Particular attention should be given to the formation of O-H(water)··· $\pi$ (pyrrole) hydrogen bonds (Table S1). The role of solvent molecules in stabilizing the crystal structure of **7** is shown in Figure 6, which also illustrates the involvement of molecules **7** in weak  $\pi$ ··· $\pi$  interactions between centrosymmetrically related benzene rings from benzothiazole fragments. The distance between centroids of the two fragments in a stack amounts to 3.925 Å, while the distance between their planes is 3.409 Å (symmetry code  $-x, 1 - y, 1 - z$ ). The planes are parallel and

the displacement of the rings in a stack is 1.945 Å. Due to the presence of supporting guest molecules, such extended hydrogen bond pattern does not significantly affect the molecular conformation, which retains a propeller shape.

Crystal data presented in Table S2 reveal that **5** and **9** are isostructural despite the fact that N-methyl imidazole has been substituted by thiazolidine. This could indicate that the replacement of the N-CH<sub>3</sub> group by a sulphur atom and hydrogenation of the five-membered ring are insignificant as far as molecular conformation and supramolecular assemblies are concerned, supposedly because neither of these two fragments is involved in hydrogen bonding. Changes in molecular conformation of **11** as compared with its parent compound (non-methylated at C5) [16] are not substantial but again might be ascribed to different interactions in crystals caused by steric hindrance. Methyl substitution in **11** prevents formation of columnar stacking interactions between benzoxazole fragments, operating in the parent compound. Instead, we observe strong competition between S and O atoms for indole N-H donor and the resulting formation of a three centre hydrogen bond to both acceptors (Table S1, Figure S27). The N⋯S(=C) distance is the longest in the reported structures. With respect to molecular conformation, the consequences of the S/O replacement are not straightforward. The oxazole derivative differs in conformation from both thiazole and benzothiazole derivatives but resembles the hydrogenated thiazole derivative **9** (Table 1).



**Fig.S27.** Competition between S and O atoms for indole N-H donor and the resulting association of molecules **11** into chains by means of a three centre hydrogen bond to both acceptors.

## References

- [S1] Owczarzak, A.; Dutkiewicz, Z.; Kurczab, R.; Pietruś, W.; Kubicki, M.; Grzeńkiewicz, A.M. Role of Staple Molecules in the Formation of S⋯S Contact in Thioamides: Experimental Charge Density and Theoretical Studies. *Crystal Growth & Design* **2019**, *19*, 7324-7335, doi: 10.1021/acs.cgd.9b01204.



**Table S1.** Hydrogen bond geometrical parameters. Intramolecular interactions are written in italics.

<i>D—H</i> ⋯ <i>A</i>	<i>D—H</i> (Å)	<i>H</i> ⋯ <i>A</i> (Å)	<i>D</i> ⋯ <i>A</i> (Å)	<i>D—H</i> ⋯ <i>A</i> (°)
<b>2</b>				
N1—H1⋯S1 <sup>i</sup>	0.86	2.65	3.445 (4)	155.1
N3—H3⋯S1 <sup>ii</sup>	0.86	2.57	3.345 (3)	150.5
C13—H13A⋯S1 <sup>iii</sup>	0.97	2.87	3.596 (5)	132.3
<i>C10—H10B</i> ⋯ <i>S1</i>	<i>0.97</i>	<i>2.78</i>	<i>3.155 (4)</i>	<i>103.6</i>
<b>4</b>				
N1—H1⋯S1 <sup>iv</sup>	0.86	2.50	3.3549 (16)	170.4
N3—H3⋯S1 <sup>v</sup>	0.86	2.52	3.3613 (15)	164.6
C13—H13⋯S1 <sup>vi</sup>	0.93	2.81	3.562 (2)	138.3
<i>C10—H10B</i> ⋯ <i>S1</i>	<i>0.97</i>	<i>2.77</i>	<i>3.2500 (17)</i>	<i>111.2</i>
<b>5</b>				
N1—H1⋯S1 <sup>vii</sup>	0.86	2.58	3.390 (2)	157.6
<i>C10—H10B</i> ⋯ <i>S1</i>	<i>0.97</i>	<i>2.81</i>	<i>3.275 (3)</i>	<i>110.6</i>
<b>7</b>				
N1—H1⋯O1W <sup>v</sup>	0.86	2.31	2.996 (3)	136.8
N11—H11⋯O1W	0.86	2.13	2.924 (3)	153.3
O1W—H1WA⋯O1ET	0.85	1.83	2.647 (3)	160.8
O1ET—H1ET⋯S1 <sup>viii</sup>	0.82	2.49	3.305 (3)	171.8
O1W—H1WB ... C <sub>g</sub> (pyrrole)	0.85	2.48	3.280	157.9
<i>C10—H10A</i> ⋯ <i>S1</i>	<i>0.97</i>	<i>2.73</i>	<i>3.229 (2)</i>	<i>112.4</i>
<i>C20—H20A</i> ⋯ <i>S1</i>	<i>0.97</i>	<i>2.73</i>	<i>3.215 (2)</i>	<i>111.6</i>
<b>8</b>				
N1—H1⋯S1 <sup>ix</sup>	0.86	2.59	3.344 (3)	146.5
<i>C10—H10A</i> ⋯ <i>S1</i>	<i>0.97</i>	<i>2.77</i>	<i>3.236 (3)</i>	<i>110.4</i>
<i>C4—H4</i> ⋯ <i>S1</i>	<i>0.93</i>	<i>2.93</i>	<i>3.760 (3)</i>	<i>149.0</i>
<i>C18—H18B</i> ⋯ <i>S1</i>	<i>0.96</i>	<i>2.81</i>	<i>3.193 (3)</i>	<i>104.9</i>
<b>9</b>				

N1—H1…S1 <sup>x</sup>	0.86	2.58	3.4186 (16)	164.7
<i>C10—H10A…S1</i>	<i>0.97</i>	<i>2.72</i>	<i>3.2047 (18)</i>	<i>111.2</i>

---

**10**

N1—H1…S1 <sup>xi</sup>	0.88	2.55	3.3896 (14)	160.5
C10—H10A…S1 <sup>v</sup>	0.99	2.96	3.6652 (16)	128.8
C12—H12…S1 <sup>viii</sup>	0.95	3.00	3.5090 (16)	114.8
C13—H13…S1 <sup>viii</sup>	0.95	2.95	3.4711 (17)	115.6
<i>C10—H10B…S1</i>	<i>0.99</i>	<i>2.73</i>	<i>3.1503 (16)</i>	<i>106.2</i>

---

**11**

N1—H1…S1 <sup>xii</sup>	0.88	2.72	3.4702 (13)	143.5
N1—H1…O1 <sup>xii</sup>	0.88	2.61	3.1495 (17)	120.7
<i>C10—H10A…S1</i>	<i>0.99</i>	<i>2.78</i>	<i>3.2540 (17)</i>	<i>109.7</i>

---

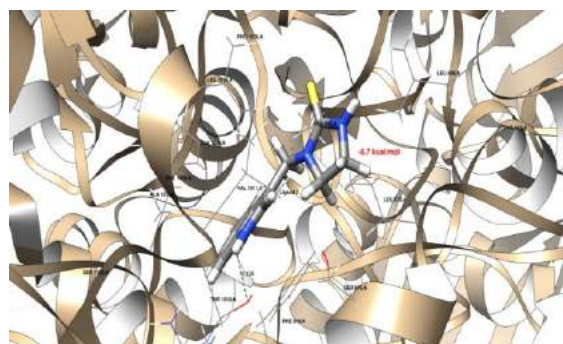
Symmetry code(s): (i)  $-x+1, -y, -z+1$ ; (ii)  $-x, -y, -z+1$ ; (iii)  $x, -y+1/2, z+1/2$ ; (iv)  $x+1/2, -y+1/2, -z+1$ ; (v)  $-x+1, -y+1, -z+1$ ; (vi)  $x, -y+1, z-1/2$ ; (vii)  $x+1/2, -y+3/2, z+1/2$ ; (viii)  $x, y+1, z$ ; (ix)  $-x+1/2, -y+1, z+1/2$ ; (x)  $x+1/2, -y+1/2, z+1/2$ ; (xi)  $-x+1/2, y+1/2, -z+1/2$ ; (xii)  $x+1, -y+3/2, z+1/2$

**Table S2.** Crystal data and structure refinement parameters for selected gramine derivatives.

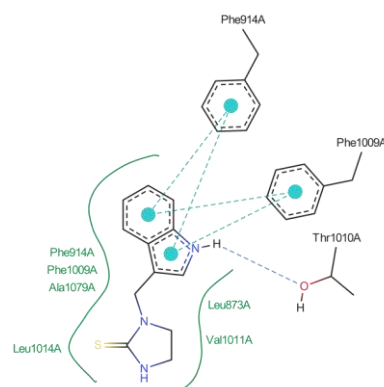
	2	4	5	7	8	9	10	11
<b>Crystal data</b>								
Chemical formula	C <sub>12</sub> H <sub>13</sub> N <sub>3</sub> S	C <sub>12</sub> H <sub>11</sub> N <sub>3</sub> S	C <sub>13</sub> H <sub>13</sub> N <sub>3</sub> S	C <sub>25</sub> H <sub>20</sub> N <sub>4</sub> S·C <sub>2</sub> H <sub>6</sub> O·H <sub>2</sub> O	C <sub>17</sub> H <sub>15</sub> N <sub>3</sub> S	C <sub>12</sub> H <sub>12</sub> N <sub>2</sub> S <sub>2</sub>	C <sub>12</sub> H <sub>10</sub> N <sub>2</sub> S <sub>2</sub>	C <sub>17</sub> H <sub>14</sub> N <sub>2</sub> OS
<i>M<sub>r</sub></i>	231.31	229.30	243.32	472.59	293.38	248.36	246.34	294.36
Crystal system space group	Monoclinic <i>P2<sub>1</sub>/c</i>	Orthorhombic <i>Pbcn</i>	Monoclinic <i>P2<sub>1</sub>/n</i>	Triclinic <i>P1</i>	Orthorhombic <i>P2<sub>1</sub>2<sub>1</sub>2<sub>1</sub></i>	Monoclinic <i>P2<sub>1</sub>/n</i>	Monoclinic <i>P2<sub>1</sub>/n</i>	Monoclinic <i>P2<sub>1</sub>/c</i>
Temperature (K)	295	293	293	293	293	293	100	130
<i>a</i> (Å)	10.4517 (8)	18.4010 (3)	9.1819 (3)	7.4924 (3)	7.1911 (2)	9.2002 (1)	7.9077 (2)	7.42703 (16)
<i>b</i> (Å)	8.4232 (6)	11.2626 (3)	14.2705 (3)	13.1185 (5)	13.9158 (4)	13.4917 (2)	7.2185 (2)	14.3167 (3)
<i>c</i> (Å)	13.5631 (11)	11.2577 (2)	9.5585 (3)	13.4710 (6)	14.6650 (4)	9.6702 (1)	19.4666 (5)	13.8146 (3)
$\alpha$ (°)	90	90	90	114.605 (4)	90	90	90	90
$\beta$ (°)	102.934 (8)	90	92.203 (3)	96.556 (4)	90	93.384 (1)	97.084 (3)	102.016 (2)
$\gamma$ (°)	90	90	90	92.830 (3)	90	90	90	90
<i>V</i> (Å <sup>3</sup> )	1163.75 (16)	2333.08 (8)	1251.53 (6)	1189.05 (9)	1467.53 (7)	1198.23 (3)	1102.70 (5)	1436.73 (5)
<i>Z</i>	4	8	4	2	4	4	4	4
<i>D<sub>x</sub></i> (Mg m <sup>-3</sup> )	1.320	1.306	1.291	1.320	1.328	1.377	1.484	1.361
Radiation type	Mo <i>K</i> $\alpha$	Cu <i>K</i> $\alpha$	Cu <i>K</i> $\alpha$	Cu <i>K</i> $\alpha$	Cu <i>K</i> $\alpha$	Cu <i>K</i> $\alpha$	Mo <i>K</i> $\alpha$	Cu <i>K</i> $\alpha$
$\mu$ (mm <sup>-1</sup> )	0.25	2.26	2.13	1.47	1.92	3.80	0.45	1.99
Crystal size (mm)	0.50 × 0.45 × 0.01	0.30 × 0.20 × 0.03	0.30 × 0.15 × 0.10	0.50 × 0.05 × 0.02	0.40 × 0.15 × 0.03	0.65 × 0.15 × 0.05	0.5 × 0.4 × 0.2	0.18 × 0.15 × 0.01
<b>Data collection</b>								
<i>T<sub>min</sub></i> , <i>T<sub>max</sub></i>	0.366, 1.000	0.595, 1.000	0.796, 1.000	0.783, 1.000	0.906, 1.000	0.335, 1.000	0.982, 1.000	0.789, 1.000
No. of measured, independent and observed [ <i>I</i> > 2 $\sigma$ ( <i>I</i> )] reflections	6864, 2008, 1047	19161, 2447, 2087	10993, 2598, 2281	19352, 4867, 4010	5861, 2993, 2724	49696, 2523, 2255	6089, 2302, 2099	5876, 2842, 2444
<i>R<sub>int</sub></i>	0.069	0.035	0.024	0.027	0.027	0.052	0.017	0.020
( <i>sin</i> $\theta$ / $\lambda$ ) <sub>max</sub> (Å <sup>-1</sup> )	0.592	0.631	0.630	0.630	0.630	0.631	0.666	0.625
<b>Refinement</b>								
<i>R</i> [ <i>F</i> <sup>2</sup> > 2 $\sigma$ ( <i>F</i> <sup>2</sup> )]	0.065	0.042	0.059	0.051	0.039	0.038	0.029	0.037
<i>wR</i> ( <i>F</i> <sup>2</sup> )	0.145	0.127	0.164	0.159	0.102	0.113	0.070	0.099
<i>S</i>	1.04	1.05	1.08	1.06	1.07	1.08	1.03	1.06

**Table S3.** Antibacterial activities of compounds **1-29**

Compound	Zone of growth inhibition [mm]			
	<i>Micrococcus luteus</i>	<i>Bacillus subtilis</i>	<i>Escherichia coli</i>	<i>Pseudomonas fluorescens</i>
<b>Gramine (1)</b>	0	0	0	0
<b>2</b>	3.3	4.5	2	4
<b>3</b>	1	1	1	1
<b>4</b>	1	2	0	1.5
<b>5</b>	3.8	5	2	4
<b>6</b>	3.5	3.3	1	2
<b>7</b>	4	2.3	1	2
<b>8</b>	1.8	1	1	1
<b>9</b>	1.3	2	1	3
<b>10</b>	3	4.2	0	4
<b>11</b>	0	0	0	0
<b>12</b>	2	3	0	5.5
<b>13</b>	7.3	9.4	0	10.5
<b>15</b>	11	3.3	7.7	0
<b>17</b>	1	1	2	1
<b>18</b>	0	0	2.5	0
<b>19</b>	0	1	2	1
<b>20</b>	1	0	2	0
<b>21</b>	3.2	4.5	1	3
<b>22</b>	0	1	3	0
<b>23</b>	1	0	3	0
<b>24</b>	0	0	3.4	0
<b>25</b>	0	1	1	1
<b>26</b>	0	0	0	0
<b>27</b>	1	0	0	0
<b>29</b>	1.3	2	1	1

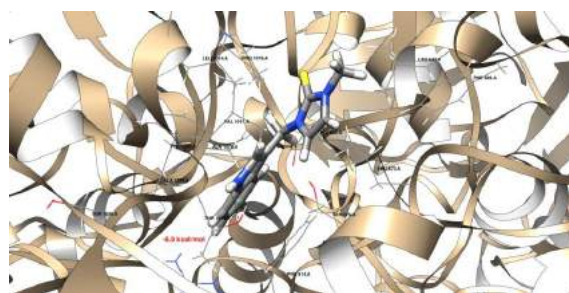


(a)

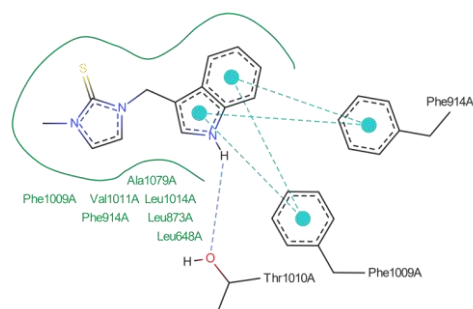


(b)

**Fig. S28.** (a) The interactions between the derivative **2** and the 1N5X protein domain. The dark-green dashed line indicates potential H-bond formation between one of the domain residues (namely THR 1010 A–2.23 Å) and the hydrogen bonded to one of the nitrogen atoms of the ligand; (b) The proposed interactions between the 1N5X protein's domain binding site and derivative **2** suggest the formation of one hydrogen bond (blue dashed line). Green solid lines signify hydrophobic contacts, and aqua dashed lines indicate pi-pi interactions.

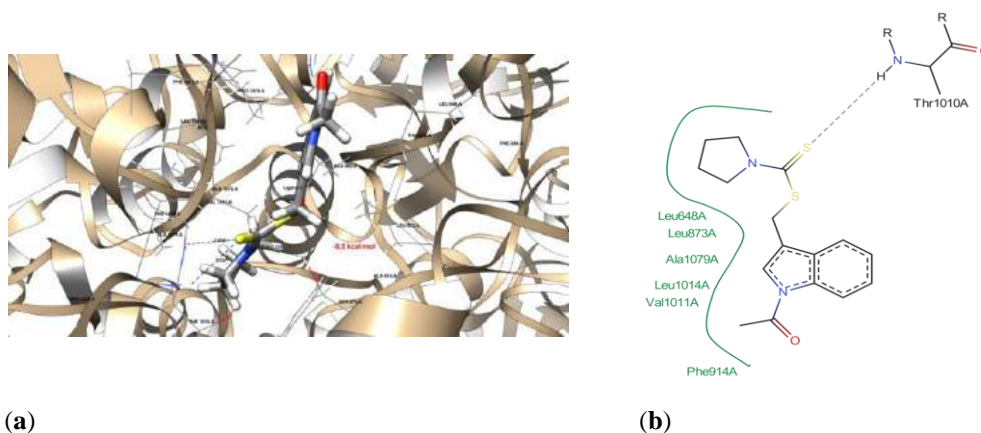


(a)

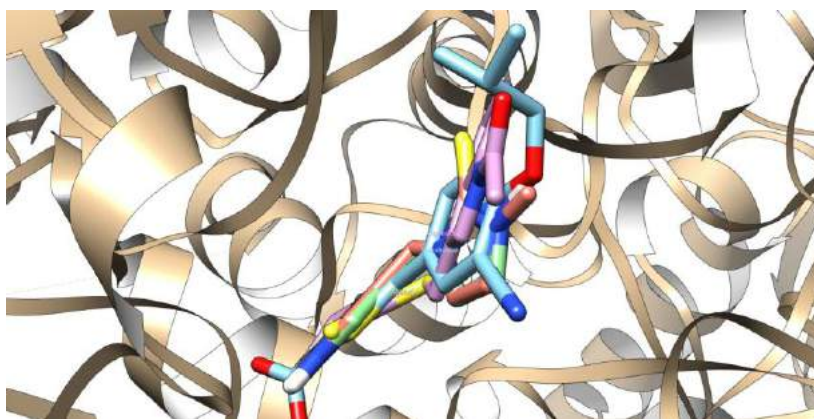


(b)

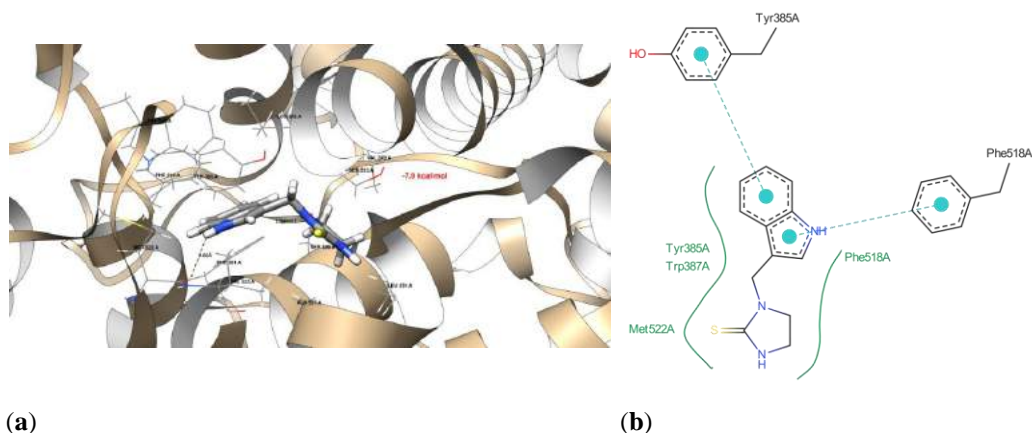
**Fig. S29.** (a) The interactions between the derivative **5** and the 1N5X protein domain. A dark-green dashed line implies potential hydrogen bond formation between domain residue THR 1010 A, and the ligand's pyrrolic-hydrogen atom (2.23 Å length); (b) The proposed interactions between the 1N5X protein's domain binding site and derivative **5** suggest the formation of one hydrogen bond (blue dashed line). Green solid lines signify hydrophobic contacts, and aqua dashed lines indicate pi-pi interactions.



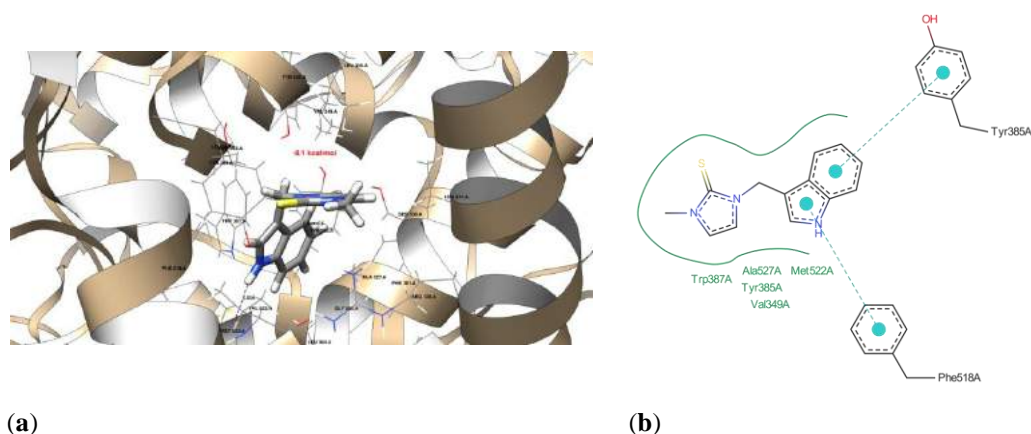
**Figure S30.** (a) The interactions between the derivative **15** and the 1N5X protein domain. A dark-green dashed line implies potential hydrogen bond formations between domain residues THR 1010 A (2.83 Å length), VAL 1011 A (2.80 Å length), and SER 876 A residue and the ligand (3.35 Å length); (b) The interactions proposed by molecular docking between the 1N5X protein's domain binding site and derivative **15**. According to the ProteinsPlus algorithm, one hydrogen bond is expected, with the possibility of three hydrogen bonds according to the UCSF Chimera software, but this hydrogen bond with THR 1010 A protein residue has the highest probability of formation. Green solid lines indicate hydrophobic contacts.



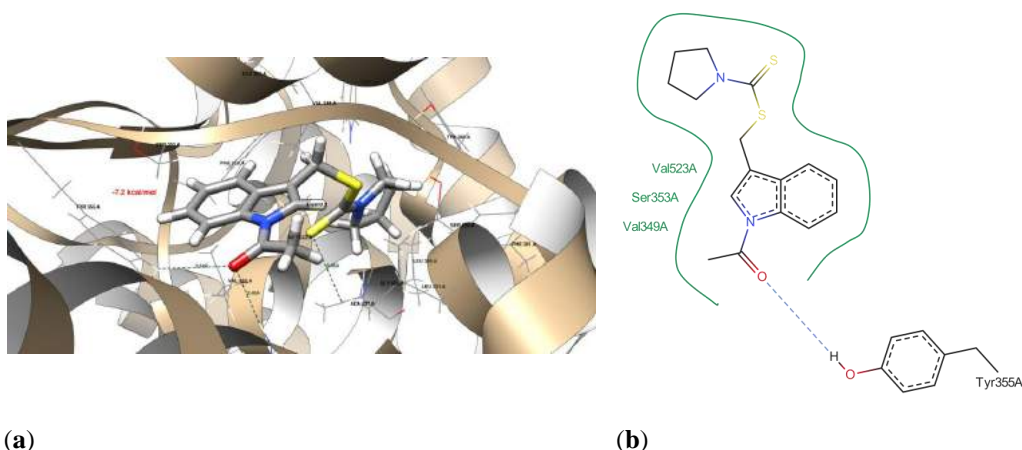
**Fig. S31.** The native ligand (febuxostat), redocked native ligand, and compounds **2**, **5**, and **15** in the binding site of the 1N5X protein domain.



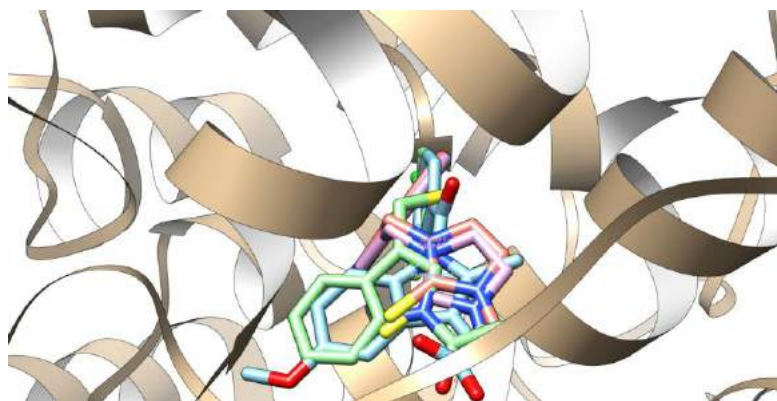
**Fig. S32.** (a) The spatial interactions between the derivative **2** and the 4COX protein domain. A dark-green dashed line implies potential hydrogen bond formation between domain residue MET 522 A (2.68 Å length) and the hydrogen bonded to the nitrogen atom of the ligand; (b) A closer look at the proposed interactions between the 4COX protein's domain binding site and derivative **2**, with green solid lines indicating hydrophobic contacts and aqua dashed lines indicating cation-pi interaction.



**Fig. S33.** (a) The spatial interactions between the derivative **5** and the 4COX protein domain. A dark-green dashed line suggests a potential hydrogen bond formation between the domain residue MET 522 A (length 2.60 Å) and the ligand; (b) The proposed interactions between the 4COX protein's domain binding site and derivative **5** are indicated by green solid lines indicating hydrophobic contacts and aqua dashed lines indicating cation-pi interaction. This model is not indicating hydrogen bond formation between MET 522 A and the ligand.



**Fig. S34.** (a) The spatial interactions between the derivative **15** and the 4COX protein domain. A dark-green dashed line suggests a potential hydrogen bond formation between the domain residue TYR 355 A and the ligand (3.54 Å length). The other can be formed between the ARG 120 A protein's residue and the ligand with a length of 2.48 Å, indicating a higher probability of formation. The last one can be formed between the ALA 527 A residue and the Ligand 3 structure (3.06 Å length); (b) The proposed interactions between the 4COX protein's domain binding site and derivative **15**. Green solid lines indicate hydrophobic contacts, and a blue dashed line indicates a hydrogen bond. It is indicating a lower number of hydrogen bonds, probably due to the fact that hydrogen bond formation between ARG 120 A and ALA 527 A residues is more difficult due to the greater angle.



**Fig. S35.** The native ligand (indomethacin), redocked native ligand, and compounds **2**, **5**, and **15** in the binding site of the 4COX protein domain.



Poznań, 29.05.2024 r.

## OŚWIADCZENIE

Oświadczamy, że w artykule pt. „New triazole-bearing gramine derivatives–synthesis, structural analysis and protective effect against oxidative haemolysis” opublikowanym w czasopiśmie *Natural Product Research*, 2022, 36(13), 3413-3419, wkład poszczególnych Autorów w powstanie publikacji jest następujący:

Lp.	Imię i nazwisko Autora	Wkład merytoryczny w powstanie publikacji	Podpis Autora
1	Prof. UAM dr hab. Beata Jasiewicz	Dyskusja wyników, współudział w opracowaniu manuskryptu	
2	Dr Arleta Sierakowska	Współudział w syntezie związków, Dyskusja wyników, współudział w opracowaniu manuskryptu	
3	Prof. UAM dr hab. Iwona Kowalczyk	Wykonanie oraz interpretacja obliczeń teoretycznych	
4	Prof. UAM dr hab. Lucyna Mrówczyńska	Wykonanie oraz interpretacja badań biologicznych, dyskusja wyników, współudział w opracowaniu manuskryptu	

Poznań, 29.05.2024 r.

## OŚWIADCZENIE

Oświadczamy, że w artykule pt. „Novel gramine-based bioconjugates obtained by click chemistry as cytoprotective compounds and potent antibacterial and antifungal agents” opublikowanym w czasopiśmie *Natural Product Research*, 2023, 1–7, wkład poszczególnych Autorów w powstanie publikacji jest następujący:

Lp.	Imię i nazwisko Autora	Wkład merytoryczny w powstanie publikacji	Podpis Autora
1	Prof. UAM dr hab. Beata Jasiewicz	Dyskusja wyników, współudział w opracowaniu manuskryptu	
2	Dr Arleta Sierakowska	Współudział w syntezie związków	
3	Mgr Kamil Ostrowski	Współudział w syntezie związków	
4	Mgr Milda Szlaużys	Współudział w syntezie związków	
5	Prof. UAM dr hab. Lucyna Mrówczyńska	Wykonanie oraz interpretacja badań biologicznych, dyskusja wyników, współudział w opracowaniu manuskryptu	

Poznań, 29.05.2024 r.

## OŚWIADCZENIE





Oświadczamy, że w artykule pt. „Synthesis and Hemolytic Activity of Bile Acid-Indole Bioconjugates Linked by Triazole” opublikowanym w czasopiśmie *Journal of Organic Chemistry*, 2023, 88(24), 16719–16734, wkład poszczególnych Autorów w powstanie publikacji jest następujący:

Lp.	Imię i nazwisko Autora	Wkład merytoryczny w powstanie publikacji	Podpis Autora
1	Prof. UAM dr hab. Beata Jasiewicz	Dyskusja wyników, współudział w opracowaniu manuskryptu	
2	Prof. UAM dr hab. Tomasz Pospieszny	Dyskusja wyników, współudział w opracowaniu manuskryptu, wykonanie oraz interpretacja obliczeń teoretycznych	
3	Dr Hanna Koenig	Współudział w syntezie związków, dyskusja wyników, współudział w opracowaniu manuskryptu	
4	Prof. UAM dr hab. Lucyna Mrówczyńska	Wykonanie oraz interpretacja badań biologicznych, dyskusja wyników, współudział w opracowaniu manuskryptu	

Poznań, 29.05.2024 r.

## OŚWIADCZENIE

Oświadczamy, że w artykule pt. „ Novel C3-Methylene-Bridged Indole Derivatives with and without Substituents at N1 : The Influence of Substituents on Their Hemolytic, Cytoprotective, and Antimicrobial Activity” opublikowanym w czasopiśmie *International Journal of Molecular Sciences*, 2024, 25(10), 5364, wkład poszczególnych Autorów w powstanie publikacji jest następujący:

Lp.	Imię i nazwisko Autora	Wkład merytoryczny w powstanie publikacji	Podpis Autora
1	Prof. UAM dr hab. Beata Jasiewicz	Dyskusja wyników, współudział w opracowaniu manuskryptu	
2	Mgr Karolina Babiczuk	Współudział w syntezie związków, dyskusja wyników, współudział w opracowaniu manuskryptu,	
3	Prof. dr hab. Urszula Rychlewska	Przeprowadzenie i analiza badań krystalograficznych, współudział w opracowaniu manuskryptu	
4	Dr Beata Warzajtis	Przeprowadzenie i analiza badań krystalograficznych, współudział w opracowaniu manuskryptu	
5	Prof. UAM dr hab. Lucyna Mrówczyńska	Wykonanie oraz interpretacja badań biologicznych, dyskusja wyników, współudział w opracowaniu manuskryptu	